Gesellschaft für Anlagen-
und Reaktorsicherheit
(GRS) gGmbH

ATHLET

Validation

GRS - P - 1 / Vol. 3
Rev. 5

Gesellschaft für Anlagen-
und Reaktorsicherheit
(GRS) gGmbH

ATHLET 3.2

Validation

G. Lerchl
H. Austregesilo
T. Hollands
P. Schöffel
D. von der Cron

February 2019

GRS - P - 1 / Vol. 3
Rev. 5

Abstract

This User's Manual has been prepared to assist users in the effective application of the ATHLET computer code. ATHLET is an advanced best-estimate system code which has been initially developed for the simulation of design basis and beyond design basis accidents (without core degradation) in light water reactors, including VVER and RBMK reactors. Furthermore, this program version enables the simulation of further working fluids like helium, liquid metals or molten salts.

The one-dimensional, two-phase fluiddynamic models are based on a five-equation model supplemented by a full-range drift-flux model, including a dynamic mixture-level tracking capability. Moreover, a two-fluid model based on six conservation equations is provided. The heat conduction and heat transfer module allows a flexible simulation of fuel rods and structures. Nuclear heat generation is calculated by a point-kinetics or by a one-dimensional kinetics model. A general control simulation module is provided for flexible modelling of BOP- and auxiliary plant systems.

Systematic code validation is performed by GRS and independent organizations.

This Validation Manual is the third volume of the ATHLET Code Documentation comprising four volumes. This manual presents an overview about the complete ATHLET validation effort spent up to now. In addition, the results of five test cases simulated with the present ATHLET program version are compared with the experimental data.

The ATHLET Code Documentation Package

The complete ATHLET Code Documentation consists of four volumes:

- **GRS-P-1 / Vol. 1 : User's Manual**
  The essential document for applying the code effectively. It contains the information necessary to perform successful calculations. It includes explanations, guidelines and instructions for modelling a reactor plant and running the code.
- **GRS-P-1 / Vol. 2 : Programmer's Manual**
  Companion document to the User's Manual. It contains instructions for code installation and comprehensive lists of subroutines and variables.
- **GRS-P-1 / Vol. 3 : Validation**
  It describes the strategy and the status of code validation. It documents the validation calculations performed prior to the release of the current code version.
- **GRS-P-1 / Vol. 4 : Models and Methods**
  Comprehensive description of the basic modelling assumptions, physical models and correlations, and numerical methods in ATHLET.

The ATHLET Code Documentation is available to all user organizations in possession of a valid license for ATHLET.

List of Contents

List of Figures

List of Tables

Nomenclature

Abbreviations and notations :

AFK	ATHLET function routine
AFW	Auxiliary feedwater system
ATLAS	ATHLET Analysis Simulator
ATWS	Anticipated transient without scram
BE	Best estimate
BL	Broken loop
BOP	Balance-of-plant
BWR	Boiling water reactor
CCFL	Counter-current flow limitation
CD	Critical discharge
CDR	Critical discharge rate
CHF	Critical heat flux
CL	Collapsed level, cold leg
CSA	Cross sectional area
CSNI	Committee on the Safety of Nuclear Installations (Nuclear Energy Agency)
CV	Control volume (finite-volume-approach)
CW	Control word
DC	Downcomer
DNB	Departure from nucleate boiling
DEB	Double end break
ECC	Emergency core cooling
EIMMB	Extended integrated mass and momentum balances
EM	Evaluation model with conservative assumptions
Eq.	Equation
Exp.	Experimental
FB	Film boiling
FEBE	Time integration module within ATHLET
FTRIX	Sparse matrix package within ATHLET
FV	Finite volume (numerical method)
FZR	Forschungszentrum Rossendorf
GCSM	General control simulation module within ATHLET
HECU	Heat conduction module within ATHLET

HCO	Heat conduction object
HCV	Heat conduction volume (heat slab)
HL	Hot leg
HTC	Heat transfer coefficient
HTEX	Heat exchanger
IAEA	International Atomic Energy Agency
IL	Intact loop
IMMB	Integrated mass and momentum balances
IP	Interfacial
ISP	International Standard Problem
KFKI	Atomic Energy Research Institute, Hungary
KW	Keyword
KKW	Kernkraftwerk (Nuclear Power Plant) :
	GKN II KKW Neckarwestheim
	KKG KKW Gundremmingen
	KKK KKW Krümmel
	KKP 1 KKW Philippsburg I
	KKU KKW Unterweser
	KRB KKW Brokdorf
LOCA	Loss-of-coolant accident
LP	Lower plenum
LWR	Light water reactor
MC	Multi-component
ML	Mixture level
MRP	Main recirculation pump
NB	Nucleate boiling
NC	Non-condensable
NEA	Nuclear Energy Agency
NEUKIN	Neutron kinetics module in ATHLET
NPP	Nuclear power plant
ODE	Ordinary differential equation(s)
OECD	Organization for Economic Co-operation and Development
OTSG	Once-through steam generator
PC	Priority chain
	Personal computer
PORV	Pressurizer relief valve
PW	Pseudo-keyword
PWR	Pressurized water reactor
RBMK	Graphite-moderated boiling water reactor (Russian type)

RUB	Ruhr-Universität Bochum
RV	Reactor vessel
SET	Separate effect test
SG	Steam generator
SJP	Single junction pipe
SSC	Steady state calculation
TB	Transition boiling
TFD	Thermo-fluiddynamics
TFO	Thermo-fluiddynamic object
THZ	Hochschule Zittau/Görlitz (FH)
TUM	Technische Universität München
UH	Upper head
UK	United Kingdom
UP	Upper plenum
VVER	Same as WWER
WWER	Pressurized water reactor with horizontal steam generators (Russian type)
2E-	Two energy equations system
1M-	Mixture momentum equations system
2M-	Two momentum equations system

Control Volume:
Basic network element; spatial entity where mass and energy are distributed homogeneously.

Junction:
Basic network element; connection between CV's where mass and energy are transported.

Simulation Model:
Totality of simulation program and input model.

Input Model:
Totality of input data for all modules applied in the particular simulation (including balance-of-plant models and user-supplied GCSM controllers).

1 Overview of ATHLET

The thermal-hydraulic computer code **ATHLET** (**A**nalysis of **TH**ermal-hydraulics of **LE**aks and **T**ransients) is being developed by the Gesellschaft für Anlagen- und Reaktorsicherheit (**GRS**) for the analysis of operational conditions, abnormal transients and all kinds of leaks and breaks in nuclear power plants. The aim of the code development is to cover the whole spectrum of design basis and beyond design basis accidents (without core degradation) for **PWRs, BWRs, SMRs and future Gen IV reactors** with one single code. The main code features are:

- advanced thermal-hydraulic modeling (compressible fluids, mechanical and thermal non-equilibrium of vapor and liquid phase)
- availability of diverse working fluids: light or heavy water, helium, sodium, lead or lead-bismuth eutectic, supercritical carbon dioxide, molten salts as well as user-provided single-phase (non-boiling) working fluids
- heat generation, heat conduction and heat transfer to single- or two-phase fluid considering structures of different geometry, e.g. rod or pebble bed
- interfaces to specialized numerical models such as 3D neutron kinetic codes or 3D CFD codes for coupled multiphysical or multiscale simulations
- control of ATHLET calculation by callbacks to programming language independent user code enabling the coupling of external models
- plug-in technique for user provided code extensions
- modular code architecture
- separation between physical models and numerical methods
- numerous pre- and post-processing tools
- portability
- continuous and comprehensive code validation

ATHLET is applied by numerous institutions in Germany and abroad.

The development and validation of ATHLET is sponsored by the German Federal Ministry for Economic Affairs and Energy (BMWi) based on decisions by the German Bundestag.

1.1 Range of Applicability

ATHLET has been developed and validated to be applied for all types of design basis and beyond design basis incidents and accidents without core damage in light water reactors, like PWR, BWR, VVER, and RBMK. For accidents with core damage, **ATHLET-CD** (**C**ore **D**egradation) has been developed providing extensions for the simulation of the mechanical fuel behavior, core melting and relocation, debris bed formation as well as fission product release and transport within the reactor system. ATHLET-CD uses the same input deck as ATHLET supplemented by data required by the core degradation models.

The range of working fluids covers **light and heavy water** enabling the transition between subcritical and **supercritical fluid states**. In addition, further coolants can be simulated as working fluids: **helium, sodium** as well as non-boiling fluids **liquid lead, lead-bismuth eutectic**, **molten salts** and **user-provided fluids**. These extensions, aiming at the simulation of future Generation IV reactor designs, are still subject to further development and validation.

1.2 Code Structure

ATHLET is written in Fortran. The code structure is highly modular and allows an easy implementation of different physical models. The code is composed of several **basic modules** for the calculation of different phenomena emphasizing the operation of a nuclear power reactor:

- Thermo-Fluiddynamics (TFD)
- Heat Conduction and Heat Transfer (HECU)
- Neutron Kinetics (NEUKIN)
- Control and Balance of Plant (GCSM)

The TFD system of ordinary differential equations is solved fully implicitly with the numerical integration method FEBE. Other independent modules (e.g. large models with own time advancement procedure) can be coupled without structural changes in ATHLET by means of dedicated interfaces.

1.3 Fluiddynamics

The TFD module of ATHLET employs a modular network approach for the representation of a thermal-hydraulic system. A given system configuration can be simulated just by connecting

basic fluiddynamic elements, called **thermo-fluiddynamic objects (TFOs)**. There are several TFO types, each of them is applied with a selected fluiddynamic model. All object types are classified into three basic categories:

- **Pipe objects** employ a one-dimensional TFD-Model describing the transport of fluid. After nodalization according to input data, a pipe object can be understood as a number of consecutive nodes (**control volumes**) connected by flow paths (**junctions**). A special application of a pipe object, called single junction pipe, consists of only one junction, without any control volumes.
- **Branch objects** consist of only one control volume. They employ a zero-dimensional TFD-model of non-linear ordinary differential equations or algebraic equations.
- **Special objects** are used for network components that exhibit a complex geometry, e.g. the cross connection of pipe objects aligned in parallel for the generation of a multidimensional network.

This object structure has been developed in order to allow the coupling of models of different physical formulation and spatial discretization, which are to be employed in certain network domains.

ATHLET offers two different sets of model equations for the simulation of the fluid-dynamic behavior:

- The **5-equation model** with separate conservation equations for liquid and vapor mass and energy, supplemented by a mixture momentum equation. It accounts for thermal and mechanical non-equilibrium and includes a mixture level tracking capability.
- The **Two-fluid model** with fully phase-separated conservation equations for liquid and vapor mass, energy, and momentum (without mixture level tracking capability).

The spatial discretization is performed on the basis of a **finite-volume staggered-grid approach**. The mass and energy equations are solved within control volumes, and the momentum equations are solved over junctions connecting the centers of the control volumes. The solution variables are the pressure, vapor temperature, liquid temperature and vapor mass quality within a control volume, as well as the mass flow rate (5-eq. model) or the phase mass velocities (6-eq. model) in a junction, respectively.

Two types of control volumes are available. Within the so-called ”ordinary” control volume, a homogeneous mass and energy distribution is assumed. Within the ”non-homogeneous” control volume, a **mixture level** is modelled. Above the mixture level, steam with water droplets, below the mixture level, liquid with vapor bubbles may exist. The combination of ordinary and

non-homogeneous control volumes provides the option to simulate the motion of a mixture level through vertical components.

A full-range **drift-flux model** is available for the calculation of the relative velocity between the fluid phases. The model comprises all flow patterns from homogeneous to separated flow occurring in vertical and horizontal two-phase flow. It also takes into account countercurrent flow limitations in different geometries.

Moreover, both fluid-dynamic options allow for the simulation of **non-condensable gases**. This applies for water as well as for the liquid metal and molten salt working fluids. Fluid properties are provided for hydrogen, nitrogen, oxygen, air, helium and argon. Additional mass conservation equations can be included for the description of **boric acid** or **zinc borate** transport within a coolant system as well as for the transport and release of **nitrogen dissolved** in the liquid phase of the coolant.

Both the 5-equation model and the two-fluid model employ the one-dimensional conservation equations for mass, momentum and energy. By means of a spatially two- or three-dimensional TFO arrangement, these models allow for a simplified multidimensional simulation. In order to enhance the capability of ATHLET with regard to the simulation of complex, multidimensional flow phenomena, a **thermal-hydraulic 2D/3D model** has been developed. It extends the balance equations of the two-fluid model. Both the fully 2D and 3D momentum equations for liquid and vapor are available, though validation is still in progress.

For pipe objects applying the 5-equation model, there is also the possibility to use the method of integrated mass and momentum balances (**EIMMB**), an option for fast-running calculations, mainly in the frame of a nuclear plant analyzer. With the application of the EIMMB-Method, the solution variables are now the average object pressure, the mass flows at pipe inlet and outlet, and the local qualities and temperatures. The local pressures and mass flow rates are obtained from algebraic equations as a function of the solution variables.

Another fluid-dynamic option, applied exclusively for the steady state calculation, consists of a 4-equation model with balance equations for liquid mass, vapor mass, mixture energy and mixture momentum. The solution variables are the pressure, vapor mass quality and enthalpy of the dominant phase within a control volume, and the mass flow rate in a junction. The entire range of fluid conditions, from subcooled liquid to superheated vapor including thermal non-equilibrium is taken into account, assuming the non-dominant phase to be at saturation.

1.4 Numerical Methods

The **time integration** of the thermo-fluiddynamic model is performed with the general purpose ODE-solver **FEBE** (Forward-Euler, Backward-Euler). It provides the solution of a linear system

of ordinary differential equations (ODE) of first order, splitting it into two subsystems, the first being integrated explicitly, the second implicitly. Generally, the **fully implicit** option is used in ATHLET. Each thermo-fluiddynamic object provides a subset of the entire ODE system, which is integrated simultaneously by FEBE.

The linearization of the underlying model equation system is done numerically by calculation of the Jacobian matrix. A **block sparse matrix package** (FTRIX) is available to handle the repeated evaluation of the Jacobian matrix as well as the solution of the resulting system of linear equations in an efficient way. Alternatively, scalable solvers from the PETSc and MUMPS libraries can be used for the numerical calculations via the Numerical Toolkit (NuT) plug-in.

A **rigorous error control** is performed based on an extrapolation technique. According to the error bound specified by the user, the time step size and the order of the method (>2) are adequately determined by FEBE for every integration step.

1.5 Heat Conduction and Heat Transfer

The simulation of the heat conduction in **structures, heat exchangers, fuel rods, electrical heaters and spheres** (pebble bed) is performed by the basic module **HECU**. It permits the user to assign heat conduction objects (HCOs) to all thermal-fluiddynamic objects of a given network.

The one-dimensional heat conductor module HECU provides the simulation of the temperature profile and the energy transport in solid materials. The model has the following characteristics:

- The shape of a HCO is constant in time.
- The model can simulate the one-dimensional temperature profile and heat conduction in plates normal to the surface, as well as in hollow or full cylinders and spheres in the radial direction.
- Optionally, two-dimensional heat conduction can be simulated considering the axial direction of plates and cylinders.
- In each HCO, up to three material zones can be modelled. A material zone is simulated by a user-defined number of temperature layers. The material zones can be separated by a geometrical gap and a corresponding heat transfer coefficient. Furthermore, the model enables the calculation of the temperature in TRISO coated particles.
- The HCOs can be coupled on left and/or right side to TFOs by consideration of the energy transport between heat conductor surface and the surrounding fluid. It is also possible to

simulate a fluid temperature as boundary condition for the HCO by means of control (GCSM) signals.

- The HCOs are automatically split into heat conduction volumes (HCVs) according to the nodalization of the adjacent TFOs and to user input.
- Heat generation can be considered in material zones. The specific heat generation rate per volume unit is assumed to be distributed uniformly either within a material zone or a temperature layer.
- Radiation heat transfer between different HCOs can be taken into account.

The **heat transfer package** covers a wide range of single phase and two-phase flow conditions of water. Correlations for critical heat flux and minimum film boiling temperature are included. Evaporation and condensation directly at heating or cooling surfaces are calculated. A quench front model for bottom and top reflooding is also available. Special heat transfer correlations are available for supercritical water, liquid metal working fluids and helium considering specific geometries (e.g. bundle or pebble bed).

1.6 Nuclear Heat Generation

The nuclear heat generation is generally modelled by means of the neutron kinetics module **NEUKIN**. For the simulation of electrically heated rods or for a simplified, straight-forward representation of a reactor core, the total generated power as a function of time or any other quantity can optionally be given.

The generated **nuclear reactor power** consists of two parts: the prompt power from fission and decay of short-lived fission products, and the decay heat power from the long-lived fission products. The steady state part of the decay heat and its time-dependent reduction after a reactor scram are provided in form of a GCSM signal. The time-dependent behavior of the prompt power generation is calculated either by a point-kinetics model or by an one-dimensional neutron kinetics model. An input-specified fraction of the total power is assumed to be produced not in the fuel but directly in the coolant.

The **point-kinetics model** is based on the application of the well-known kinetics equations for one group of prompt and for six groups of delayed neutrons. The reactivity changes due to control rod movement or reactor scram are given by a GCSM signal. The reactivity feedback effects for fuel temperature, moderator density and moderator temperature are calculated either by means of dependencies given by input tables or with reference reactivity coefficients. If the

boron tracking model is applied, the reactivity feedback due to changes in the boron concentration will be also taken into account.

The **one-dimensional kinetics model** solves the time-dependent neutron diffusion equations with two energy groups of prompt neutrons and six groups of delayed neutrons. The active core zone can be subdivided into zones with different materials. A reflector zone is also considered.

The model includes the coarse-mesh spatial approximation of the neutron flux by means of second order polynomials. It also accounts for moderator and Doppler reactivity feedback by temperature and density dependent cross sections. Control rod movement and reactor scram are simulated by means of local changes of group cross sections as a function of rod position.

The module NEUKIN also offers a general interface for coupling of **3D neutronic models**. Several 3D codes for rectangular and hexagonal geometries have been successfully coupled to ATHLET with this interface, e.g. QUABOX/CUBBOX, TORT-TD, PARCS or DYN3D.

1.7 Simulation of Components

Specific models are provided for the simulation of **valves, pumps, accumulators, steam separators, steam and gas turbines, compressors, steam condensers, single and double ended breaks, fills, leaks, and boundary conditions** for pressure and enthalpy. The steam separator model is an empirical approach for the calculation of carry-over and carry-under flows by means of input functions of the inlet mass flow rates, of the void fraction in the separator region, and of the mixture level outside the separator. Abnormal separator conditions like flow reversal or flooding can be simulated.

In general, major plant components (e.g. pressurizer, steam generators) can be modelled by connecting thermo-fluiddynamic objects (TFOs) and heat conduction objects (HCOs) via input data. Simplified compact models for those components are also available as special objects.

Critical flow, e.g. **discharge** flow**,** is calculated by a one-dimensional thermal non-equilibrium model with consideration of the given flow geometry. The module CDR1D generates automatically tables of critical mass fluxes applied in ATHLET for the interpolation of the critical mass flow rates. Optionally, a homogeneous equilibrium model and the Moody discharge model are available.

1.8 Simulation of Control and Balance of Plant

The simulation of balance-of-plants (**BOP**) systems within ATHLET is performed by the basic module **GCSM** (General Control Simulation Module). GCSM is a block-oriented simulation language for the description of control, protection and auxiliary systems.

The user can model control circuits or even simplified fluid systems just by connecting basic functional blocks (e.g. switch, adder, integrator). Most of the system variables calculated within the fluiddynamics, neutron kinetics or within other ATHLET modules can be selected as input to these functional blocks (process variables). The output of such control blocks can be fed back to the thermo-fluiddynamics in form of hardware actions (e.g. valve cross sectional area, control rod position) or boundary conditions (e.g. temperature, heat and mass sources).

The GCSM module allows for the representation of fluiddynamic systems (e.g. steam line, condensate system) in a very simplified way (quasi stationary approach) with the advantage of requiring very little computing time in comparison with the fluiddynamics module.

GCSM also provides an interface to a library that contains detailed models with fixed structure and own input data for plant components (e.g. heat exchanger or even containment model) or for control systems (e.g. power control or system pressure control for typical power plants). The **GRS containment codes CONDRU and COCOSYS** have been coupled to ATHLET by means of this interface. In addition, GCSM comprises a flexible interface that enables the coupling of ATHLET with user provided code, that implements external models, new controllers types, specific signals, or complete BOP models.

1.9 Code Handling

ATHLET provides a free-format, hierarchically structured input. Both the generation and the maintenance of the ATHLET input decks are facilitated by several copy functions and by the use of a flexible parameter technique during input data processing, which helps to avoid the repeated typing of identical or similar input data. An extended checking of both the input data and the program processing helps the user to discover input errors or modelling weaknesses affecting both code performance and physical results.

ATHLET provides a **restart capability**. The program execution can be **parallelized** on computers with shared memory architecture using the Fortran OpenMP standard. ATHLET runs under different computer operational systems (MS Windows ®, Unix).

The ATHLET Program Package comprises a series of **auxiliary programs** to support both the ATHLET users and developers in the application and development of ATHLET:

- AGM: **A**THLET **G**CSM **M**odeler for graphical setup and testing of control systems and generation of GCSM input data.
- AIG: **A**THLET **I**nput **G**raphics for graphical representation of the TFO and HCO network specified in the input model.
- GIG: **G**CSM **I**nput **G**raphics for graphical representation of the structure of GCSM controllers.
- Several programs for the post-processing of plot data (concatenation, merging, algebraic operations,...)
- APTPlot: Generates time and locus diagrams exploiting the structure of the input model.
- ATLAS: Dynamic visualization of the simulation results on the basis of AIG and GIG pictures.
- Several programs for the analysis of the Jacobian matrix (interdependencies, Eigenvalues,..), mainly for code development and debug purposes.

Furthermore, ATHLET can be applied as process model of the **ATLAS plant simulator** providing full interaction and extended data visualization. ATLAS is also a component of the AC² software package.

ATHLET is also closely linked with the GRS computer programs **SUSA** and **MCDET**. Both enable uncertainty and sensitivity analyses of ATHLET simulation results.

1.10 Code Coupling

ATHLET is part of the **AC² software package**, which comprises the GRS codes ATHLET, ATHLET-CD and COCOSYS, complemented by the interactive simulator software ATLAS.

To allow **multiphysical or multiscale simulations**, ATHLET has been coupled successfully to various computer codes by means of dedicated coupling interfaces. The following figure depicts the essential interfaces that are realized for ATHLET. Depending on the characteristic time constants of the coupled processes, the coupling techniques used range from weak form (e.g. data transfer after completed time step) to strong or semi-implicit form (i.e. mutual iteration of the codes' results for each substep of the FEBE extrapolation algorithm, used for coupling with CFD codes).

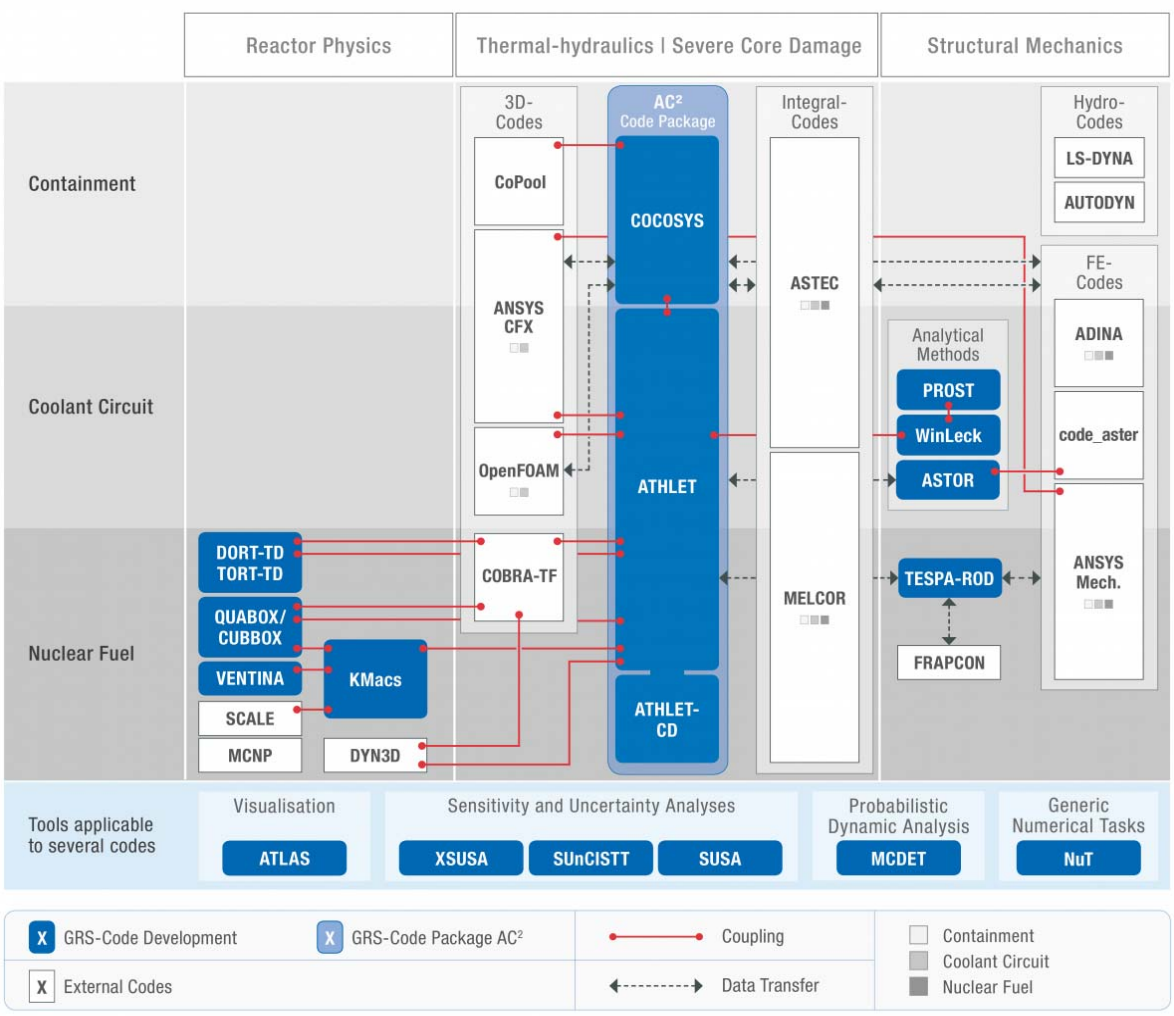

Moreover, ATHLET can be extended by user provided feature implementations. The **plug-in concept** enables the users to apply ATHLET more individually by either requesting a specific extension from GRS or even by developing the needed feature on their own. Such plug-ins have to be created as separate shared libraries on Linux systems or DLLs under Windows. In case a plug-in binary is placed within the *plugin* directory of an ATHLET installation, ATHLET will register it at startup and invoke it if the applied input file demands its use. The parts or phases of the simulation that can be extended by plug-ins are specified by ATHLET.

Another option for controlling the simulation by user code is offered by using the shared library version (MS Windows: dll / Linux: so) of ATHLET. This library provides the main entry of ATHLET via the exported routine symbol athlet_. This variant allows to implement a user program that calls ATHLET as a subroutine. In this case the simulation process can be controlled in an *"event oriented"* manner by associating the so called **callback routines** before calling ATHLET. An *event* can be considered as a certain and named point in the simulation flow, like *input done*, *begin of timestep*, *end of timestep*. These points have been made available as the so called **hooks**, at which a user might associate routines that instruct ATHLET what to do at this

point before continuing the simulation. Hashmaps, which include pointers to exported ATHLET variables, are accessible by both the user code and ATHLET. They enable inter-code data transfer of e.g. physical fields or GCSM control block states.

1.11 Validation

The development of ATHLET was and is accompanied by a systematic and comprehensive validation program. The validation is mainly based on pre- and post-test calculations of separate effects tests, integral system tests including the major **International Standard Problems**, as well as on actual plant transients. A well balanced set of tests has been derived from the **CSNI Code Validation Matrix** emphasizing the German combined ECC injection system. The tests cover phenomena which are expected to be relevant for all types of events of the envisaged ATHLET range of application for all common LWRs including advanced reactor designs with up-to-date passive safety systems. The validation of ATHLET for alternative working fluids relevant for future Gen IV reactors is underway.

2 General Validation Strategy

2.1 Objectives and Definitions

Computer codes like ATHLET aim to simulate the system behavior of nuclear power plants as realistic as possible ('best estimate'). These computer codes are used to investigate

- incidents and accidents of different scenarios and their consequences,
- the effectiveness of emergency procedures.

The process carried out by comparing code predictions with experimental measurements or measurements in a reactor plant (if available) is called validation. A code or code model is considered validated when sufficient testing has been performed to ensure an acceptable level of predictive accuracy over the range of conditions for which the code may be applied. Accuracy is a measure of the difference between measured and calculated quantities taking into account uncertainties and biases in both. Bias is a measure, usually expressed statistically, of the systematic difference between a true mean value and a predicted or measured mean. Uncertainty is a measure of the scatter in experimental or predicted data /CSN89/. The acceptable level of accuracy is judgmental and will vary depending on the specific problem or question to be addressed by the code. The procedure for specifying, qualitatively or quantitatively, the accuracy of code predictions is also called code assessment.

The international literature often distinguishes between the terms 'validation' and 'verification'. A mathematical model, or the corresponding computer code, is verified if it is demonstrated that the code behaves as intended, i.e. that it is a proper mathematical representation of the conceptual model, and that the equations are correctly encoded and solved. Verification may include the demonstration of convergence of the calculated results during a process of reduction of time steps and the size of the nodes of simulation. Also the comparison of selected results with exact mathematical solutions and with the results obtained by similar codes may fall under the term verification. In this context, the comparison with measured values is not part of the verification process, it is rather a validation task. The term verification, however, is often used synony-

mously with validation and qualification /CSN89/. Especially in the past, the term verification was used in the frame of the ATHLET code validation work, including comparisons between calculations and measurements.

2.2 Validation Matrices for Light Water Reactors

The validation of codes is mainly based on pre-test and post-test calculations of separate effects tests, integral system tests, and transients in commercial plants. An enormous amount of test data, usable for code validation, has been accumulated in the last decades. In the year 1987 the Committee on the Safety of Nuclear Installations (CSNI) of the Nuclear Energy Agency (NEA) in the Organization for Economic Co-Operation and Development (OECD) issued a report compiled by the Task Group on the Status and Assessment of Codes for Transients and ECC /CSN87/. It contains proposed validation matrices for LOCA and transients, consisting of the dominating phenomena and the available test facilities, and the selected experiments. The Task Group on Thermal Hydraulic System Behavior updated the integral test matrices /ANN96/ and extended their work to separate effects tests /AKS94/.

The systematic validation of the ATHLET computer code is based on a well balanced set of integral and separate effects tests derived from the CSNI proposal, emphasizing however the German combined ECC injection system which has been investigated in the UPTF, PKL and LOBI facilities.

The validation methodology distinguishes between the validation of individual code models and the assessment of the overall system simulation. The individual code models are validated against separate effects tests in full or at least large scale test facilities. The overall assessment is based on pre- and post-test calculations of integral tests, and comparisons with available plant transients.

To systemize the selection of tests for code validation, the so-called 'Cross Reference Matrices' have been first established. Based on these matrices, phenomenologically well founded sets of experiments have been defined, for which comparison of measured and calculated parameters form a basis for establishing the uncertainty range of test calculation results. The matrices also permit identification of areas where further research may be justified.

In the Cross Reference Matrices (figs. 2 - 1 to 2 - 11), the relevant physical phenomena which are believed to occur during transients or loss-of-coolant accidents in different types of NPPs are listed, together with the experimental facilities suitable for reproducing these effects and

the test types of interest. The relationship phenomenon versus test type indicates which phenomena are expected to occur in which test types. The relationship test facility versus phenomenon indicates the suitability of the test facilities for code validation of the different phenomena, and the relationship test type versus test facility indicates which test types are performed in which test facilities.

The matrices for Western PWRs and BWRs are focused mainly on integral system tests and operational data from power plants. For PWR facilities, six individual matrices were prepared (figs. 2 - 1 to 2 - 6), differentiating among:

- large breaks
- small and intermediate leaks for PWRs with U-tube steam generators
- small and intermediate leaks for PWRs with once-through steam generators
- transients
- transients under shut-down conditions
- accident management for a non-degraded core.

The matrix for small and intermediate breaks in PWRs with once-through steam generators (fig. 2 - 3) has been developed to address particular phenomena which are unique to this reactor type. For BWR facilities, two individual matrices have been established (figs. 2 - 7 to 2 - 8) differentiating between loss-of-coolant accidents and transients.

For Russian WWER facilities, three matrices have been compiled by the OECD /LIE01/ differentiating between large breaks, small and intermediate breaks, and transients (figs. 2 - 9 to 2 - 11). Different to the matrices for Western NPPs they include test facilities for the execution of separate effects tests. Furthermore, they distinguish between the plant types WWER-440/213 and WWER-1000. (This matrices are out-of-date. The more current state of the performed WWER related tests is given in tables 2 - 2, 2 - 4 and 2 - 7.)

The NPP types PWR, BWR or WWER are included under 'Test Facility', since the analyses of transients and accidents in real power plants are potentially valuable with respect to scaling and simulation problems.

The relationship phenomenon versus test type is rated at one of three levels:

- occurring: which means that the particular phenomenon does occur in that kind of test (plus sign in the matrix),
- partially occurring: only some aspects of the phenomenon occur (open circle in the matrix),

- not occurring (dash in the matrix).

The relationship phenomenon versus test facility is rated at one of four levels:

- suitable for code assessment: a facility is designed in such a way as to simulate the phenomenon assumed to occur in the plant, and it is sufficiently instrumented to reveal the phenomenon (plus sign in the matrix),
- limited suitability: the same as above, but with restrictions due to imperfect scaling or insufficient instrumentation (open circle in the matrix),
- not suitable (dash in the matrix),

The relationship test type versus facility is also rated at one of three levels:

- performed: the test type is useful for code assessment purposes (plus sign in the matrix),
- performed but of limited use: this kind of test has been performed in the facility, but it has limited usefulness for assessment purposes due to poor scaling or lack of instrumentation (open circle in the matrix),
- not performed (dash in the matrix).

For WWER plants two further relationships are included to account for the different reactor designs:

- plant type versus phenomenon and
- plant type versus test facility.

The matrices for WWER reactor types date from 2001. At this time the suitability in particular of the PSB-WWER facility for several phenomena could be only estimated. Therefore, a new rating 'expected to be suitable' had been introduced. Meanwhile, numerous experiments have been performed proving the suitability of the facilities for code assessment (see tables in chap. 2.2.1).

MATRIX I: CROSS REFERENCE MATRIX FOR LARGE BREAKS IN PWRs		**Test Type**			**Test Facility**						
Test type vs. phenomenon + occurring o partially occurring - not occurring **Test facility vs. phenomenon** + suitable for code assessment o limited suitability - not suitable **Test type vs. test facility** + performed o performed but of limited use - not performed or planned		Blowdown	Refill	Reflood	CCTF 1:25	LOFT 1:50	BETHSY 1:100	PKL 1 : 145	LOBI 1:712	SEMISCALE 1:1600	UPTF 1:1 (1)
Phenomena	Break flow	+	+	+	o	o	o	o	o	o	o
	Phase separation (condition or transition)	o	+	+	+	+	+	+	+	+	+
	Mixing and condensation during injection	o	+	+	o	o	o	o	o	o	+
	Core wide void + flow distribution	o	+	+	o	o	o	o	o	-	o
	ECC bypass and penetration	o	+	o	+	+	-	o	o	-	+
	CCFL (UCSP)	o	+	+	o	o	o	o	o	-	+
	Steam binding (liquid carry over, ect.)	-	o	+	o	o	-	o	o	o	o
	Pool formation in UP	-	+	+	o	o	o	o	o	o	+
	Core heat transfer incl. DNB, dryout, RNB	+	+	+	o	+	+	+	o	o	-
	Quench front propagation	o	o	+	+	+	+	+	-	+	-
	Entrainment (Core, UP)	o	o	+	o	o	+	o	o	o	+
	Deentrainment (Core, UP)	o	o	+	o	o	o	o	o	o	+
	1- and 2-phase pump behavior	+	o	o	-	o	-	o	+	+	-
	Noncondensable gas effects	-	o	o	-	-	o	-	-	-	o
Test Facility	CCTF	-	o	+							
	LOFT	+	+	+	Important test parameters: - Break location/break size - Pumps off/pumps on - Cold leg injection/combined injection						
	BETHSY	-	-	+							
	PKL	o	+	+							
	LOBI	+	+	-							
	SEMISCALE	+	+	+	(1) UPTF integral tests						
	UPTF	o	+	+							

Fig. 2 - 1: Cross Reference Matrix for Large Breaks in PWRs

MATRIX II: CROSS REFERENCE MATRIX FOR SMALL AND INTERMEDIATE BREAKS IN PWRs		**Test Type**							**Test Facility**								
Test type vs. phenomenon + occurring o partially occurring - not occurring **Test facility vs. phenomenon** + suitable for code assessment o limited suitability - not suitable **Test type vs. test facility** + performed o performed but of limited use - not performed or planned		Stationary test addressing energy transport on primary side	Stationary test addressing energy transport on secondary side	Small leak overfeed by HPIS, secondary side necessary	Small leak without HPIS overfeeding, secondary side necessary	Intermediate leak, secondary side not necessary	Pressurizer leak	U-tube rupture	PWR 1:1	LOFT 1:50	LSTF 1:50	BETHSY 1:100	PKL-III 1:145	SPES 1:430	LOBI-II 1:712	SEMISCALE 1:1600	UPTF TRAM 1:1 (2)
Phenomena (3)	Natural circulation in 1-phase flow, primary side	+	+	+	o	-	+	+	+	+	+	+	+	+	+	+	-
	Natural circulation in 2-phase flow, primary side	+	-	o	+	+	o	-	-	+	+	+	+	+	+	+	o
	Reflux condenser mode and CCFL	+	-	-	+	+	-	-	-	o	+	+	o	o	o	o	+
	Asymmetric loop behavior	-	-	+	+	-	o	+	-	-	o	+	+	+	o	o	+
	Break flow	-	-	+	+	+	+	+	-	+	+	+	+	+	+	+	o
	Phase separation without mixture level formation	+	-	o	+	+	+	o	-	o	+	+	+	+	+	o	+
	Mixture level and entrainment in SG second side	-	+	+	+	+	+	+	-	-	+	+	+	o	o	-	-
	Mixture level and entrainment in the core	+	-	-	+	+	+	-	-	o	+	+	+	o	o	o	o
	Stratification in horizontal pipes	+	-	-	+	+	-	-	-	+	+	o	o	+	o	o	+
	Phase separation in T-junct. and effect on break flow	-	-	-	+	+	-	-	-	o	o	o	o	o	o	-	+
	ECC-mixing and condensation	-	-	o	+	+	+	+	-	o	o	o	o	o	o	o	+
	Loop seal clearing	-	-	-	+	+	o	-	-	+	+	+	+	+	+	+	+
	Pool formation in UP/CCFL (UCSP)	+	-	-	o	+	+	-	-	o	o	o	o	o	-	o	+
	Core wide void and flow distribution	+	-	-	o	+	+	-	-	o	o	o	o	-	-	-	o
	Heat transfer in covered core	+	+	+	+	+	+	+	o	+	+	+	+	+	+	+	-
	Heat transfer in partly uncovered core	+	-	-	o	+	-	-	-	+	+	+	+	o	o	o	-
	Heat transfer in SG primary side	+	o	o	+	+	o	o	-	o	+	+	+	+	+	o	-
	Heat transfer in SG secondary side	o	+	+	+	+	+	+	-	o	+	+	+	o	+	o	-
	Pressurizer thermohydraulics	o	-	o	o	+	+	+	o	o	o	o	o	o	o	-	+
	Surge line hydraulics	o	-	-	o	+	+	o	-	o	o	o	o	o	o	o	+
	1- and 2-phase pump behavior	-	-	-	o	+	-	-	o	o	o	o	o	o	+	+	-
	Structural heat and heat losses (1)	+	-	o	+	+	o	o	-	o	o	o	o	o	o	o	o
	Noncondensable gas effects	+	-	-	-	-	-	-	-	-	o	o	o	-	-	o	+
	Boron mixing and transport	+	-	+	+	+	+	+	-	-	-	-	-	-	-	-	o
Test Facility	PWR	-	-	o	-	-	+	+									
	LOFT	-	-	+	+	+	+	-									
	LSTF	+	+	+	+	+	+	+									
	BETHSY	+	+	+	+	+	+	+									
	PKL-III	+	+	+	+	+	+	+									
	SPES	+	+	+	+	-	-	-									
	LOBI-II	+	+	+	+	+	+	+									
	SEMISCALE	o	o	+	+	+	+	+									
	UPTF, TRAM	-	-	-	-	+	+	-									

(1) Problem for scaled test facilities
(2) UPTF integral tests
(3) For intermediate breaks phenomena included in large break reference matrix may be also important

Fig. 2 - 2: Cross Reference Matrix for Small and Intermediate Breaks in PWRs

MATRIX III: CROSS REFERENCE MATRIX FOR SMALL AND INTERMEDIATE BREAKS IN PWRs WITH OTSG (IN ADDITION TO THE MATRIX FOR PWRs WITH UTSG)		**Test Type**							**Test Facility**				
Phenomenon + suitable for code assessment o limited suitability - not suitable **Test type vs. test facility** + performed o performed but of limited use - not performed or planned		Stationary test addressing energy transport on primary side	Stationary test addressing energy transport on secondary side	Small leak overfeed by HPIS, secondary side necessary	Small leak without HPIS overfeeding, secondary side necessary	Intermediate leak, secondary side not necessary	Pressurizer leak	OTSG-tube rupture	PWR	Univ. Maryland (lowered loop) 1:500	MIST (lowered loop) 1 : 817	OTIS (raised loop) 1 : 1686	GERDA (raised loop) 1 : 1686
Phenomena (2)	Natural circulation in 1-phase flow, primary side	+	+	+	o	-	+	+	+	+	+	+	+
	Natural circulation in 2-phase flow, primary side	+	-	o	+	+	o	o	-	+	+	-	+
	Boiler condenser mode	+	-	-	+	+	-	-	-	+	+	+	+
	Asymmetric loop behavior	-	-	+	+	-	o	+	-	+	+	-	-
	Break flow	-	-	+	+	+	+	+	-	+	+	+	o
	Phase separation without mixture level formation	-	-	o	+	+	+	o	-	+	+	-	-
	Mixture level and entrainment in SG secondary side	-	+	+	+	+	+	+	-	o	+	o	o
	Mixture level and entrainment in the core	-	-	-	+	+	+	-	-	-	-	-	-
	Stratification in horizontal pipes	-	-	-	+	+	-	-	-	o	o	-	-
	Phase separation in T-junct. and effect on break flow	-	-	-	+	+	-	-	-	-	-	-	-
	ECC-mixing and condensation	-	-	o	+	+	+	+	-	o	o	-	o
	Loop seal clearing	-	-	-	+	+	o	-	-	+	o	-	-
	Pool formation in UP/CCFL (UCSP)	-	-	-	o	+	+	-	-	-	-	-	-
	Core wide void and flow distribution	-	-	-	o	+	+	-	-	o	o	-	-
	Heat transfer in covered core	+	+	+	+	+	+	+	o	o	o	+	+
	Heat transfer in partly uncovered core	-	-	-	o	+	-	-	-	-	-	-	-
	Heat transfer in SG primary side	+	o	o	+	+	o	o	-	+	+	o	o
	Heat transfer in SG secondary side	o	+	+	+	+	+	+	-	o	o	o	o
	Pressurizer thermohydraulics	-	-	o	o	+	+	+	o	o	o	-	-
	Surge line hydraulics	-	-	-	o	+	+	o	-	-	-	-	-
	1- and 2-phase pump behavior	-	-	-	o	+	-	-	o	o	o	-	-
	Structural heat and heat losses (1)	+	-	o	+	+	+	o	-	o	o	o	o
	Noncondensable gas effects	+	-	-	-	-	-	-	-	+	+	+	+
	Boron mixing and transport	+	-	+	+	+	+	+	-	-	-	-	-
	Intermittent two-phase natural circulation	-	-	-	+	+	o	o	-	+	+	+	+
	Natural circulation-core, vent valve, downcomer	+	o	+	+	+	+	+	o	+	+	+	+
	Refill of loops	-	-	+	+	o	+	-	-	+	+	o	+
	Superheating in secondary side	+	+	+	+	+	+	+	+	+	+	+	+
Test Facility	PWR	-	-	o	-	-	+	o	(1) Problem for scaled test facilities (2) For intermediate breaks phenomena included in large break reference matrix may also be important				
	Univ. Maryland	+	+	+	+	-	+	+					
	MIST	+	+	+	+	-	+	+					
	OTIS	+	+	+	+	-	+	-					
	GERDA	+	+	+	+	-	+	-					

Fig. 2 - 3: Cross Reference Matrix for Small and Intermediate Breaks in PWRs with OTSG

MATRIX IV: CROSS REFERENCE MATRIX FOR TRANSIENTS IN PWRs		**Test Type**								**Test Facility**							
Test type vs. phenomenon + occurring o partially occurring **Test facility vs. phenomenon** + suitable for code assessment o limited suitability - not suitable **Test type vs. test facility** + performed o performed but of limited use - not performed or planned		ATWS	Loss of feed water, non ATWS	Loss of heat sink, non ATWS (3)	Station blackout	Steam line break	Feed line break	Reactivity disturbance	Over-cooling	PWR 1:1	LOFT 1:50	LSTF 1:50	BETHSY 1:100	PKL-III 1:134	SPES 1:430	LOBI-II 1:712	SEMISCALE 1:1000
Phenomena	Natural circulation in 1-phase flow	+	+	+	+	+	+	o	o	+	o	+	+	+	+	+	+
	Natural circulation in 2-phase flow	+	+	+	+	-	-	o	-	-	o	+	+	+	+	+	+
	Core thermohydraulics	+	+	+	+	o	o	+	o	o	+	+	+	+	+	+	+
	Thermohydraulics on primary side of SG	+	o	o	+	o	o	o	+	o	o	+	+	+	+	+	o
	Thermohydraulics on secondary side of SG	+	+	+	+	+	+	o	+	o	o	+	+	+	o	+	o
	Pressurizer thermohydraulics	+	+	+	+	o	o	o	+	o	o	o	o	o	o	o	o
	Surge line hydraulics (CCFL, choking)	+	+	+	+	o	o	o	o	o	o	o	o	o	o	o	o
	Valve leak flow (1)	+	+	+	+	+	+	+	+	-	o	o	o	o	o	o	o
	1- and 2-phase pump behavior	+	+	+	+	o	o	o	+	o	o	+	o	o	o	+	+
	Thermohydraulic-nuclear feedback	+	-	-	-	-	-	+	-	+	+	-	-	-	-	-	-
	Structural heat and heat losses (2)	o	o	o	o	o	o	o	o	-	o	o	o	o	o	o	o
	Boron mixing and transport	-	-	-	-	o	-	-	o	-	-	-	-	-	-	-	-
	Separator behavior	o	-	-	-	+	-	-	-	-	-	-	-	-	o	o	-
Test Facility	PWR	-	-	-	-	-	-	-	o								
	LOFT	+	+	+	o	-	-	+	+								
	LSTF	-	+	-	+	+	+	-	+								
	BETHSY	-	+	+	-	+	+	-	-								
	PKL-III	-	+	+	+	+	+	-	+								
	SPES	-	+	-	+	-	-	-	-								
	LOBI-II	+	+	+	+	+	+	-	-								
	SEMISCALE	-	+	+	+	+	+	-	+								

(1) Valve flow behavior will be strongly design-dependent, specific experimental data should be used if possible
(2) Problem for scaled test facilities
(3) Isolation of one or more steam generators

Fig. 2 - 4: Cross Reference Matrix for Transients in PWRs

MATRIX V: CROSS REFERENCE MATRIX FOR TRANSIENTS AT SHUT-DOWN CONDITIONS IN PWRs		**Test Type**				**Test Facility**		
Test type vs. phenomenon + occurring o partially occurring - not occurring **Test facility vs. phenomenon** + suitable for code assessment o limited suitability - not suitable **Test type vs. test facility** + performed o performed but of limited use - not performed or planned		Loss of RHR with no opening	Loss of RHR with openings	Loss of RHR with dam in HL	Boron dilution at shut-down	LSTF	BETHSY	PKL III
Phenomena	Pressurization due to boiling	+	+	+	-	+	+	+
	Reflux condenser mode and CCFL	+	+	o	-	+	+	o
	Asymmetric loop behavior	-	o	+	-	+	+	+
	Flow through openings (manholes, vents)	-	+	+	-	+	+	-
	Mixture level formation in upper plenum and hot legs	+	+	+	-	+	+	+
	Mixture level and entrainment in the core	+	+	+	-	+	+	+
	SG siphon draining	-	-	+	-	+	-	-
	Asymmetry due to the presence of a dam	-	-	+	-	+	-	-
	Stratification in horizontal pipes	+	+	+	-	+	o	+
	Phase separation in T-junctions and effect on flow	-	+	+	-	o	o	o
	ECC mixing and condensation	+	+	+	-	o	o	o
	Loop seal clearing and filling	+	+	+	-	+	+	-
	Pool formation in UP/CCFL (UCSP)	-	-	-	-	-	-	-
	Core 3D thermalhydraulics	+	+	+	+	o	o	o
	Heat transfer in covered core	+	+	+	-	+	+	+
	Heat transfer in partially uncovered core	+	+	+	-	o	o	-
	Heat transfer in SG primary side	+	+	+	-	+	+	+
	Heat transfer in SG secondary side	+	+	+	-	+	+	+
	Pressurizer thermalhydraulics (1)	-	x	x	-	o	o	o
	Surge line thermalhydraulics (1)	-	x	x	-	o	o	o
	Structural heat and heat losses	-	-	-	-	-	-	o
	Noncondensable gas effects	+	+	+	-	+	+	+
	Boron mixing and transport	-	-	-	+	-	-	-
	Thermalhydraulics-nuclear feedback	-	-	-	+	-	-	-
Test Facility	LSTF	+	+	+	-			
	BETHSY	-	+	-	-			
	PKL III	+	-	-	-			

(1) x is dependent on opening location:
+ pressurizer manhole open
- pressurizer manhole closed

Fig. 2 - 5: Cross Reference Matrix for Transients at Shutdown Conditions in PWRs

MATRIX VI: CROSS REFERENCE MATRIX FOR ACCIDENT MANAGEMENT FOR A NON-DEGRADED CORE IN PWRs		Test Type					Test Facility						
Test type vs. phenomenon + occurring o partially occurring - not occurring **Test facility vs. phenomenon** + suitable for code assessment o limited suitability - not suitable **Test type vs. test facility** + performed o performed but of limited use - not performed or planned		High pressure primary side feed and bleed	Low pressure primary side feed and bleed	Secondary side feed and bleed	RCP-Restart in a highly voided PCS	Primary to secondary break with multiple failures	LOFT 1:50	LSTF 1:50	BETHSY 1:100	PKL-III 1:145	SPES 1:430	LOBI-II 1:712	UPTF TRAM 1:1 (2)
Phenomena	Natural circulation in 1-phase flow, primary side	+	-	+	-	+	+	+	+	+	+	+	-
	Natural circulation in 2-phase flow, primary side	+	+	+	-	+	+	+	+	+	+	+	o
	Reflux condenser mode and CCFL	-	-	+	-	+	o	+	o	o	o	o	+
	Asymmetric loop behavior	+	+	+	+	+	-	o	+	+	+	o	+
	Break flow	+	+	o	+	+	+	+	+	+	o	+	o
	Phase separation without mixture level formation	+	+	+	+	+	o	+	+	+	+	+	+
	Mixture level and entrainment in SG secondary side	-	-	+	-	+	-	+	+	+	o	o	-
	Mixture level and entrainment in the core	+	+	+	o	+	o	+	+	+	o	o	o
	Stratification in horizontal pipes	+	+	+	o	+	+	+	o	o	o	o	+
	Phase separation in T-junct. and effect on break flow	+	+	o	-	+	o	o	o	o	o	o	+
	ECC-mixing and condensation	+	+	+	-	+	o	o	o	o	o	o	+
	Loop seal clearing	o	o	+	o	+	+	+	o	o	+	+	+
	Pool formation in UP/CCFL (UCSP)	+	+	+	-	+	o	o	o	o	o	-	+
	Core wide void and flow distribution	+	+	+	+	+	o	o	o	o	-	-	o
	Heat transfer in covered core	o	o	+	-	+	+	+	+	+	+	+	-
	Heat transfer in partly uncovered core	+	+	+	+	+	+	+	+	+	o	o	-
	Heat transfer in SG primary side	-	-	+	o	+	o	+	+	+	+	+	-
	Heat transfer in SG secondary side	-	-	+	o	+	o	+	+	+	o	+	-
	Pressurizer thermohydraulics	+	+	o	o	+	o	o	o	o	o	o	+
	Surge line hydraulics	+	+	o	o	+	o	o	o	o	o	o	+
	1- and 2-phase pump behavior	o	o	+	+	+	o	o	o	o	o	+	-
	Structural heat and heat losses (1)	+	+	+	+	+	o	o	o	o	o	o	o
	Noncondensable gas effects	o	+	+	+	+	-	o	o	+	-	-	+
	Accumulator behavior	-	+	+	-	o	o	+	+	+	+	+	+
	Boron mixing and transport	+	+	+	+	+	-	-	-	-	-	-	o
	Thermohydraulic-nuclear feed back	-	-	-	+	-	-	-	-	-	-	-	-
	Separator behavior	-	-	-	-	-	-	-	-	-	-	-	-
Test Facility	LOFT	-	-	+	-	-							
	LSTF	+	+	+	-	o							
	BETHSY	+	+	+	-	+							
	PKL-III	o	+	+	+	-							
	SPES	+	+	+	-	+							
	LOBI-II	+	+	+	-	+							
	UPTF, TRAM	o	+	-	-	-							

(1) problem for scaled test facilities
(2) UPTF integral tests

Fig. 2 - 6: Cross Reference Matrix for Accident Management for a Non Degraded Core in PWRs

MATRIX VII: CROSS REFERENCE MATRIX FOR LOCAs IN BWRs		**Test Type**						**Test Facility**						
Test type vs. phenomena + occurring o partially occurring - not occurring **Test facility vs. phenomenon** + suitable for code assessment o limited suitability - not suitable **Test type vs. test facility** + performed o performed but of limited use - not performed or planned		Large steam line break with fast depressurization	Large break below water level with fast depress.	Small break without depress. before ADS actuation	Intermediate break with slow depress.	Spray line break	Refill - reflood	BWR 1:1 (1)	TBL 1:382, 2 chan., full pow., full height	ROSA III 1:424, 4 channels	TLTA 1:624, 1 chan., full power	FIST 1:624, 1 chan., full pow., full height	FIX 2 1:777, 1 chan., full pow., full height	PIPER1 1:2200, 1 chan., full height
Phenomena	Break flow	+	+	+	+	+	o	-	o	o	o	o	o	+
	Channel and bypass axial flow and void distribution	+	+	+	+	+	+	o	+	o	+	+	+	+
	Core wide radial void distribution	o	o	+	+	+	+	o	o	+	o	o	o	-
	Parallel channel effects-instabilities	-	-	+	+	+	+	-	o	+	-	-	-	o
	ECC bypass	-	-	o	o	o	+	-	o	o	o	o	-	+
	CCFL at UCSP and channel inlet orifice	o	+	-	+	+	+	-	o	o	-	o	o	o
	Core heat transf. incl. DNB, dryout, RNB. surf. to surf radiation	+	+	o	+	o	+	-	+	+	+	+	+	+
	Quench front propagation for both fuel rods and channel walls	-	-	-	-	-	+	-	+	+	+	+	-	+
	Entrainment and deentrainment in core and upper plenum	+	+	o	o	o	+	-	-	o	o	o	-	o
	Separator behavior incl. flooding, steam penetration and carryover	+	+	o	o	o	-	o	+	o	o	+	o	o
	Spray cooling	-	-	o	o	o	+	-	o	o	o	o	-	+
	Spray distribution	-	-	o	o	o	+	-	-	o	-	-	-	-
	Steam dryer - hydraulic behavior	+	-	o	o	-	-	o	o	o	o	o	-	o
	One and two phase pump recirc. behavior incl. jet pumps	o	o	+	+	+	o	o	o	o	o	o	o	-
	Phase separation and mixture level behavior	+	+	+	+	+	+	-	o	+	o	+	+	o
	Guide tube and lower plenum flashing	+	+	-	o	o	-	-	+	+	+	+	+	+
	Natural circulation - core and downcomer	-	-	+	o	o	+	+	+	o	o	+	+	+
	Natural circulation core bypass, hot and cold bundles	-	-	+	o	o	+	-	o	o	o	o	o	o
	Mixture level in core	-	-	+	o	o	+	-	+	+	+	+	+	o
	Mixture level in downcomer	+	+	+	+	+	+	-	+	o	o	+	+	o
	ECC mixing and condensation	-	-	+	o	+	+	-	o	o	o	o	-	o
	Pool formation in upper plenum	o	o	-	o	o	+	-	o	o	o	o	o	o
	Structural heat and heat losses	o	o	o	+	+	+	-	+	o	o	o	o	o
	Phase separ. in T-junction and effect on break flow	-	-	+	o	+	-	-	-	-	-	-	-	+
Test Facility	BWR	-	-	-	-	-	-							
	TBL	+	+	+	+	-	+							
	ROSA III	+	+	+	+	-	+							
	TLTA	+	+	-	+	-	+							
	FIST	+	+	+	+	-	+							
	FIX 2	-	+	-	+	-	-							
	PIPER 1	-	+	+	+	-	+							

(1) These are non-LOCA data but may be used for assessment

Fig. 2 - 7: Cross Reference Matrix for LOCAs in BWRs

MATRIX VIII: CROSS REFERENCE MATRIX FOR TRANSIENTS IN BWRs		Test Type									Test Facility			
Test type vs. phenomenon + occurring o partially occurring - not occurring **Test facility vs. phenomenon** + suitable for code assessment o limited suitability - not suitable **Test type vs. test facility** + performed o performed but of limited use - not performed or planned		Stationary test measuring power flow map	Recirculation pump trip	Core stability	Loss of main heat sink	Feed water flow or temperature disturbance, e. g. LOFW	Loss of feed water (LOFW) up to time of const. pressure	Inadvertent increase in steam flow	ATWS	Station blackout (Loss-of-Offsite Power)	BWR 1:1	ROSA III 1:424, 4 channels	FIST 1:642, 1 channel, full power, full height	FIX2 1:777, 1 channel, full power, full height
Phenomena	Natural circulation in one- and two-phase flow	+	+	+	+	-	-	-	+	+	+	o	+	o
	Collapsed level bahavior in downcomer	-	+	o	+	+	+	+	+	+	+	o	+	+
	Core thermal hydraulics	o	+	+	+	o	o	o	+	+	o	+	+	+
	Valve leak flow	-	-	-	+	-	-	-	+	+	o	o	o	-
	Single phase pump behavior (1)	o	+	o	+	o	o	+	+	+	o	o	o	o
	Parallel channel effects and instabilities	-	+	+	o	-	-	-	+	+	o	+	-	-
	Nuclear thermalhydraulic feedback including spatial effects	o	o	+	-	o	o	o	+	-	+	-	-	-
	Nuclear thermalhydraulic instabilities	-	o	+	-	-	-	o	+	-	+	-	-	-
	Downcomer mixing	-	-	-	-	+	+	-	+	+	o	o	-	-
	Boron mixing and distribution	-	-	-	-	-	-	-	+	-	-	-	-	-
	Steam line dynamics	-	-	-	+	-	-	+	+	+	o	-	o	-
	Void collapse and temp. distribution during pressurization	-	-	-	+	-	-	-	+	+	o	+	+	+
	Critical power ratio	-	+	+	+	+	+	+	+	+	o	+	+	+
	Rewet after DNB at high press. and high power incl. high core flow	-	+	-	+	-	-	o	+	o	-	o	+	+
	Structural heat and heat losses	-	o	-	o	-	o	o	o	o	-	o	o	o
Test Facility	BWR	+	+	+	+	+	+	+	-	o				
	ROSA III	-	+	+	+	-	+	-	-	+				
	FIST	-	o	-	+	-	+	+	o	+				
	FIX 2	-	+	-	+	-	-	-	-	-				

(1) Two-phase pump bahavior is of interest for certain special ATWS and inadvertent increase of steam flow transients

Fig. 2 - 8: Cross Reference Matrix for Transients in BWRs

MATRIX IX:
CROSS REFERENCE MATRIX FOR LARGE BREAKS IN WWERs

CSNI
+ covered by
o partially covered
- not covered

Plant type vs. phenom.
+ fully specific to WWER
o partially specific
- not specific

Test type vs. phenom.
+ occuring
o partially occuring
- not in list

Test facility vs. phenom.
+ suitable for code assessment
o limited suitability
- not suitable

Plant type vs. phenom.
x expected to be suitable

Test type vs. test facility
+ already performed
o performed but of limited use
- not performed

Plant type vs. test facility
+ covered by
o partially covered
- not covered

Phenomena	CSNI	Plant Type: WWER-440/213	Plant Type: WWER-1000	Test Type: Blowdown	Test Type: Reflood	Test Type: Refill	System Tests: PSB-WWER	System Tests: PM-5	System Tests: SB	System Tests: ISB-WWER	Separate Effects Tests: Data bank (EREC)	LWL	REWET-II	IVO-CCFL	SKN	SVD-1	SVD-2	TVC-440	EVTUS	KS	TOPAZ	SG-NPP
Break flow	+	-	-	+	+	+	x		+	x	+											
Phase separation	o	+	o	o	+	+	x			x				o								
Mixing and condensation during injection	o	+	+	o	+	+	x			x												
2-phase flow in SG primary and secondary side	-	o	o	o	o	o	x			x												
Core wide void + flow distribution	o	+	+	o	+	+	x	o		-												
ECC downcomer bypass and penetration	o	+	+	o	o	+	-			-												
UP injection and penetration	-	+	+	o	+	+	x		+	x			+				+	+				
CCFL (UCSP)	o	+	+	o	+	+	x	+		x				+								
Steam binding (liquid carry over, ect.)	o	o	o	-	+	o	x		+	x												
Pool formation in UP	o	+	+	-	+	+	x	+		x												
Core heat transfer incl. DNB, dryout, RNB	o	+	+	+	+	+	x	o	+	x		+			+	+	+	o	o	+		
Quench front propagation	o	+	+	o	+	o	x		+	x			+			+	x	+	o		+	
Entrainment (Core, UP)	-	+	o	o	+	o	x	o	+	x			+				x	o				
Deentrainment (Core, UP)	-	+	o	-	+	o	x	o	+	x			+				x	o				
1 - and 2-phase pump behavior	-	+	+	+	o	o	x			-												
Noncondensable gas effects	-	o	o	-	+	+	x			+												x
ISB-WWER		o	+	-	-	-																
PSB-WWER			+	-	-	-																
SB		+	+	+	+	+																
PM-5			+		+																	

Test Facility

Test Facility System

Important test parameters:
- Leak location/leak size
- Pumps off/pumps on
- ECC injection mode
- Accumulator pressure

Fig. 2 - 9: Cross Reference Matrix for Large Breaks in WWERs

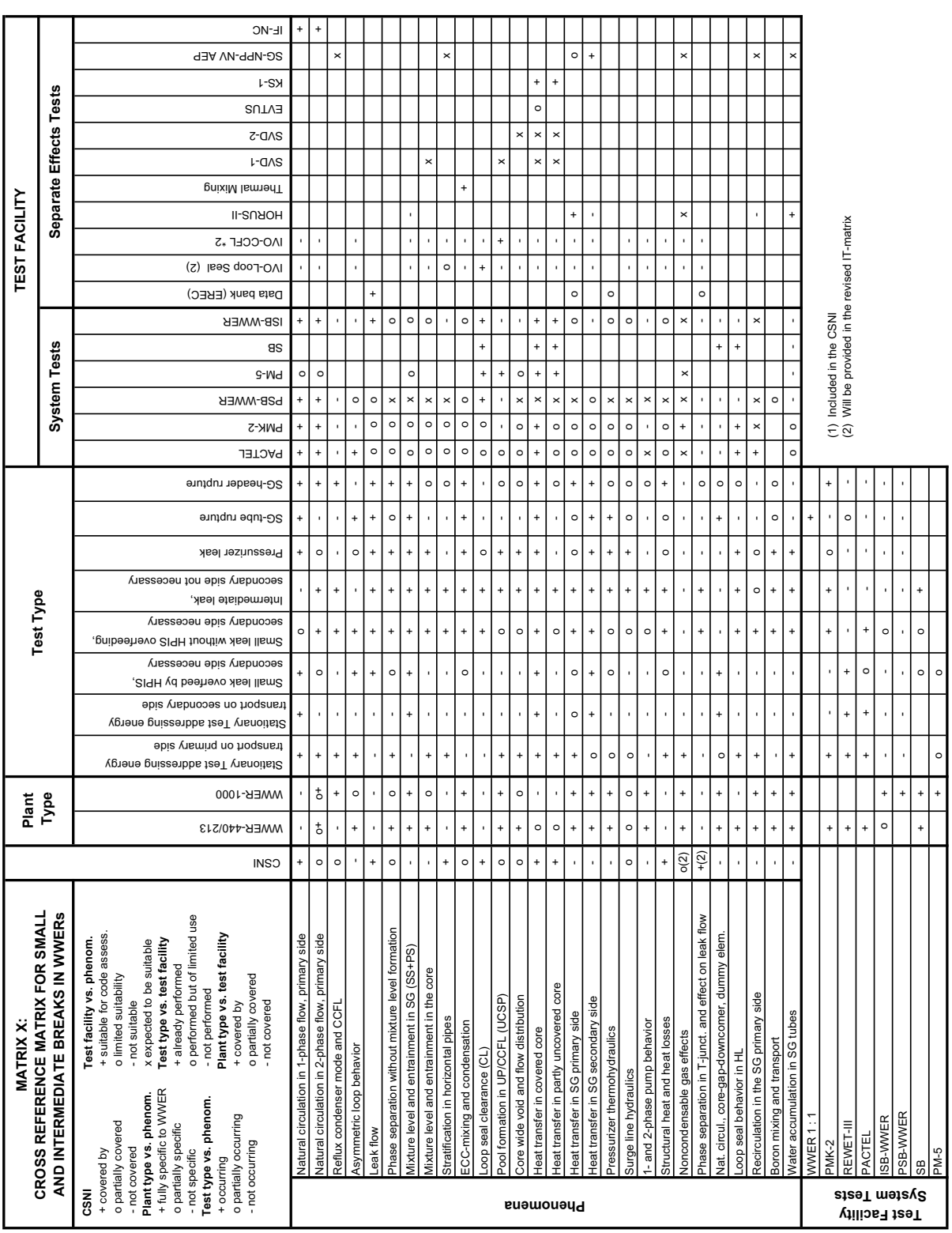

Fig. 2 - 10: Cross Reference Matrix for Small and Intermediate Breaks in WWERs

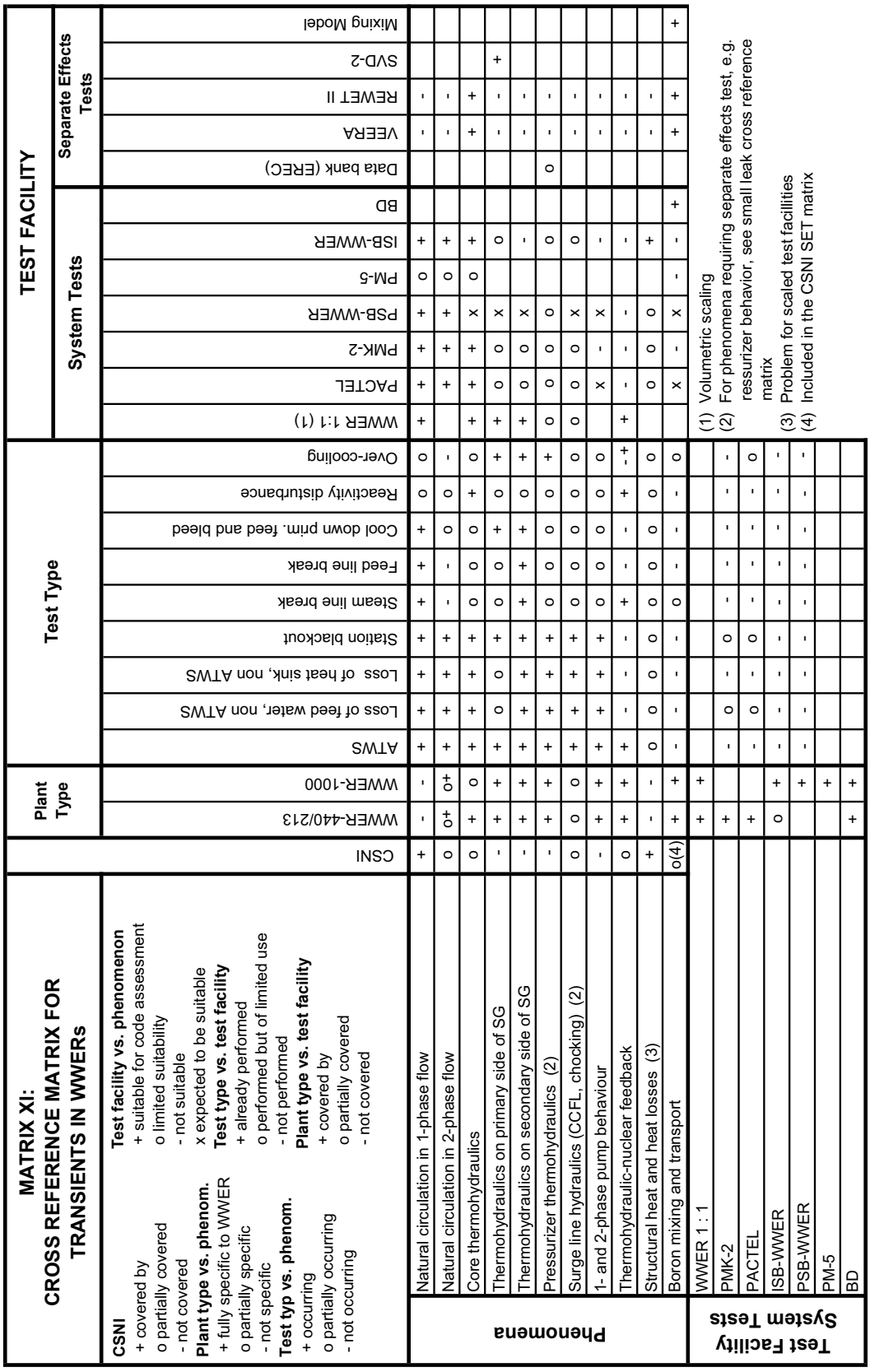

Fig. 2 - 11: Cross Reference Matrix for Transients in WWERs

2.2.1 Integral Tests Validation Matrices for ATHLET

Based on the Cross Reference Matrices (figs. 2 - 1 to 2 - 11), well balanced sets of tests were selected for the ATHLET validation based on the criteria presented in the CSNI report /ANN96/. The criteria for selection are:

- each phenomenon should be addressed in test facilities of different scale,
- all test types should be included.

If feasible, each thermal-hydraulic phenomenon and each test type should be addressed by at least two facilities of different scale. A total of approximately 50 test types results in about 100 integral tests for code validation. The validation work is shared between GRS and independent organizations.

During the selection process, a number of additional factors were considered, including:

- typicality of facility and experiment to expected reactor conditions,
- quality and completeness of experimental data (measurement and documentation),
- relevance to safety issue,
- test selected must clearly exhibit the addressed phenomena,
- high priority to International Standard Problems (ISP), counterpart and similar tests (for more explanations see /ANN96/),
- challenge to system codes.

Where counterpart tests or similar tests were identified between two or more facilities, they were included in order to address questions relating to scaling and facility design compromises. For the accident management matrix, priority was given on how realistically the test represents typical accident management procedures.

A periodic updating of the matrices may be necessary to include new relevant experimental facilities and tests, and to include improved understanding of existing data as a result of further validation.

The integral tests selected for the ATHLET validation are presented in tables 2 - 1 to 2 - 13. An overview of the different integral test facilities indicating the number of selected tests for each category (e.g. large breaks, small breaks, etc.), and the current status of calculated experiments is shown in tables 2 - 14 and 2 - 15.

Table 2 - 1: Large Breaks in PWRs (Matrix I)

Test Facility	Test No.	Brief Description	Calculation done by	ATHLET Version	Reference
UPTF	-2	Double ended cold leg break, cold ECC injection, EM-case			
UPTF	-27B	Double ended cold leg break, cold ECC injection, BE-case	RUB	Mod1.2B	/WEI01/
UPTF	-18	Double ended cold leg break, combined ECC injection, EM-case	TÜV-Bayern	Mod1.0D	/GAS91/
UPTF	-28	Double ended cold leg break, combined ECC injection, BE-case			
UPTF	-19	50% Break in the cold leg, combined ECC injection,EM-case			
UPTF	-24	Vent valve test, double ended cold leg break, EM-case, downcomer and cold leg ECC			
CCTF	C2-19/79	Double ended cold leg break, combined ECC, EM-case	FZR	Mod1.2C	/KRE01/
CCTF	C2-20/80	Double ended cold leg break, combined ECC, BE-case	TÜV-Bayern	Mod1.0D	/KRY91/
CCTF	C2-04/62	Double ended cold leg break, cold ECC, EM-case, base case	FZR	Mod1.2C	/KRE01/
CCTF	C2-12/71	Double ended cold leg break, cold ECC, BE-case	Battelle	Mod1.2B	/SCH00/
LOFT	L2-5	Double ended cold leg break, loss of external power, decoupled pump flywheel	Battelle	Mod1.2B	/SCH00/
LOFT	LP-LB-1	Double ended cold leg break, loss of external power	GRS	DRUFAN Current	/WAH86/ Chap. 5.3
LOBI	A1-06	Double ended cold leg break, combined ECC injection	Battelle	Mod1.0 B	/SCH89/
LOBI	A1-66	Double ended cold leg break, cold ECC injection	Battelle	Mod1.0 B	/SCH89/
PKL-II	B2	Double ended cold leg break, combined ECC injection	TÜV Nord	Mod1.2C	/WIE00/
PKL-II	B5	Double ended cold leg break, cold leg ECC injection	TÜV Nord	Mod1.2C	/WIE00/

Table 2 - 2: Large Breaks in WWERs (Matrix IX)

Test Facility	Test No.	Brief Description	Calculation done by	ATHLET Version	Reference
PSB WWER	XT-2x25-02	2 x 25% break in hot leg	Kurchatov	Mod2.0A	/MOS05b/

Table 2 - 3: Small and intermediate breaks in PWRs (Matrix II)

Test Facility	Test No.	Brief Description	Calculation done by	ATHLET Version	Refer-ence
UPTF TRAM	A7	5% cold leg break, hot leg ECC injection	GRS	Mod1.1D	/DRÄ98/
UPTF TRAM	A6	5% cold leg break, cold leg ECC, similar to LSTF-SB-CL-18	GRS	Mod1.1A	/BUR94/ /PAP96/
ATLAS	SB-DVI-09	50% Break of a DVI Line of the APR-1400 (ISP-50)	GRS	Mod2.2A	/AUH13a/
ATLAS	A1.1	Station Blackout (SBO) with asymmetric cooling via one steam generator	GRS	Mod3.0B	/HOL16/
ATLAS	A5.1	1% cold leg break, failure of HPI and secondary side depressurization (counterpart test to LSTF SB-CL-32)	GRS	Mod3.1A	/HOL16/
LOFT	LP-SB-1	2% hot leg break, main coolant pumps switched off	GRS	DRUFAN	/POI84/
LOFT	LP-SB-2	2% hot leg break, main coolant pumps running	GRS	DRUFAN	/POI84a/
LOFT	LP-SB-3	1% cold leg break	GRS	Mod1.0D	/DRÄ91/
LOFT	L3-2	15% cold leg break			
LSTF	SB-CL-18	5% cold leg break, ISP-26	GRS	Current	Chap. 5.1
LSTF	SB-CL-21	5% cold leg break, similar to BETHSY 6.2 TC and LOBI BL-34			
LSTF	SB-CL-32	1% cold leg break, failure of HPI and secondary side depressurization	GRS	Mod3.0A	/HOL16/
LSTF	IB-HL-01	17% hot leg break (Test 1 of OECD ROSA-2 Project)	GRS	Mod2.2B	/AUH13/
LSTF	IB-CL-03	17% cold leg break (Test 2 of OECD ROSA-2 Project)	GRS	Mod2.2B	/AUH13/
LSTF	IB-CL-05	13% cold leg break (Test 7 of OECD ROSA-2 Project)	GRS	Mod2.2B	/AUH13/
PKL-III	A 4.1	1% cold leg break, LP, HP ECC, pressurizer level test	GRS	Mod0	/AUS89/
PKL-III	AC-1	Reflux condenser mode (similar to LOBI A1-92)			
PKL-III	B 3.2B	Natural circulation with different mass inventories and flow resistances (similar to LSTF ST-NC-08)			
PKL-III	B 3.5.1	Cooldown of a PWR with 100K/h under reflux condenser mode with 4 SG at 2% power			
PKL-III	B 4.3	System behavior during nitrogen injection under reflux condenser conditions	TÜV Nord	Mod1.1C	/WIE98/

PKL-III	B 4.1	System behavior during nitrogen injection under single phase natural circulation conditions in primary side	GRS	Mod1.1B	/RIN95/
PKL-III	C 6.1	24 cm^2 cold leg break, cooldown of a PWR with 100K/h, isolation of 2 SG, nitrogen injection from 2 accumulators	TÜV Nord	Mod1.2A	/WIE98/
PKL-III	C 3.2	Reflux condenser with 0.8MPa and increasing SG Power (1%-20%)			
PKL-III	D 2.1	Small CL leak, start of natural circulation with HP, LP, accumulator injection into two loops	GRS	Mod1.2D	/STF02/
PKL-III	D 2.2	Small HL leak, start of natural circulation with LP injection into four loops	GRS	Mod1.2D	/RIN03/
PKL-III	E 2.2	Small CL leak, start of natural circulation with HP and LP injection into two CLs	GRS	Mod2.0A	/STF04/
PKL-III	E 2.3	Small HL leak, start of natural circulation with HP injection into two HLs and accumulator injection into 4 HLs	GRS	Mod2.0B	/STF06a/
PKL-III	F 1.2	Concentration of low borated water at heat exchanger exits during two-phase natural circulation and reflux condenser			
PKL-III	H 2.1	Station Blackout (SBO)	GRS	Mod3.0A	/HOL16/
PKL-III	H 2.2, Run 2	Station Blackout (SBO)	GRS	Mod3.0A	/HOL16/
PKL-III	H 4.1	Cool-down under natural circulation conditions with isolated, water-filled steam generators	GRS	Mod3.0A	/HOL16/
BETHSY	4.1a	Two phase natural circulation with different mass inventories in the primary circuit	GRS	Mod1.0D	/TEH91/
BETHSY	5.1a	Variation of mass inventories in the secondary circuit	GRS	Mod1.1A	/RIN93a/
BETHSY	3.4a	Natural circulation with 2 isolated SGs, similar to PKL III B3.1	Battelle	Mod1.1A	/SCH94/
BETHSY	4.3b	Multiple steam generator u-tube rupture	GRS	Mod1.1A	/RIN93/
BETHSY	4.1a TC	Two phase natural circulation with constant core power 5%	Battelle	Mod1.1C	/SCH98/
BETHSY	6.2 TC	5% cold leg break, without HP ECC, similar to LSTF-SB-CL-18 and LOBI-BL-34	Battelle	Mod1.1C	/SCH98/
BETHSY	7.2 c	Reflux condenser mode with nitrogen in primary circuit	Battelle	Mod1.1C	/SCH98/
LOBI II	A2-77A	Primary side behavior with different mass inventories	GRS	Mod1.0D	/KIR89/
LOBI II	A1-82	LOCA with 1% cold leg break, hot leg HP ECC injection	GRS	Mod1.2D	/RIN01a/
LOBI	A2-81	LOCA with 1% cold leg break, cold leg HP ECC injection, ISP-18	GRS	Mod1.0D	/BUR89/
LOBI II	A1-91	1% cold leg break, with hot ECC injection	Battelle	Mod1.0B	/SCH89/
LOBI II	BL-01	5% cold leg break	GRS	Mod1.0D	/KYN89/
LOBI II	A1-83	10% cold leg break			

LOBI	B-R1M	25% cold leg break	Battelle	Mod1.0B	/SCH89/
LOBI II	BL-34	6% cold leg break, similar to LSTF-SB-CL-21 and BETHSY 6.2 TC			

Table 2 - 4: Small and intermediate breaks in WWERs (Matrix X)

Test Facility	Test No.	Brief Description	Calculation done by	ATHLET Version	Refer-ence
PMK		ATWS with stuck open pressurizer relief valve, loss of feedwater	GRS/KFKI	Mod1.2A	/HOC99/
PMK		7,4% cold leg break with N_2 injection, secondary side bleed and feed	GRS/KFKI	Mod1.1B	/GYO95/
PMK		7,4% cold leg break without N_2 injection, secondary side bleed and feed	GRS/KFKI	Mod1.1B	/GYO95/
PMK		7,4% cold leg break , secondary side bleed and feed, IAEA SPE-4	GRS/Kurt.	Mod1.1A	/STE95/
PMK		0,5% cold leg break , secondary side bleed and feed	NRI/GRS	Mod1.1D	/VOJ00a/
PMK		Surge line break	NRA/GRS	Mod1.2A	/VOJ01/
ISB		Small break in cold leg, Russian Standard Problem No. 1 (SSP-1)	FZR	Mod1.1A	/KRE96/
ISB		Intermediate break in cold leg without HP injection, Russian Standard Problem No. 2 (SSP-2)	GRS	Mod1.1C	/STE98/
ISB		Intermediate break in cold leg with HP injection, Russian Standard Problem No. 3 (SSP-3)	INRNE/GRS	Mod1.2A	/VOJ00b/
ISB		11,2% break of connection pipe to the upper plenum, 1 HP injection	NRI/GRS	Mod1.1D	/VOJ00a/
ISB		11,2% break of connection pipe to the upper plenum, 2 HP injections	NRI/GRS	Mod1.1D	/VOJ00a/
ISB		0,5% break in cold leg with HP injection	NRI/GRS	Mod1.1D	/VOJ00a/
PACTEL	ITE-06	Natural circulation , ISP-33	GRS THZ	Mod1.0E	/STE94/ /LIS93/
PACTEL	SBL-03	0,04% break, 3,3% power			
PACTEL	SBL-04	1% break, 3,3% power			
PACTEL	SBL-07	0,04% break 3,3% power, pressurizer isolation			
PACTEL	SBL-22	Small break in lower plenum, one and two phase natural circulation, reflux condenser mode	THZ	Mod1.1C	/LIS97/
PACTEL	LSR-10	Loop seal refilling test	THZ	Mod1.1 B	/LIS96/
PACTEL	SIR-11	Stepwise reduction of coolant inventory			
PACTEL	SIR-20	Natural circulation with lower pressure at 4,0MPa (prim. side) and 1,2MPa (sec. side), reduction of water inventory	THZ	Mod1.1 D	/VAN98/
PACTEL	SIR-21	Natural circulation with lower pressure at 1,6MPa (prim. side) and 0,3MPa (sec. side), reduction of water inventory	THZ	Mod1.1 D	/VAN98/

PSB WWER	XT-3-02	3% leak in cold leg	Kurchatov	Mod2.0A	/MOS05a/
PSB WWER	OECD / Nr.1	11% leak in upper plenum	GRS	Mod2.0A	/VOJ06/
PSB WWER	OECD / Nr.4	1.4% primary to secondary leak in hot collector top	GRS	Mod2.1A	/STG05/

Table 2 - 5: Small and intermediate breaks in PWRs with once-through steam generators (Matrix III)

Test Facility	Test No.	Brief Description	Calculation done by	ATHLET Version	Reference
GERDA	160 702	20% break in pump seal	ABB/GRS	Mod1.0D	/STF91/

Table 2 - 6: Transients in PWRs (Matrix IV)

Test Facility	Test No.	Brief Description	Calculation done by	ATHLET Version	Reference
LOFT	L9-3	ATWS, loss of feedwater			
LSTF	ST-NC-41	Stepwise cooldown procedure with SG isolated and empty on the secondary side (Test 6 of OECD ROSA-2 Project, Counterpart test to PKL-III G2.1)	GRS	Mod2.2B	/AUH13/
PKL-III	A1.2	Asymmetric cooldown of a PWR with one pump and 3 isolated SG			
PKL-III	A2.1	Cooldown of a PWR with 4 SG and loss of offsite power, similar to LOBI A1-87			
PKL-III	A2.2	Cooldown of a PWR with station blackout, 3 SG			
PKL-III	A3.2	Restart of a main coolant pump, with upper head steam/gas cushion			
PKL-III	A5.2	Loss of feedwater of 1 SG			
PKL-III	B3.1	Cooldown with one of four steam generators	GRS	Mod 1.0E	/SEN 94/
PKL-III	F4.1	Inherent boron dilution under reflux-condenser conditions as function of primary coolant inventory	GRS	Mod 2.1B	/AUS10/
PKL-III	F4.2	Inherent boron dilution (GRS-LOBI Scenario)	GRS	Mod 2.1B	/AUS10/
PKL-III	G2.1 Run 3	Stepwise cooldown procedure with SG isolated and empty on the secondary side	GRS	Mod 2.2B	/AUS13/
PKL-III	G3.1	10% steam line break; OECD/PKL 2 Benchmark	GRS	Mod 2.2A	/DEL11/
PKL-III	G4.1 Run 2	Systematic study on heat transfer under reflux-condenser conditions	GRS	Mod 2.2B	/AUS13/

LOBI-II	A1-87	Cooldown of a PWR			
LOBI-II	A2-90	Loss of offsite power, ATWS	GRS	Mod3.0A	/LER12/
LOBI-II	BT-01	10% steam line break	GRS	Mod1.0D	/GEP90/
LOBI-II	BT-12	Steam line break	Battelle	Mod1.0B	/SCH89/
GKN-2		Load rejection (2.4.92)	GRS	ATLAS	/HOC98/
GKN-2		Reactor trip (18.10.91)	GRS	ATLAS	/HOC98/
GKN-2		Trip of one main coolant pump (20.5.93)	GRS	ATLAS	/HOC98/
KKU		Load rejection (17.2.99)	GRS	ATLAS	/DRÄ00/
KKU		Turbine trip, reactor trip (6.6.98 and 14.10.98)	GRS	ATLAS	/DRÄ00/
KKU		Planned reactor cooldown (26. - 27.6.99)	GRS	ATLAS	/DRÄ00/
KKP-2		Pump failure (1 of 4; 19.11.98)	GRS	ATLAS	/DRÄ02/
KKP-2		Fault of load control (21.5.99)	GRS	ATLAS	/DRÄ02/
KKP-2		Turbine trip (28.2.01)	GRS	ATLAS	/DRÄ02/
KKP-2		Reactor trip (8.10.00)	GRS	ATLAS	/DRÄ02/
KKP-2		Planned reactor cooldown (23.7.00)	GRS	ATLAS	/DRÄ02/
KBR		Simulation of a SG tube rupture (start-up test; 21.11.86)	GRS	ATLAS	/HOC95/
KBR		Turbine trip (14.8.93)	GRS	ATLAS	/HOC95/
KBR		Load rejection (11.3.91)	GRS	ATLAS	/HOC95/
KBR		Inadvertent closing of a feedwater control valve, reactor trip (25.4.95)	GRS	ATLAS	/HOC95/

Table 2 - 7: Transients in WWERs (Matrix XI)

Test Facility	**Test No.**	**Brief Description**	**Calculation done by**	**ATHLET Version**	**Refer-ence**
PACTEL	LOF-01	Loss of feedwater (1 loop, 75 KW power)	THZ	Mod1.1A	/LIS94/

PACTEL	LOF-04	Loss of feedwater (3 loop, 166 KW power)	THZ	Mod1.1A	/LIS94/
Greifswald (U4)		Quick electrical power reduction by 100 MW	GRS	Mod1.0D	/POI91/
Greifswald (U4)		Commissioning test: loss of two main coolant pumps	GRS	Mod1.0D	/POI91/
Dukovany		Failure of 1, 2, 3, and 6 main circulation pumps	NRI/GRS	Mod1.1A	/ARN97/
Dukovany		Reactor scram and turbine trip caused by EP1 signal	NRI/GRS	Mod1.1D	/VOJ00a/
Bohunice		Transient following the signal 'Pressure in primary system below 8.3 MPa'	NRA/GRS	Mod1.1D	/VOJ01/
Kosloduj (U6)		Coast down of two neighboring out of four main circulation pumps	INRNE/GRS	Mod1.2A	/VOJ00b/

Table 2 - 8: Transients at shut-down conditions in PWRs (Matrix V)

Test Facility	**Test No.**	**Brief Description**	**Calculation done by**	**ATHLET Version**	**Refer-ence**
PKL-III	B 4.5	Loss of residual heat removal system during mid-loop operation	GRS	Mod1.2B	/STF01/
PKL-III	E 3.1	Loss of residual heat removal system during 3/4-loop operation; OECD/PKL Benchmark	GRS	Mod2.0B	/STF06/
PKL-III	F 2.1	Loss of residual heat removal system with different water inventories and varied upper head by-passes	GRS	Mod2.1B	/WIB08/
BETHSY	6.9a	Loss of residual heat removal system during mid-loop operation, pressurizer manways open			
BETHSY	6.9c	Loss of residual heat removal system during mid-loop operation, pressurizer and SG outlet ple-num manways open, ISP 38	GRS/Kurt.	Mod1.1D	/MOS97/
BETHSY	6.9d	Loss of residual heat removal system during mid-loop operation, primary system half open			

Table 2 - 9: Transients at shut-down conditions in WWERs

Test Facility	**Test No.**	**Brief Description**	**Calculation done by**	**ATHLET Version**	**Refer-ence**
PMK		Primary circuit opened, water level reduction	GRS/KFKI	Mod1.1B	/GYO95/
PMK		Primary circuit opened, isolation of a cold leg	GRS/KFKI	Mod1.1B	/GYO95/

Table 2 - 10: Accident management for non-degraded core in PWRs (Matrix VI)

Test Facility	Test No.	Brief Description	Calculation done by	ATHLET Version	Refer-ence
Primary bleed and feed procedures					
TRAM	B1	Steam release from the pressurizer at constant system pressure	GRS	Mod1.1C Mod1.1D	/KIR96/ /SCK98/
TRAM	B2	Steam release from the pressurizer with depressurization			
TRAM	B3	Steam release from the pressurizer with depressurization, alternative ECC injection			
PKL-III	B1.6	Loss of off-site and on-site power			
PKL-III	C1.2	Small leak with station blackout, primary side accident management-procedures	GRS	Mod1.1C	/RIN96/
PKL-III	C5.2	Loss of offsite power, primary side bleed and feed followed by secondary side bleed and feed	GRS	Mod1.1D	/STF98/
LOBI II	BT-02	Primary feed and bleed procedures after a complete loss off feedwater	Battelle	Mod1.0E	/SCH93/
BETHSY	5.2a	Two phase natural circulation with empty SG secondary side and primary accident management procedures			
BETHSY	5.2c	Primary feed and bleed procedures after a complete loss off feedwater	FZR	Mod1.1D	/KRE98a/
Secondary bleed and feed procedures					
PKL III	B1.2	Complete loss of feedwater, injection of water due to flashing in feedwater line, mobile pump	GRS GRS	Mod1.1B Mod1.1D	/GEP96/ /SCK98/
PKL III	C2.2	Primary depressurization after a SG tube rupture			
PKL III	C4.2	Complete loss of feedwater, injection of water due to flashing in feedwater line and feedwater tank,			
PKL III	D1.2	System behavior during a station blackout with small leak and secondary accident management-procedures	GRS	Mod1.2B	/STF99/
PKL III	G7.1	1.5% hot leg break with failure of high pressure injection and secondary side depressurization (Counterpart test to LSTF SB-HL-18)	GRS	Mod2.2B	/AUS13/

LOBI II	BT-17	Complete loss of feedwater, isimilar to PKL III B1.2	Battelle	Mod1.0E	/SCH93/
BETHSY	9.1b	0.5% break in the cold leg without high pressure injection (ISP-27)	GRS	Mod1.1A	/POI92/
BETHSY	5.2d	Station black-out in combination with auxiliary feedwater failure	GRS	Mod1.1B Mod1.1D	/RIN94/ /SCK98/
BETHSY	9.3	SG tube rupture with loss of feedwater and failure of high pressure injection	FZR	Mod1.1D	/KRE98b/
LSTF	SB-PV-09	1.9% pressure vessel upper head break with total failure of high pressure injection	GRS	Mod2.1A	/AUS07/
LSTF	SB-PV-10	0.1% break in bottom of pressure vessel and failure of high pressure injection asymmetrical steam generator secondary side depressurization as AM action	GRS	Mod2.1A	/AUS10/
LSTF	SB-HL-18	1.5% hot leg break with failure of high pressure injection and asymmetrical steam generator secondary side depressurization as AM action (OECD ROSA-2 Project Test 3)	GRS	Mod2.2B	/AUS13/

Table 2 - 11: Accident management procedures for WWERs (secondary feed and bleed)

PACTEL	SBL-31	0.22% cold leg break, 3 loops, secondary side bleed and feed	THZ	Mod1.2A	/VAN99/
PACTEL	SBL-33	0.44% cold leg break, 3 loops, secondary side bleed and feed	THZ	Mod1.2B	/VAN99a/

Table 2 - 12: Small, intermediate and large breaks in BWRs (Matrix VII)

Test Facility	**Test No.**	**Brief Description**	**Calculation done by**	**ATHLET Version**	**Refer-ence**
ROSA III	Run 912	5% pipe rupture in the recirculation line, failure of the high pressure core spray system, ISP-12	TÜV Bayern	Mod1.0E	/GAS93/
ROSA III	Run 984	2,8% pipe rupture in the recirculation line in a BWR facility	GRS	Mod1.0C	/HRU92/
ROSA III	Run 916	50% pipe rupture in the recirculation line, failure of the high pressure core spray system	GRS	Current	Chap. 5.2
ROSA III	Run 983	200% pipe rupture in the recirculation line, failure of one emergency diesel for the low pressure injection system	GRS	Mod1.0A/ FLUT	/POI89/
ROSA III	Run 952	100% steam line rupture	GRS	Mod1.0E	/HRU93/
FIST	6SB2C	2,8% pipe rupture in the recirculation line, similar to ROSA III Run 984	GRS	Mod1.0E	/HRU95/
FIST	6MSB1	100% steam line rupture	GRS	Mod1.1A	/ARI95/

Table 2 - 13: Transients in BWRs (Matrix VIII)

Test Facility	Test No.	Brief Description	Calculation done by	ATHLET Version	Refer-ence
ROSA III	Run 971	Loss of offsite power, failure of the high pressure core spray system	TÜV Bayern	Mod1.0E	/BOR93/
FIST	6PMC1	ATWS	GRS	Mod 2.1B	/AUS 10/
KRB		Turbine trip (2.10.87)	GRS	ATLAS	/POI94/
KRB		Reactor trip (18.10.90)	GRS	ATLAS	/POI94/
KRB		Temperature transient at pressure vessel bottom (8.5.93)	GRS	ATLAS	/POI94/
KKK		Loss of main heat sink (17.1.91)	GRS	ATLAS	/HOP93/
KKK		Reactor trip (29.10.91)	GRS	ATLAS	/POI96/
KKK		Steam line isolation (18.7.90)	GRS	ATLAS	/POI96/
KKP-1		Loss of main heat sink (22.3.96)	GRS	ATLAS	/POI99/
KKP-1		Reactor trip (6.3.96 and 3.12.96)	GRS	ATLAS	/POI99/
KKP-1		Planned reactor cooldown (11.1.96)	GRS	ATLAS	/POI99/

Table 2 - 14: Summary of ATHLET validation integral experiments and incidents for western design facilities (total / performed analyses)

Facility or Plant	Scale	Pressurized Water Reactors					Boiling Water Reactors	
		Large breaks	Small and medium breaks	Transients	Transients with loss of RHRS	AM	LOCAs	Transients
UPTF/ TRAM	**1:1**	6 / 2	2 / 2			3 / 1		
CCTF	**1:25**	4 / 4						
LOFT	**1:50**	2 / 2	4 / 3	1 / 0				
LSTF	**1:50**		5 / 4			3 / 3		
BETHSY	**1:100**		7 / 7		3 / 1	5 / 4		
PKL	**1:145**	2 / 2	13 / 8	12 / 7	3 / 3	8 / 5		
ATLAS	**1:288**		1 / 1					
LOBI	**1:712**	2 / 2	8 / 6	4 / 3		2 / 2		
GERDA*	**1:1686**		1 / 1					
ROSA-III	**1:424**						5 / 5	1 / 1
FIST	**1:642**						2 / 2	1 / 1
German Konvoi				3 / 3				
KBR				4 / 4				
KKU				3 / 3				
KKP-2				5 / 5				
KKP-1								3 / 3
KRB								3 / 3
KKK								3 / 3
TOTAL		**16 / 12**	**41 / 32**	**32 / 25**	**6 / 4**	**21 / 15**	**7 / 7**	**11 / 11**

*) PWR with once-through steam generators

Table 2 - 15: Summary of ATHLET validation integral experiments for Russian design facilities (total / performed analyses)

Facility	Scale	Large breaks	Small and medium breaks	Transients	Transients with loss of RHRS	AM
PMK	**1:2070**		6 / 6		2 / 2	
ISB	**1:3000**		6 / 6			
PACTEL	**1:305**		9 / 5	2 / 2		2 / 2
PSB WWER	**1:300**	1 / 1	3 / 3			
Greifswald (U4)	**1:1**			2 / 2		
Dukovany	**1:1**			2 / 2		
Bohunice	**1:1**			1 / 1		
Kosloduj (U6)	**1:1**			1 / 1		
TOTAL		**1 / 1**	**24 / 20**	**8 / 8**	**2 / 2**	**2 / 2**

2.2.2 Separate Effects Test Validation Matrices for ATHLET

Whereas integral experiments are usually designed to follow the behavior of a reactor system in various off-normal conditions or accidents, separate effects tests (SETs) focus on the behavior of a single component, or on the characteristics of one thermal-hydraulic phenomenon. Main advantages of separate effects tests are:

- the existence of clear boundary conditions,
- measurement instrumentation can be chosen to study one particular phenomenon,
- reduced possibility of compensating modelling errors during code validation,
- systematic evaluation of accuracy of a code model across a wide range of conditions up to full reactor plant scale,
- steady state rather than transient observations possible.

The construction of a separate effects test matrix is an attempt to collect the best sets of available test data for code validation, assessment and improvement, from the wide range of experiments that have been carried out world-wide in the field of thermal-hydraulics.

At the beginning of the code assessment work it was considered that sufficient comparison with separate effects tests data would be undertaken and documented by code developers. Therefore, only limited further validation against separate effects test data would be necessary. This expectation has shown to be unrealistic. It is now recognized that continued comparison of calculations with separate effects test data would be necessary to investigate particular applications of codes, especially where a quantitative evaluation of prediction accuracy is required, as well as for code model improvement. A key issue concerning the application of best estimate codes to plant calculations is quantitative code assessment. Quantitative code assessment is intended to allow predictions of nuclear power plant behavior to be made with a well defined uncertainty. Most methods for achieving this quantification of uncertainty rely on assigning uncertainties to the modelling by the code of individual phenomena, for instance by the determination of reasonable ranges which key model parameters can cover and still produce results consistent with data. This interest has placed a new emphasis on separate effects tests over and above that originally envisaged for model development.

A further incentive to conduct separate effects tests in addition to tests carried out in integral facilities is the difficulty encountered in scaling predictions of phenomena from integral test facilities (which are small scaled) to plant applications. Where a phenomenon is known to be highly scale dependent and difficult to model mechanistically, there is a strong case for conducting separate effects tests at full scale. In general, it is desirable to have a considerable overlap of

data from different facilities, since successfully predicting data from different facilities provides some confirmation that a phenomenon is well understood. While both integral test data and separate effects test data are appropriate for code validation, for model development and improvement there should be a preference for separate effects test data.

A total of 67 thermal-hydraulic phenomena of interest in LWR LOCA and transients are listed in table 2 - 16. This table is taken from the OECD/CSNI report on the separate effects test matrix /AKS94/. All representative phenomena occurring during a LOCA or transient are included. However, several phenomena are combined under a general heading in some cases, such as various instances of counter-current flow limitation, and of critical flow. It should also be realized that some phenomena are dependent on each other, for instance spray effects and condensation. There are different types of phenomena, varying from those such as interphase friction which is a very basic attribute of a two-phase flow, to those such as loop seal clearing, which is essentially a system phenomenon, localized in its occurrence but very dependent on events and conditions elsewhere in the loop. In such cases, the influences from the loop have to be provided as boundary conditions. A detailed description of these phenomena can be found in /AKS94/.

This list of phenomena forms one axis of the SET facility cross reference matrix. The second axis of the matrix consists of the 187 facilities identified as potential sources of separate effects test data. For each test facility, the phenomena addressed by the corresponding experimental research programme have been indicated in these matrix tables, yielding the SET cross reference matrix for test facilities and thermal-hydraulic phenomena.

A number of specific experiments were selected from those facilities which are included in the cross-reference matrices described above. These selected tests versus phenomena establish the individual code validation matrix (table 2 - 17). An overview of the different separate effects test facilities indicating the number of selected tests as well as the current status of calculated experiments is shown in table 2 - 18.

Table 2 - 16: List of relevant phenomena for LWR transients and LOCAs

0	Basic Phenomena	1 2 3 4 5 6 7 8 9	Evaporation due to depressurization Evaporation due to heat input Condensation due to pressurization Condensation due to heat removal Interfacial friction in vertical flow Interfacial friction in horizontal flow Wall-to-fluid friction Pressure drops at geometric discontinuities Pressure wave propagation
1	Critical flow		Breaks (1), Valves (2), Pipes (3)
2	Phase separation / vertical flow with or without mixture level		Pipes / plena (1), Core (2), Downcomer (3)
3	Stratification in horizontal flow	1	Pipes
4	Phase separation at branches	1	Branches
5	Entrainment / De-entrainment	1 2 3 4 5 6	Core Upper plenum Downcomer Steam generator tube Steam generator mixing chamber (PWR) Hot leg with ECC injection (PWR)
6	Liquid-vapor mixing with condensation	1 2 3 4 5 6	Core Upper plenum Downcomer Lower plenum Steam generator mixing chamber (PWR) ECC injection in hot and cold legs (PWR)
7	Condensation in stratified conditions	1 2 3 4	Pressurizer (PWR) Steam generator primary side (PWR) Steam generator secondary side (PWR) Horizontal pipes
8	Spray effects	1 2 3	Core (BWR) Pressurizer (PWR) OTSG secondary side
9	Countercurrent flow / CCFL	1 2 3 4 5 6	Upper tie plate Channel inlet orifices (BWR) Hot and cold leg Steam generator tube (PWR) Downcomer Surge line (PWR)
10	Global multidimensional fluid temperature, void and flow distributions	1 2 3 4	Upper plenum Core Downcomer Steam generator secondary side
11	Heat transfer: Natural or forced convection Subcooled / saturated nucleate boiling DNB / Dryout Post critical heat flux Radiation Condensation	1 2 3 4 5 6	Core, steam generator, structures Core, steam generator, structures Core, steam generator, structures Core, steam generator, structures Core Steam generator, structures
12	Quench front propagation / rewetting	1 2	Fuel rods Channel walls and water rods (BWR)
13	Lower plenum flashing		
14	Guide tube flashing (BWR)		
15	One and two phase impeller-pump behavior		
16	One and two phase jet-pump behavior (BWR)		
17	Separator behavior		
18	Steam dryer behavior		
19	Accumulator behavior		
20	Loop seal filling and clearance (PWR)		
21	ECC bypass / downcomer penetration		
22	Parallel channel instabilities (BWR)		
23	Boron mixing and transport		
24	Non-condensable gas effects (PWR)		
25	Lower plenum entrainment		

Table 2 - 17: Separate Effect Tests Matrix

Test Facility	Test No.	Brief Description	Calculation done by	Code Version	Refer-ence
ACHILLES		Reflooding in bundle with 69 electrically heated rods (6 tests)	GRS	Mod2.2B	/TIB15/
Bartolomej	1 ... 21	Subcooled and saturated nucleate boiling at high pressure	GRS	Mod2.1B	/TRB09/
BATTELLE	SWR 2R	Break of a steam line, ISP-6	GRS	DRUFAN	/STF89/
BATTELLE	SL1	Break of a feedwater line	GRS	DRUFAN	/RIN83/
KWU-Karlstein	RS 37 C	Blowdown heat-transfer			
CREARE	1/5	CCFL in downcomer	RUB	Mod1.1D	/WEI98/
CREARE	1/15	CCFL in downcomer	RUB	Mod1.1D	/WEI98/
CREARE	1/30	CCFL in downcomer	RUB	Mod1.1D	/WEI98/
ECTHOR		Clearance of a water filled loop seal by a forced air flow through the loop	RUB	Mod1.0E	/SCA93/
FEBA	Series I	Reflooding in a 5x5 full length rod bundle	RUB	Mod2.2B	/TIB15/
FLECHT-SEASET	31701	US SP 9A: Bundle reflood at high flooding rate	GRS GRS	Mod1.2D Mod3.0A	/TES01/ /TIB15/
	31805	US SP 9B: Bundle reflood at low flooding rate	GRS GRS	Mod1.2D Mod3.0A	/TES01/ /TIB15/
GE VESSEL	5702-16	Blowdown test with top leak	GRS	Mod0.0B	/KIR87/ /SKO88/
GE VESSEL	5803-2	Blowdown test with bottom leak	GRS	Mod0.0B	/KIR87/ /SKO88/

HDR	V 45	Break of a steam line	GRS	DRUFAN	/STF89/
HDR	V 21.1	Break of a feedwater line	GRS	Mod1.0D	/POI92a/
HDR	V 21.3	Break of a feedwater line			
HDR-COCO	E 33.1131	Steam condensation at ECC water: 0.4 MPa, Steam surplus, Rt=0.8	GRS	Mod1.0E	/TES93/
HDR-COCO	E 33.1142	Steam condensation at ECC water: 0.4 MPa, Steam deficiency, Rt=1.2	GRS	Mod1.0E	/TES93/
HDR-COCO	E 33.1168	Steam condensation at ECC water: 0.4 MPa, Steam deficiency, Rt=3.0	GRS	Mod1.0E	/TES93/
HDR-COCO	E 33.1241	Steam condensation at ECC water: 2.5 MPa, Steam surplus, Rt=0.8			
HDR-COCO	E 33.1246	Steam condensation at ECC water: 2.5 MPa, Steam deficiency, Rt=1.6			
HDR-COCO	E 33.2331	Steam condensation at ECC water: 7.0 MPa, Steam surplus, Rt=0.8			
HDR-COCO	E 33.2338	Steam condensation at ECC water: 7.0 MPa, Steam deficiency, Rt=3.0			
IVO		Clearance of a water filled loop seal, test sloping inlet D=80mm, WWER 440	GRS	Mod1.0A	/SKO88a/
IVO		Clearance of a water filled loop seal, test straight inlet D=80mm, WWER 1000	GRS	Mod1.0A	/SKO88a/
IVO		Clearance of a water filled loop seal, D=850mm, WWER 1000	GRS	Mod1.0A	/SKO88a/ /SON94/
IVO-CCFL		CCFL in fuel element head and fuel bundle (air-water)	RUB	Mod1.0B	/WEI00/
HORUS	PCHS 5,9,10,11	Injection of steam in WWER SG tube; closed exit collector; condensation	THZ	Mod1.1B	/FJO94/
HORUS	PCHS 23,25,30,36	Injection of steam in WWER SG tube; closed exit collector; condensation	THZ	Mod1.2B	/GOC00/
HORUS	POHS 1,3,5	Injection of steam in WWER SG tube; open exit collector; condensation	THZ	Mod1.1B	/FES93/
HORUS	PCHG 7	Injection of steam in WWER SG tube with N_2 gas; closed exit collector; condensation	THZ	Mod1.1C	/FJO 96/
HORUS	POHG 9	Injection of steam in WWER SG tube with N_2 gas; open exit collector; condensation	THZ	Mod1.1C	/FJO 96/
HORUS	PCHN 5,6,8,10	Injection of steam and N_2 gas in WWER SG tube; closed exit collector; condensation	THZ	Mod1.2B	/GOC00/
KFA		Onset of flow instabilities in research reactors at low pressure	GRS	Mod2.1B	/TRB09/

MARVIKEN	Test 22	Blowdown test with critical flow in subcooled fluid conditions	GRS	Mod0.0A	/RIN87/
NEPTUNUS	Y 05	Pressurizer transient, d=800mm	GRS	Mod1.0 B	/HOB89/ /CEC90/
OMEGA Bundle	Test 9	PWR rod bundle behavior during blowdown	GRS	Mod1.1C	/GLA94a/
PATRICIA	GV 2	SG swell level (8 steady state tests, 3 transient tests)	RUB	Mod1.1D	/WEI 96/
PERICLES		3 Boil-off tests (steady state) in rectangular bundle, p=0.3-0.55 MPa	GRS	Mod1.0B	/CEC90/
PERICLES		Reflooding in an array of 3 bundles of 7x17 rods each (6 tests)	GRS	Mod2.2B	/TIB15/
ROCOM	T6655	Density driven mixed experiments (3 runs)	GRS	Mod2.1C	/HOR09/
ROCOM	Tests 1.1-1.3	Coolant mixing in downcomer during a MSLB scenario (Complementary tests to PKL-3 G3.1 in the frame of the OECD/NEA PKL-2 Project	GRS	Mod3.0A	/AUS13/
ROCOM	Tests 2.1, 2.2	Coolant mixing in downcomer during a MSLB scenario (Complementary tests to PKL-3 H in the frame of the OECD/NEA PKL-3 Project	GRS	Mod3.0B Current	/PAN15/ /CEU15/ Chap. 5.5
RS 77		Thermodynamic nonequilibrium, evaporation	GRS	Mod1.1A	/RUA96/
SCTF	S3-09/713	Double ended cold leg break, cold leg ECC, EM-case			
SCTF	S3-10/714	Double ended cold leg break, cold leg ECC, BE-case			
SCTF	S3-11/715	Double ended cold leg break, combined ECC, BE-case			
SCTF	S3-13/717	Double ended cold leg break, combined ECC, EM-case			
SCTF	S3-14/718	Double ended cold leg break, cold leg ECC, flat power profile			
SCTF	S3-16/720	Double ended cold leg break, cold leg ECC, steep power profile			
SUPER MOBY DICK		Phase separation with lateral outlet			

SUPER MOBY DICK		Critical flow; d=5.2 mm, d=15.5 mm	GRS	DRUFAN	/BUR85/
THETIS		8 Boil-off Tests (steady state) in circular bundle, p=0.5-4.0 MPa	GRS	Mod1.0B	/CEC90/
KfK T-Junction Test Facility		T-junction tests	GRS	Mod1.1C	/SKO95/
TOSHIBA - Vessel		Blowdown test with vessel boil-off	GRS	Mod1.0E	/STO92/
TPTF	Nr.6	6 Boil-off tests in bundles, (p=3.0, 7.0, 11.9 MPa)	GRS	Mod1.0D	/RIN91/
TPTF		Test in horizontal pipe, stratified flow	GRS	Mod1.1C	/SON94/ /BAE96/
Techn. Univer-sität Hannover		CCFL in bundle			
UPTF	5A	CLI, CCFL Downcomer			
UPTF	5B	CLI, CCFL Downcomer, break in cold leg			
UPTF	6	CLI, CCFL Downcomer	RUB GRS	Mod1.2D Mod3.1A	/WEI02/ /HOL16/
UPTF	7	CLI, CCFL in downcomer	RUB GRS GRS	Mod1.2D Mod2.1A Mod3.0A	/WEI02/ /WIB06/ /AUS13/
UPTF	8A	Flow regime dependent condensation in cold/hot leg during HLI and CLI, resp.	GRS	Mod1.2B	/RIN01/
UPTF	9	Flow regime dependent condensation for combined ECC injection			
UPTF	10B	Liquid entrainment in steam flow from core to SG	RUB	Mod1.1D	/WEI98/
UPTF	10C	CCFL core / UP	RUB GRS	Mod1.1D Mod 2.1B	/WEI98/ /AUS10/
UPTF	11	CCFL in hot leg, reflux condensation	GRS	Mod1.0D	/SON90/
UPTF	15 Run123	HLI, CCFL in fuel element head plate during ECC injection into intact HL, large break			

UPTF	20	UPI, CCFL in fuel element head plate during upper plenum injection	Pitscheider GRS	Mod1.0C Mod2.1B	/THI90/ /SCH08/
UPTF	22	DCI, Vent valve test			
UPTF	23	DCI, Vent valve test			
UPTF	25A	CLI, Entrainment in DC			
UPTF	25B	CLI, Entrainment in DC			
UPTF	26 Run 230	HLI, CCFL behavior in hot leg, effect of scoop injection in hot leg	GRS	Mod1.0D	/SON90a/
UPTF	29	Upper plenum deentrainment			
UPTF	30	HLI, CCFL in fuel element head plate during HP injection into intact HL, small leak	GRS	Mod1.0D	/BUR92/
UPTF	Z1	Liquid entrainment in steam flow from downcomer to cold leg during reflood phase; steam condensation during cold water injection			
UPTF	Z3	CCFL in Downcomer during the postulated large break in cold leg	GRS RUB GRS	Mod1.0D Mod1.2D Mod3.1A	/BUR92a/ /WEI02/ /HOL16/
UPTF TRAM	A1	Core cooling flow in hot leg ECC injection			
UPTF TRAM	A2	Stratified flow in hot leg ECC	Pitscheider	Mod1.0E	/FEI 93/
UPTF TRAM	A4	Reflux condenser with ECC injection			
UPTF TRAM	A5	Clearance of a water filled loop seal	RUB	Mod1.1A	/WEI96/
UPTF TRAM	C1	ECC injection in the cold leg of a water-filled PWR; thermal mixing in cold leg and downcomer	GRS GRS	Mod1.2E Mod2.2B	/LER02/ /SCH12/
UPTF TRAM	C2	ECC injection in steam-filled cold leg; influence of N_2 on condensation	GRS	Mod1.2B	/BUR01/
UPTF TRAM	C3	Mixing of mass flows with different temperatures	GRS	Mod1.2E	/BUR03/

Table 2 - 18: Summary of ATHLET validation separate effects tests (total / performed analyses)

Test Facility	Nr. of Tests	Test Facility	Nr. of Tests	Test Facility	Nr. of Tests
ACHILLES	1 / 1	Bartolomej	1 / 1	Battelle	2 / 2
CREARE	3 / 3	ECTHOR	1 / 1	FEBA	1 / 1
FLECHT	2 / 2	GE VESSEL	2 / 2	HDR	3 / 2
HDR-COCO	7 / 3	HORUS	6 / 6	IVO	3 / 3
IVO-CCFL	1 / 1	KFA	1 / 1	KfK T-Junction	1 / 1
KWU-Karlstein	1 / 0	MARVIKEN	1 / 1	NEPTUNUS	1 / 1
OMEGA	1 / 1	PATRICIA	1 / 1	PERICLES	2 / 2
ROCOM	4 / 4	RS77	1 / 1	SCTF	6 / 0
S MOBY DICK	2 / 1	THETIS	1 / 1	TOSHIBA-V.	1 / 1
TPTF	2 / 2	TU Hannover	1 / 0	UPTF	20 / 10
UPTF-TRAM	7 / 5				
TOTAL	**87 / 61**				

2.3 Validation for Passive Safety Systems

Particularly advanced Gen III+ and IV reactor designs rely more and more on passive safety systems for accident control and mitigation. Their range of applicability comprises ECC injection, residual heat removal, pressure reduction, flow limitation, etc.. The functional capability of passive safety systems is based on physical key principles such as gravitation, buoyancy, condensation and evaporation. Compared to active systems typically used in former reactor types, passive systems exhibit different operational conditions and by far smaller driving forces. In addition, their instantaneous working point is not defined but determined by the overall conditions in the facility. Thus, a separate code validation for passive safety systems or even further code elaboration becomes indispensable.

In the frame of the longtime general code validation procedure, ATHLET proved to be capable to capture basic phenomena that are characteristic for the operation of passive systems, e.g. single and two-phase natural convection processes or condensation/evaporation in heat exchangers of different shape. Unfortunately, only few experimental data of separate effect tests investigating in detail the practicality of passive safety systems are available until now. However, ATHLET could be validated against several dedicated test cases. Table 2 - 19 provides an overview of selected experiments. Some of the test cases are also included in the tables of the preceding chapters of the manual in hand.

Table 2 - 19: Validation cases for passive safety systems

Facility	Test	Brief Description	Calculation done by	Code Version	Reference
INKA	2_12_1 1_10_85_13_1	Stationary and transient emergency condenser tests simulating heat removal and primary side steam condensation in the KERENA BWR design	GRS	Mod3.0B	/BUC15/
NOKO Juelich	Emergency condenser capacity	Analysis of an emergency condenser employing one slightly inclined heat exchanger pipe bundle	GRS	Mod3.0B	/SCH15/
ATLAS	Test A1.2	Passive Auxiliary Feedwater System during a Station Blackout	GRS	Mod3.0B	/AUS16/
UPTF TRAM	A6	Cold leg accumulator injection after 5% cold leg break	GRS	Mod1.1A	/BUR94/

2.4 Validation for GEN IV Reactors

Originally, ATHLET has been developed to be applied for the analysis of the behavior of Light Water Reactors (LWR) under transient or accident conditions. Meanwhile, the new working fluids heavy water, helium and the liquid metals lead, lead-bismuth eutectic (LBE) and sodium have been implemented into the code, together with new models and correlations related to these coolants. These extensions are required for the modelling of a new generation of NPPs, called GEN IV reactors, which use different fluids in the coolant circuits. Presently, the following reactor types are considered as the most promising ones:

- (Very) high temperature gas cooled reactor (V)HTGR (helium cooled)
- Sodium cooled fast reactor SFR (coolant is liquid sodium)
- Lead cooled fast reactor LFR (liquid lead or LBE)

The new core designs aim at different advantages compared to LWRs, among them

- increased overall efficiency of the NPP,
- improved fuel utilization and sustainability,
- improved passive or even inherent safety,
- improved reliability,
- reduced risk of proliferation.

Another innovative reactor design is the so-called Accelerator Driven Sub-critical System (ADS) with LBE as coolant and target. This design enables the transmutation of long-lived fission products into short-lived ones.

In addition to the new coolants, the design of these reactors is quite different to those of common LWRs. In particular, the geometry of and the coolant flow inside the reactor vessel differ strongly from LWRs. Moreover, the nuclear core of (V)HTGRs may consist of graphite pebbles or may have a graphite block structure.

Different to LWRs, no systematic validation matrices have been set-up for GEN IV reactor's design and thermal-hydraulic phenomena up to now. Nevertheless, all major system codes have been extended for these types of reactors, and validation work is underway.

The validation of the ATHLET extensions for GEN IV reactors has just started. Besides many test calculations in the frame of the ATHLET development proving the capability of the code

to model the new coolants and to produce 'reasonable' results, some verification work has been performed up to now (table 2 - 20). One subject of this work was the simulation of different transients and accident scenarios in the MYRRHA/XT-ADS concept which is planned to be built at the Belgian Nuclear Research Center SCK-CEN /PAL13/. Up to now, no measured date are available, the ATHLET results have been compared with those obtained with the RELAP5 computer code.

Table 2 - 20: Validation cases for GEN IV reactors

Test Facility	Test No.	Brief Description	Calculation done by	Code Version	Reference
KASOLA, code-to-code comparison	Drainage test	Emergency drainage of the KASOLA test facility, working fluid Sodium	GRS	Mod3.0A	/HRI15/
MHTGR-350, code-to-code comparison	OECD MHTGR benchmark	OECD code benchmark for prismatic MHTGR-350-MW core designs	GRS	Mod3.0B	/CRO15/
MYRRHA, code-to-code comparison		Simulation of nominal conditions and accidental scenarios in the spallation loop of MYRRHA facility (LBE)	GRS	Mod3.0A	/PAL13/
TALL	T.01.09	European FP7 project THINS, ATHLET - ANSYS CFD coupled calculations of transition from forced to natural convection, working fluid LBE	GRS, TUM	Mod3.0A	/PAP15/

2.5 Validation for Coupled Code Systems

In the past, various interfaces were developed in order to couple ATHLET with other codes. This work enables multi-scale and multi-physical simulations and, by that, extends the code's scope of application. Figure 2 - 12 depicts available code couplings. Regarding the interface concept, pure data transfer interfaces, e.g. for provision of appropriate boundary conditions for subsequent code application, and true coupling interfaces based on simultaneous code execution can be distinguished. Depending on the characteristic time constants of the coupled physical processes, the coupling is realized in weak or strong form, where the latter refers to mutual data transfer on ATHLET sub-timestep level, sometimes also including mutual iteration of both codes' results to comply with defined convergence criteria.

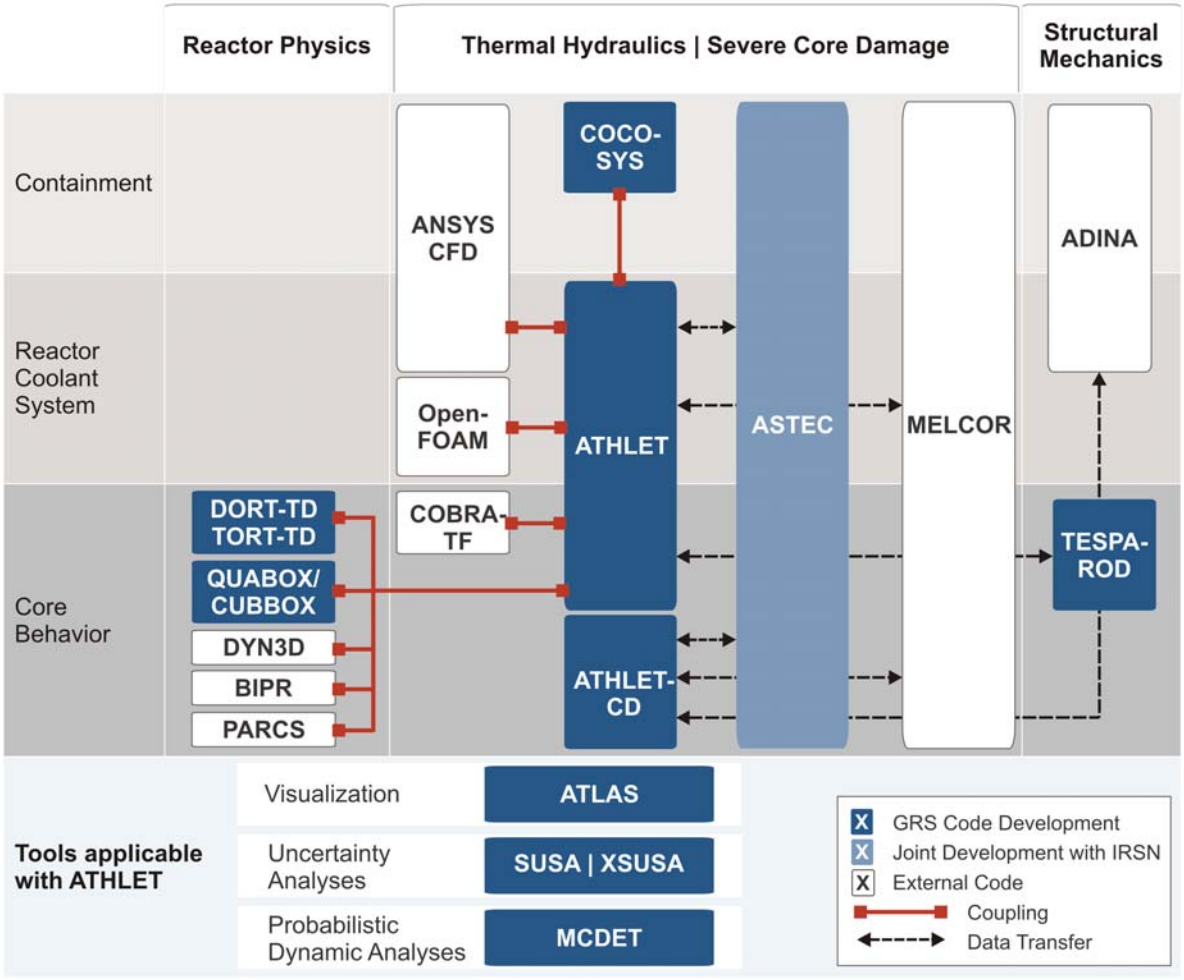

Fig. 2 - 12: Codes coupled with ATHLET

2.5.1 Coupling with CFD Codes

In a series of reactor transients and accidents, 3D flow phenomena relevant for nuclear safety issues occur in various parts of a NPP. Examples for this are boron dilution events or the main

steam line rupture leading to a strongly asymmetric coolant distribution in the reactor pressure vessel which may propagate into the nuclear core. For these cases, the degree of coolant mixing of deborated and borated water or of hot and cold water, resp., particularly in the downcomer and the lower plenum is of essential significance for the distribution of the boron concentration and the coolant temperature at the core entry, which in turn determines the local nuclear power production in the core.

TH system codes like ATHLET are based on balance equations solved in 1D direction. Although simulation networks with 3D topology can be generated and applied for safety analyses, their solution remains of 1D type neglecting mixed and turbulent terms in the momentum equation. Computational fluid dynamics (CFD) codes, in turn, are able to model complex flow processes by means of true 3D approaches with high resolution in space and time. Unfortunately, CFD simulations require very high computation time. Thus, the application of these tools for the complete NPP to be analyzed is presently not feasible.

Since 3D processes, in general, are significant only in some location of the NPP, coupled system and CFD code packages are developed and applied, where only the crucial part of the facility is modelled in detail with a CFD code and the remaining (much larger) part is modelled with the system code.

For that purpose, ATHLET has been coupled with the CFD code ANSYS CFD. The validation of this coupled code system is presently underway. Besides many test calculations in the frame of the development of the coupling proving its feasibility, the implementation on a computer cluster, and the correctness of the achieved results (by comparison with stand-alone calculations), some validation work has been performed up to now. Table 2 - 21 provides an overview.

2.5.2 Coupling with 3D neutronics codes

For ATHLET, coupling interfaces to several 3D neutronics codes are provided (see figure 2 - 12). The development of multi-physics methodologies requires comprehensive validation procedures. For that purpose, NEA/OECD defined and conducted benchmarks that permit the verification of best-estimate neutronics / thermal-hydraulics coupled code systems for LWR. The benchmarks were addressed to complex transients with core plant interaction. Examples are the PWR coolant transient benchmark /KOL11/ or the BWR turbine trip benchmark /LAN04/.

A selection of cases employed for the validation of the ATHLET / neutronics code coupling against PWR and BWR of both western and Russian design is presented in table 2 - 22.

Table 2 - 21: Validation cases for coupling with ANSYS CFD

Test Facility	Test No.	Brief Description	Calculation done by	Code Version	Reference
Double T-junction (PSI)	Double T-junction experiment	Fluid-fluid mixing in a double T-junction	GRS	Mod3.0A	/PAP14/
LSTF	ROSA V, Test 1.1	PTS issue during the injection of cold emergency coolant into the cold leg of a PWR filled with hot water	GRS	Mod2.2B	/PAP12/
TALL	T.01.09	Transition from forced to natural convection after pump trip. TALL facility comprises 3D test section and employs working fluid LBE. (European FP7 project THINS)	GRS, TUM	Mod3.0A	/PAP15/

Table 2 - 22: Validation cases for coupling with 3D neutronics codes

Facility	Test	Brief Description	Calculation done by	Code Version	Reference
Kalinin-3 VVER-1000	MCP trip	Switching-off of one of the four operating main circulation pumps at nominal power (OECD/NEA Kalinin-3 coolant transient benchmark)	GRS/KI (QUABOX/ CUBBOX, BIPR)		/NIK11/
Kursk-1 RBMK-1000	Vapor reactivity coefficient measurement (2010)	Modelling of vapor reactivity coefficient measurement in RBMK-1000	SEC NRS / GRS (QUABOX/ CUBBOX)	Mod2.2A	/KHR15/
Peach Bottom-2 (GE BWR/4)	Turbine trip transient	BWR turbine trip (OECD/U.S. NRC BWR TT benchmark)	GRS (QUABOX/ CUBBOX)		/LAN04/
PWR Boron Transient	Code-to-code	Postulated boron transient in PWR	GRS (QUABOX/ CUBBOX, TORT-TD)		/VEL09/
Three Mile Island-1 PWR	Code-to-code	Overcooling transient after main steam line break at 114% of nominal power (OECD PWR MSLB Benchmark)	GRS (QUABOX/ CUBBOX)		/LAN03/
VVER-1000	Code-to-code	Main steam line break outside the containment (OECD/NEA VVER-1000 coolant transient benchmark V1000CT-2)	GRS/KI (BIPR)		/KOL11/

3 International Standard Problems

Assessing the safety of nuclear installation requires the use of a number of highly specialized tools: computer codes, experimental facilities and their instrumentation, special measurement techniques, methods for testing components and materials, and so on. A highly effective way of increasing confidence in the validity and accuracy of such tools is provided by International Standard Problem (ISP) Exercises in which they are gauged against one another and/or agreed standards /NEA89, NEA00/. The OECD/CSNI Nuclear Energy Agency promoted International Standard Problems mainly for OECD countries, the IAEA mainly for Eastern European Countries.

For example, predictions of different computer codes or different users using the same computer code version for a given physical problem may be compared with each other and with the results of a carefully controlled experiment which could also be a real plant transient. This kind of comparative exercise is clearly suitable for an international venture. Moreover, ISPs enable code users to gain experience and to demonstrate their competence. ISPs are performed as 'open' or 'blind' problems. In an open Standard Problem the results of the experiment are available to the participants before performing the calculations, while in a blind Standard Problem the results are locked until the calculation results are made available for comparison.

The objectives of International Standard Problems are to /NEA89/:

1. Contribute to a better understanding of postulated and actual events;
2. Compare and evaluate the capability of best estimate computer codes to predict controlled experiments and actual plant transients, and thus improve confidence in them as assessment tools for safety questions;
3. Suggest necessary improvements in the code;
4. Improve the ability of the code users;
5. Provide information for quantifying code uncertainties and hence safety margins in design or licensing criteria;
6. Suggest necessary experiments to reduce technical ambiguities which are discovered by the ISP.

The selection and analysis of ISPs should be based on the following:

1. Selections must be made with respect to relevance to the stated objectives and to safety priorities;
2. Both integral and separate effects experiments (as well as actual plant transients) may be considered;
3. Best estimate computer codes should preferably be used;
4. The analysis should be fully documented.

While code validation is primarily a task for institutions developing codes requiring considerable financial resources for performing a large number of calculations and comparing relevant experimental results with calculated data, ISP exercises can be considered as a supplementary activity validating appropriate code applications through the analyses of experts also different from the code developers. The application of the same code by different code users provides insight into the so-called user effect on calculated results /AKS95/. The list of thermal-hydraulic International Standard Problems performed by OECD/CSNI is given in table 3 - 1.

Table 3 - 1: OECD/CSNI International Standard Problems on thermal-hydraulic tests

ISP	Date	Title	CSNI Report No.
1	1975	Edwards' Pipe (discharge, pressure waves)	-
2	1975	Semiscale: Test 11 (LB LOCA blowdown)	-
4	1978	Semiscale MOD1: Test S-02-6 (6% SB LOCA)	16, 50
5	1979	LOFT: Test L1-4 (isothermal non-nuclear blowdown)	29 (+ addendum)
6	1979	Battelle: Test SWR-2R (steam line break)	30
7	1979	ERRSEC (reflooding experiment of LOCA, SET)	55
8	1979	Semiscale MOD1: Test S-06-03 (LB LOCA, counterpart test to LOFT L2-3)	38
9	1981	LOFT: Test L3-1 (2.5% LOCA)	66
10	1981	PKL-I: Test K9 (LB LOCA refill and reflood)	64
11	1984	LOFT: Tests L3-6/L8-1 (2.5% LOCA)	73
12	1982	ROSA-III: Run 912 (5% LOCA in BWR)	100
13	1983	LOFT: Test L2-5 (LB LOCA)	101
15	1983	FIX-II: Experiment 3025 (31% LOCA in BWR)	102
18	1987	LOBI-MOD2: Experiment A2-81 (1% LOCA)	133
19	1987	PHEBUS: Test 218 (nuclear fuel behavior during LB LOCA)	131
20	1988	DOEL-2: Steam generator tube rupture event	154

21	1989	Piper-One: Test PO-SB-07 (1.6% and 2.8% LOCA in BWR)	162
22	1990	SPES: Test SP-FW-02 (loss of feedwater transient)	174 and NEA/CSNI/R(92)7
25	1991	ACHILLES: N_2 injection from accumulators and best estimate reflood rates (effect of accumulatot gas during LOCA reflood)	NEA/CSNI/R(91)11
26	1992	LSTF: Test SB-CL-18 (5% cold leg LOCA)	NEA/CSNI/R(91)13
27	1992	BETHSY: Test 9.1b (0.5% LOCA with Loss of HP Injection)	NEA/CSNI/R(92)20
33	1992	PACTEL: Test ITE-06 (WWER-440 natural circulation behaviour)	NEA/CSNI/R(94)24
38	1995	BETHSY: Test 6.9c (loss of residual heat removal system during mid-loop operation	NEA/CSNI/R(97)38
42	2003	PANDA: Long term passive containment cooling system performance, 6 phases	NEA/CSNI/R(2003)6 NEA/CSNI/R(2003)7
43	2001	Univ. of Maryland College Park: Boron dilution, 2 tests	NEA/CSNI/R(2000)22
50	2010	ATLAS: 50 % Break of DVI Line	NEA/CSNI/R(2012)6

Experiments selected to support ISP exercises are usually exceptionally well documented; they play a prominent role in the ATHLET validation matrices. GRS has participated in almost all thermal-hydraulic ISPs using ATHLET (or former DRUFAN, all essential models have been incorporated into ATHLET). The official comparison reports acknowledge the high quality of the obtained results and good agreement with experimental data compared with other computer codes. All ISP participations using ATHLET / DRUFAN are given in table 3 - 2.

Table 3 - 2: Participations with ATHLET / DRUFAN in OECD/NEA/CSNI International Standard Problems

ISP	Facility	Country	Year	Subject	Program	Ref.
1	Edwards' Pipe	UK	1975	Discharge, pressure waves	DRUFAN-01	/GAR73/
6	Battelle	Germany	1979	BWR steam line break	DRUFAN-01	/WIN78/
8	Semiscale	USA	1979	LB LOCA	DRUFAN-01	
11	LOFT	USA	1984	SB LOCA	DRUFAN-02	
13	LOFT	USA	1984	LB LOCA	DRUFAN-02	/BUT84/
18	LOBI	EC	1987	SB LOCA	DRUFAN-02	/STA87/
26	ROSA-IV-LSTF	Japan	1989	5% SB LOCA	ATHLET 1.0/FLUT N08 [1)]	/KUK92/
27	BETHSY	France	1991	0.5% SB LOCA with AM	ATHLET 1.0/FLUT N08 [1)]	/CLE92/
33	PACTEL	Finland	1994	WWER Natural Circulation	ATHLET 1.0	/PUR94/
38	BETHSY	France	1996	Mid-Loop Operation	ATHLET 1.1	/LAV95/
50	ATLAS	Korea	2010	50 % Break of DVI Line	ATHLET 2.2A	/CHO12/

[1)] for refill and reflood phase of LOCA

The OECD/CSNI International Standard Problems focussed on the investigation of the thermal-hydraulic phenomena appearing in western type of NPPs. For the analysis of phenomena and processes related to NPPs with Russian design, several experiments of WWER integral test facilities have been declared as Standard Problems. In table 3 - 3 a list of WWER-related Standard Problems calculated with ATHLET is given.

Table 3 - 3: Participations with ATHLET in WWER Standard Problems

SP	Facility	Country	Year	Subject	Program	Ref.
SPE-4	PMK-2	Hungary	1993	SB LOCA, sec. side feed and bleed	ATHLET 1.1	/IAE95/
SSP-1	ISB	Russia		SB LOCA	ATHLET 1.1	/ELE95/
SSP-2	ISB	Russia		Intermediate break LOCA, no HP inj.	ATHLET 1.1	/ELE97/
SSP-3	ISB	Russia		Intermediate break LOCA, with HP inj.	ATHLET 1.1	*/STE99/

* No official Final Report released

4 Quality Assurance Procedures

4.1 Source Code Maintenance

The ATHLET source code is written mostly in FORTRAN complemeted with some C-features. Programming changes and new modelling developments follow both the GRS internal quality assurance policy /GRS13/ and the ATHLET programming guidelines presented first in /ATH92/. A Python-script is used to prepare the auto-generated code documentation of the programmer's manual.

The ATHLET development and validation work is done on several computer platforms like PCs with Windows OS, or Linux clusters with different OS. ATHLET libraries and executables are generated using current versions of both the Intel Fortran Compiler and the GNU Fortran Compiler.

The ATHLET source code, executables, sample cases and code documentation are stored within in a repository of the version control system Subversion (SVN):

- ../A_Vers/fort for the ATHLET source code (only if provided),
- ../A_Vers/mod for the ATHLET modules (only if provided),
- ../A_Vers/project for the executables,
- ../A_Vers/plugins for code extensions, features and coupling purposes,
- ../A_Vers/athlet-conroller for external controller-code examples,
- ../A_Vers/external external dependencies
- ../A_Vers/samples for sample cases,
- ../A_Vers/docu for code documentation,

where “A_Vers” indicates the corresponding ATHLET program version tag within the SVN-repository. A daily backup is performed for all directories.

The version management software Subversion (SVN) of the CollabNet enterprise is applied for both the quality assurance and version management as well as for the storage of the ATHLET releases. The ability to properly compile and run the program is continuously verified by means of the continuous integration software Jenkins.

4.2 Release Procedures

During the development of new models or methods, or after modifications of the code structure, resp., more or less extensive test calculations may be required which are performed by the code developers. The test cases are dedicated to the code modifications which have been performed. They may be either selected from the validation matrices, or specially created by the code developer to specifically examine the current code modification. Only if these tests are successfully finished, a new developer's version of ATHLET is committed to the SVN archive. Thus, the code development is accompanied by a continuous verification and validation effort.

Prior to the release of a new ATHLET code version, either for use inside GRS (intermediate 'frozen' code versions), or for use outside GRS (general releases), a set of experiments out of the validation matrices is calculated to check finally the overall capability of the new code version. These test cases are:

- samples (standardized calculation examples),
- relevant separate effects tests, and
- the 'basis' validation cases.

The use of samples and separate effects tests depends on type and amount of changes in the code between two releases. The selected test cases ensure that changes applied to solve one modelling problem do not affect other individual models or the overall simulation capability. A further intention is to compare the results of the new version with those of earlier versions.

The basis validation consists of 5 integral tests which cover as much thermal-hydraulic phenomena as possible:

- PWR tests:
  - LOFT LP-LB-1 (200% break in cold leg, cold leg ECC water injection)
  - LSTF-SB-CL-18 (5% break in cold leg, cold leg ECC water injection)
  - Rocom Test 2.1 (Coolant mixing in RPV after MSLB)

- BWR tests:
  - ROSA III-916 (50% break in recirculation line)
- WWER tests:
  - ISB-WWER SSP 2 (rupture of one UP ECC injection line)

The comparison of the calculated and experimental data of these listed integral tests are documented in chap. 5 of this report.

Besides the comparison with the experimental data, three kinds of tests are performed on the base of one or more validation calculations:

- restart tests,
- optimization tests, and
- check of portability.

The restart capability is checked to ensure that all necessary data are stored in the restart file. Usually, a validation calculation is performed in one run, with one or more restart time points defined during the transient. Afterwards, a restart time point is selected, and a restart run is performed. The code must continue the calculation after a restart with identical results in comparison to the original run, if the input is not changed.

ATHLET can be executed in parallel mode utilizing several CPUs sharing a common memory (SMP computer architecture). This parallelization is based on the OpenMP standard. Parallel ATHLET simulations must provide results which are identical to those achieved with serial applications. Moreover, data conflicts like race conditions must be certainly avoided. These requirements are periodically proven through the comparison of appropriate test cases.

Most of the FORTRAN compilers available on different platforms offer several levels of compiler optimization. Optimization is a valuable tool to improve runtime performance, i.e. to reduce the computational time for a given code application. Some options, like loop optimizations or in-lining, can affect processing sequences and can cause significant deviations of calculated results. The adopted procedure for ATHLET is to run one or more validation calculations on a given platform with the debug option (no optimization) of the corresponding compiler, and then to repeat the calculations with the optimization level recommended for the applied compiler (default). Both calculations must produce quasi-identical results. Eventual noticeable deviations are investigated thoroughly. They can indicate incorrect programming, or even compiler malfunctions. Some examples have been reported in /TRB 96/.

One main feature of ATHLET - including all of its tools - is the portability to different computing platforms. Prior to a code release, a subset of the test cases described above is run on different platforms available at GRS at that time. Also the complete software environment is checked on those computers where it is intended to be applied.

ATHLET can also be used on computer platforms not available within GRS. If problems occur either during the implementation or during the application of the code package, support is provided by the developer team. Exploiting the experiences of the external users, the ATHLET programs are either improved to run on the new platforms (e.g. through the introduction of compiler directives in the source code), or the implementation guidelines are supplemented by related hints to support the users for future cases.

5 Selected Validation Calculations for Current Version

This chapter presents the analyses of the integral experiments included in the basis validation matrix. These examples cover a wide range of thermal-hydraulic phenomena and give an insight into the actual performance of the current code version when applied to new challenging experimental findings.

At present, five assessment calculations are included in this chapter:

- LSTF Run SB-CL-18
- ROSA III - Run 916
- LOFT LP-LB-1
- ISB Test SSP-2
- ROCOM Test 2.1

The test facilities cover a scaling range from 1:3000 up to 1:50. The post-test calculations include the simulation of an ATWS transient, using the fast-running EIMMB option of the code, three small break calculations for three different reactor types (PWR, BWR and WWER), and a large break LOCA simulation. Both the 5-eq. and the 6-eq. model as well as the local and integrated mass and momentum balance method are applied. In some cases, models are applied even if the related physical process does not appear in the experiment or has no measurable effect on the results - provided the calculated results are not affected. With this, the applicability of these models and the plausibility of the results shall be proven.

Besides that, several code features are applied for these calculations, among others :

- one-dimensional modelling of the break region for the calculation of the critical discharge rates,
- mixture level tracking model,
- quench front propagation model,

- simulation of non-condensable gases.

A detailed list of the model options applied for the individual calculations is given in the corresponding chapters below.

All calculations were carried out on Intel ® Xeon ® CPU E5-2430 0 @ 2.20 GHz processors. The Intel Fortran compiler ifort version 16.0.4 was used. Please note that calculation results may vary depending on employed compiler, hardware architecture and operating system.

5.1 LSTF Run SB-CL-18

5.1.1 Test Facility

The LSTF (Large Scale Test Facility) is a 1/48 volumetrically scaled model of a Westinghouse-type 3423 MWt four loop PWR. The LSTF has the same major component elevations as the reference PWR to simulate the natural circulation phenomena, and large loop pipes (hot and cold legs of 207 mm in diameter) to simulate the two-phase flow regimes and phenomena of significance in an actual plant. The LSTF equipment can be controlled in the same way as that of the reference PWR to simulate long term operational transients. Furthermore, the LSTF is designed to be operated at the same high pressures and temperatures as the reference PWR.

Figure 5 - 1 and table 5 - 1 show the structure and major dimensions of the LSTF, respectively. The four primary loops of the reference PWR are represented by two equal-volume loops. A detailed LSTF system description is presented in Ref. /JAE85/.

The hot and cold legs are sized to conserve the volume scaling and the ratio of the length to the square root of pipe diameter $L/D^{0.5}$ for the reference PWR in expectation that the flow regime transitions in the primary loops can be simulated appropriately by taking this scaling approach.

Over 2500 instruments are available for making various types of measurements in LSTF. Most numerous (about 70%) are the thermocouples that measure the fluid (TE) and wall (TW) temperatures and temperature differences (DT). There are also about 400 conduction probes (CP) distributed throughout the primary and secondary systems which indicate the presence or absence of liquid or vapor. Other conventional instruments include among others pressure (PE) and differential pressure (DP) transducers, liquid level meters (LE) based on differential pressure measurements, and flow meters (FE) using an orifice, venturi or nozzle. Advanced two-phase flow instruments include drag discs (MF) and three-beam gamma densitometers (DE) for measurement of momentum flux and fluid density, respectively.

Table 5 - 1: Major design characteristics of LSTF and PWR

			LSTF	PWR	PWR/LSTF
Pressure		(MPa)	16	16	1
Temperature		(K)	598	598	1
No. of fuel rods			1064	50952	48
Core height		(m)	3.66	3.66	1
Fluid volume V		(m^3)	7.23	347	48
Core power P		(MW)	10	3423(t)	342
P/V		(MW/m^3)	1.4	9.9	7.1
Core inlet flow		(t/s)	0.0488	16.7	342
Downcomer gap		(m)	0.053	0.260	4.91
Hot leg	D	(m)	0.207	0.737	3.56
	L	(m)	3.69	6.99	1.89
	$L \cdot D^{-0.5}$	($m^{-0.5}$)	8.15	8.15	1.0
	$A \cdot L$	(m^3)	0.124	2.98	24.0
No. of loops			2	4	2
No. of tubes in steam generator			141	3382	24
Length of steam generator tube (average) (m)			20.2	20.2	1.0

5.1.2 Test Conditions and Procedure

The major initial conditions of the LSTF 5% cold leg break test, Run SB-CL-18, and a detailed description can be found in /JAE89/. Both the initial steady state conditions and the test procedures were designed to minimize the effects of LSTF scaling compromises on the transients during the test.

The most important design scaling compromise is the 10 MW maximum core power limitation, 14% of the scaled reference PWR rated power. The steady-state condition is restricted to a core mass flow rate that is 14% of the scaled value, to simulate the reference PWR temperature distribution in the primary loop. The desired primary coolant flow rate was established by reducing the pump speed with the flow control valves in the cross-over legs fully open. The primary loop flow rate was then increased at the time of break to improve the similarity of the LSTF to the reference PWR by increasing the pump speed.

The primary-to-secondary heat transfer must also be maintained at 10 MW, i.e., 14% of the scaled value. Since the LSTF steam generators are geometrically scaled to the reference PWR, the 14% primary-to-secondary heat transfer rate is established by raising the secondary temperature such that the primary pressure and temperature are representative of the reference PWR.

Major operational set points and conditions including emergency core cooling system (ECCS) actuation logic for this test are shown in /RIN90/.

After the break occurred at time zero, the primary system depressurizes quickly. At a pressurizer pressure of 12.97 MPa, the reactor scrams. Loss of offsite power concurrent with the reactor scram is assumed and the primary coolant pumps are tripped to begin coastdown and the core power begins to decrease along the pre-programmed decay curve. The power decay curve used in the test takes into account the actinides and delayed neutron effects and gives a slower decrease than the ANS standard. The SG auxiliary feedwater is assumed to fail to simplify the transient.

At a pressurizer pressure of 12.27 MPa, the safety injection signal is sent that trips ECCS to be actuated at respective pressure set points. However, the high pressure charging system and the high pressure injection system are assumed to fail in the test. The accumulator system and the low pressure injection system (LPIS) are specified to initiate coolant injection into the primary system at pressures of 4.51 and 1.29 MPa, respectively. The accumulator-cold system injects into the cold leg A and the accumulator-hot system into the cold leg B. The water temperatures of ACC-cold and ACC-hot tanks are the same and the ratio of accumulator injection flow rate into cold leg A and into cold leg B is 3:1. This injection method is adopted for good simulation of ECC injection flow rate to each cold leg in the LSTF.

The break point is located in the loop B cold leg (loop without the pressurizer) between the reactor coolant pump and the reactor pressure vessel. The break orientation is horizontal.

5.1.3 Experimental Results

The chronology of events for Run SB-CL-18 is shown in table 5 - 2. The experiment was initiated by opening the break valve at time zero. At that time, the speed of the main coolant pumps was increased to establish a primary coolant flow similar to the scaled value. The reactor scram signal was sent at a pressurizer pressure of 12.97 MPa, 9 s after break, and this signal closed the turbine throttle valve. The turbine bypass system was inactive due to the assumption of loss-of-offsite power occurring concurrently with scram. The loss of offsite power terminated the

main feed water, and also tripped the reactor coolant pumps to initiate coastdown. The reactor coolant pumps completely stopped at about 265 s after break.

The safety injection signal was sent at a pressurizer pressure of 12.27 MPa, 12 s after break. However, the high pressure charging and high pressure safety injection systems were not activated because of the failure assumptions. The secondary pressure increased after the closure of the turbine throttle valve, but was maintained at approximately 8 MPa due to the SG relief valve operation.

The core was temporarily uncovered between about 120 s and 155 s after break, and the heater rods in most of the core experienced superheating of up to about 190 K. This temporary core uncovery occurred during water accumulation in the loop seals. The core liquid level was depressed concurrently with the level drop in the cross-over leg downflow sides. The core level drop was amplified by the manometric effect caused by an asymmetric coolant holdup in the SG upflow and downflow sides. At about 140 s after the break, loop seal clearing occurred in both loops and the core liquid level recovered rapidly. After the loop seals cleared, the break flow changed from low quality to high quality two-phase flow, and the depressurization of the primary loop was accelerated. By about 180 s after the break, the primary loop pressure decreased below the SG secondary side pressure. Thereafter, the steam generators no longer served as heat sinks and the energy removal from the primary system was through the discharge of coolant from the break. It is noted that the loop seal clearing occurred before the reversal in primary and secondary pressures.

The core was uncovered again after about 420 s due to vessel inventory boil-off, and the heater rods in the upper part of the core showed superheating of up to about 80 K. Due to depressurization of the primary system, the accumulators were automatically actuated at 455 s to fill the system with the ECC water. The core was covered with two-phase mixture again after about 540 s by the ECC water injection.

The maximum peak cladding temperature in the test was approximately 740 K, observed during the temporary core uncovery just before the loop seal clearing.

Table 5 - 2: Chronology of events for Run SB-CL-18

Event	Time (s)
Break	0
Reactor trip	9
Safety Injection Signal	12
Main Steam Line Valve Close	14
SG Feedwater stop	16
High Pressure Charging Injection	-
High Pressure Safety Injection	-
Auxiliary Feedwater ON	-
First Core Uncovery	120 - 155
Loop Seal Clearing (Loop A/B)	140
Primary/Secondary Pressure Reversal	180
Reactor Coolant Pumps (PC-A/B) stop	265
Second Core Uncovery	420 - 540
Accumulator Injection ON	455

5.1.4 Input Dataset

5.1.4.1 Nodalization

The figures 5 - 2 and 5 - 3 show the nodalization used for the ATHLET analysis of the LSTF SB-CL-18 test /RIN90/. Except for the fuel rods, the heat conduction volumes for the simulation of the facility structures are not included in these figures. The nodalization includes the following numbers of network elements:

CVs for primary system:	179
CVs for secondary system	26
CVs for emergency cooling system	12
Junctions in total	261
ODEs for thermo-fluiddynamic	1393
Heat conduction volumes	261
ODEs for heat conduction	999

Thermo-fluid objects

The following aspects were considered for the choice of nodalization of the fluid system /RIN90/:

- Core
  The simulation of the partial dryout required a fine axial division of the core. The level of division is matched to the the axial core power distribution. A one channel modelling of the core turned out to be not sufficient. The used two channel representation enables the simulation of the inhomogeneous fluid conditions in the core in a realistic way. One channel includes the high and middle powered bundle (PV-CORI). The low powered bundles are combined in the cold outer channel (PV-CORO). An exchange between these channels is considered via a cross connection object (PV-CORE-CC).

- Core bypasses
  In the LSTF facility, three core bypasses exist which promote the pressure balancing between the upper plenum and the downcomer:

  a) Upper head bypass
     This bypass carries nominally 0.3% of the core mass flow via 8 spray nozzles and the control rod tubes (TFOs PV-DC-A-4, -B-4 and PV-BYP-UHI, -UHO).

  b) Upper downcomer - upper plenum bypass
     This bypass has no matching part in the Westinghouse reactor. It is an undesired leakage of the LSTF facility. The flow area is unknown. It depends on the thermal and mechanical load of the vessel. From JAERI specification, a bypass mass flow of 0.085% of the nominal core mass flow is used here for the calculations (TFOs PV-BYP-DCA and -DCB).

  c) Downcomer - hot leg bypass
     This bypass carries nominally 0.1% of the core mass flow and simulates the reactor bypass at the break through of the hot leg through the downcomer (TFOs PV-BYP-HLA and -HLB).

- Downcomer
  To consider the asymmetric cold leg ECC injection and the influence of the break location, the downcomer is split into two parallel channels (PV-DC-A-x and -B-x) interconnected via the TFOs PV-DC-CC-x.

- Circuits
  The bends in the circuit are flow limiting cross-sections. Correct modelling of the counter current flow limitation requires a detailed nodalization of the elbow in the hot leg and in the pump seal. The flow channel in the main coolant pump is modelled in a sophisticated man-

ner in order to simulate the overflow baffle of the pump case. This baffle enables the swell of emergency cooling water at the cold side of the leg.

- U-tube steam generator
  A difference in the behavior of the long and the short U-tubes is observed in the experiment. The U-tubes are modelled by two channels accounting the results from the experiment. The SG inlet and outlet plena are nodalized considering the strong differences in the cross sections. The cross sections in the main coolant pipes, the SG plena, and the U-tube bundles are related like 1.0 : 6.1 : 4.6. The SG plena represent a strong cross section increase and a distinctive phase separation can be expected. A splitting of the SG plena into 4 parts is used to get a realistic mass distribution.

- Upper downcomer - upper plenum
  A fine nodalization is applied for the realistic modelling of the bypass in this part.

- ECC piping
  The fluid temperatures in the ECC injection nozzles indicate that, before the ECC injection started, the ECC water in the injection lines was considerably warmer than the accumulator water. Therefore, the injection lines are sub-divided into 5 CVs and a linear initial temperature profile is specified to approach the measured temperature time history.

Heat conduction objects

- Heater rods
  The radial power distribution of the heater rods is represented by three different groups of heater rods:

360 rods	14118 W	radial peaking factor 1.51
180 rods	9350 W	radial peaking factor 1.00
524 rods	6171 W	radial peaking factor 0.66

  These heater rods are distributed to the two core channels according to the radial power distribution in the core (HCOs HPV-CORI-x and HPV-CORO-x). Every heater rod HCO is sub-divided into 9 HCVs.

- Steam generator U-tubes
  The 151 U-tubes of one SG are sub-divided into two groups representing 57 long and 84 short U-tubes, each with 14 HCVs and 12 HCVs, resp.

- Structures
  The major wall and internal structures of the reactor vessel, coolant pipes, pressurizer, and the steam generators are represented by HCOs, considering the heat losses to the environment.

5.1.4.2 Model Options

Following model options are applied:

- For the primary side of the test facility, the 6 eq. model is applied with the exception of the pressurizer and the break, where the 5 eq. model is chosen. The secondary side is completely simulated with the 5 eq. model.
- The T-junction model is applied to the entrance section of the break pipe. The critical discharge mass flow is calculated with the CDR1D model.
- The T-junction model is also applied at both ends of the pressurizer surge line to simulate the vapor pull-through when the mixture level reaches the surge line nozzle, as well as the vapor flow and liquid entrainment in case of a pressurizer in-surge.
- The multi-component model is used for the simulation of the nitrogen cushion in the accumulator.
- The condensation rates are calculated with the ATHLET direct condensation model.
- Evaporation and condensation at heating and cooling surfaces are considered.

5.1.5 Results of the ATHLET Calculation

The figures 5 - 4 to 5 - 49 compare ATHLET results with the corresponding experimentally measured parameters for a variety of physical quantities, proving the quality of the ATHLET simulation. In the figures, 'A:' denotes the ATHLET result, generally followed by the thermo-fluid or heat conduction object name and the index of the network element inside. 'E:' denotes the experimental result followed by the designation of the measurement which is a combination of a two-letter prefix indicating the type of measurement and a number unique to each instrument location. Detailed information on the measurements and instrumentation system can be found in /JAE89a/.

The calculated primary side pressure (fig. 5 - 4) agrees very well with the experiment with two exceptions. In the early phase of the depressurization (20 to 60 s), the pressure drops too far for two reasons: The core is represented only by one inner and one outer channel. Since there is no hot channel simulation, the beginning of evaporation in the core is calculated late. The second reason is the over-prediction of the heat flow to the secondary side in that time period, which can be derived from the too fast increase of the pressure on the secondary sides of the steam generators (figs. 5 - 5 and 5 - 6) after the closure of the main steam valves. Also during the late phase of the accumulator injection, the pressure drops too far caused by the overes-

timation of the steam condensation on the cold ECC water. The pressures on the steam generators secondary side are governed by the three times opening of the steam generator relief valves, and after that by the heat flow to the primary side.

The loop mass flows were measured only in the two loop seals (figs. 5 - 7 and 5 - 8). As already mentioned, the pump speed was temporarily increased immediately after break initiation to establish the scaled nominal loop mass flow. Due to the assumption of loss of offsite power the pumps were tripped and coasted down. The increase of the loop mass flows at about 150 s is caused by the clearance of the pump seals. After that, two phase flow occurs at the measurement position which could not been exactly measured by the venturi meters.

Due to the overprediction of the steam condensation at the cold ECC water, the accumulator injection is terminated later than in the experiment (figs. 5 - 9, 5 - 10, 5 - 12, and 5 - 13) and too much liquid is injected.

The break mass flows are compared in fig. 5 - 11. The experimental data are derived from the level increase in the leakage catch tank. Unfortunately, it is not accurate enough to verify the calculated break mass flow. For example, the density measurement upstream the break orifice (fig. 5 - 18) indicates entrained liquid between 550 s and 650 s. This should lead to an increase of the leak mass flow, which is actually not measured, and not calculated, too. The break is located behind a bend at its outside (see arrow in fig. 5 - 1). It can be expected that the centrifugal force of the stratified liquid flow from the accumulator injection point towards the reactor vessel leads to an increased liquid fraction upstream the break and consequently to an increased leak flow. Parameter studies performed varying the leak mass flow (e.g. with a lowered elevation of the break nozzle), showed that the two periods of core uncovery sensitively depend on the leak flow.

The figs. 5 - 14 to 5 - 18 compare the densities in both the hot and cold legs of the two loops, as well as upstream the break orifice. The calculation matches very well the measurement, with the exception of the liquid entrainment at the break nozzle, which is clearly underestimated by ATHLET.

After the main coolant pump coastdown, the differential pressures of figs. 5 - 19 to 5 - 34 are determined by the liquid distribution in the test facility, since there are only low fluid velocities in the primary system. In general, the agreement of the calculation with the experiment is good, in some locations even excellent. For example, the two periods of core uncovery (around 140 s and 550 s, fig. 5 - 19) are described well by ATHLET. Also the time point of pump seal clearance is calculated well (figs. 5 - 28 and 5 - 34). On the other hand, the liquid inventories in the downcomer and especially in the steam generator inlet plena are clearly overestimated after 650 s, due to the too long time period of accumulator injection already mentioned.

In fig. 5 - 35 the measured fluid temperature in the upper head is compared with the ATHLET result calculated above the mixture level (which is initiated at ca. 20 s). After ca. 400 s, the steam becomes superheated due to the heat flow from the hot structures, which is satisfactorily reflected by the calculation. A similar behavior can be observed in the upper downcomer (fig. 5 - 38), where the mixture level model is not applied. Therefore, too much liquid is entrained by ATHLET and the superheating is under-predicted. The calculated fluid temperature at the core entry (fig. 5 - 36) shows a significant subcooling after 650 s, probably caused by the too large accumulator injection. The measured temperatures in the ECC nozzles (figs. 5 - 43 and 5 - 44) indicate that the water in the ECC injection lines is initially clearly warmer than that in the accumulators. This is considered in the calculation by a relatively fine nodalization of the injection lines (5 CVs) and by the specification of an adequate initial temperature profile. Nevertheless, the fluid temperatures in the cold legs downstream the ECC injection points are calculated significantly too low (figs. 5 - 41 and 5 - 42).

The fuel rod temperatures show the core heat-up during two periods of core uncovery. The first core uncovery is caused by manometric forces due to the asymmetric liquid holdup in the steam generator U-tubes and in the pump seals, and it is terminated after pump seal clearing at about 140 s. The second core uncovery around 500 s which is observed only in the upper part of the core is caused by boil-off of the vessel inventory and terminated by the accumulator injection. In figs. 5 - 45 to 5 - 49, the cladding temperatures calculated for the hot rod of the inner core channel are compared with the minimum and maximum values measured at different levels. The calculated temperature excursions are within the measurement spread, but the maximum values are underestimated. Besides the general uncertainties concerning the liquid distribution during the transient, the further reasons are possibly deviations of the break mass flow as well as the too large accumulator injection. In addition, the representation of the hot bundle by a separate core channel could improve the calculated maximum cladding temperature.

Finally, the figs 5 - 50 to 5 - 52 document the performance of the ATHLET simulation concerning numerical effort and conservation of the coolant mass balance. No numerical problems appeared and the maximum mass error of ca. 4 kg is negligible compared to the initial primary side mass inventory of about 5500 kg (without accumulators).

Summarizing the comparison of the ATHLET calculation with the experimental results, it can be stated that, in general, the calculated parameters show a good, some of them even excellent agreement with the measurements. ATHLET is able to simulate all main phenomena appearing during that type of transient investigated by this LSTF experiment.

5.1.6 Figures

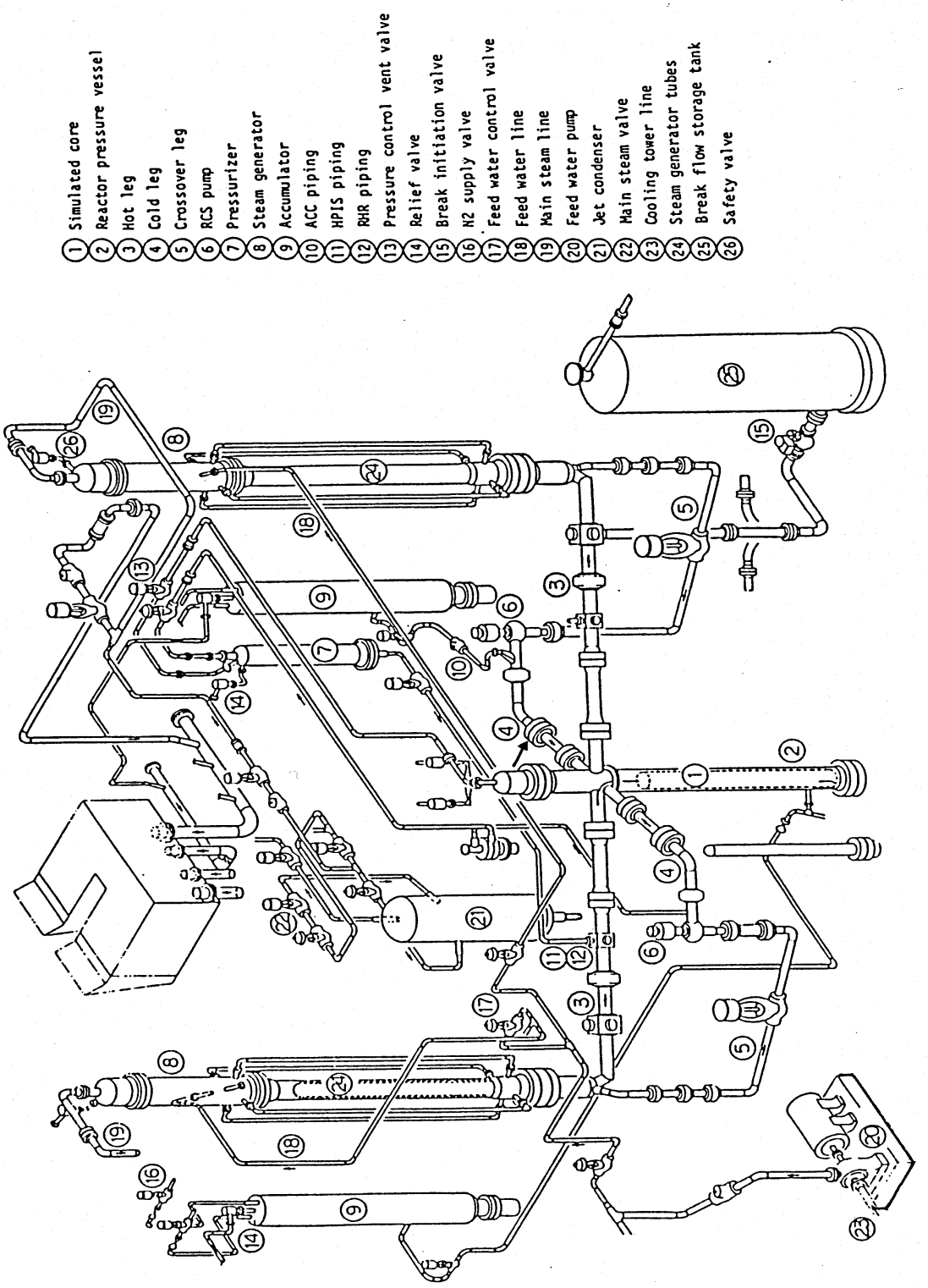

Fig. 5 - 1: General structure of LSTF

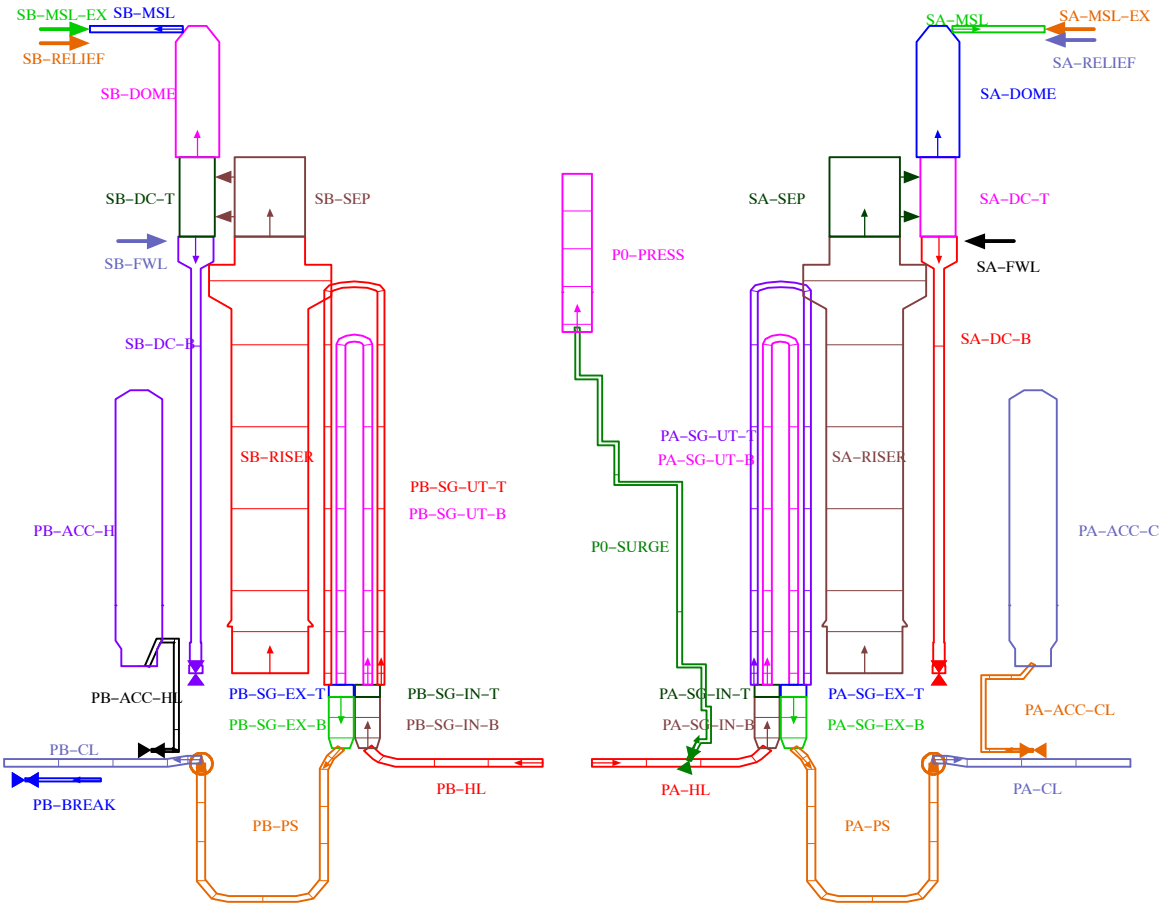

Fig. 5 - 2: LSTF: Nodalization of the loops

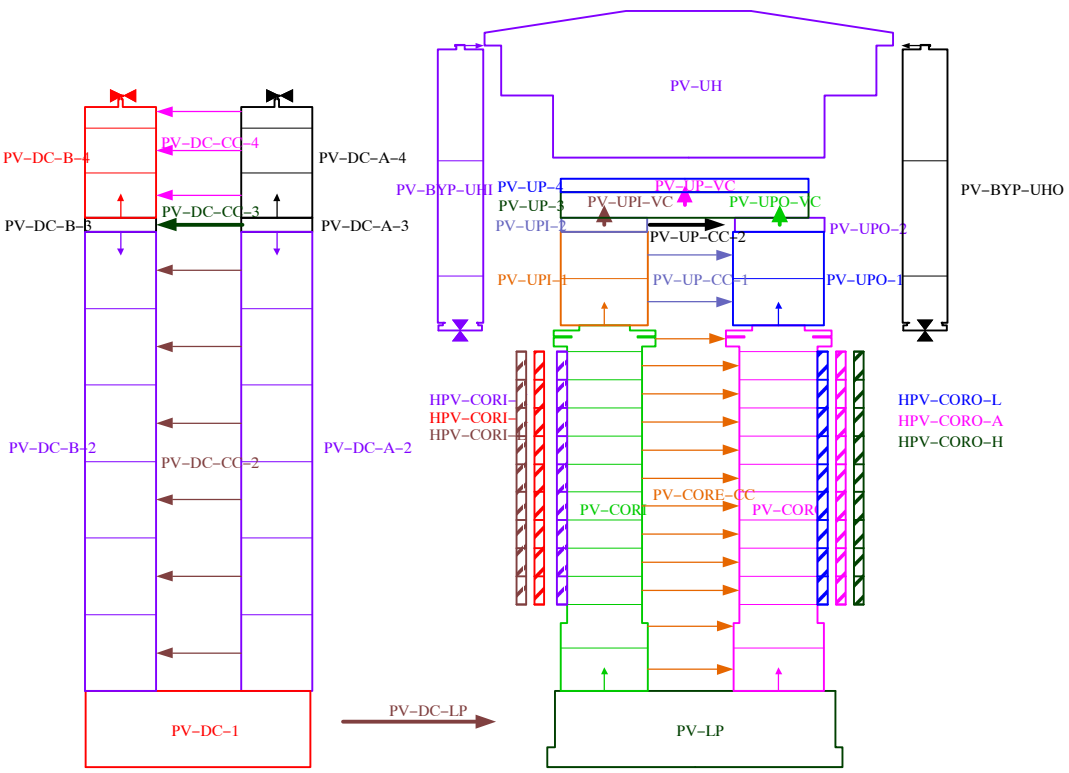

Fig. 5 - 3: LSTF: Nodalization of the pressure vessel

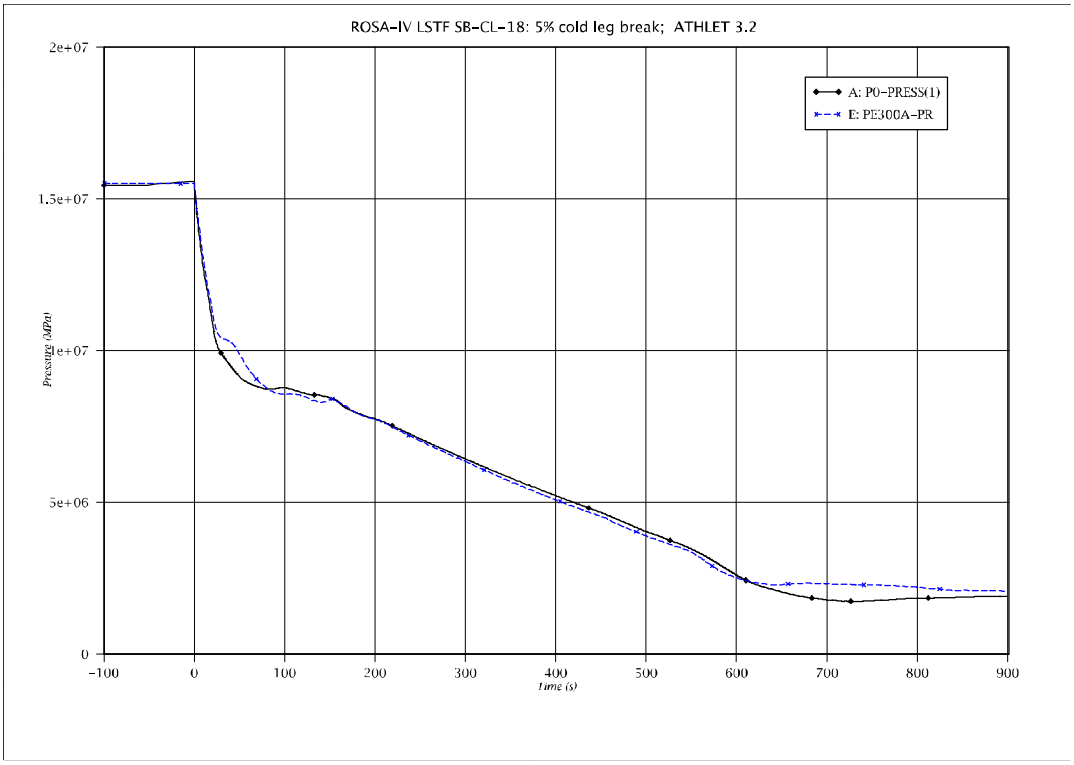

Fig. 5 - 4: Pressure in pressurizer

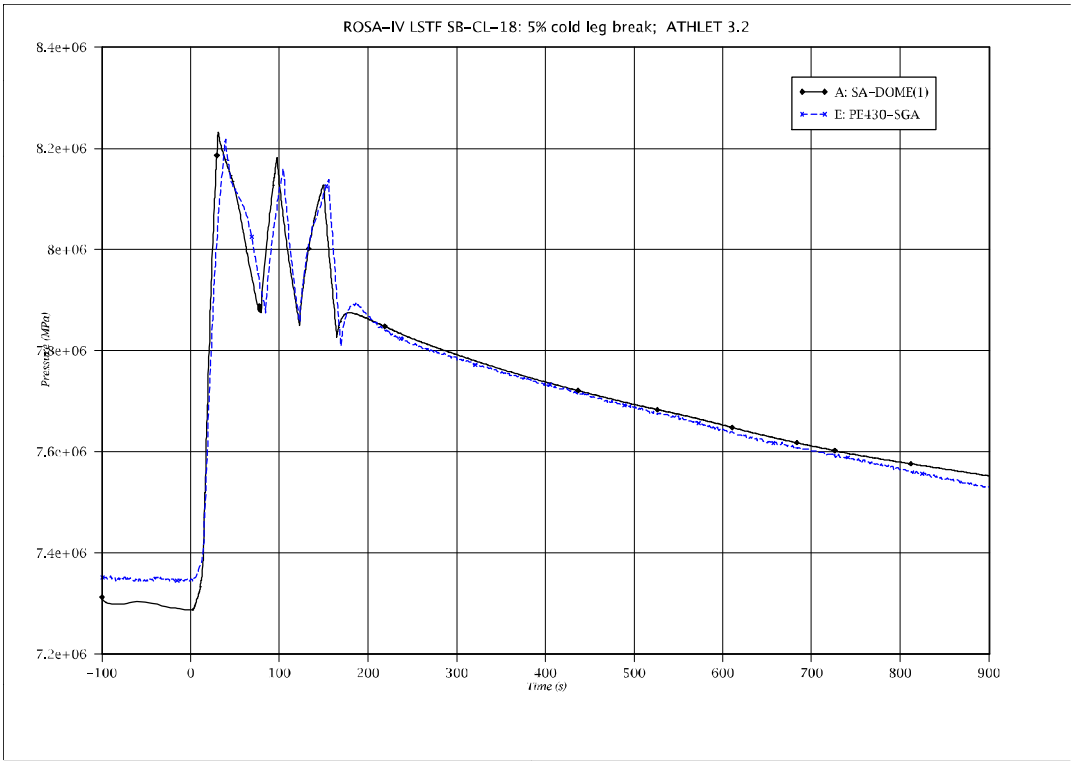

Fig. 5 - 5: Pressure in IL SG dome

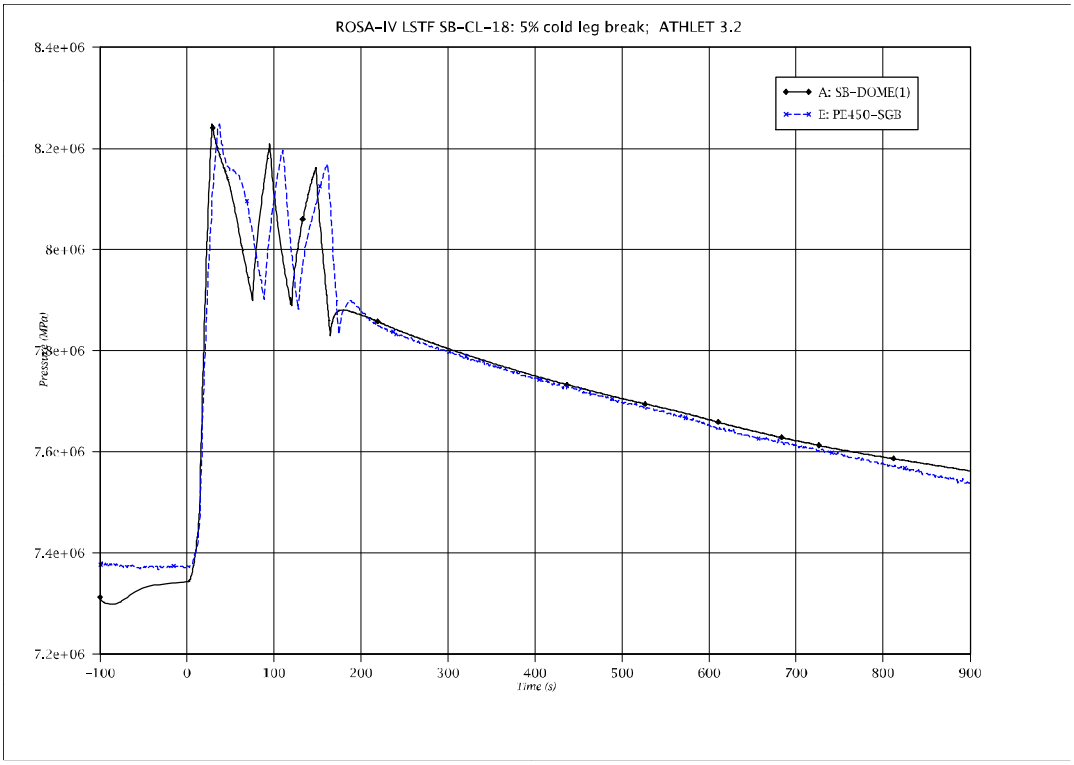

Fig. 5 - 6: Pressure in BL SG dome

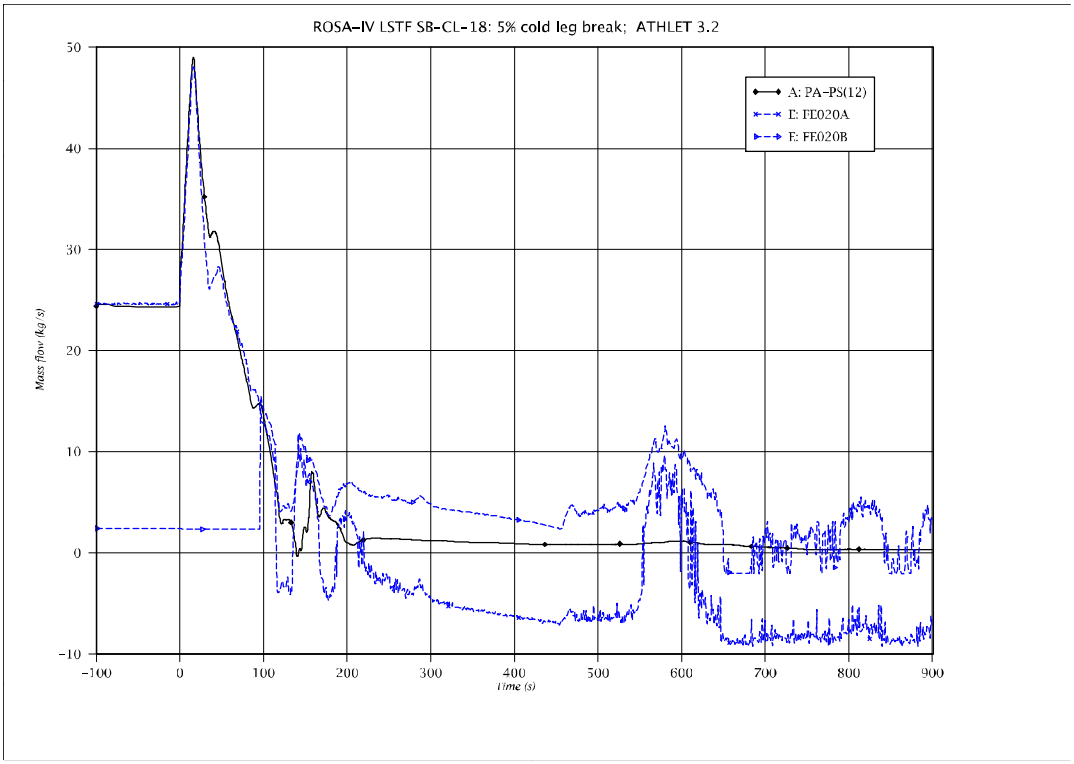

Fig. 5 - 7: Mass flow in loop seal of IL

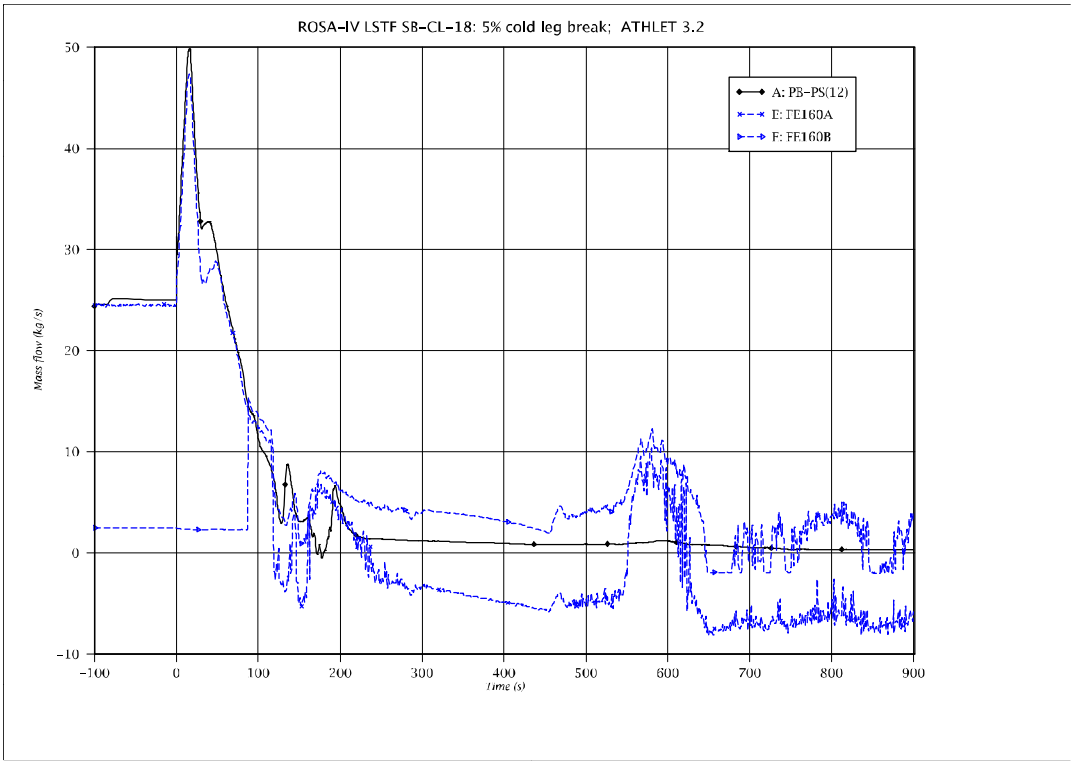

Fig. 5 - 8: Mass flow in loop seal of BL

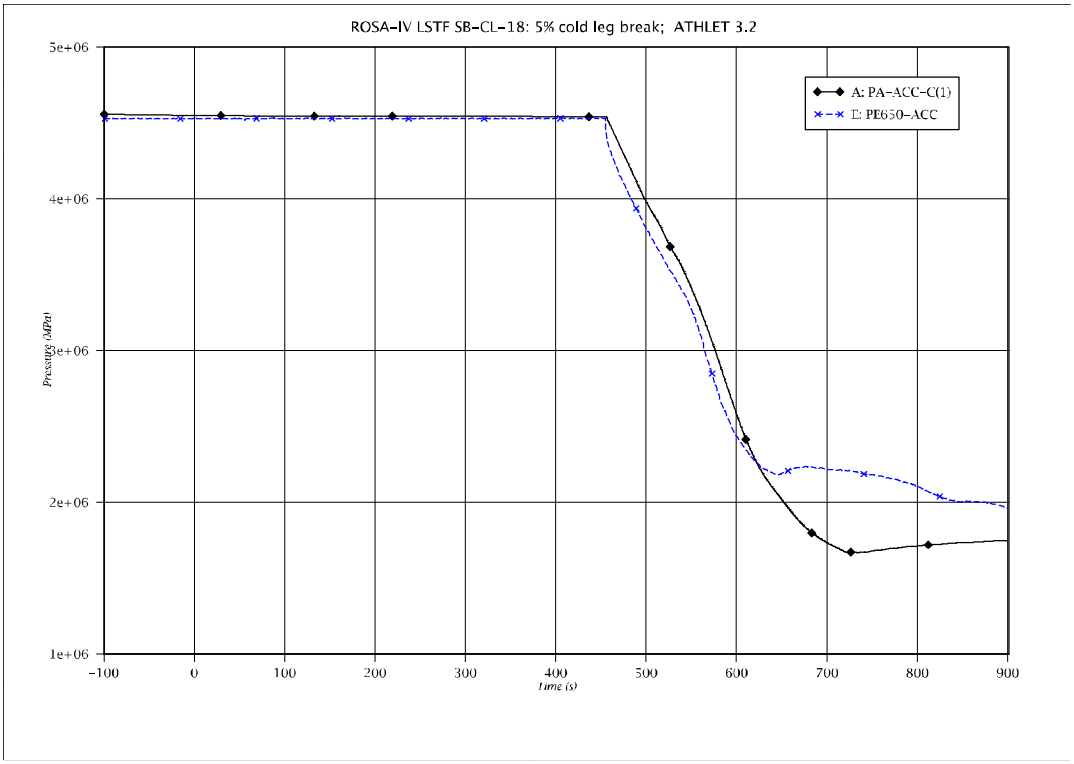

Fig. 5 - 9: Pressure in IL accumulator

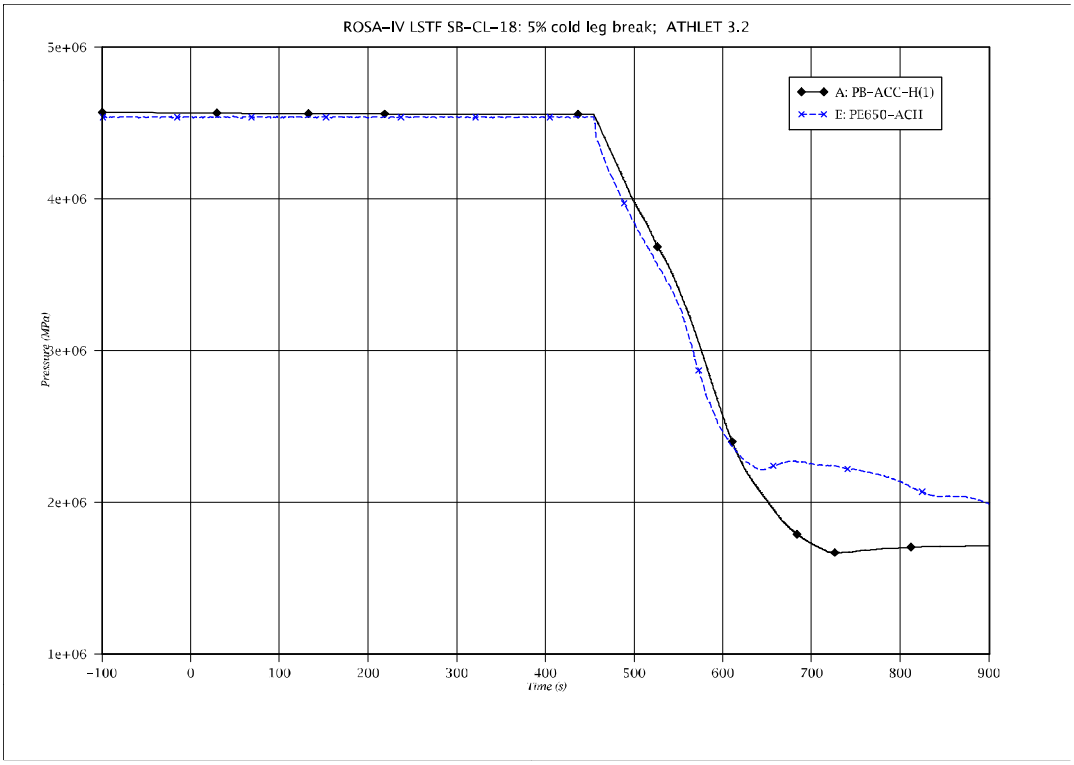

Fig. 5 - 10: Pressure in BL accumulator

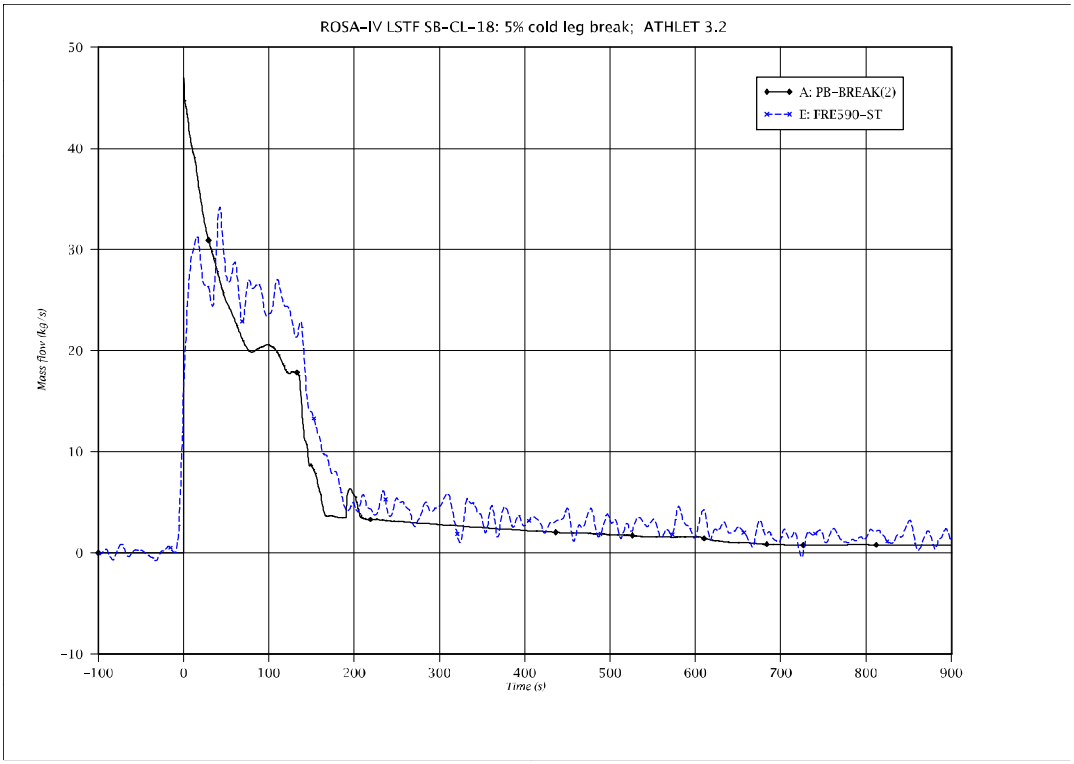

Fig. 5 - 11: Break mass flow

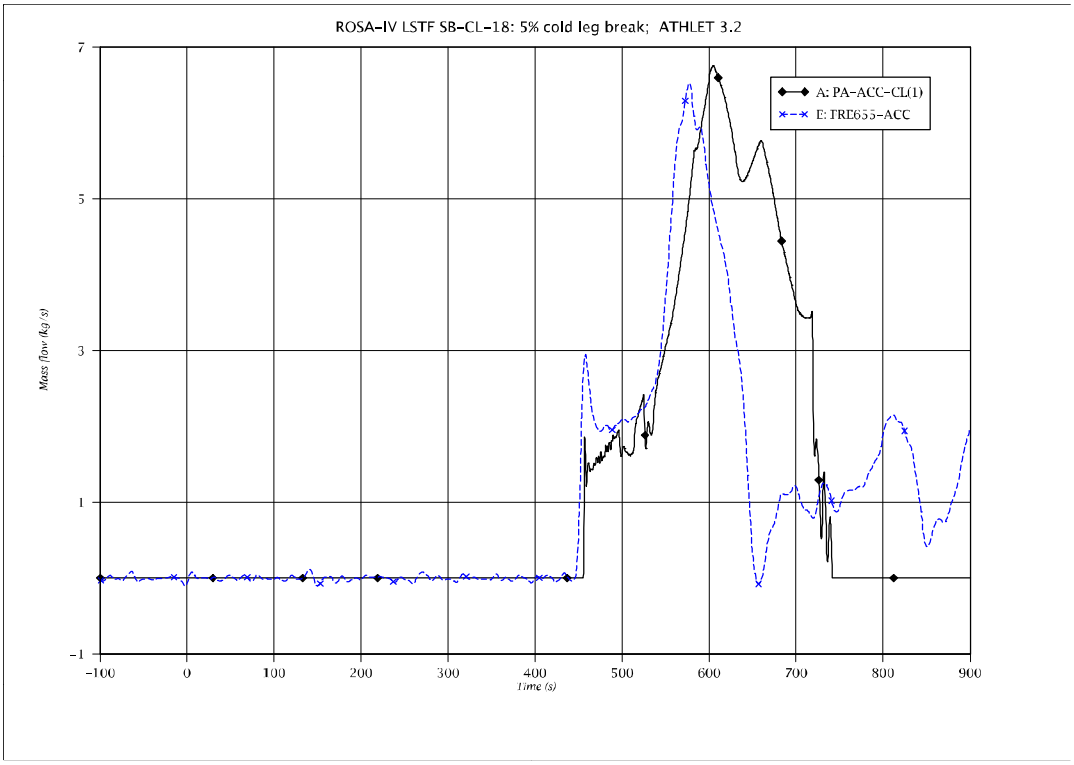

Fig. 5 - 12: Injection mass flow of IL accumulator

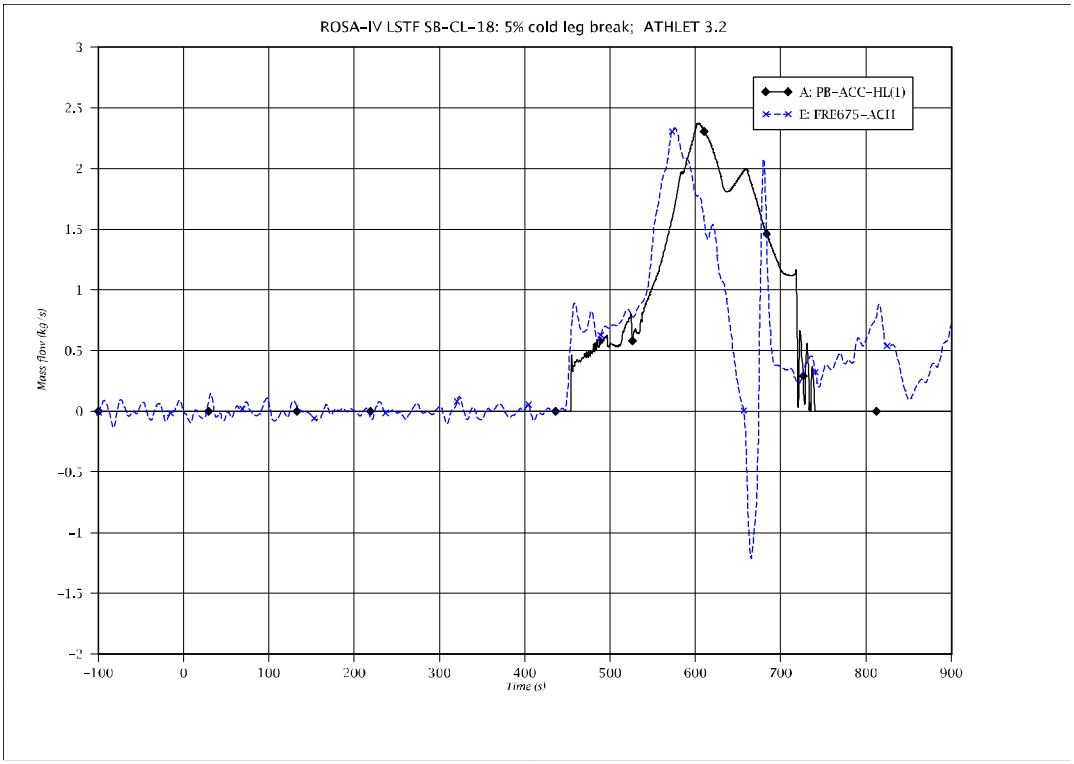

Fig. 5 - 13: Injection mass flow of BL accumulator

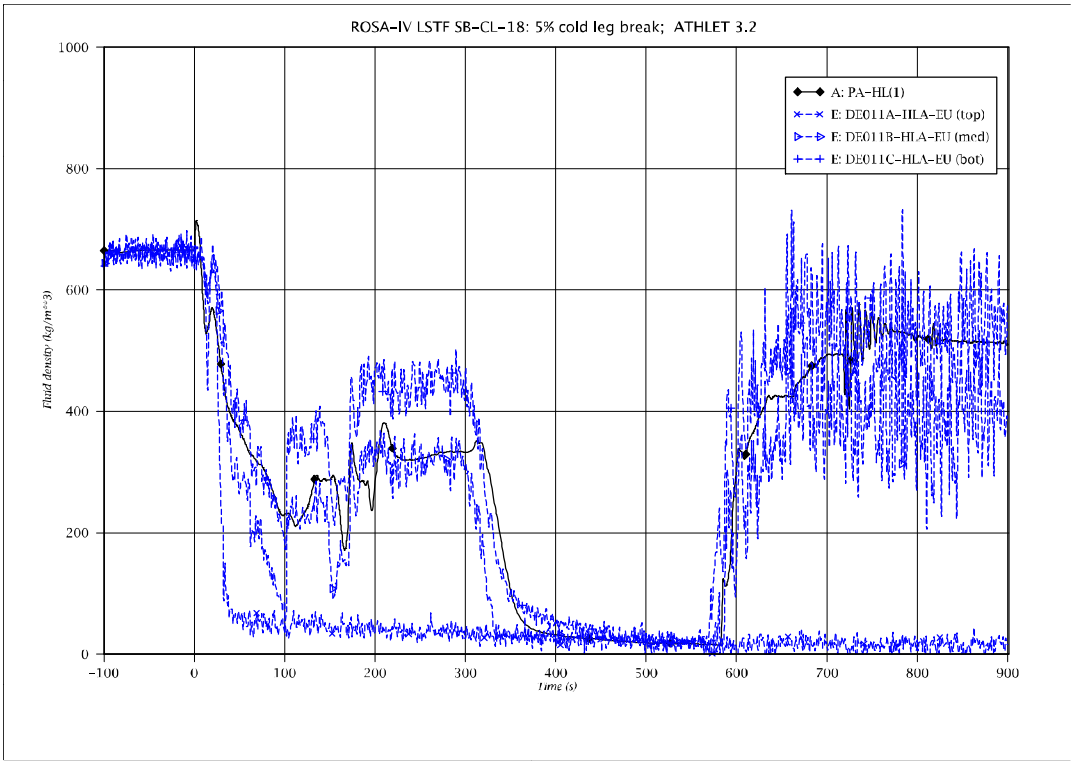

Fig. 5 - 14: Fluid density in IL hot leg

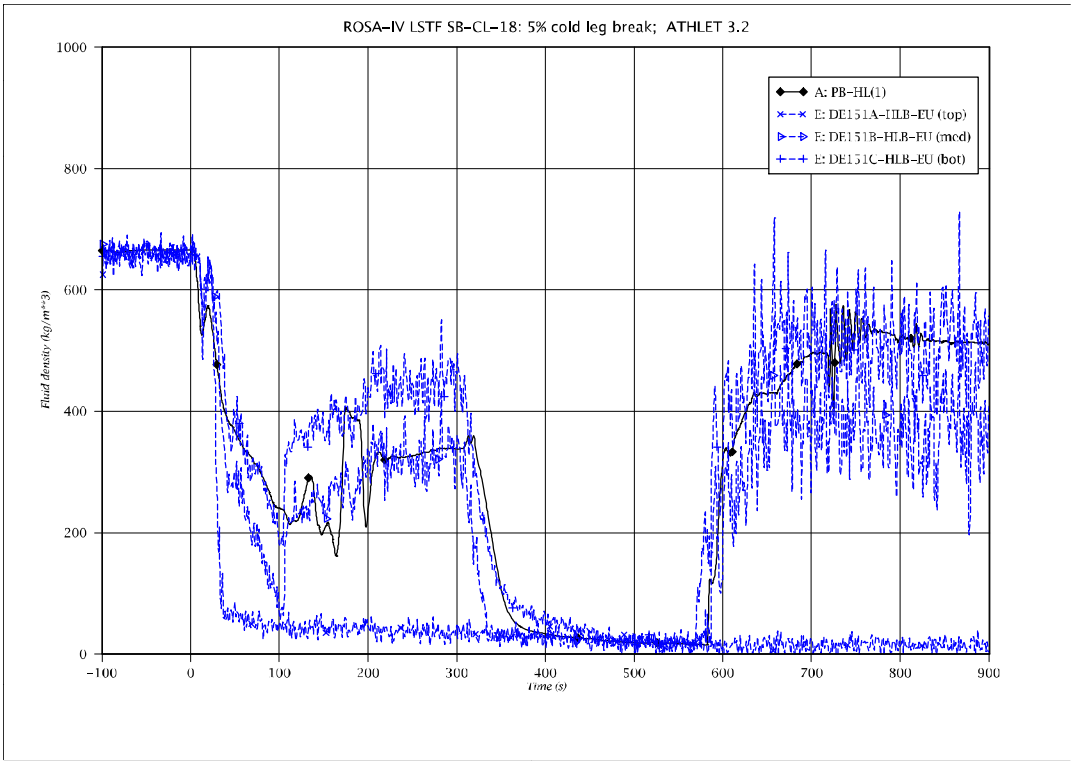

Fig. 5 - 15: Fluid density in BL hot leg

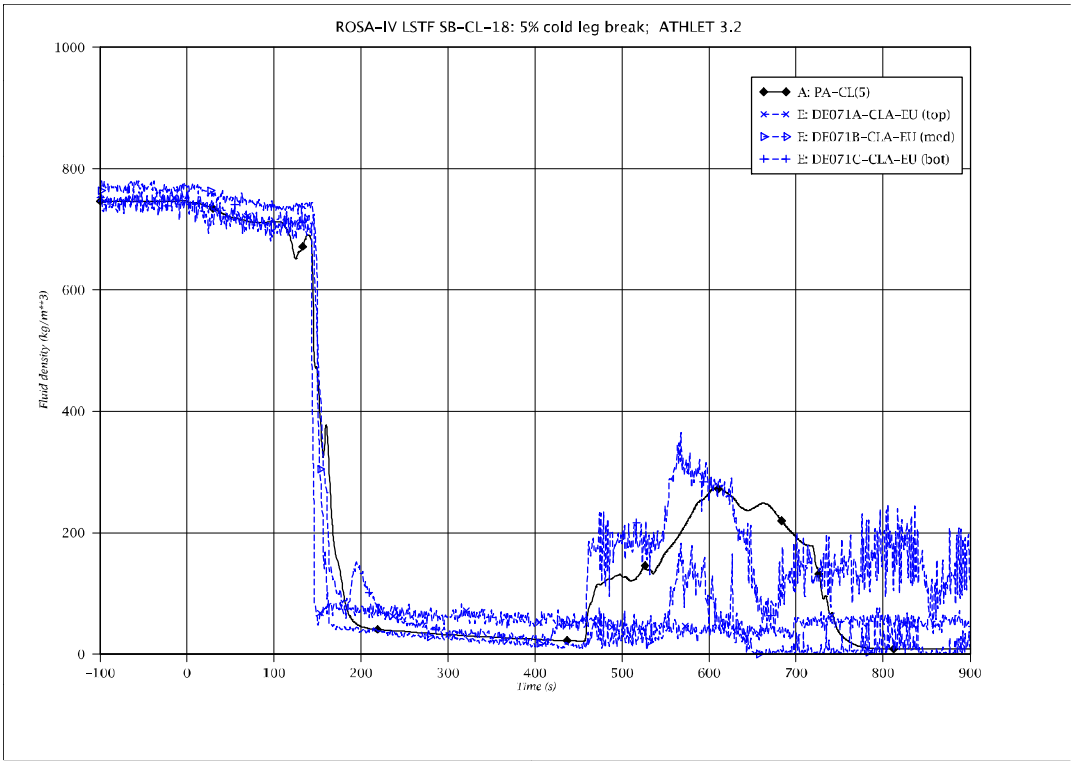

Fig. 5 - 16: Fluid density in IL cold leg

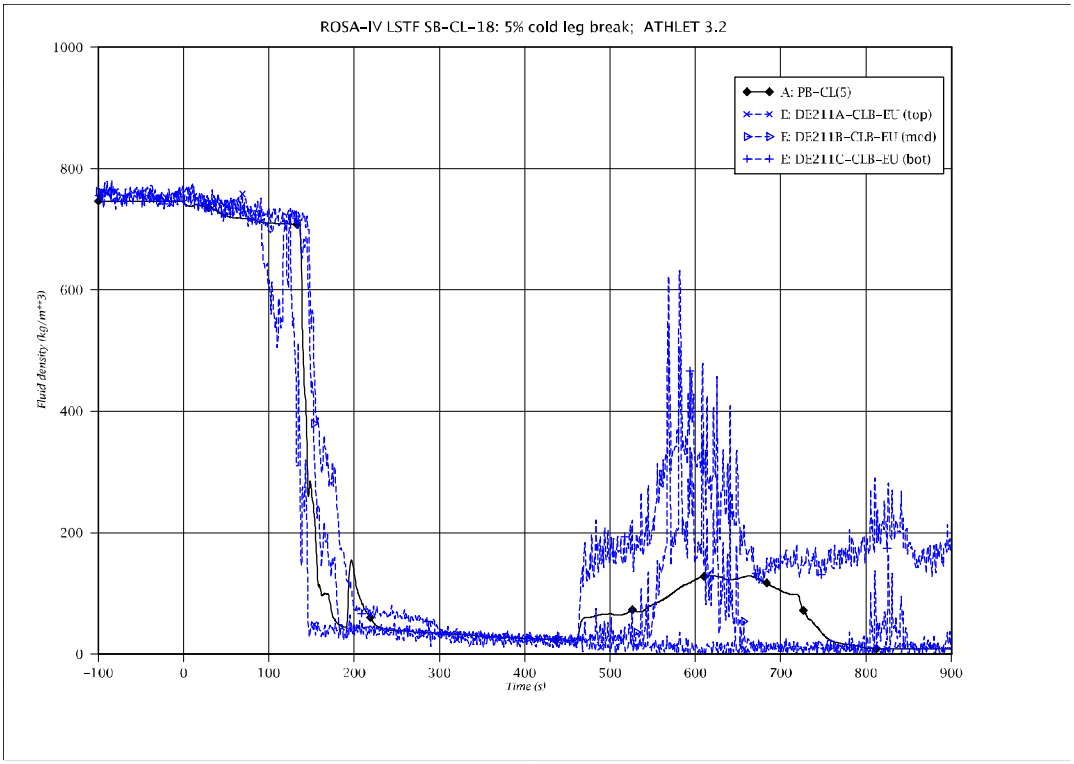

Fig. 5 - 17: Fluid density in BL cold leg

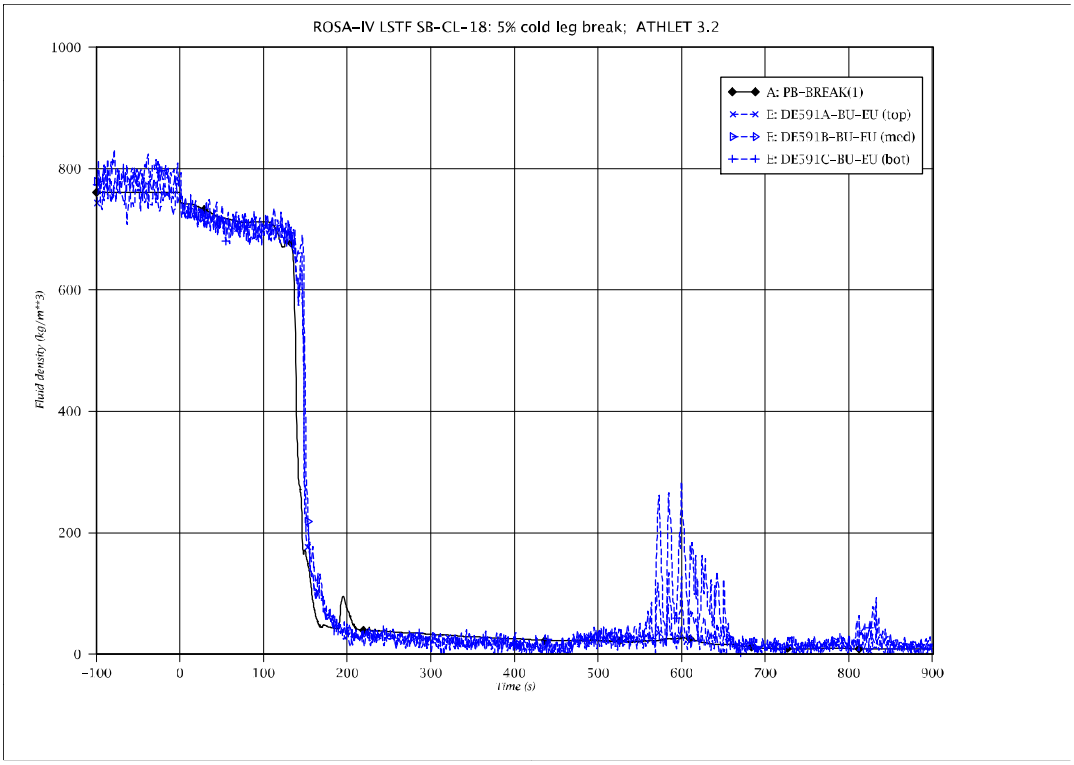

Fig. 5 - 18: Fluid density upstream break orifice

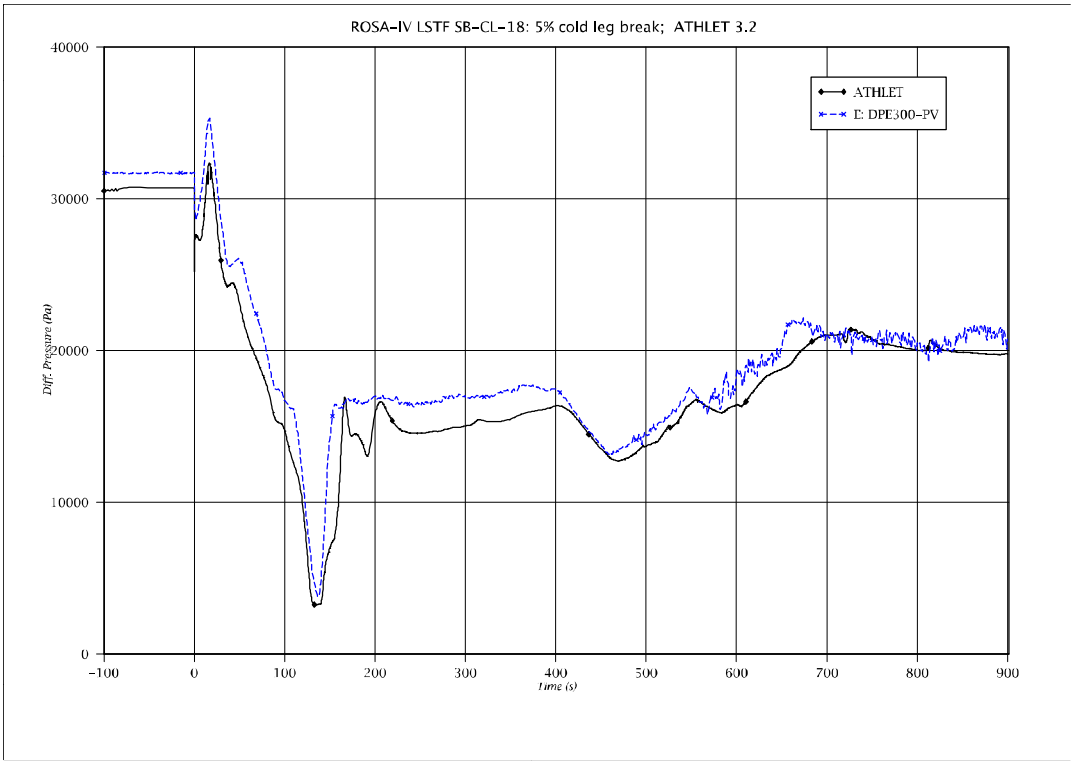

Fig. 5 - 19: Differential pressure across core (outer channel)

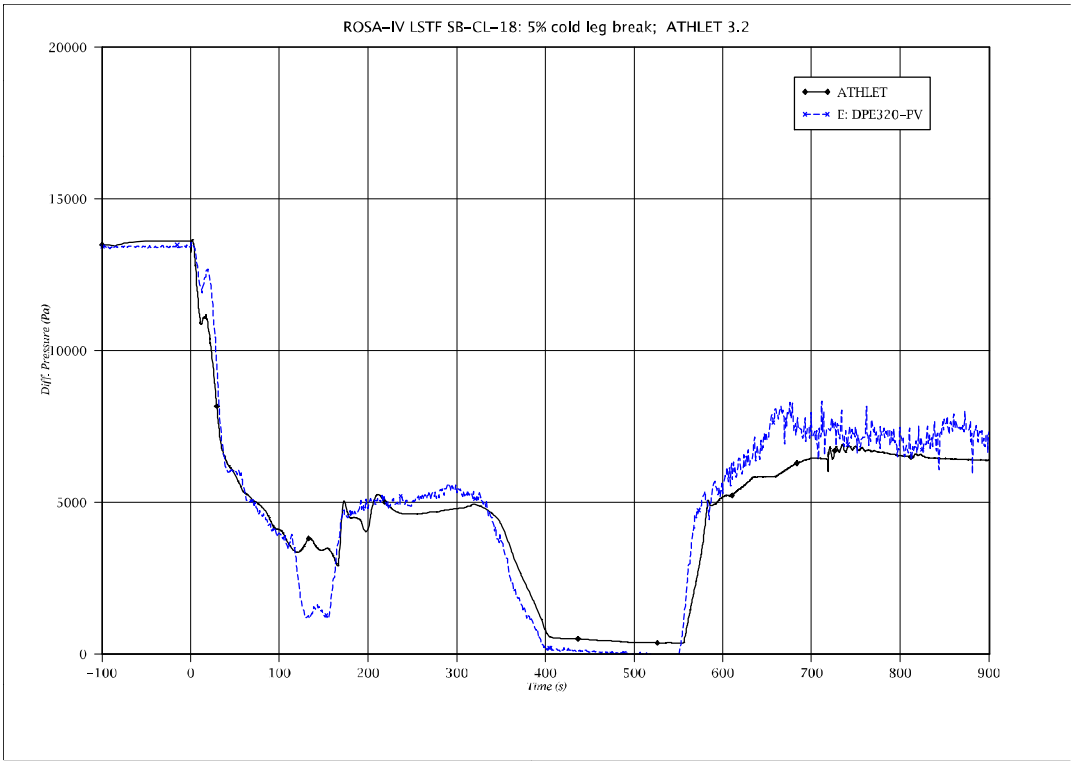

Fig. 5 - 20: Differential pressure across upper plenum

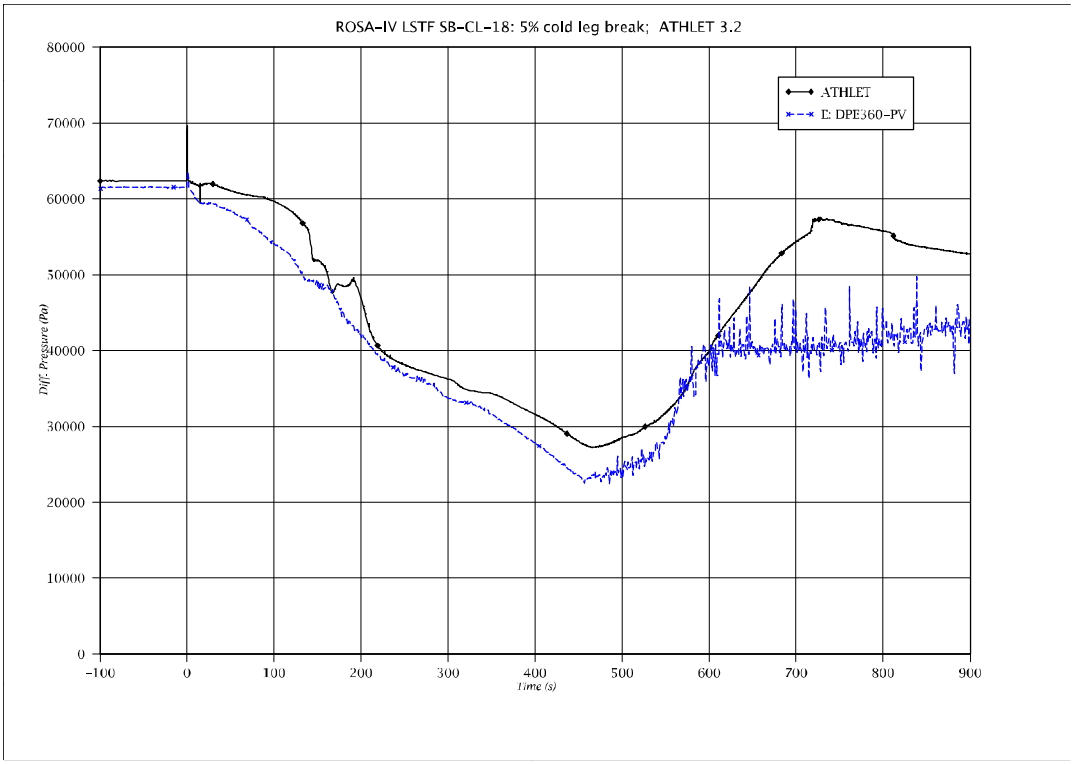

Fig. 5 - 21: Differential pressure across downcomer

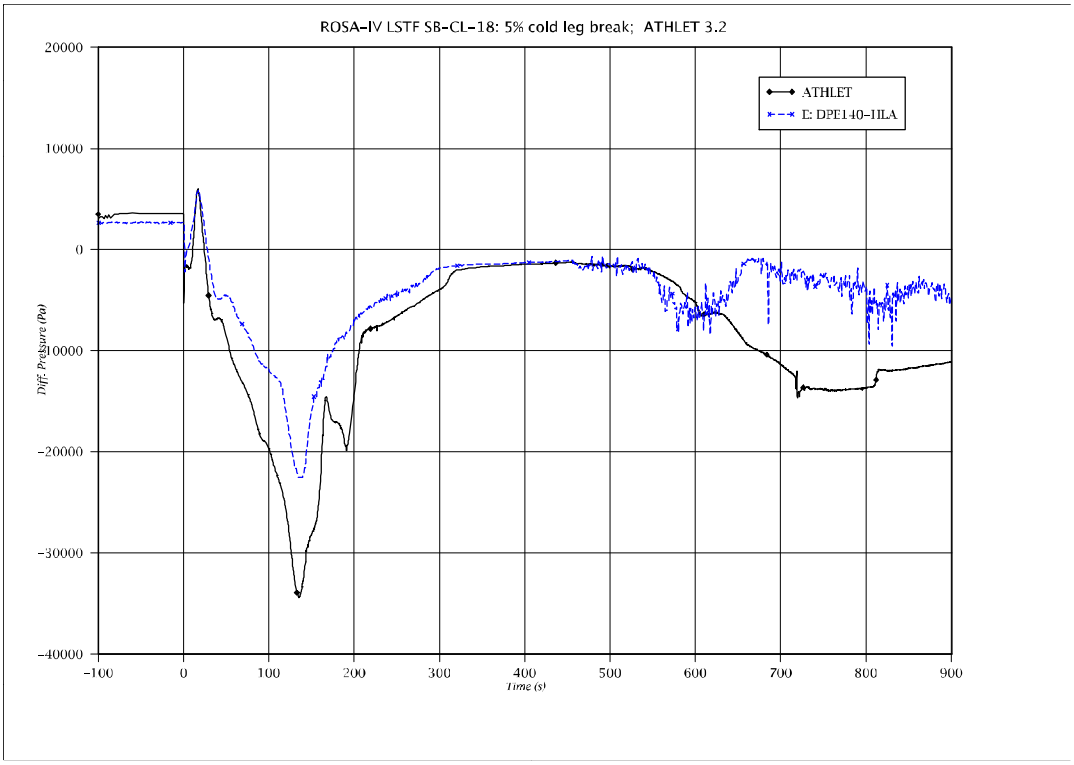

Fig. 5 - 22: Differential pressure downcomer - upper plenum

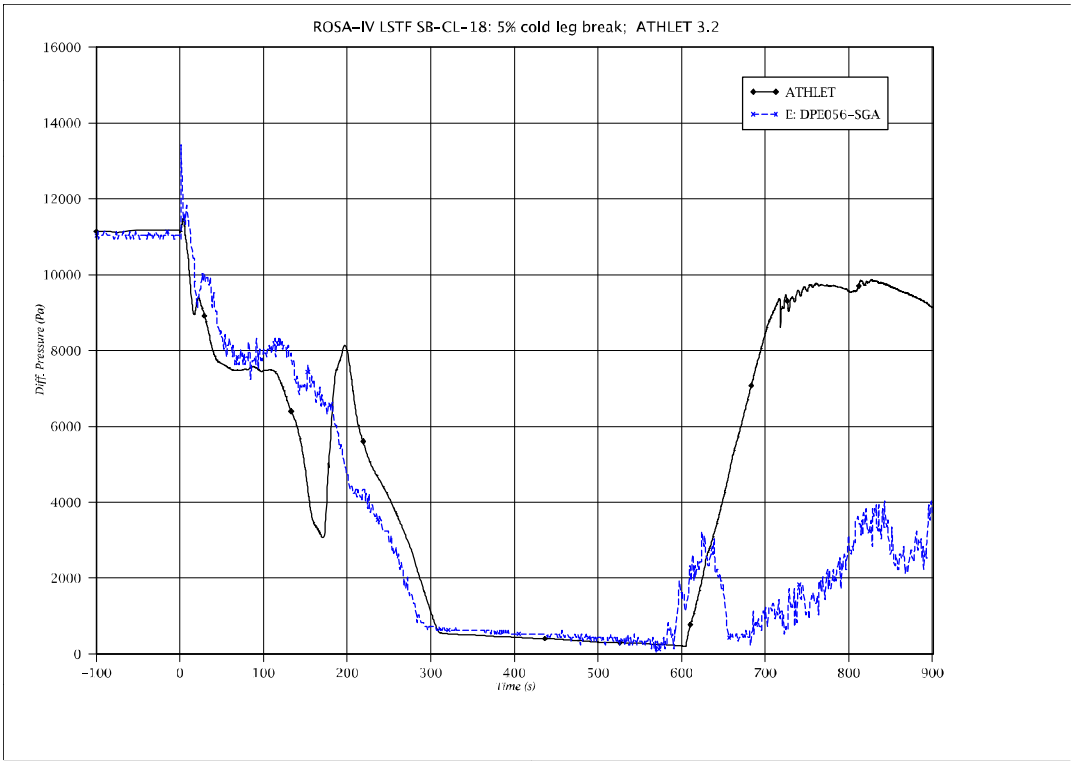

Fig. 5 - 23: Differential pressure across IL SG inlet plenum

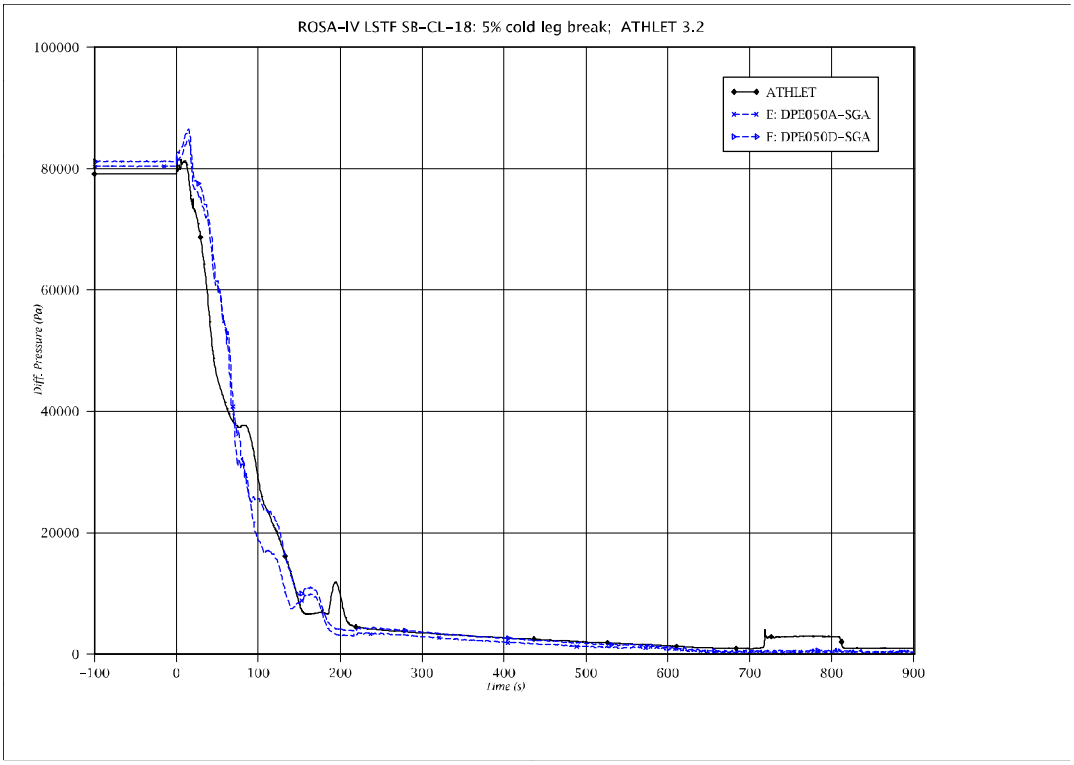

Fig. 5 - 24: Differential pressure across IL SG, highest U-tube, upflow

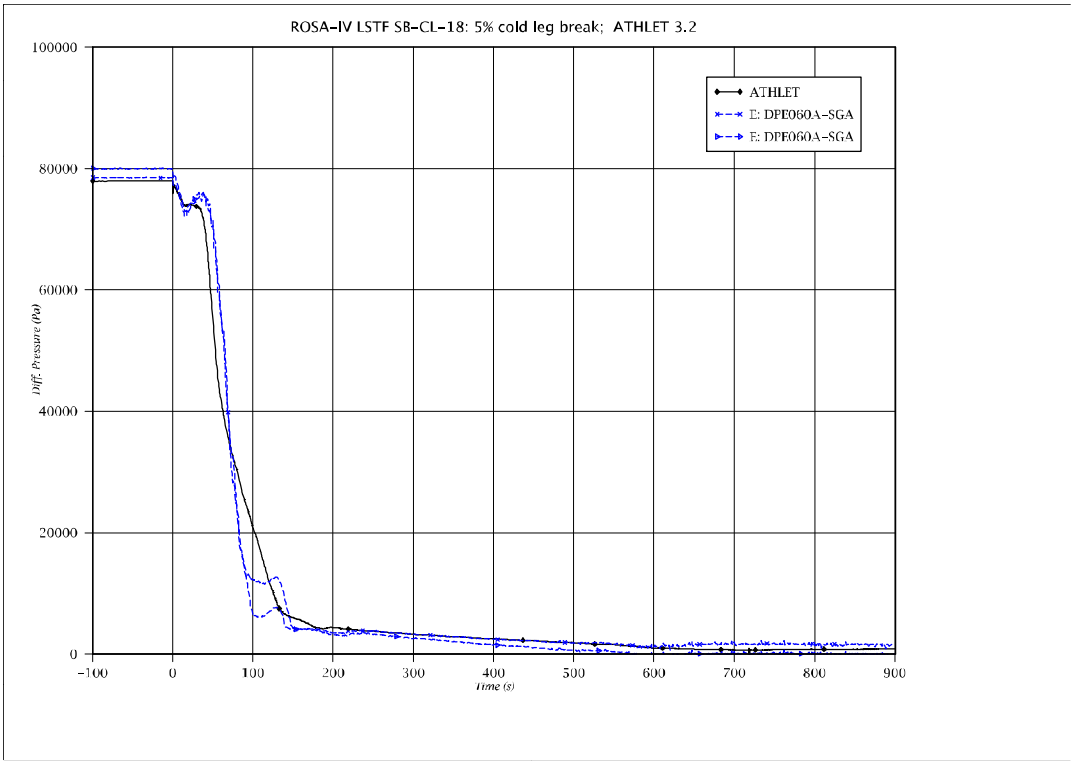

Fig. 5 - 25: Differential pressure across IL SG, highest U-tube, downflow

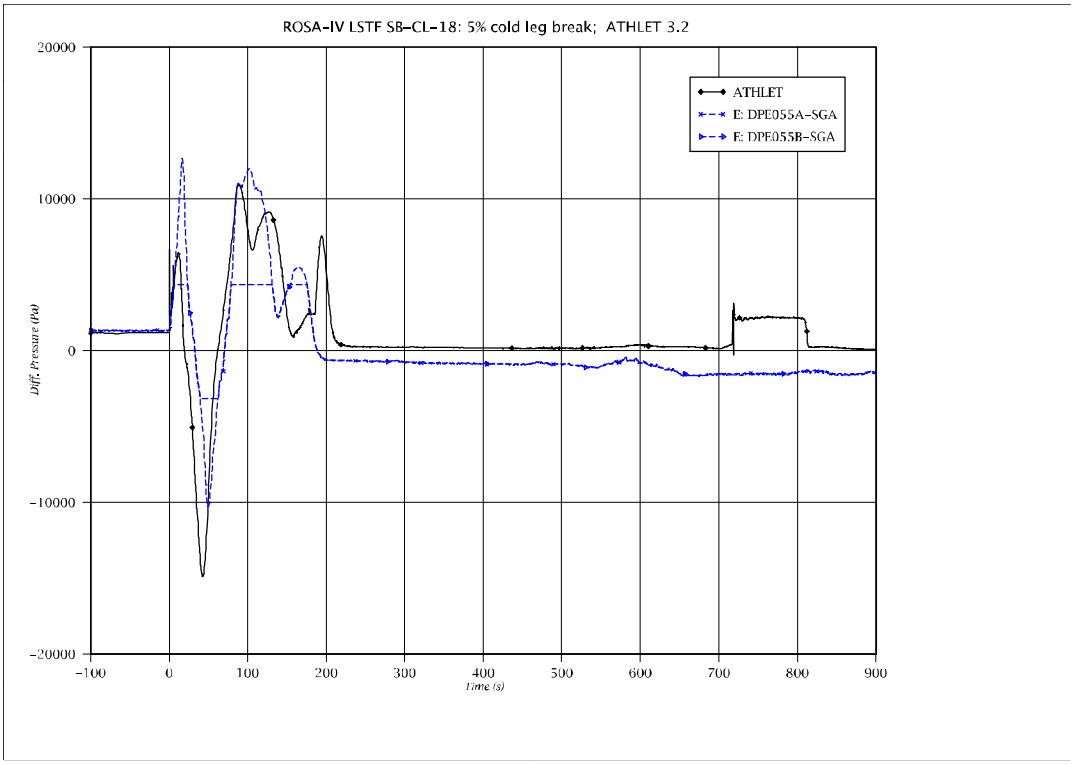

Fig. 5 - 26: Differential pressure IL SG inlet - outlet plenum

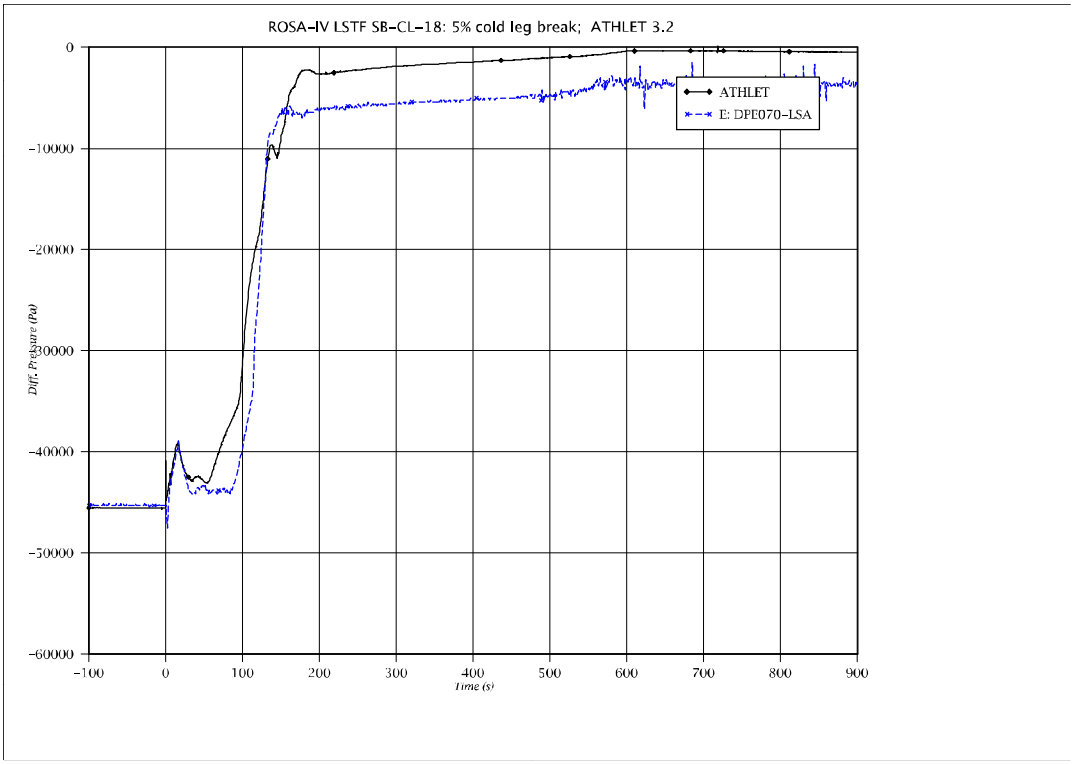

Fig. 5 - 27: Differential pressure across IL loop seal, downflow

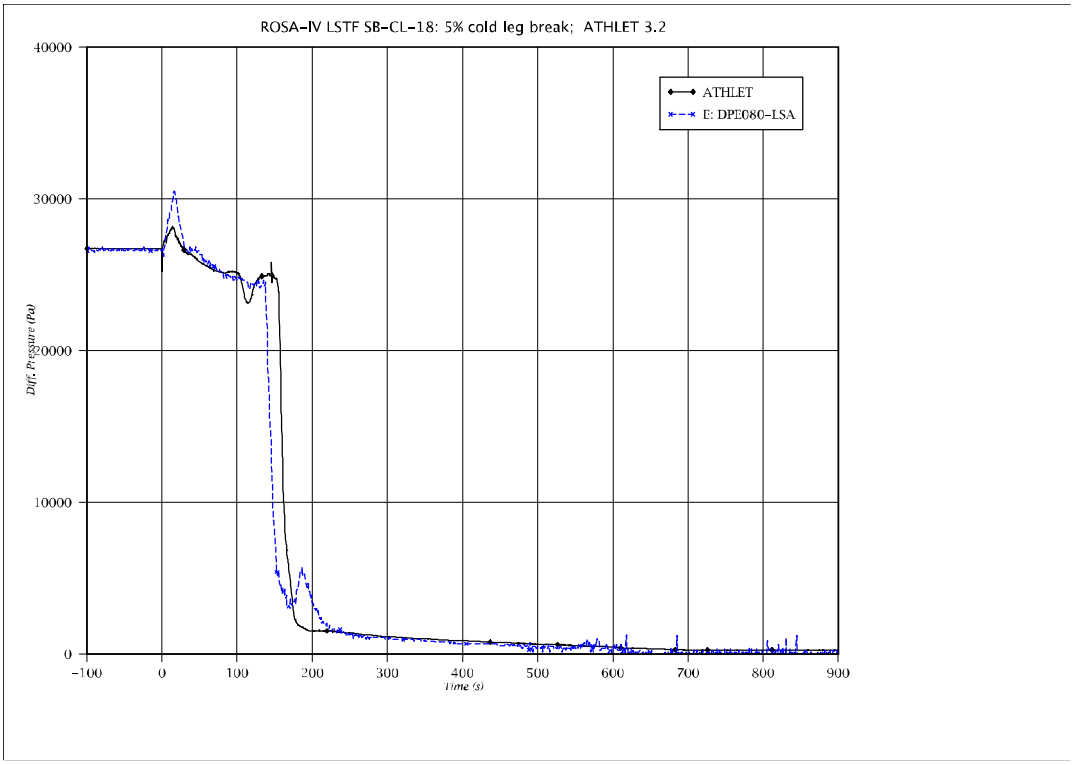

Fig. 5 - 28: Differential pressure across IL loop seal, upflow

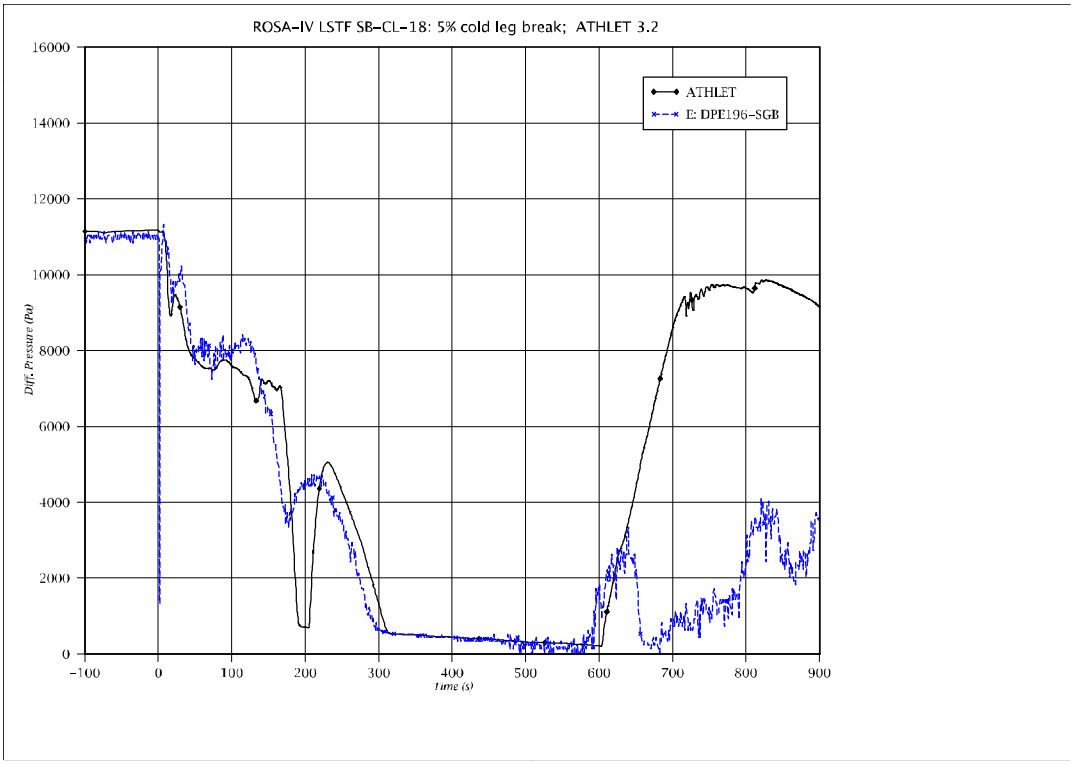

Fig. 5 - 29: Differential pressure across BL SG inlet plenum

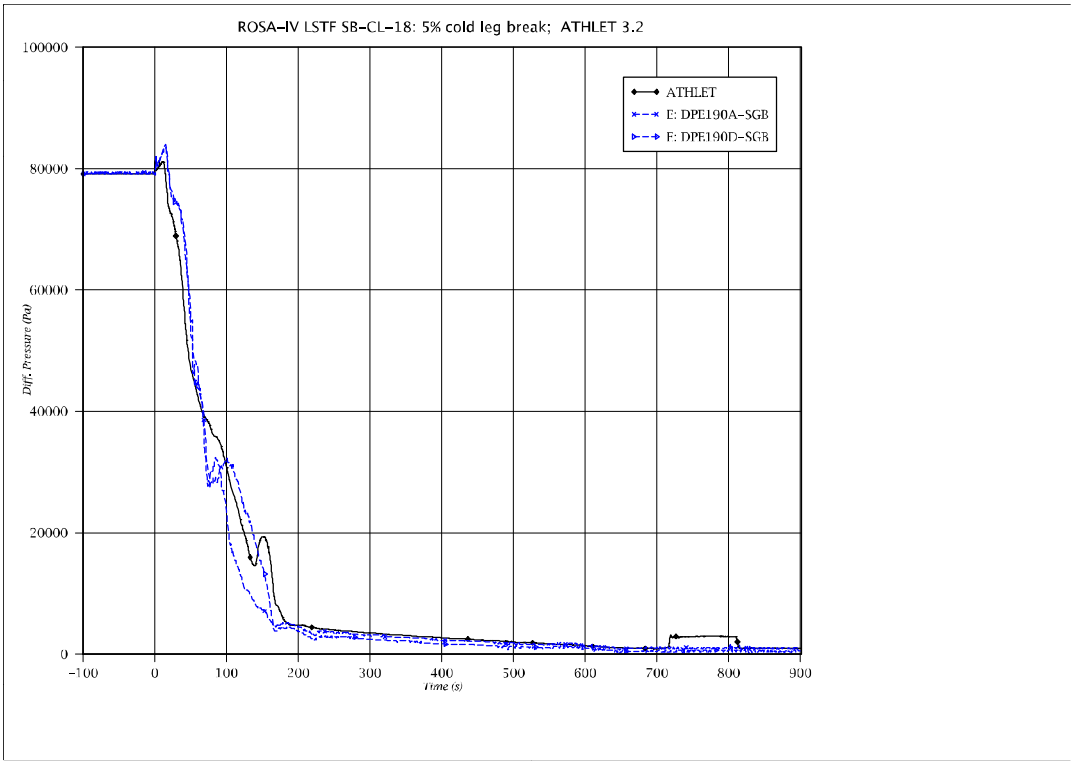

Fig. 5 - 30: Differential pressure across BL SG, highest U-tube, upflow

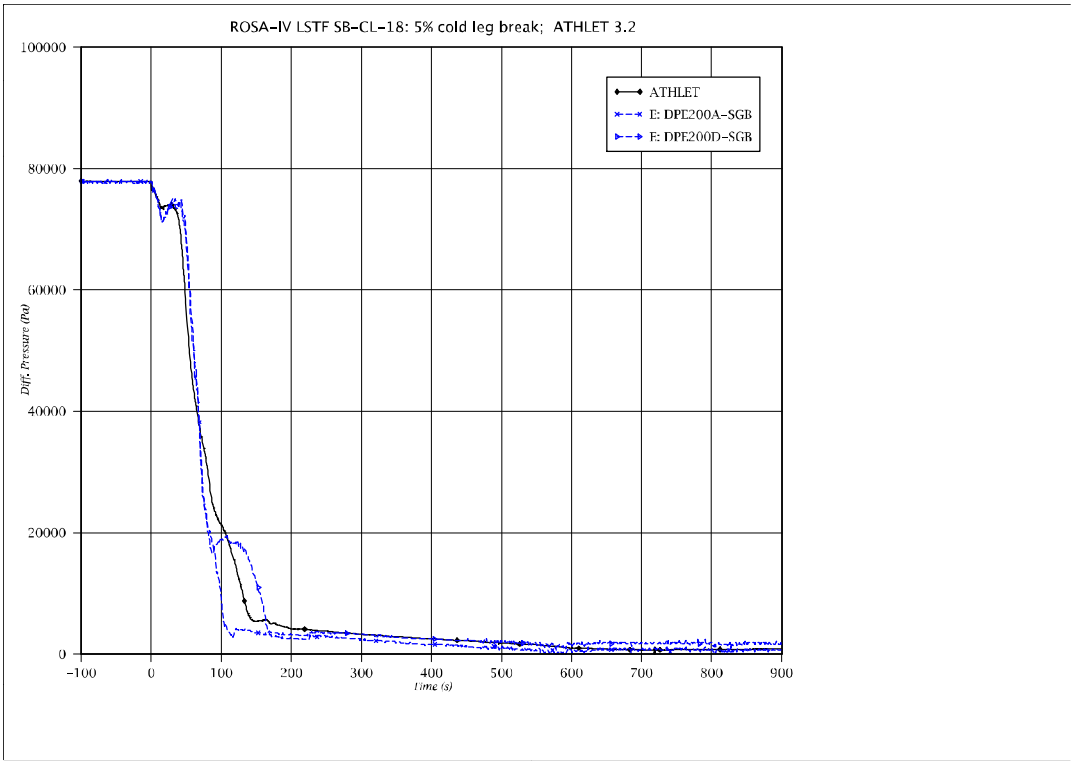

Fig. 5 - 31: Differential pressure across BL SG, highest U-tube, downflow

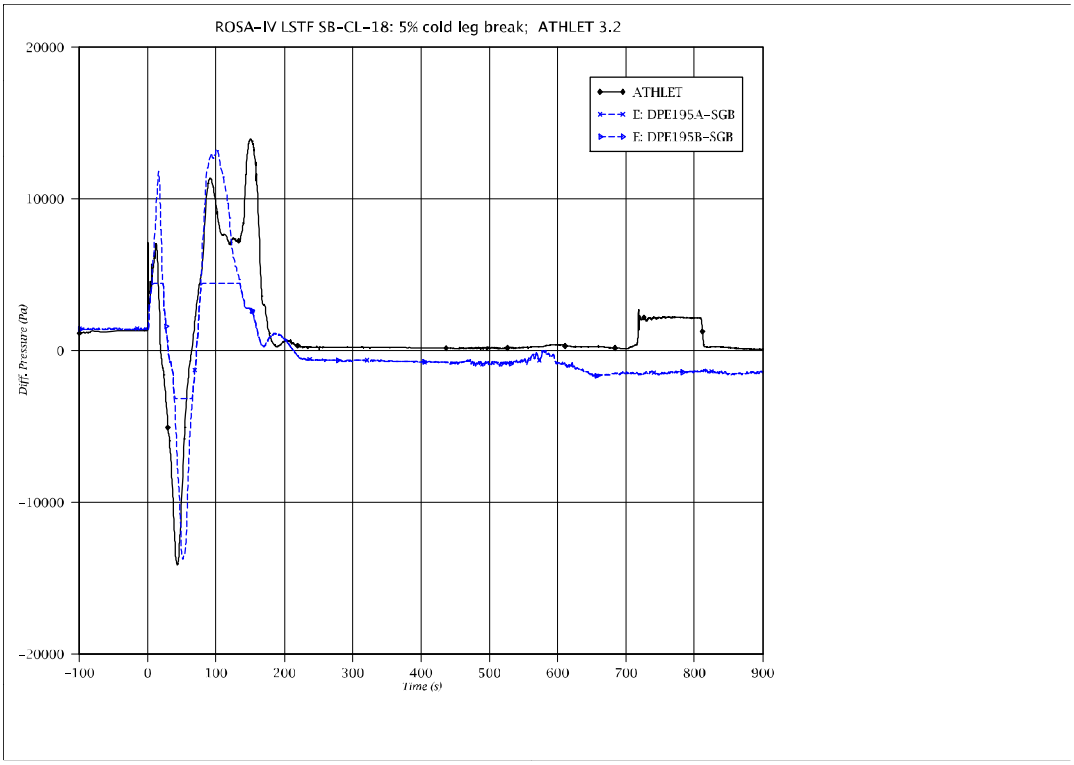

Fig. 5 - 32: Differential pressure across BL SG inlet - outlet plenum

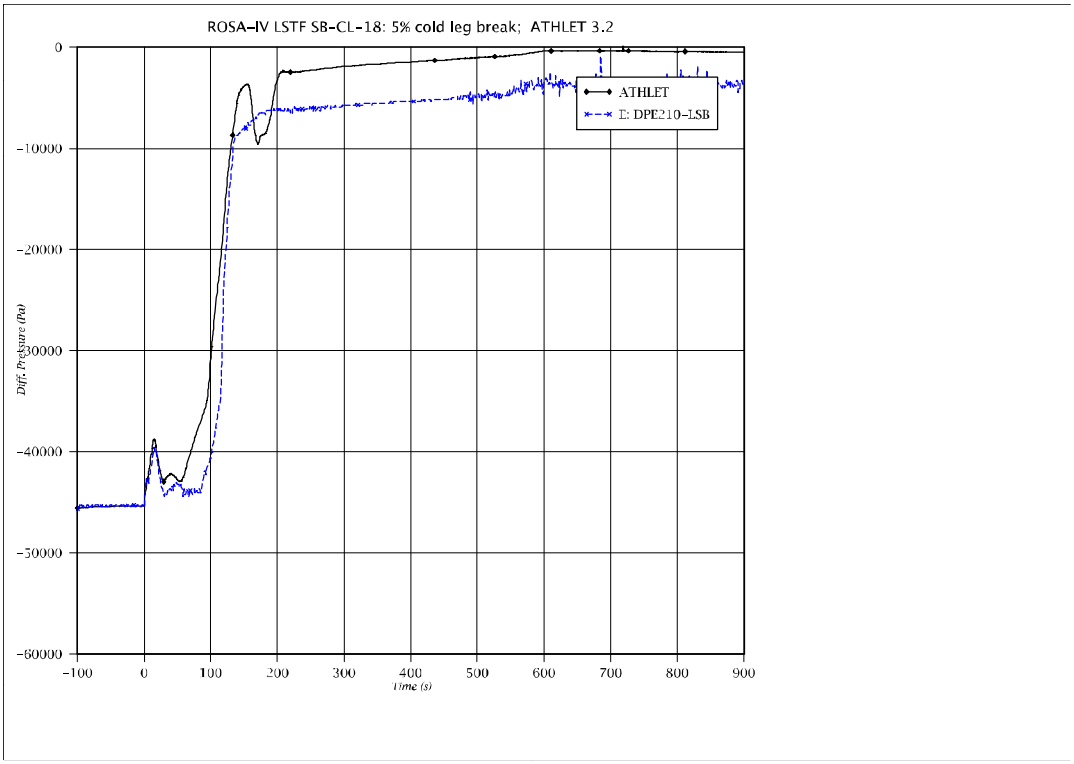

Fig. 5 - 33: Differential pressure across BL loop seal, downflow

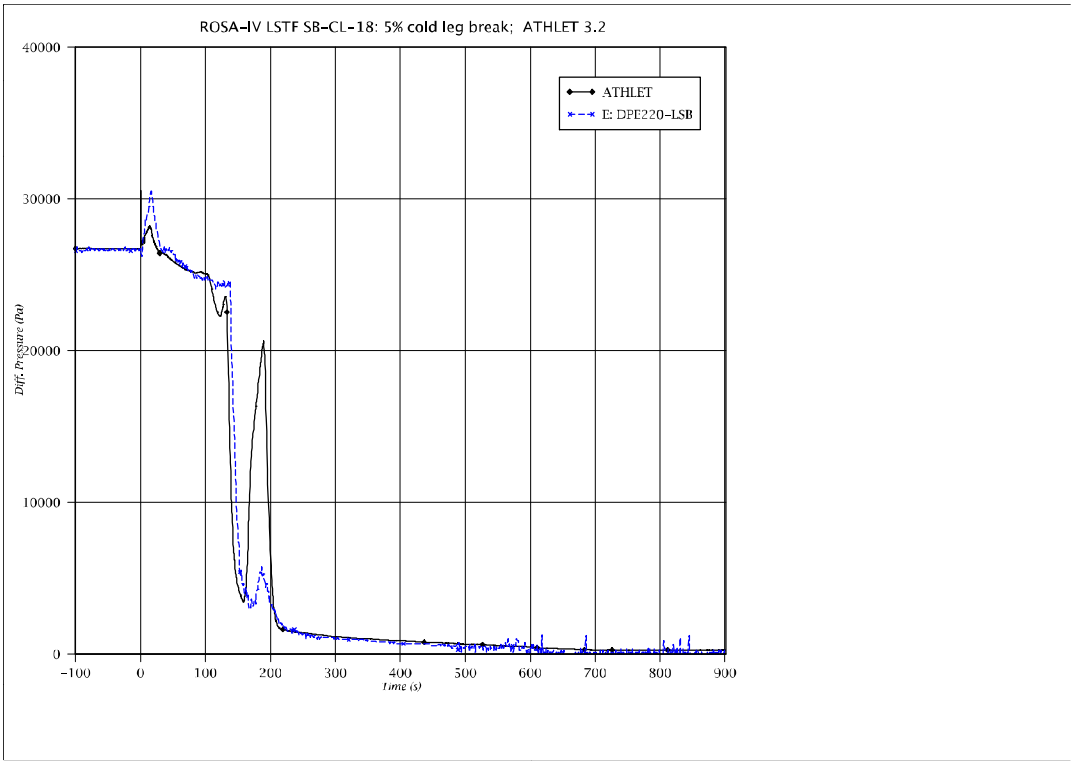

Fig. 5 - 34: Differential pressure across BL loop seal, upflow

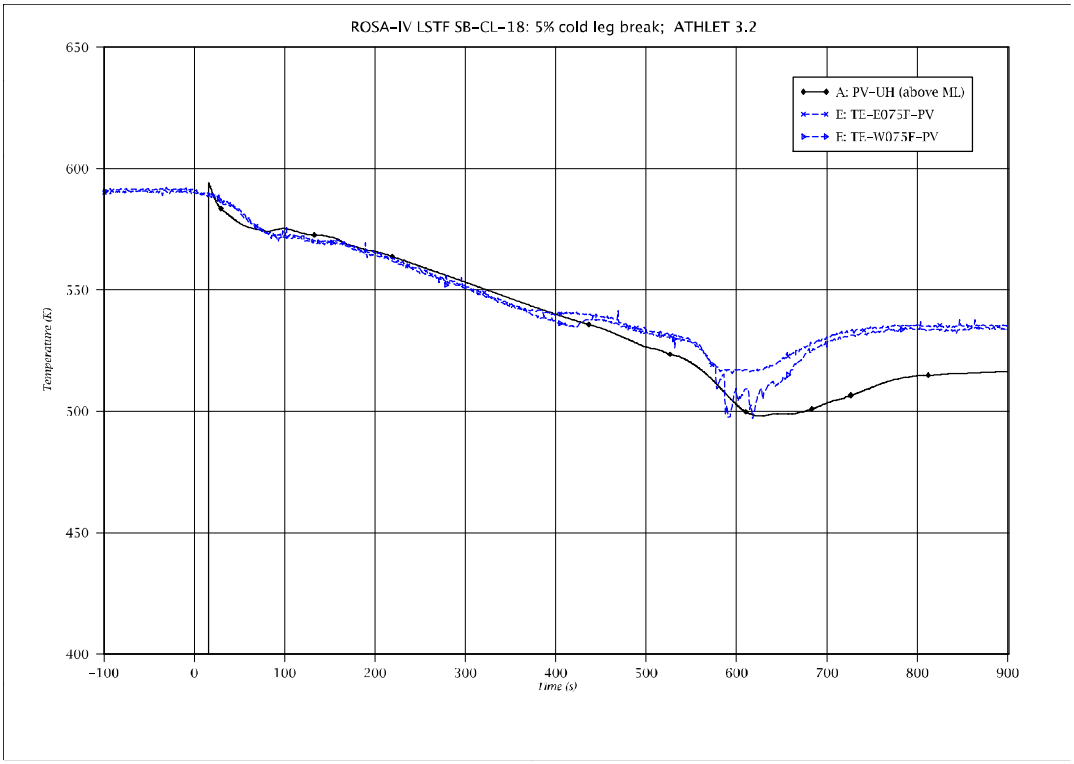

Fig. 5 - 35: Fluid temperature in upper head (above mixture level)

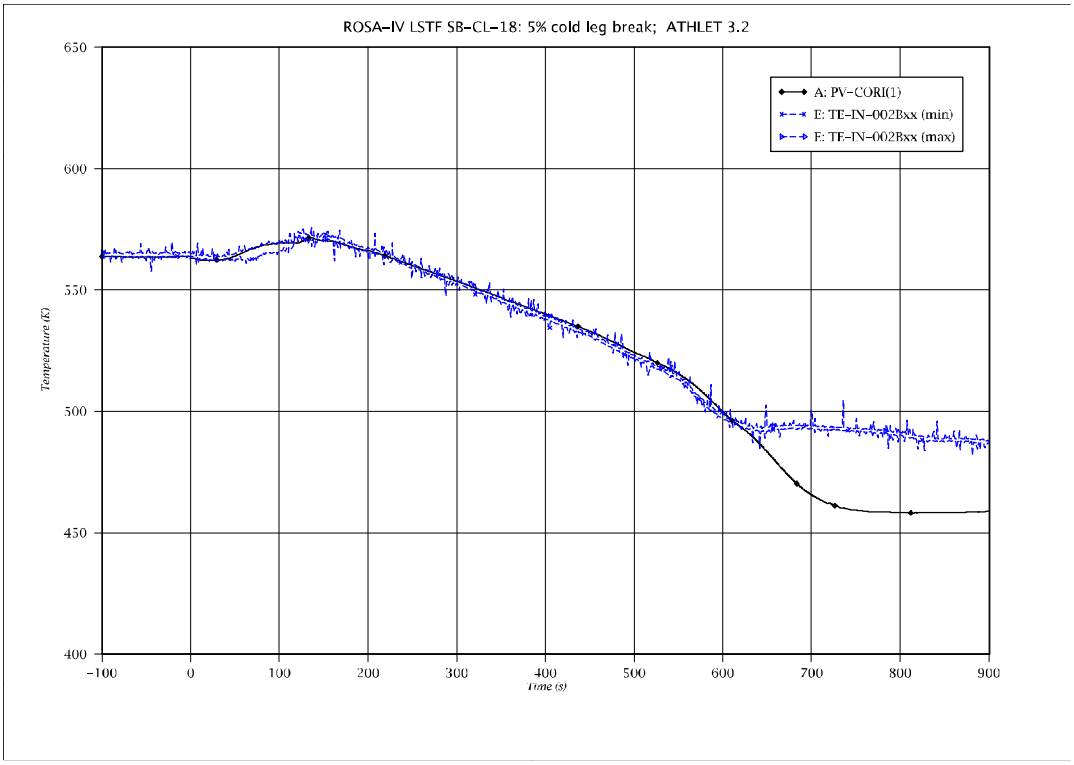

Fig. 5 - 36: Fluid temperature at core entry (inner channel)

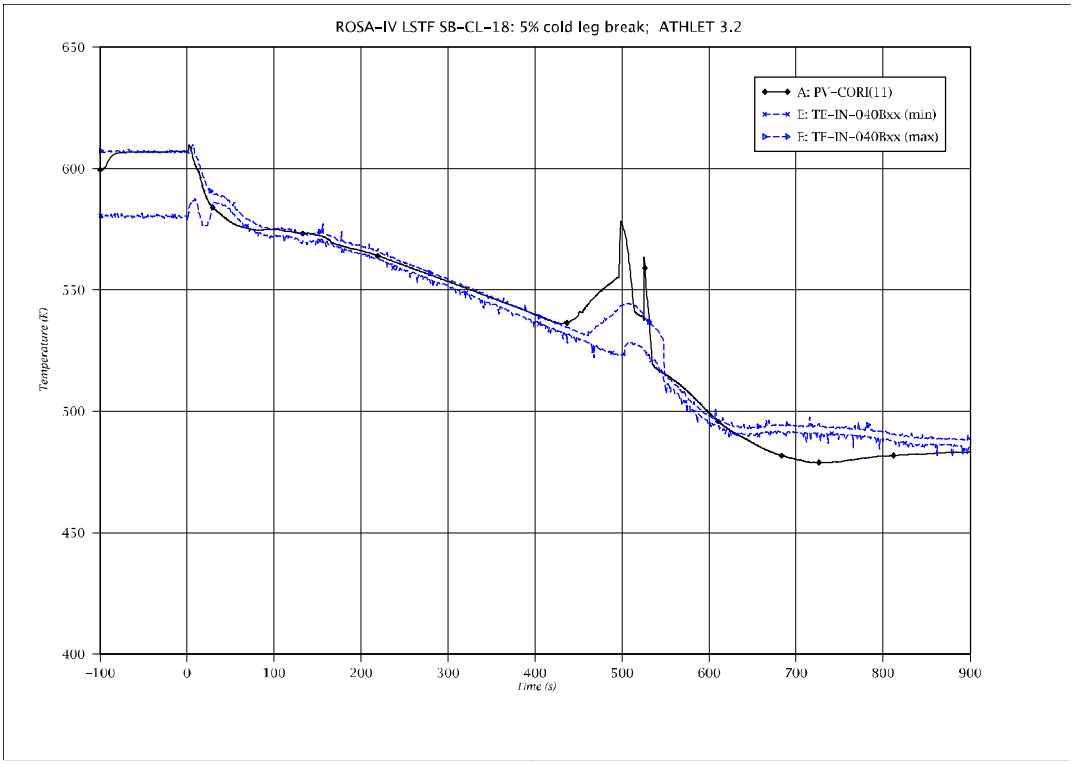

Fig. 5 - 37: Fluid temperature at core exit (inner channel)

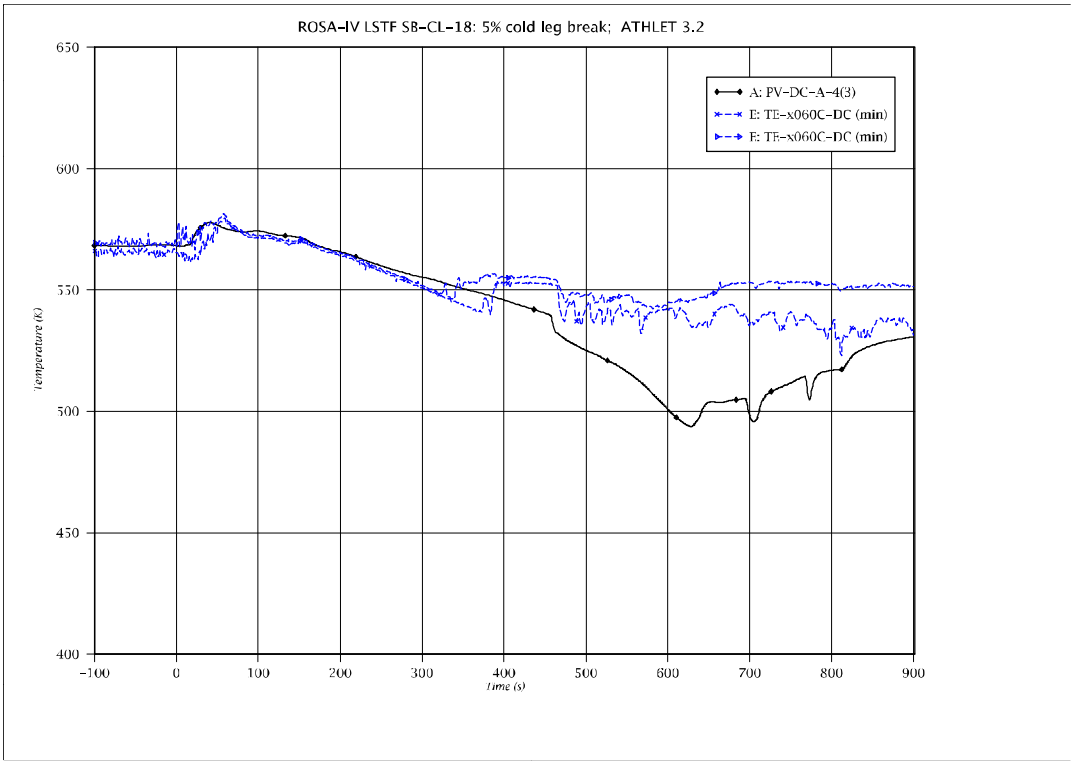

Fig. 5 - 38: Fluid temperature in upper DC

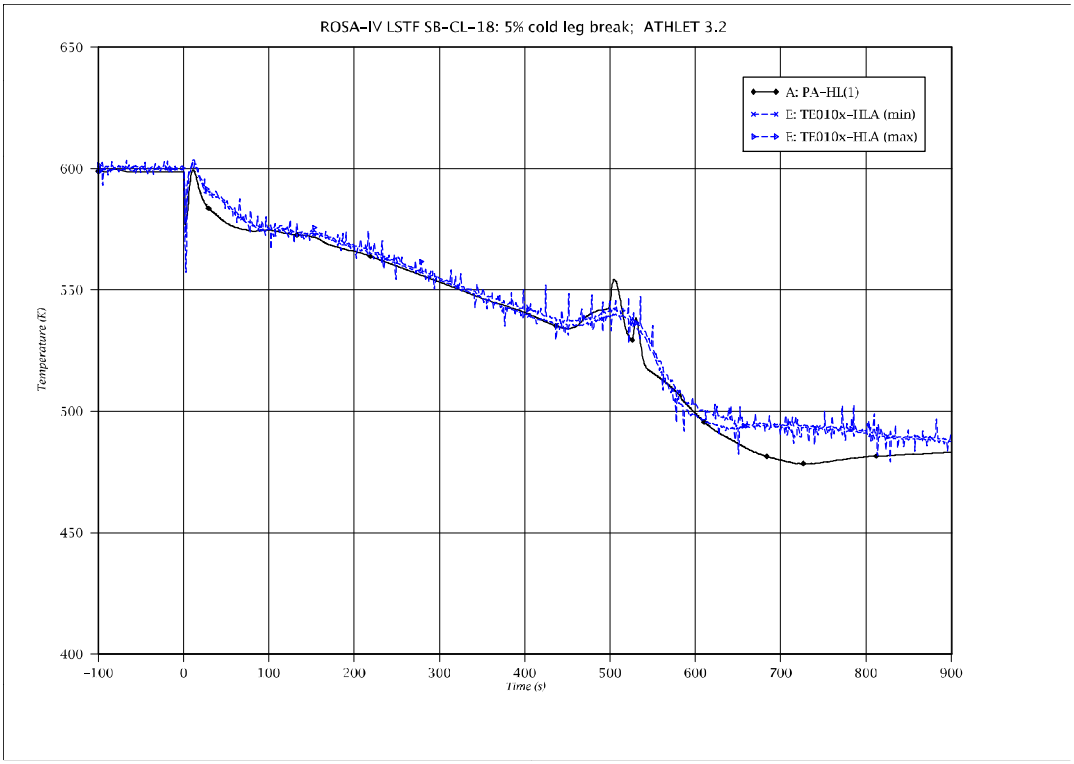

Fig. 5 - 39: Fluid temperature in IL hot leg vessel side

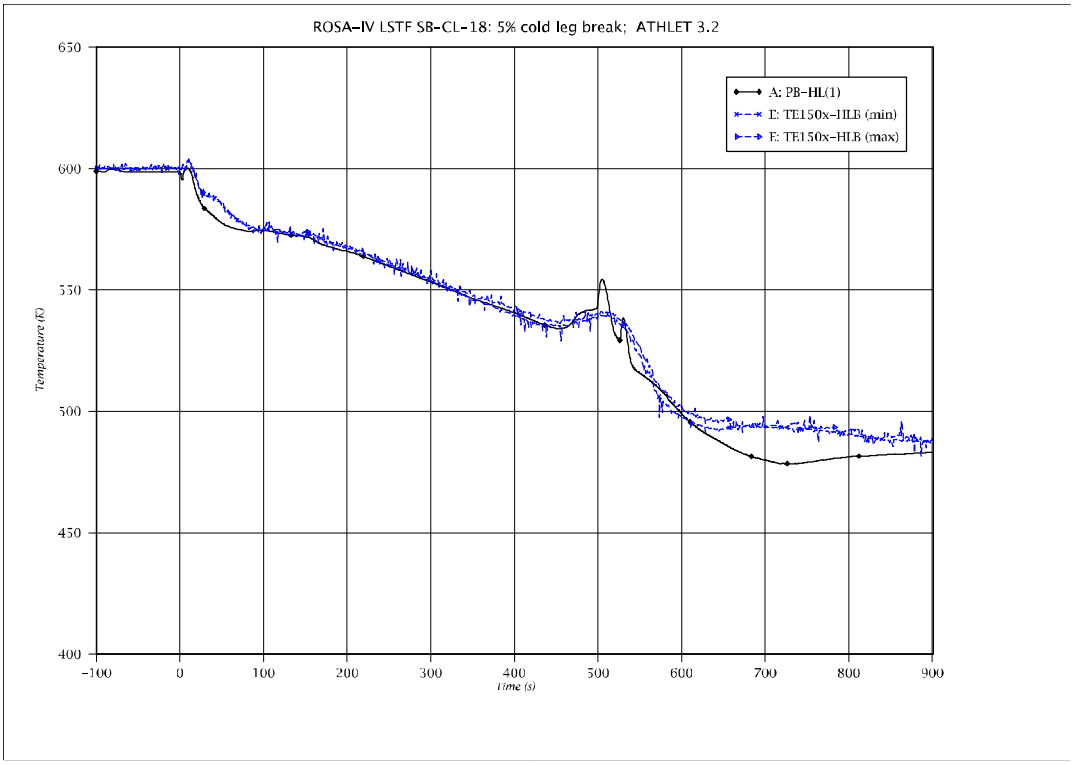

Fig. 5 - 40: Fluid temperature in BL hot leg vessel side

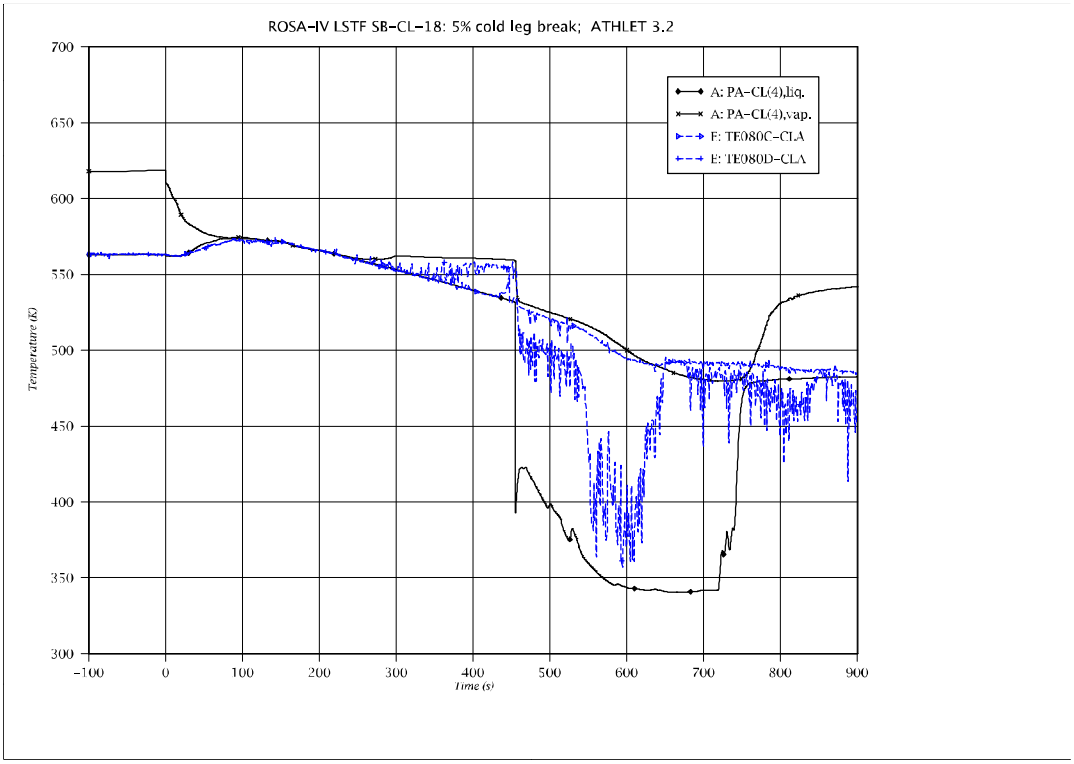

Fig. 5 - 41: Fluid temperature in IL cold leg vessel side

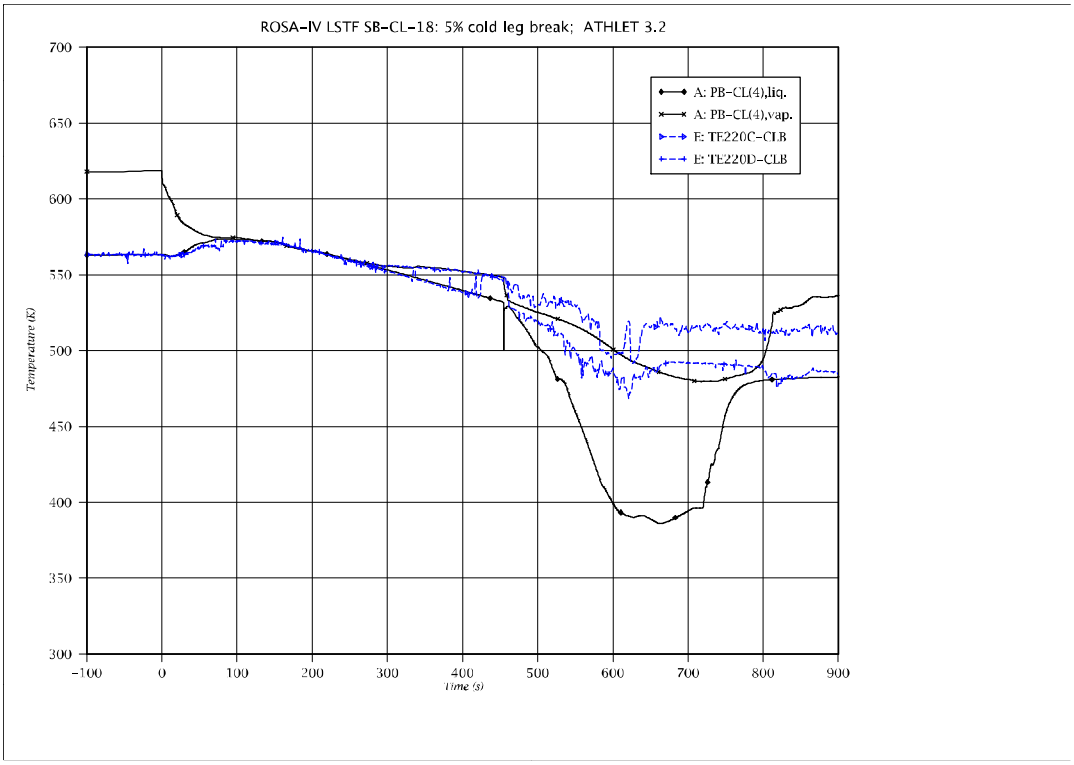

Fig. 5 - 42: Fluid temperature in BL cold leg vessel side

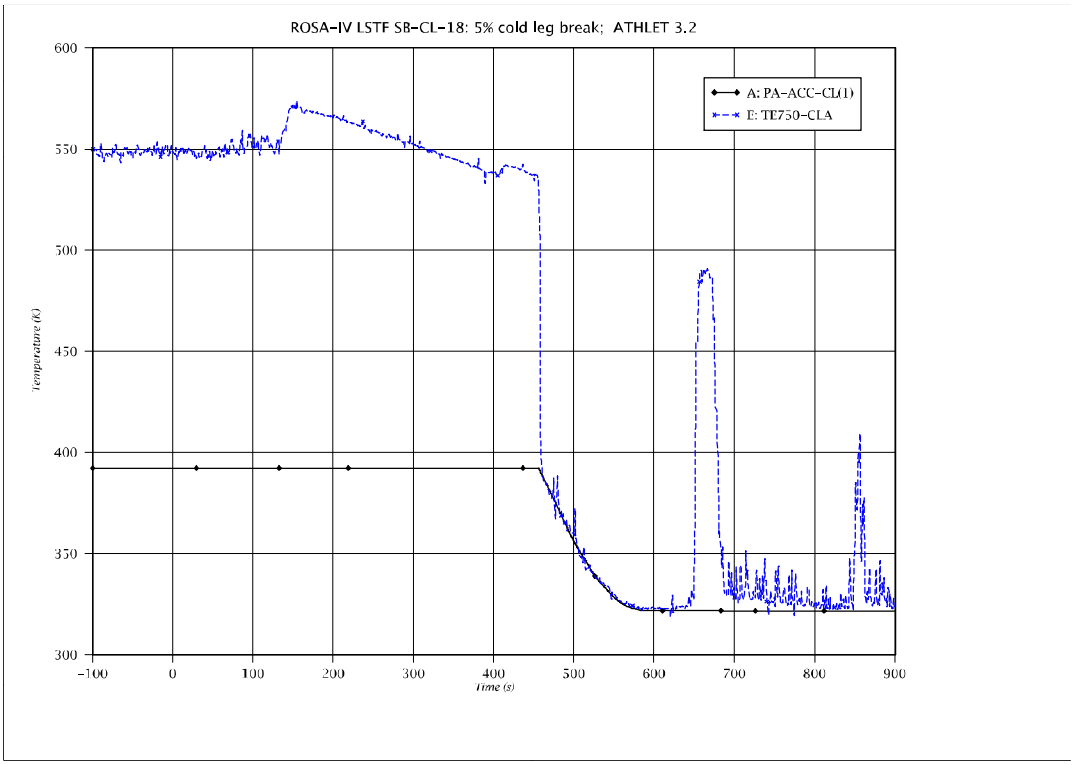

Fig. 5 - 43: Fluid temperature in IL ECC nozzle

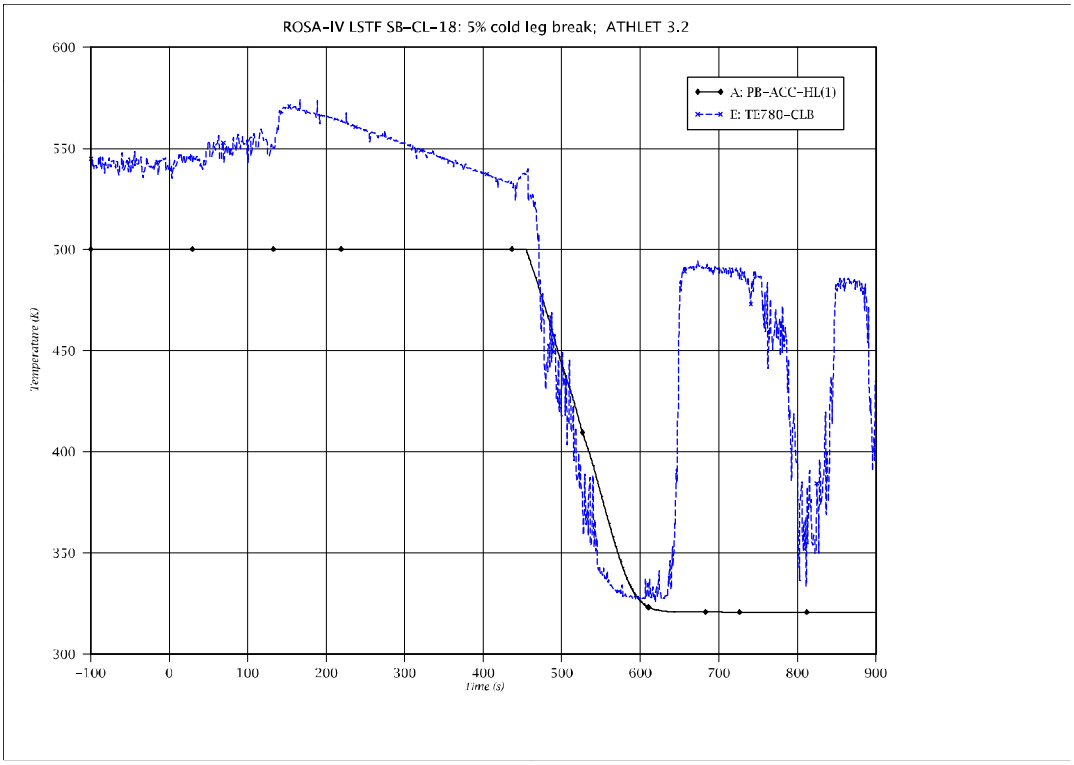

Fig. 5 - 44: Fluid temperature in BL ECC nozzle

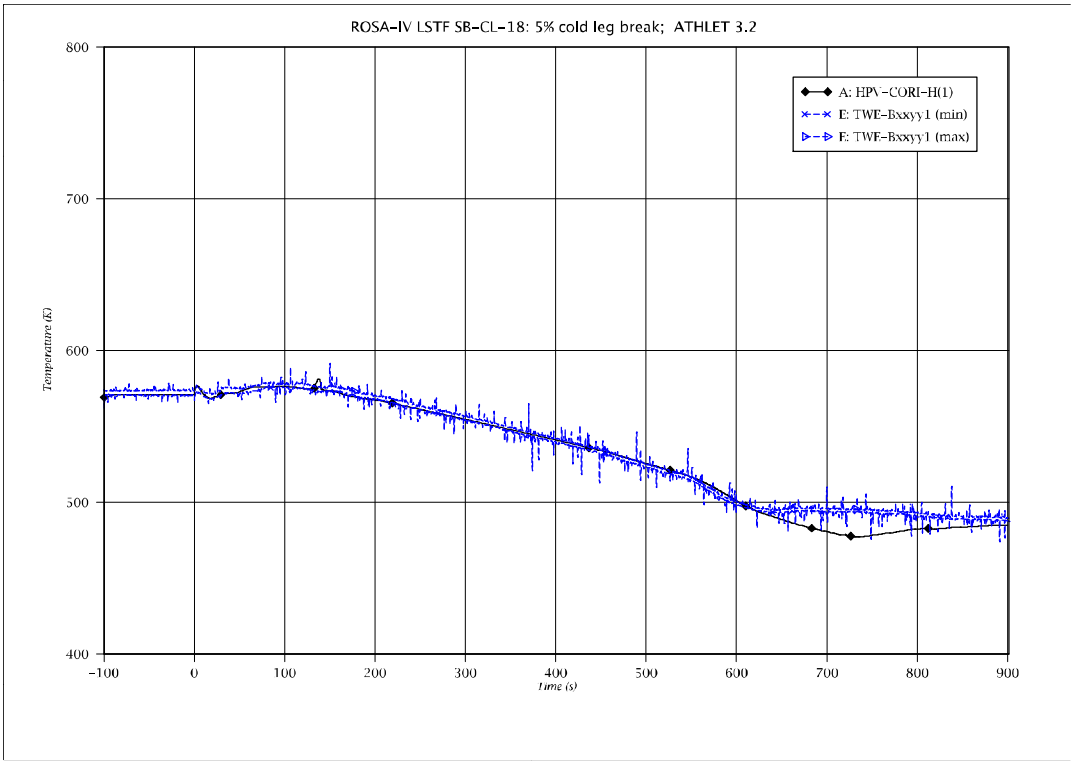

Fig. 5 - 45: Hot rod cladding temperature (HPV-CORI-H #1; bottom)

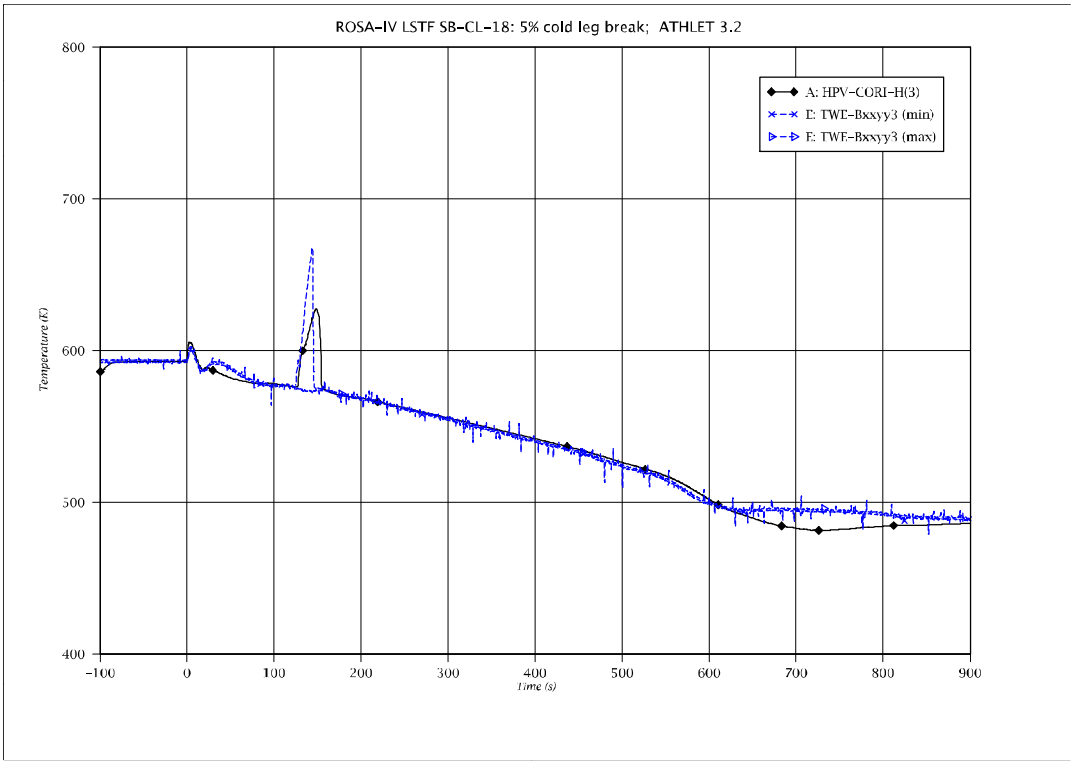

Fig. 5 - 46: Hot rod cladding temperature (HPV-CORI-H #3)

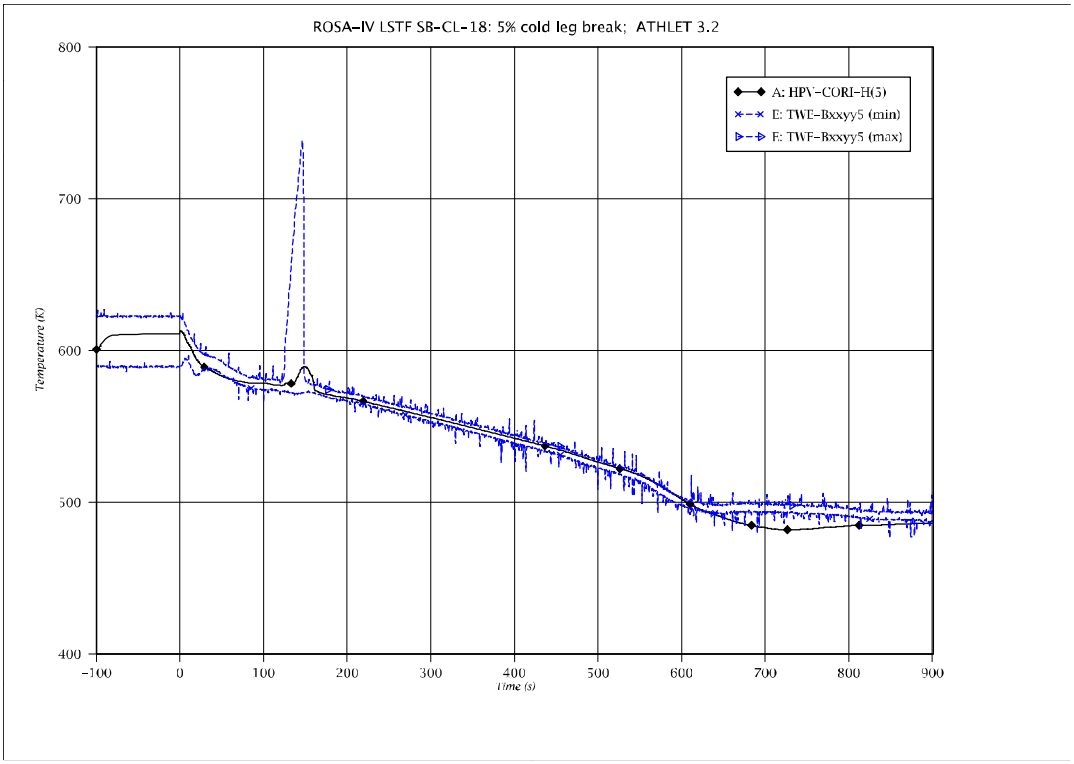

Fig. 5 - 47: Hot rod cladding temperature (HPV-CORI-H #5)

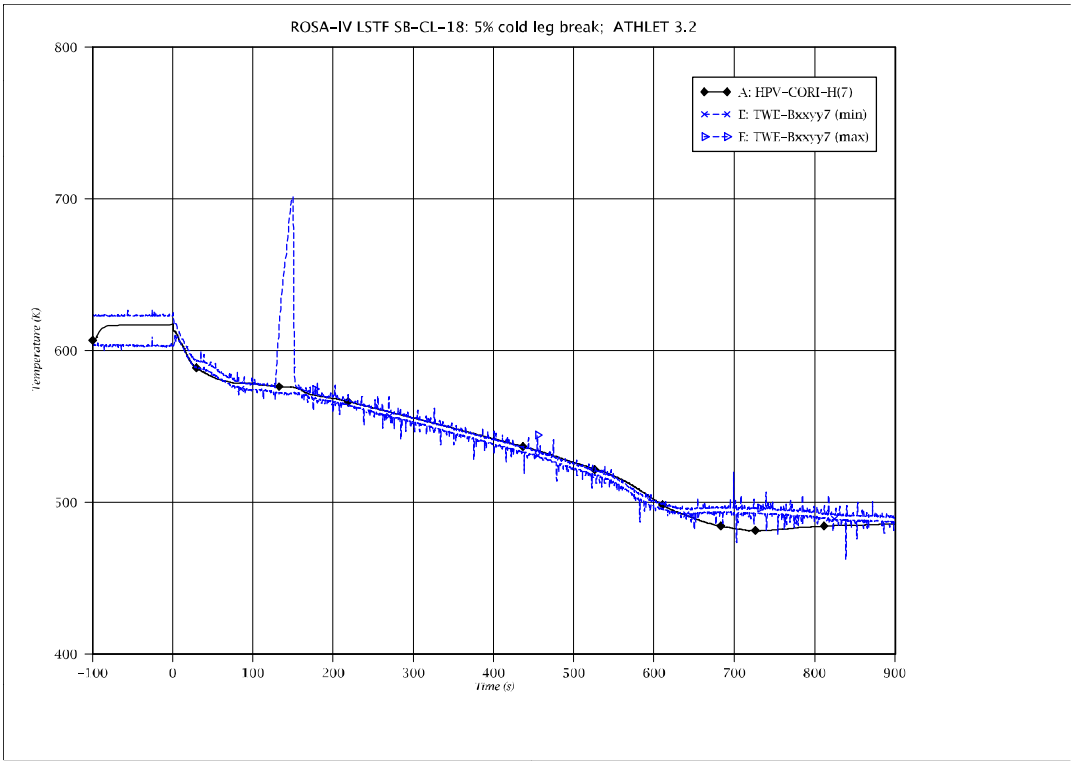

Fig. 5 - 48: Hot rod cladding temperature (HPV-CORI-H #7)

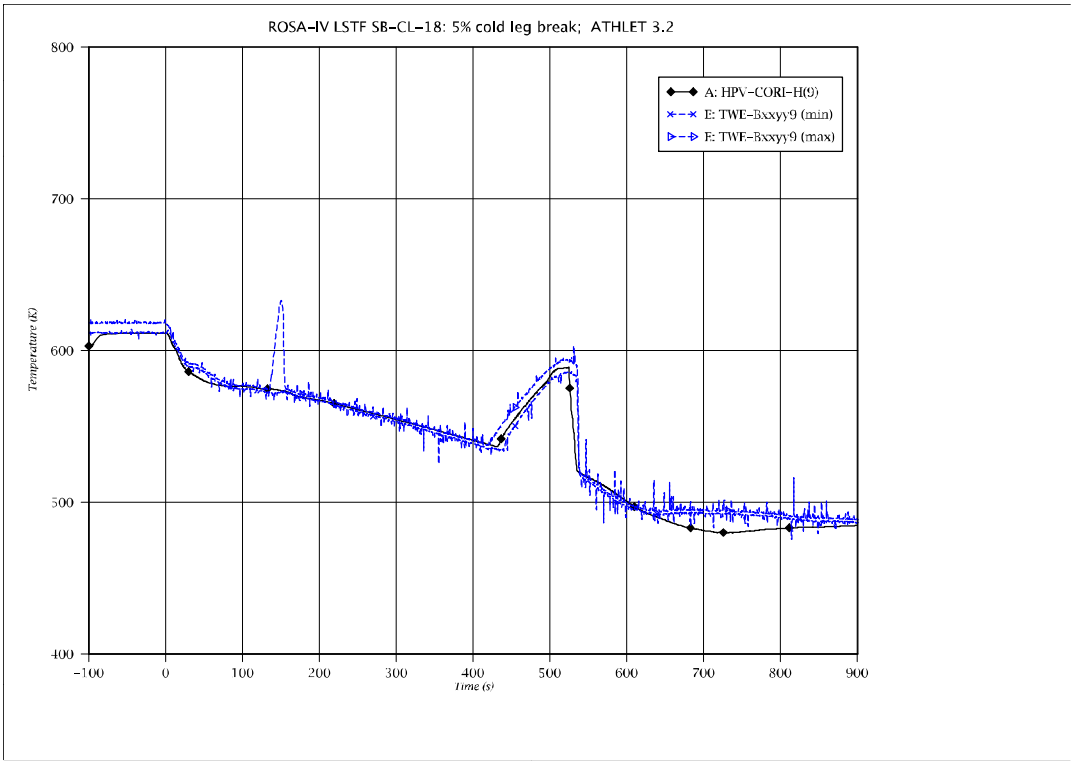

Fig. 5 - 49: Hot rod cladding temperature (HPV-CORI-H #9; top)

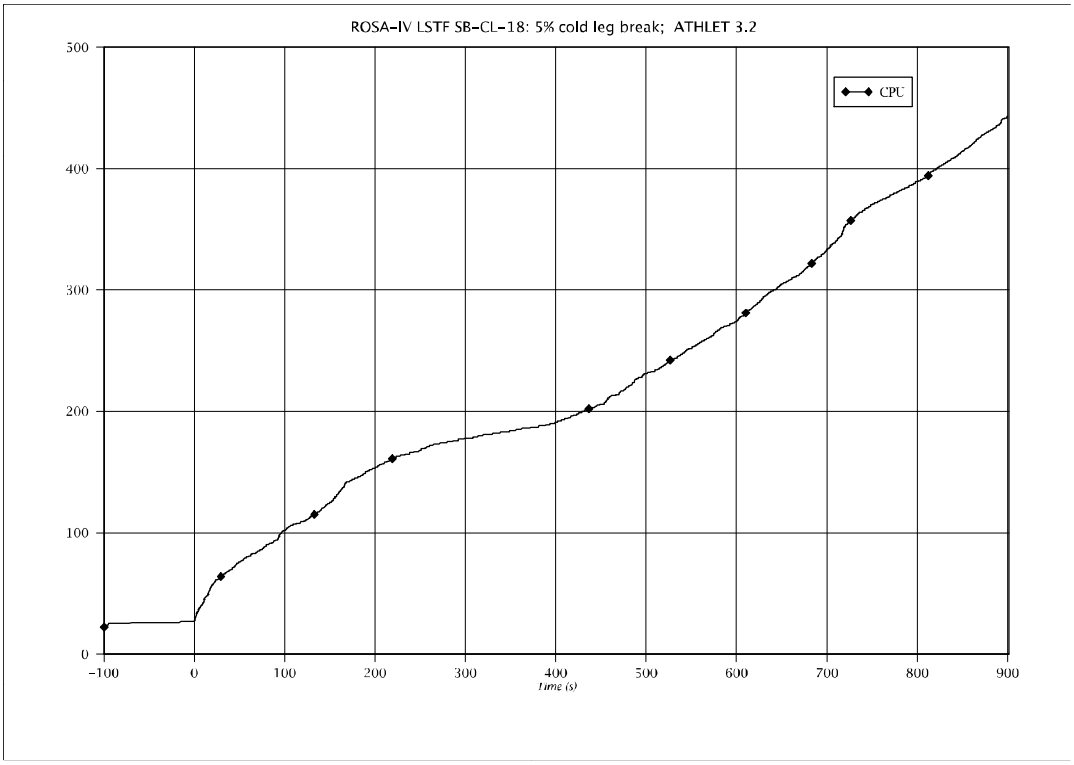

Fig. 5 - 50: CPU time consumption

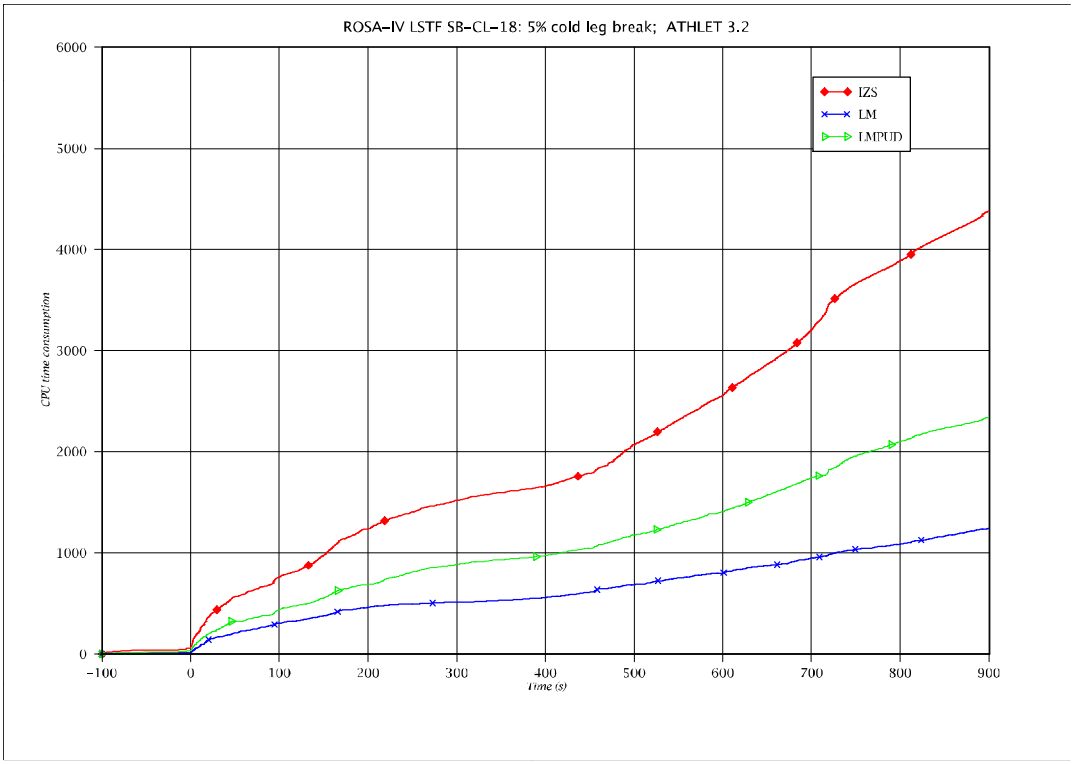

Fig. 5 - 51: Number of time steps (IZS) and Jacobian complete (LM) and partial updates (LMPUD)

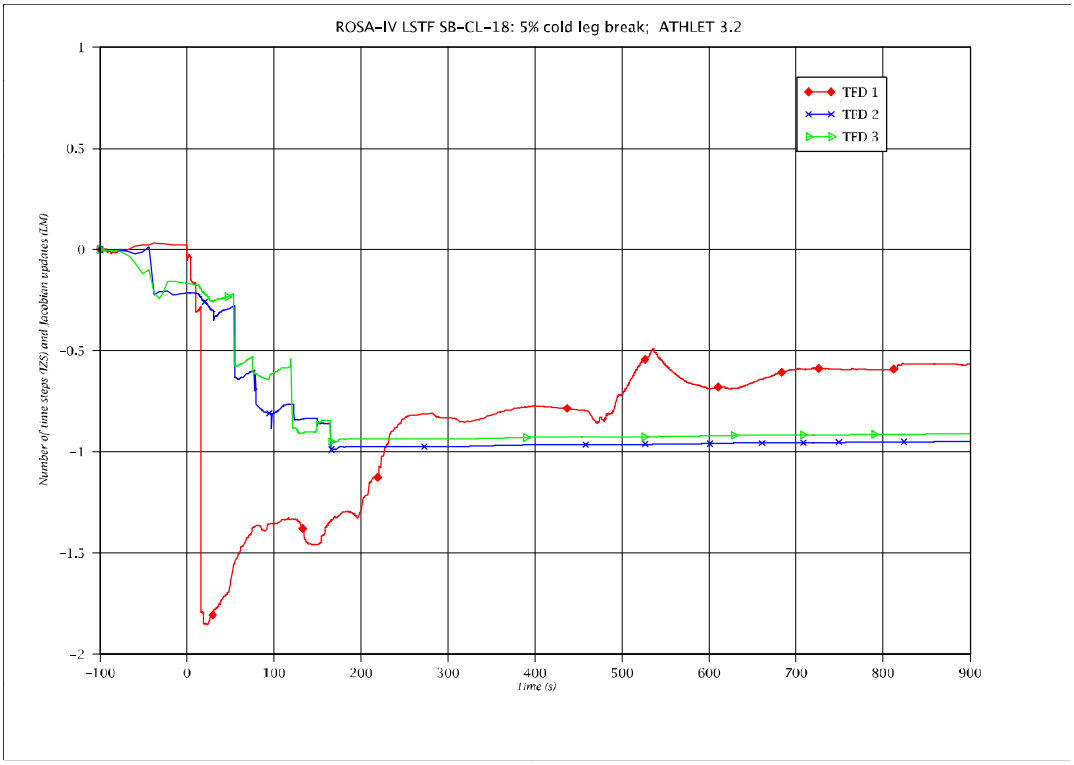

Fig. 5 - 52: Mass error in the TFD systems

5.2 ROSA-III - Run 916

5.2.1 Test Facility

The ROSA-III facility is a volumetrically scaled (1/424) BWR system with an electrically heated core designed to study the response of the coolant system, the core, and the ECCS during a postulated LOCA. The facility is instrumented such that various thermal-hydraulic parameters are measured and recorded during the test. The test facility consists of four subsystems. These subsystems are the pressure vessel, the steam line and the feedwater line, the recirculation loops, and the ECCS. Figure 5 - 53 illustrates the configuration of the facility.

The ROSA-III pressure vessel includes various components simulating the internal structures of the reactor vessel in the BWR system. The interior of the vessel is divided into the core, the lower plenum, the upper plenum, the downcomer annulus, the steam separator, the steam dome, and the steam dryer. The core consists of four model fuel assemblies of half length and a control rod simulator. Each fuel assembly contains 62 heater rods and 2 supporting rods spaced in a 8 x 8 square array and supported by spacers and upper and lower tie plates. The heater rods are heated electrically with a chopped cosine power distribution along the axis. The effective heated length is 1880 mm, one half of the active length of a BWR fuel rod. The electric power supplied to the 'hot' model fuel assembly 'A' is 1.4 times larger than the power supplied to each of the other assemblies. The heater rods in each assembly are divided into three groups in terms of heat generation rate. The relative power generation rate of a heater rod in each group is 1.1, 1.0, and 0.875 respectively. The orifice plates are inserted at the core inlet to control the core inlet flow.

The steam line is connected to the steam dome of the pressure vessel. A control valve is installed in the steam line to control the steam dome pressure in steady state before the initiation of the tests. The steam line has a branch in which the automatic depressurization system is installed. The feedwater is supplied from the feedwater tank through the feedwater line and the feedwater sparger in the downcomer annulus. The recirculation lines consist of two loops. Each line is furnished with a recirculation pump and two jet pumps. The jet pumps are installed outside the pressure vessel to simulate the relative volume and the relative height to the core.

Two break simulators and a quick shut-off valve are installed in one of these loops to simulate the various break conditions. Each break simulator consists of a nozzle to determine the break size and a quick opening valve to initiate the test. The break mode (the double-ended or the split), the break size, and the break location can be changed. The diameter of the largest nozzle available is 26.2 mm. Several flow nozzles of different size are prepared to vary the break size.

The ROSA-III facility is furnished with all kinds of the ECCS available in the BWR system, i.e., the high pressure core spray (HPCS), the low pressure core spray (LPCS), the low pressure coolant injection (LPCI), and the automatic depressurization (ADS) systems. The HPCS and the LPCS provide the cooling water from the top of the core. The LPCI injects the cooling water into the core shroud. Each ECCS consists of a pump, a tank, piping, and a control system. More detailed information of the facility design is available in references /ANO80, ANO81/.

5.2.2 Test Conditions and Procedures

Run 916 was a 50 % break test at the recirculation pump suction in one of the two recirculation lines /YON85/. A sharp-edged orifice was used as a break plane. The break area is determined by inserting an orifice or a nozzle upstream of the QOBV. Blowdown is initiated by opening the blowdown valve B.

The initial conditions of Run 916 are listed in table 5 - 3. The subcooling at core inlet is 11.2 K, the estimated quality at the core outlet is 14.2 %. The core power is 3.963 MW before the break initiation which is 44 % of the 9 MW steady state power based on the conservation of the power to volume ratio in the reference BWR. The core power is changed during the transient after the break initiation. The power is kept constant for the first 9.0 seconds and reduced along a curve simulating the total heat transfer rate in the core of the reference BWR (the delayed neutron fission power, the decay power of fission products and actinides and the stored heat in the nuclear fuel) neglecting the stored heat of ROSA-III heater rod. The maximum linear heat generation rate of the peak power rod is 16.7 kW/m before the break initiation.

The steam flow before MSIV closure is limited by an orifice of 18.0 mm ID (inner diameter) installed upstream of the MSIV CV-130. The feedwater supply is terminated at 2 s after the break by closing the valve AV-112 in the feedwater line. However, feedwater remained in the piping between the valve AV-112 and the feedwater sparger, and flashed during the transient after the pressure dropped below the saturation pressure.

The coolant recirculation pumps are tripped at the break initiation. The liquid level signals in the downcomer are used to actuate the ECCS and to close the MSIV. The downcomer level in the steady state operation is set at the scram level L3 (5.00 meters above the bottom of the pressure vessel) and L1 and L2 levels are 4.25 meters and 4.76 meters, respectively. The L2 level signal is used to close the MSIV with a time delay of 3 s and to actuate HPCS with time delay of 27 s. The L1 level signal is used to actuate LPCS, LPCI and ADS with time delay of 40 s, 40 s and 120 s, respectively. The above lag times of 3 s, 27 s, 40 s and 120 s are used in a safety analysis of the reference BWR. LPCS and LPCI could inject cooling water after the primary sys-

tem pressure is reduced below 2.16 MPa and 1.57 MPa, respectively. Specified system pressures for actuating LPCS and LPCI were decided from the pump characteristics used in the safety analysis of the reference BWR. The test was terminated after the whole core was quenched at 255 s after the break initiation.

Table 5 - 3: Initial conditions for ROSA-III test Run 916

Parameter	Measured value	ATHLET
Steam dome pressure (MPa)	7.32	7.32
Lower plenum (°C)	277.7	280.9
Core inlet mass flow (kg/s)	16.5	16.6
Core power (kW)	3963	3960
Max. linear heat generation rate channel A (kW/m)	16.7	16.7
Max. linear heat generation rate channel B (kW/m)	11.9	11.9
Feedwater temperature (°C)	216	216
Feedwater mass flow (kg/s)	2.1	2.1
Steam mass flow (kg/s)	2.03	2.1
Water level in PV (m)	5.0	4.8
ECCS water temperature (°C)	40	40

5.2.3 Input Dataset

5.2.3.1 Nodalization

The figure 5 - 54 shows the nodalization used in the ATHLET calculation /POI89a/. The heat conduction volumes for the simulation of the facility structures are not included in this figure. The nodalization includes the following numbers of network elements:

Branches	11
Pipes	30
CVs	167
Junctions	180
ODEs for thermo-fluiddynamic	863
Heat conduction volumes	159
ODEs for heat conduction	833

The downcomer and the steam dome are divided in 7 TFOs. This fine nodalization is required to simulate all connecting pipes, the separator and the dead end of the lower downcomer. For all downcomer objects the mixture level model is applied.

The geometry of the loops is exactly represented. The hydraulic parameters of the recirculation pumps in the loops are determined by homologous curves. Only the single phase head curves are known for the ROSA-III pumps, therefore the two phase curves have been derived from the Semiscale pump data. Since no momentum curves are available the pump speed history has been specified as a table according to the experimental measurement.

The TFOs NOZZLEI/B, JETPUMPI/B, and DISSUSORI/B simulate the jet pumps of the intact and the broken loop. The pressure recovery in the diffusor pipe is calculated via the standard momentum equation, the momentum mixing and the suction effect, however, are simulated with a GCSM controlled pump model taking into account the given jet pump characteristics.

The objects LPBOTTOM, LPCON, LPBOTR and LPTOP represent the lower plenum. This fine nodalization is required to simulate the phase separation processes below the flow limiting cross areas in a realistic way. The 4 rod bundles are modelled by two channels. The object CORE1 represents the bundles B, C and D with a radial power factor of 0.91, CORE2 simulates bundle A with a radial power factor of 1.27. The objects COREOUT and COREIN simulate the head of the bundle and bundle inlet plenum.

The heater rods are modelled by one hot rod and the remaining number of averaged rods. A realistic modelling of the axial power shape is given by 24 axial CV's (arranged from bottom to top), each three of them assigned to one CV. The heater rods are divided in 3 radial materials (heat conductor, isolation and cladding).

The upper plenum and the separator are modelled by the objects RISER and SEPARATOR. The RISER is divided in 4 CVs in order to simulate the phase separation below the separator.

The TFO BYPASS comprises the guide tubes, the reflector and the bundle bypass. COREINBY represents the holes connecting the bundle inlet plenum with the bypass.

The GCSM controlled fill components FEEDWATER and STEAML simulate the steady state feedwater injection and the steady state as well as transient steam removal, resp. The actual volume of the feedwater line is represented by the TFO FEEDWL to consider the flashing and injection process after the pressure has dropped below the feedwater saturation pressure. The ECC injection is performed via the fills HPCS, LPCS, and LPCI2, where the high pressure injection is assumed to fail.

In all vertical objects including flow limiting flow areas, a fine nodalization in the region below these areas is used. In this way, a correct simulation of possibly counter-current flow limitations can be ensured.

In addition to the heater rods, all relevant structures are considered. To reduce the number of HCVs (to save CPU time) some of them are concentrated to a reduced number of HCOs conserving both the volume and the surface of the structures.

5.2.3.2 Model Options

Following model options are applied:

- The 5 eq. model with the flooding based drift model is applied for all TFOs. Corresponding to the geometry, the pipe, bundle, or annulus drift flux option is selected.
- The relative velocity in the bundle inlet diaphragm is calculated with a special flooding based drift model correlation for bundle inlet orifices of boiling water reactors.
- The critical discharge mass flow is calculated with the CDR1D model. A contraction factor of 0.8 is applied for vapor discharge flow.
- The T-junction model is applied for the entrance from the downcomer to the broken loop recirculation line.
- The friction losses are calculated with the Martinelli-Nelson model applying a constant Darcy-Weissbach friction factor of 0.012.
- The condensation rates are calculated with the ATHLET direct condensation model.
- Evaporation and condensation at heating and cooling surfaces are considered.
- The quench front model is applied to the heater rods.

5.2.4 Results of the ATHLET Calculation

The figures 5 - 55 to 5 - 103 compare ATHLET results with the corresponding experimentally measured parameters for a variety of physical quantities. 'A:' denotes the ATHLET result, generally followed by the thermo-fluid or heat conduction object name and the index of the network element inside. 'E:' denotes the experimental result followed by the designation of the measurement. Table 5 - 4 lists the sequence of events of both the experiment and the ATHLET calculation.

Table 5 - 4: Sequence of events for ROSA-III test Run 916

Event	Measured time (s)	ATHLET
Break opening, MRP tripped	0	0
Closure of FW supply	1.6 - 3.2	1.6 - 3.2
L2 level trip signal (level < 4.76 m)	5.6	5.7
L1 level trip signal (level < 4.25 m)	10.3	10.8
Main steam line closure	7.5 - 12.2	7 - 12
Jet pump suction nozzle uncovery	13.4	13.6
Recirculation line nozzle uncovery	18	16
Dryout at top of the core	22	20
Lower plenum flashing	38	36
ADS actuation	131	130
FW line flashing	142	143
LPCS initiation	143	142
LPCI initiation	183	185

Figure 5 - 55 compares the pressure in the upper plenum, which is representative for all other pressure measurements. After the break has been initiated, the pressure decreases until the main steam valve is closed (at ca. 10 s). The following pressure increase is terminated by the uncovery of the broken loop main circulation line due to the low mixture level in the downcomer, leading to an increasing vapor flow through the break (see density at break, fig. 5 - 60). In the following time period till about 35 s, ATHLET overestimates the pressure drop, which can be explained by a too early transition to vapor flow at the MRP side of the break (fig. 5 - 61) and a slightly too low density at the RV side of the break (fig.5 - 60). In addition, the dryout of the top core region is overestimated (e.g. figs. 5 - 96 and 5 - 100) which reduces the steam production there. In the time period until about 100 s, the calculated pressure approaches the measurement. Around 140 s, the feedwater injection line starts to flash and the LPCS injection is initiated which reduces the depressurization.

The figures 5 - 56 to 5 - 58 show the total break mass flow and the contributions from the RV and the MRP side of the break. Although the density at the MRP side of the break as well as the differential pressure across the BL MRP are overestimated by ATHLET (figs. 5 - 61 and 5 - 72), the break mass flow from the MRP side seems to be underestimated. A good agreement between calculation and measurement can be stated for the main steam mass flow in fig. 5 - 59.

The fluid densities at the jet pump exits and upstream of the break are presented in figs. 5 - 60 to 5 - 63. At the jet pump exits, the calculation corresponds well with the experiment until 200s, after that the density increase due to the ECC injection (LPCS and LPCI) is clearly overpredicted. As already mentioned, ATHLET calculates the first appearance of steam at the pump

side of the break about 10 s too early. Between 40 and 160 s and once again after 250 s, the calculated density is clearly higher than the measured value.

During operational conditions, i.e. before the opening of the break, the pressure differences depend on the mass inventory as well as the flow losses. Since the mass inventory is well known at that time, a good consistency between calculation and experiment proves that the flow loss coefficients are correctly supplied. After the main recirculation pumps have been switched off, the pressure differences across vertical sections indicate mainly the liquid inventory (except near the leak).

The figs. 5 - 64 to 5 - 78 compare the pressure differences across various parts of the pressure vessel and the recirculation loops. In general, the ATHLET results correspond very well with the measurements, in several locations even excellently. For example, the pressure difference between the lower and the upper plenum (including the core) is exactly calculated (fig. 5 - 64) proving that the total liquid inventory in the RV is correctly calculated.. This is pointed out here because the calculated fuel rod cladding temperatures indicate a wrong liquid inventory in that section or at least a wrong liquid distribution within the core (s. below).

Major differences between calculation and experiment can be observed for the pressure differences from the jet pump drives to suctions (figs. 5 - 68 and 5 - 70). Under steady state conditions, the comparison is difficult since there are strong pressure gradients in the vicinity of the jet pump nozzles which, of course, are not resolved by the ATHLET discretization. During the transient, the deviation for the IL jet pump, which is nearly constant in time, seems to be caused by a measurement bias, whereas for the BL jet pump, the deviation may be caused by a too low mass flow towards the break (fig. 5 - 58).

Altogether, the comparison of the pressure differences demonstrates that the steady state flow losses as well as the liquid distribution during the transient are calculated well by ATHLET.

The figures 5 - 79 to 5 - 87 compare the calculated liquid and vapor temperatures with the measured fluid temperatures. As long as there is no vapor (liquid) in an ATHLET control volume, the vapor (liquid) temperature equals the saturation temperature. In general, both the calculated and measured fluid temperatures are close to the saturation values. Subcooled liquid can be observed only during the initial phase of the transient in the lower downcomer and lower plenum due to the injection of subcooled feedwater, and after the start of the ECC injection into the upper plenum and the core bypass. The latter is clearly overpredicted by ATHLET (e.g. fig. 5 - 84), what indicates that the calculated condensation rates during ECC injection are too low. Even in the lower plenum (fig. 5 - 79), ATHLET calculates subcooled ECC water whereas in the experiment all liquid temperatures remain close to saturation. Superheated vapor appears in pure vapor areas due to heat-up by the fuel bundles (e.g. fig. 5 - 86) or by hot structures (e.g. fig. 5 - 81).

Comparing the calculated and the measured fluid temperatures, one has to consider that the measurement shows the temperature history in a small spatial area (e.g. a sub-channel in the core) whereas ATHLET supplies values averaged over the entire control volume which represents - for example - not only the complete core channel flow area but even a finite axial range. Strong spatial temperature gradients in the core region or in the vicinity of the ECC injection points complicate the comparison between the calculation and the experiment.

The figures 5 - 88 to 5 - 103 show the cladding temperature of each an average and a hot rod in the hot channel box A (`HV-ROD2x`) and the channel boxes B, C, D (`HV-ROD1x`) at the axial positions 2 (close to top of core) to 6 (close to bottom of core). The figures point out that the liquid inventory and distribution in the core is not exactly calculated by ATHLET, although the pressure difference between the upper and lower plenum agrees excellently with the experiment (fig. 5 - 64). Within the first 50 s after the break, an early dry-out and rewetting is calculated in the top core region, in contrast to the experiment (e.g. fig. 5 - 88). At ca. 65 s, dry-out starts in the experiment at top of the core and propagates down through the core. Only for the hot rods in pos. 2 the ATHLET results agree well with the experiment. For lower positions the dry-out is calculated late and the cladding temperatures are clearly underestimated.

Finally, the figs 5 - 104 to 5 - 106 document the performance of the ATHLET simulation concerning numerical effort and conservation of the coolant mass balance. No numerical problems appeared and the maximum mass error of ca. 0.5 kg is negligible compared to the initial mass inventory of about 775 kg.

Summarizing the comparison of the ATHLET calculation with the experimental results, it can be stated that, in general, the calculated hydraulic parameters show a good, some of them even excellent agreement with the measurements. The main deviations concern the fuel cladding temperatures, in particular in the lower core region, which are underpredicted due to a too large liquid inventory in the core.

5.2.5 Figures

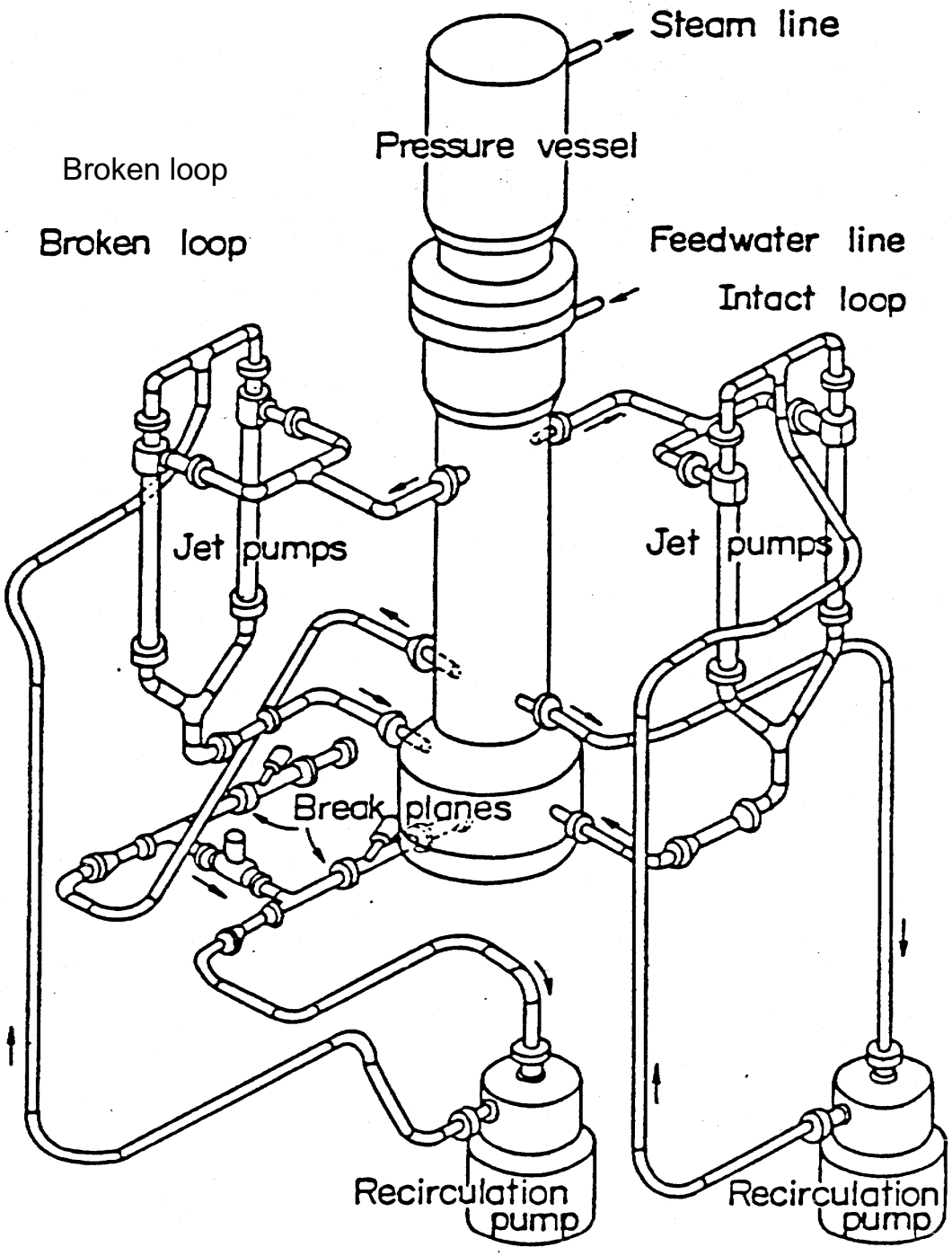

Fig. 5 - 53: Test Facility ROSA III Run 916

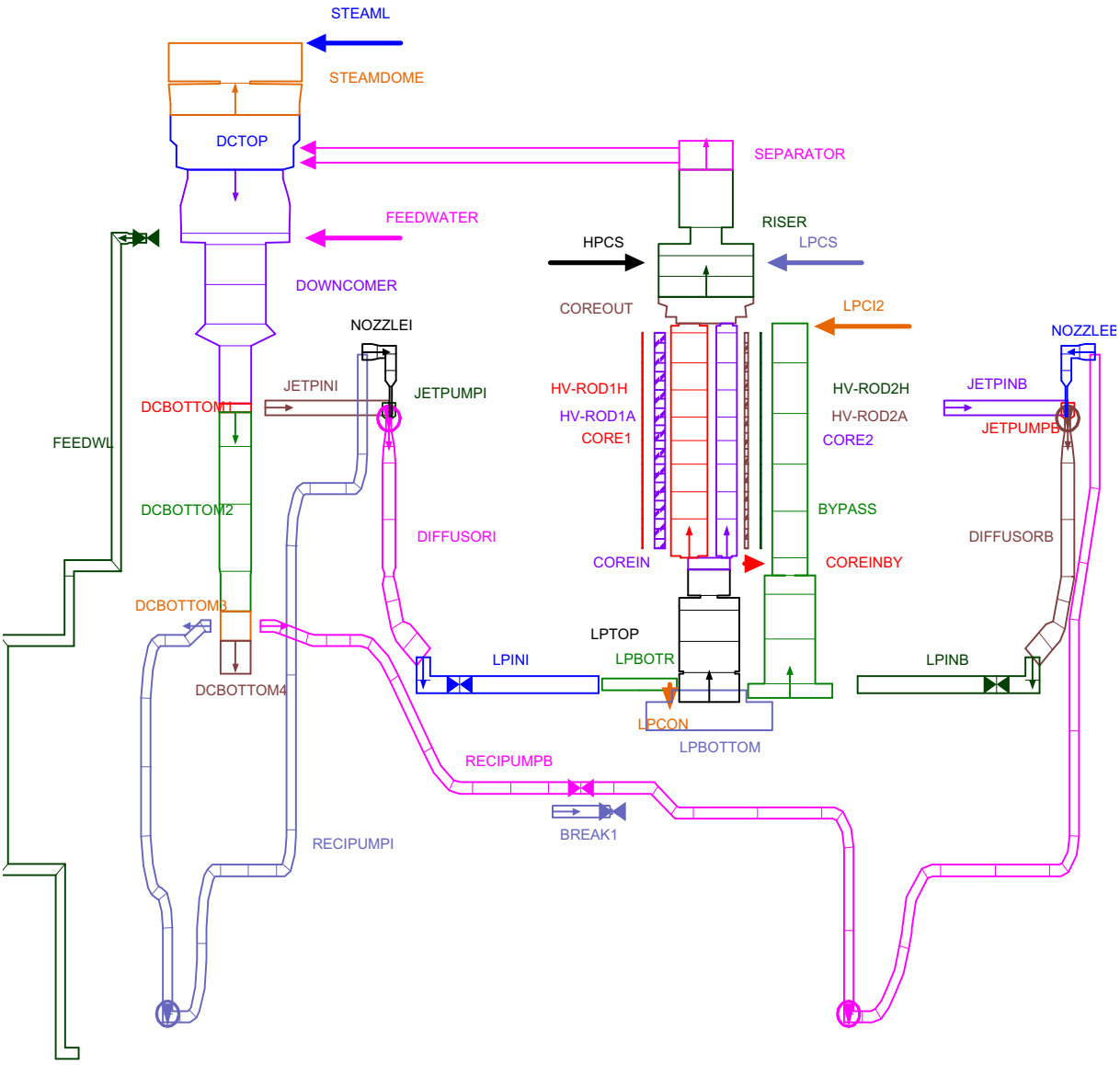

Fig. 5 - 54: Nodalization of ROSA III for ATHLET

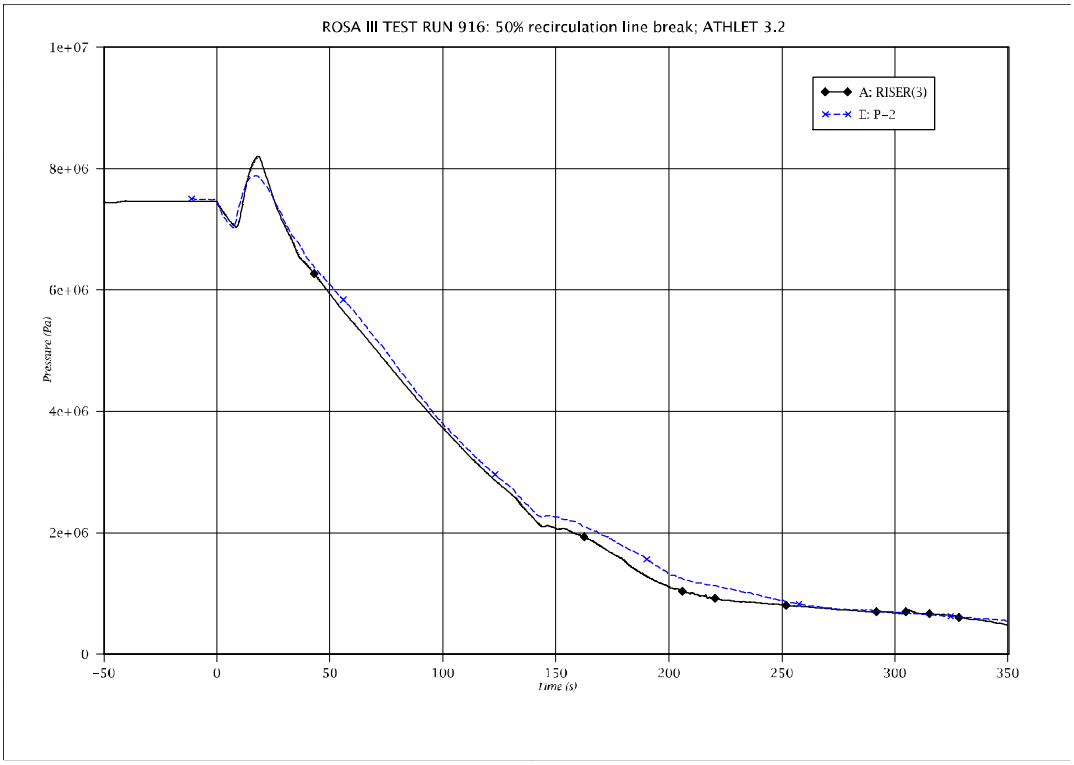

Fig. 5 - 55: Pressure in upper plenum

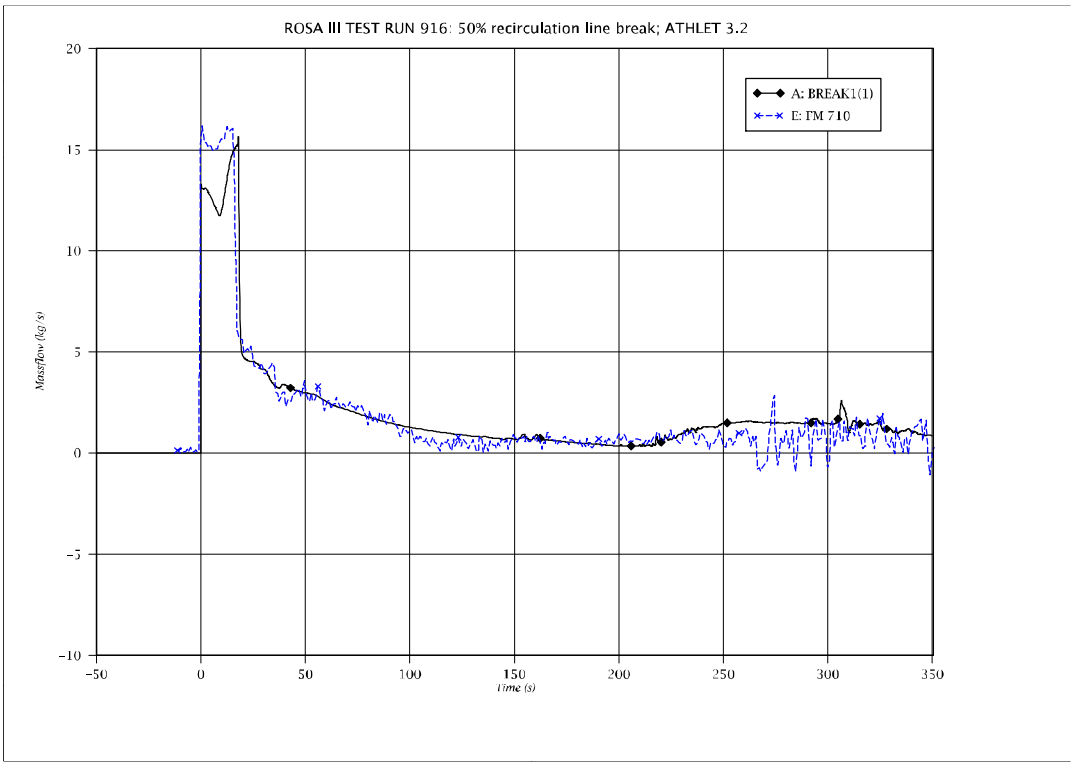

Fig. 5 - 56: Total break mass flow

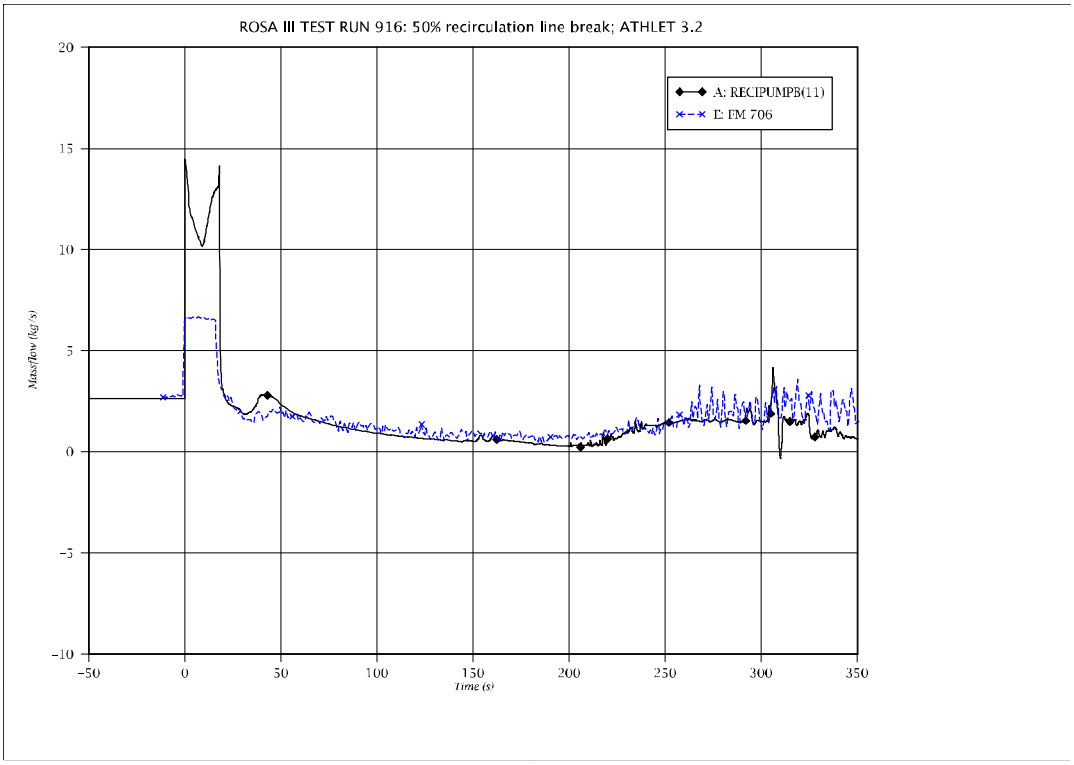

Fig. 5 - 57: Mass flow at PV side of break (low range measurement)

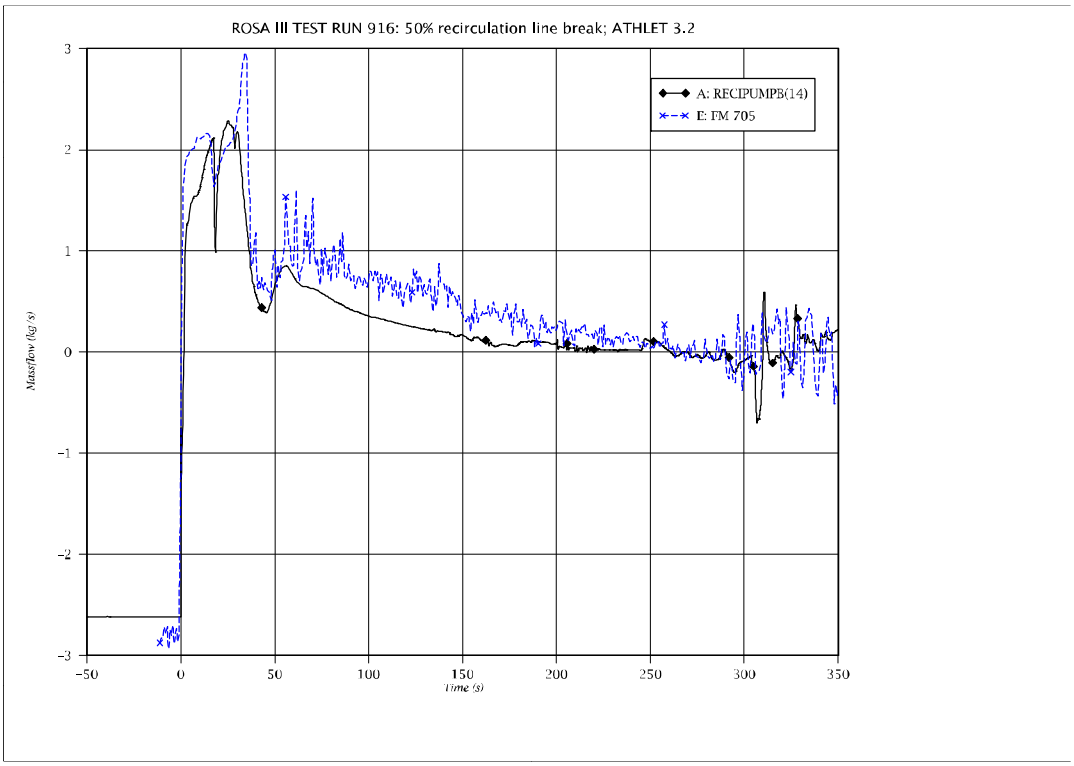

Fig. 5 - 58: Mass flow at MRP side of break (low range measurement)

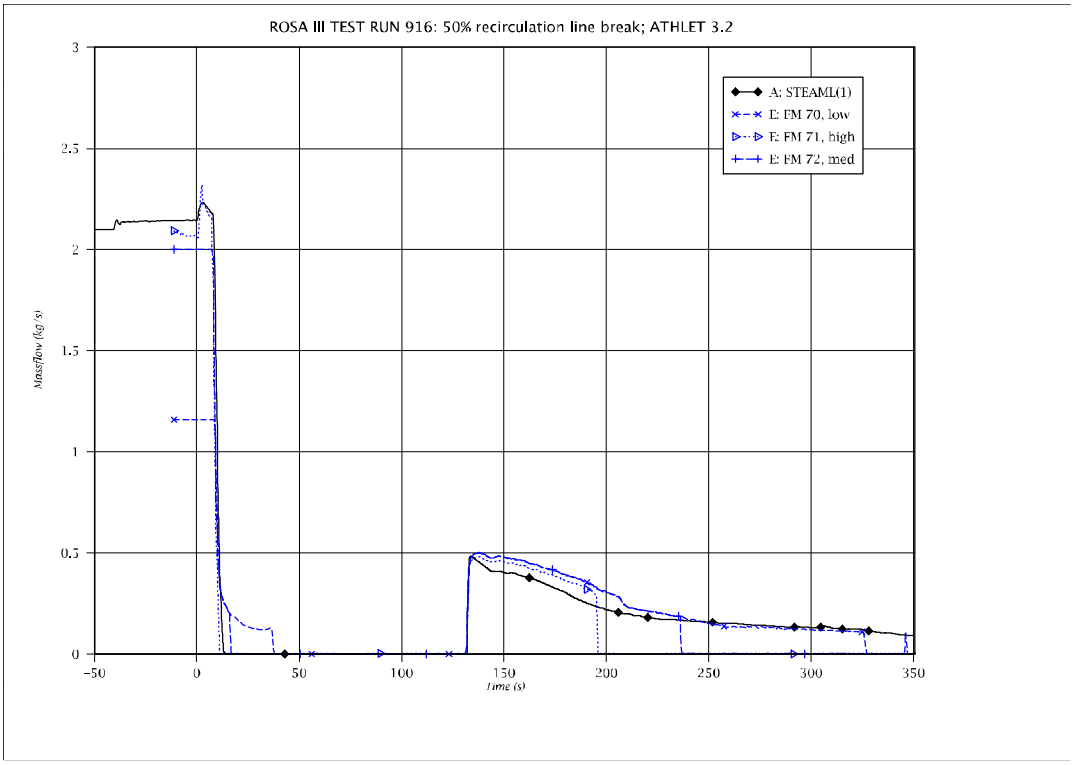

Fig. 5 - 59: Mass flow in main steam line

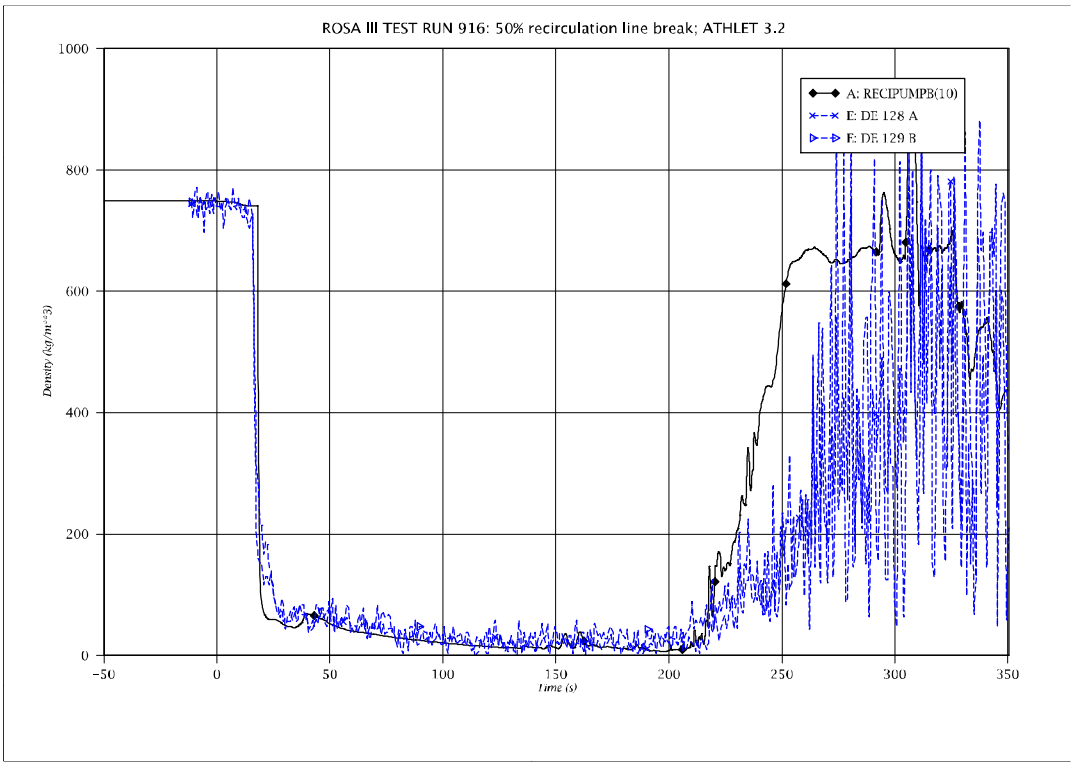

Fig. 5 - 60: Fluid density at break (RV side)

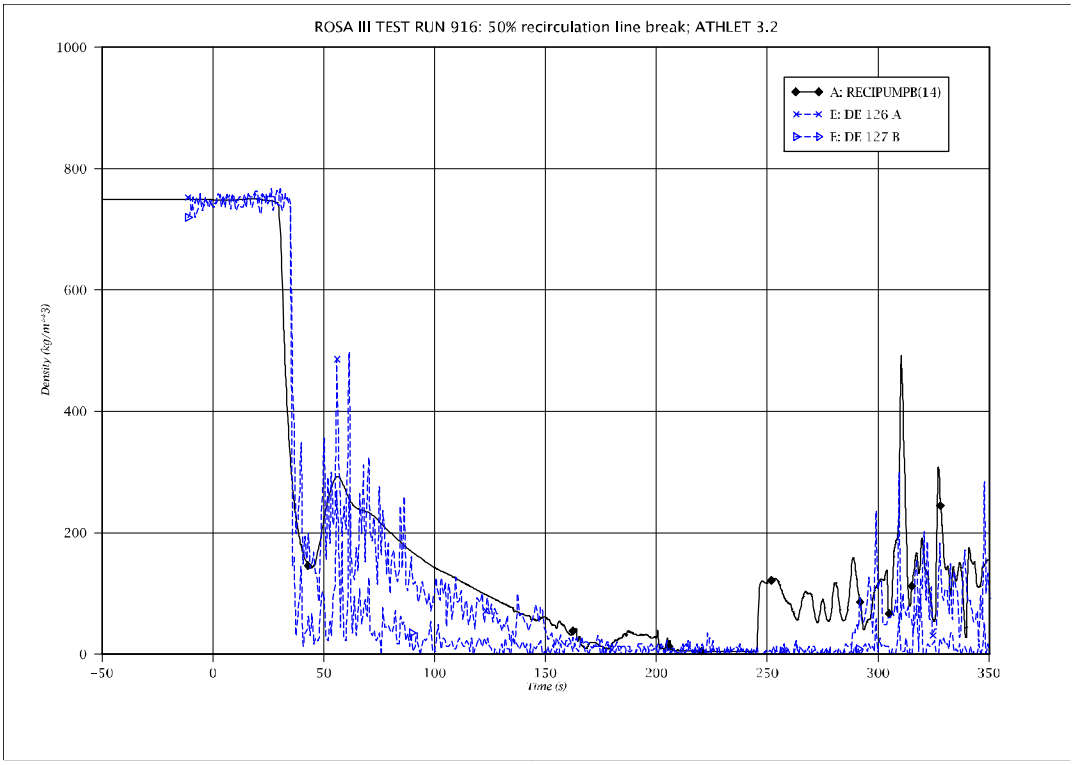

Fig. 5 - 61: Fluid density at break (MRP side)

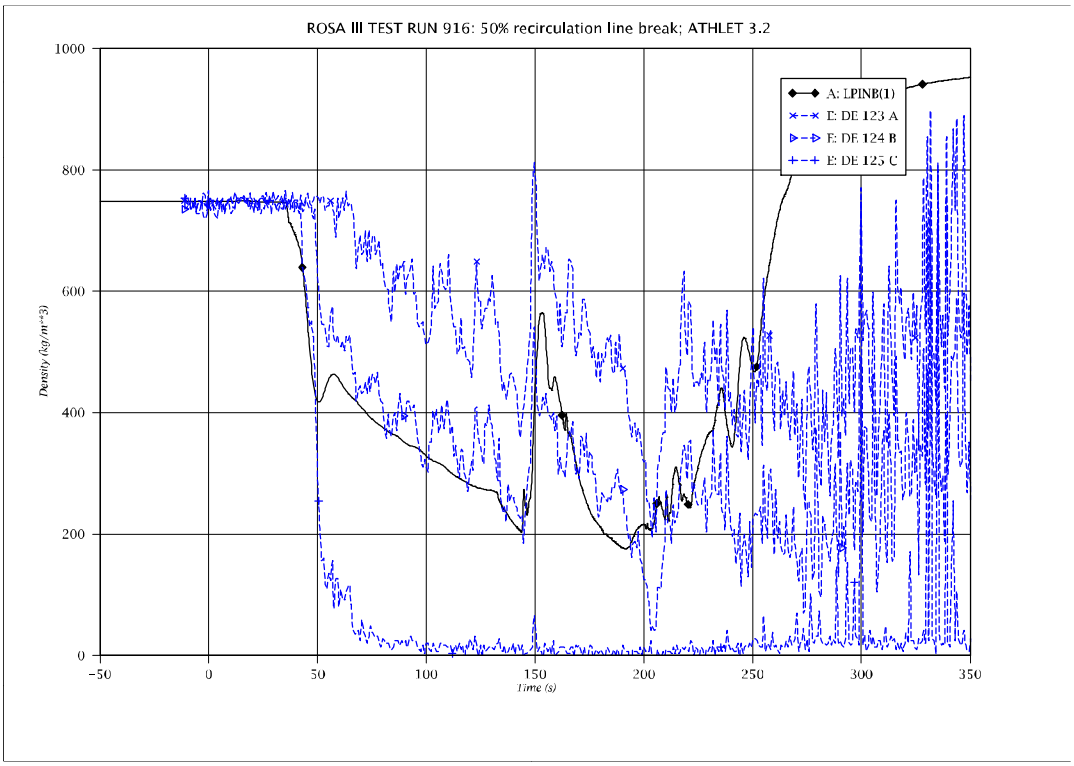

Fig. 5 - 62: Fluid density at BL jet pump exit

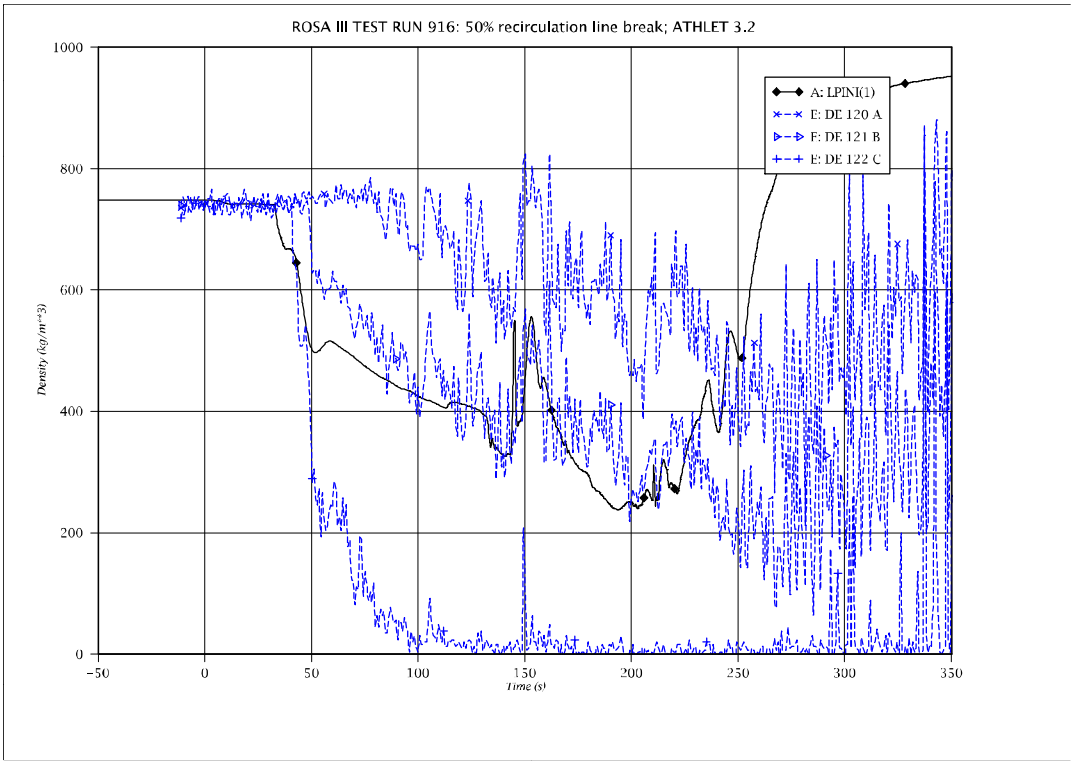

Fig. 5 - 63: Fluid density at IL jet pump exit

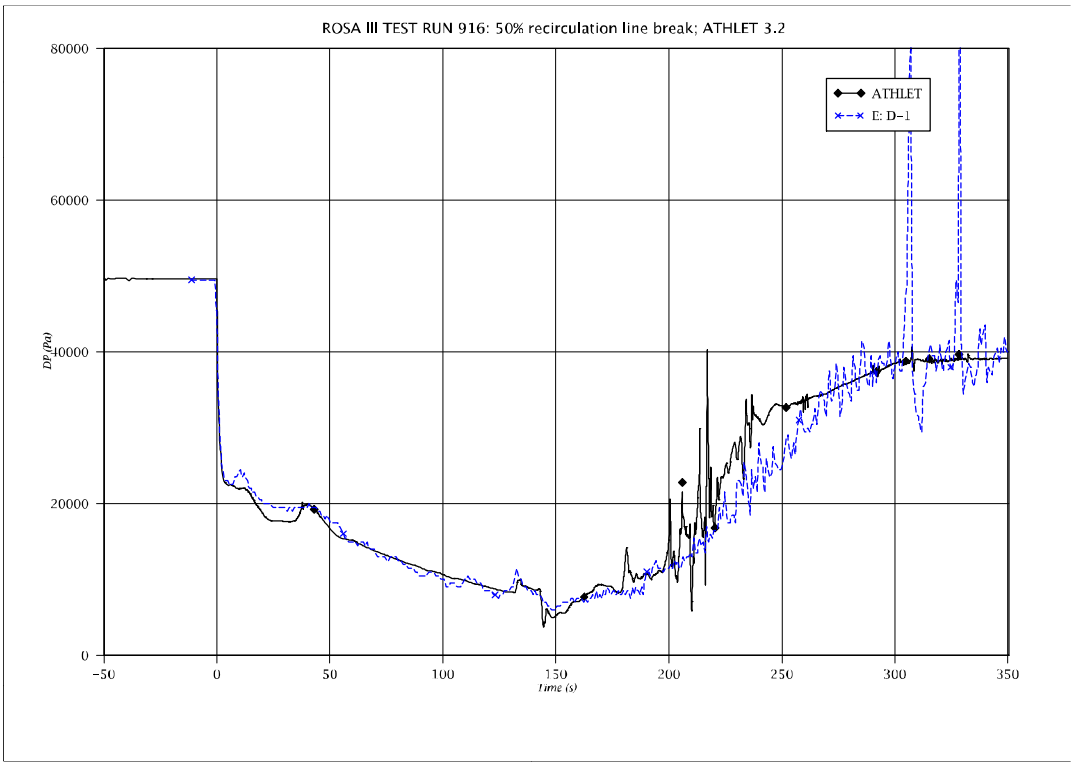

Fig. 5 - 64: Differential pressure between lower and upper plenum

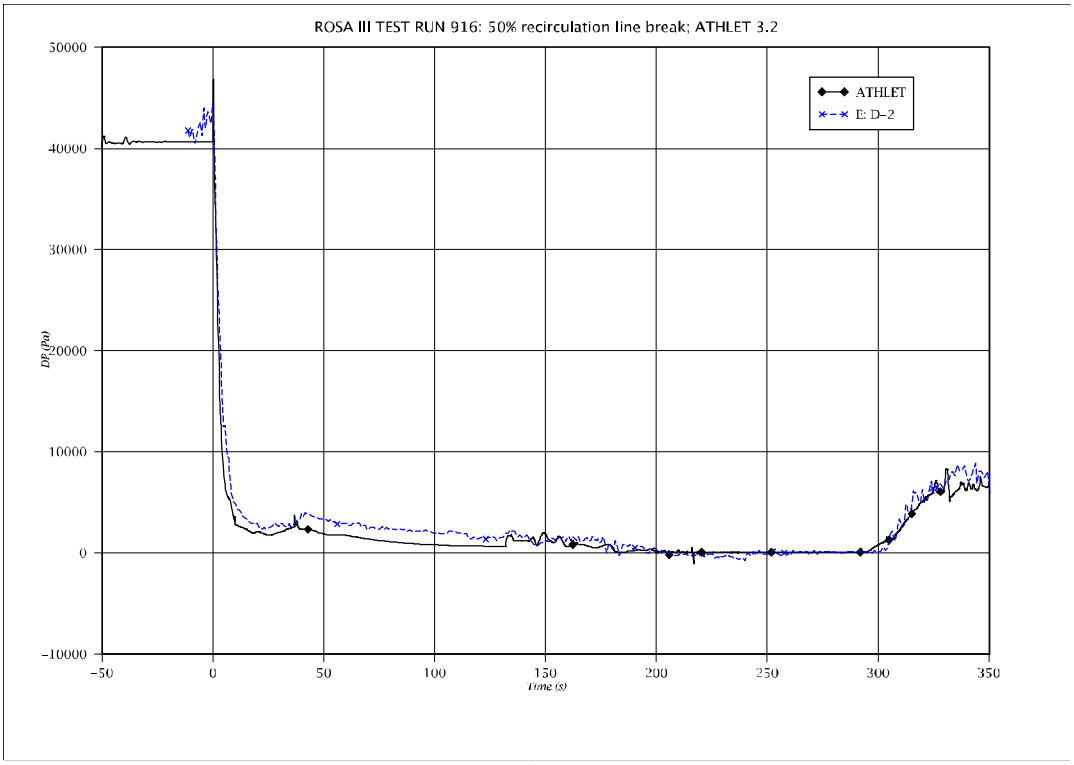

Fig. 5 - 65: Differential pressure between upper plenum and PV top

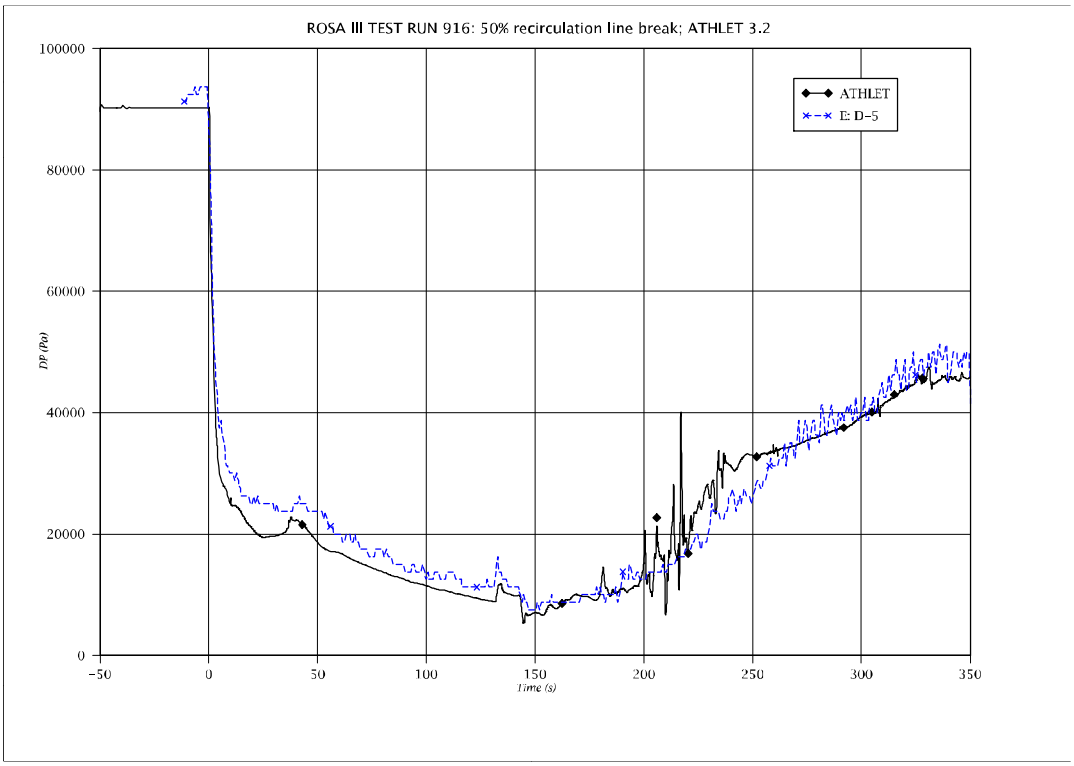

Fig. 5 - 66: Differential pressure between lower plenum and PV top

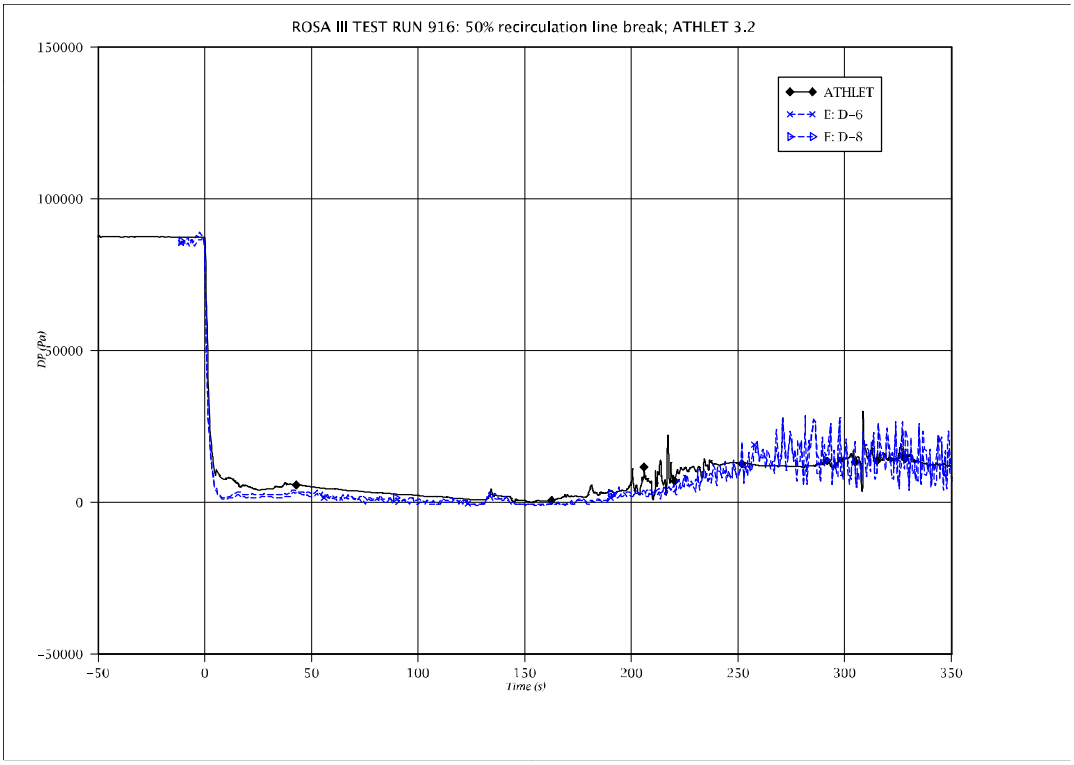

Fig. 5 - 67: Differential pressure IL jet pump discharge to suction

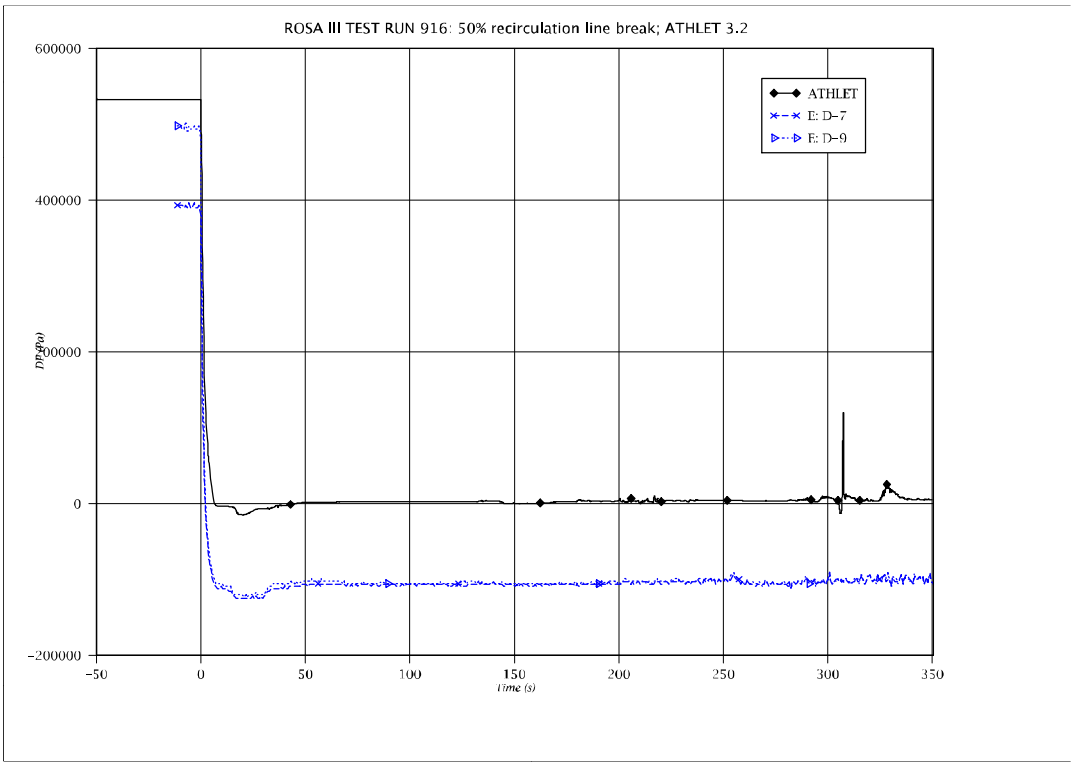

Fig. 5 - 68: Differential pressure IL jet pump drive to suction

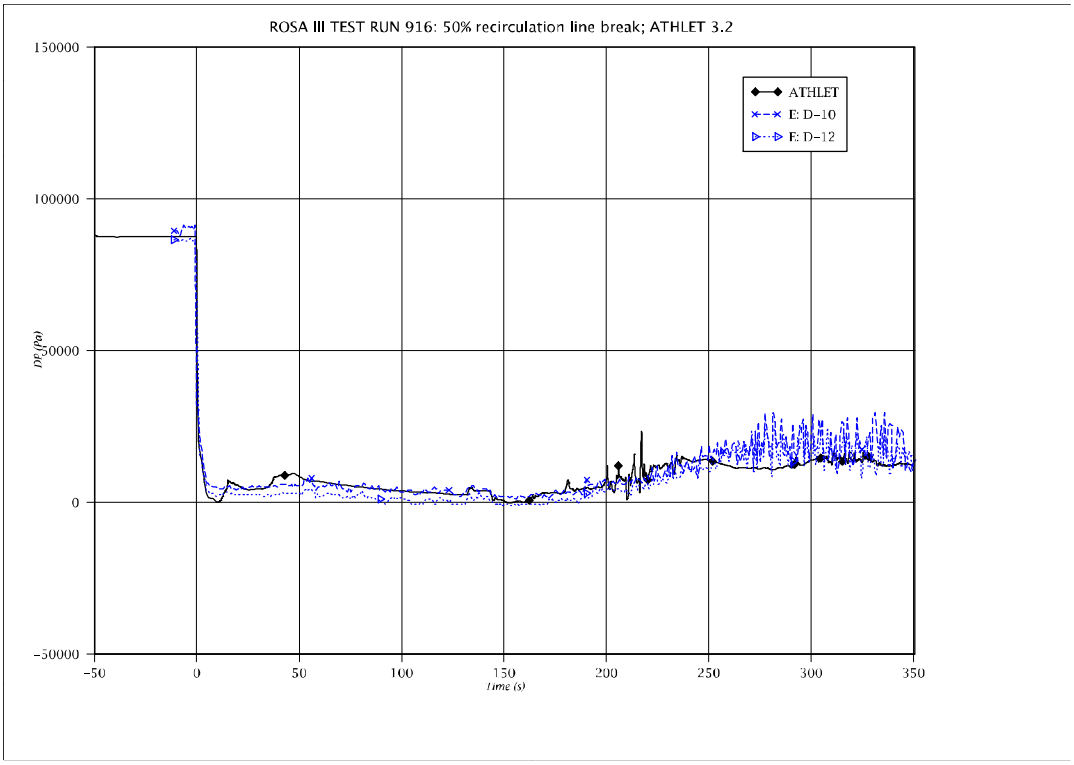

Fig. 5 - 69: Differential pressure BL jet pump discharge to suction

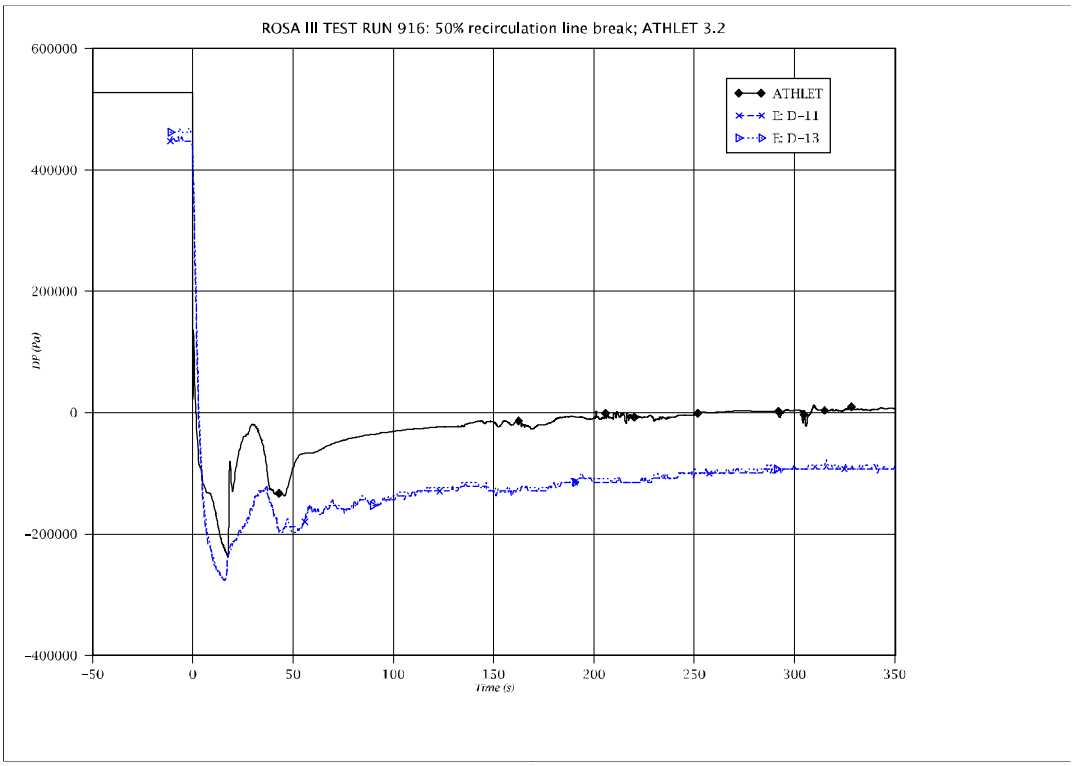

Fig. 5 - 70: Differential pressure BL jet pump drive to suction

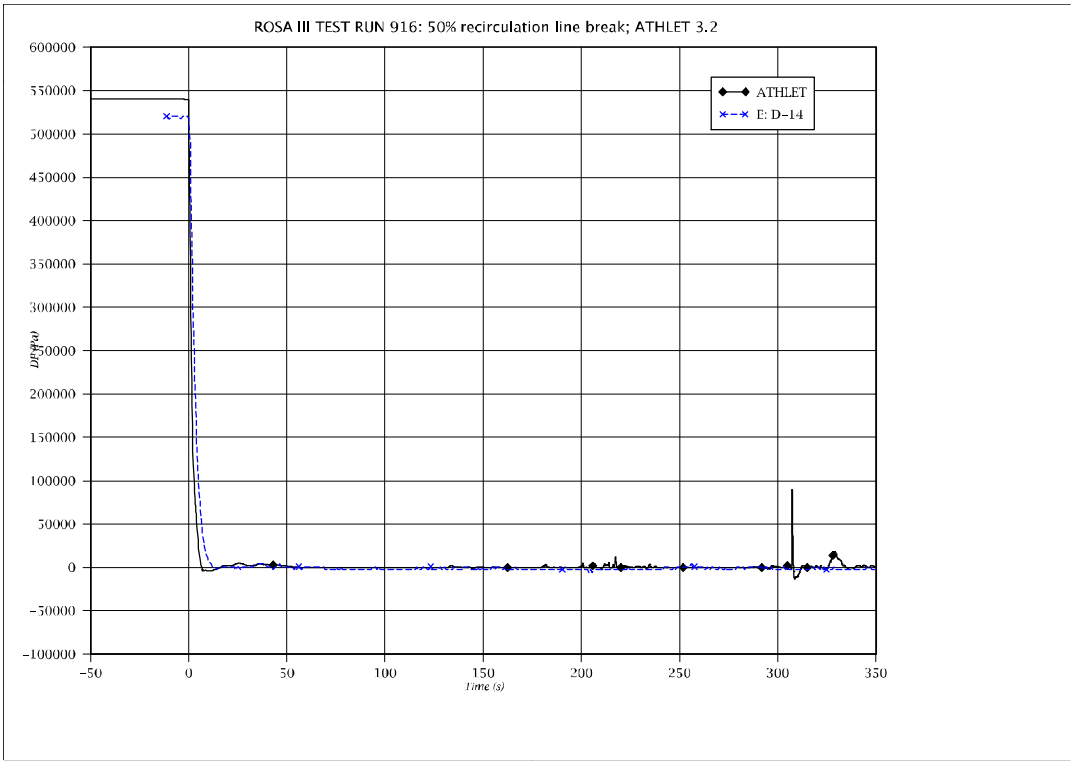

Fig. 5 - 71: Differential pressure across IL MRP

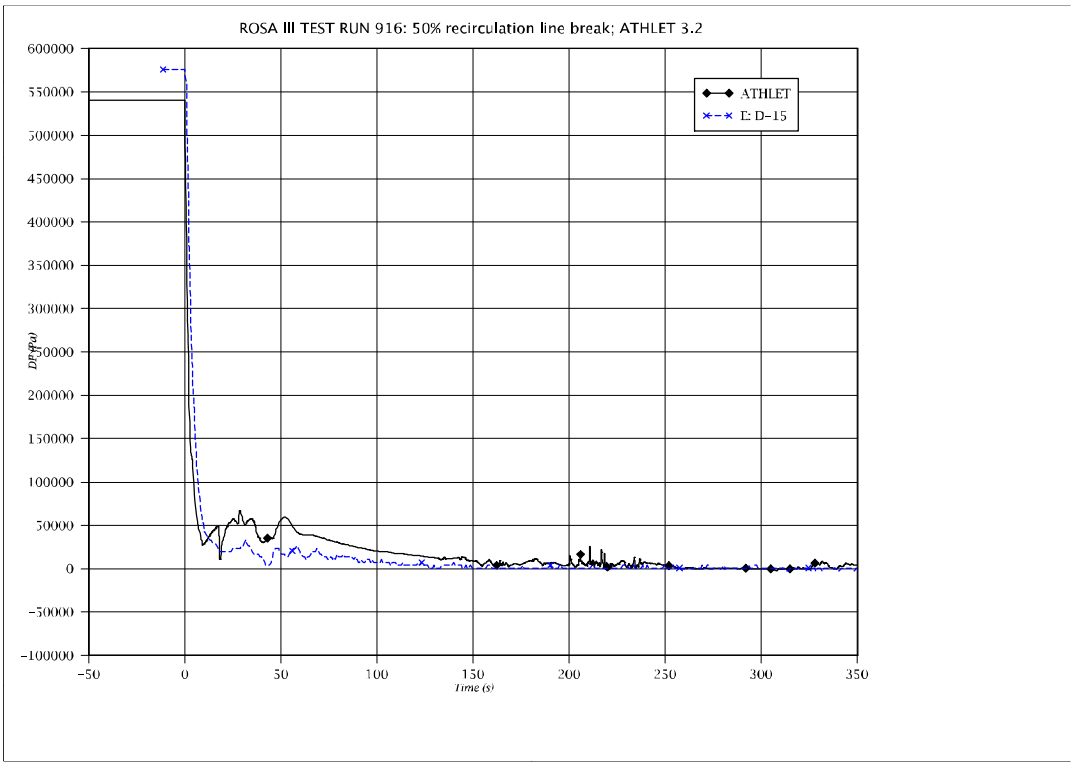

Fig. 5 - 72: Differential pressure across BL MRP

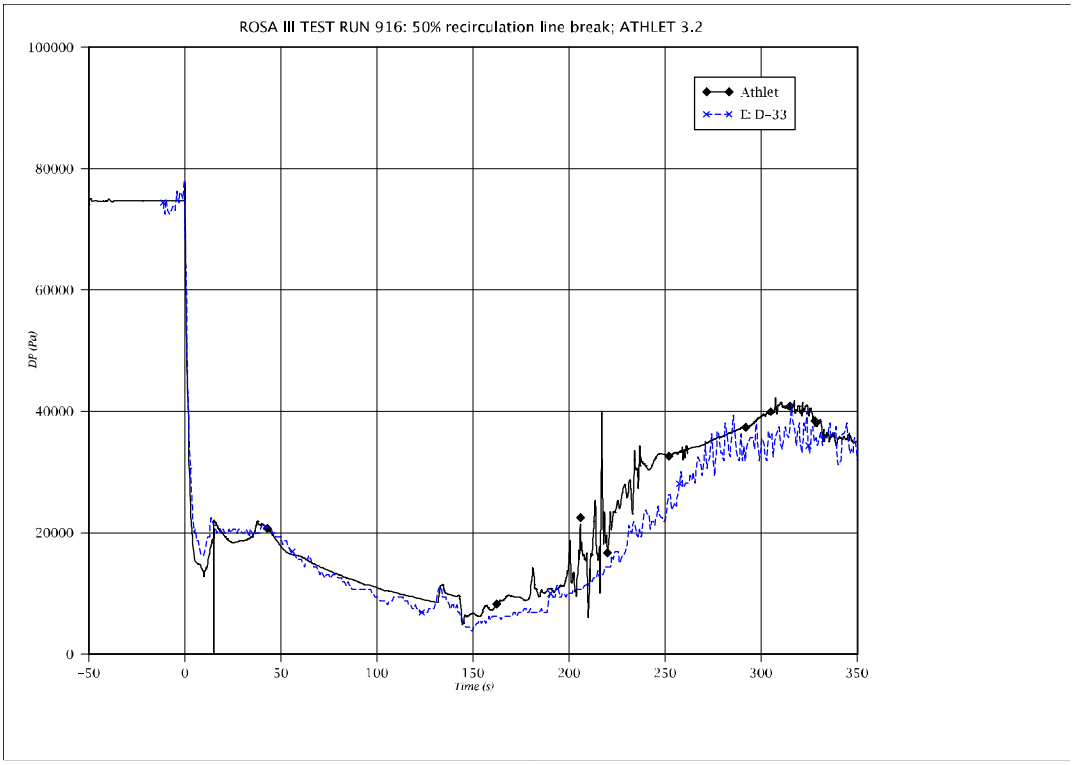

Fig. 5 - 73: Differential pressure between lower plenum and DC middle

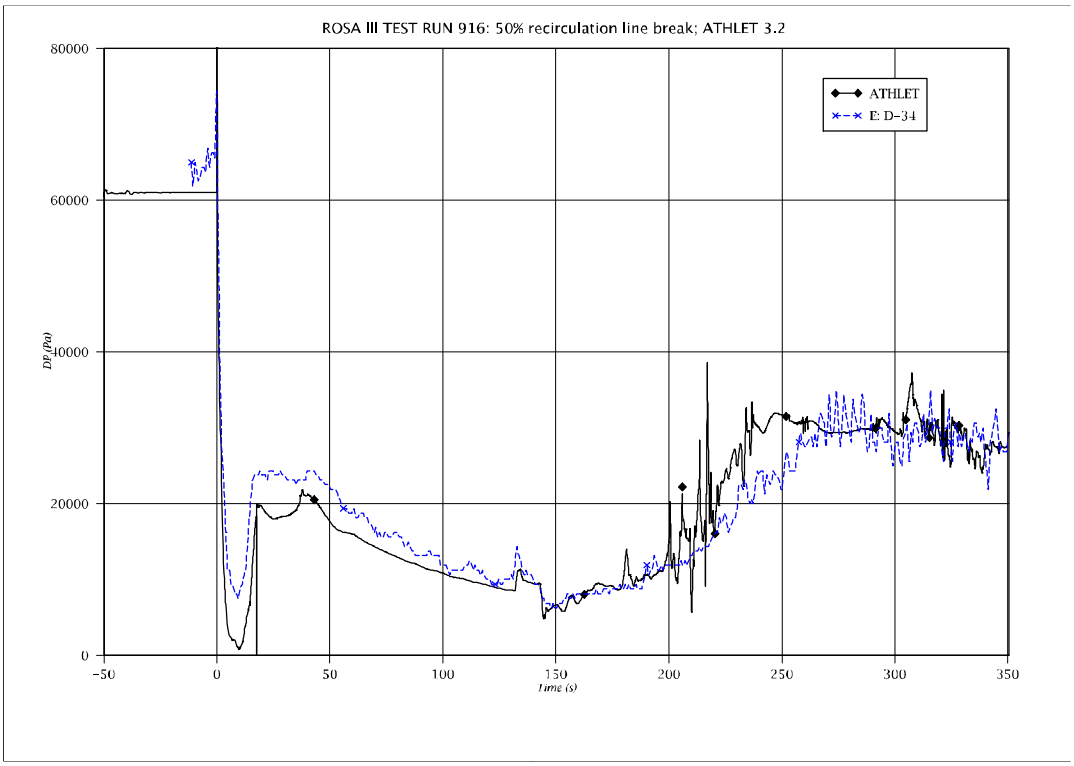

Fig. 5 - 74: Differential pressure between lower plenum and DC bottom

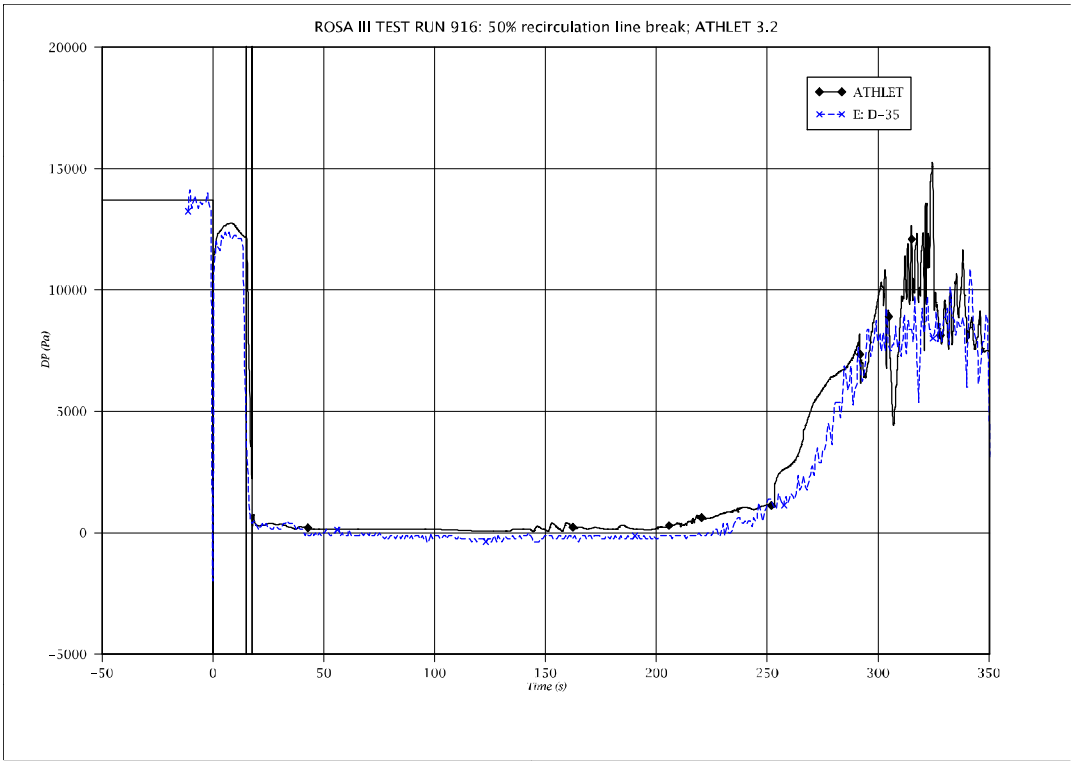

Fig. 5 - 75: Differential pressure between DC bottom and DC middle

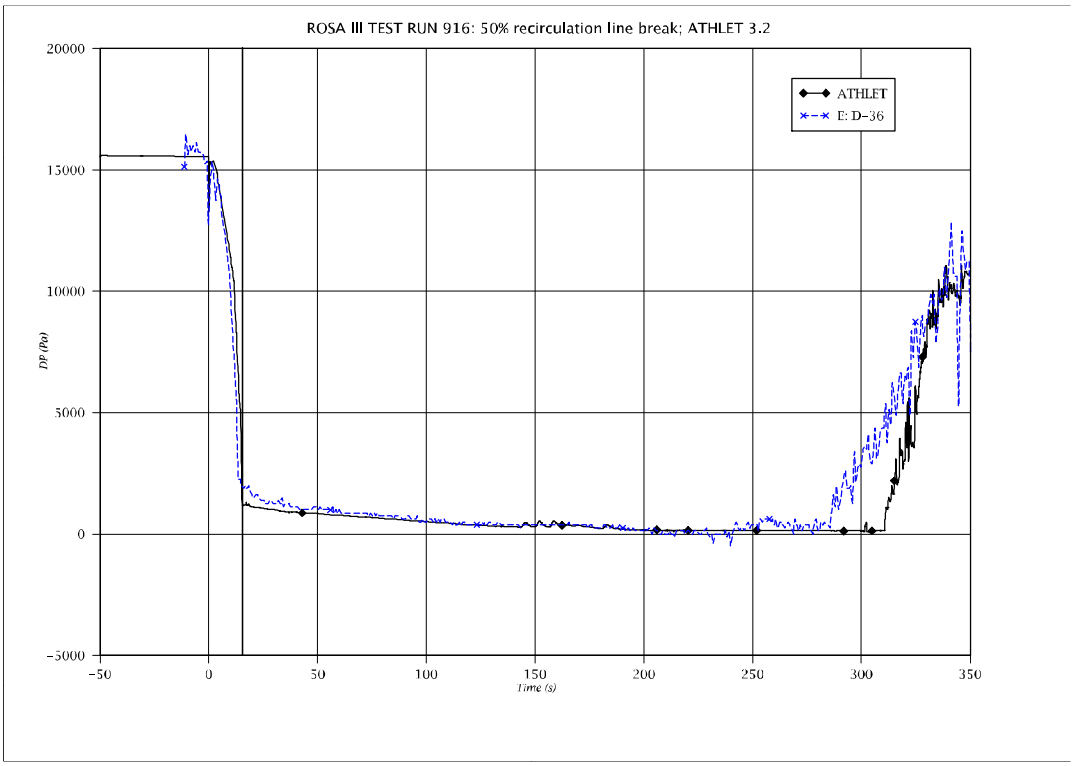

Fig. 5 - 76: Differential pressure between DC middle an PV top

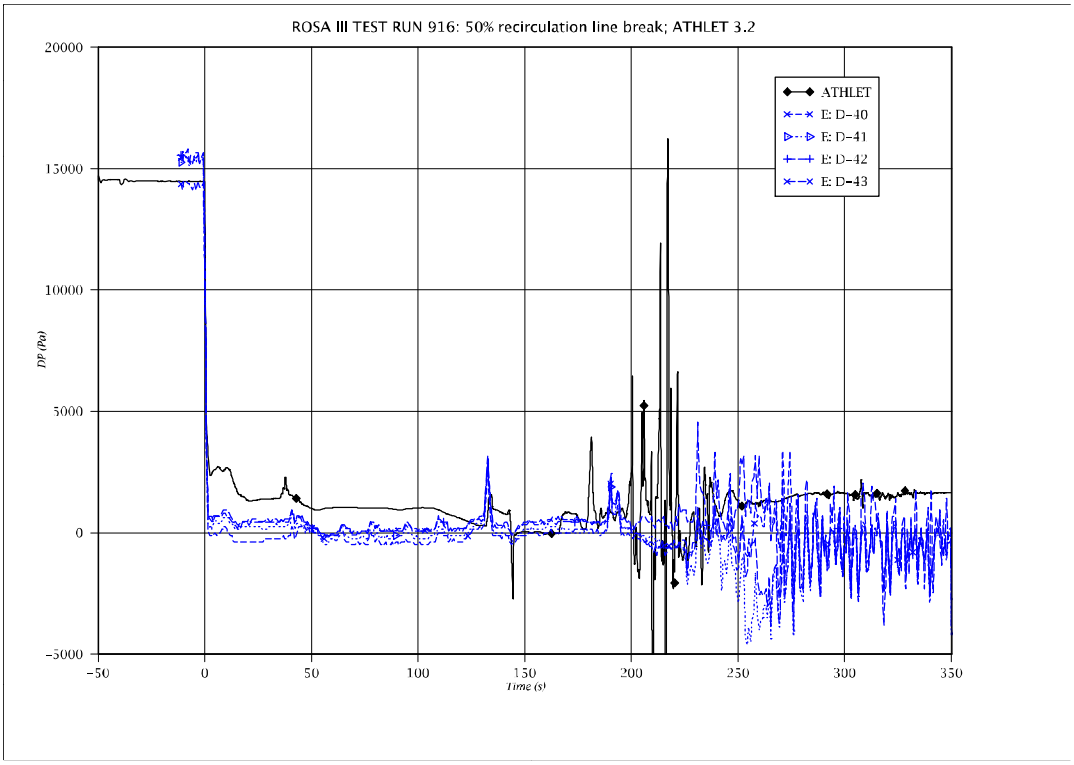

Fig. 5 - 77: Differential pressure across channel inlet orifice

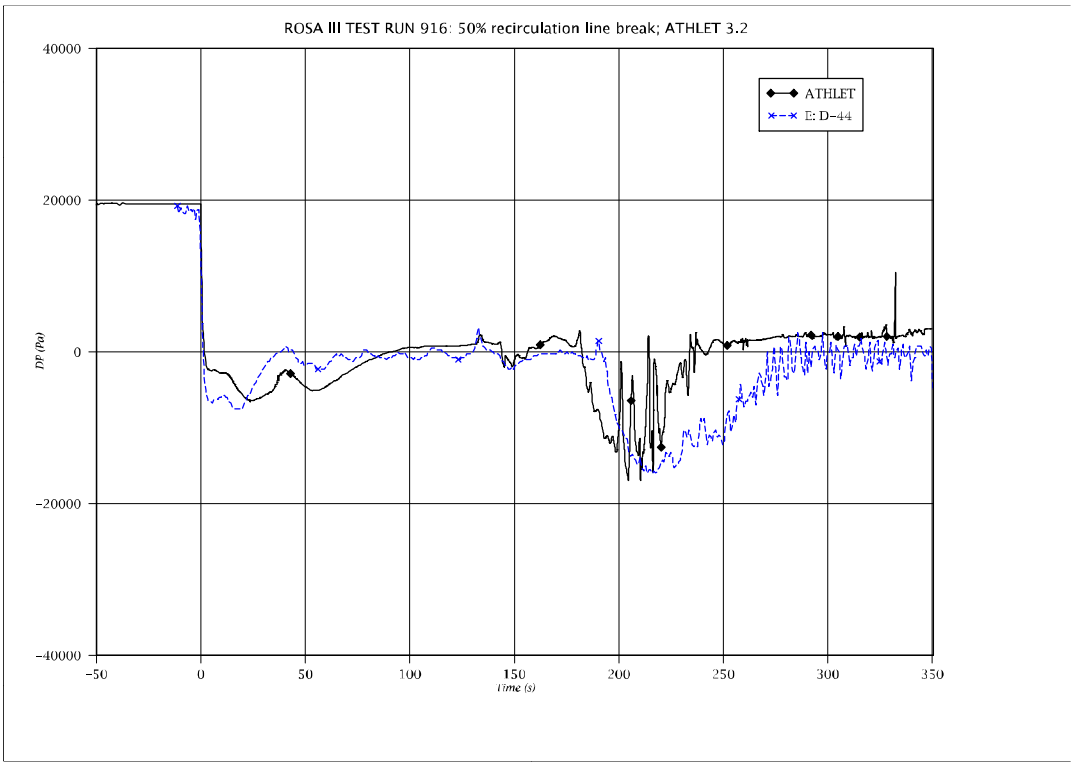

Fig. 5 - 78: Differential pressure across bypass hole

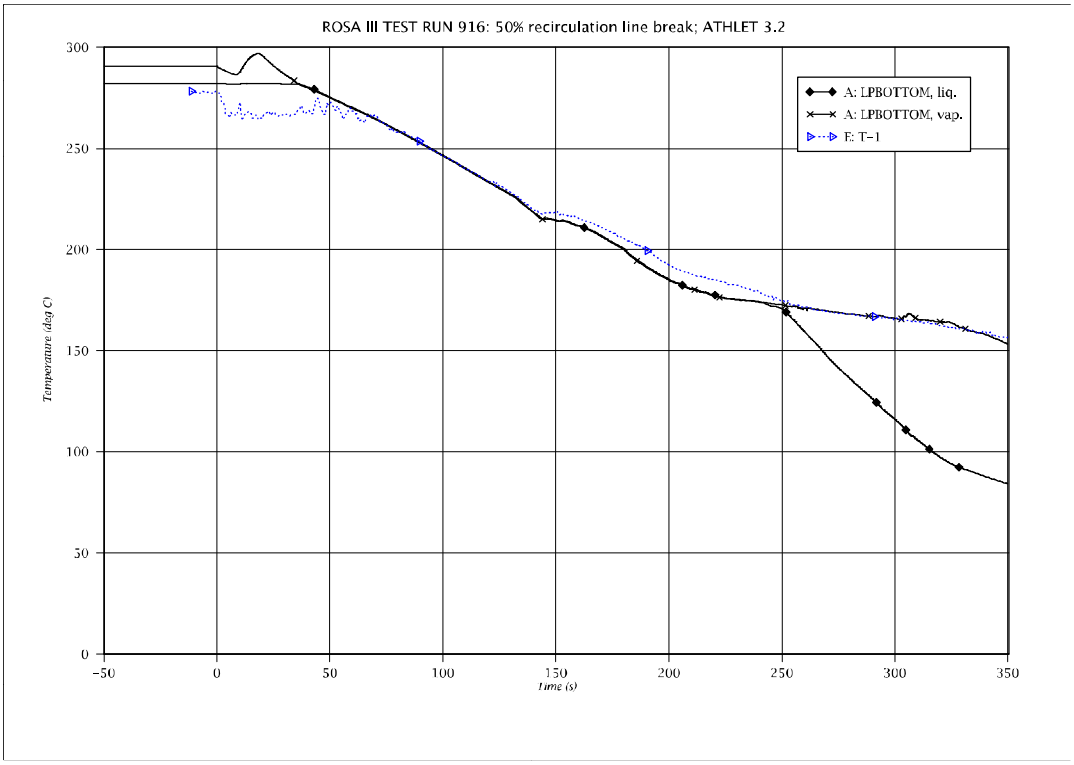

Fig. 5 - 79: Fluid temperature in lower plenum

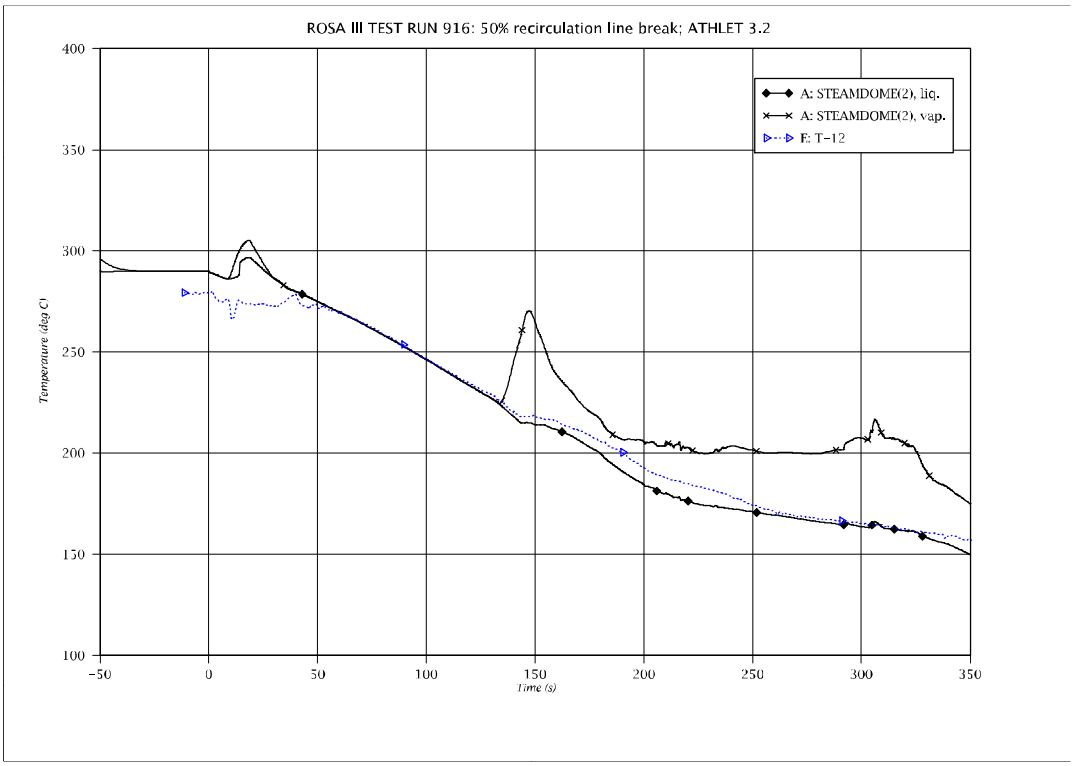

Fig. 5 - 80: Fluid temperature in steam dome

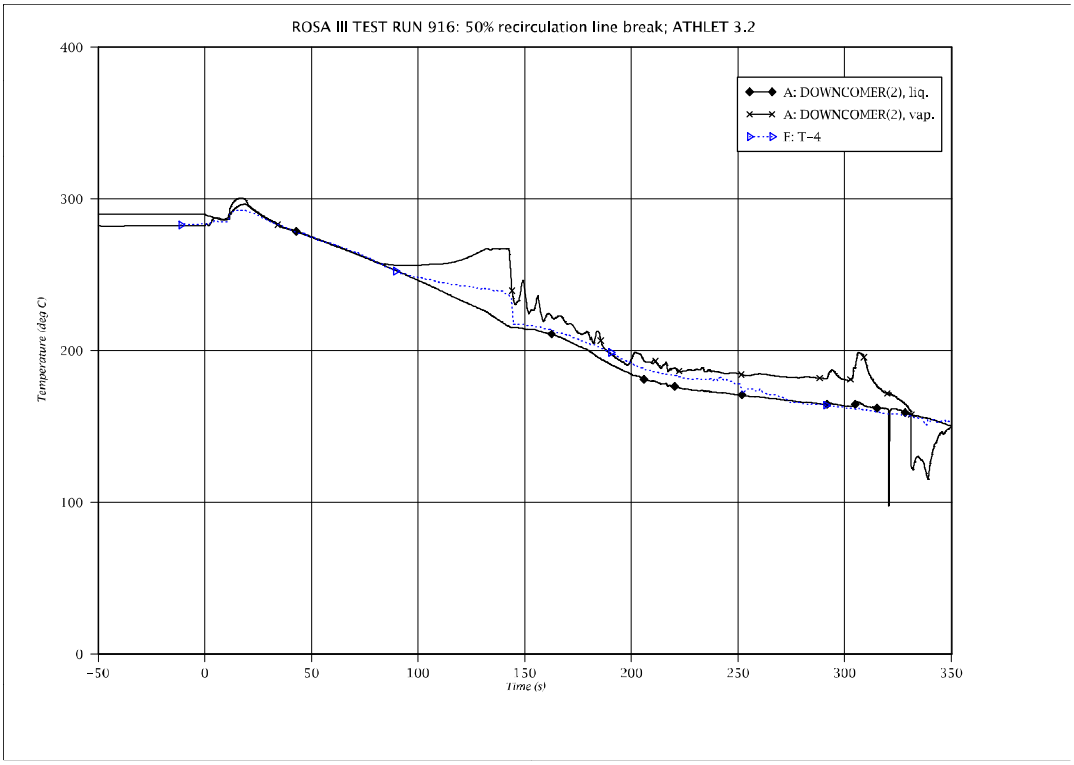

Fig. 5 - 81: Fluid temperature in upper DC

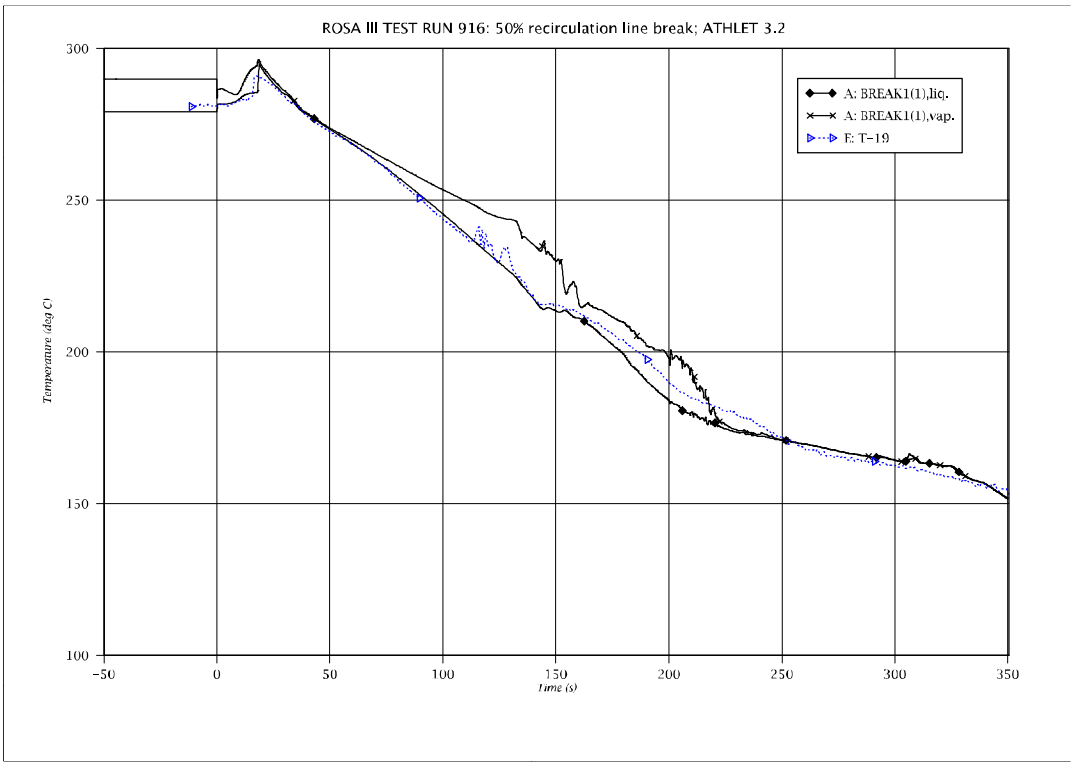

Fig. 5 - 82: Fluid temperature upstream of break

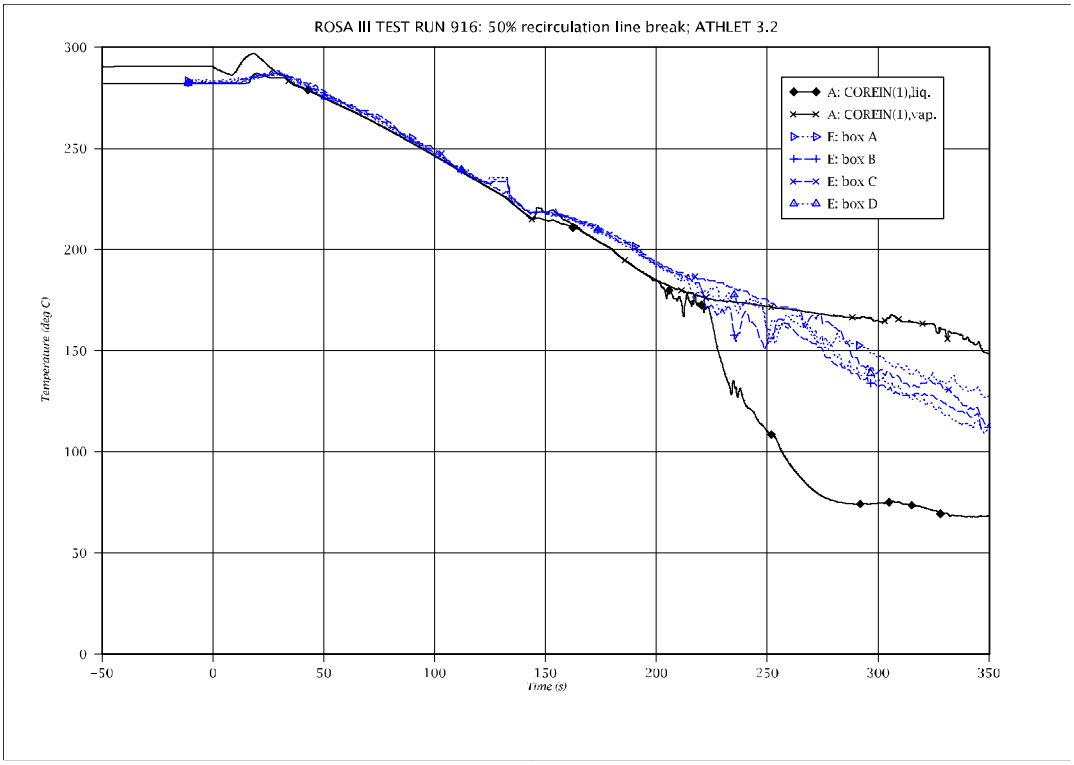

Fig. 5 - 83: Fluid temperature at core channel inlet boxes

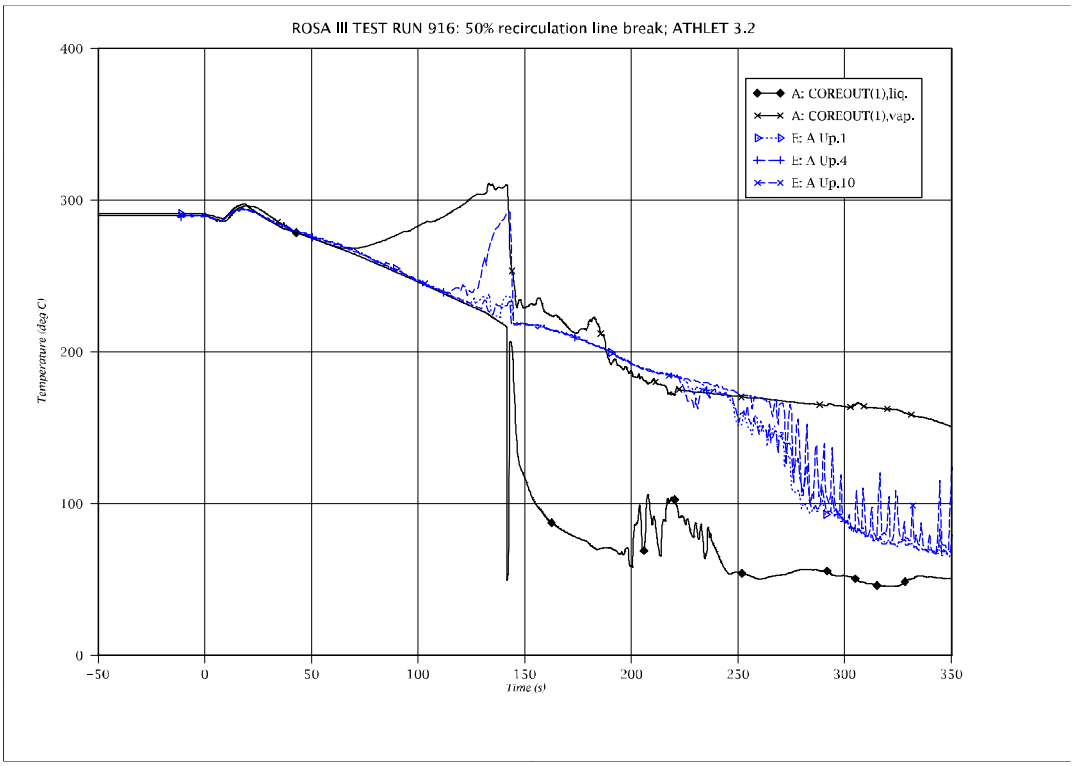

Fig. 5 - 84: Fluid temperature above tie plate

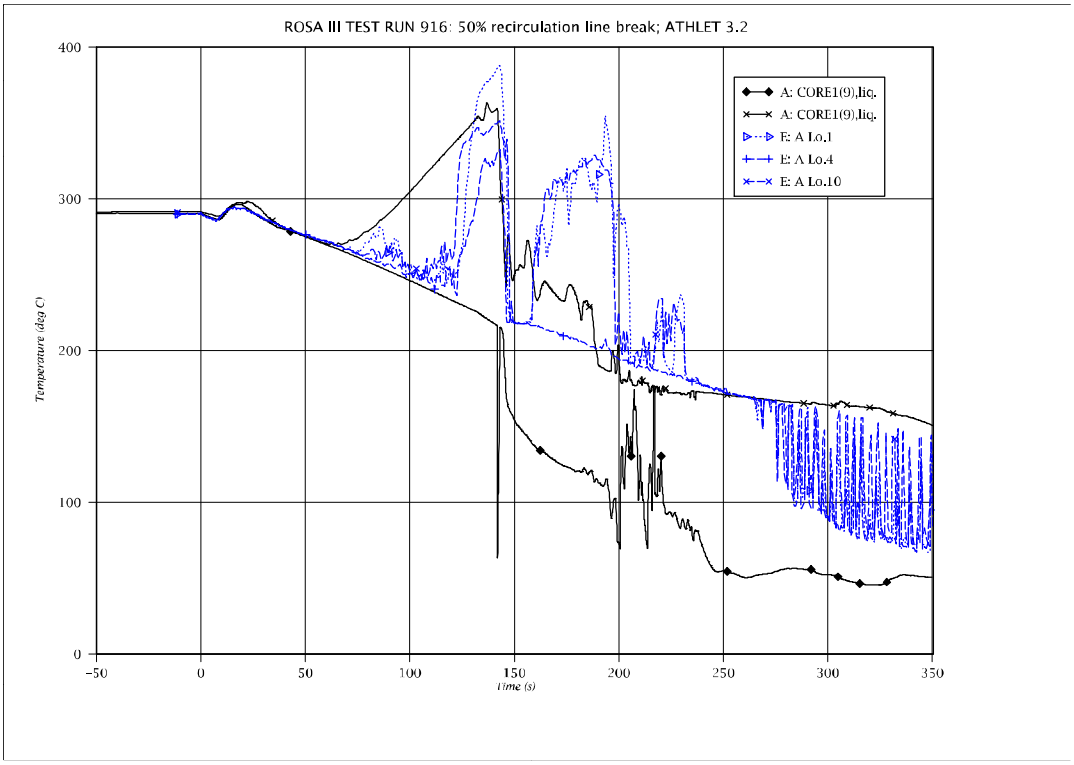

Fig. 5 - 85: Fluid temperature below tie plate

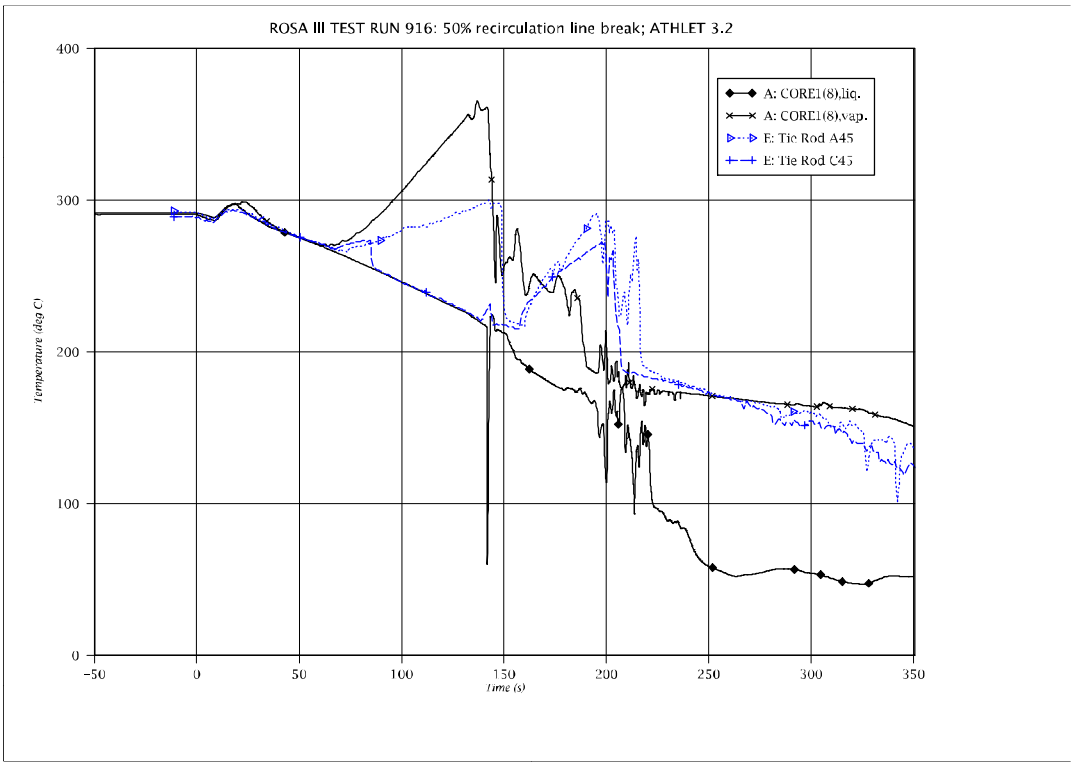

Fig. 5 - 86: Fluid temperature in the core (level 1)

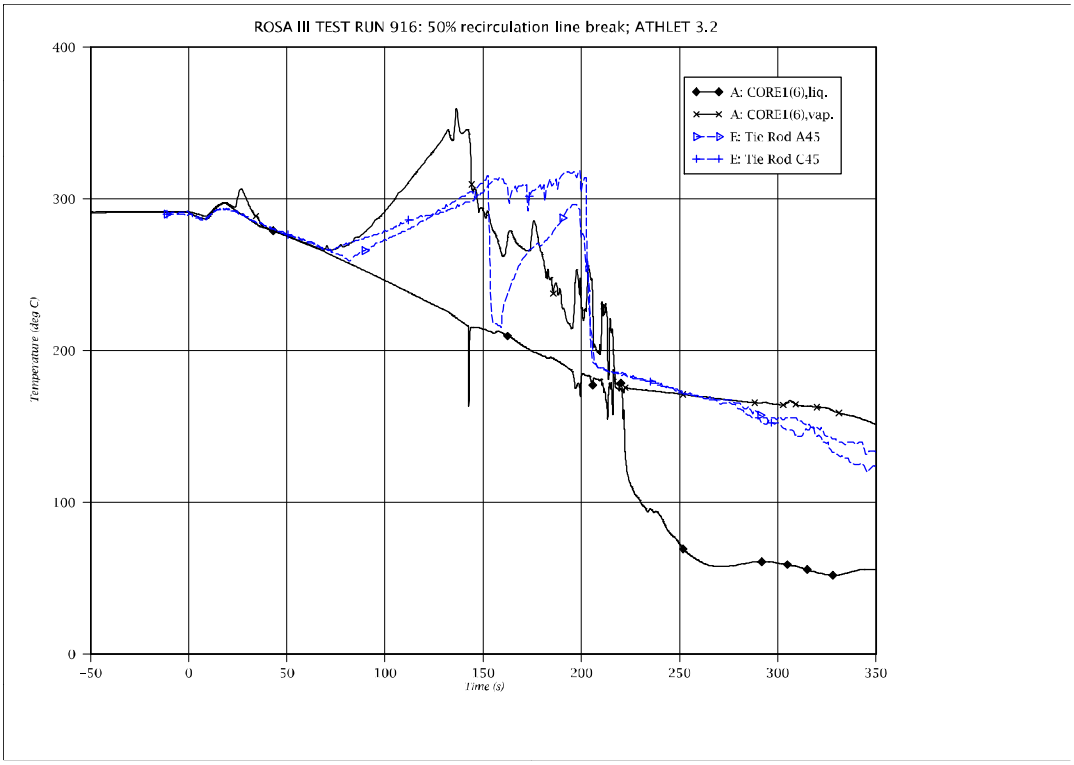

Fig. 5 - 87: Fluid temperature in the core (level 3)

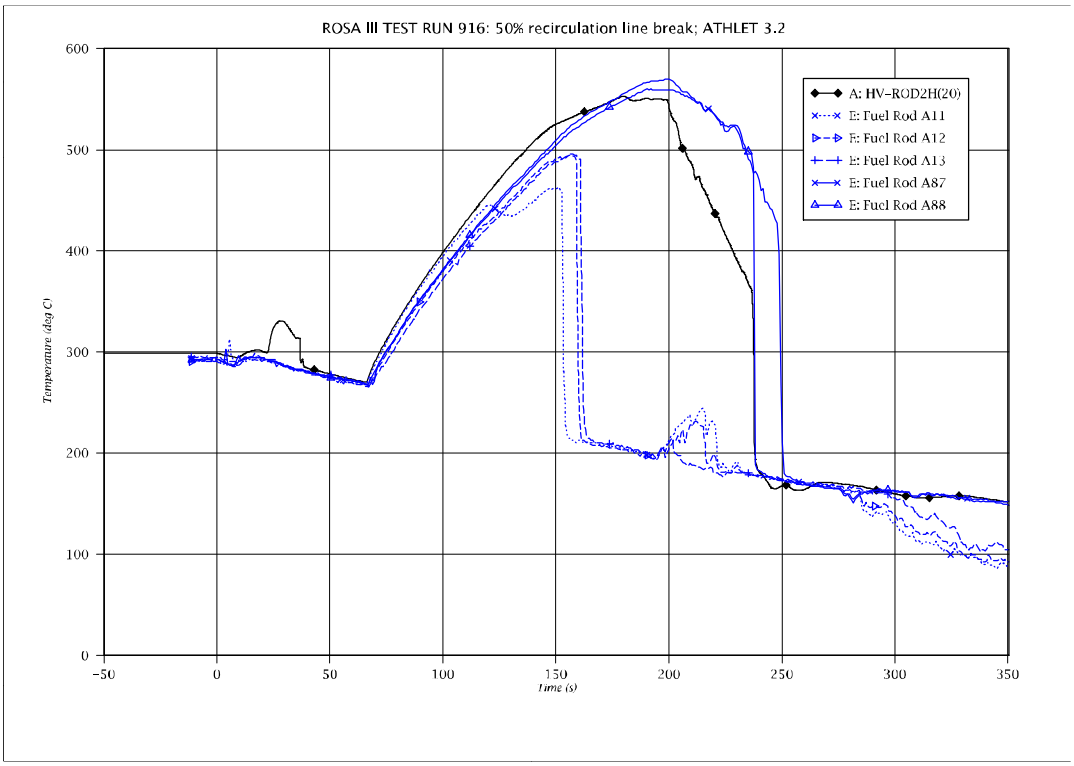

Fig. 5 - 88: Cladding temperature of fuel hot rods A at pos. 2

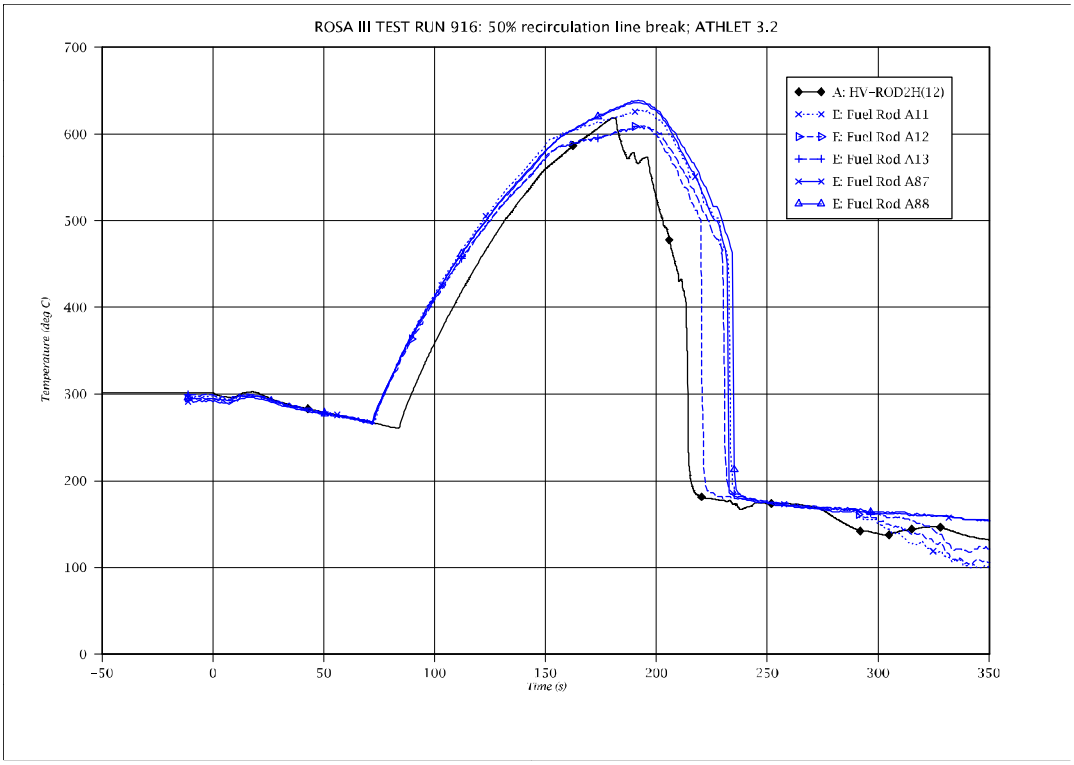

Fig. 5 - 89: Cladding temperature of fuel hot rods A at pos. 4

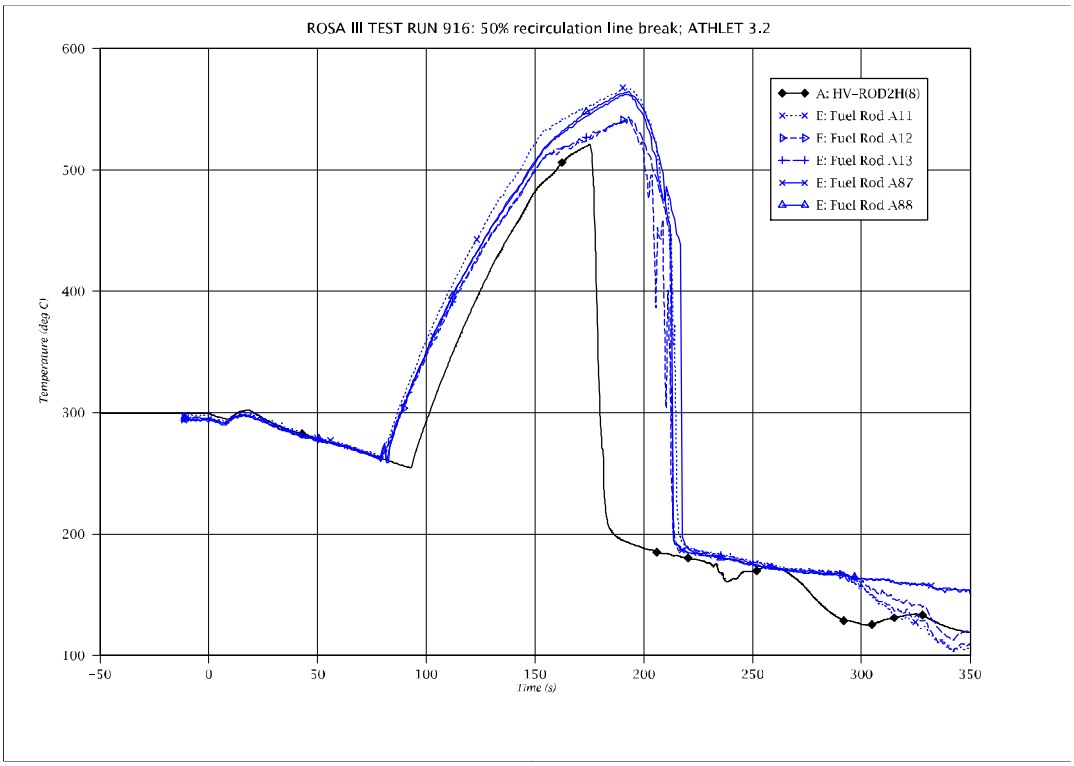

Fig. 5 - 90: Cladding temperature of fuel hot rods A at pos. 5

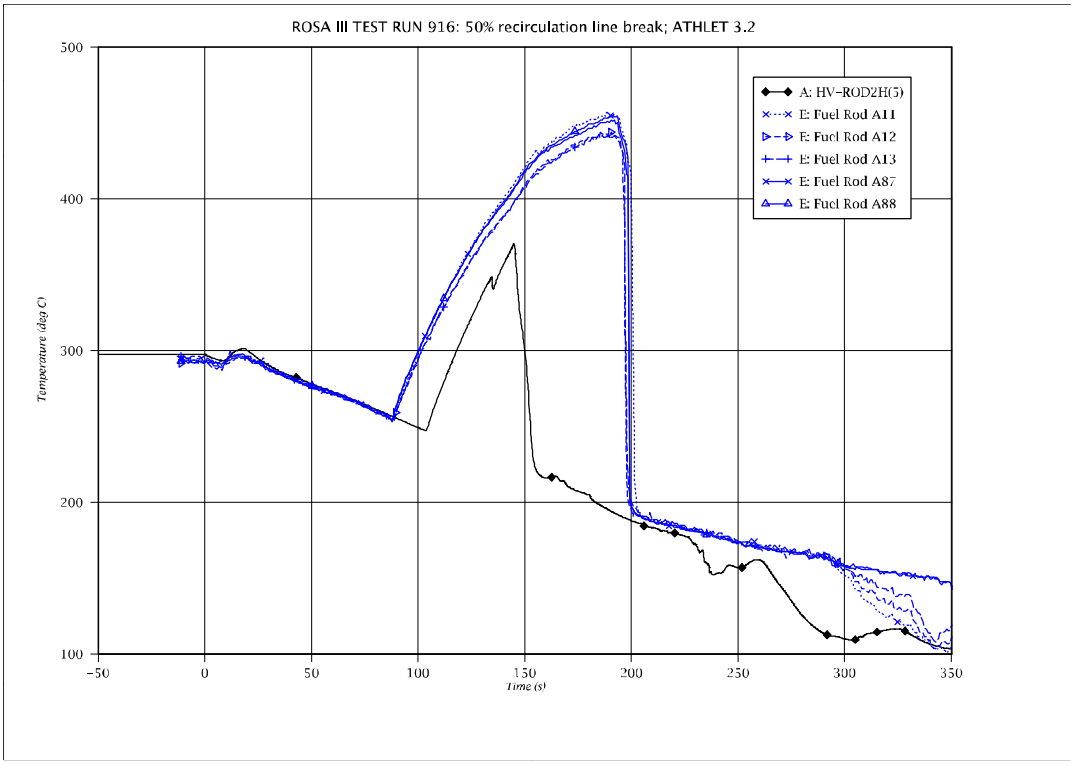

Fig. 5 - 91: Cladding temperature of fuel hot rods A at pos. 6

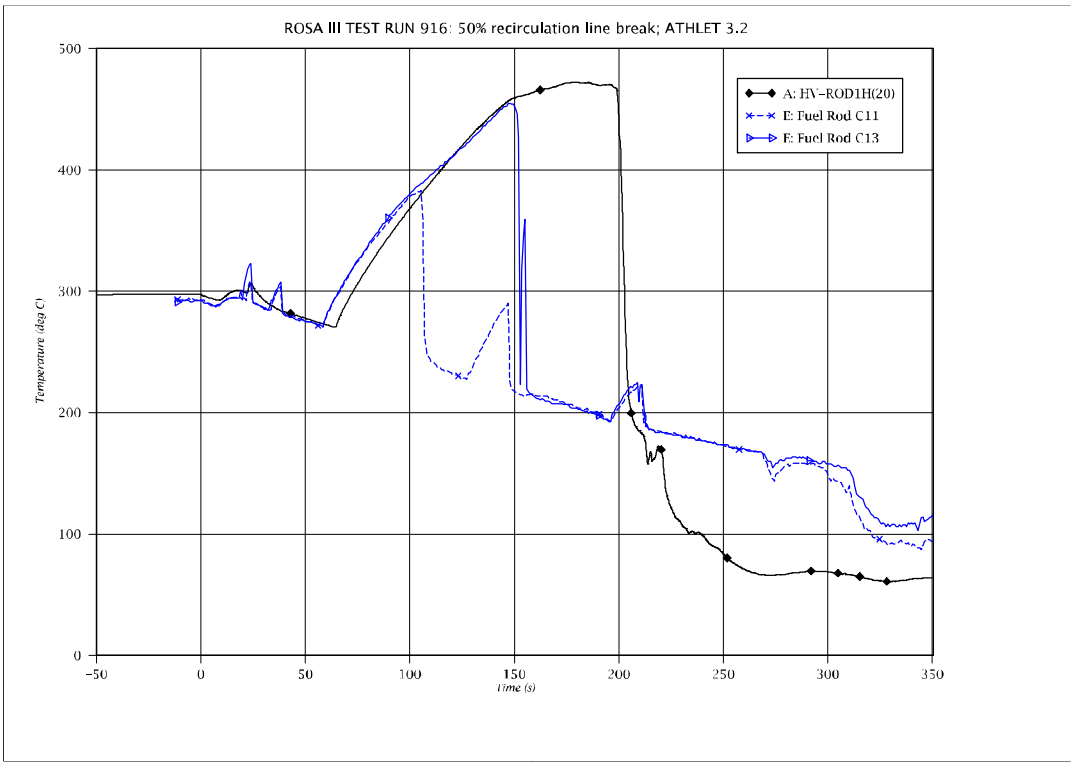

Fig. 5 - 92: Cladding temperature of fuel hot rods C at pos. 2

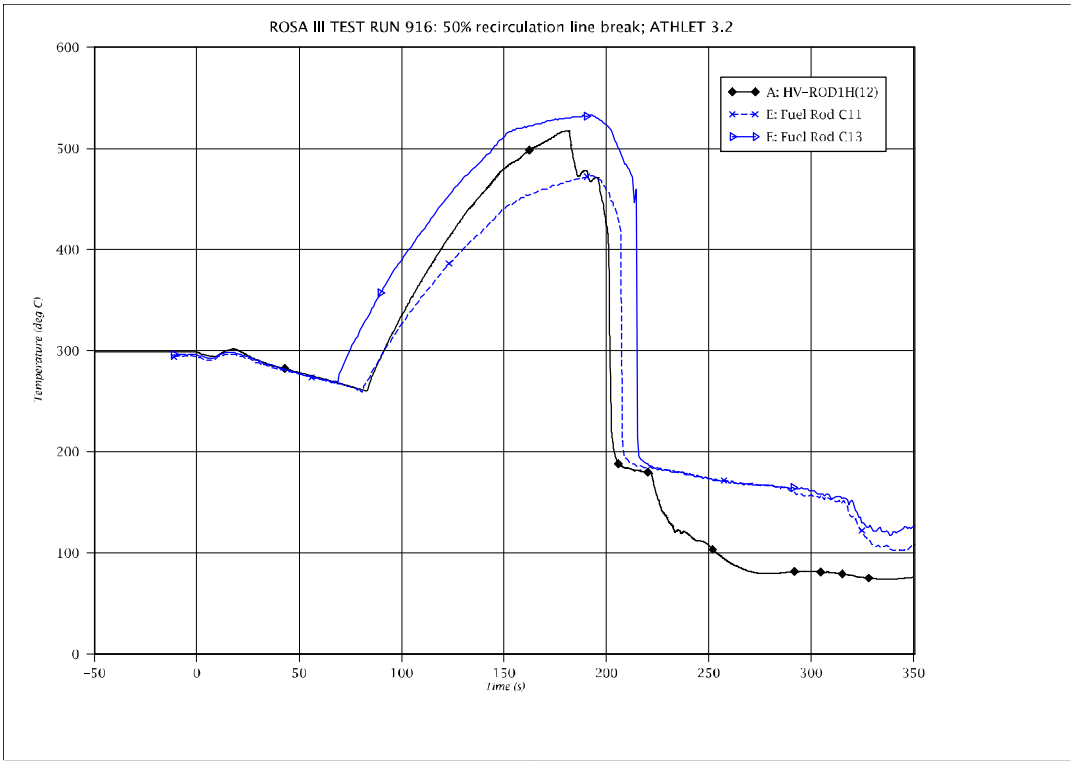

Fig. 5 - 93: Cladding temperature of fuel hot rods C at pos. 4

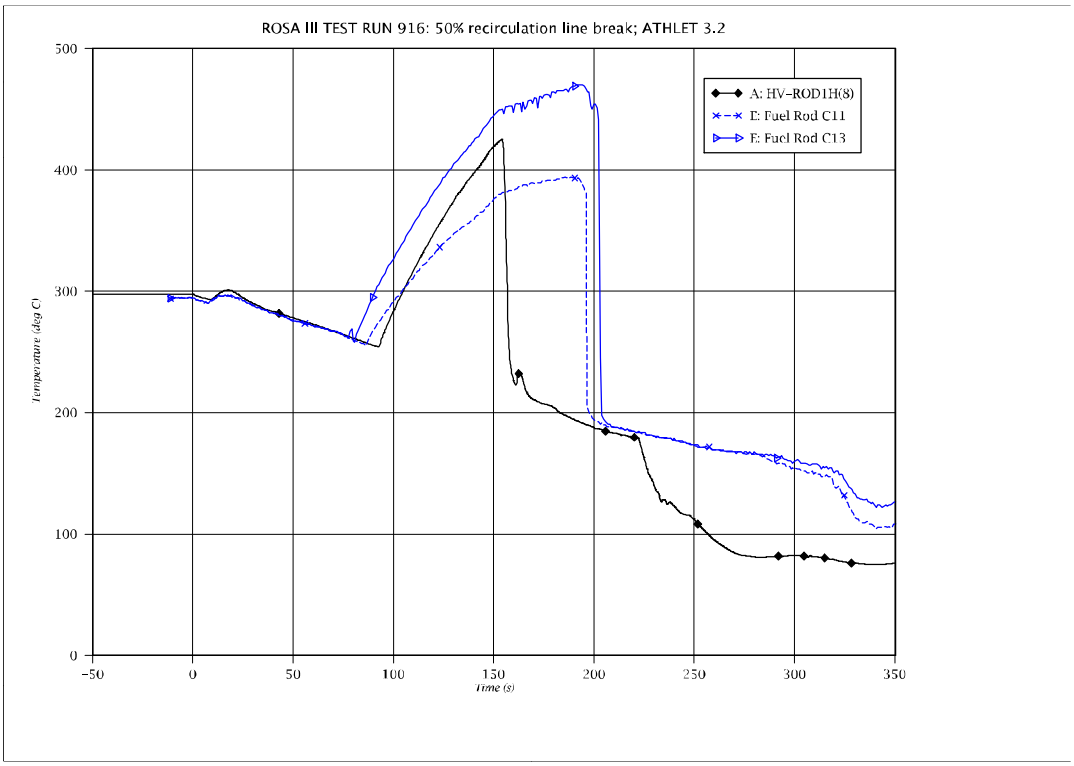

Fig. 5 - 94: Cladding temperature of fuel hot rods C at pos. 5

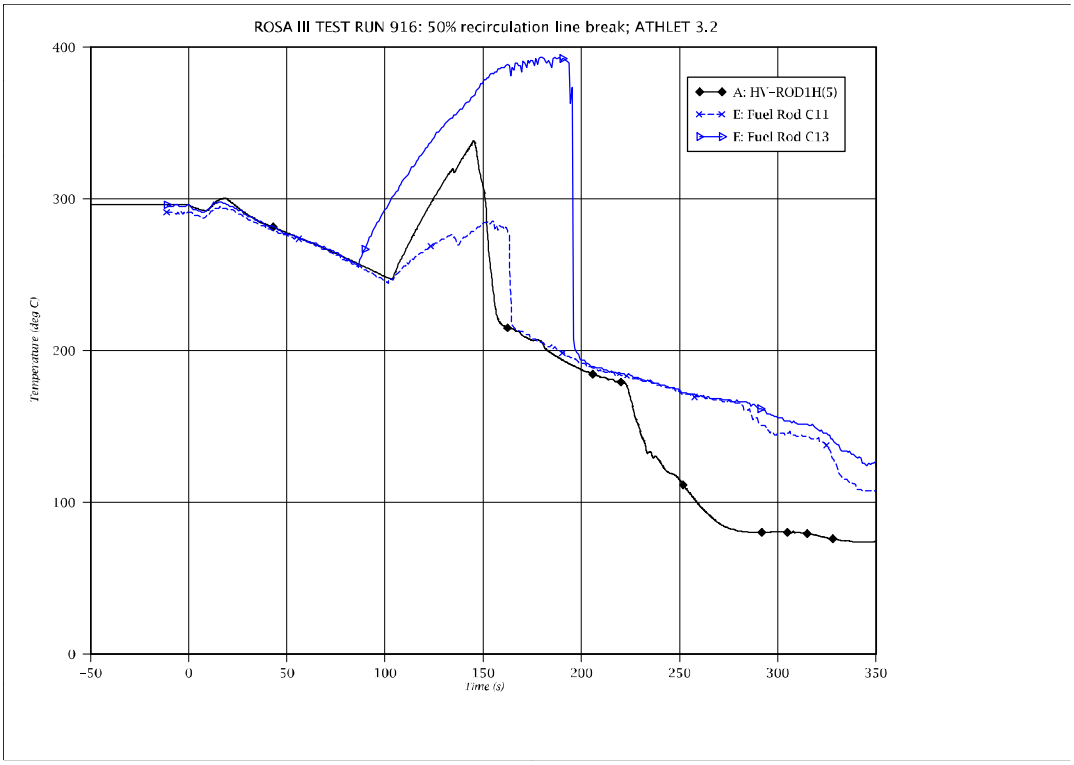

Fig. 5 - 95: Cladding temperature of fuel hot rods C at pos. 6

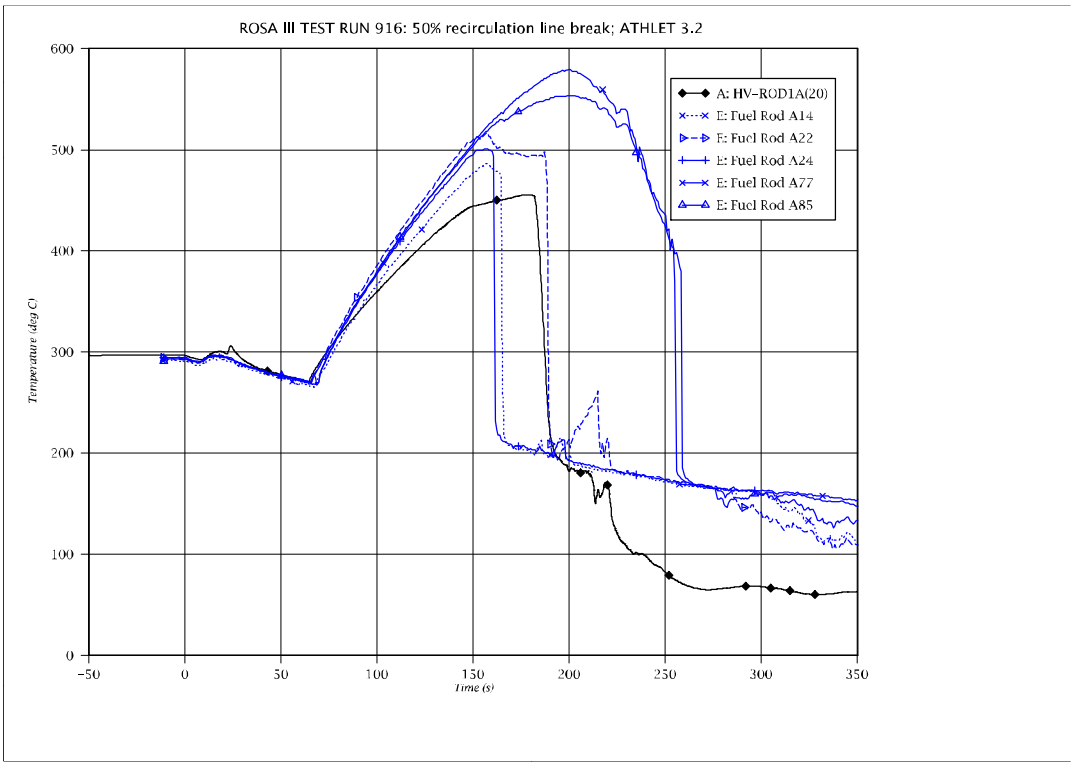

Fig. 5 - 96: Cladding temperature of fuel average rods A at pos. 2

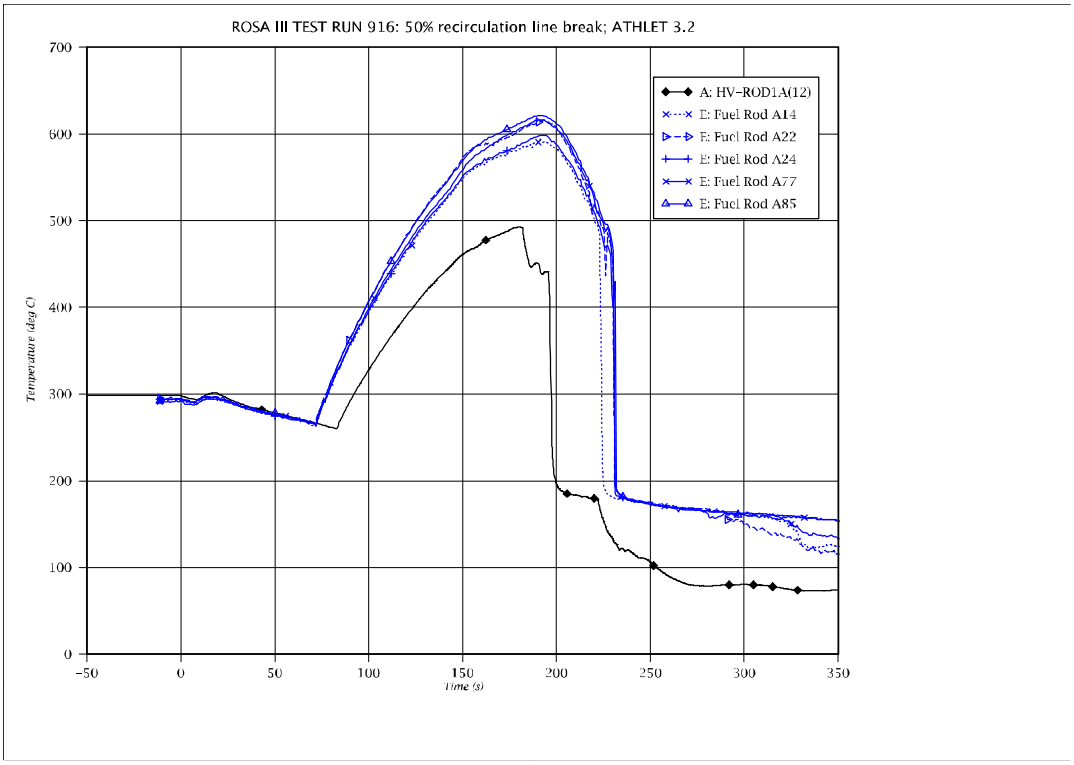

Fig. 5 - 97: Cladding temperature of fuel average rods A at pos. 4

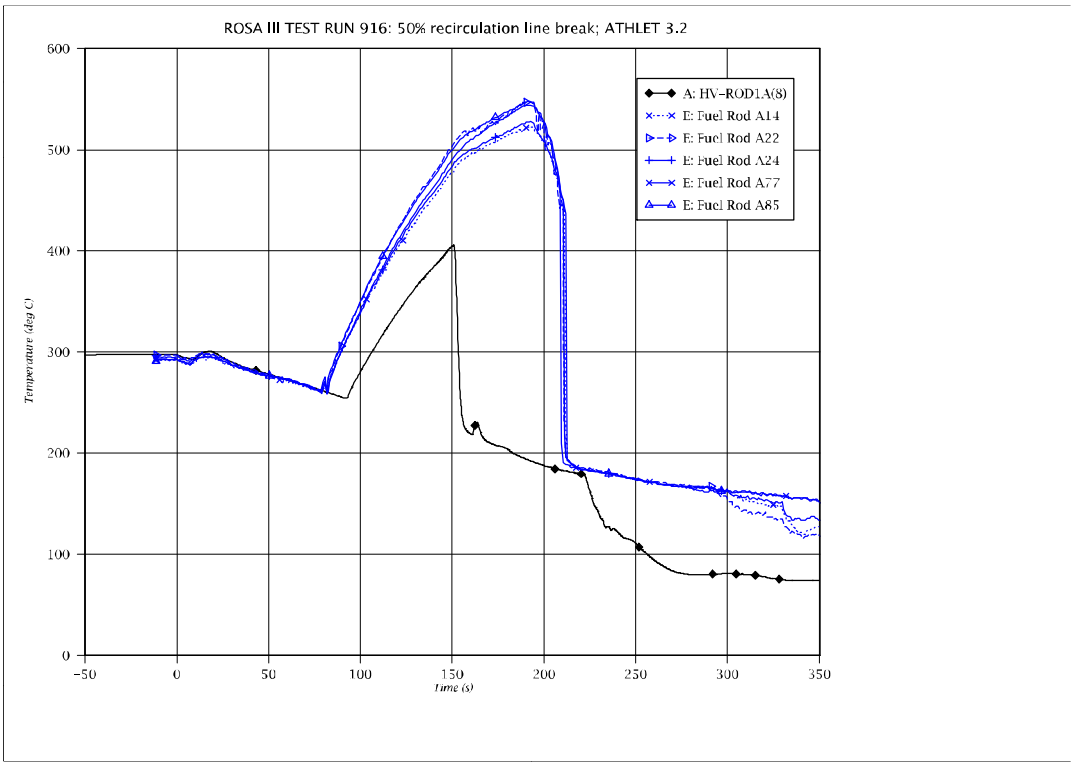

Fig. 5 - 98: Cladding temperature of fuel average rods A at pos. 5

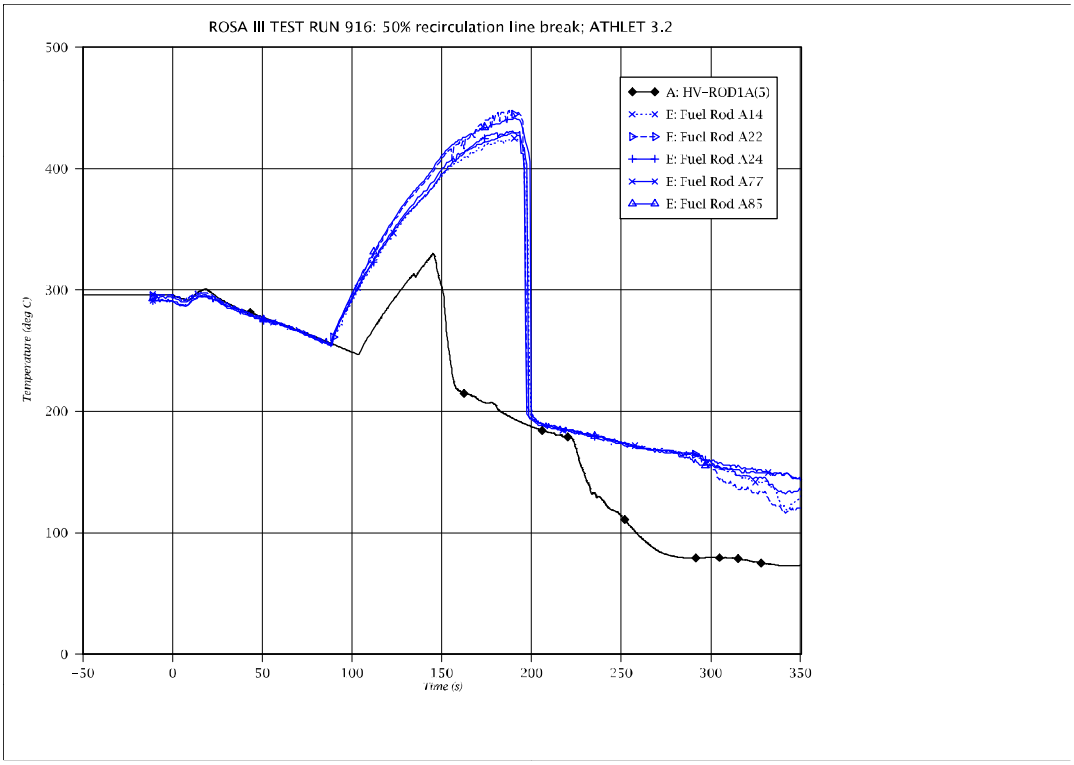

Fig. 5 - 99: Cladding temperature of fuel average rods A at pos. 6

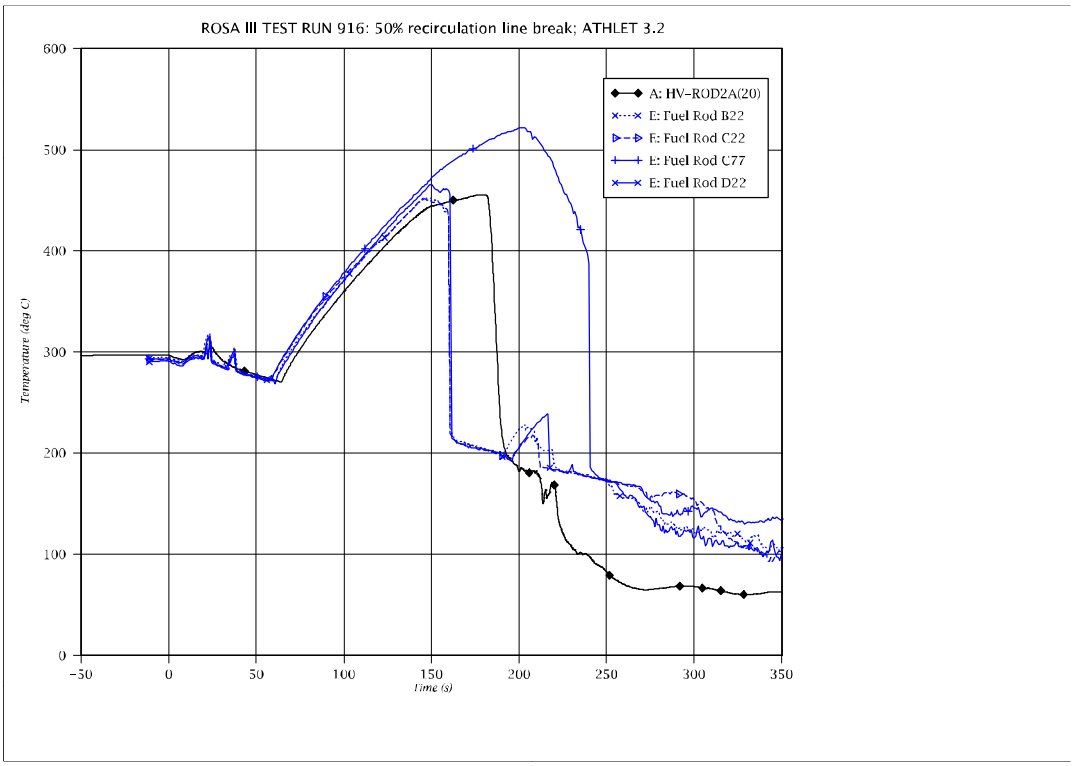

Fig. 5 - 100: Cladding temperature of fuel average rods B, C, D at pos. 2

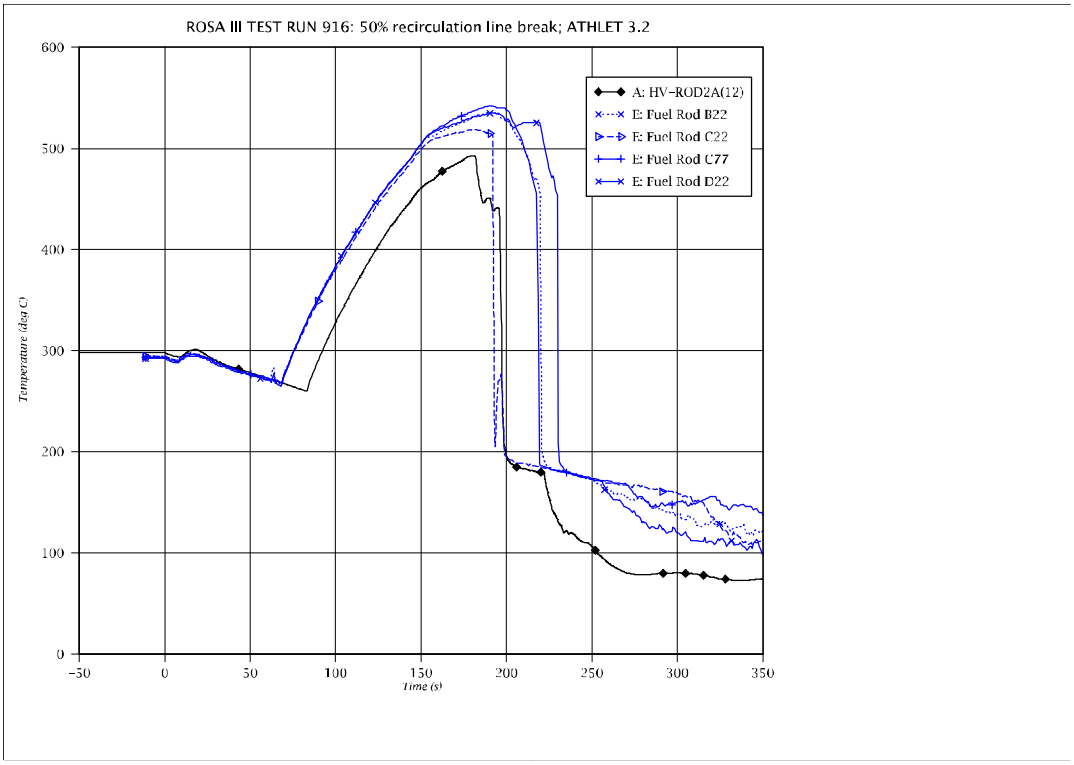

Fig. 5 - 101: Cladding temperature of fuel average rods B, C, D at pos. 4

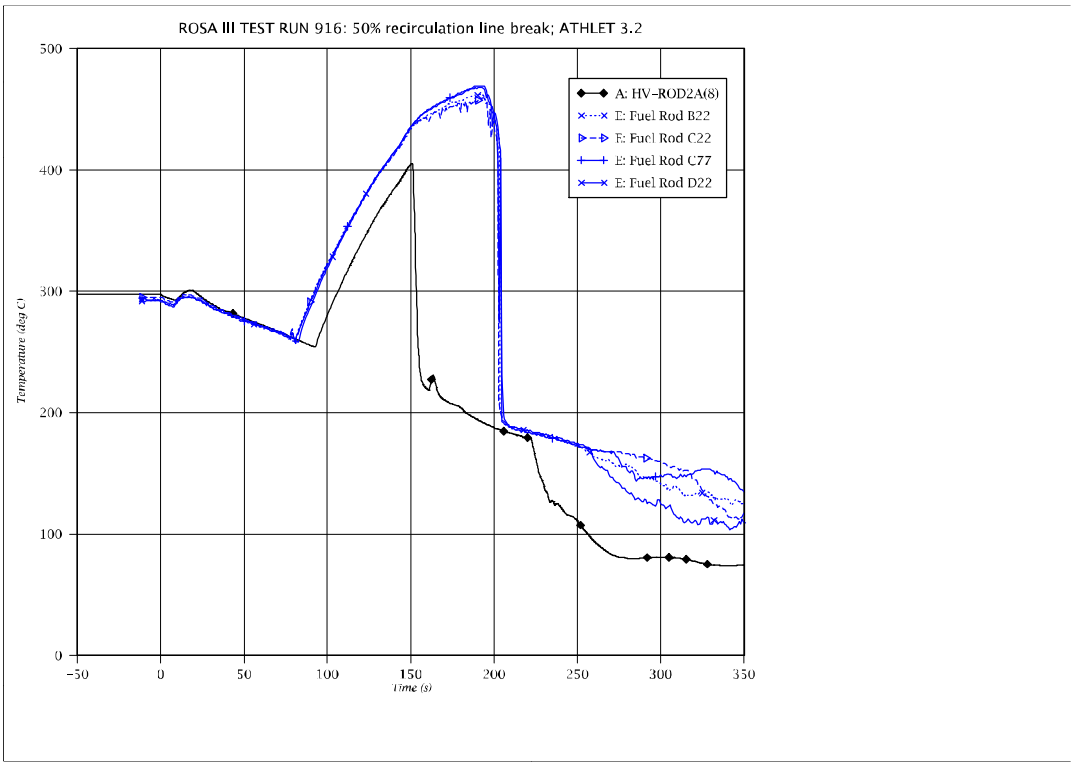

Fig. 5 - 102: Cladding temperature of fuel average rods B, C, D at pos. 5

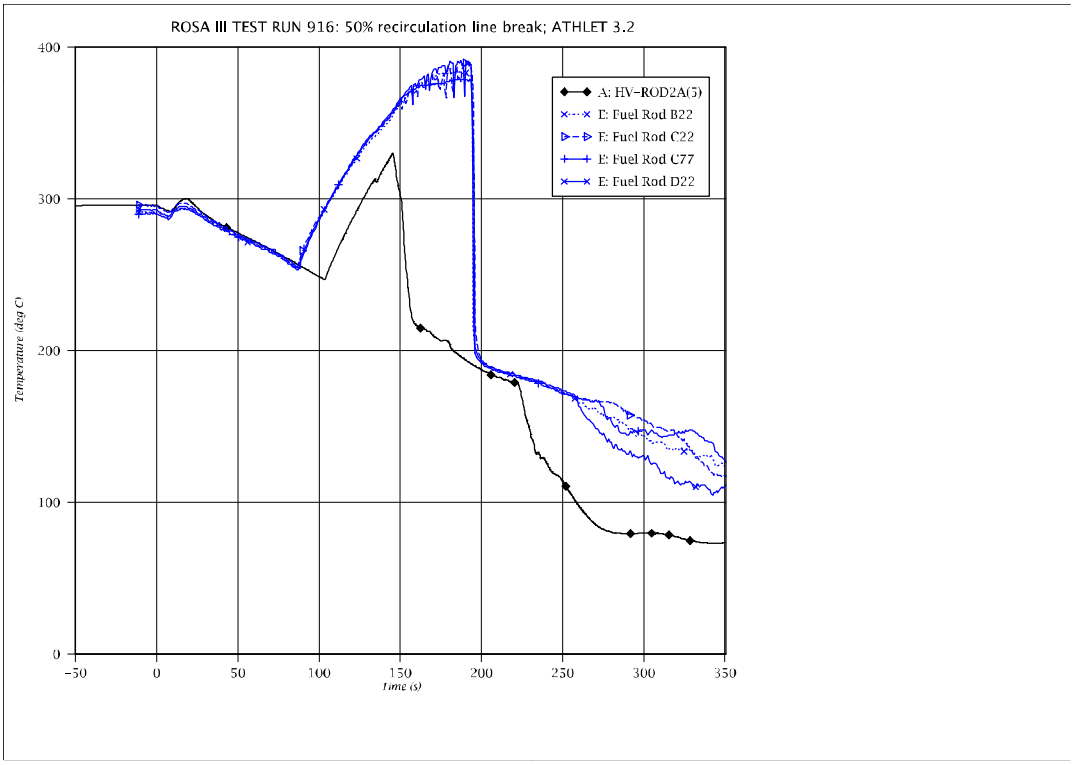

Fig. 5 - 103: Cladding temperature of fuel average rods B, C, D at pos. 6

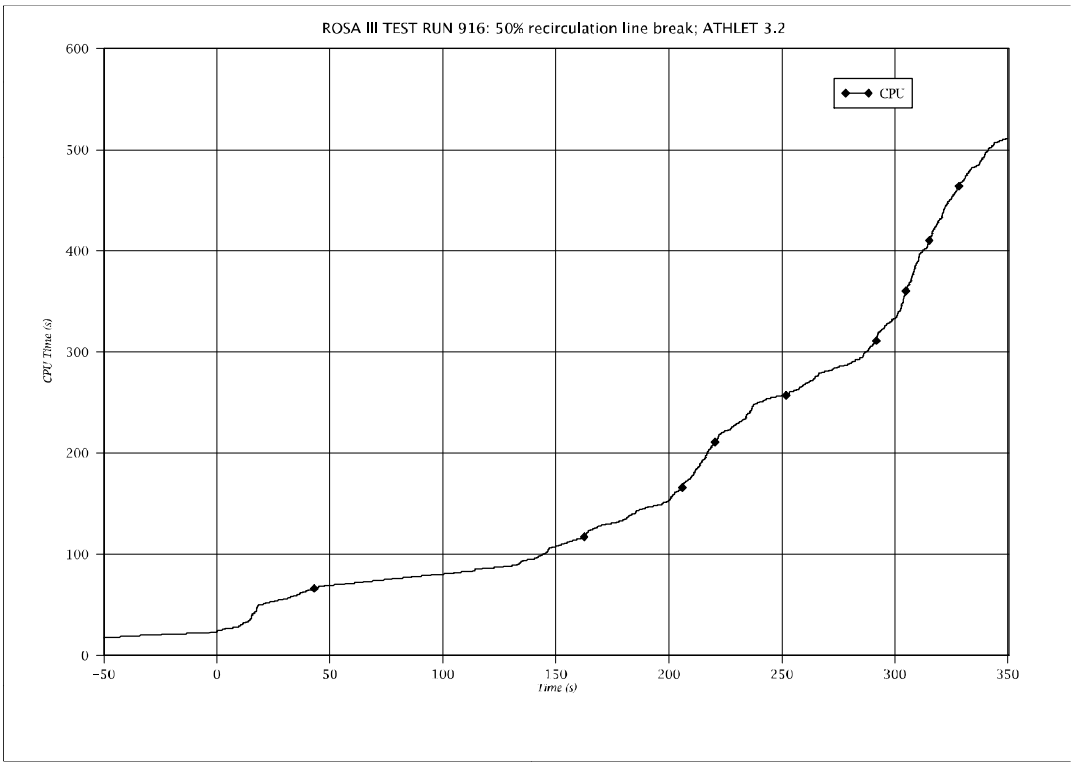

Fig. 5 - 104: CPU time consumption

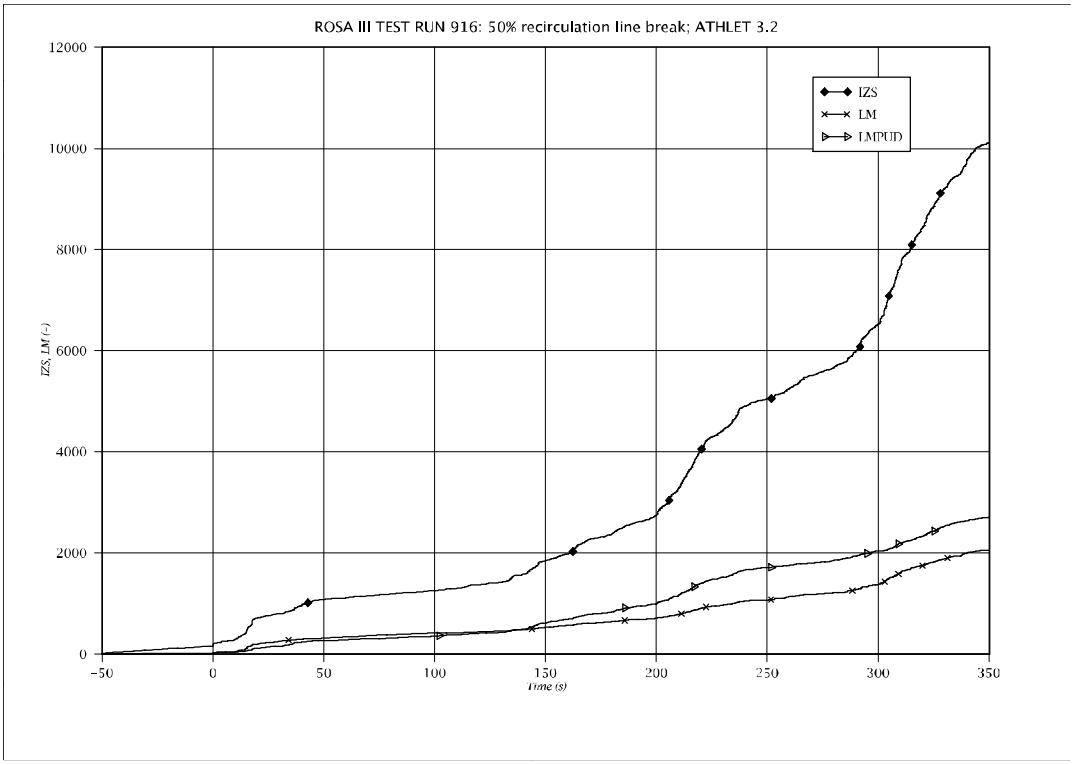

Fig. 5 - 105: Number of time steps (IZS) and Jacobian complete (LM) and partial updates (LMPUD)

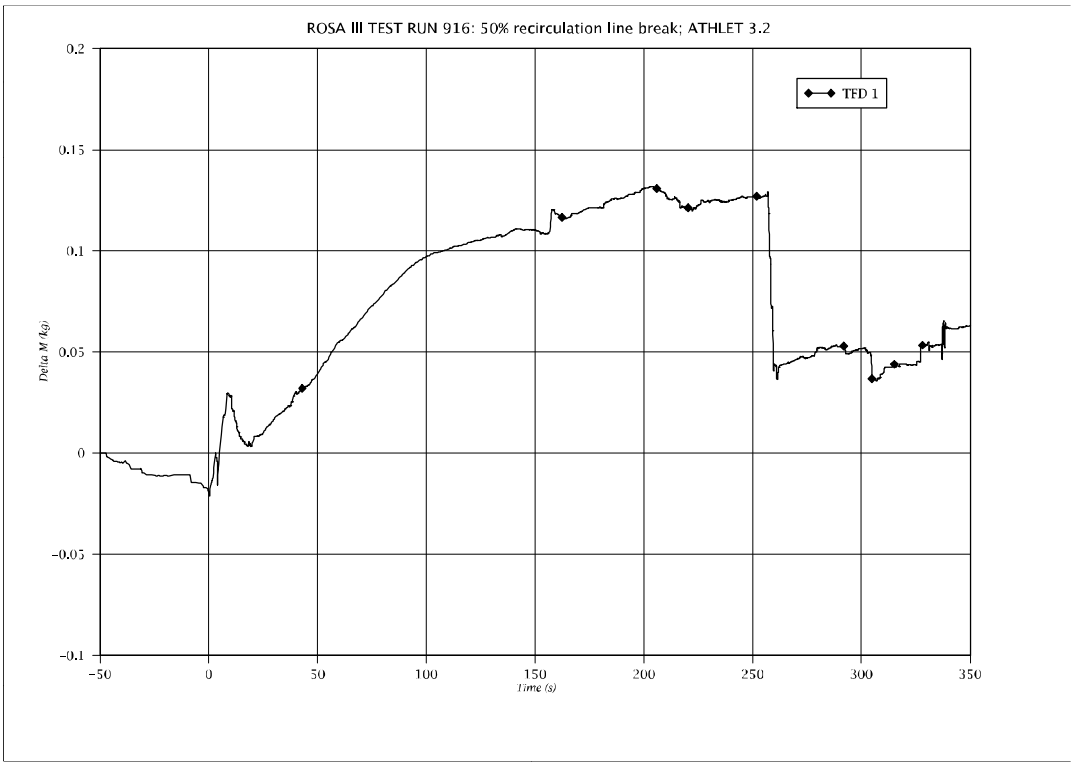

Fig. 5 - 106: Mass error

5.3 LOFT LP-LB-1

5.3.1 Test Facility

The LOFT test facility is a 50 MWt PWR system design to simulate the major components and system responses of a commercial PWR during LOCAs or operational transients sequences. It provides a unique link between the smaller full-powered facilities (e.g. LOBI and SEMI-SCALE), the decay-powered facilities (e.g. PKL, ROSA IV and BETHSY) and commercial PWRs. Another main advantage of LOFT stems from its nuclear core.

The nuclear reactor is 1/47 volumetrically scaled to an American type 1000 MWe PWR. The experimental assembly includes five major subsystems which have been instrumented in a way that system variables can be measured and recorded during the experiments. The subsystems include the reactor vessel, the operating or intact loop, the broken loop, the blowdown suppression system and the emergency core cooling system. More detailed information on the LOFT system configuration can be found in /REE78/.

The configuration of the major LOFT components is shown in fig. 5 - 107. The operating (intact) loop simulates three loops of a commercial four-loop PWR, and contains a steam generator, two primary coolant pumps in parallel, one pressurizer, a venturi flowmeter, and connection piping. The broken loop consists of a hot leg and a cold leg, and the blowdown suppression tank header. Each leg contains a quick-opening blowdown valve, and an orifice to represent the break plane. Steam generator and main coolant pumps are inactive simulators representing just the volume and flow resistances of those components. Before break initiation, there is no fluid flow in the broken loop. A recirculation line establishes a small flow through the broken loop to maintain the fluid temperature equal to the intact loop cold leg temperature. They were isolated prior to the initiation of the experiment.

The LOFT reactor vessel shown in fig. 5 - 108 has an annular downcomer, a lower plenum, lower core support plates, a nuclear core, and an upper plenum. The downcomer is connected to the cold legs of the intact and broken loops, and the upper plenum is connected to the hot legs. The core consists of 1300 enriched-uranium fuel rods arranged in five square and four triangular fuel modules. The fuel rods are designed to commercial PWR specifications, except that they are only 1.68 m (5.5 ft.) long, and several fuel rods have special instrumentation. All fuel rods in the core were unpressurized for the test LP-LB-1.

Each one of the two LOFT ECC system consists of an accumulator, a high pressure injection system (HPIS) and a low pressure injection system (LPIS).

LOFT started operation in 1976. From 1976 till the end of the fiscal year 1982, a total of 30 nuclear and 7 non-nuclear experiments were run in the US Nuclear Regulatory Commission's (NRC) program. A summary of NRC LOFT program experiments and research findings can be found in /NAL85/. In February 1983, participants from 9 OECD countries agreed to form an international consortium with the objective to conduct a series of experiments in LOFT, in order to provide thermal-hydraulic, fuel, and fission product transport information used to assess computer codes, define safety margins, identify previously unanticipated phenomena and develop techniques for accident recovery. A total of 8 experiments have been performed within this frame, among them the large break LOCA test LP-LB-1.

5.3.2 Test Conditions and Procedures

The experiment LP-LB-1 (LOFT Project Large Break test no. 1; /ADA84/), performed in February 1984, simulated a double-ended offset shear of a cold leg primary coolant pipe in a commercial PWR, and was initiated from conditions representative of a PWR operating near its licensing limits. The boundary conditions for the experiment included:

- The reactor has been operating at steady state power long enough to establish near equilibrium decay heat levels.
- There is a loss of off-site power coincident with the LOCA, thus the primary coolant pumps coasted down after break initiation and pumped ECC injections delayed for a period of time corresponding to the delay assumed for a commercial plant to start the emergency diesel generators and deliver power to the ECC pumps.
- Minimum UK ECC injection assumptions were used as the basis for the ECC injections. Both LPIS's are operating, none of the HPIS's are available, and only two of the 4 accumulators are available to inject into the intact loop. The LPIS and the accumulators have been connected to the cold legs. Since all ECC water injected into the broken loop of a commercial PWR is assumed to be lost out of the break, in experiment LP-LB-1, the accumulator injection mass was about 70% and the total pumped injection flow rate was about 50% of that used in previous LOFT large break LOCA simulations. The accumulator injection line remains open so that the cushion nitrogen is injected into the primary system until the pressure equilibrium is reached.
- The reactor coolant pumps were tripped and disconnected from their flywheels within 1 s after experiment initiation in order to maximize the fraction in the core that has not been rewet at the end of blowdown.

A summary of the measured initial conditions and the corresponding ATHLET values is given in tab. 5 - 5.

Table 5 - 5: Initial conditions for LOFT test LP-LB-1

Parameter	Measured value	ATHLET
Primary coolant system		
Core ΔT (K)	29.8 ± 1.4	29.7
Hot leg pressure (MPa)	14.90 ± 0.08	14.88
Cold leg temperature (K)	556 ± 1	556
Mass flow rates (kg/s)	305.8 ± 2.6	305.8
Reactor Vessel		
Power level (MW)	49.3 ± 1.2	49.4
Max. linear heat generation rate (kW/m)	51.7 ± 3.6	51.5
Pressurizer		
Liquid volume (m^3)	0.56 ± 0.02	0.55
Steam volume (m^3)	0.37 ± 0.02	0.38
Water temperature (K)	615 ± 5.8	614.7
Pressure (MPa)	14.92 ± 0.11	14.86
Liquid level (m)	1.04 ± 0.04	1.10
Broken Loop		
Cold leg temperature (K)	552 ± 6	552
Hot leg temperature (K)	561 ± 1	561
Emergency Core Cooling System		
Accumulator liquid volume (m^3) (incl. injection line)	1.18 ± 0.02	1.18
Accumulator pressure (MPa)	4.21 ± 0.06	42.1
Accumulator liquid temperature (K)	305 ± 6	305

5.3.3 Experimental Results

The blowdown valves were opened to initiate the experiment. The reactor scrammed on indication of low pressure in the intact loop hot leg, the primary pumps were tripped and then decoupled from their flywheel, and the cladding temperatures deviate from saturation, all within 1 s. The primary system depressurized, and saturated fluid conditions were reached at 1 s in the broken loop hot leg and at 3.5 s in the broken loop cold leg. The maximum cladding temperature during blowdown, 1261 K, was reached at 13 s, and was followed by a slight decrease in temperature and then a gradual heat-up which continued until 27 s, during the refill of the lower plenum. A top-down quench occurred in the upper third of the core starting at 13 s, which lasted until about 22 s, by which time the entire core had started to heat up. Around 30 s, a precursory cooling follows which gradually reduces the cladding temperatures. The core started to quench at 35 s, and was completely quenched at 72 s. The ECC injection initiated at 18 and 32 s from the accumulator and LPIS, respectively. The experiment was terminated at 132s .

The chronology of significant events as measured in the experiment is presented in tab. 5 - 6.

Table 5 - 6: Chronology of events for LOFT test LP-LB-1

Event	Time (s)
Blowdown valves opened	0.
Reactor scrammed	0.13 ± 0.01
RCP tripped	0.24 ± 0.01
RCP disconnected from flywheels	0.63 ± 0.01
Control rods on bottom	1.83 ± 0.01
Max. cladding temperature reached (blowdown)	12.9 ± 0.5
Pressurizer emptied	15 ± 1
Accumulator injection initiated	17.5 ± 0.05
LPIS pumps turned on	24.8 ± 0.5
Max. cladding temperature reached (reflood)	26.8 ± 0.5
LPIS initiated	32 ± 1
Accumulator emptied	40 ± 1
Accumulator injection complete	46 ± 2
Core reflood complete	50 ± 2
Core quench complete	72 ± 2
Experiment terminated	132

5.3.4 Input Dataset

5.3.4.1 Nodalization

The figure 5 - 109 shows the major parts of nodalization used for the ATHLET analysis of the LOFT test LP-LB-1. Except for the fuel rods, the heat conduction volumes for the simulation of the facility structures are not included in this figure. The nodalization includes the following numbers of network elements:

Branches	13
Pipes	38
CVs	142
Junctions	170
ODEs for thermo-fluiddynamic	1027
Heat conduction volumes	253
ODEs for heat conduction	1019

All relevant parts of the LOFT facility except the blowdown suppression tank are simulated. The following briefly describes the main features of the ATHLET input dataset:

Thermo-fluid objects

- Core
  The core is represented by two channels. The hot channel (PV-COR-H) simulates the central bundle and includes two groups of fuel rods (HPV-COR-H1 and -H2) with radial peaking factors of 1.40 and 1.20. The peripheral bundles are simulated by the pipe PV-COR-N with three groups of fuel rods (HPV-COR-N1 to -N3) with radial peaking factors of 1.20, 1.00, and 0.73. An exchange between these two channels is considered via a cross connection object (PV-COR-CC).
- Core bypasses
  The numerous core bypasses of the LOFT facility are represented by three 3 core bypasses in the ATHLET input model:
  a) Upper downcomer - upper head bypass
     This bypass carries nominally 2% of the loop mass flow (TFOs PV-DU1 and PV-DU2).
  b) Bypass through the core filler pieces
     This bypass carries nominally 3% of the loop mass flow (TFO PV-COR-BYP).
  c) Reflood assist bypass (RABS)
     This is a connection line between the broken loop hot and cold leg which should be closed during the experiment. Actually, a leakage of 3% of the nominal flow was assumed by the experimenter (TFO RABS).
- Downcomer
  To consider the asymmetric cold leg ECC injection and the influence of the break location, the downcomer is split completely into two parallel channels (PV-DC1-x and -DC2-x) interconnected via the cross connection object PV-DC-CC. Above the nozzles, it is interconnected via the SJP PV-DC12-TJ.
- Circuits
  The IL steam generator secondary side is nodalized in detail to simulate both the heat removal during the steady and heat addition during the transient phase of the experiment. The two parallel main coolant pumps and related pipings are combined to one pump. The pump head is calculated by means of homologous head curves, the pump speed is supplied as measured.

Heat conduction objects

- Fuel rods
  The radial power distribution of the fuel rods is represented by five different groups of fuel

rods.

Central fuel bundle:

184 rods	53.32 kW	radial peaking factor 1.40
20 rods	45.70 kW	radial peaking factor 1.20

Peripheral fuel bundle:

288 rods	45.70 kW	radial peaking factor 1.20
304 rods	38.08 kW	radial peaking factor 1.00
504 rods	27.75 kW	radial peaking factor 0.73

Every heater rod is sub-divided in axial direction into 18 HCVs. The axial power profile is input equally for all rods, the axial peaking factor is 1.6 at 0.55 m above bottom of the rod.

- Structures
  The major wall and internal structures of the reactor vessel, coolant pipes, pressurizer, and the steam generator are represented by HCOs. The heat losses to the environment are neglected.

5.3.4.2 Model Options

Following model options are applied:

- For the primary side of the test facility the 6 eq. model is applied with the exception of the pressurizer and the break, where the 5 eq. model is chosen. The secondary side is completely simulated with the 5 eq. model.
- The T-junction model is applied at both ends of the pressurizer surge line to simulated the vapor pull-through when the mixture level reaches the surge line nozzle, as well as the vapor flow and liquid entrainment in case of a pressurizer in-surge.
- The critical discharge mass flow is calculated with the CDR1D model.
- The multi-component model is used for the simulation of the nitrogen cushion in the accumulator and the nitrogen injection into the primary system. Nitrogen is assumed to be solved in the accumulator water with a concentration of 600 ppm.
- Evaporation and condensation at heating and cooling surfaces are considered.
- The heat generation in the core is determined by the point neutron kinetics model.
- The boron tracking model is applied. The initial boron concentration equals 513 ppm for the primary coolant, and 3000 ppm for the accumulator and LPIS.
- The gap conductance coefficient between the cladding and the fuel is calculated with the gap conductance model; the gap width of the cold rod is input as 0.095 mm.

5.3.5 Results of the ATHLET Calculation

The figures 5 - 110 to 5 - 150 compare ATHLET results with the corresponding experimentally measured parameters for a variety of physical quantities, proving the quality of the ATHLET simulation. In the figures, 'A:' denotes the ATHLET result, generally followed by the thermo-fluid or heat conduction object name and the index of the network element inside. 'E:' denotes the experimental result followed by the designation of the measurement.

After the simultaneous opening of the two blowdown valves, the system pressure rapidly drops to the saturation pressure of the hot core exit temperature of about 102 bar. Flashing initiates in the hot part of the primary system and the depressurization is slowed down. Figure 5 - 110 compares measurement and calculation of the pressure in the IL hot leg which is representative for the primary side except the pressurizer and the vicinity of the break. During two time periods, ATHLET calculates the pressure too low: between 10 and 20 s, where the experiment shows a bend in the pressure history while ATHLET calculates a more linear pressure decrease, and between 35 and 55 s, which is possibly caused by an overestimated steam condensation during ECC injection. The same applies to the pressure in the pressurizer (fig. 5 - 111). The calculated pressures at different positions of the BL (figs. 5 - 112 and 5 - 113) agree well with the measurement, except PE-BL-4 which is the pressure in the cold leg break nozzle. At this position, strong pressure gradients have to be expected accompanied with flow contraction due to the abrupt reduction of the flow area. None of the effects can be resolved by the finite volume approach used by ATHLET. After closing the feedwater and main steam line, the pressure on the steam generator secondary side decreases due to reverse heat flow from secondary to primary side. This decrease is slightly over-predicted by ATHLET (fig. 5 - 114).

The figures 5 - 115 to 5 - 118 show the mass flows in both the hot and cold legs of the two loops, and the figures 5 - 119 to 5 - 122 the corresponding fluid densities. The densities are measured with three-beam densitometers with the beams A (bottom of pipe) to C (top of pipe). The signals are averaged using a specific algorithm. Where available, the averaged values (designation -105,...) are compared with ATHLET results, otherwise the available single beam signals are shown. The BL mass flows agree satisfactorily with the experiment, in particular if the measurement uncertainties are taken into account. Nevertheless, the rapid decrease of the density and - as a result - of the mass flow in the BL cold leg around 5 s is not calculated. No reason could be found for this process. The calculated IL mass flow seem to have a too strong reverse tendency between 5 and 20 s. Together with the possibly overestimated ECC bypass to the leak (fig. 5 - 119), this may be the reason for the underestimated core inventory and the late quenching of the fuel rods, which will be discussed later. Figure 5 - 121 shows the density in the IL cold leg, where the ECC water is injected to. The coolant density in the injection control volume is compared with the measurement which is actually upstream of the injection point. Therefore,

and due to the premature start of the ECC injection in ATHLET, the calculated result is too high. (In the CV upstream of the injection CV, no ECC water arrives due to the coarseness of the finite volume approach.) The density between the steam generator exit and the pump seal is shown in fig. 5 - 123. In the calculation, the density decreases not as fast as it is measured. This can be explained by the fact that the calculated density is the average in the CV while the experiment supplies a very local value.

The figures 5 - 124 to 5 - 128 represent differential pressures along different sections of the two loops. Unfortunately, no measurement is available in the RV or in the steam generators indicating mass inventories in these vertical components. Hence, the comparison between experiment and calculation can only prove whether the flow losses in the loops are correctly represented by the input model. For the intact loop, a good agreement between calculation and measurement can be stated. Some of the instruments seem to have bias deviations, e.g. the differential pressure across the main coolant pumps (fig. 5 - 126). Nevertheless, a more positive value as indicated by the instrument on and after 10 s would improve the liquid inventory in the core. Parameter studies with heavily manipulated homologous head curves to reduce the pressure drop in the reverse turbine operation region improved the quench behavior in the core significantly. On the other hand, the acceleration of the pump rotors between 22 and 44 s (fig. 5 - 129) points to a pressure drop across the pumps. (Pump speed is supplied as time table.)

Many of the differential pressure measurements in the broken loop are on short distance and dominated by abrupt flow area changes, others failed in this experiment. Strong spatial pressure gradients and flow contractions restrict the worth of comparison with calculated results. For that reasons, only two measurements are compared with ATHLET results. The tendency of pressure difference across the SG simulator exit orifice (fig. 5 - 127) is met quite well by ATHLET but the value is overestimated which can be caused by the fact that this a short distance measurement, too. Across the pump simulator, a good agreement can be stated (fig. 5 - 128).

The accumulator and low pressure injection rates are compared in figs. 5 - 130 and 5 - 131, where the latter is supplied as time table. Due to the too low primary pressure in the ATHLET calculation at that time, the accumulator injection starts too early. After the accumulator liquid level has reached the inlet elevation of the accumulator stand pipe, nitrogen enters the injection pipe which reduces significantly the flow losses and the injection rate increases clearly. ATHLET calculates this process accurately. According to the measurement, the accumulator liquid level drops down to 1.75m (fig. 5 - 132) which is below the experiment specification. On the contrary, the ATHLET result corresponds to the specification.

Some of the fluid temperature measurements in the reactor vessel are compared with ATHLET in figs. 5 - 133 to 5 - 135. In general, ATHLET calculates somewhat too high values in the upper section of the RV and too low values in the lower part. The calculated fluid temperatures in the

loops agree satisfactorily with the experimental data (figs. 5 - 136 to 5 - 140), although the superheating of the vapor is not correctly met in detail. The subcooling of the liquid in the IL cold leg during the ECC injection is calculated well indicating the good quality of both the injection jet and bulk condensation model.

Finally, the fuel cladding temperatures in different fuel bundles and for different rod power classes and elevations are compared. The figures 5 - 141 to 5 - 145 present data for the central bundle, the figures 5 - 146 to 5 - 150 for the peripheral bundles. Not going into the details of every plot, the following can be stated:

- The first temperature peak of most of the available measurements are calculated satisfactorily.
- The early top-down quench of the upper third of the core observed in the experiment is underestimated, but the generally improved cooling conditions during that time period is seized by the simulation.
- ATHLET calculates the precursory cooling of the cladding, which starts in the experiment around 30 s, clearly too late. Therefore, the second peak of the cladding temperature is frequently overestimated and the calculated quench time is too late at several fuel positions. The reason is probably a too little coolant inventory in the core at that time as it was discussed already before.
- The thermocouples in the peripheral fuel assemblies indicate repeatedly spontaneous rewetting of single cladding locations. These are local effects which can be caused by gaps in the core filler blocks where coolant may flow from the core bypass channels to the outer core sections. These gaps are not simulated.
- The best overall agreement is achieved in the axial mid-section of the fuel rods. The wider spread of the experimental and calculated data is observed at both the bottom and top end of the fuel rod, where for the first, the steep gradient of the axial power profile may contribute, and the latter can be expected to be influenced by penetrating liquid from the section above the core (which is significantly larger than that of the standard PWR design).

The figs. 5 - 151 to 5 - 153 document the performance of the ATHLET simulation concerning numerical effort and conservation of the coolant mass balance. No numerical problems appeared. The maximum mass errors of ca. 1 kg for both primary side and secondary side, resp., is negligible compared to the initial mass inventory of about 6000 kg on primary side (without accumulator), and of about 3300 kg on secondary side.

Summarizing the comparison of the ATHLET calculation with the experimental results, it can be stated that - although the core coolant inventory is underestimated during the reflood phase

of the accident - the calculated parameters are in satisfactory to good agreement with the measurements. ATHLET is able to simulate all main phenomena appearing during a double ended 200% offset break in the main coolant pipe of a PWR, as it was investigated by this LOFT experiment.

5.3.6 Figures

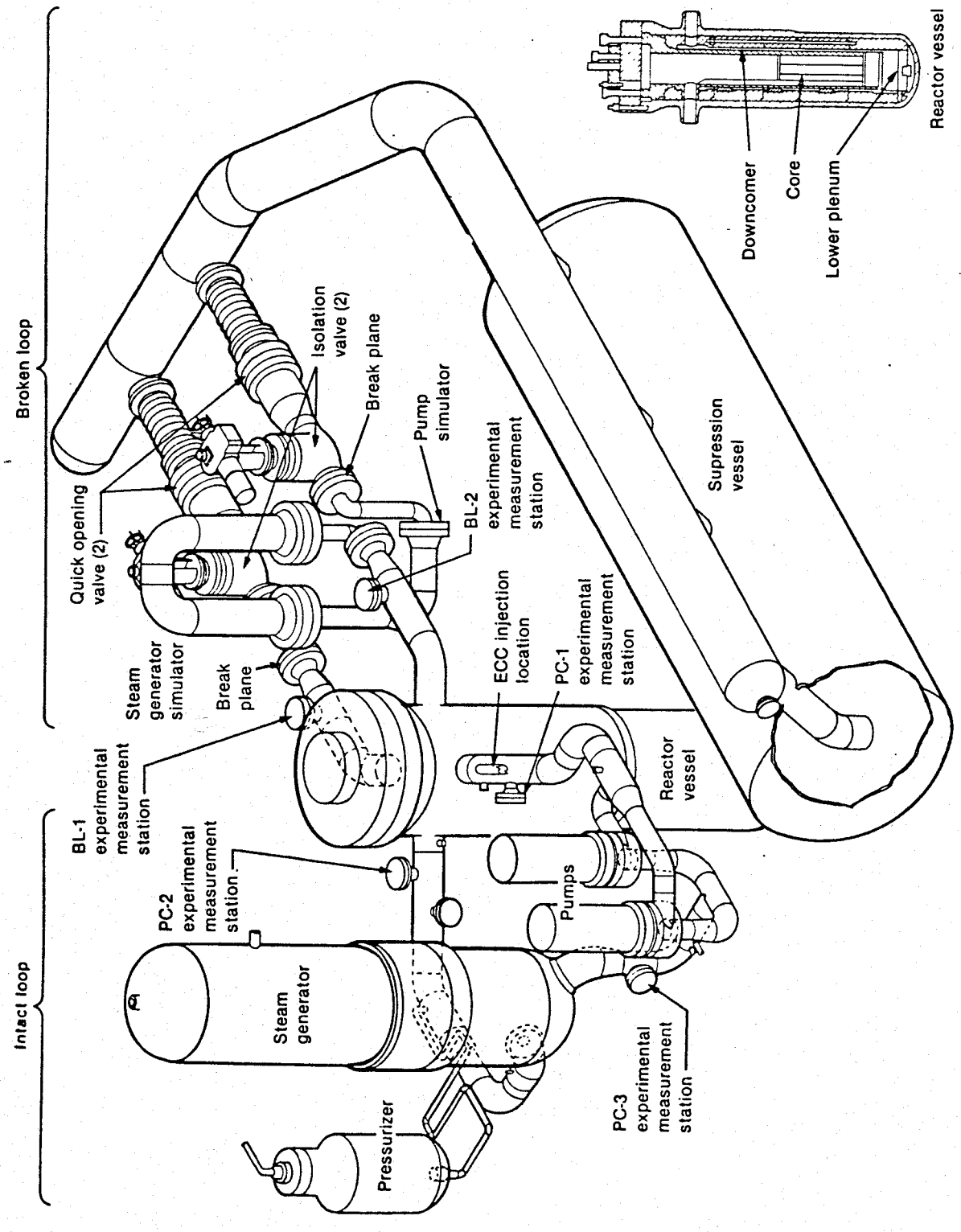

Fig. 5 - 107: LOFT components and main instrumentation locations

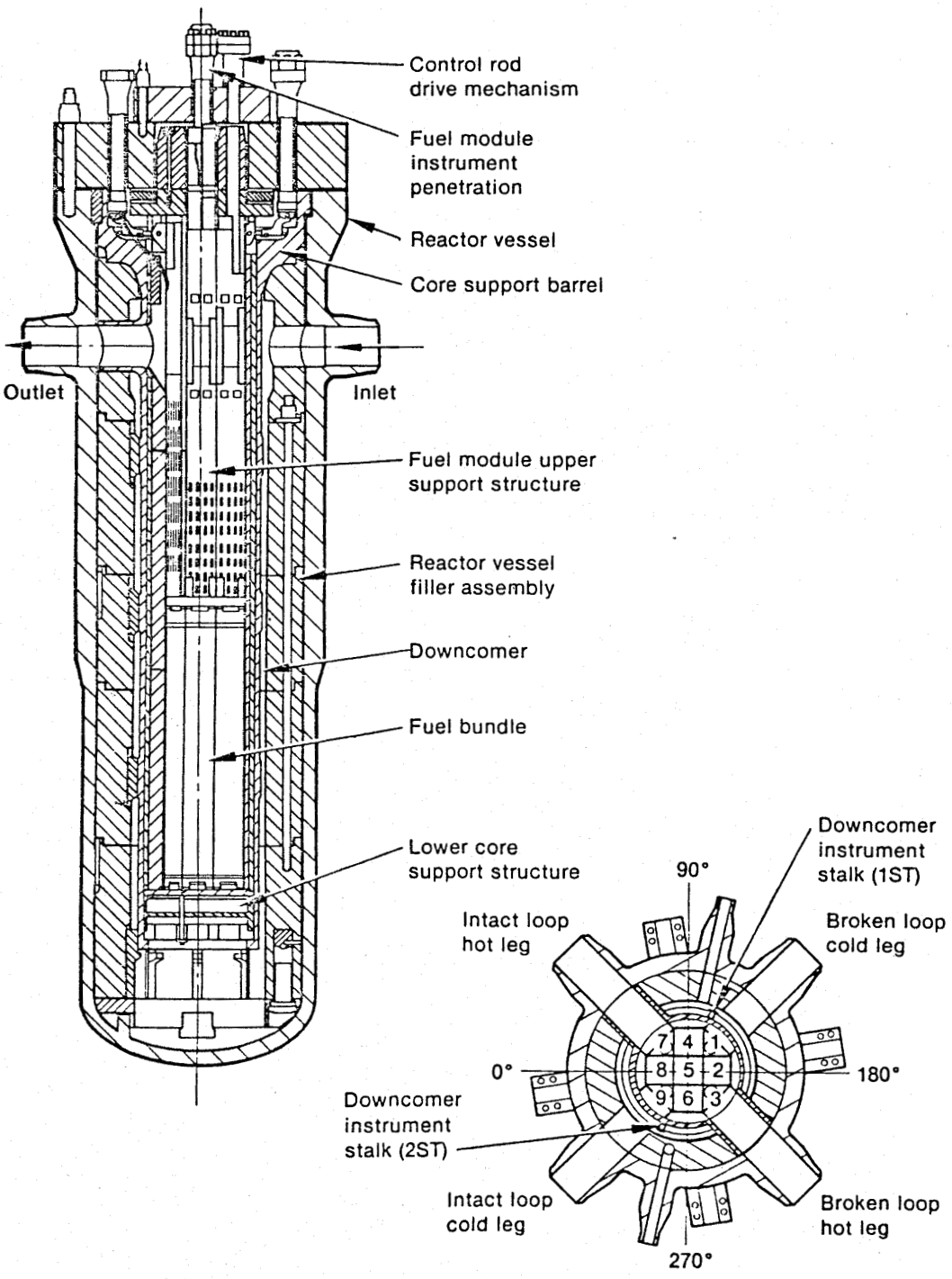

Fig. 5 - 108: LOFT reactor vessel assembly

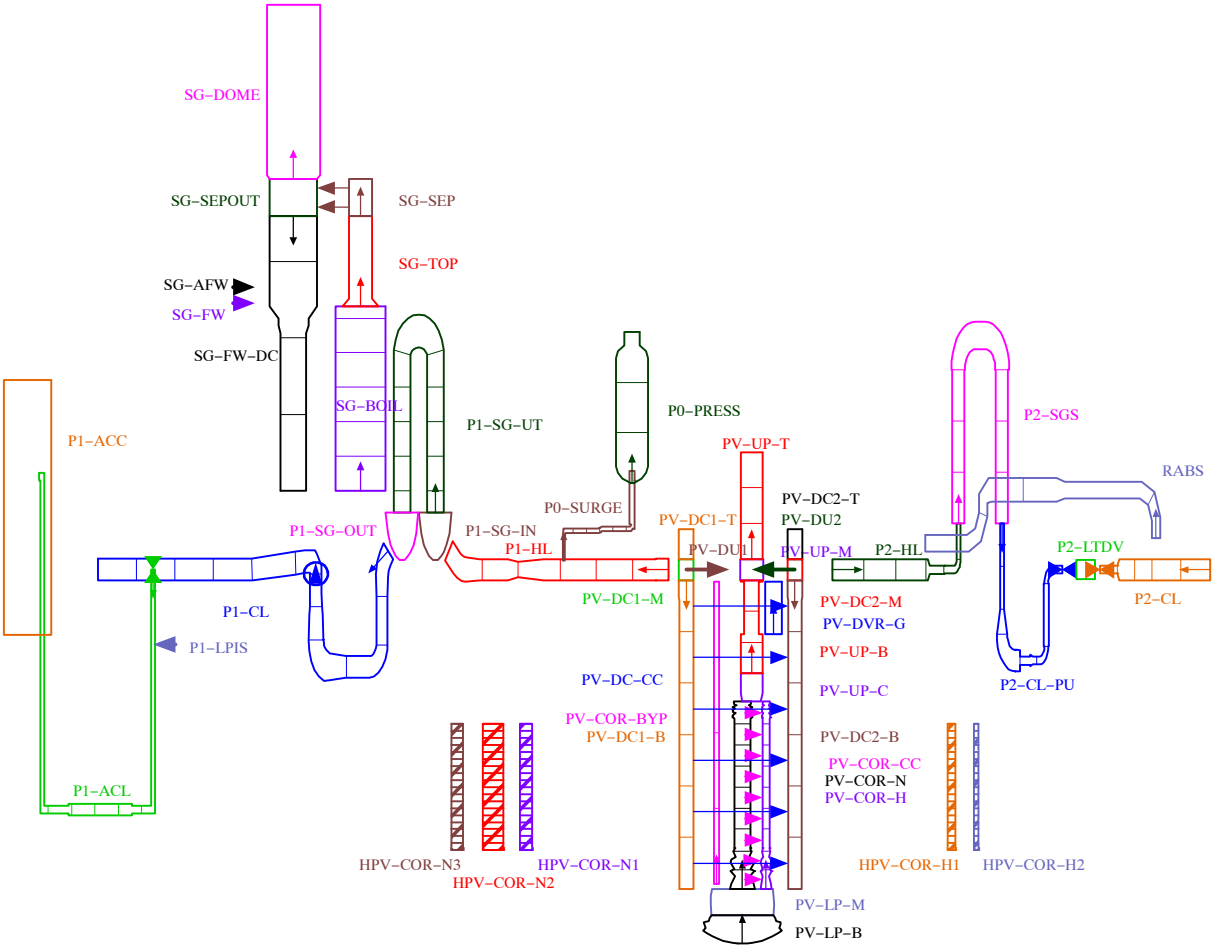

Fig. 5 - 109: Nodalization of LOFT LP-LB-1 for ATHLET

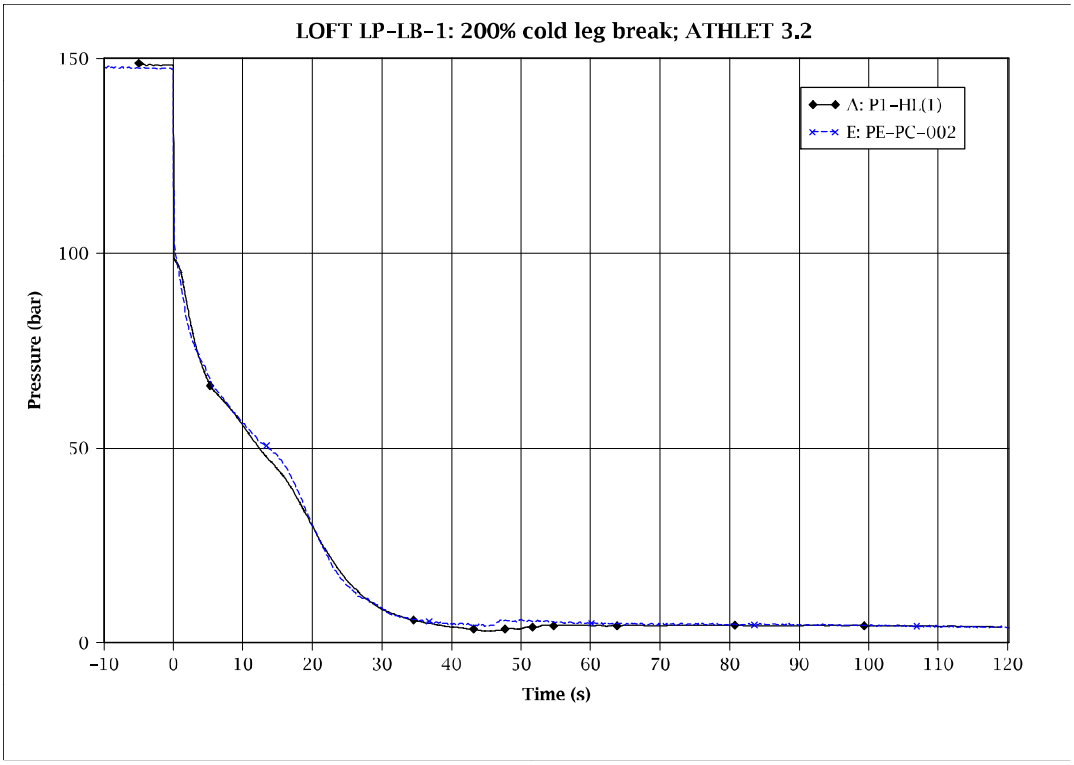

Fig. 5 - 110: Pressure in IL hot leg

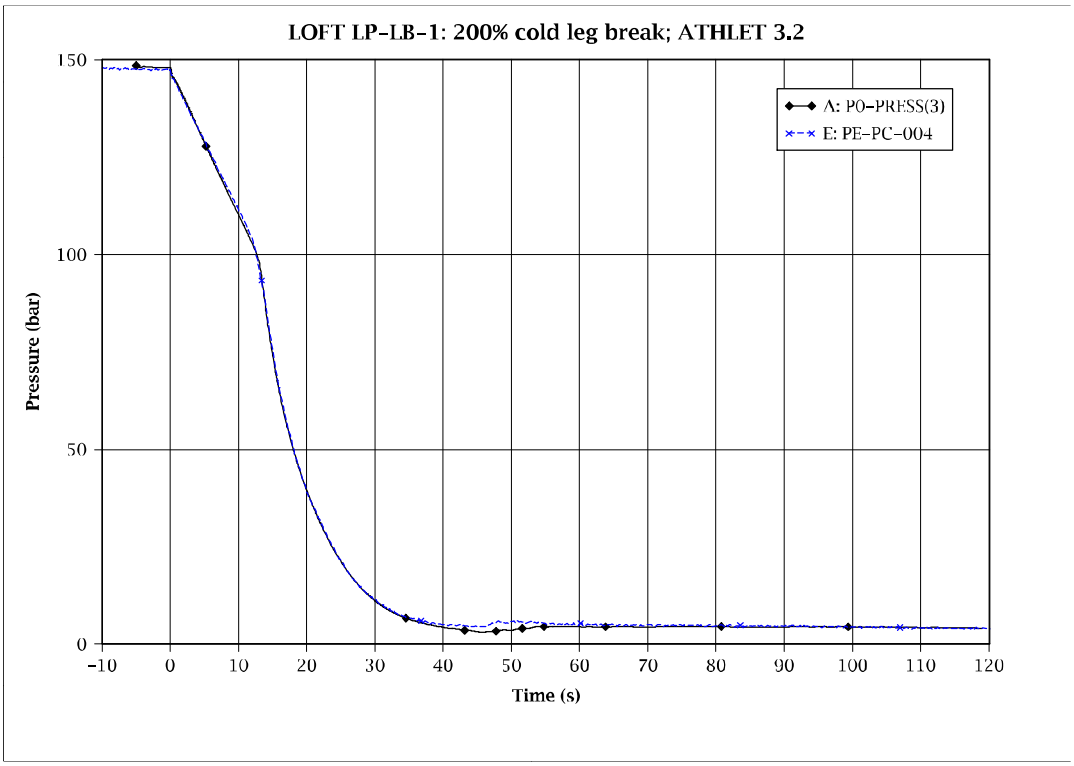

Fig. 5 - 111: Pressure in pressurizer

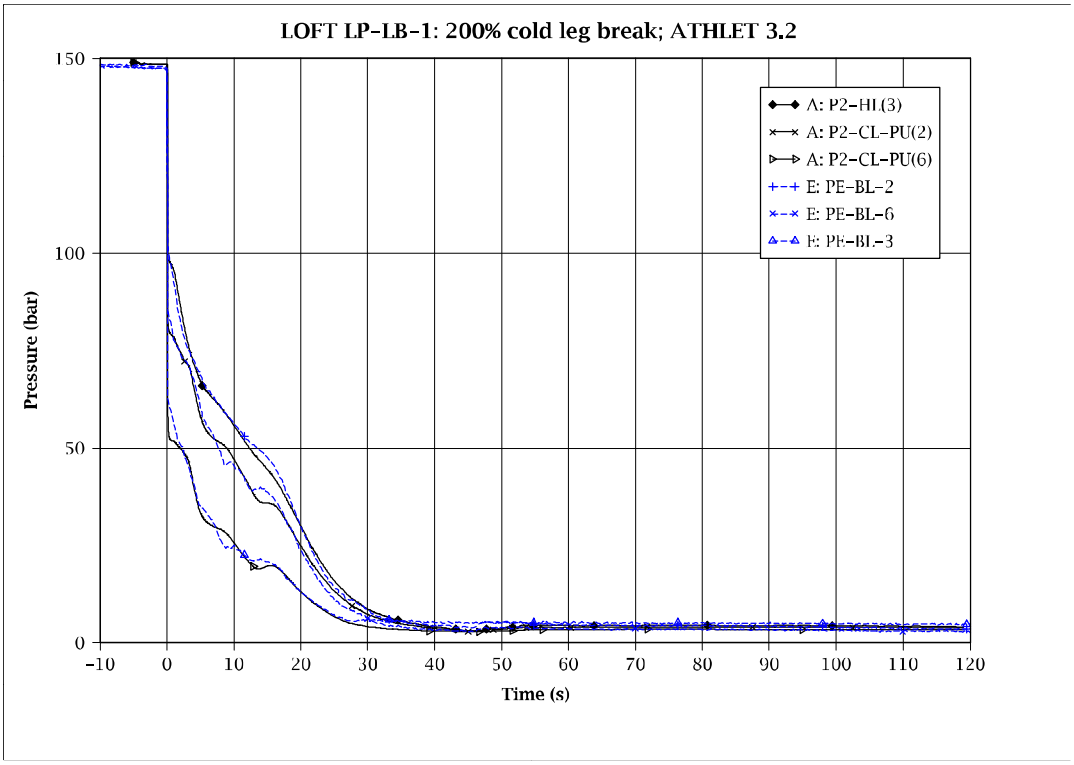

Fig. 5 - 112: Pressure in BL

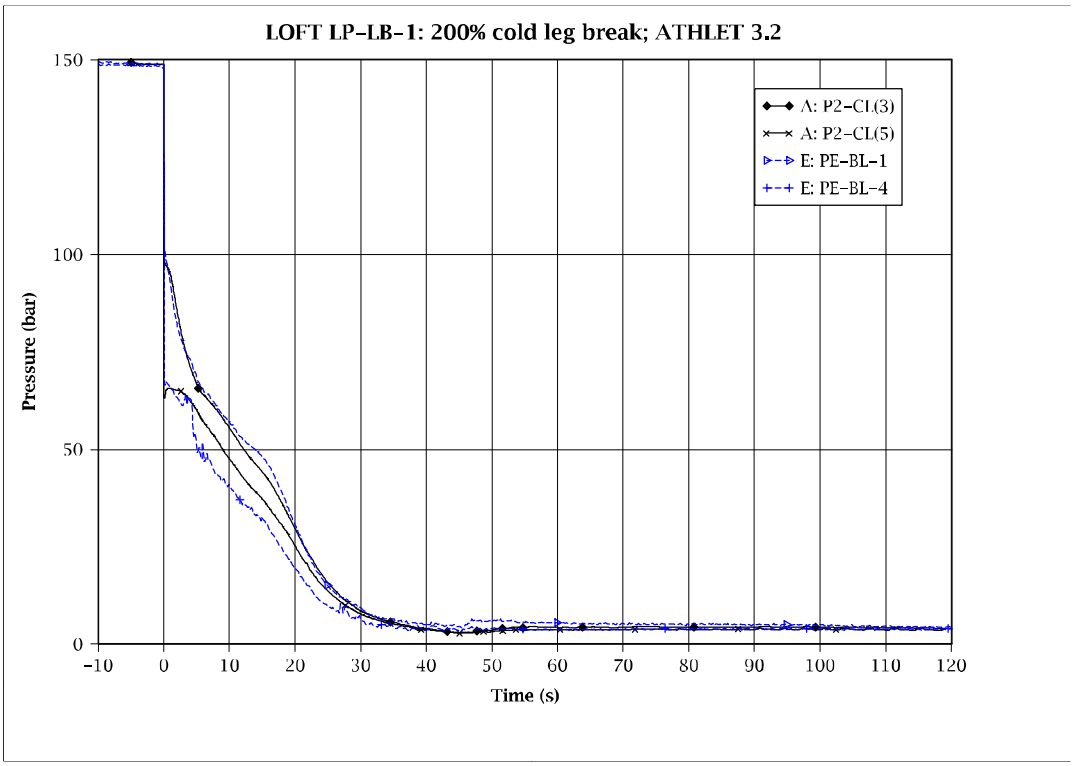

Fig. 5 - 113: Pressure in BL cold leg (RV side)

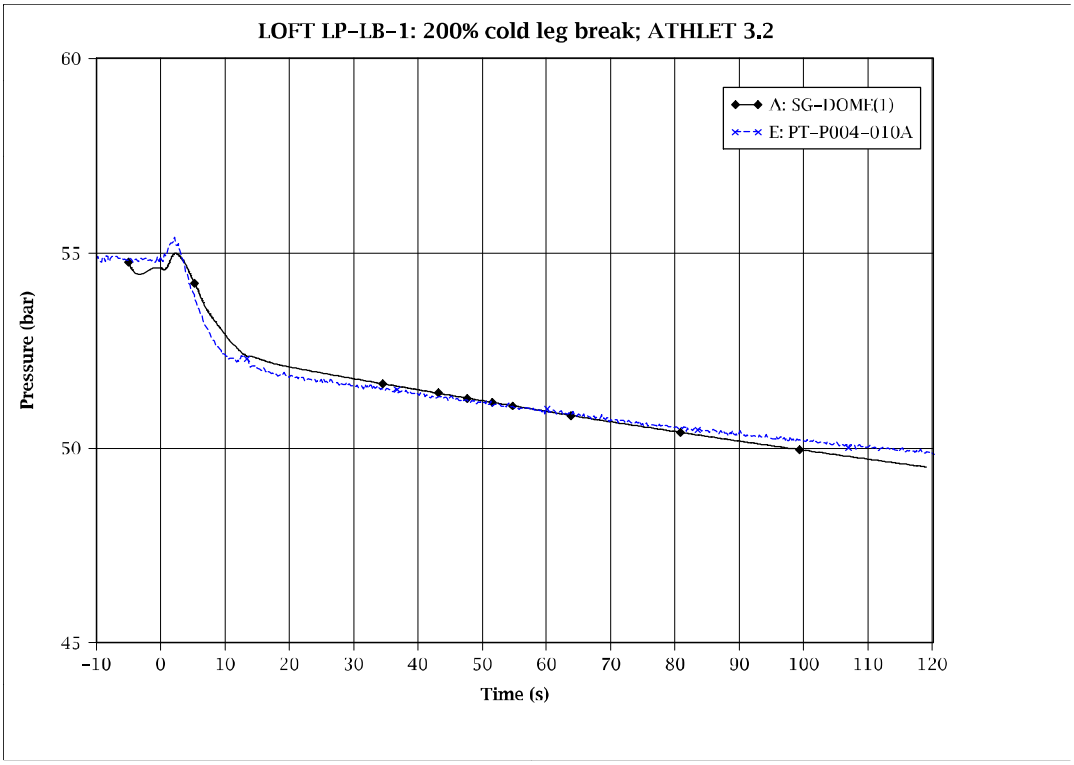

Fig. 5 - 114: Pressure on secondary side

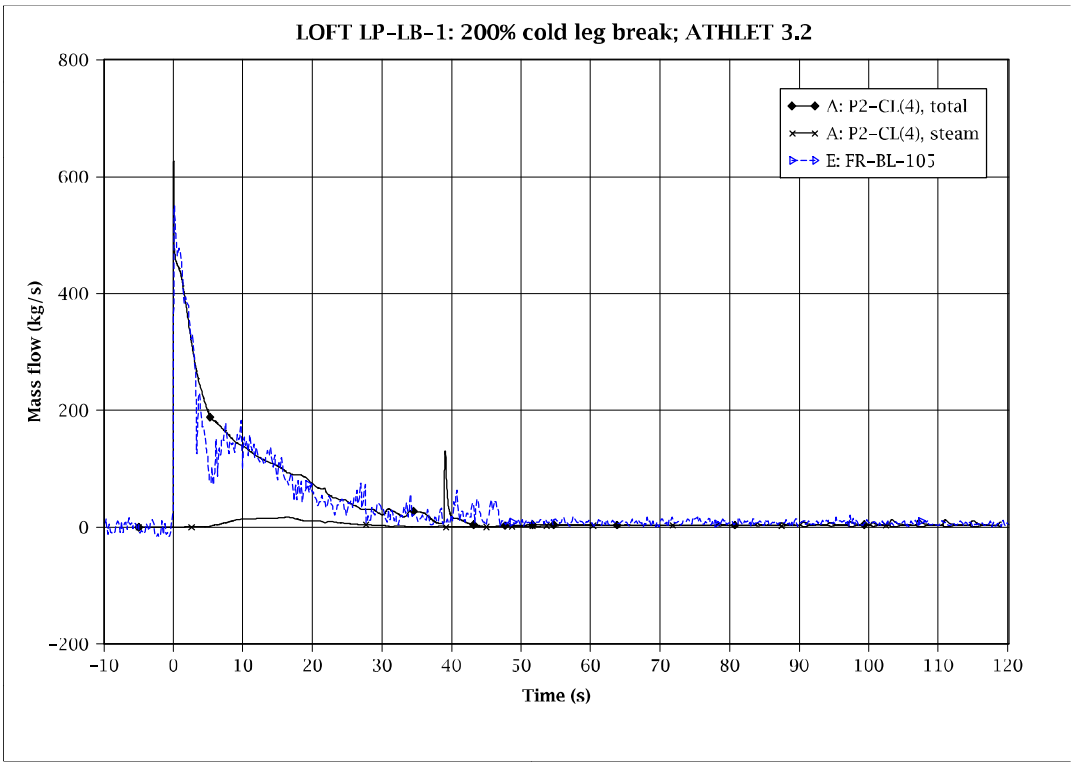

Fig. 5 - 115: Mass flow in BL cold leg

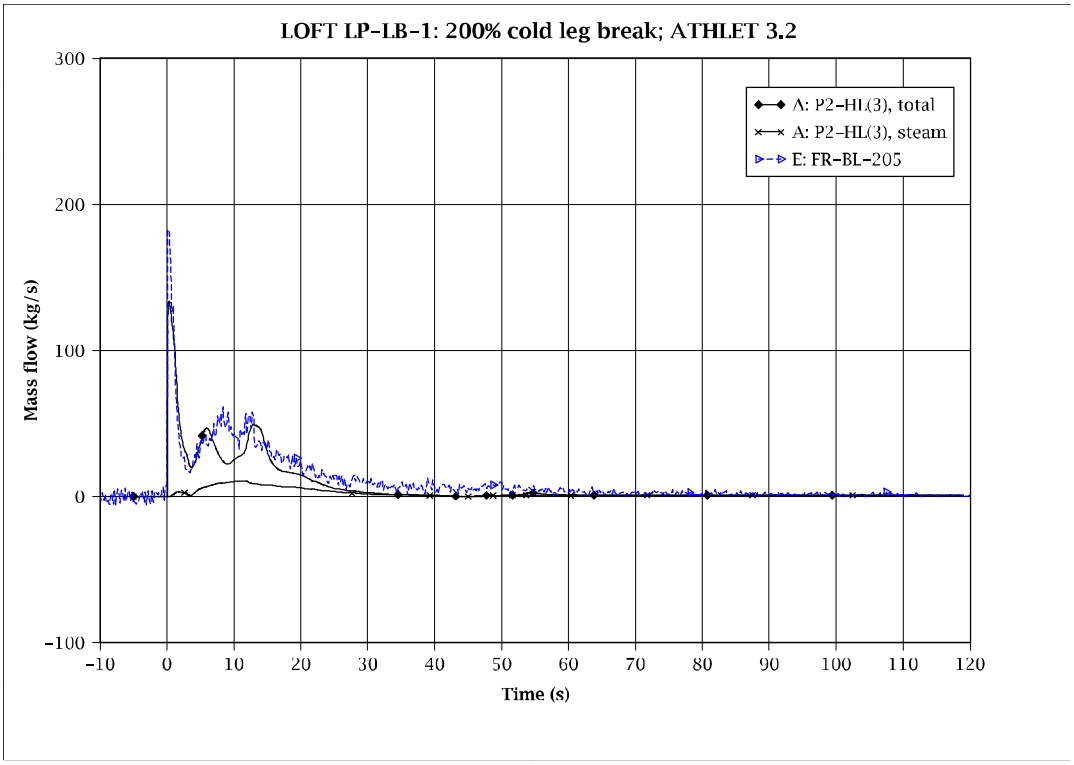

Fig. 5 - 116: Mass flow in BL hot leg

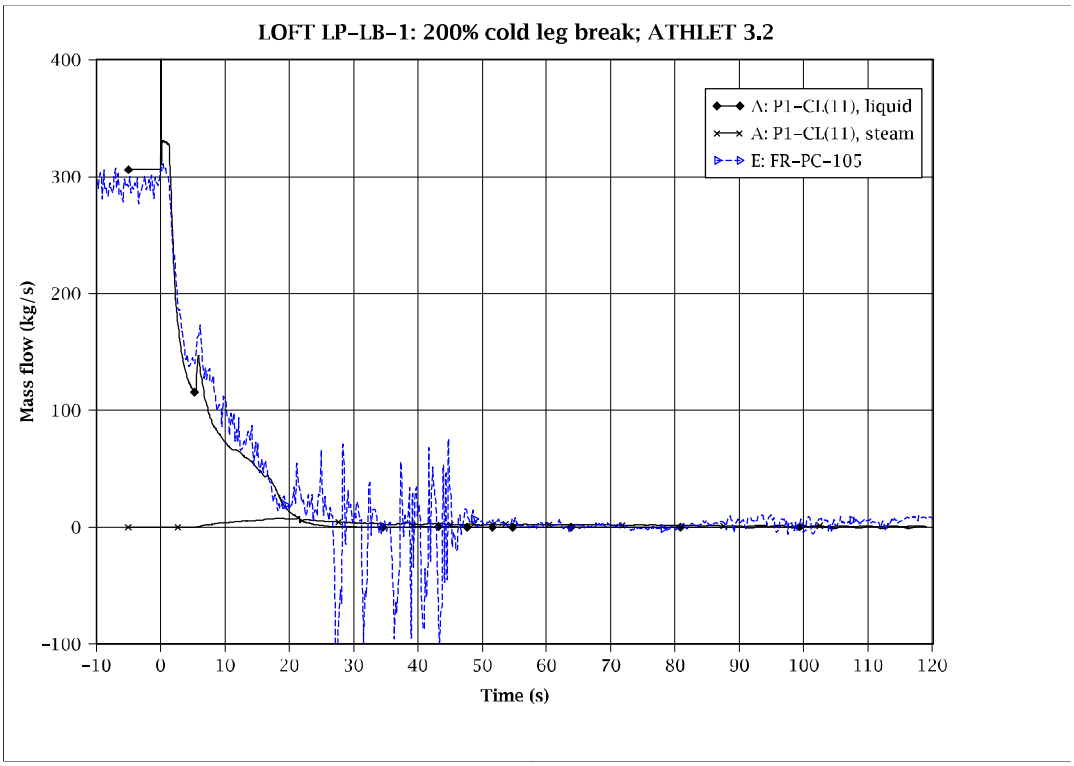

Fig. 5 - 117: Mass flow in IL cold leg

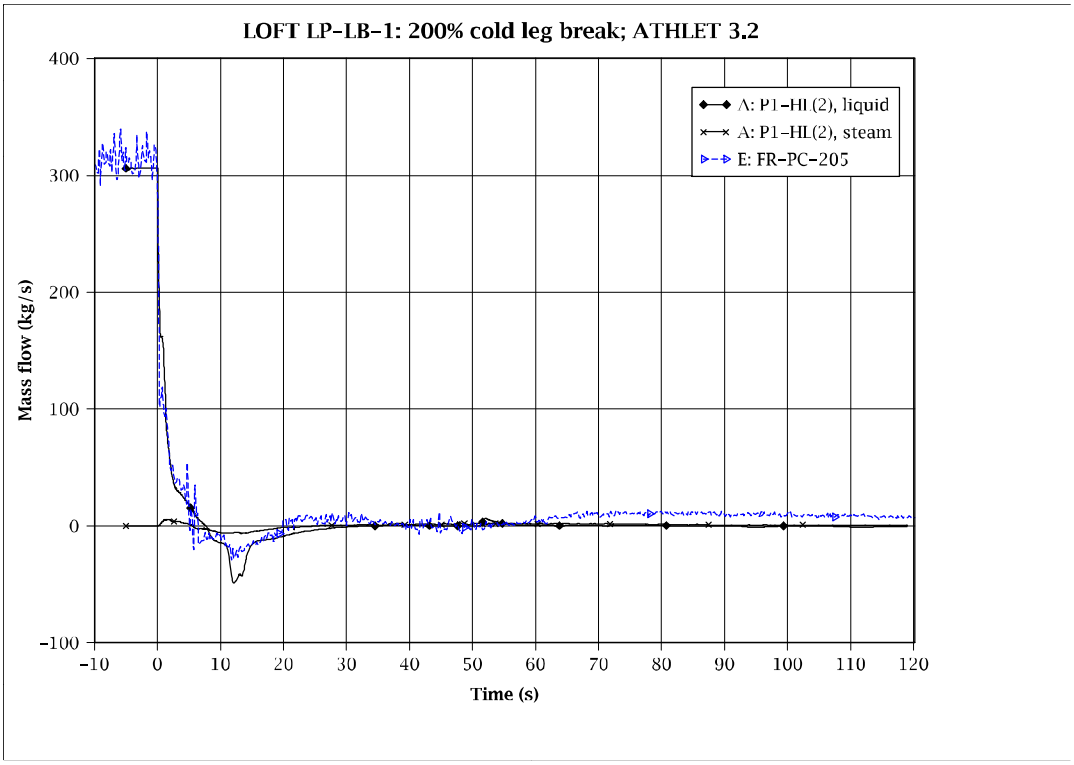

Fig. 5 - 118: Mass flow in IL hot leg

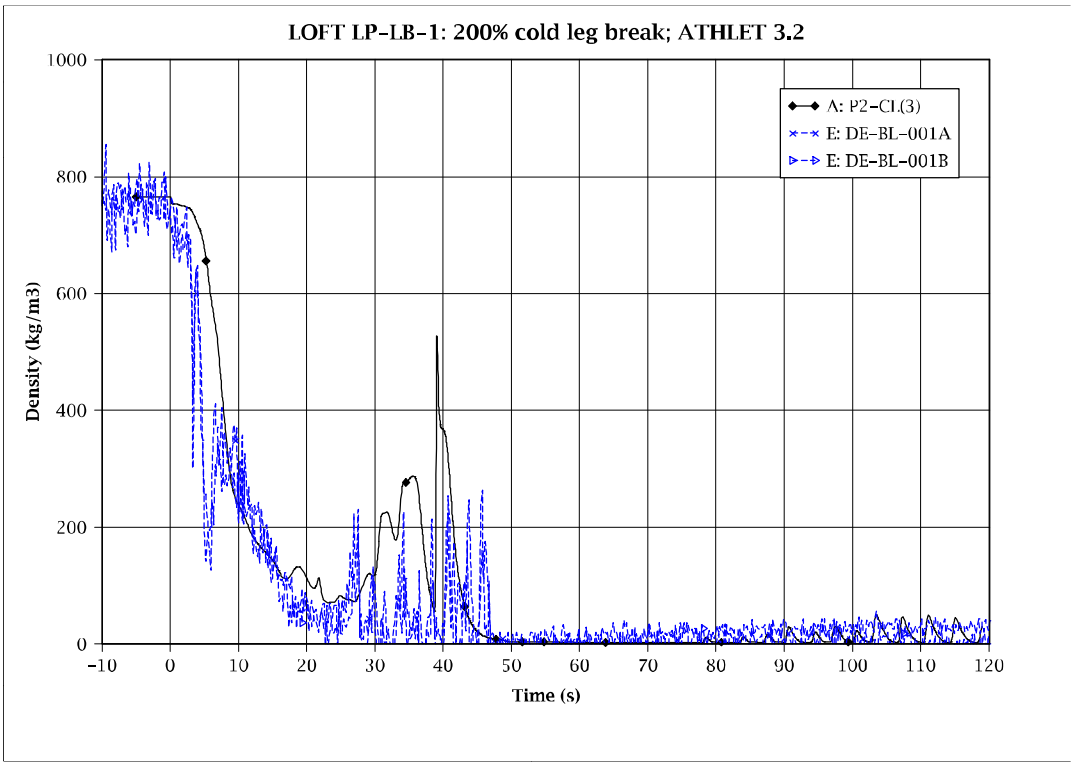

Fig. 5 - 119: Fluid density in BL cold leg

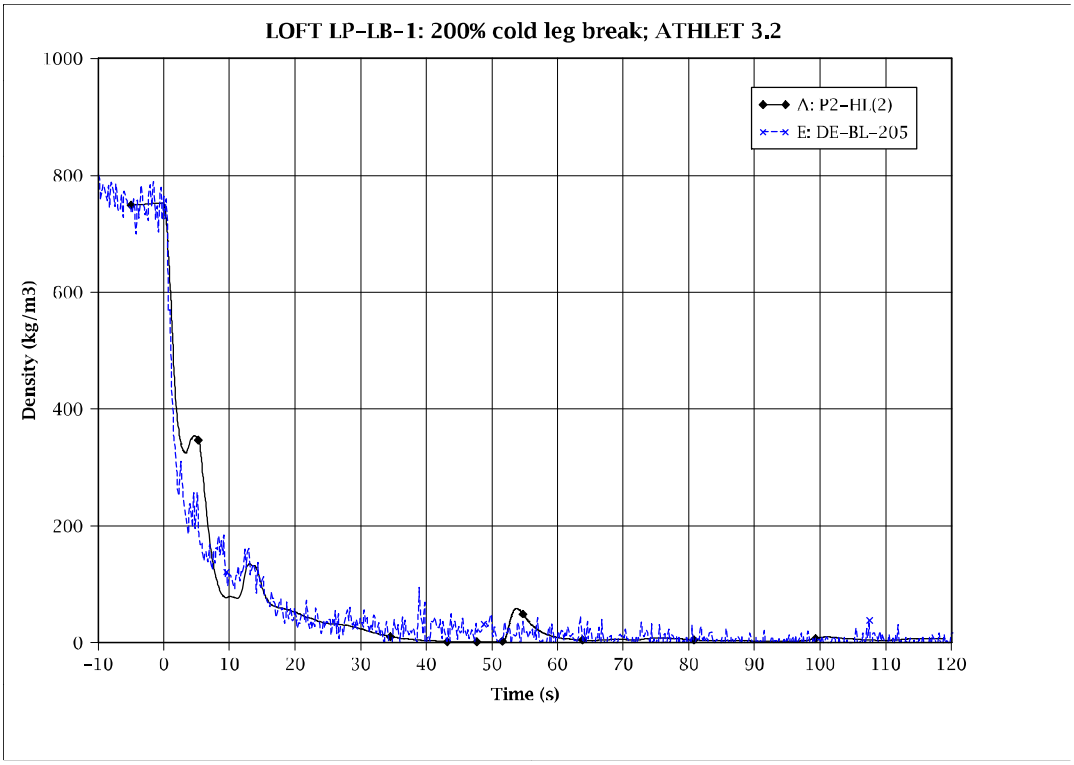

Fig. 5 - 120: Fluid density in BL hot leg

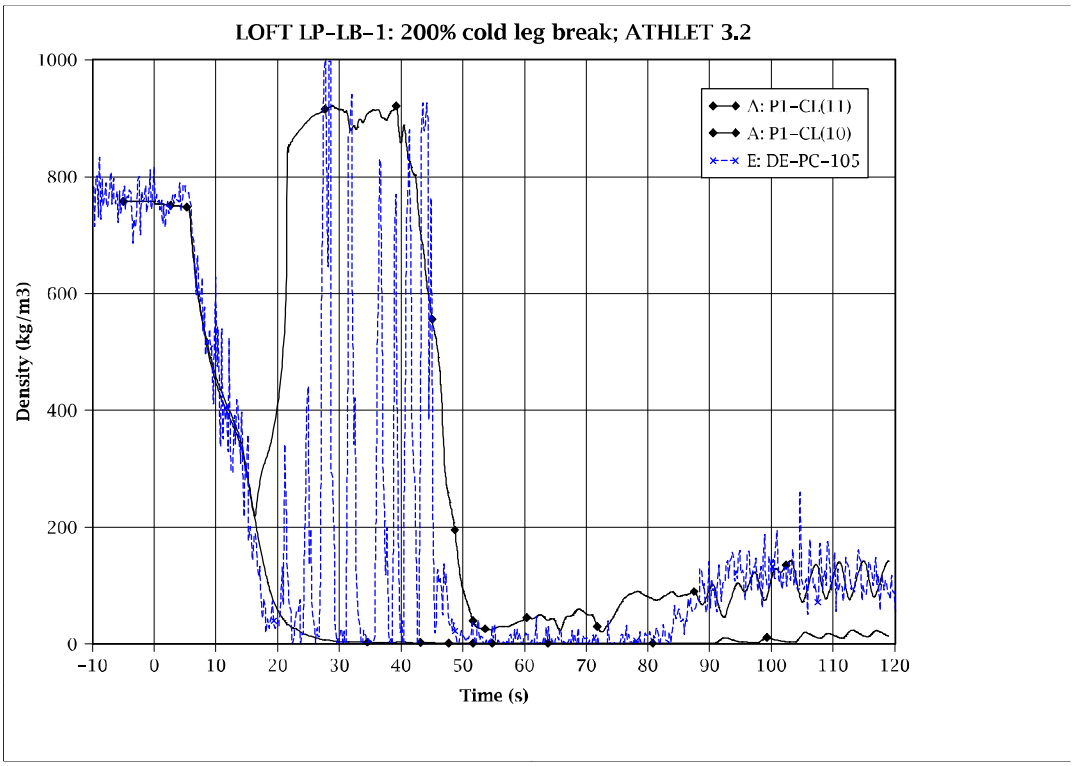

Fig. 5 - 121: Fluid density in IL cold leg

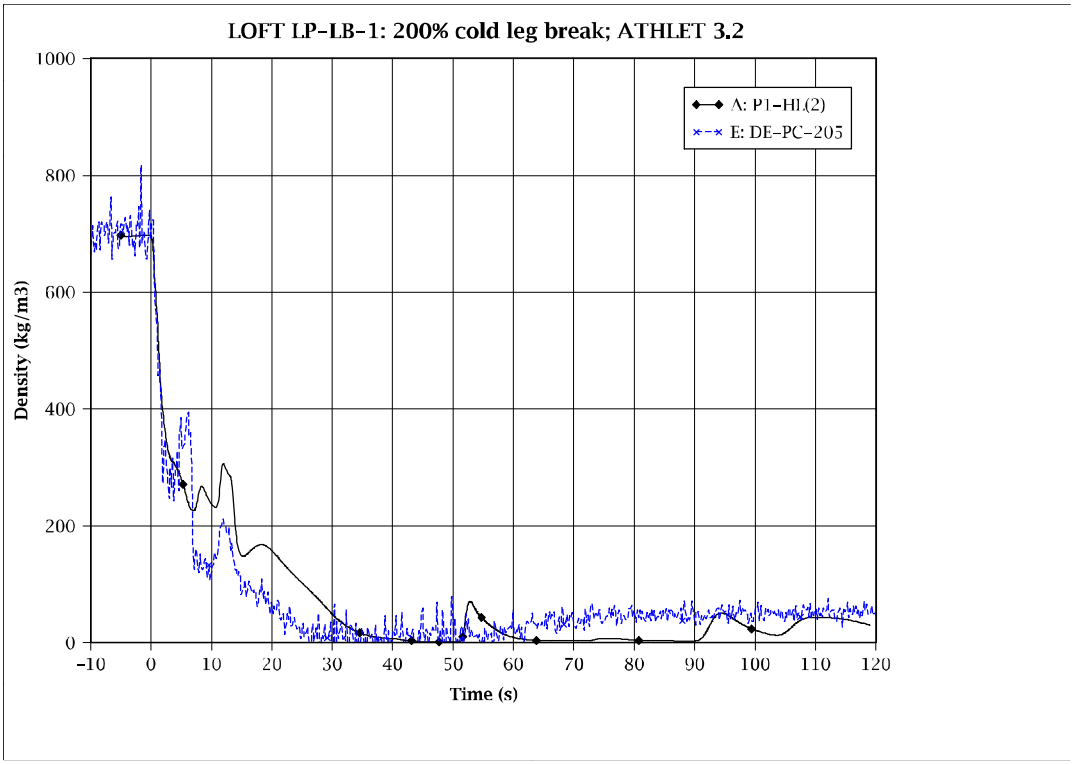

Fig. 5 - 122: Fluid density in IL hot leg

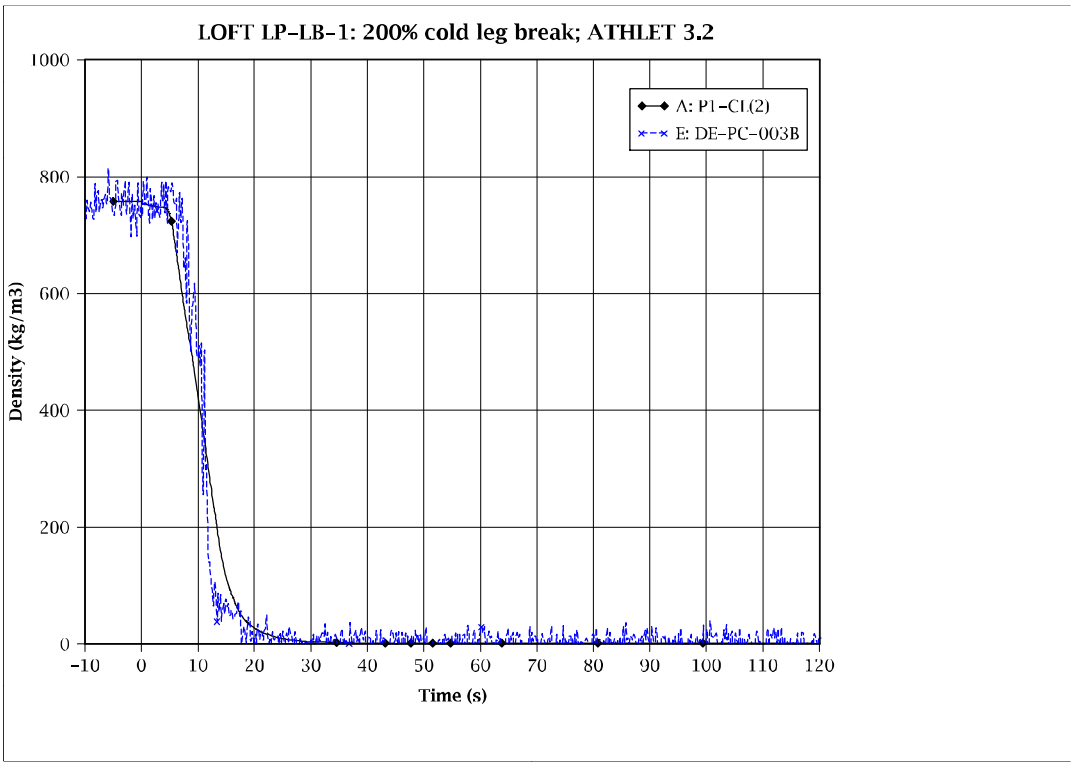

Fig. 5 - 123: Fluid density in IL SG outlet

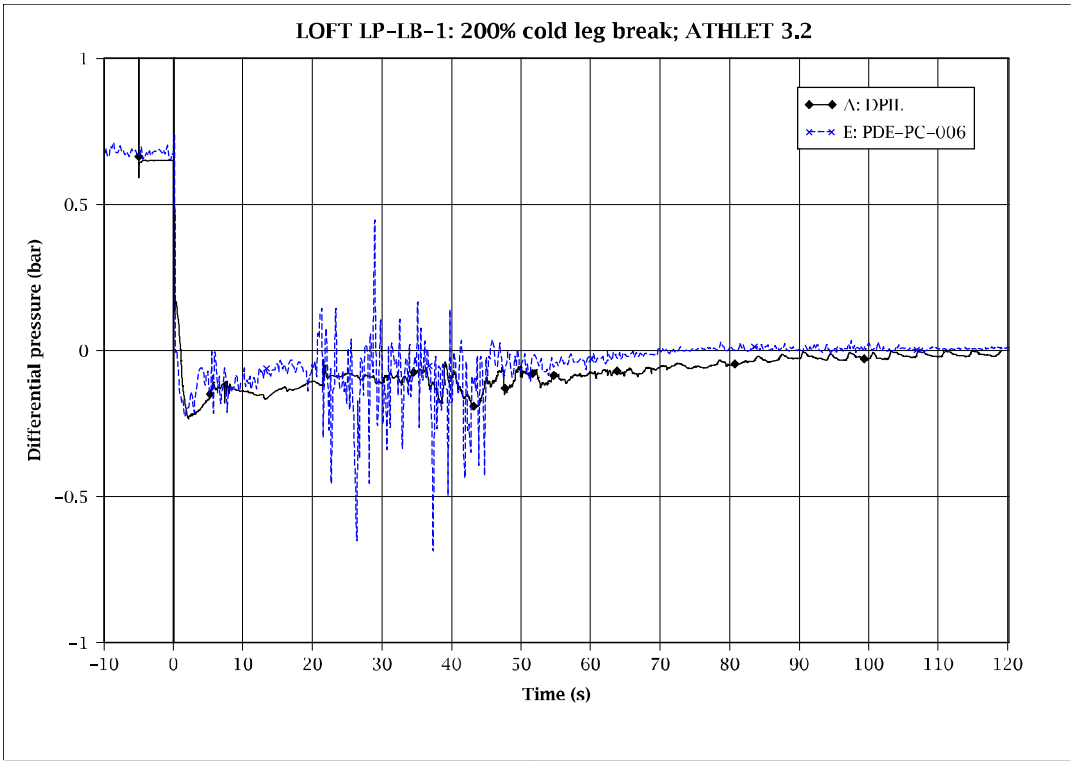

Fig. 5 - 124: Differential pressure in IL (CL nozzle - HL nozzle)

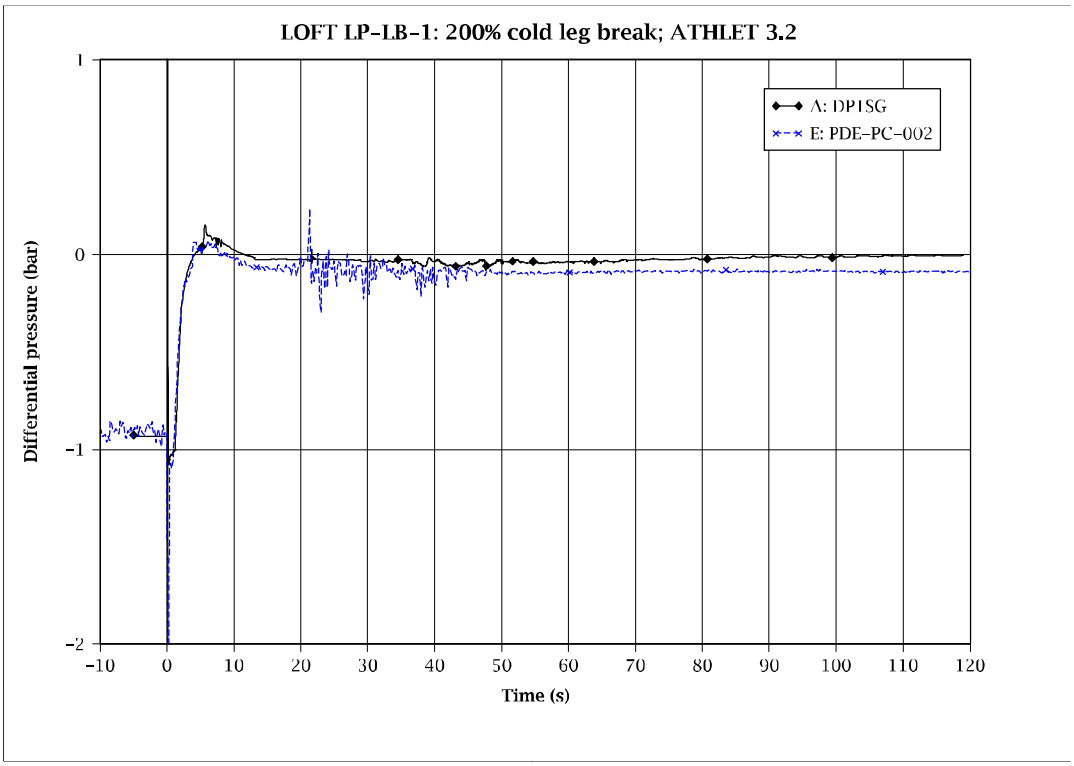

Fig. 5 - 125: Differential pressure across IL steam generator

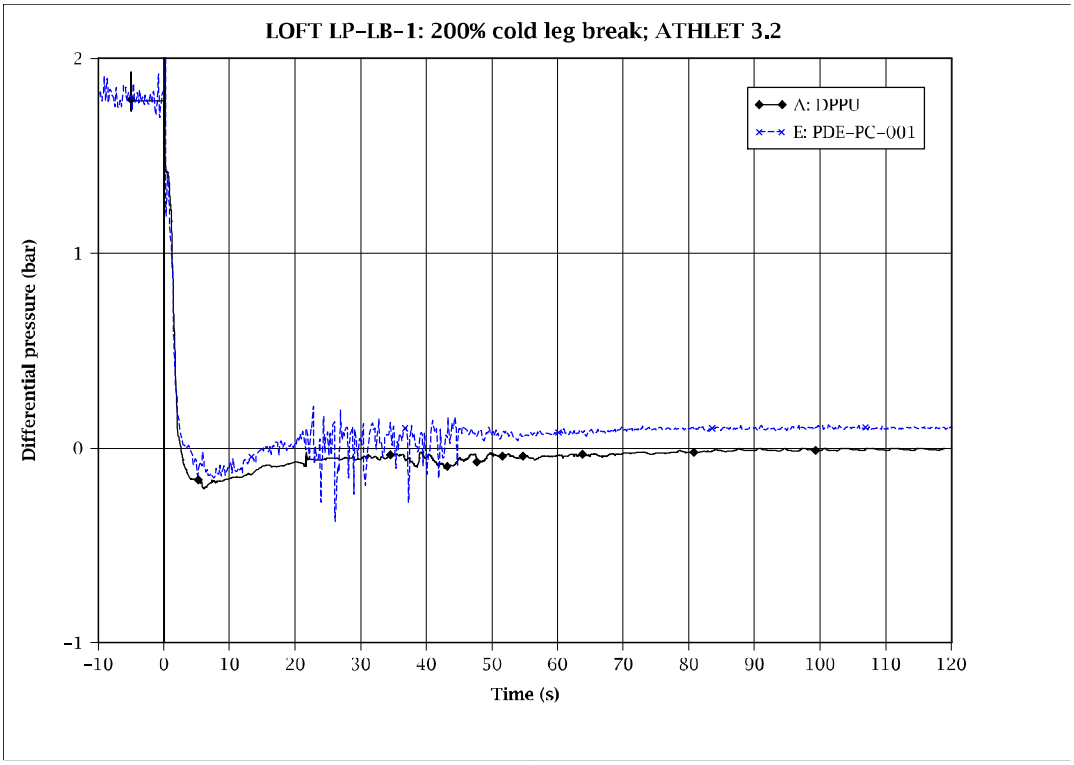

Fig. 5 - 126: Differential pressure across IL pumps

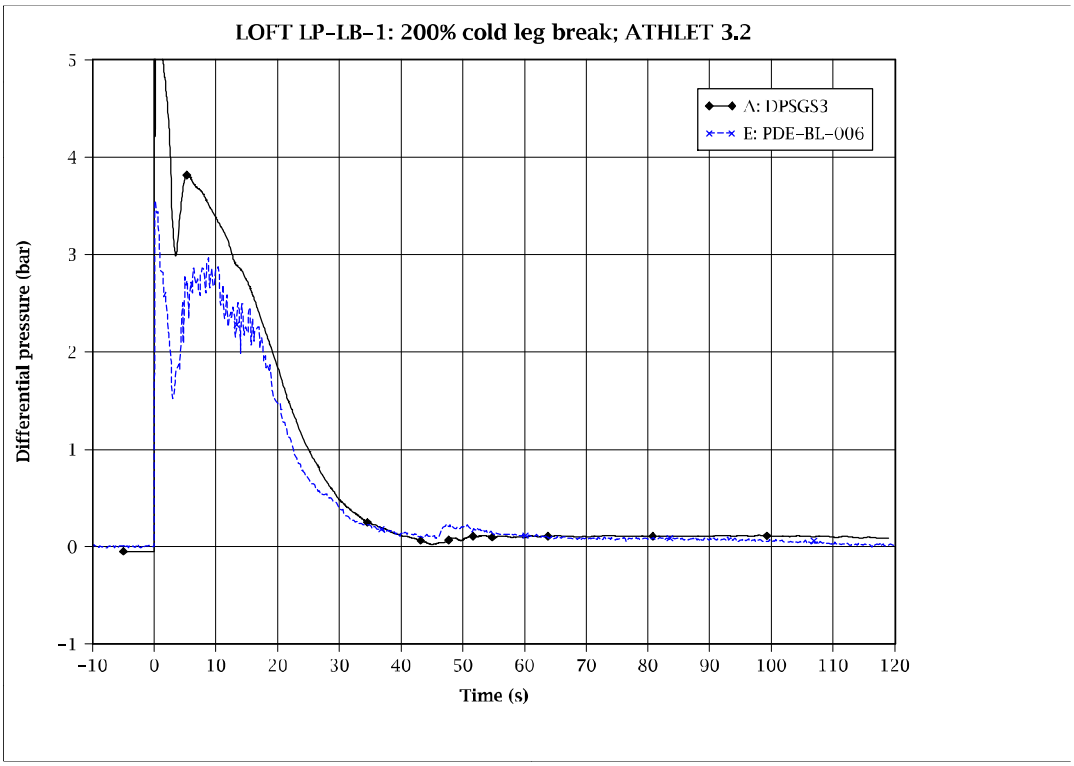

Fig. 5 - 127: Differential pressure across BL steam generator outlet orifice

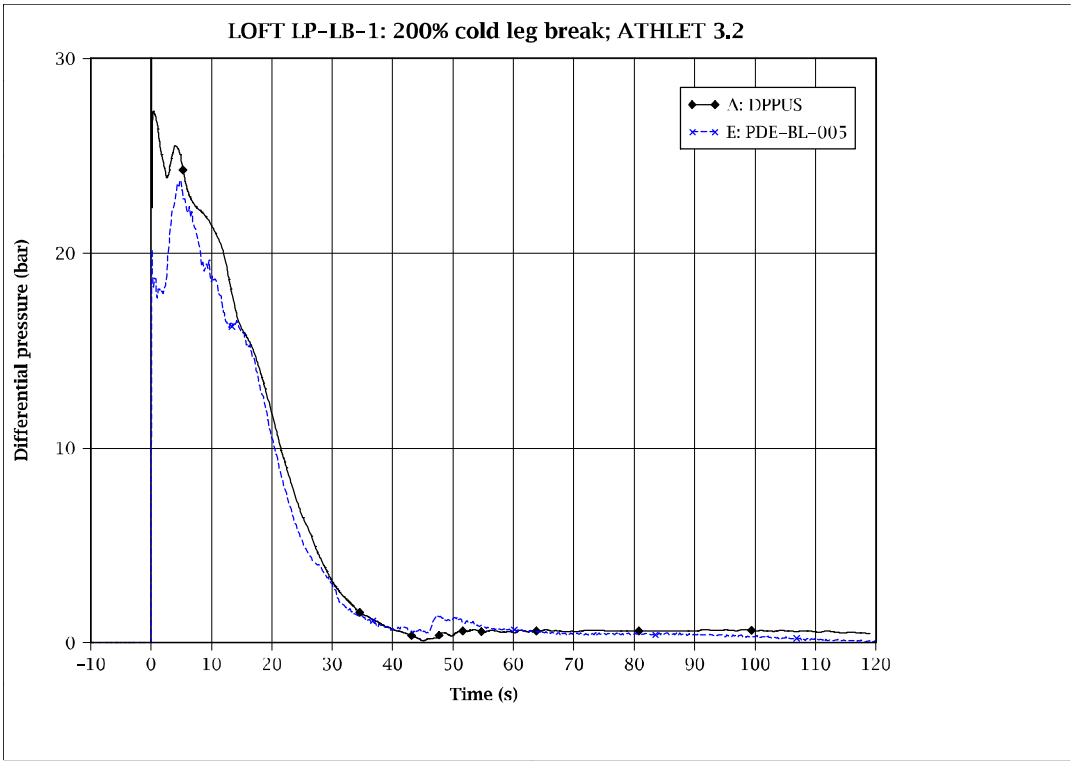

Fig. 5 - 128: Differential pressure across BL pump simulator

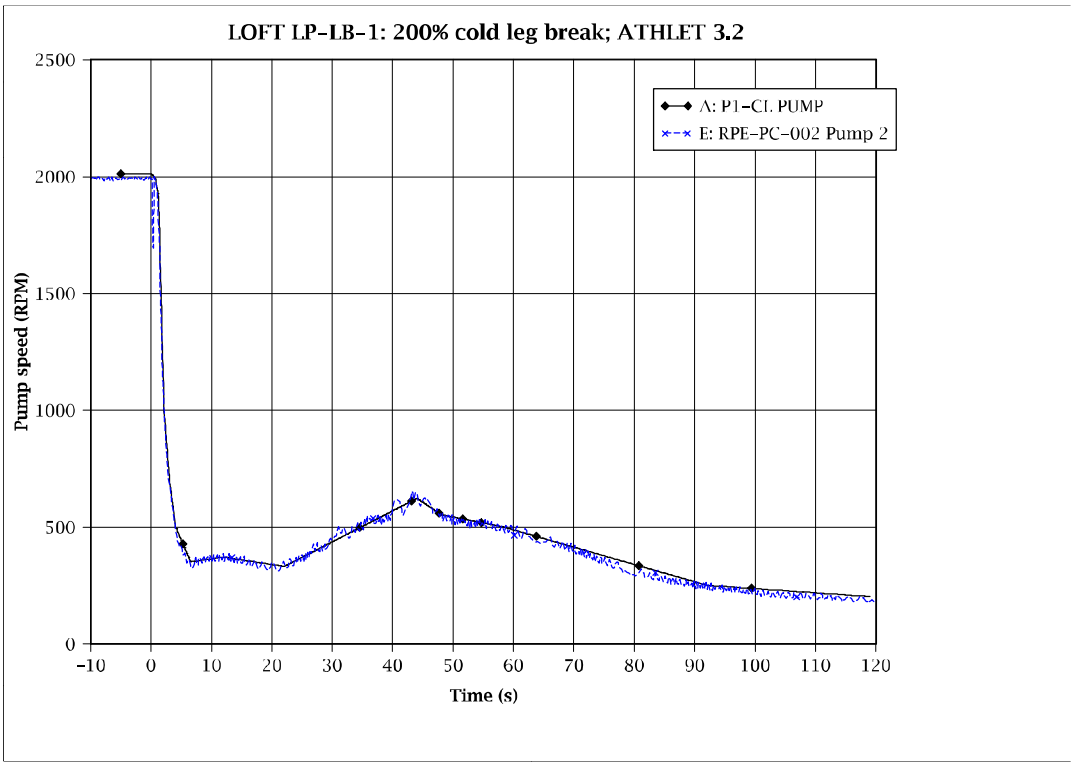

Fig. 5 - 129: Speed of primary coolant pumps

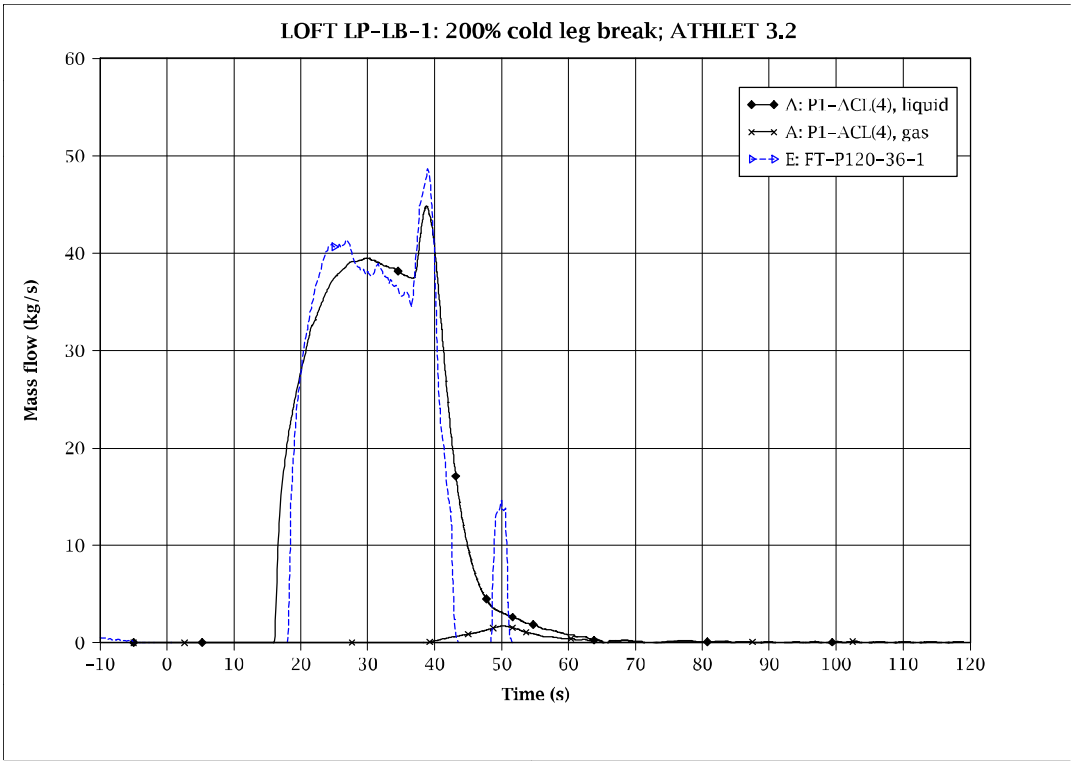

Fig. 5 - 130: Accumulator injection mass flow

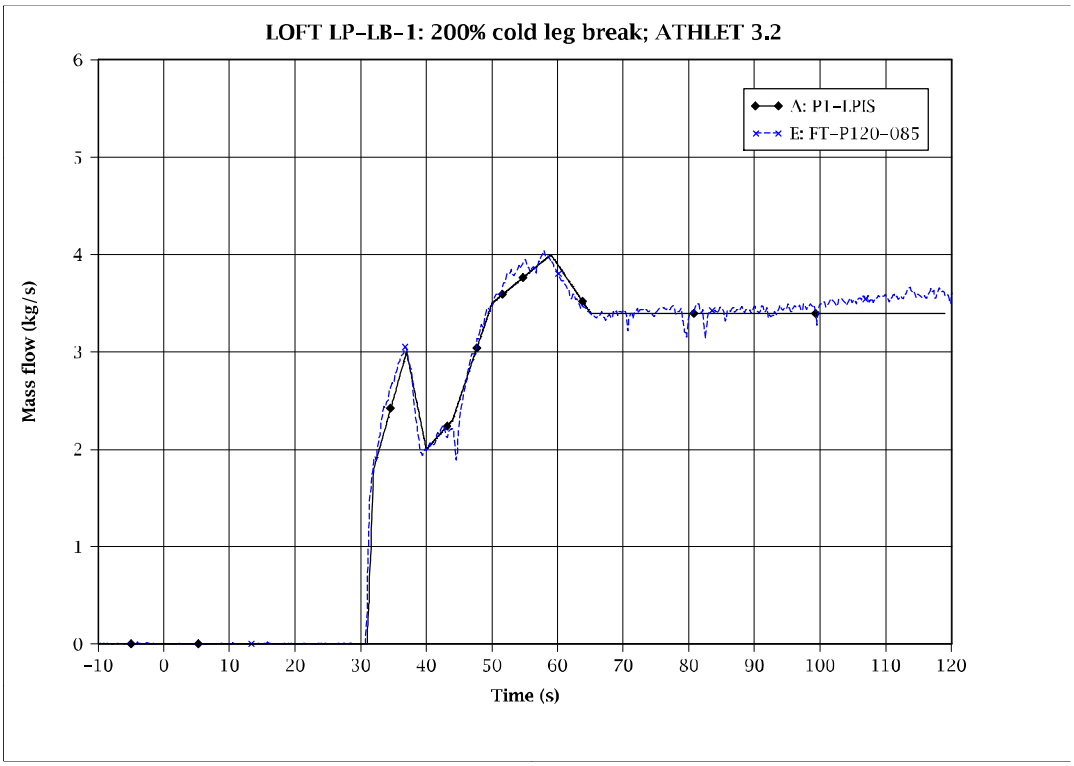

Fig. 5 - 131: LPIS injection mass flow

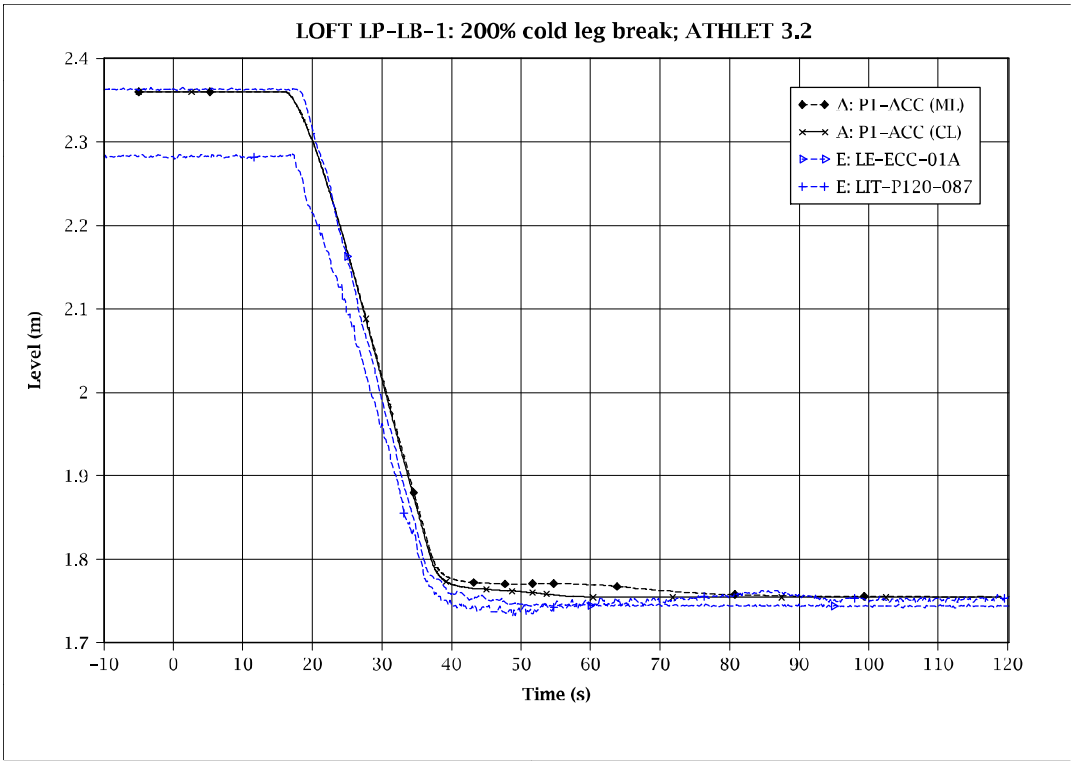

Fig. 5 - 132: Liquid level in accumulator

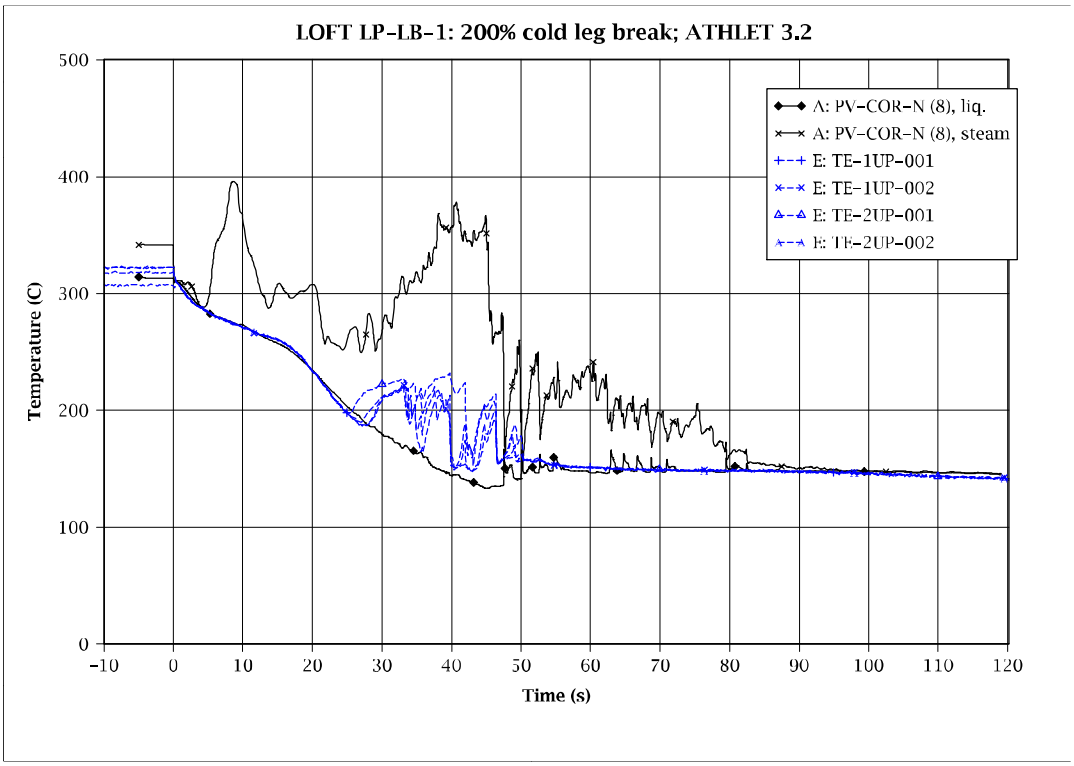

Fig. 5 - 133: Fluid temperature in upper end box

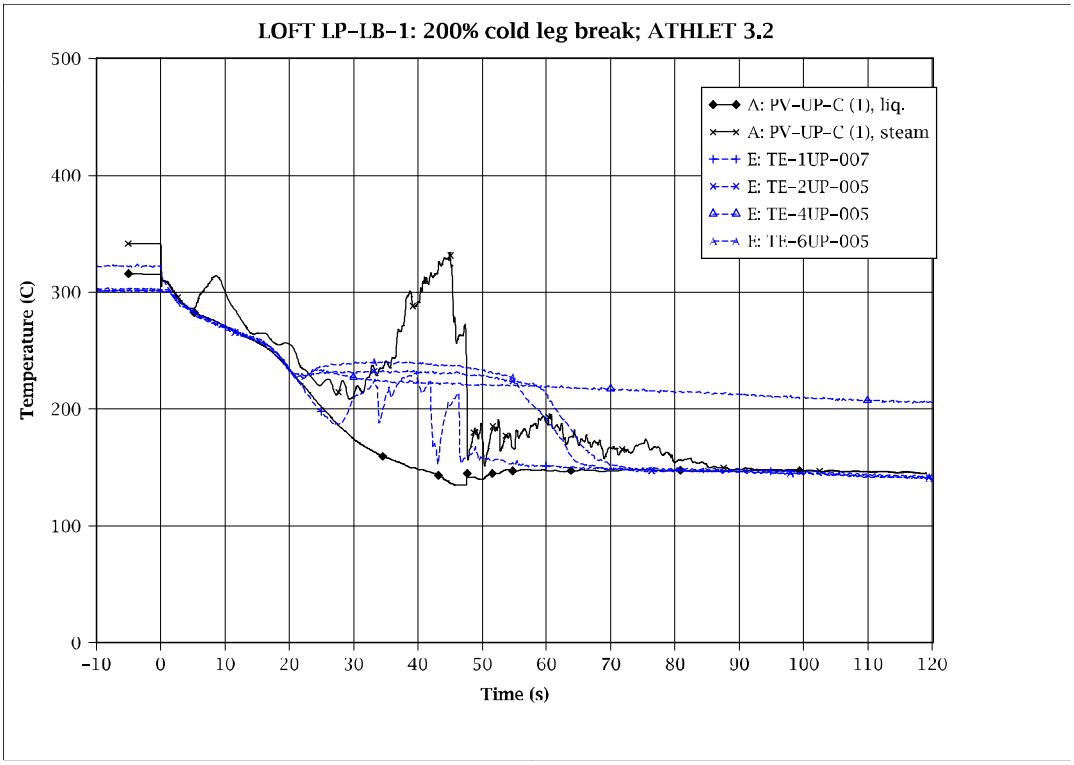

Fig. 5 - 134: Fluid temperature in upper plenum

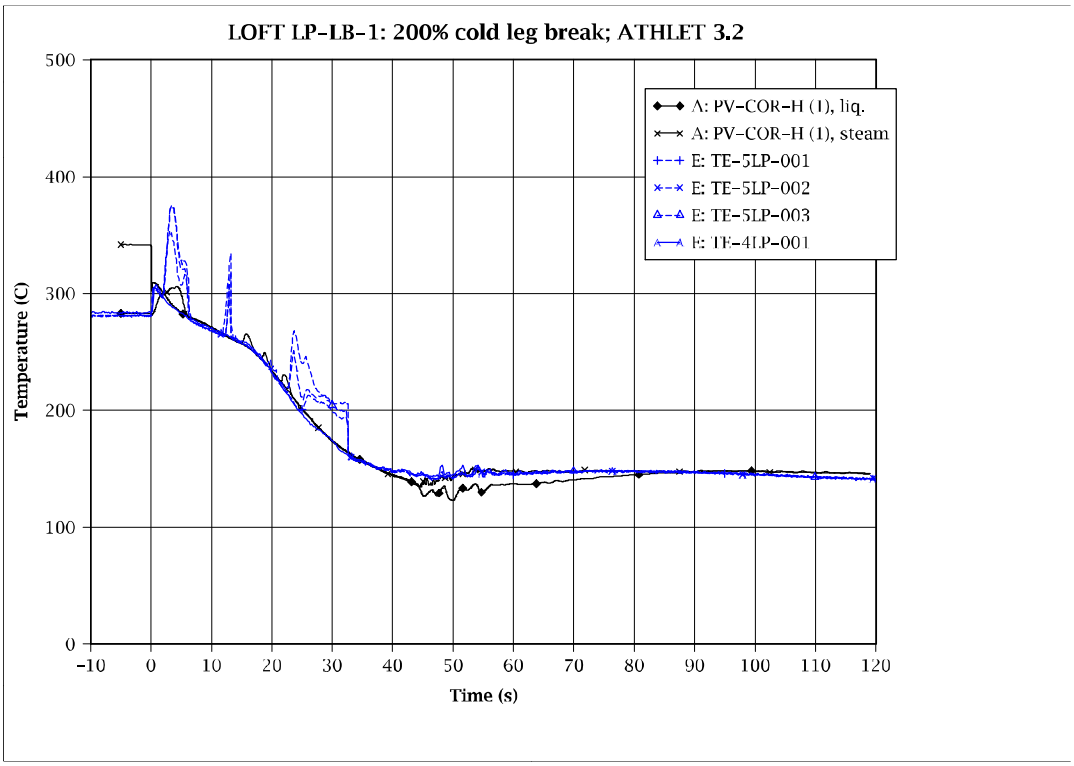

Fig. 5 - 135: Fluid temperature in lower end box

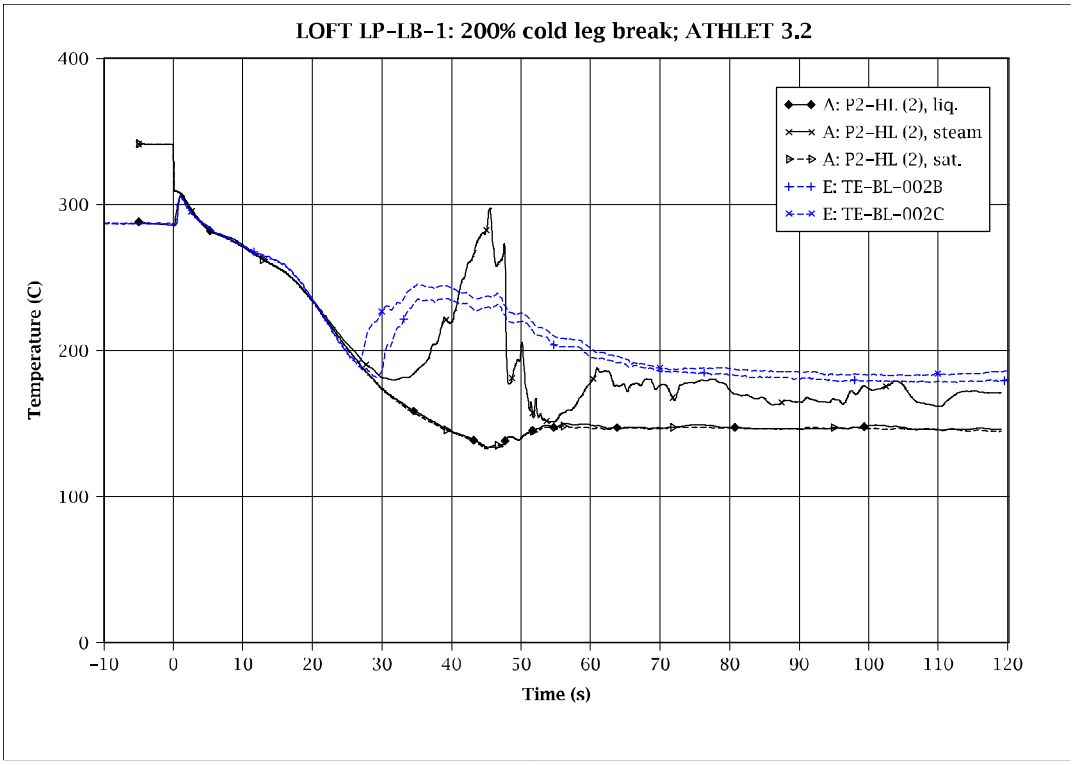

Fig. 5 - 136: Fluid temperature in BL hot leg

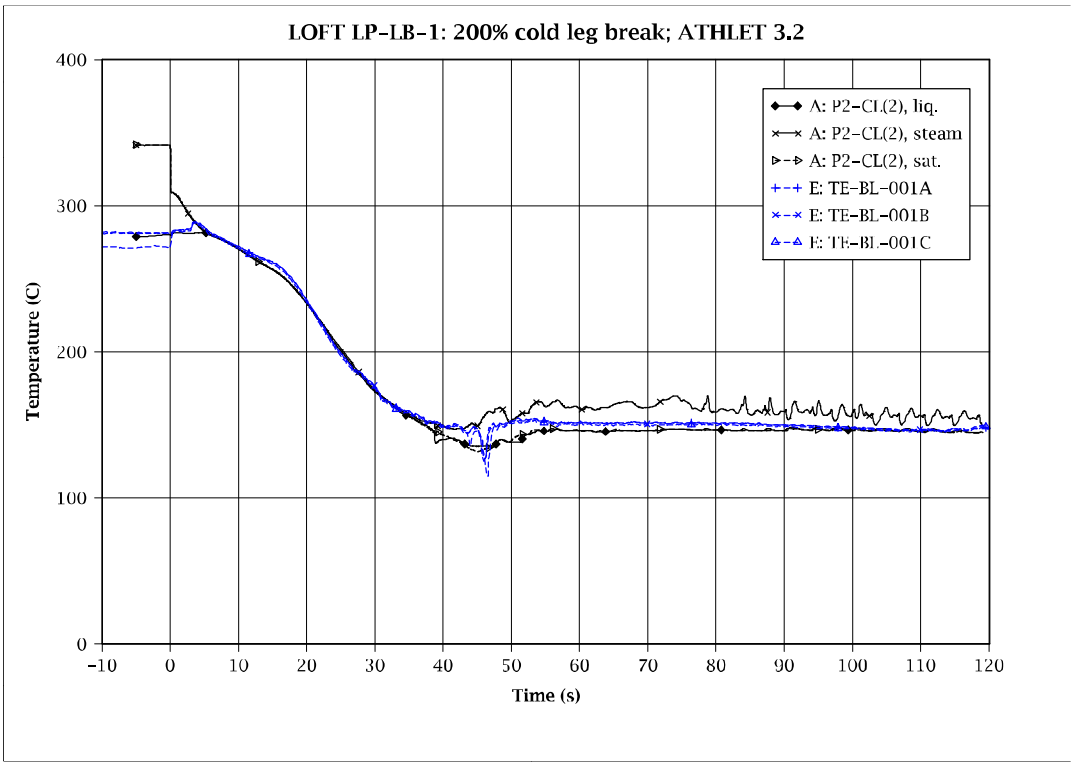

Fig. 5 - 137: Fluid temperature in BL cold leg

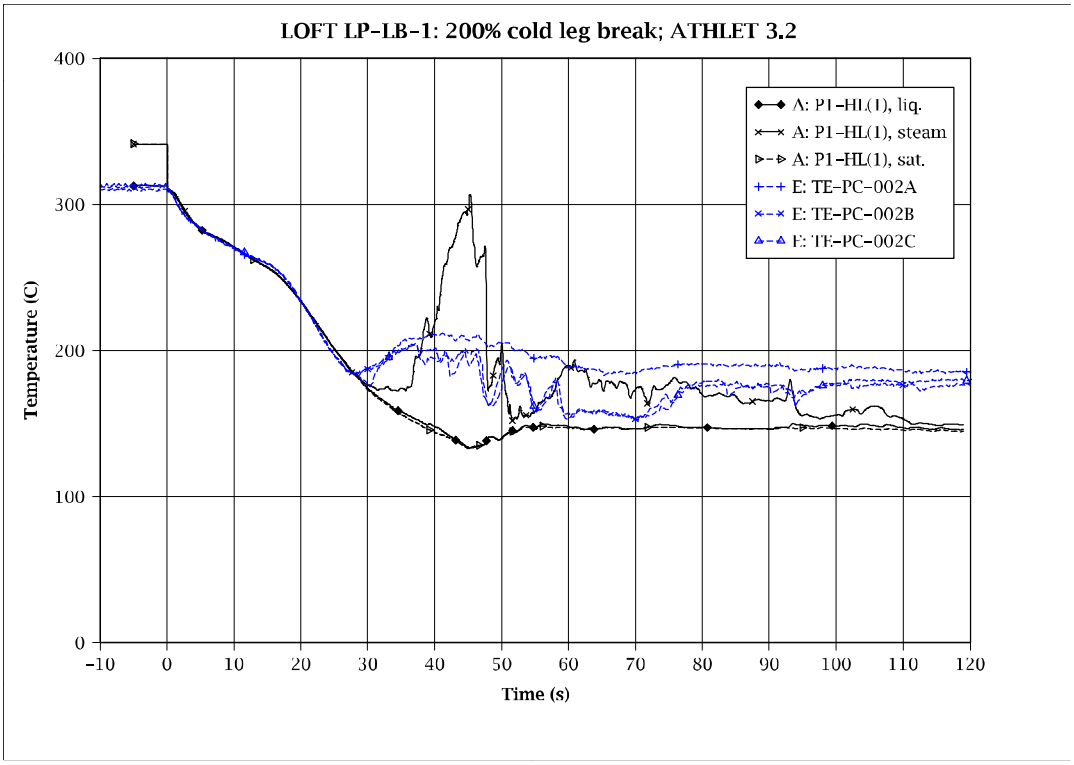

Fig. 5 - 138: Fluid temperature in IL hot leg

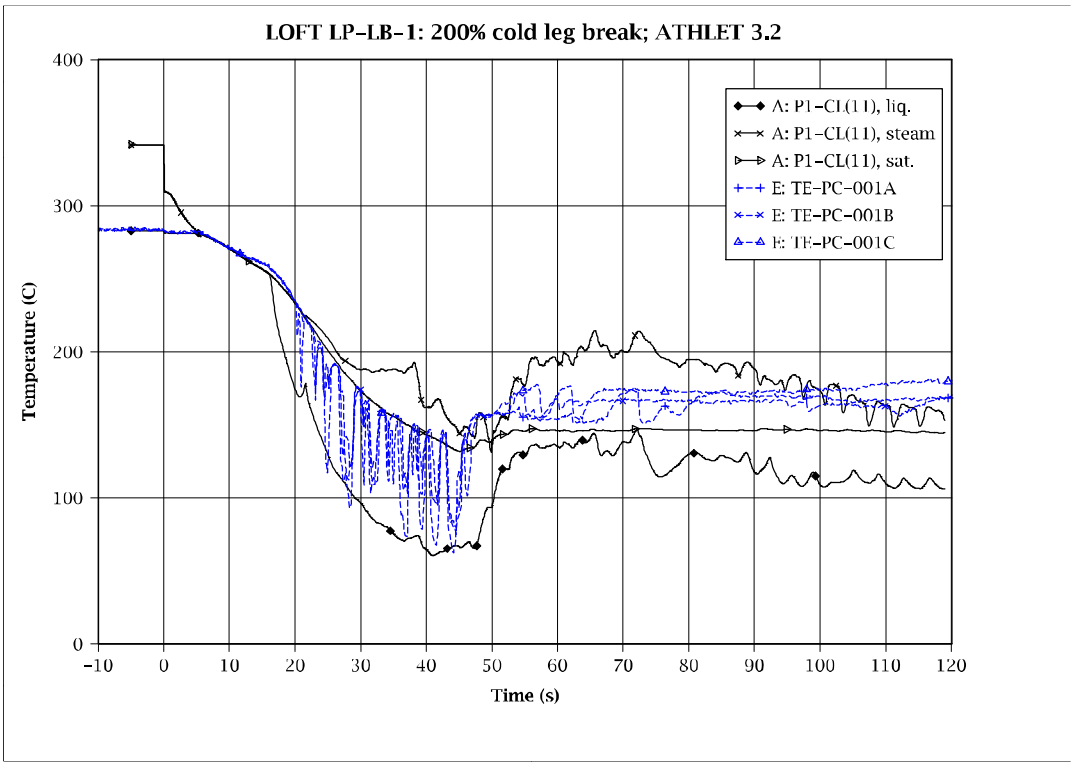

Fig. 5 - 139: Fluid temperature in IL cold leg

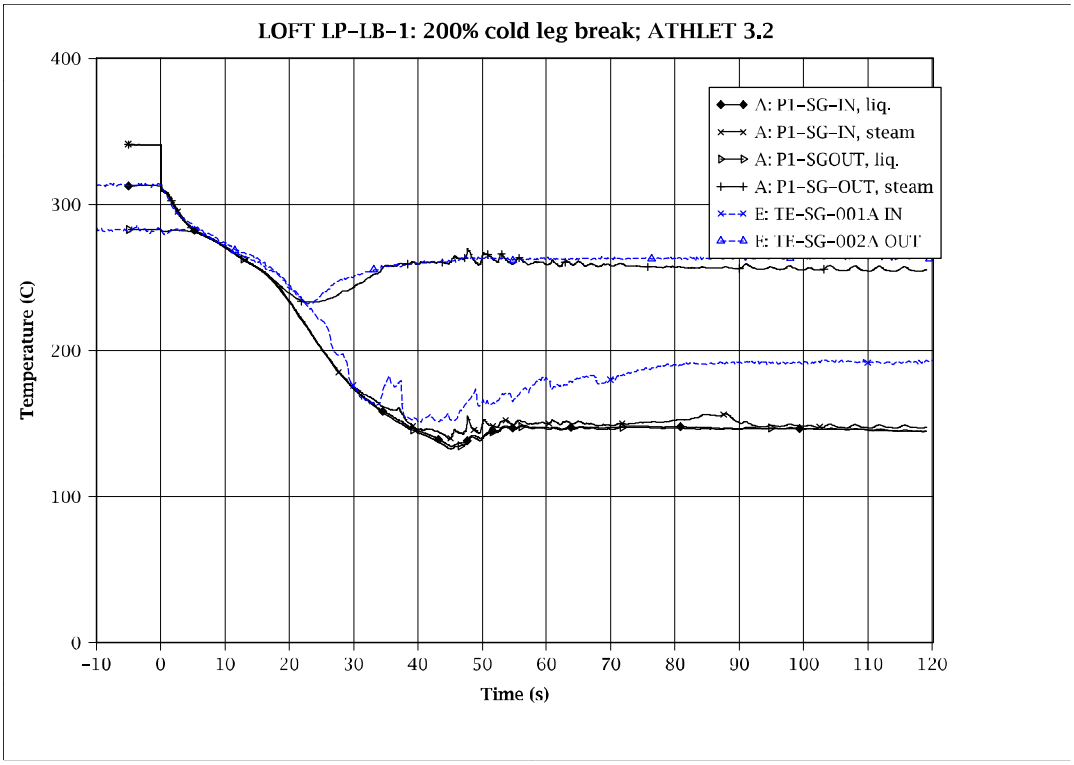

Fig. 5 - 140: Fluid temperature in IL steam generator inlet and outlet

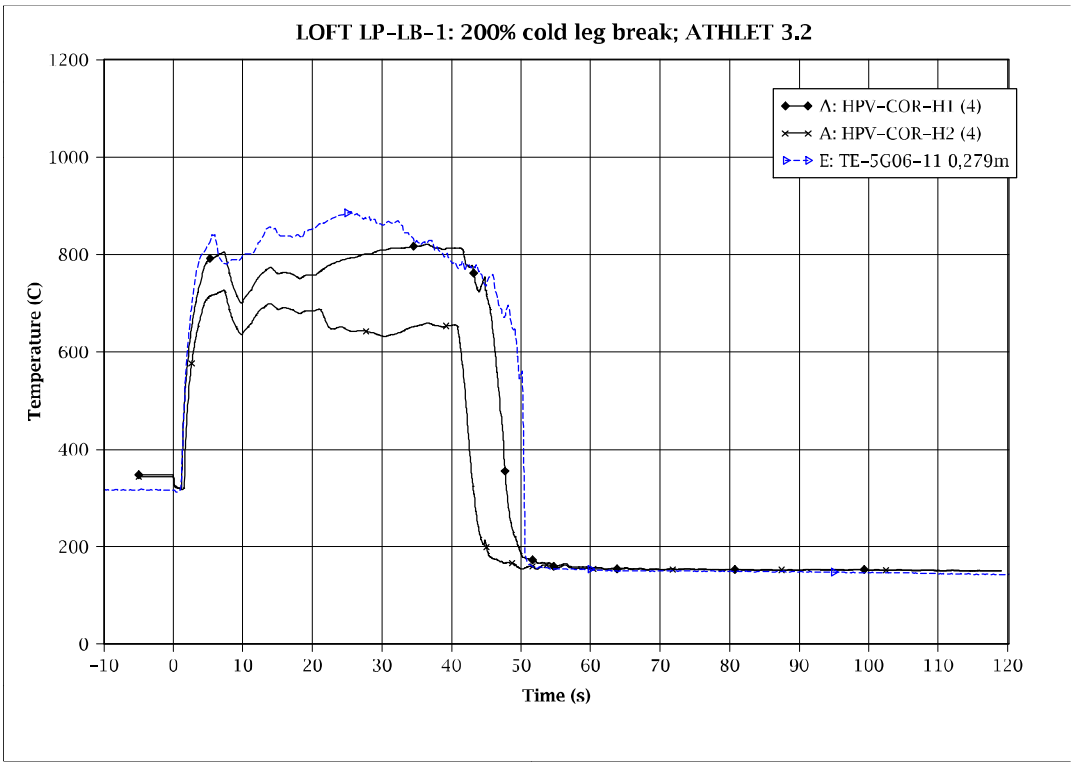

Fig. 5 - 141: Cladding temperature in central fuel assembly (0.28m)

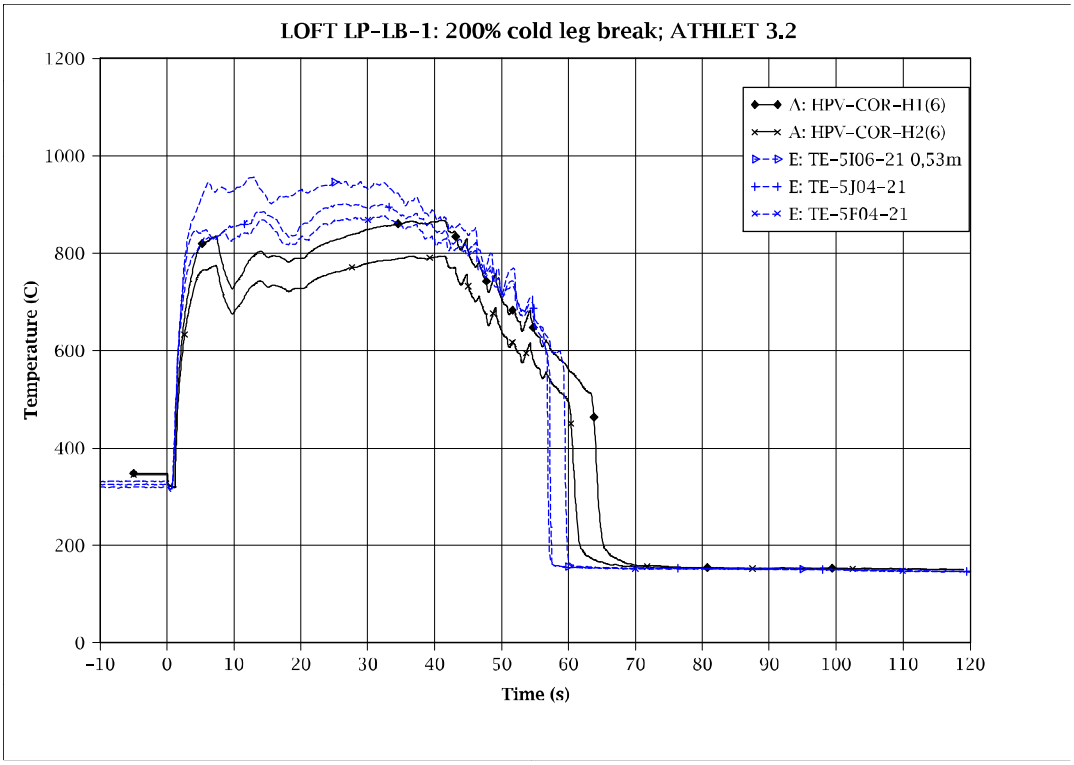

Fig. 5 - 142: Cladding temperature in central fuel assembly (0.53m)

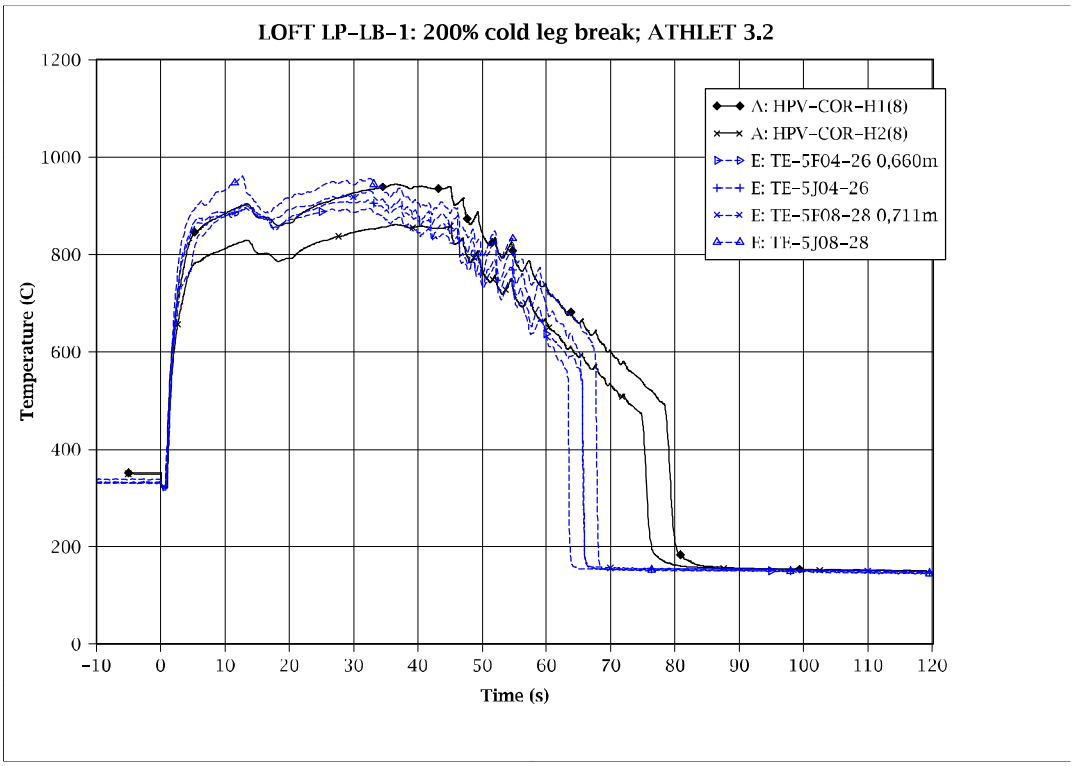

Fig. 5 - 143: Cladding temperature in central fuel assembly (0.66 and 0.71m)

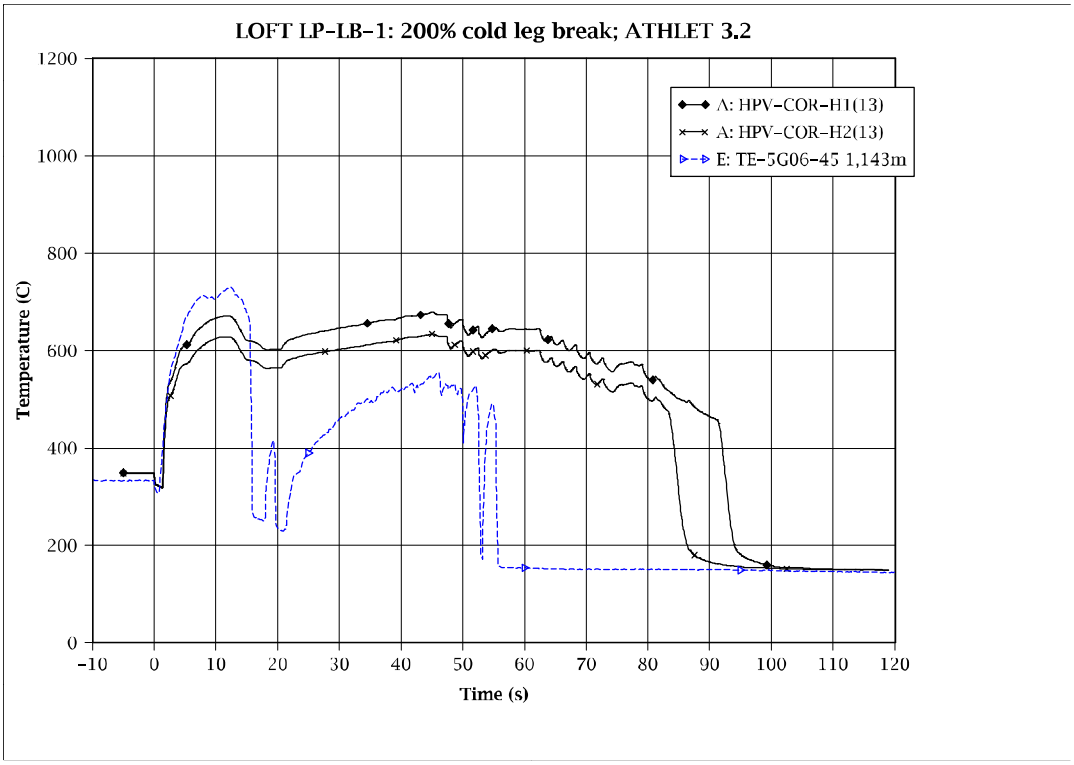

Fig. 5 - 144: Cladding temperature in central fuel assembly (1.14m)

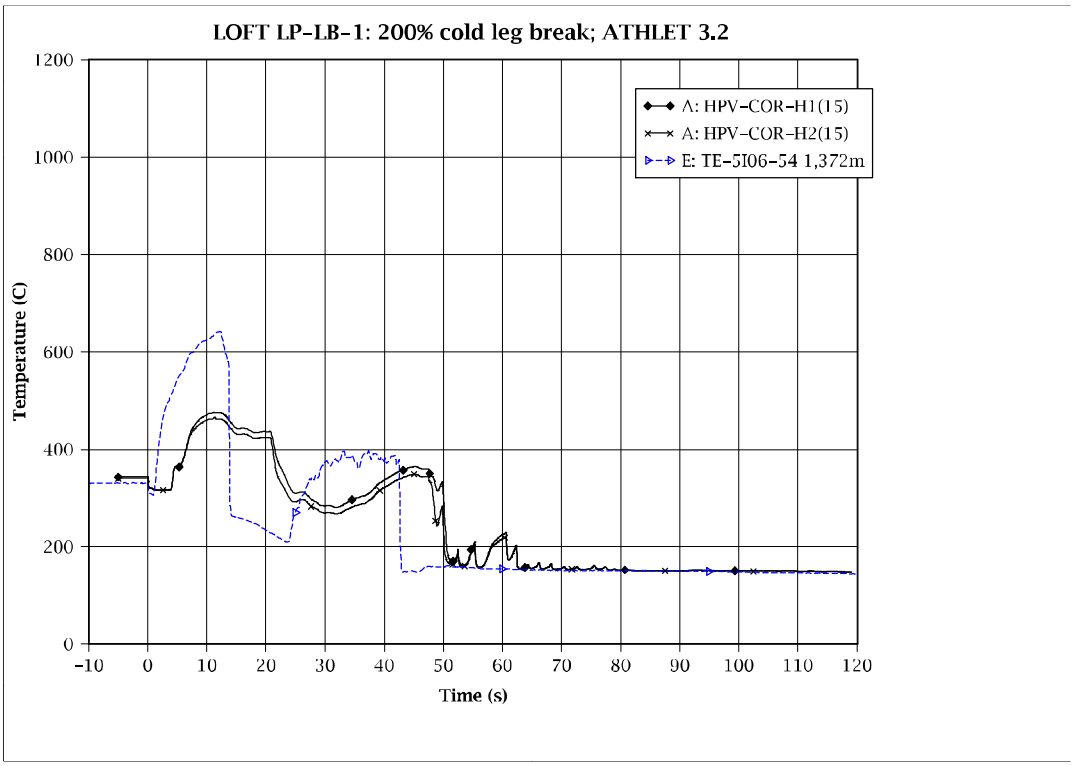

Fig. 5 - 145: Cladding temperature in central fuel assembly (1.37m)

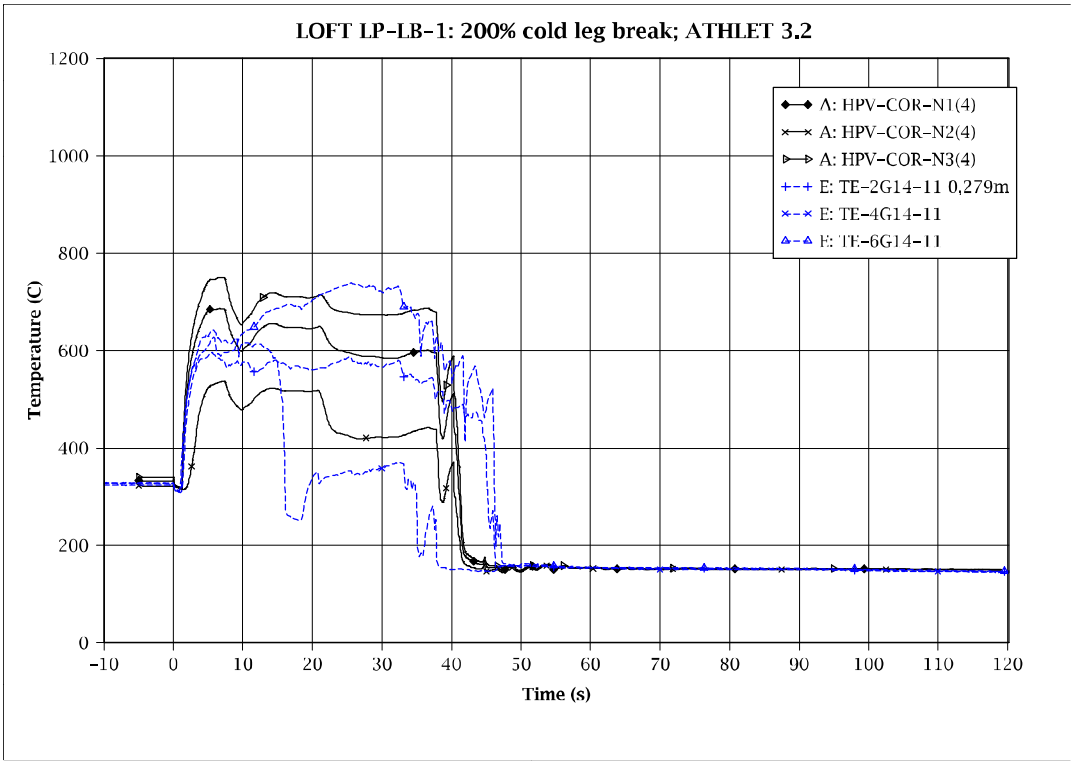

Fig. 5 - 146: Cladding temperature in peripheral fuel assemblies (0.28m)

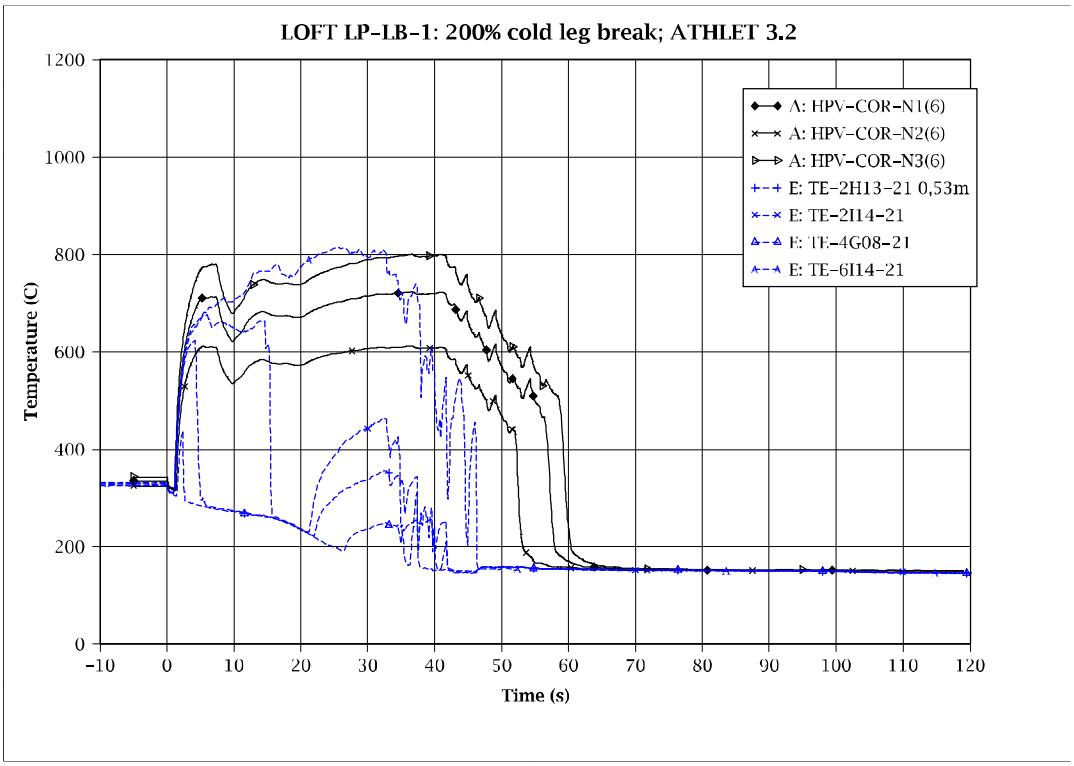

Fig. 5 - 147: Cladding temperature in peripheral fuel assemblies (0.53m)

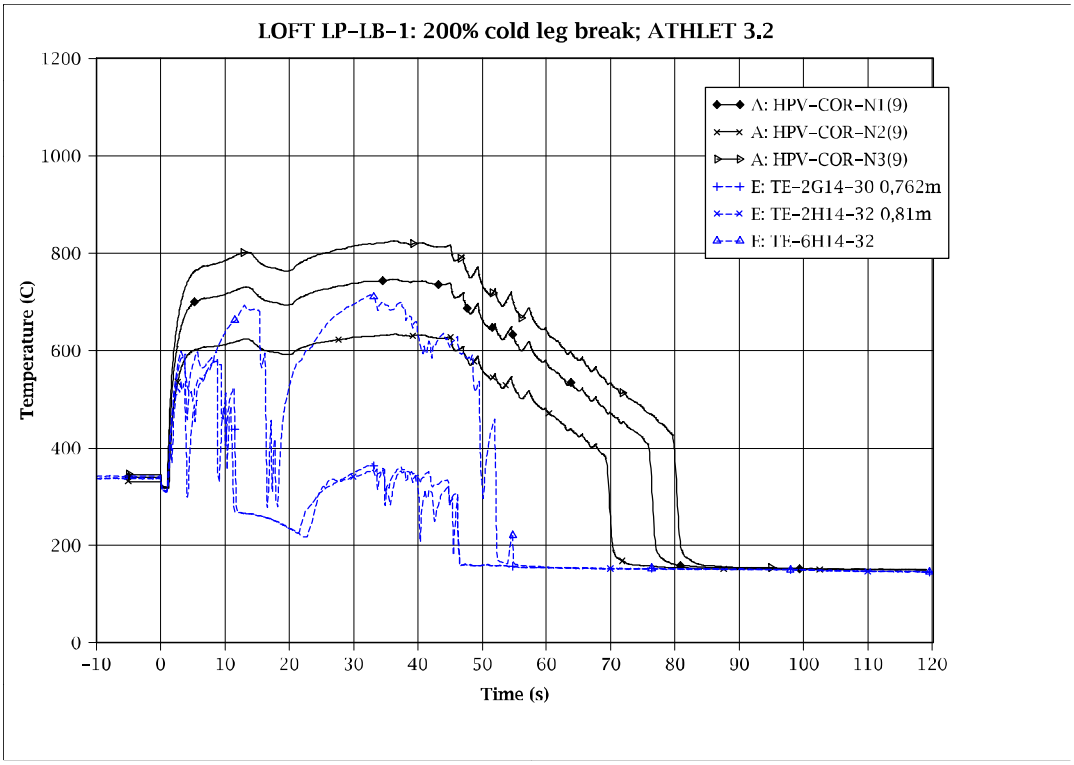

Fig. 5 - 148: Cladding temperature in peripheral fuel assemblies (0.76 and 0.81m)

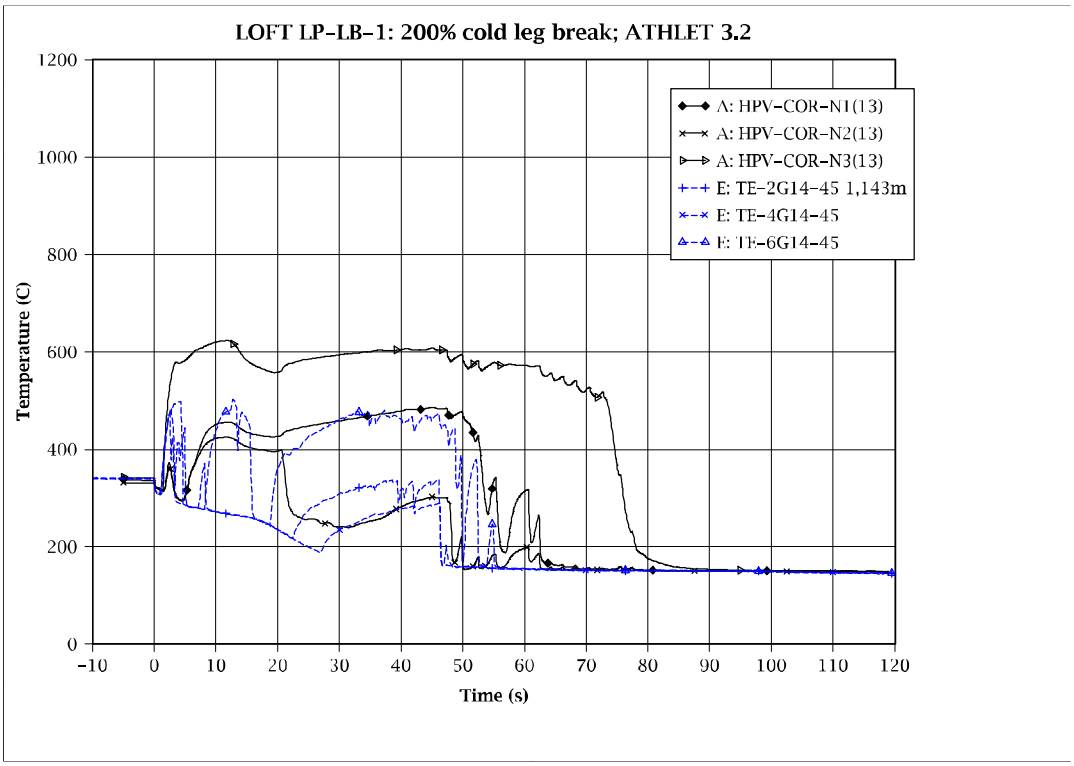

Fig. 5 - 149: Cladding temperature in peripheral fuel assemblies (1.14m)

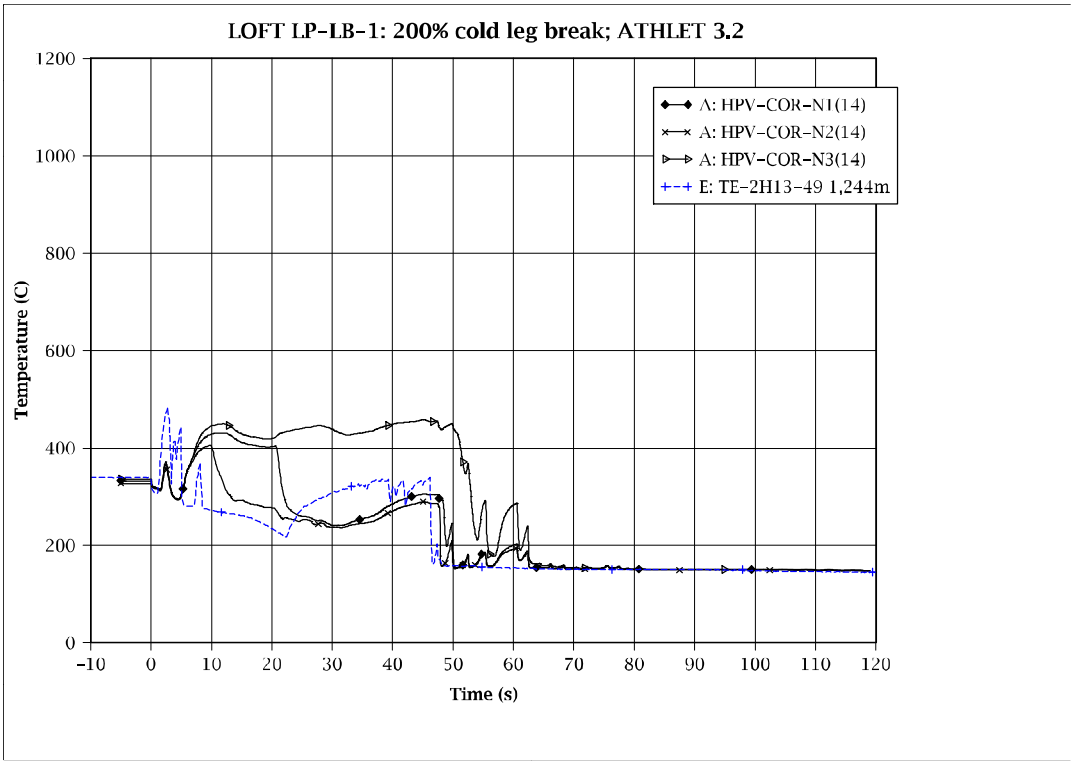

Fig. 5 - 150: Cladding temperature in peripheral fuel assemblies (1.24m)

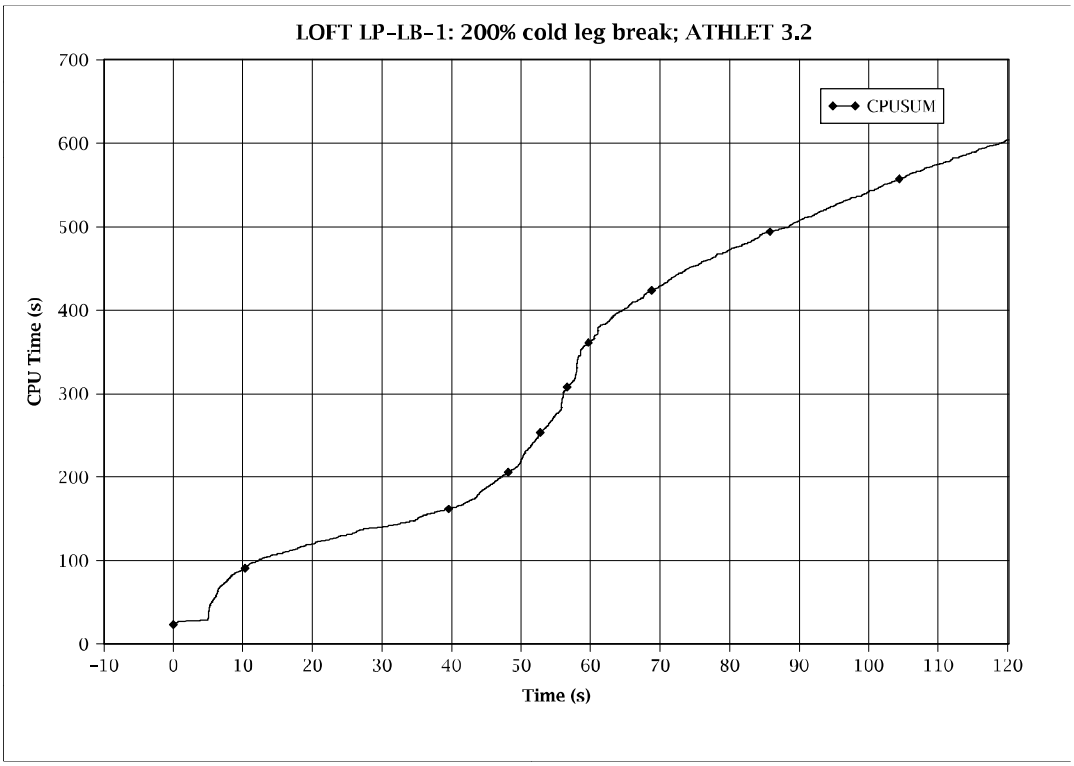

Fig. 5 - 151: CPU time consumption

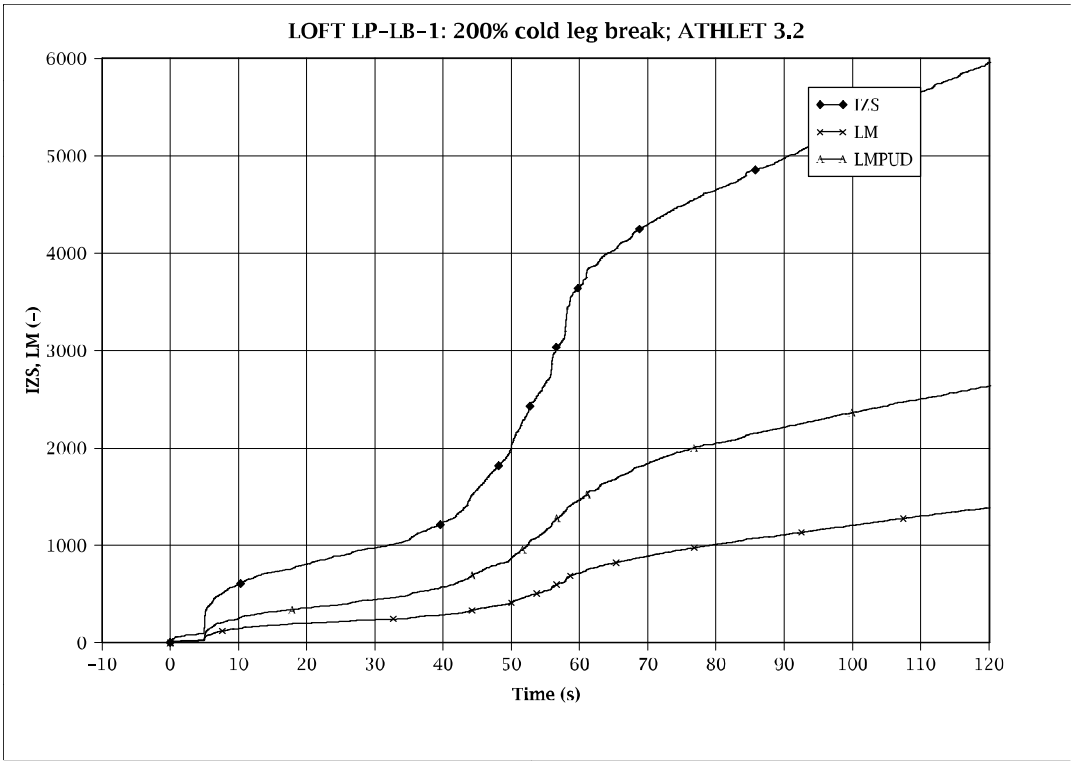

Fig. 5 - 152: Number of time steps (IZS) and Jacobian complete (LM) and partial updates (LMPUD)

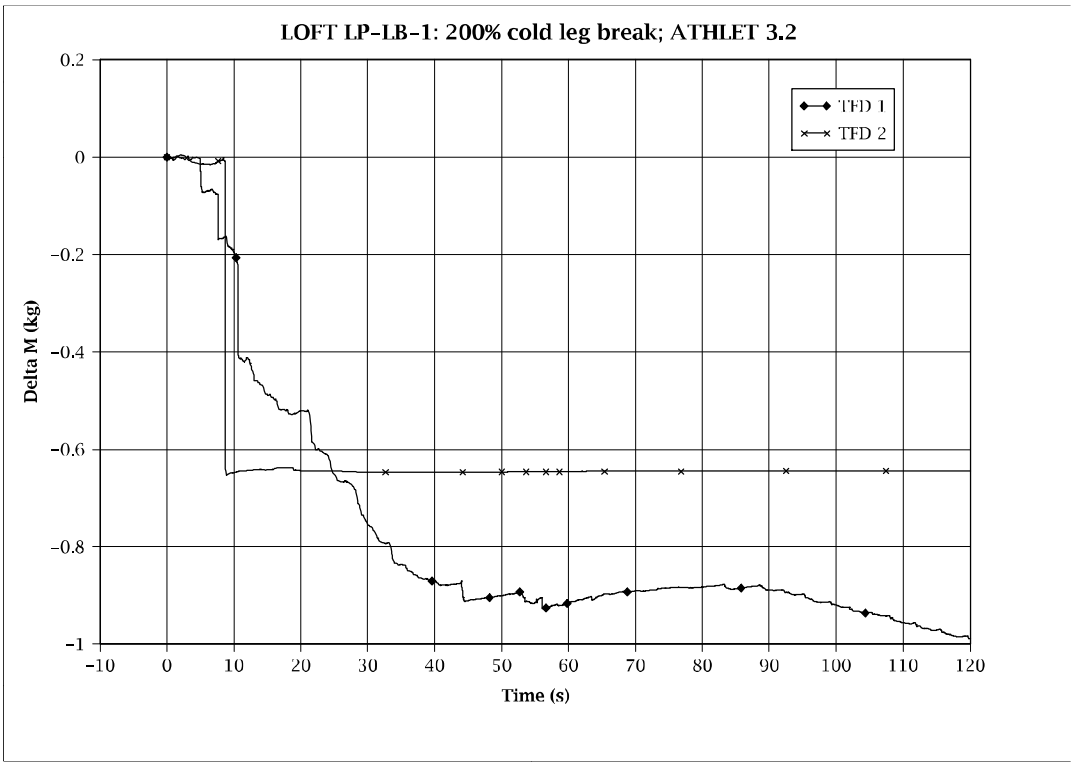

Fig. 5 - 153: Mass error

5.4 ISB-WWER Test SSP-2

5.4.1 Test Facility

The test facility ISB-WWER, designed and constructed by the Electrogorsk Research and Engineering Centre, is a full-pressure scaled-down model of the Russian reactor WWER-1000. The volume scaling is 1:3000 and the elevations are kept 1:1. The original four-loop primary circuit with horizontal steam generators is represented by a two-loop circuit with four vertical steam generators. The first loop represents a single loop (also called broken loop) with one steam generator and the second loop represents a triple loop (also called intact loop) with three parallel connected steam generators. The volume ratio between both loops is 1:3. The main circulation pumps are installed as bypasses around the loop seals, and are isolated from the loops during the experiments.

The primary circuit further consists of an electrically heated pressurizer model, which can be connected to the single as well as to the triple loop, and models of the three independent emergency core cooling systems: high pressure injection system, hydro-accumulators and low pressure injection system. The four hydro-accumulators of the WWER-1000 dispose of own connections to the reactor pressure vessel. This is a special feature of WWER. Two of the four accumulators are connected to the downcomer and the other two to the upper plenum of the reactor.

The reactor model is divided into the following parts:

- an external downcomer simulating the vertical downcomer annulus as well as the lower plenum of the reactor vessel,
- the core simulator based on a bundle of 19 directly heated fuel rod simulators with a length of 3.5 m,
- the upper plenum section simulating the upper plenum as well as the upper head of the reactor vessel, and
- the bypass section simulating the core coolant bypass channels; it allows to adjust the bypass flow of the core in the range of 3 to 20 % of the nominal mass flow rate.

The core simulator is connected to the downcomer and to the upper plenum via horizontal U-shaped tube junctions. The bypass is located between one lower and one upper connection line. The secondary circuit is not modelled in detail. The vertical steam generators are designed only to remove the power from the primary circuit. An isometric view of the main components of the ISB-WWER test facility is given in figure 5 - 154 and the principle scheme of ISB-WWER is shown in figure 5 - 155. An overview of the main design characteristics of the facility is given in table 5 - 7.

The standard instrumentation of the ISB-WWER facility includes transducer for pressures, differential pressures, temperatures, mass flows, and for the electrical parameters of the fuel rod simulator and the other heating devices. The most important parameters for the described experiment are the pressure in the primary circuit (P13) and on the secondary side of the steam generators (P1 - P4). The transducers for the differential pressure are placed as a complete chain around the whole primary loops. The temperature is measured by thermocouples. Most important locations are the inlet and outlet temperatures of reactor vessel and steam generators as well as the surface temperatures of core heater claddings and the U-tubes in the steam generators. There are also thermocouples in additional locations for heat loss information. The flow rates in the loops are measured in both the single and the triple loop cold leg by differential pressure flowmeter (FL7 and FL9). In addition, the secondary side feed water mass flow rate is also measured. The electrical heat power for core, bypass and pressurizer heaters is defined by measured voltage and current. Special devices - the so-called needle shaped conductivity probes - are used as local void fraction sensors in 14 places. These probes provide especially useful local information about the time of structural changes of the flow. This includes the time of the transition from one-phase to two-phase flow and vice-versa, the time of significant changes of the void fraction and of the passing of a mixture level.

All measured signals are recorded and pre-processed by a data acquisition system. The channel information is scanned by the basic PC system with a maximum sampling rate of 18 Hz, and stored on hard disk.

A more detailed description of the test facility is given in /GAX95/.

5.4.2 Test Conditions and Procedures

The Second Russian Standard Safety Problem (SSP-2) was carried out in Electrogorsk Research and Engineering Centre of Nuclear Plants Safety in 1995/96. The scenario of the experiment simulates the rupture of an ECC injection line. As the initiating event, the rupture of one line connected to the upper plenum was assumed. The result is a 11% break (in terms of main circulation line cross section) in the upper plenum of the reactor vessel, close to a medium size LOCA. In addition, the trip of all four main circulation pumps by blocking signal was assumed, and the emergency core cooling systems were assumed to be not available. The description of initial and boundary conditions is given in more detail in /GAX97, STE98/.

The given scenario for the experiment is the following:

- t = 0 s Start of transient;
  Break line opening (5.2 mm diameter, l/d=10 at upper plenum)
- t = 5 s Start of electrical power reduction at the core and the bypass section;
  Steam generator secondary side feed water injection and steam release is switched off (closing valves W-3, W-5, W-7, W-9, S-7, S-9, S-11, S-13)
- t = 9 s Pump trip by blocking signal (UPP13=11.0 MPa) simulated by closing valves W-33,W-34 and by opening valves W-10a, W-64, W-16, W-52, and W-65
- end The experiment is finished when the maximum cladding temperature of the core simulator achieves 723 K.

Table 5 - 7: Main characteristics of the ISB-WWER test facility

Characteristics	Value
Coolant	Water
Number of loops	2
Volume ratio of coolant loops	1:3
Maximum pressure	25 MPa
Operational pressure (nominal)	16 MPa
Temperature at core outlet (max)	400 °C
Core electrical heating power (max)	1.8 MW
Operational core heating power (nominal)	1.0 MW
Pressurizer heating power	20 kW
Core mass flow rate (max)	9.0 kg/s
Core mass flow rate (nominal)	6.0 kg/s
Cladding temperature (max)	1000 °C
Number of fuel elements in core bundle	19
Scaling factor for heights	1:1
Scaling factor for volumes	1:3000

5.4.3 Input Dataset

In the framework of participation in the Second Russian Standard Safety Problem, a new input data deck of the code version ATHLET Mod 1.1 Cycle C was developed for the ISB-WWER test facility. The basis for the geometrical information was mainly the data report /GAX95/. This input deck was continuously adapted to new ATHLET versions.

The input model for the test facility consists of 81 thermo-fluid objects and 78 heat conduction objects, comprising 382 control volumes, 423 junctions and 393 heat conduction volumes. The overall nodalization scheme is shown in figure 5 - 156.

For this small break calculation, the 5-eq. option of the code was chosen.

The modelling of the main components of the test facility is described in more detail below:

Reactor vessel model

The reactor vessel model is divided into three components: the downcomer/lower plenum, the core simulator and the upper plenum section (fig. 5 - 157).

Due to their three-dimensional nature, it is difficult to model the downcomer/lower plenum with only one-dimensional thermo-fluid-objects. Therefore, it is represented by 12 TFOs. All inlets are connected to the annulus represented by the branch PV-DC-2 and by the pipes PV-DC-1 and PV-DC-3. The pipe PV-DC-4 represents the upper head of the downcomer and the connection to the upper head of the upper plenum. They are connected by the branch PV-DC-5. The lower part is represented by PV-DC-6. The lower plenum annulus is represented by the TFOs PV-LP-1 to PV-LP-4.

The core simulator is represented by 8 TFOs. The connections from the lower plenum to the inlet section PV-COR-IN have been modelled by PV-LP-21 and PV-LP-22. The core simulator itself is named PV-COR and is connected to the branch PV-COR-OUT. The two horizontal pipes connecting the core simulator to the upper plenum have been modelled by PV-UP-11 and PV-UP-12. The external bypass PV-COR-BYP is connected to PV-LP-22 and PV-UP-12.

The upper plenum, especially the outlet annulus section, is difficult to model too. Therefore, after the simple lower part represented by PV-UP-1 and PV-UP-2, a branch PV-UP-3 has been introduced. The inner section PV-UP-36/PV-UP-6 and the outer annulus represented by PV-UP-4 and PV-UP-5 have been connected to this branch. The upper head of the reactor vessel is represented by the pipe PV-UP-7. The contents of this TFO are the grid plate and the connection pipe to the downcomer PV-DC-UP.

Main circulation loops

The hot legs of the main circulation pipes are connected to the branch PV-UP-5. The hot leg of the single loop is represented by the pipe P1-HL. The triple loop hot leg has been modelled by the common part P2-HL, the branch P2-HL-BR and the pipe P2-HL-SGT representing the connections to the three steam generators (FPARO=3). The cold legs have been modelled in

a similar way. The single loop cold leg is given by the pipes P1-CL-1 to P1-CL-3 and the bypass line P1-PUMP including the main circulation pumps. The triple loop cold leg is represented in a similar way by the pipes P2-CL-1 to P2-CL-3 and the pump bypass P2-PUMP, but in addition there are the TFOs P2-CL-SGT and P2-CL-BR with FPARO=3. The main circulation pumps (MCP) have been modelled with the ATHLET pump model. The nominal pump head has been taken as the corresponding value of the prototype WWER-1000 MCP (0.66MPa), due to the lack of information about the pumps and local form losses. The pressure losses in the primary circuit have been adjusted to the measured pressure differences at steady state conditions. The pump coastdown is simulated by a GCSM signal for pump head, on the basis of an input table.

Steam generator

The steam generators for both the single and the triple loop have been modelled similarly. An overview of their nodalization is given in figure 5 - 157. The inlet and the outlet chamber on the primary side are represented by the branches P1(2)-SG-IN and P1(2)-SG-OUT respectively. The 11 vertical U-tubes have been divided into three bundles with different lengths P1(2)-SG-UT1 to P1(2)-SG-UT3 in order to take into account the influence of the different elevations on natural circulation. The secondary side is represented by the pipe S1(2)-DRUM. The steam generator primary and secondary side are coupled by heat structures for every bundle.

Pressurizer

The pressurizer system is represented by 6 TFOs. The connection between the pressurizer itself P0-PRESS and the hot legs is modelled by the pipe P0-SURGE and P0-HL-SL, taking into account the possibility to connect the pressurizer to the single loop as well as to the triple loop. For the current calculation the pressurizer is connected to the single loop only because of the closed valve to the triple hot leg. The spray line is modelled by the TFOs P0-CL-SL and P0-PRES-SP, but it is not used for this experiment, due to the closed valves W30 and W31. The pressurizer safety valve is represented by the single junction pipe P0-PRES-RV.

Break modelling

The break line is modelled as a single junction pipe with a discharge valve assigned to it. The discharge rate is calculated by means of CDR tables. In order to take into account the stratification upstream of the leak, the option JFLO0 = -1 was chosen, as recommended in the ATHLET User's Manual.

Secondary circuit

The secondary circuit is modelled in a very simple way. Both the single loop as well as the triple loop secondary side except the steam generator drum have been modelled by the two pipes

S1(2)-MSL and S1(2)-BPL only, representing the steam line and the bypass line toward the relief valve. The feed water injection system is simulated for both loops with a single junction pipe S1(2)-FWL at the bottom of the steam generator drum. The steam lines have been completed by the isolation valve S1(2)-MSV and the safety relief valve S1(2)-BPV.

Heat conduction structures

The heat losses to the environment have been modelled by taking into account all solid component structures of the test facility. Also the heating structures as well as the heat exchange structures have been modelled by heat structure objects. To match the heat losses of the components given as boundary condition for the calculation, the outside heat transfer coefficients - considering the effect of the isolation material - were estimated by the code on the basis of calibrated temperature-dependent tables. In the period of zero-transient calculation the heat losses in those parts of the components without mass flow have been switched off and are considered only after the begin of the transient. The heater rods in the core simulator have been modelled in agreement with the single flow channel by only one heat structure HV-COR-R taking into account the number of rods using FPARH=19. Therefore, radial temperature differences inside the core simulator are not simulated. The axial rod power distribution is kept constant for all elevations. The time evolution of the power for the core rods as well as for the pressurizer heaters is given by input tables.

GCSM

Besides the definition of a series of important process variables in the process signal block, there are 16 blocks for special tasks shortly described below:

- `BLOCK-1' Set of transient initialization signals like start of transient, scram, pump coast down, ECCS and valve actions.
- `MCPUMP' Main circulation pump coast down simulation.
- `VALVES' Isolation valve opening and closing position control, including accumulator and leak simulator valve.
- `ECCS' Emergency core cooling system control, especially mass flow and enthalpy behavior. This block is not used for this transient.
- `SCRAM' Scram power behavior in the core simulator.
- `PRESHEAT' Pressurizer heater controller for primary pressure control in the zero-transient period and heater behavior for transient according to the prescribed boundary conditions.
- `BYPHEAT' Core bypass heat behavior.

- `RV-PRESS' Pressurizer safety valve controller, including estimation of critical discharge through the valve.
- `AIR' Temperature boundary conditions for the environment.
- `TDV' Time dependent volume boundary conditions.
- `FEEDW' Feedwater mass flow and enthalpy.
- `SG-STEAM' Steam generator secondary side pressure controller for the zero-transient period and steam mass flow behavior for transient according to the prescribed boundary conditions.
- `SG-SV' Steam generator safety valve controller including estimation of critical discharge through the valve.
- `HEATLOSS' Estimation of outside heat transfer coefficient for the component heat losses according to the temperature dependent boundary conditions.
- `MEASUREM' Post processing of process signals for comparison with experimental data.
- `POSTPROC' Post processing information concerning heat losses and mass balance.

5.4.4 Results of the ATHLET Calculation

Selected results of the calculation are presented in figures 5 - 158 to 5 - 183, together with the corresponding parameter experimentally measured. The transient was started by opening the leak valve in the upper plenum. The leak mass flow rate becomes critical very quickly and reaches its maximum value of 1.2 kg/s after about one second. The primary pressure decreases strongly (fig. 5 - 158) and water from the pressurizer is discharged to the hot leg of the single loop. Therefore, the temperature at the SG inlet drops for a short time due to the relatively cold water of the surge line and then increases because of the saturated conditions in the pressurizer and the higher enthalpy of the injected water (fig. 5 - 162). The temperature in the hot leg does not reach the same values as in the experiment because of the smaller flow rate in the surge line out of the pressurizer. For the same reason, the collapsed level in the pressurizer drops more slowly and the depletion will occur later. After 3 s the electrical power to the core simulator is switched off.

Due to the fast pressure decrease, flashing at the steam generator inlet can be observed, first in the single loop and at about 6 s in the triple loop. The flashing in the single loop starts earlier because of the higher initial temperatures there. After 8 s the main circulation pumps were stopped without coast-down. The mass flow in the loops decreases in the next 4 s to small val-

ues (figs. 5 - 164 and 5 - 165). That is the reason for the short temporary pressure increase in the primary circuit after about 10 s. At the same time flashing takes place in the upper plenum, and the leak mass flow, now saturated, starts to decrease.

In the secondary circuits the feedwater valves and the steam outlet valves also start closing at 8s. Therefore, the pressure on steam generator secondary side increases due to the remaining heat flow from the primary loops (fig. 5 - 160). The collapsed level in the steam generator secondary side increases because of the mass balance between feedwater and steam release. Afterwards, the pressure decreases very slowly due to the heat losses to the environment. The parameters at the steam generators of the different loops are not comparable due to different initial conditions and different valve closing behavior. In addition, the pressurizer influences the behavior of the single loop.

Due to the fact that the emergency core cooling systems were assumed to be not available, the coolant inventory decreases continuously. The primary pressure still drops rapidly. After the appearance of the first vapor at the reactor outlet, the coolant flashed in the hot leg. After 38s the pressurizer is completely empty. The state of the primary circuit after the depletion of the pressurizer is characterized by a counter-current flow. The vapor from the reactor outlet moves towards the steam generator and is condensed there. The condensate flows partially through the hot legs back to the reactor vessel. Only the remaining part of vapor condenses in the descending part of U-tubes and flows to the cold leg. Vapor appears in the cold leg of single loop after 42 s and of triple loop after 75 s respectively, and the liquid level in the cold leg decreases afterwards. The differences between the loops are mainly caused by the different secondary side parameters. Simultaneously, the primary temperature decreases and the heat sink in the steam generators looses effectiveness. Consequently, the primary pressure drop decelerates. When the primary pressure finally comes close to the secondary pressure at roughly 140 s, the condensation rate decreases and the level in the hot leg drops rapidly (fig. 5 - 166).

When the hot legs are depleted, the leak flow changed from two-phase mixture to vapor. Consequently, the pressure decrease was accelerated. This is caused by the increasing enthalpy losses via the leak. The intensification of the pressure drop initiated also an intensification of flashing in those parts of the circuit, which were still filled with two-phase mixture. The flashing in the cold leg causes a rise of the mixture level in its vertical part indicated by the pressure difference CLIDP17 and CLIDP28 for the intact and CLBDP11 for the broken loop (figs. 5 - 169 to 5 - 171). Due to the mass losses, the mixture level started to fall again after several seconds. The decrease of the level was continuing slowly. As it is indicated by the measured differential pressures and voids (figs. 5 - 172 to 5 - 174), a cold leg loop-seal clearing does not occur. Therefore, the vapor generated in the loop seal has to flow towards the steam generator on the one side and towards the downcomer on the other side. The result is a reverse vapor flow through the steam generator, which is indicated by the temperatures at the inlet and outlet of

the steam generator (figs. 5 - 162 and 5 - 163). The temperature at the inlet is a little bit higher than at the outlet because the vapor is heated by the secondary side. The vapor flowing towards the downcomer leads to a level decrease in the downcomer. The level reached the holes connecting the downcomer to the lower plenum at 182 s. At this time, an entrainment of vapor from the downcomer to the core is presumed, as indicated by the differential pressure across the lower core region (fig. 5 - 167). Finally, the inventory of the downcomer was pushed into the core simulator and out of the leak.

As expected when no emergency core cooling system is operating, an overheating of the fuel rod simulators can be observed (figs. 5 - 176 to 5 - 179). The first short temperature increase occurs near the outlet of the bundle at about 160 s when the hot legs were depleted. But this temperature increase reaches 70 K only, and the rod is cooled again due to the increased mass flow from the downcomer. The final rise of the maximum cladding temperature starts at 197 s, 10 s later than in the experiment, due to the larger core mass inventory in this period. At 219 s the temperature reached 723 K and the defined criterion to stop the calculation was reached (fig. 5 - 176).

The comparison of the calculated results with the measured experimental data shows in general a good agreement. The main phenomena were reproduced by the code. Nevertheless, there are some disagreements between experimental and calculated results:

- Different from the experiment, the calculated natural circulation in the broken loop reached smaller values and stopped completely after 150 s (fig. 5 - 165).
- The steam generator secondary side U-tube surface temperatures deviate from the measured ones, especially in the triple loop (figs. 5 - 180 and 5 - 181).
- The calculated core bypass temperature increases considerably after pump trip, possibly due to an incorrect modelling of pressure losses (fig. 5 - 183).

Additionally it must be taken into account that, in contrast to the calculated results, the void measurement is a strong local one and delivers information for a special location. Therefore, the comparison with the calculated values depends on the nodalization chosen.

The results illustrate the capability of ATHLET to analyze thermal-hydraulic problems for WWER plant configurations.

5.4.5 Figures

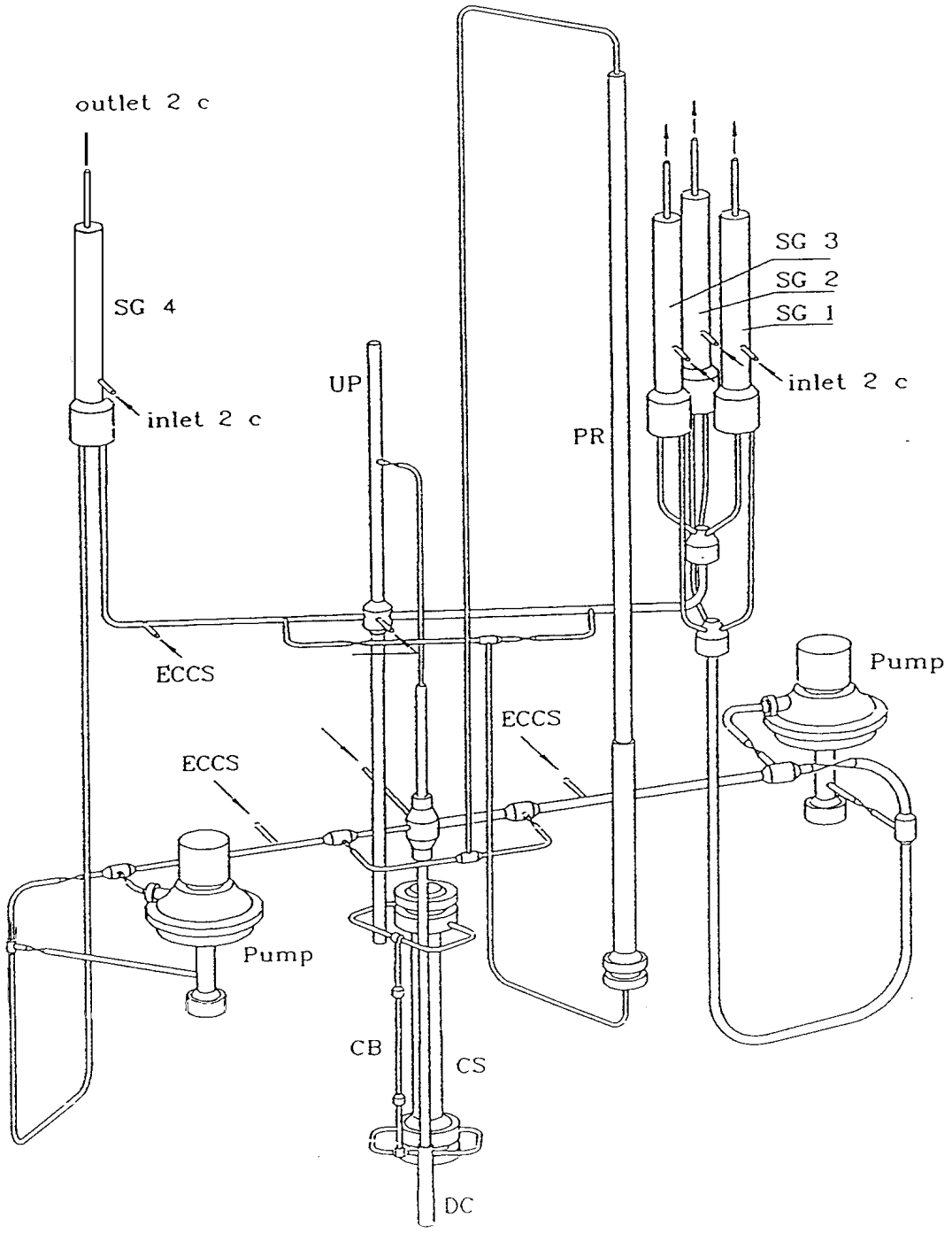

Fig. 5 - 154: Isometric view of ISB-WWER facility main components

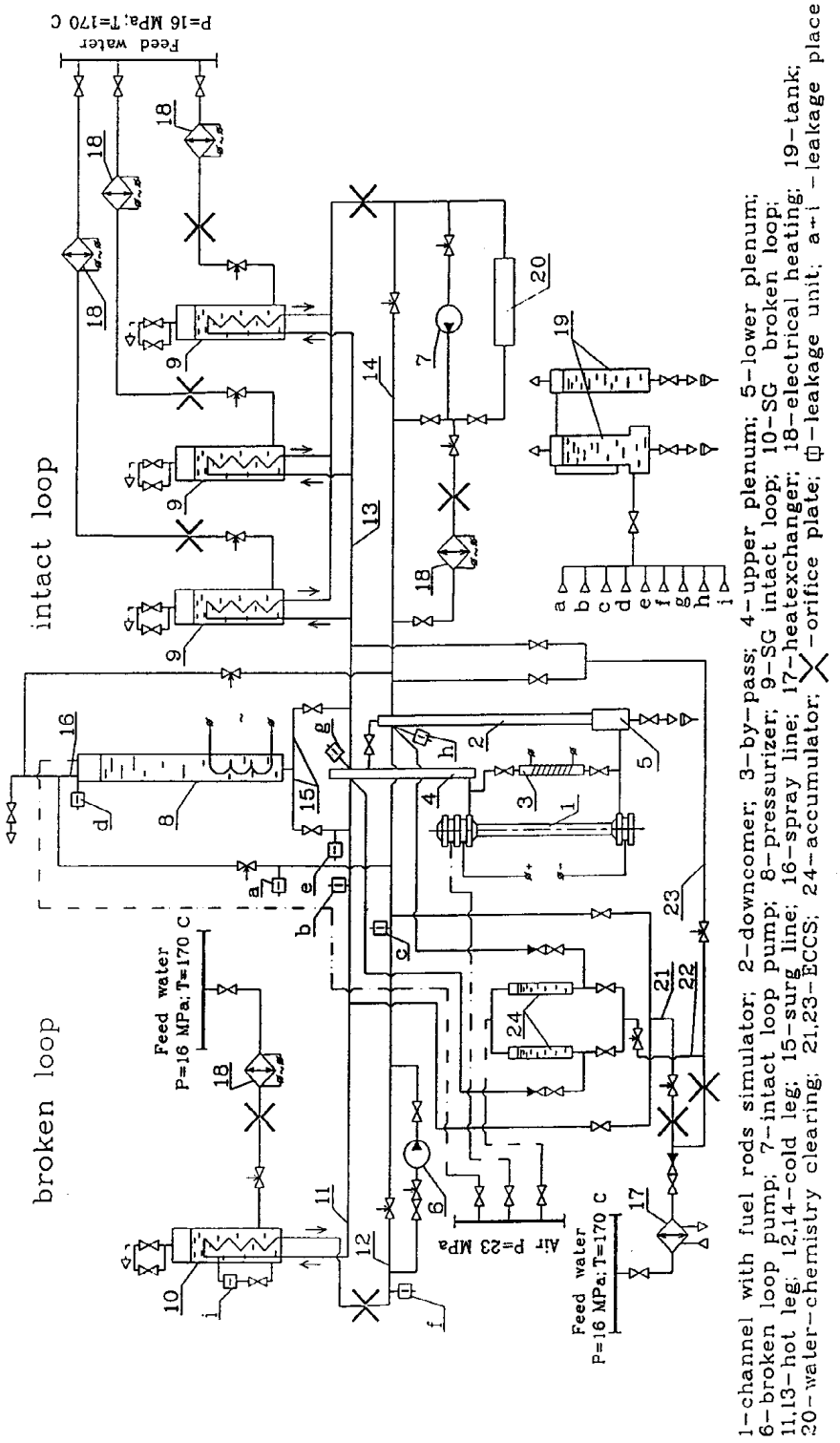

Fig. 5 - 155: Basic scheme of ISB-WWER test facility

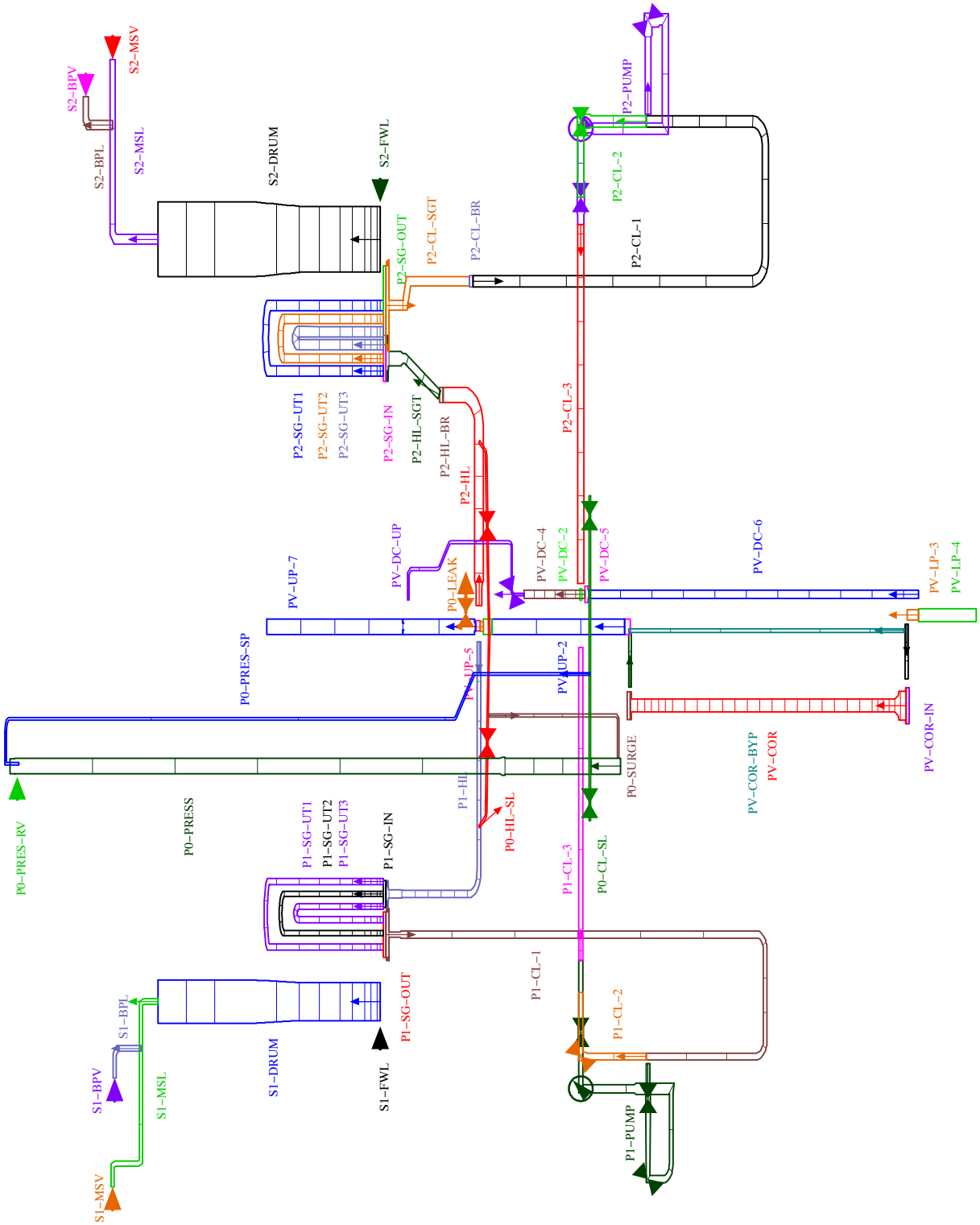

Fig. 5 - 156: ATHLET nodalization scheme of ISB2-WWER facility (overview)

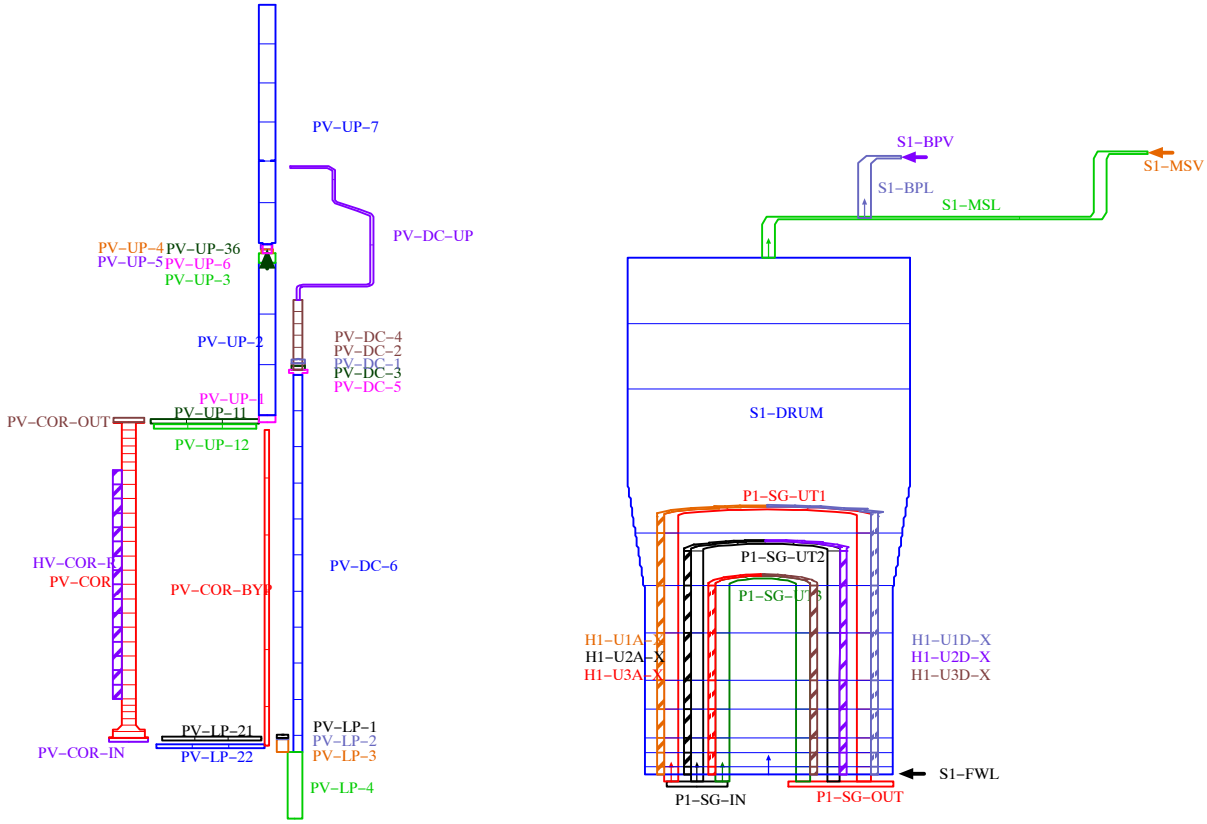

Fig. 5 - 157: ATHLET nodalization scheme of reactor vessel and steam generator

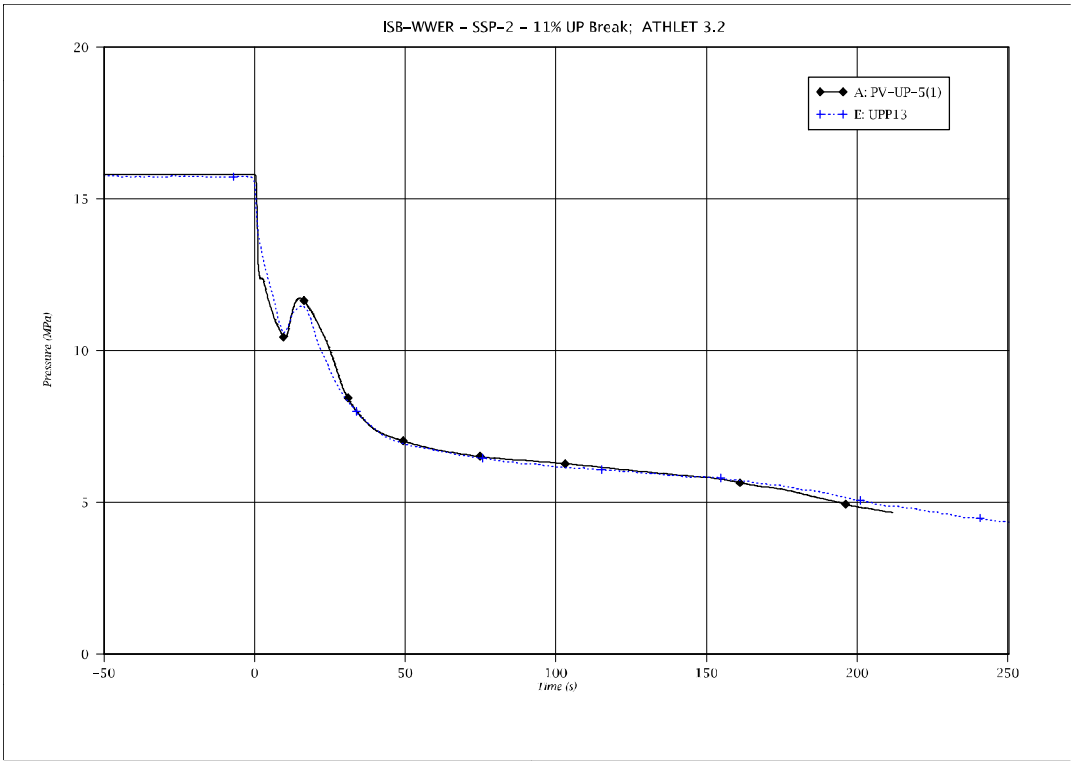

Fig. 5 - 158: Pressure in upper plenum

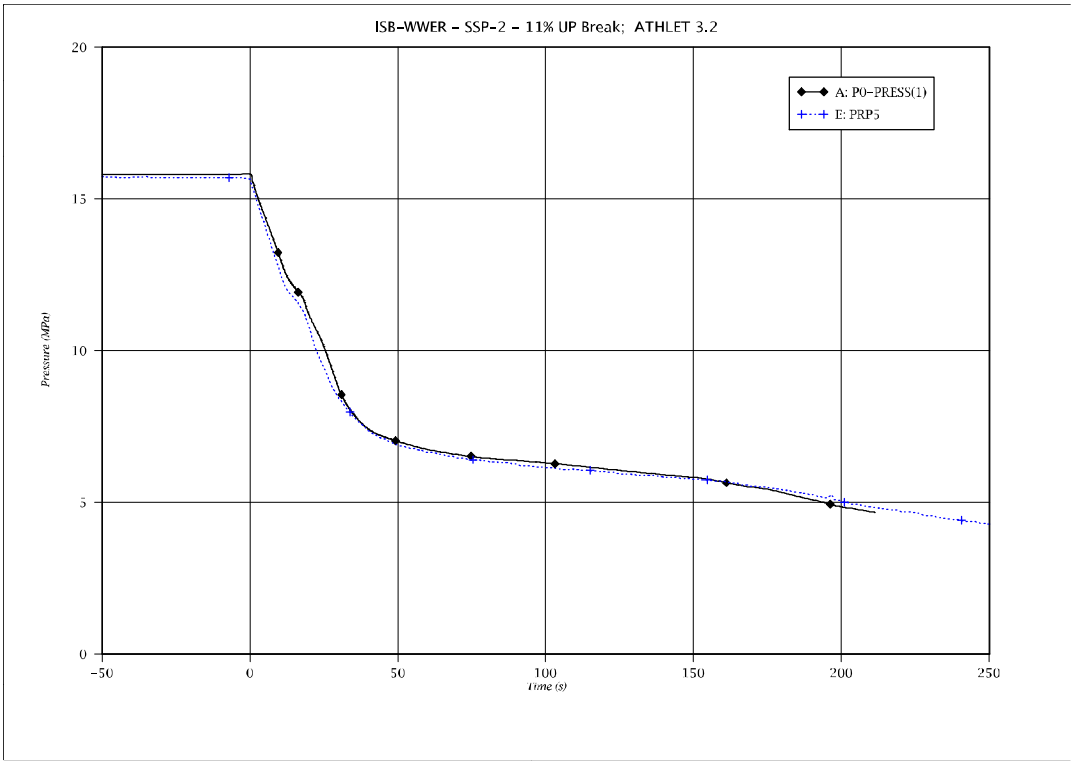

Fig. 5 - 159: Pressurizer pressure

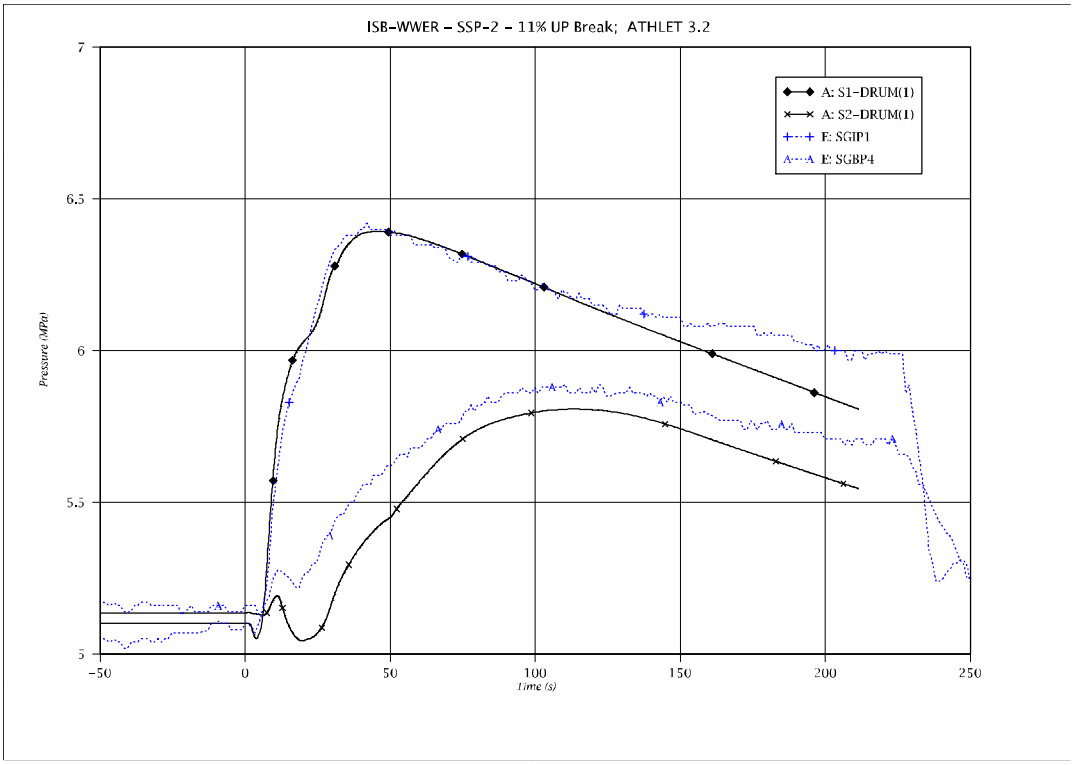

Fig. 5 - 160: Secondary pressure

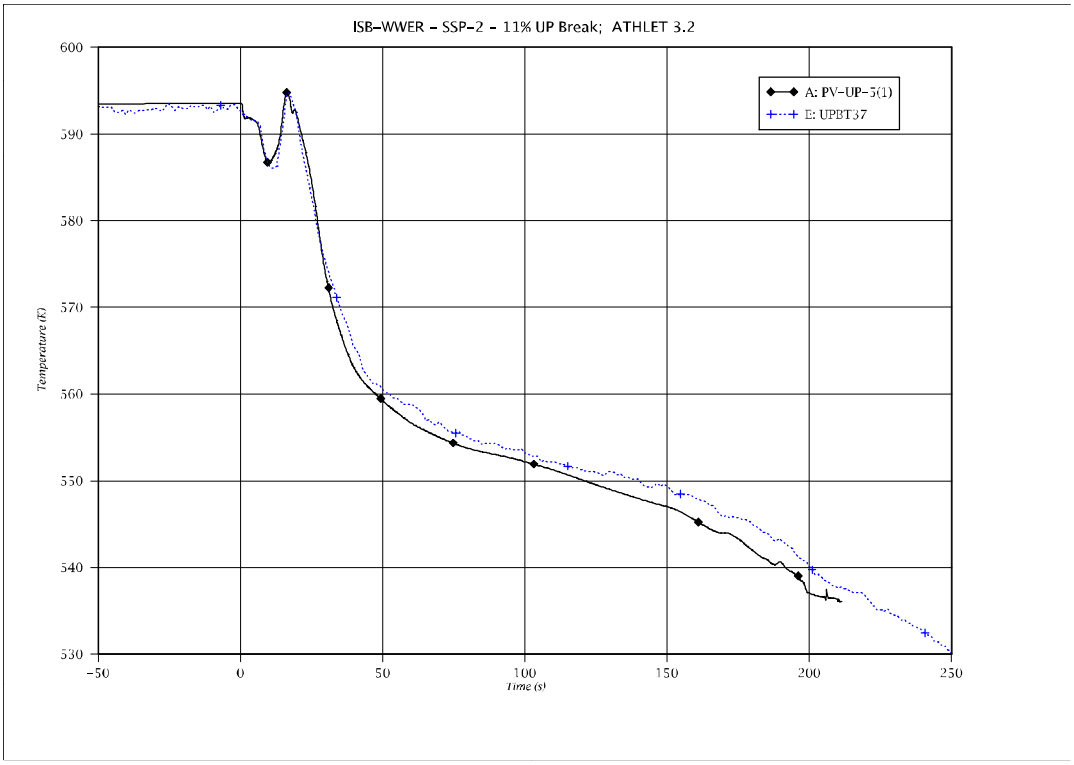

Fig. 5 - 161: Temperature at upper plenum outlet

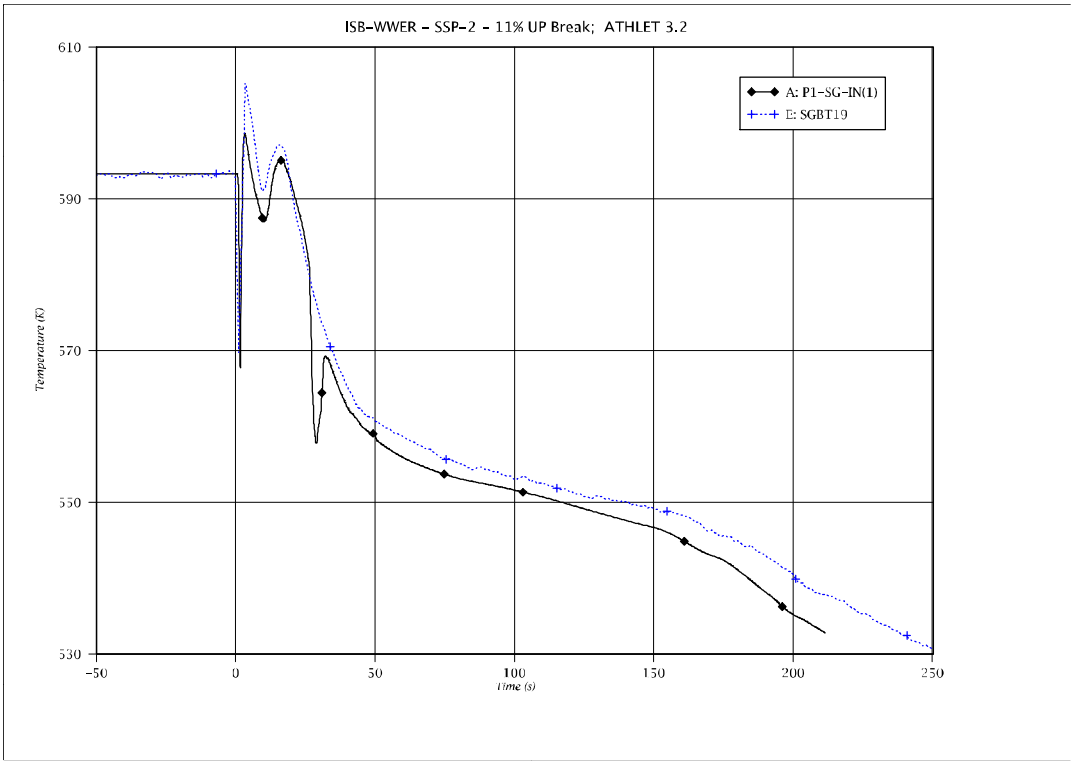

Fig. 5 - 162: SG inlet temperature (single loop)

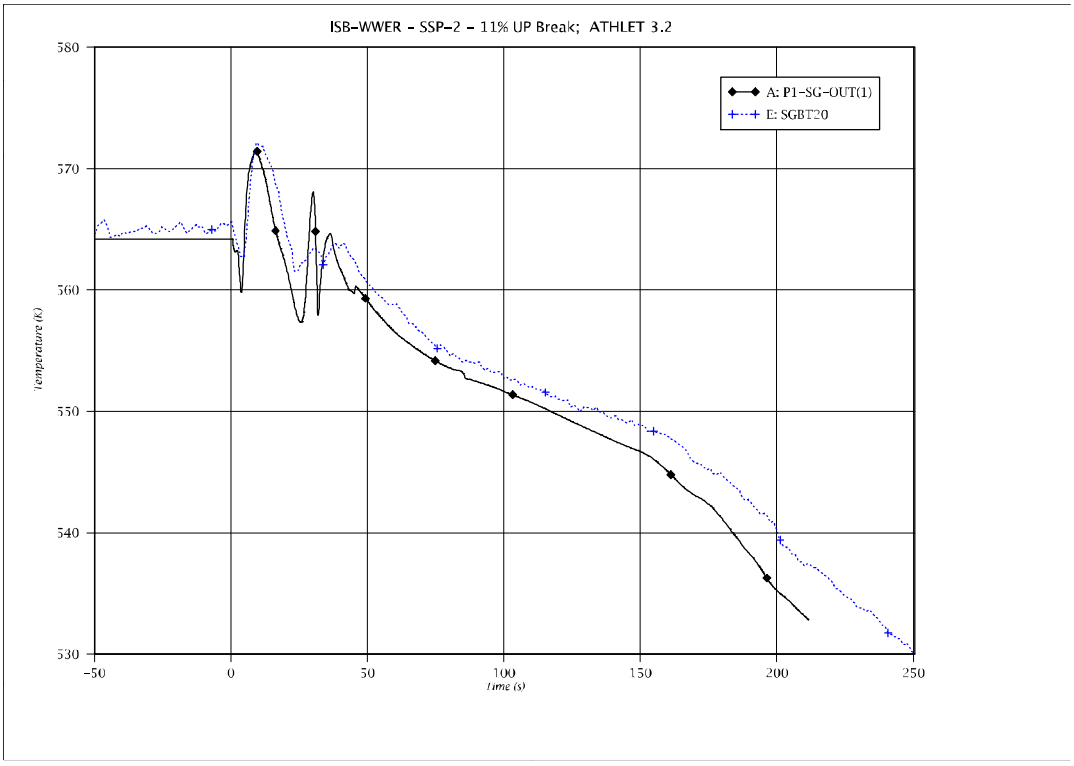

Fig. 5 - 163: SG outlet temperature (single loop)

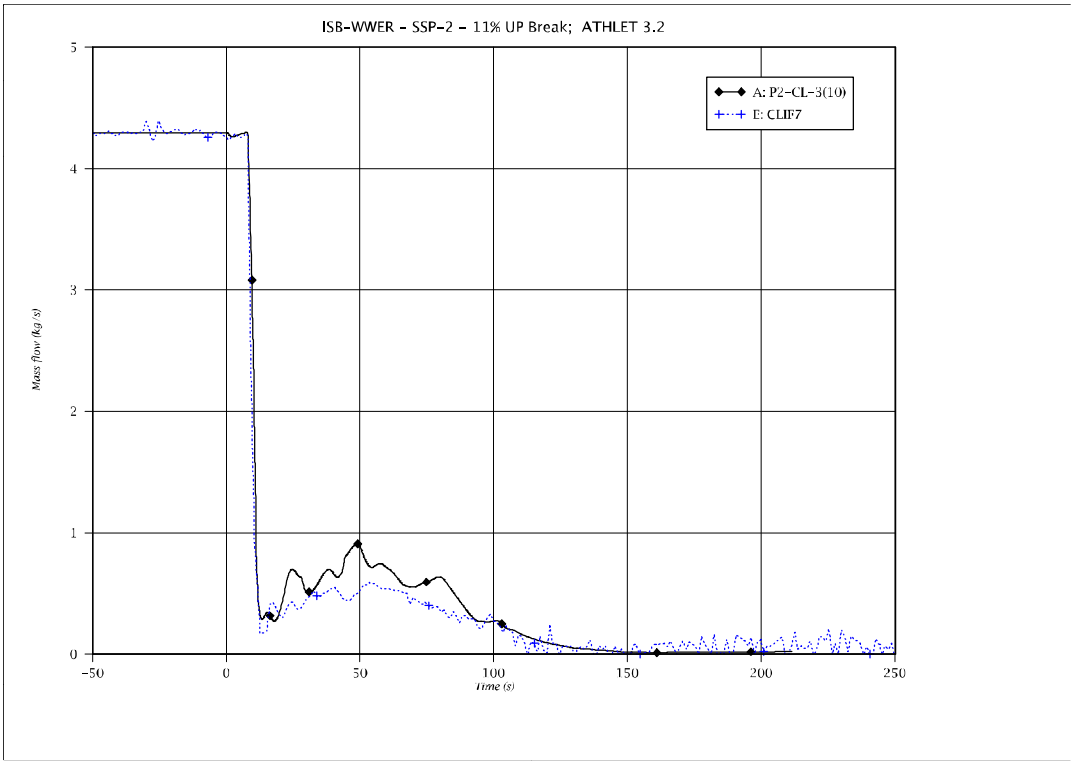

Fig. 5 - 164: Mass flow rate in cold leg (triple loop)

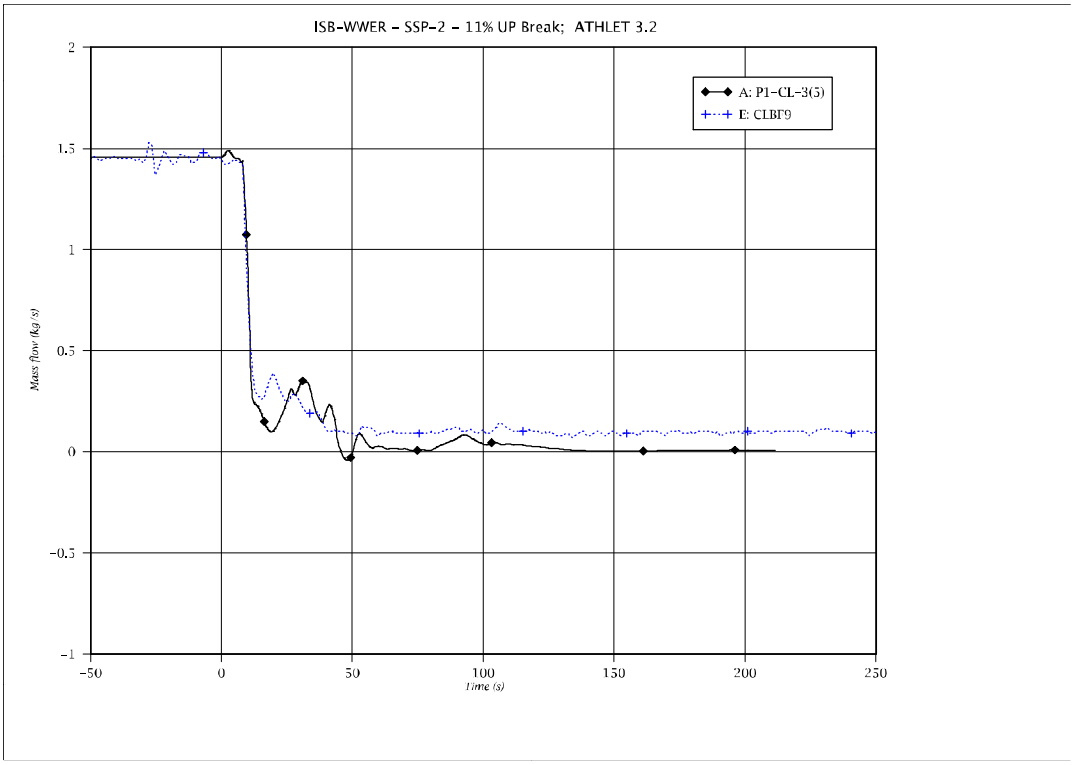

Fig. 5 - 165: Mass flow rate in cold leg (single loop)

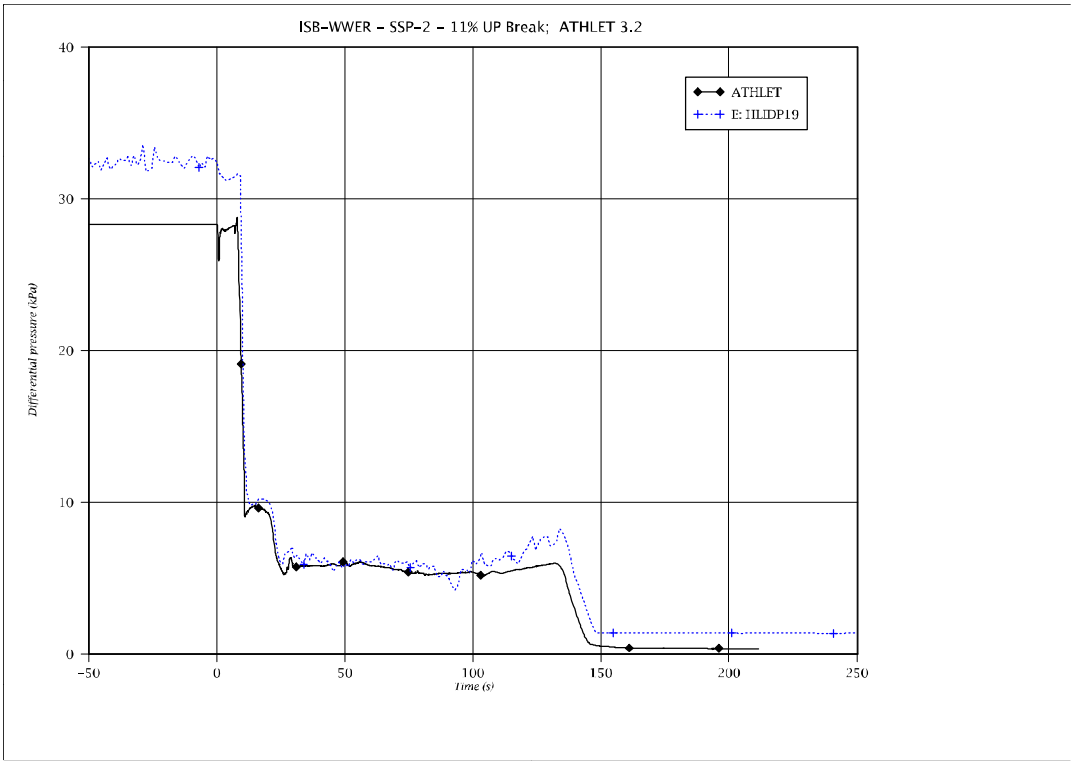

Fig. 5 - 166: Differential pressure in vertical part of triple loop hot leg

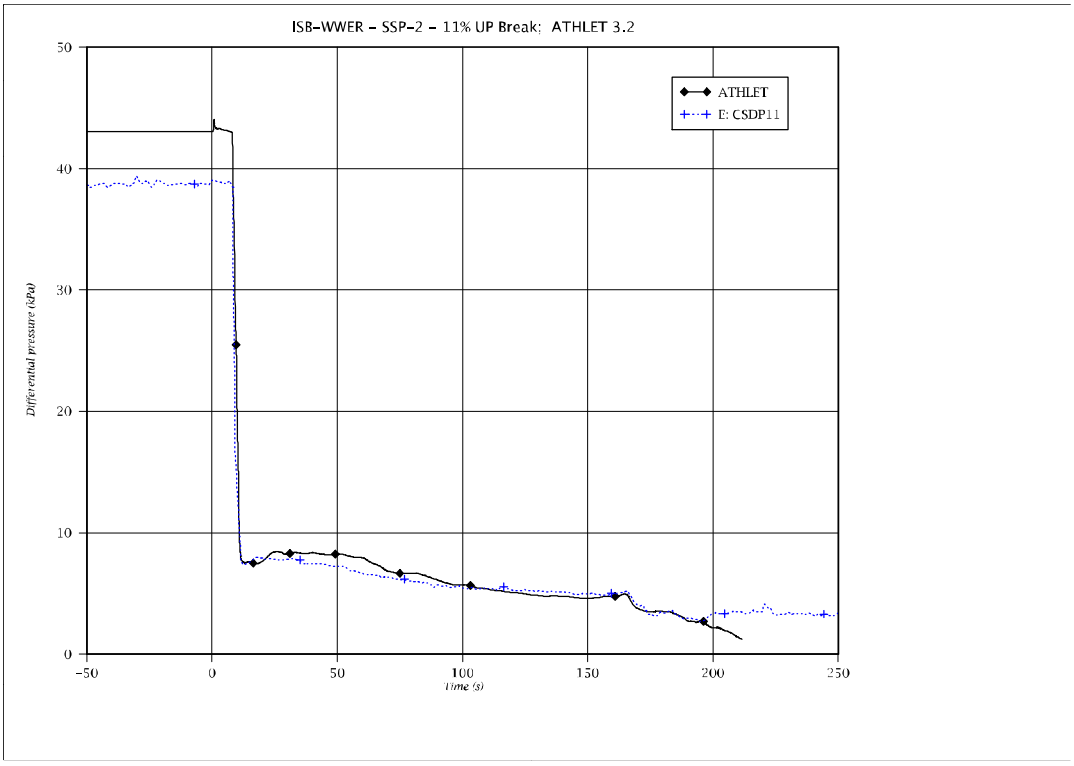

Fig. 5 - 167: Differential pressure across lower core region

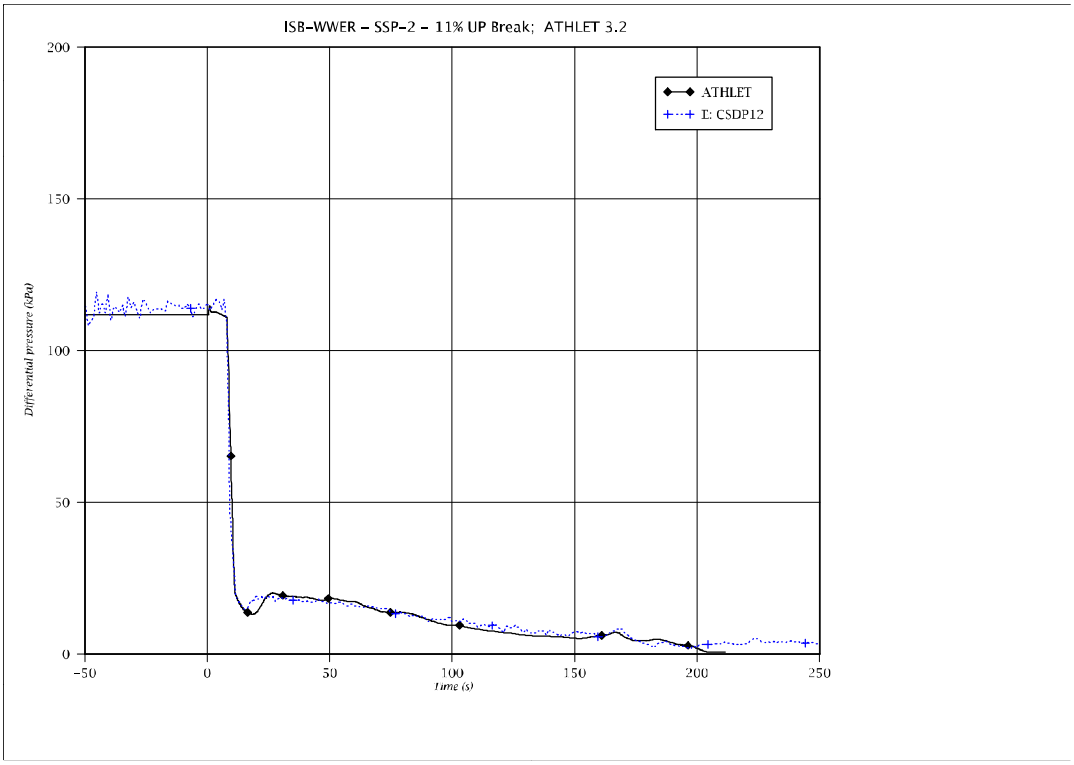

Fig. 5 - 168: Differential pressure across upper core region

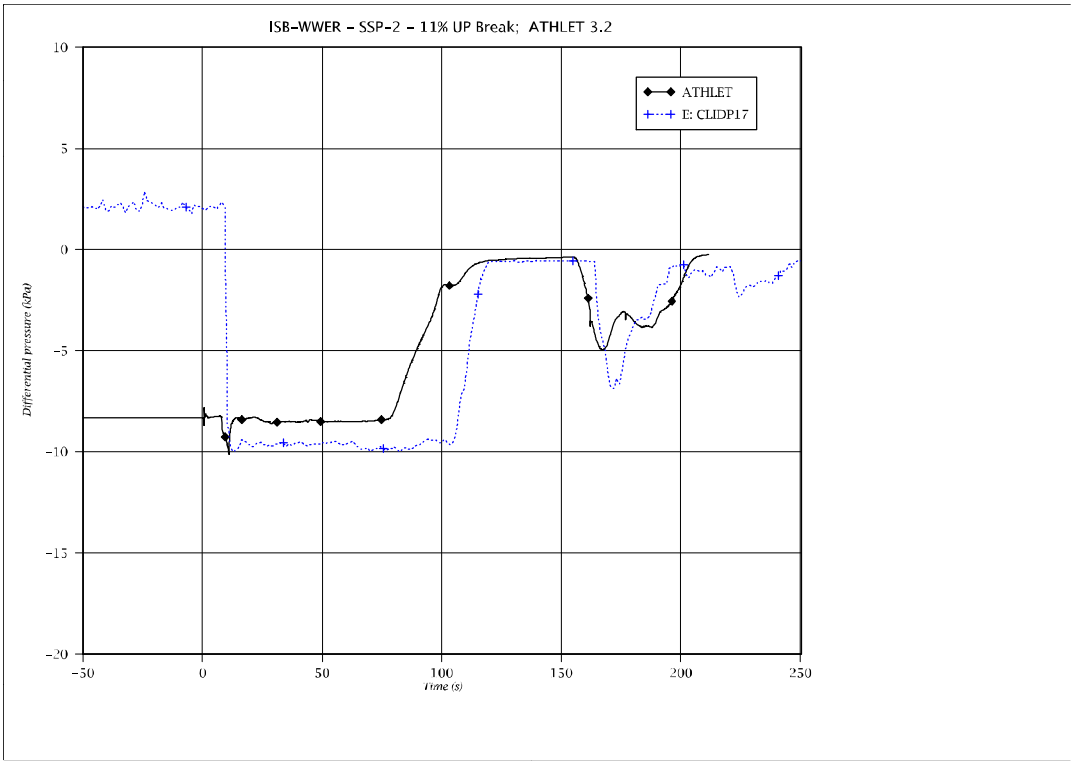

Fig. 5 - 169: Differential pressure in vertical part of triple loop cold leg (downflow)

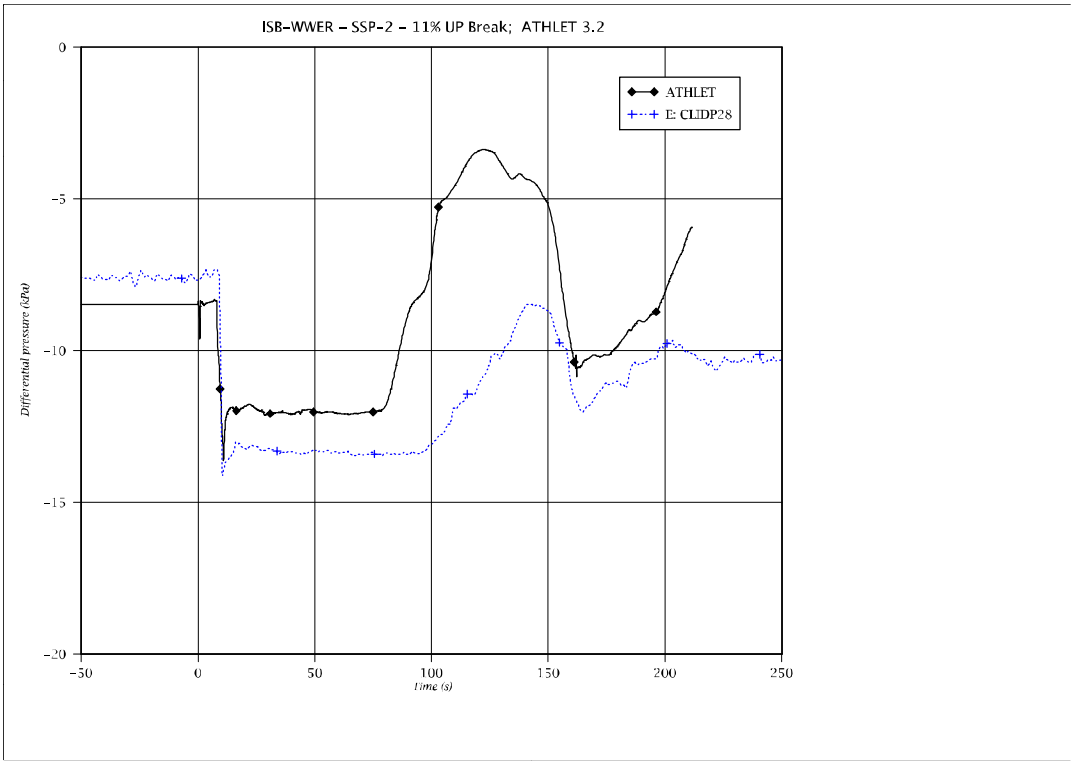

Fig. 5 - 170: Differential pressure in vertical part of triple loop cold leg (upflow)

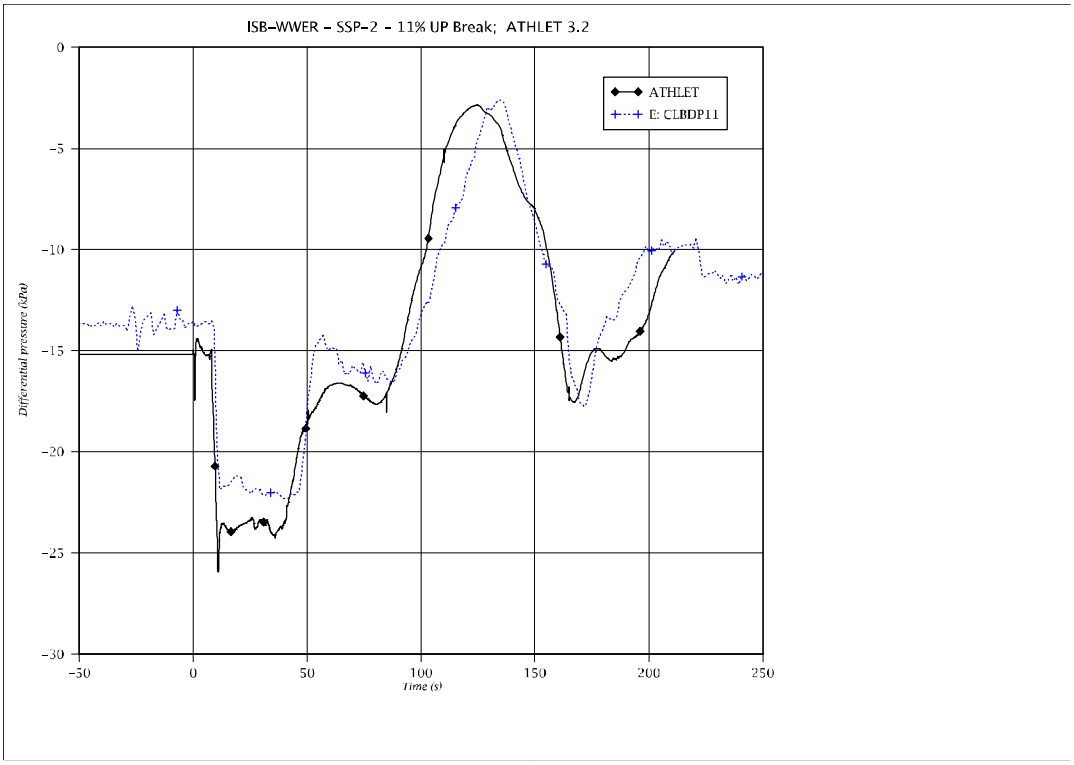

Fig. 5 - 171: Differential pressure in vertical part of single loop cold leg (downflow)

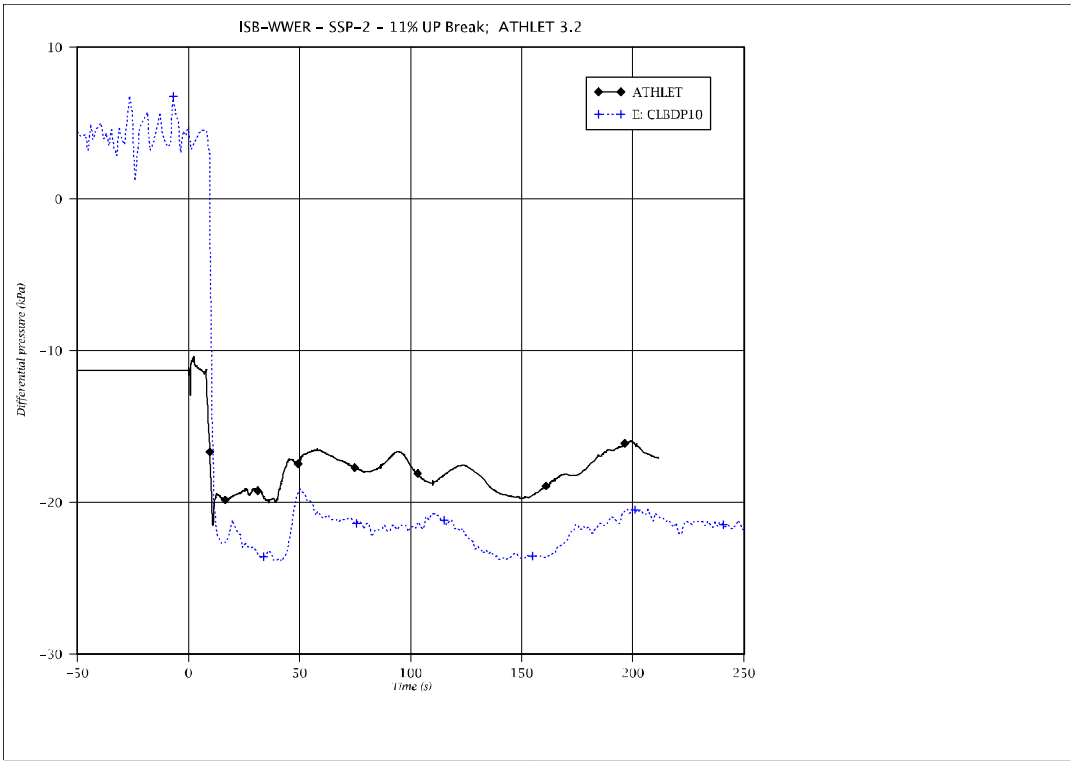

Fig. 5 - 172: Differential pressure in vertical part of single loop cold leg (upflow)

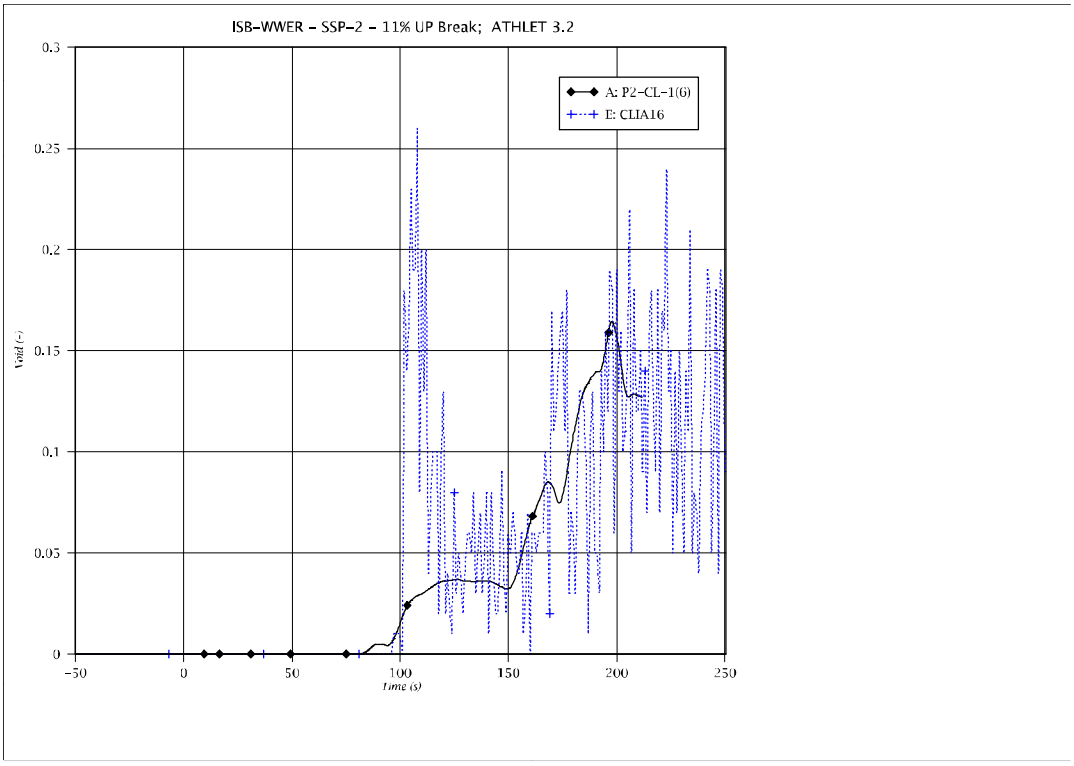

Fig. 5 - 173: Void at vertical part of triple loop cold leg (downflow)

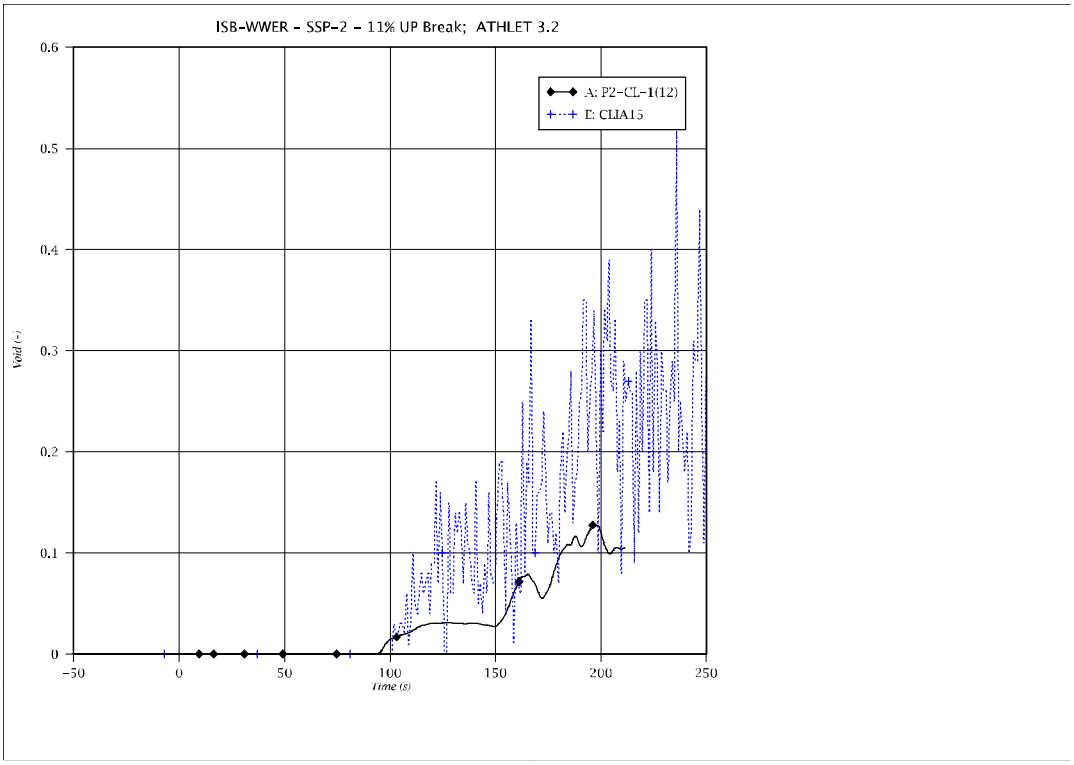

Fig. 5 - 174: Void at vertical part of triple loop cold leg (upflow)

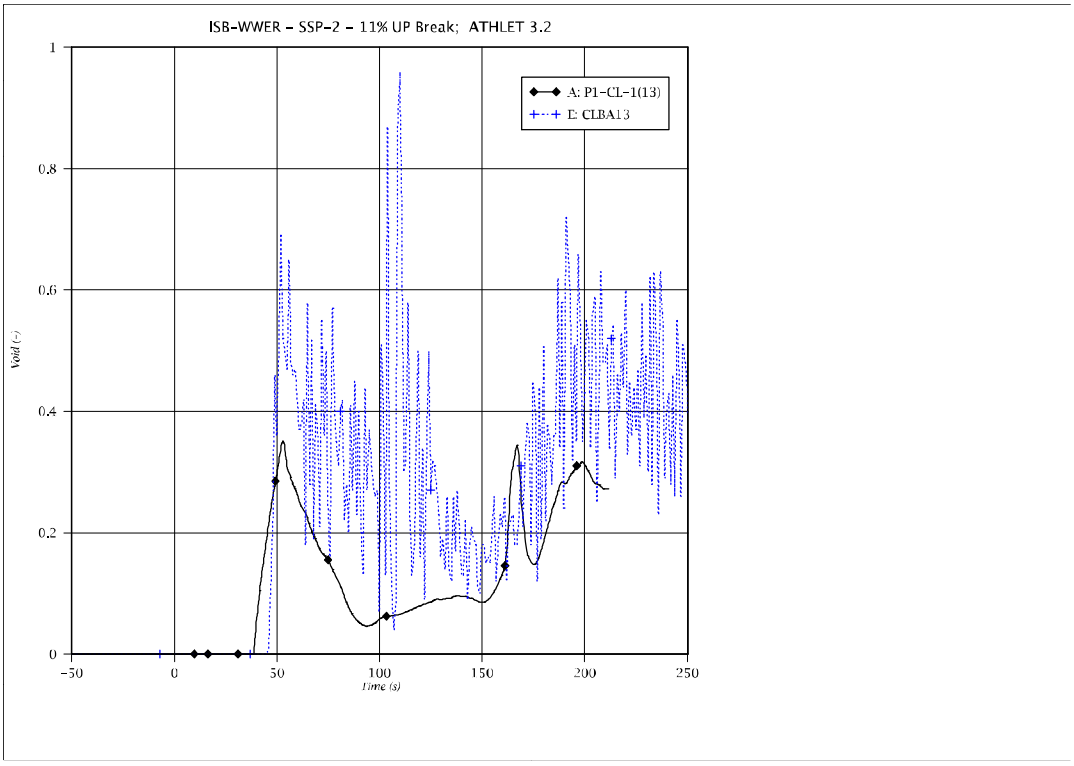

Fig. 5 - 175: Void at vertical part of single loop cold leg (upflow)

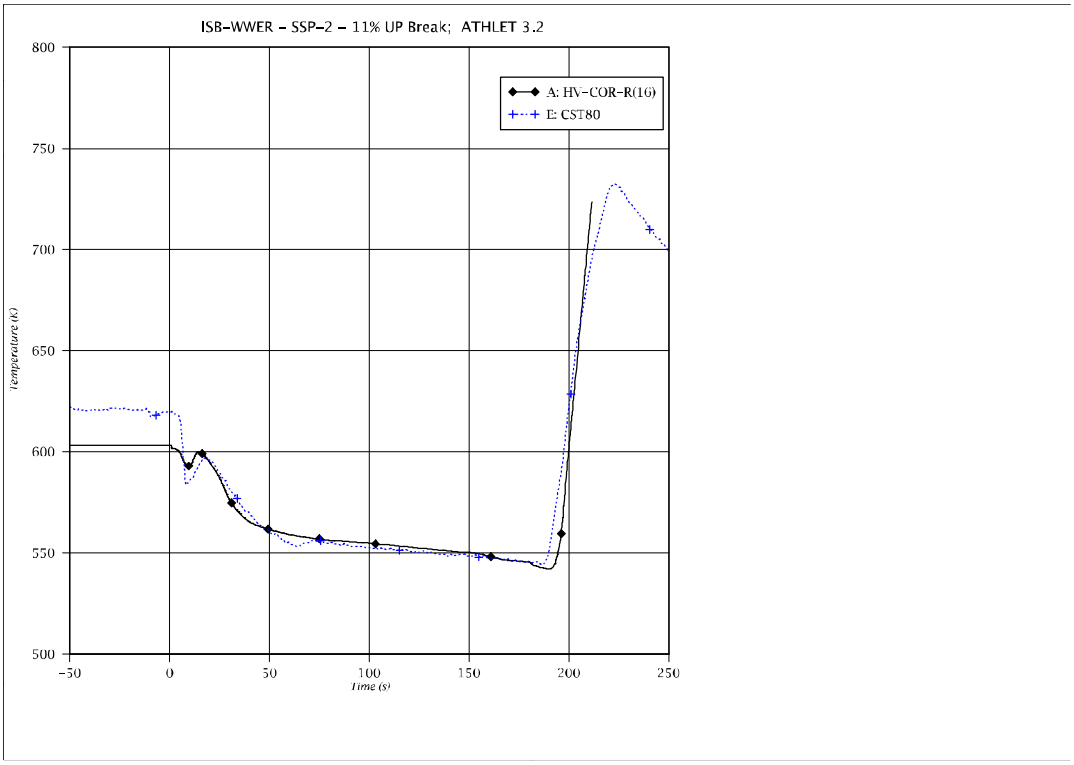

Fig. 5 - 176: Cladding temperature at elevation -1742 mm

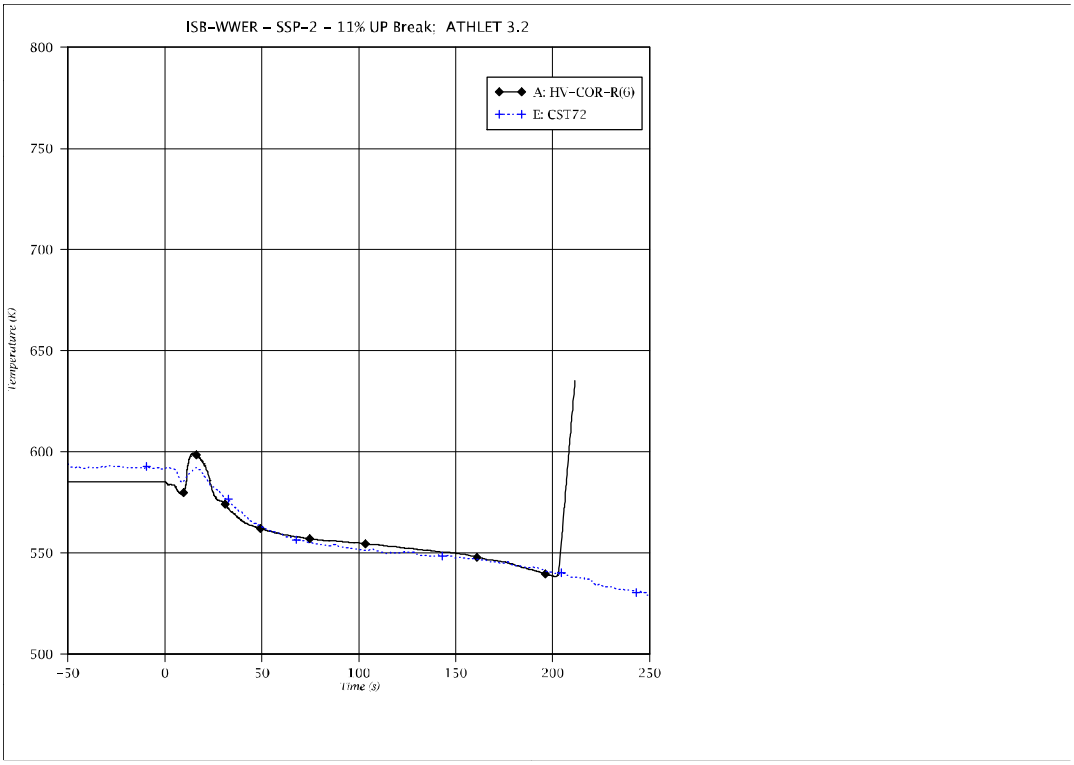

Fig. 5 - 177: Cladding temperature at elevation -3885 mm

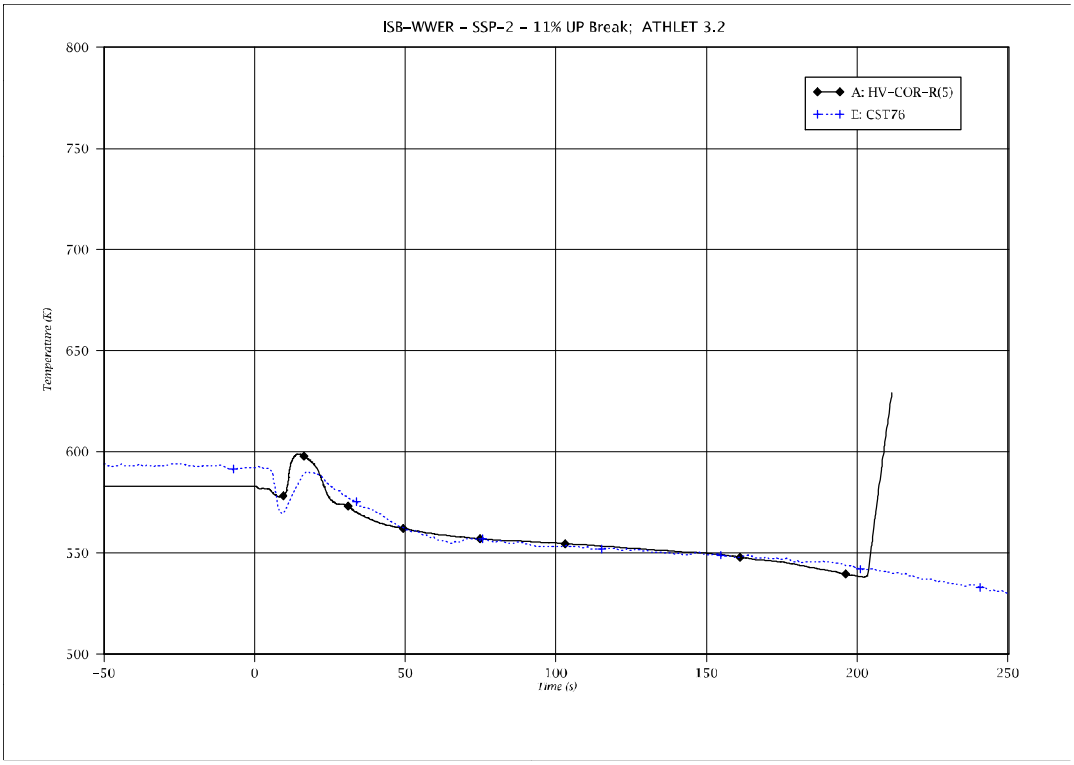

Fig. 5 - 178: Cladding temperature at elevation -4140 mm

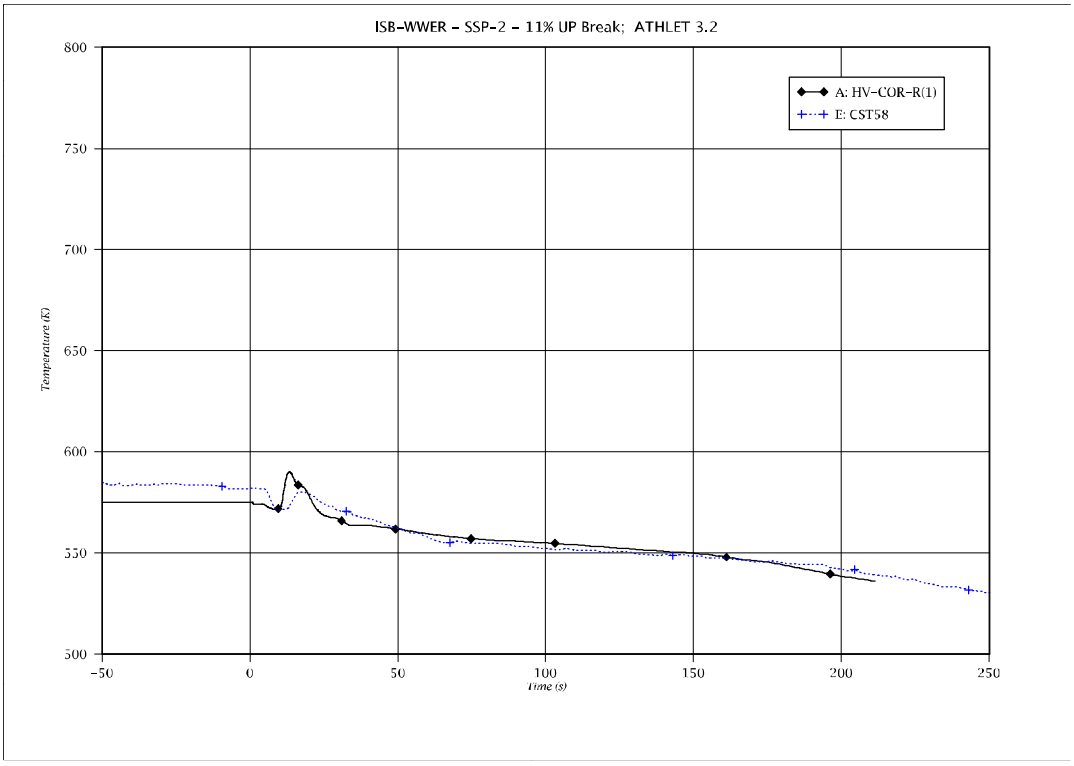

Fig. 5 - 179: Cladding temperature at elevation -5015 mm

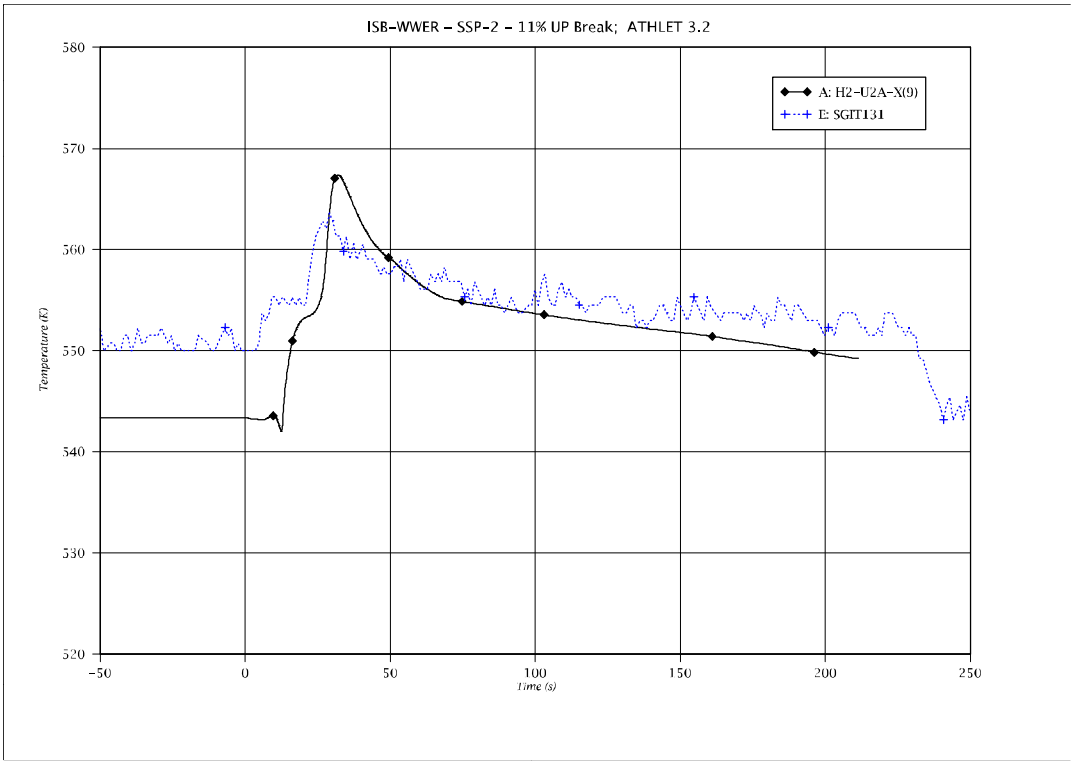

Fig. 5 - 180: U-tube surface temperature at elevation -4923 mm (triple loop)

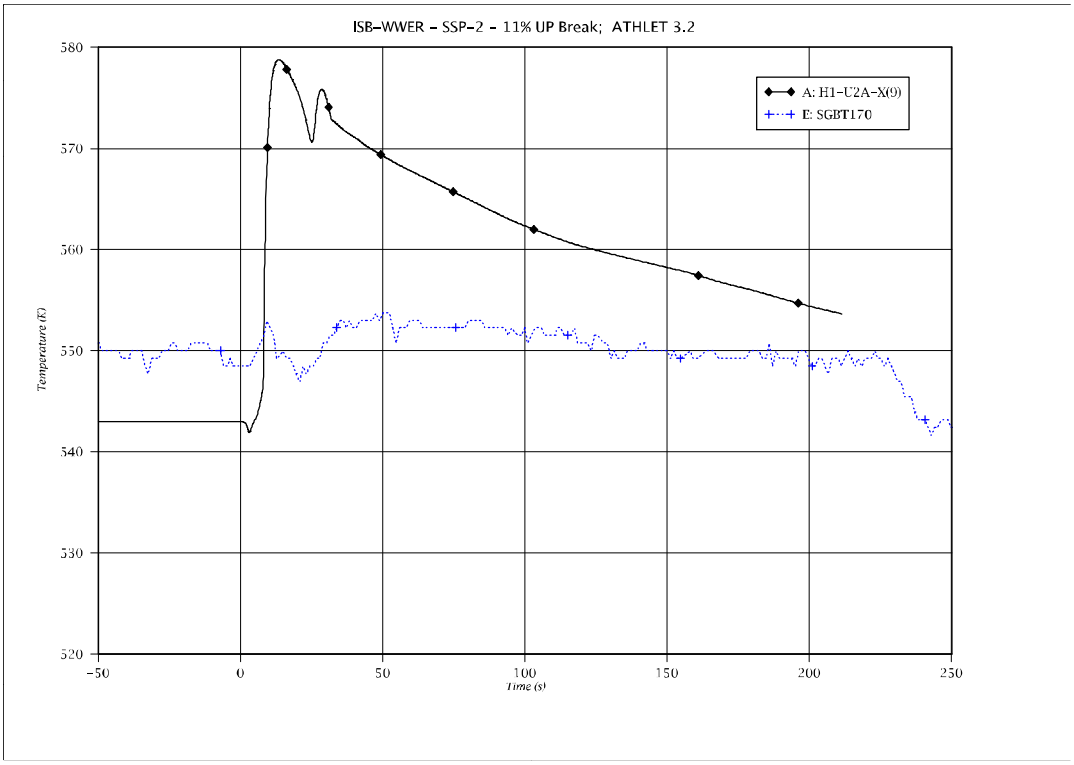

Fig. 5 - 181: U-tube surface temperature at elevation -4924 mm (single loop)

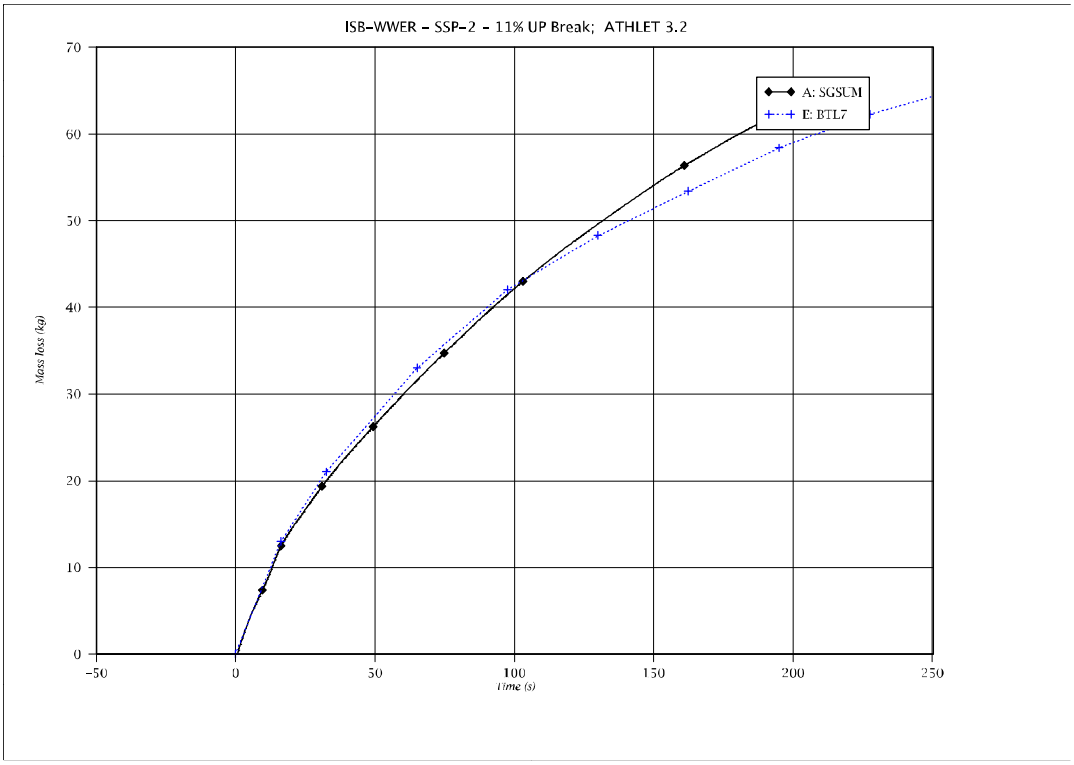

Fig. 5 - 182: Integrated break mass flow rate

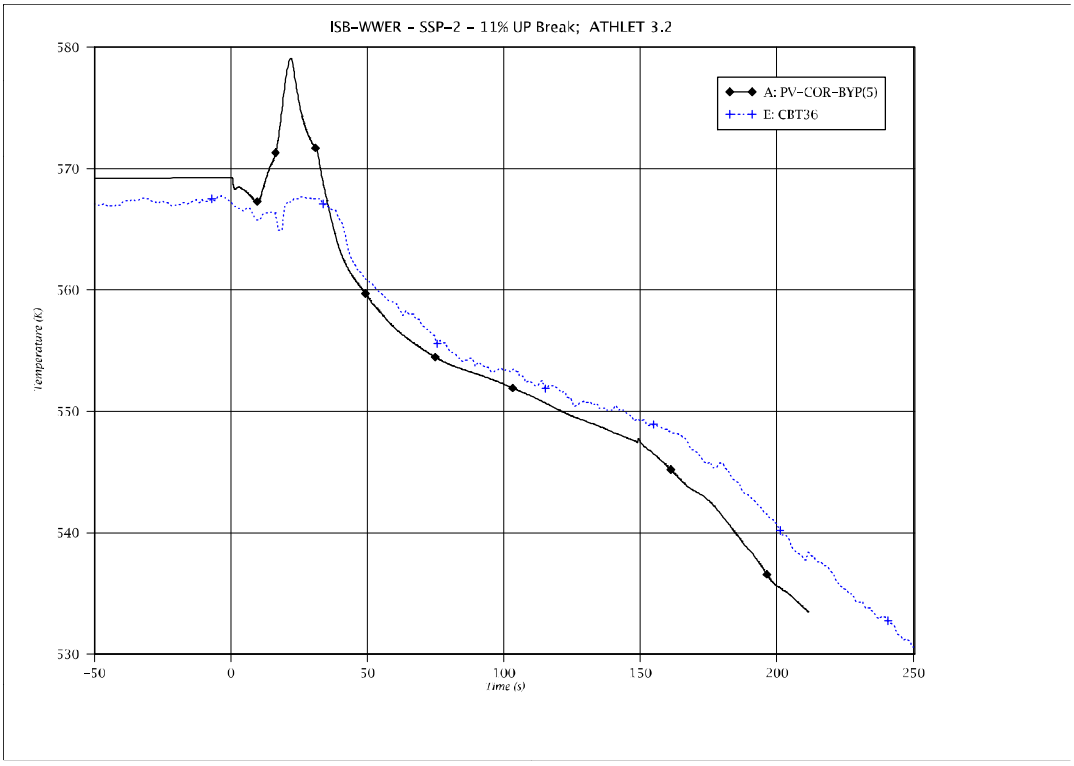

Fig. 5 - 183: Temperature in core bypass at elevation - 1570 mm

5.5 ROCOM Test T2.1

5.5.1 Test Facility

The four-loop integral test facility Rossendorf Coolant Mixing (ROCOM) replicates according to a linear scale of 1:5 a German KONVOI-type PWR with all details important for the coolant mixing along the flow path; from the cold-leg nozzles up to the core inlet. Special attention was given to components, which significantly influence the velocity field, such as the core barrel with the lower core support plate and core simulator, the perforated drum in the lower plenum, and the RPV inlet and outlet nozzles /KLI12/. Each of the loops includes a pump which can adjust the coolant mass flow. The test facility was constructed to provide a validation basis focusing on mixing processes for multidimensional computer codes, such as Computational Fluid Dynamics (CFD) and system codes /KLI12/.

The experiments are carried out with water at atmospheric pressure and room temperature. The temperature difference between the primary coolant and the emergency core coolant is represented through a density difference reached by means of the added sugar solution. The coolant mixing behavior is measured exploiting the local electrical conductivity of the fluid. Additives such as salt or brine tracer are used to label the water and subsequently study its distribution within the system. This is monitored by the specially designed electrical conductivity Wire Mesh Sensor (WMS) which provides high-resolution measurements of the tracer concentration both in space and time, /PRA03/ and /KLI08/. Several sensors are installed at the RPV inlets, at two concentrical layers close to the inner and outer DC wall, stretched along nearly the entire length of the DC, and at the Core Inlet (CI). Figure 5 - 184 shows the Reactor Pressure Vessel (RPV) model of the ROCOM facility and the locations of each installed WMS. The geometry of the core and the upper plenum is simplified within the ROCOM facility and considered only by means of its hydraulic resistance. The core consists of 193 rod correspondents simulating the 193 fuel assembly of the KONVOI reactor. Each of the core channels is equipped with one WMS at the CI, integrated into the lower core support plate. The DC wire mesh sensors are subdivided into 64 azimuthal and 29 axial measuring planes.

Additional to the geometrical similarity also the dynamical similarity must be fulfilled by the experimental facility in order to replicate the buoyant and turbulent flow processes. In the particular experimental scenario, however, since the density difference is the driving force for the natural circulation phenomena, the similarity based on the Froude number had to be fulfilled. The dimensionless Fr number is defined in eq. 5 - 1.

$$Fr = \sqrt{\rho \frac{w^2}{\Delta\rho g L}} \qquad (5-1)$$

In equation 5 - 1, *L* represents the characteristic length, *w* the velocity, *ρ* the density and *g* the gravitational acceleration. The dynamic similarity imposed a velocity scaling factor of for the ROCOM experiment T2.1.

5.5.2 Test Conditions and Procedure

The ROCOM experiment T2.1 was carried out as a counterpart test in the frame of the OECD PKL-2 project, dedicated to the fast cool-down transient induced by a main steam line break /OEC12/. The scenario of the experiment can be divided in two main phases. The first phase starts immediately after the main steam line break on the secondary side, resulting in an increase of the heat transfer due to the enhanced evaporation in one Steam Generator (SG) following the pressure decrease. As a result the corresponding primary loop is strongly affected. This first phase lasts until the entire fluid inventory of the affected SG evaporates. The second phase on the other hand is characterized by the activation of the Emergency Core Cooling (ECC) system, which injects cold and highly borated water into the cold legs. The ROCOM experiment T2.1 was dedicated to the first phase also called the over-cooling phase. The over-cooling phase can for example trigger a recriticality process due to boron dilution while the ECC injection in the second phase can lead to a Pressurized Thermal Shock phenomenon.

Table 5 - 8: Initial and boundary conditions of the ROCOM experiment T2.1

Cooling Circuit Loop	1	2	3	4
Volumetric flow rate, [l/s]	5.24	2.47	2.47	2.47
Relative density, [-]	1.067	1.0	1.00	1.00
Temperature, [˚C]	199.3	241	241	241
Pressure [MPa]	4.1	4.1	4.1	4.1
Experimental procedure				
Time	**Experimental log**			
Experiment preparation	Preparation of the water/sugar solution with the desired density value; labelling of the water with salt			
t = -30 s	Establishing stationary flow conditions in loops 2, 3, 4			
t = 0 s	Injection of the higher density water into loop 1			
t = 150 s	End of injection			

Constant Boundary Conditions (BC) of the quasi-stationary experiment were fixed based on the results of the G3.1 PKL-2 /OEC12/ experiment. A summary of the initial and BC is presented in table 5 - 8.

The leak was postulated during the Test T2.1 in the steam line of the steam generator of loop 1. The over-cooled fluid with the increased density was therefore modelled in this loop. Loop

1, the Affected Loop (AL) was plugged behind the main coolant pump. The fluid mass flow rate with the appropriate density (“over-cooled fluid”) was directly pushed into the cold leg of the AL, between the main pump and the DC inlet (see fig. 5 - 185). The injected water mass was consistently discharged from the corresponding hot leg during the experiment. In the other three loops the fluid was circulated with the main coolant pumps.

5.5.3 Input Dataset

Figures 5 - 186 to 5 - 188 show the nodalization used for the ATHLET analysis of the ROCOM T2.1 test. For the simulation of the ROCOM experiment T2.1, a multi-dimensional numerical grid was used for the nodalization of the RPV DC region, consisting of sixteen azimuthally distributed control volumes (CV) and thirteen axial CV. The cold legs are connected to the PV-DCM region of the DC, as exemplified in fig. 5 - 186. The DC region consists from top to bottom of the components called PVDC-T, PV-DCM, PV-DCB and PLM. SJP or cross-connection elements link on the circumference the DC the components PVDC-T, PV-DCM and PV-DCB and the curved region of the DC, consisting of the PLM components

The complex set-up of the lower core plate was considered in the ATHLET model of the ROCOM facility. The core was divided into 33 parallel hydraulic channels arranged in two cylindrical rings around the central channel. Each channel has an axial resolution of five computational cells. A schematic drawing of the sixteen azimuthal DC elements and the 33 core channels together with the location of the broken loop is presented in fig. 5 - 187. In this figure, a fixed number of fuel assemblies is assigned to each core channel. On average, each TFO of the outer core ring, channel 1A to 8B in fig. 5 - 187, corresponds to 6.25 core channels of the original ROCOM facility. The ATHLET thermo-fluid objects of the inner core ring, channel 9A to 16B in fig. 5 - 187, correspond each to 5.25 of the actual core channels of the ROCOM facility. The central TFO, channel 17 in fig. 5 - 187, corresponds to 9.00 actual core channels of the real ROCOM facility.
The LP of the RPV is geometrically approximated by a cylindrical grid that consists of two axial layers. The upper layer contains two rings with 16 segments and one central region while the lower layer contains one single central element. In order to capture the complex coolant flow that is guided by the curved shape of the calotte, the outer LP region is modeled by a 2D grid with 16 azimuthal CV, elongating the grid of the vertical DC region. Figure 5 - 188 shows a schematic representation of the multidimensional nodalization of the LP. A sieve drum mounted in the LP of the real ROCOM facility is modelled in the nodalization only by an increase of the local form loss coefficient between the outer and the inner LP ring.

For a better representation of the multidimensional flow phenomena anticipated in the RPV the native 2D/3D component model available in ATHLET was applied. All pipes of ROCOM’s pri-

mary coolant loops have been modelled employing 1D thermo-fluid components. The UP is modelled as a single volume, a BRANCH component, connected with all core channels and each of the four hot legs.

Summary of network data:

Number of branches:	40
Number of pipes:	303
Number of CVs:	804
Number of junctions:	1337

Thermo-fluid objects

The following aspects were considered for the choice of nodalization of the fluid system:
Core
The experimental facility includes 193 dummy flow channels corresponding to the fuel elements of a real KONVOI-type PWR, simulating the pressure drop over the core region. The 193 dummy flow channels are collapsed within 33 TFO components.
Downcomer
To consider the asymmetric influence of the main steam line break location in SG1, the DC is split into sixteen parallel channels interconnected via TFOs forming a 2D numerical grid, as presented in fig. 5 - 186.
Circuits
All four coolant loops are accurately modelled within ATHLET. The main coolant pumps and the steam generators are modelled according to the real design data of the ROCOM experimental facility.

5.5.3.1 Model Options

Following model options are applied:
The 6 eq. model is applied for the simulation of the ROCOM T2.1 experiment. The 2D/3D model equations were applied to the components PVDC-T1A to PVDC-T8B, PV-DCM1A to PV-DCM8B, PV-DCB1A to PV-DCB8B and PLM1A to PLM8B of the DC region (fig. 5 - 186) and PLM11A to PLM81B, PLM12A to PLM82B and PLM00A (fig. 5 - 188) of the LP region. All model parameters required by the 2D/3D-Module were selected according to the default or recommended values, as documented in the current ATHLET User's Manual. In addition the special cold water injection model was activated for the affected loop, in order to account locally for the thermal mixing phenomena between CL and RPV.

5.5.4 Results of the ATHLET Calculation

The discussion of the ATHLET simulation results begins with the general presentation of key time points in the experiment progress. These include:

d) The denser liquid injected into the AL reaches the DC at approx. Problem Time (PT) 12.4s.

e) A helicoidal flow of the denser liquid downwards within the DC creating two strands of denser liquid, approx. PT 15.1s to 18.4s.

f) The denser liquid reaches the LP. At the same time the two denser liquid strands merge to form a continuous plume of dense liquid below the RPV inlet nozzle of the AL, approx. PT 24.7s.

g) The denser liquid reaches the Core Inlet (CI), approx. PT 24.7s.

h) Replacement of the lighter liquid by denser one in the core, starting approx. with PT 26.5s and lasting until the end of the experiment. The replacement occurs from the core periphery towards its center, approx. starting at PT 55.0s.

The assessment of the simulation results will start with the qualitative comparison against the measurement data in the DC and the LP regions of the RPV, according to the locations indicated in fig. 5 - 184. A direct comparison between the results of the computer simulation and the WMS captured data is presented in figs. 5 - 189 and 5 - 190. The color scheme used to represent the temperature field in the DC and at the core inlet is set up as follows: the color “blue” always corresponds to the value of 514 K, while the color “red” corresponds to the value 472 K and 488 K in the DC region and at the CI respectively. In the second part of this assessment the temperature trends reconstructed from the WMS electrical conductivity data at key locations in the RPV will be compared against the calculated results, see figs. 5 - 191 to 5 - 210.

As depicted in fig. 5 - 191, the time point at which the denser liquid reaches the DC is well predicted by ATHLET, key point d). The interpretation of the measurement data reveals a non-uniformly mixture of the coolant at the RPV inlet nozzle in the first few seconds of the experiment. This detail influences the degree of coolant mixing in the DC of the RPV. Owing to ATHLET’s one-dimensional description of the coolant flow in the cold legs, this effect could not be observed in the numerical simulation, but it will have an impact on the temperature distribution in the DC region.

In the experiment the denser liquid creates a plume of approx. 90° azimuthal width below the RPV inlet nozzle of the AL. This flow behavior can be observed in the experiment between PT 12.4s and 15.1s. Subsequently, the denser liquid flows downwards to the LP in form of two diverging strands, a behavior characteristic for the time-interval PT 15.1s to 24.7s. The ATHLET

simulation, employing the genuine multidimensional flow description, captures well the effect of the liquid strand separation over an azimuthal sector of approx. 90° at PT 15.1s. Still the two resulting strands flow in a more compact pattern towards the LP in the simulation than in the experiment.

At the key point f) denser liquid reaches the LP over almost the entire periphery and it starts to enter the core, key point g) in fig. 5 - 189. The ATHLET simulation calculates a more compact plume pattern of the denser liquid reaching the LP, as the two denser liquid strands already merged around PT 18.4s, approx. 6s sooner than in the experiment. Still the time point when the first over-cooled liquid reaches the core tie plate is well predicted by ATHLET. In the experiment the denser liquid momentum transport along the curved shapes of the LP results in a temperature distribution as the denser liquid reaches the CI, with colder liquid at the periphery than at the core center. The core channels diagonally opposite to the AL are reached sooner than the ones neighboring the AL. A sequence qualitatively captured by ATHLET, where flow channels of the inner ring diagonally across the core are reached by the lower temperature coolant as seen at PT 26.5s presented in fig. 5 - 190. The fact that the ATHLET core channels 1A to 3B seem not to be reached by the lower temperature coolant is the result of two separate effects: the first represents the lower predicted azimuthal distribution of the two colder liquid strands within the DC compared to the experiments, while the second represents the overestimation of the dampening effect the momentum transport within the LP.

Starting with the time point when the core is reached by the denser liquid, a continuous replacement of the lighter liquid by denser one is observed until the end of the experiment, key point h). The lighter liquid is displaced at this stage from the periphery of the core towards its center, resulting in a cold liquid bulk in the core center at PT 149.5s, as seen in fig. 5 - 190. The time point at which the denser liquid bulk is starting to form in the core center is well captured by the simulation, around PT 55.0s. Nevertheless, the pattern of the denser liquid bulk is not as sharp as it appears in the measurement data, due to an enhanced mixing in the relative coarse computational grid of the LP.

The interpretation of the measured temperature field in the DC between PT 26.5s and 55.0s reveals a transient behavior of temperature stratification in this region. It can be noticed that a temperature front is built up and then quickly decreases as the denser fluid stored in the DC is continuously pushed towards the core. This effect can be better observed by analyzing the temperature trend of the average temperature calculated at the upper and the lower DC region, represented in fig. 5 - 192. The curve labeled as *AVETDCTOP* corresponds to the average temperature in the upper DC region while *AVETDCBOT* represents the average temperature in the lower DC region. The average temperatures were calculated on the basis of all azimuthal measuring points at the two mentioned levels provided by the installed WMS.

Both temperature trends show a sudden decrease, first noticed in the upper region around PT 20.0s and some seconds later also in the lower DC region close to the LP. This sudden temperature decrease is reversed by the recirculation in the LP, thus resulting in a temperature in-

crease to a quasi-steady value. A similar behavior was predicted by the ATHLET simulations in the upper DC region. The simulation employing the genuine multidimensional flow model predicts very well the flow behavior in this region. The difference between the simulated and measured temperature profiles in the case of the ATHLET model is also influenced by the predicted degree of mixing at the RPV nozzle. The one-dimensional description of the cold legs, assumes a homogenous coolant temperature for the entire cross section which is in partial contradiction to the experimentally observed temperature layering in the first seconds after the injection of the over-cooled liquid in the affected loop. On the other hand the relatively large discrepancy between the numerical analysis and the measured data in the lower DC region, depicted in fig. 5 - 191 and 5 - 192, is caused by the simulated temperature stratification in the DC an effect not confirmed by the ROCOM experiment.

The temperature trends at the CI of all ATHLET core channels are presented in figs. 5 - 193 to 5 - 210, together with the average and the minimum CI temperature derived over all core channels in figs. 5 - 211 and 5 - 212. Concerning ATHLET's predictive capabilities for the temperature trends in the channels close to the AL and diagonally across the core it can be noticed that the overall behavior is well captured.

Figures 5 - 213 and 5 - 214 give an overview over the total CPU time (CPU), the number of time steps (IZS), the number of total (LM) and partial (LMPUD) updates of the Jacobian matrix used by ATHLET employing the 2D/3D model for the simulation of the transient ROCOM T2.1 experiment.

Summarizing the comparison of the ATHLET calculation with the experimental results, it can be stated that, in general, the calculated parameters show a good, some of them even excellent agreement with the measurements. The main deviations concern the predicted temperature stratification in the DC region and the overall overprediction of the thermal mixing in the LP region due to the relative coarse nodalization of the RPV component.

5.5.5 Figures

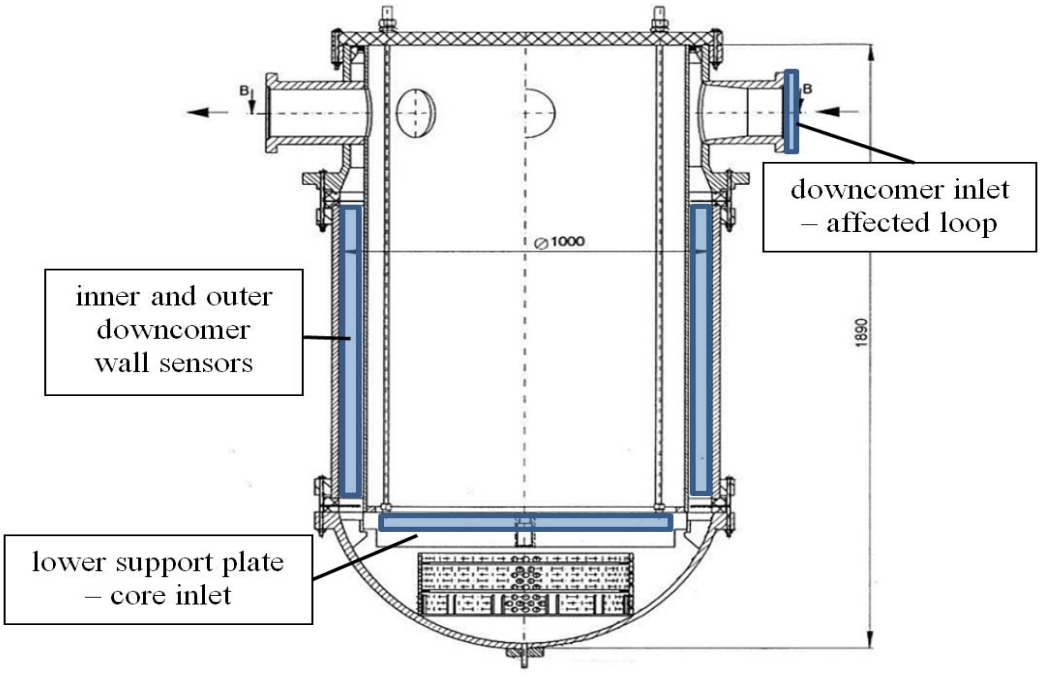

Fig. 5 - 184: RPV of the ROCOM facility showing the location of relevant WMS, edited based on /KLI12/

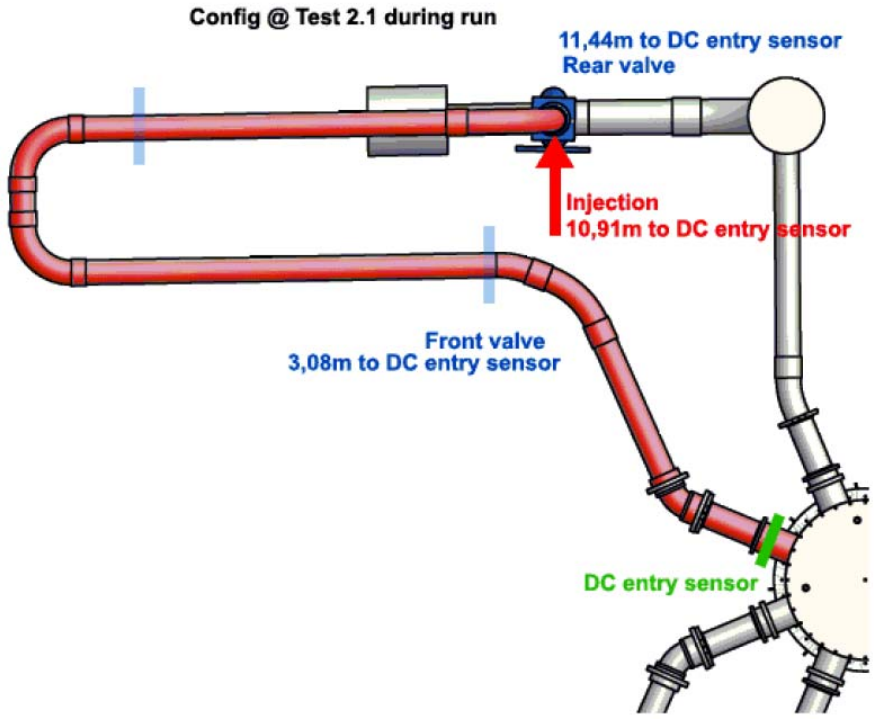

Fig. 5 - 185: Configuration of loop 1 (affected loop) during the ROCOM experiment T2.1 /KLI12/

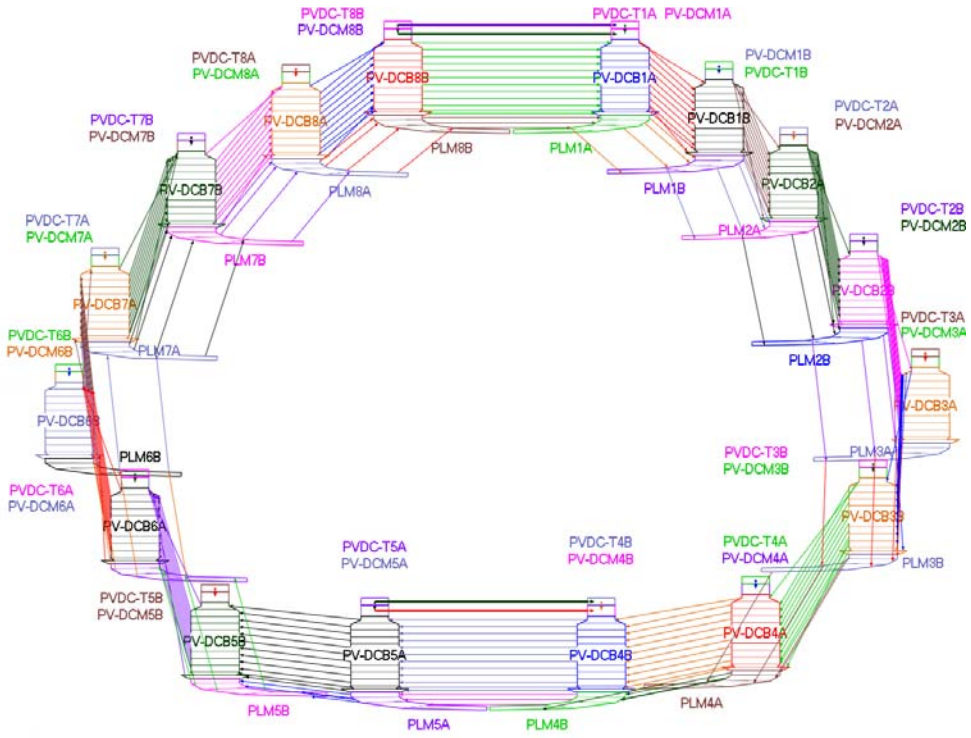

Fig. 5 - 186: Schematic representation of nodalization employed in the DC region and the curved region of the LP

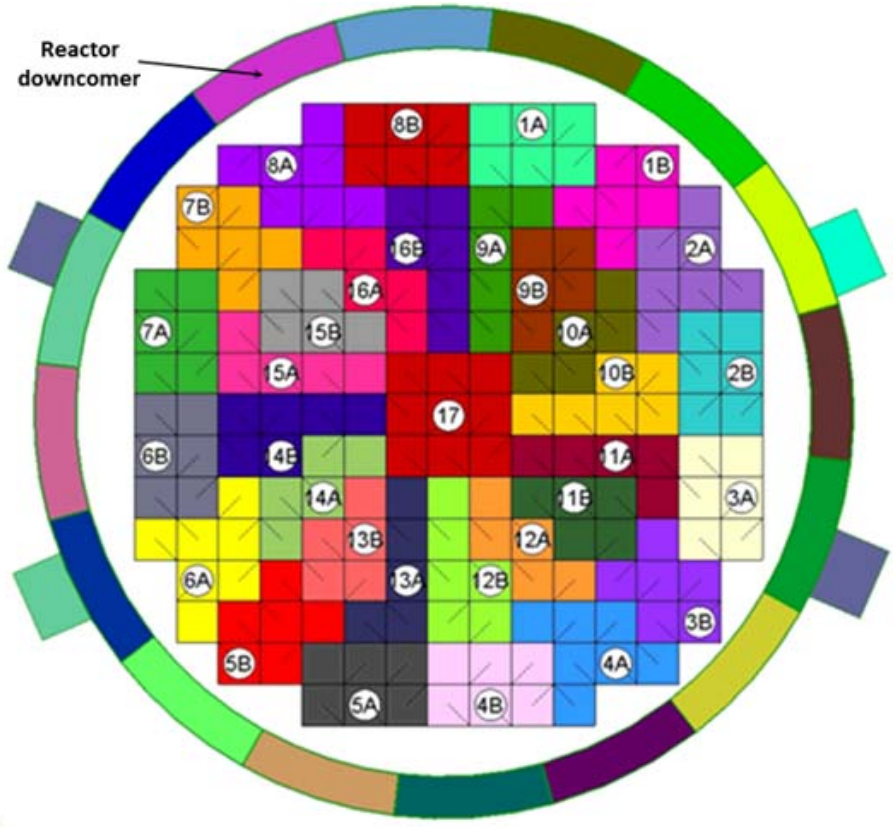

Fig. 5 - 187: Schematic drawing of the sixteen azimuthal CV representation of the DC and the thirty-three core channels

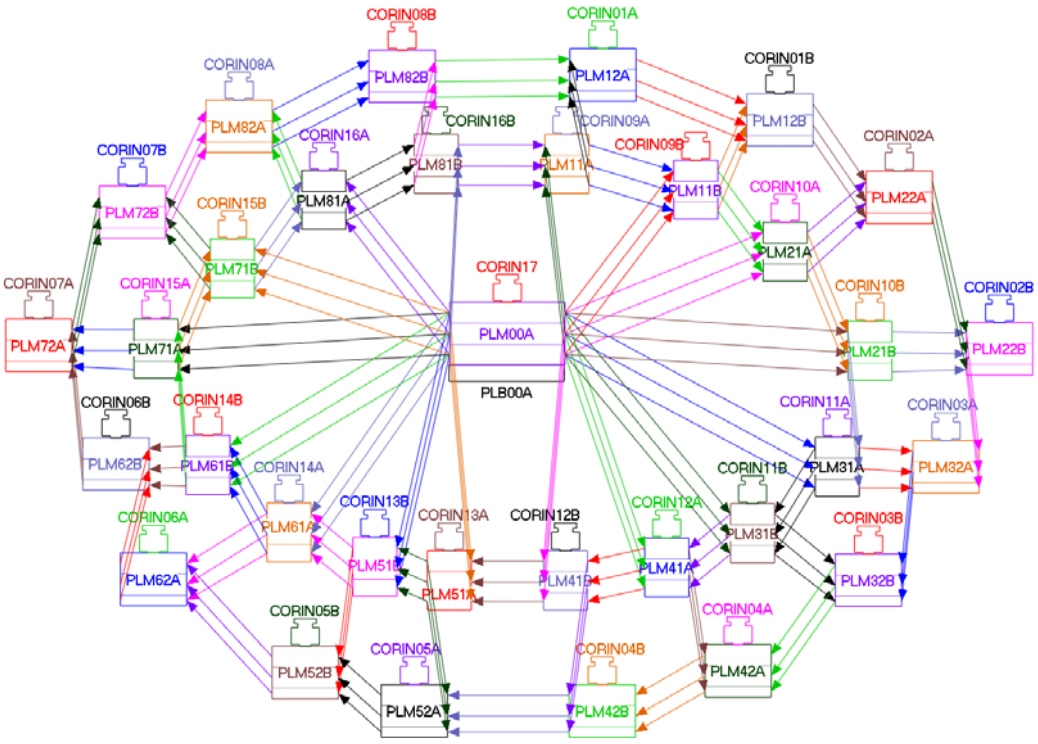

Fig. 5 - 188: Schematic representation of nodalization employed in the LP

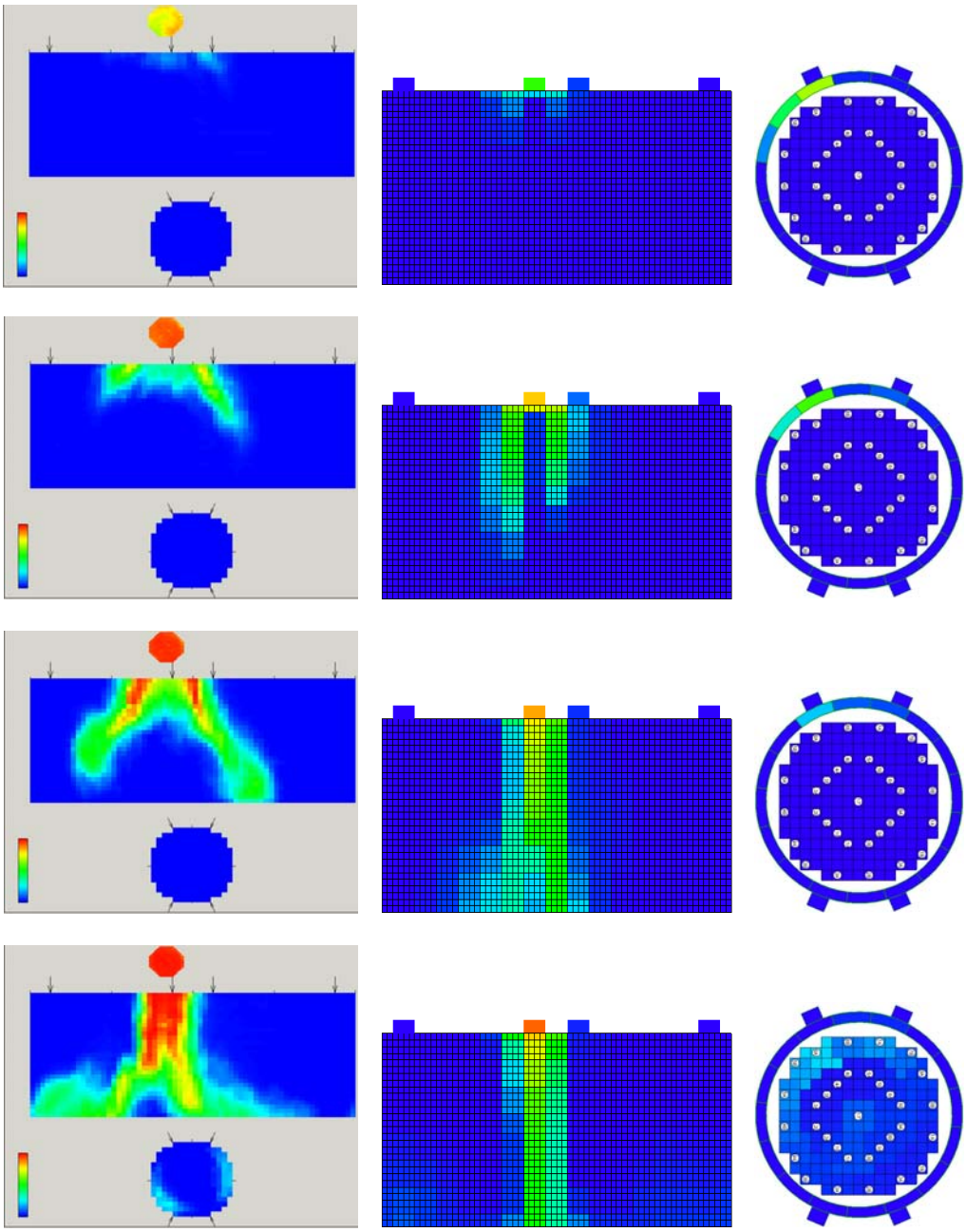

Fig. 5 - 189: Comparison of the temperature fields derived from measured data (left) and simulated data in the DC (mid) and at the CI (right) at temporal key points of the experiment (PT 12.4s, 15.1s, 18.4s and 24.7s).

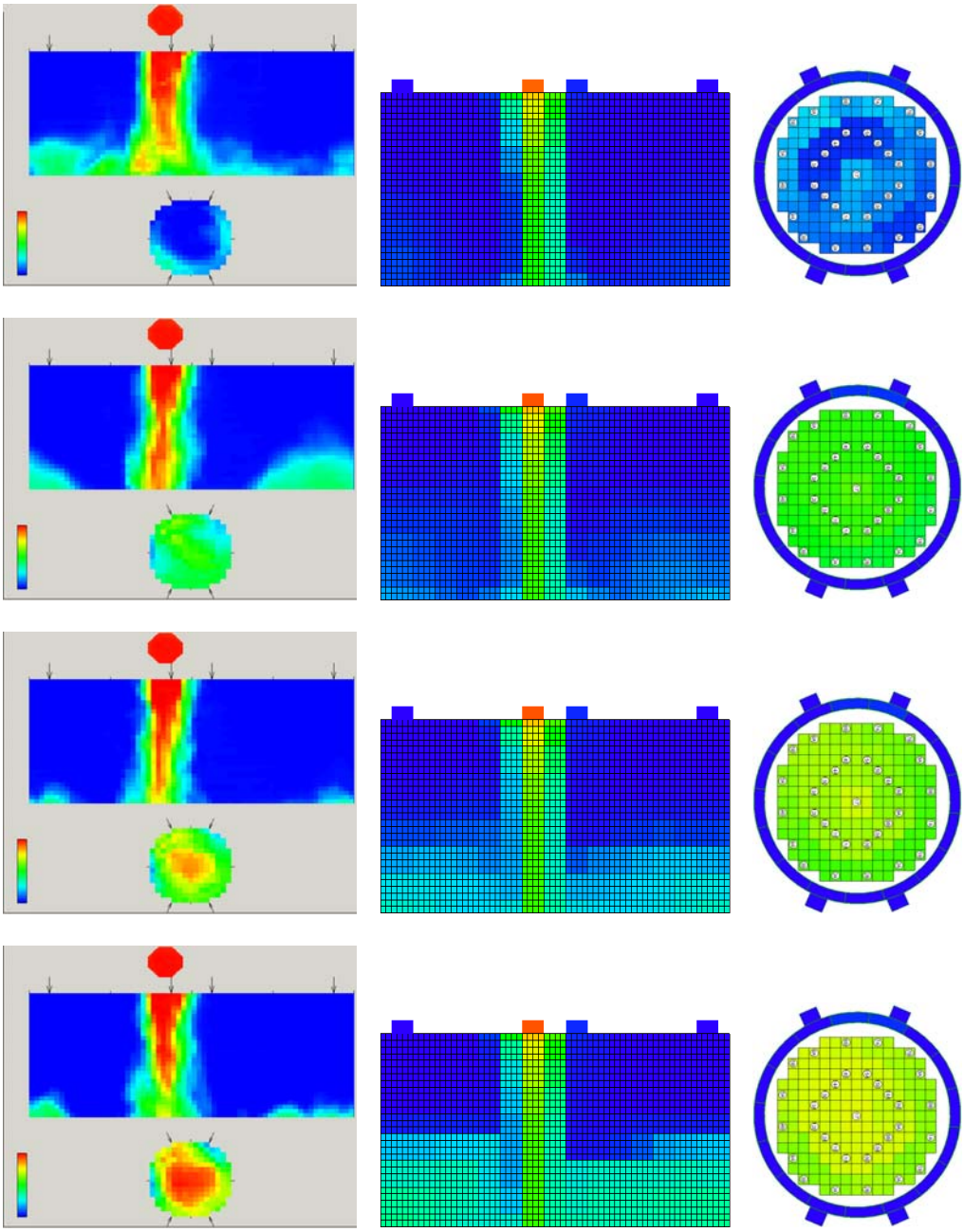

Fig. 5 - 190: Comparison of the temperature fields derived from measured data (left) and simulated data in the DC (mid) and at the CI (right) at temporal key points of the experiment (PT26.5s, 37.9s, 55.0s and 149.5s)

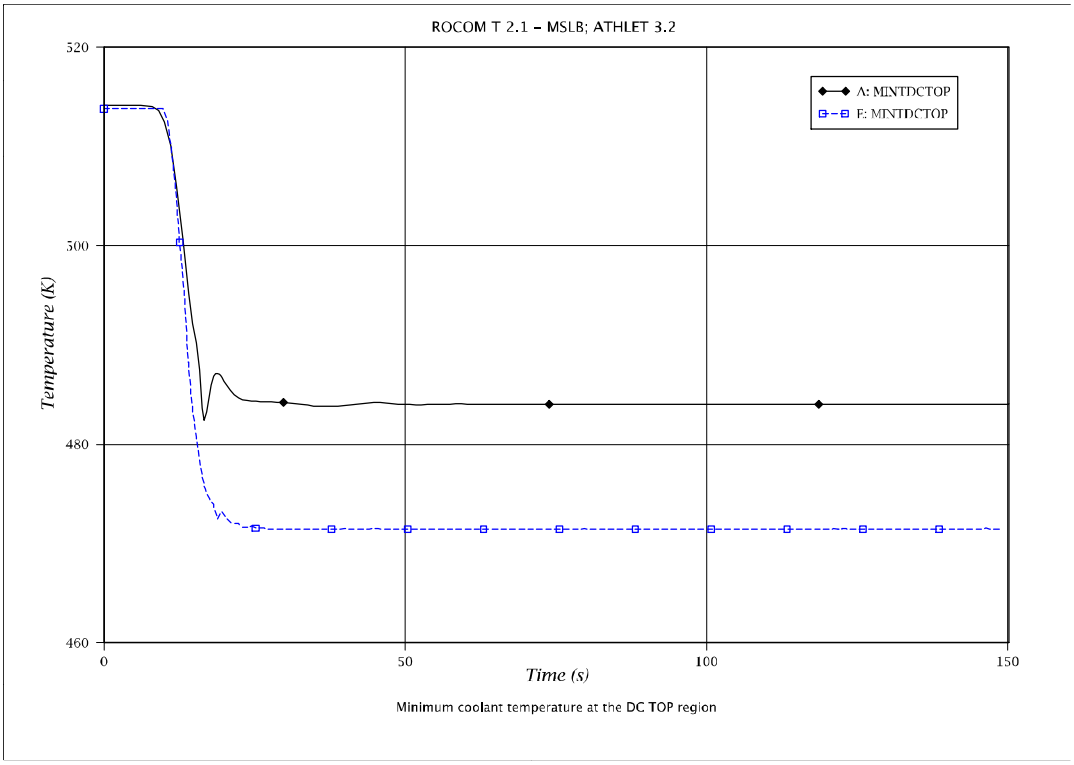

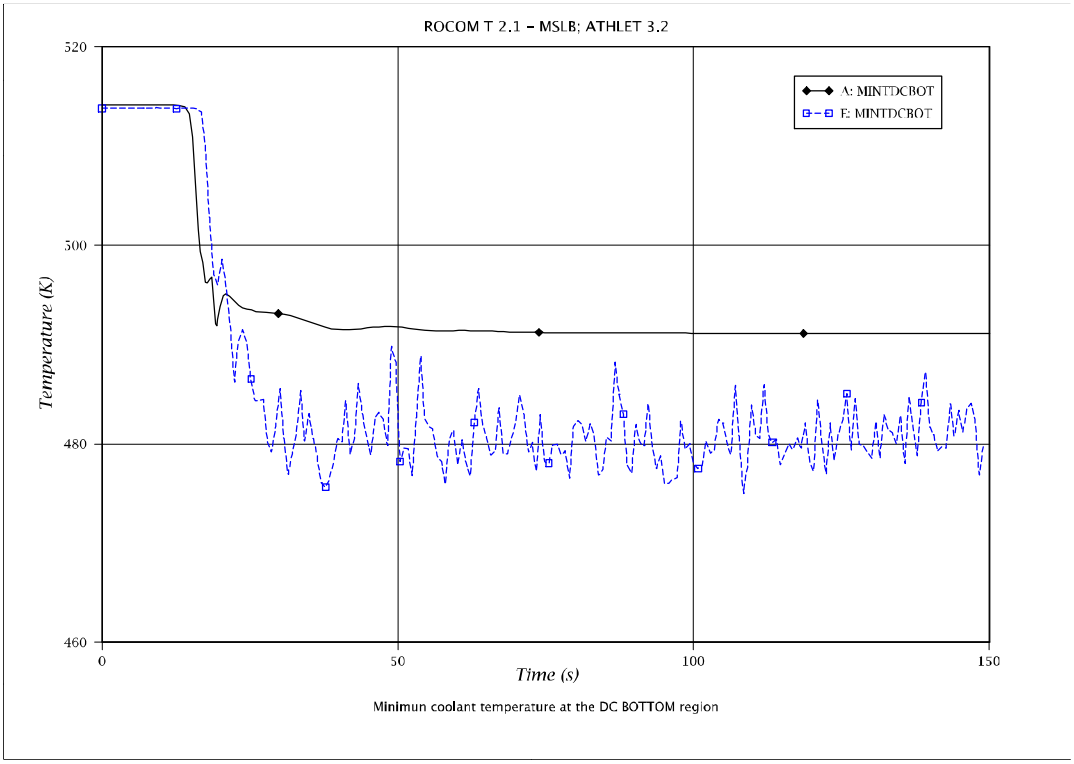

Fig. 5 - 191: Minimum temperature trends in the DC upper and lower region

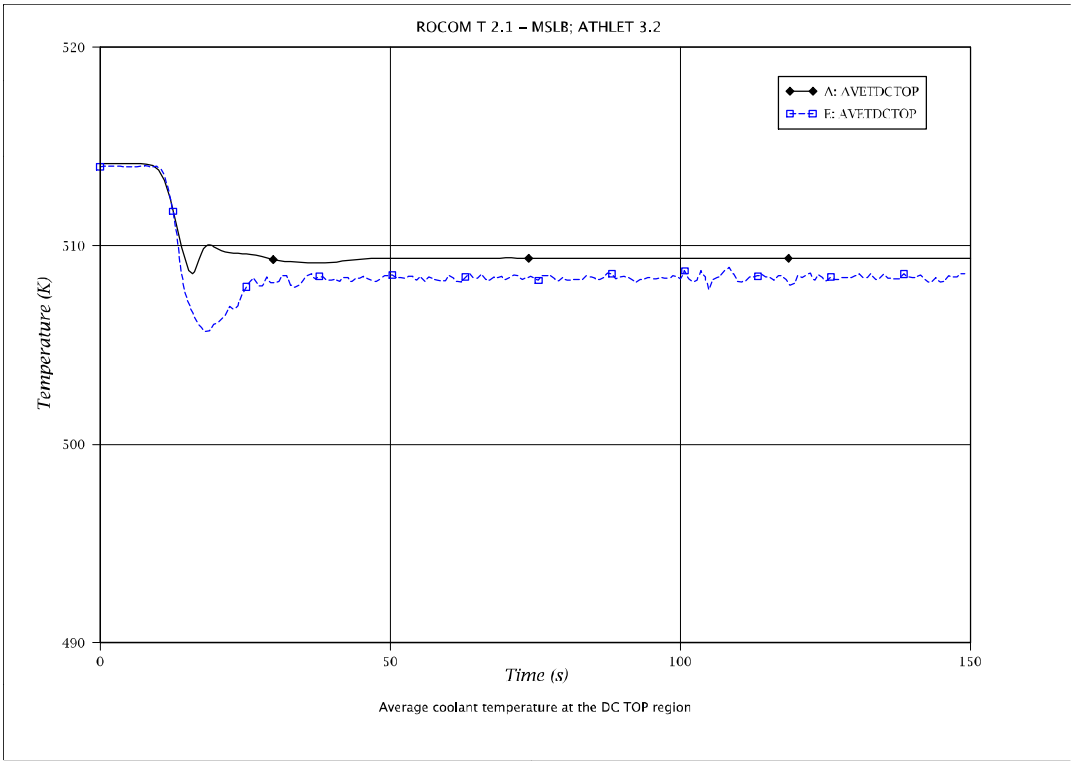

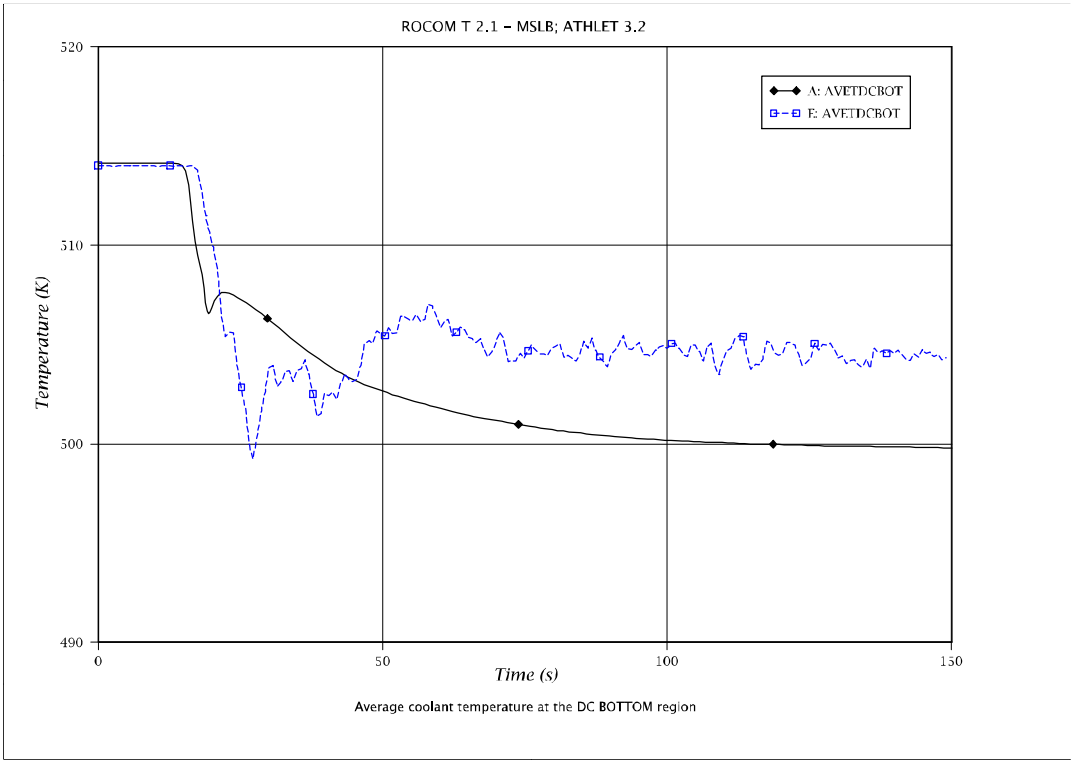

Fig. 5 - 192: Average temperature trends in the DC upper and lower region

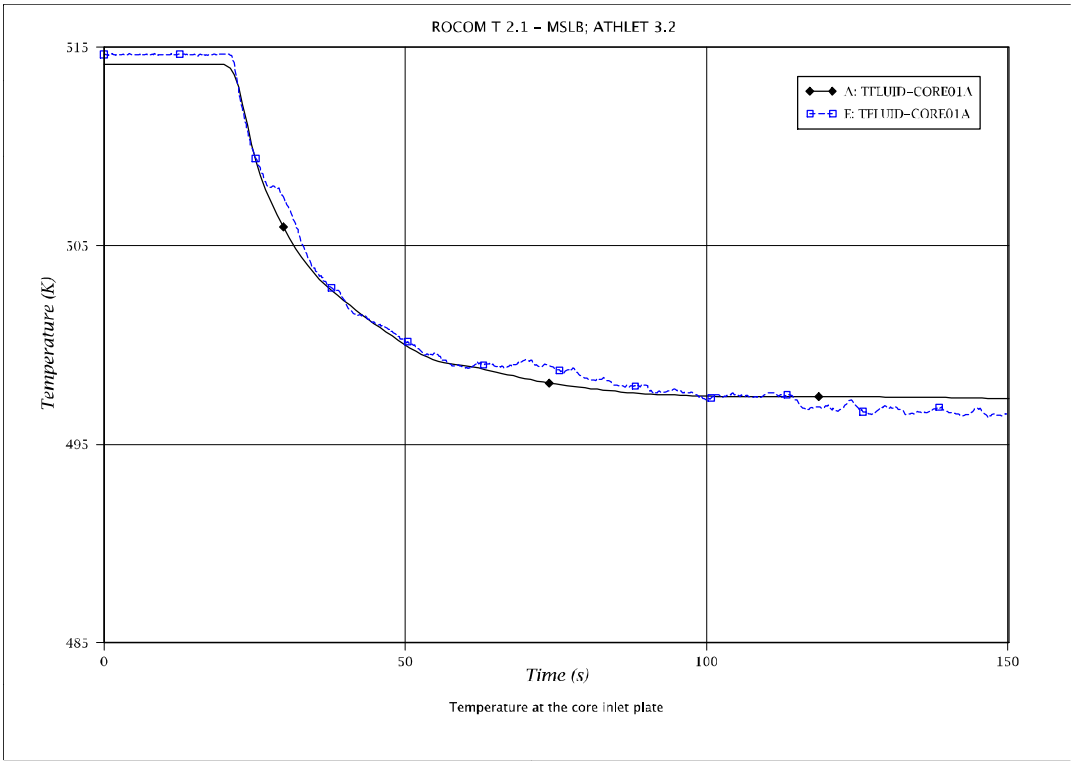

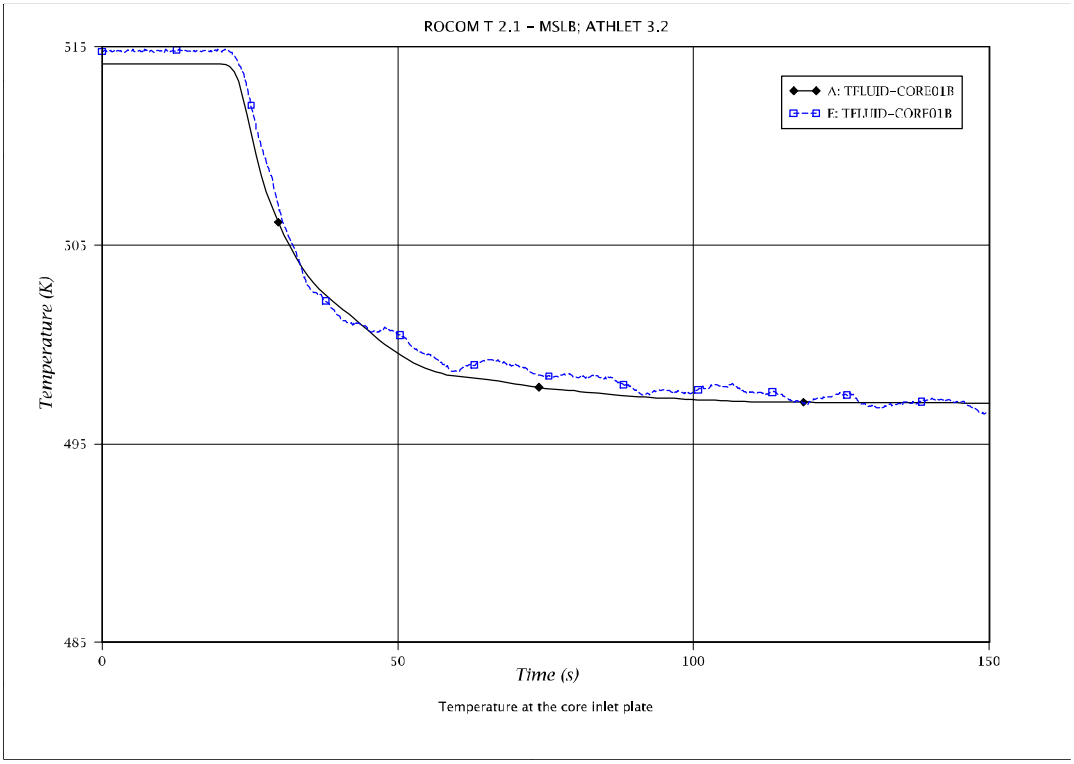

Fig. 5 - 193: Temperature at core inlet: channel 1A and 1B

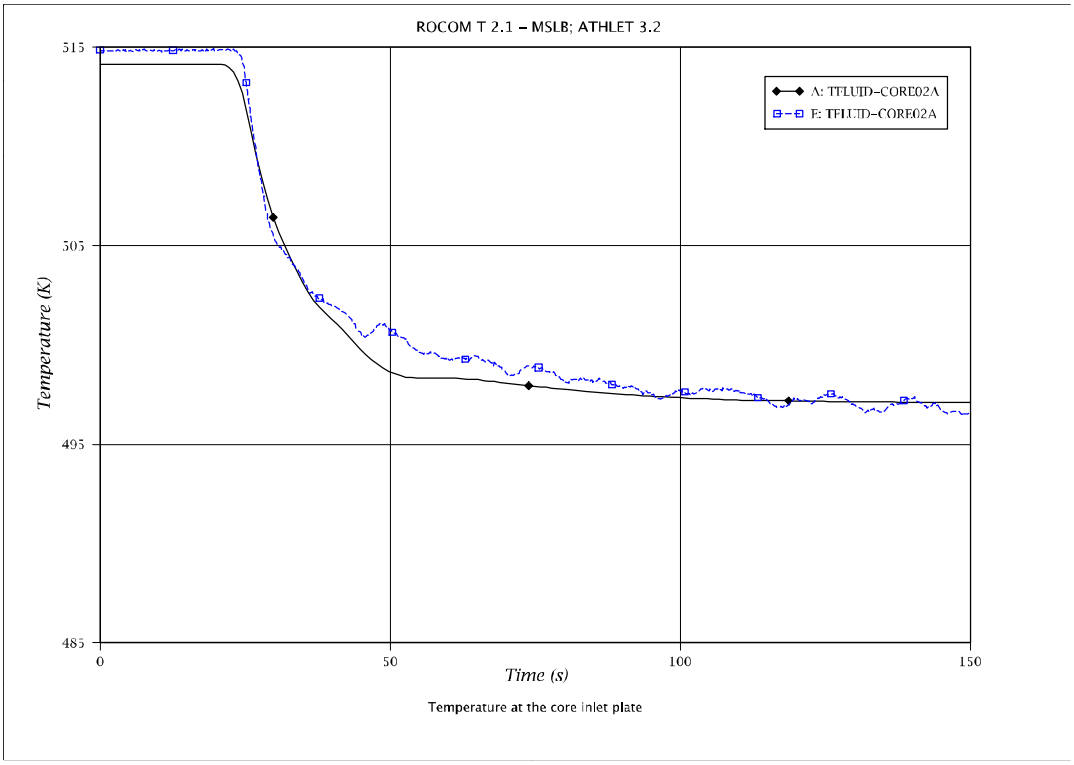

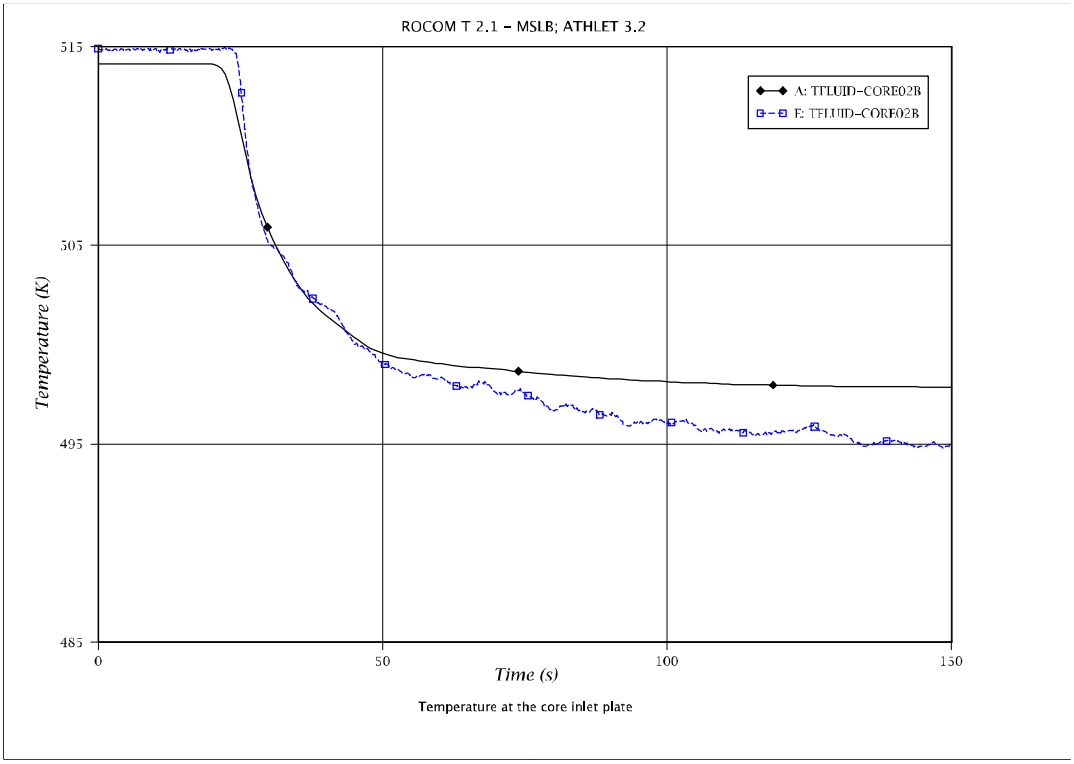

Fig. 5 - 194: Temperature at core inlet: channel 2A and 2B

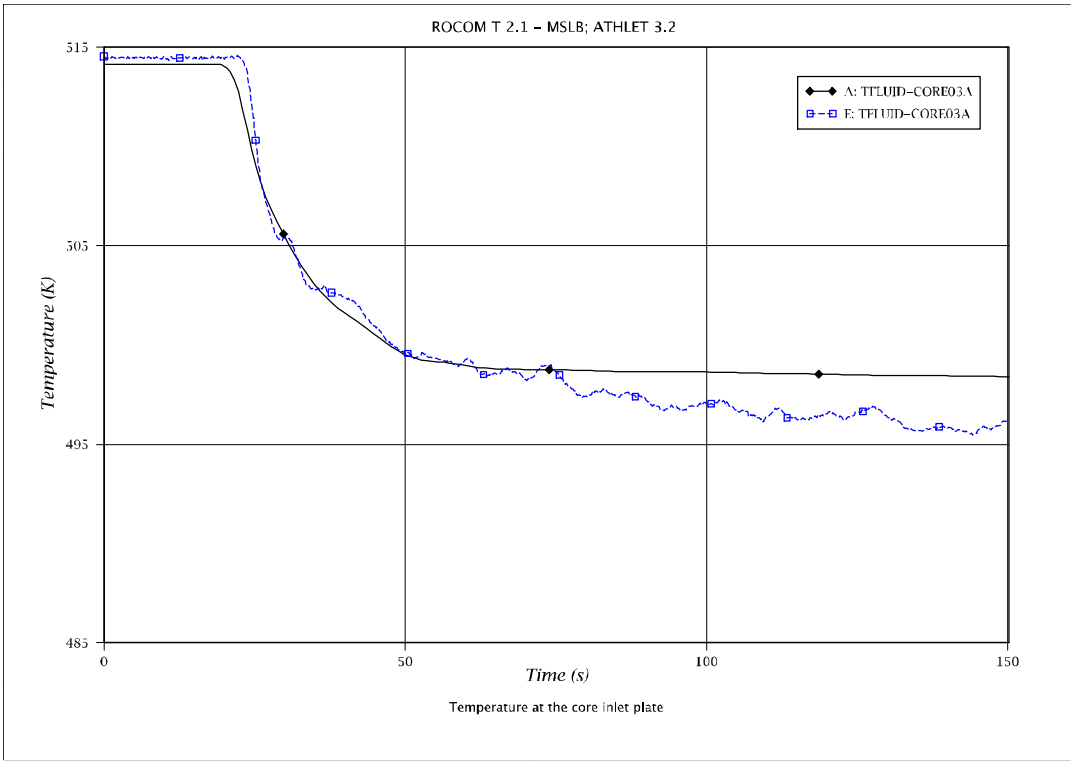

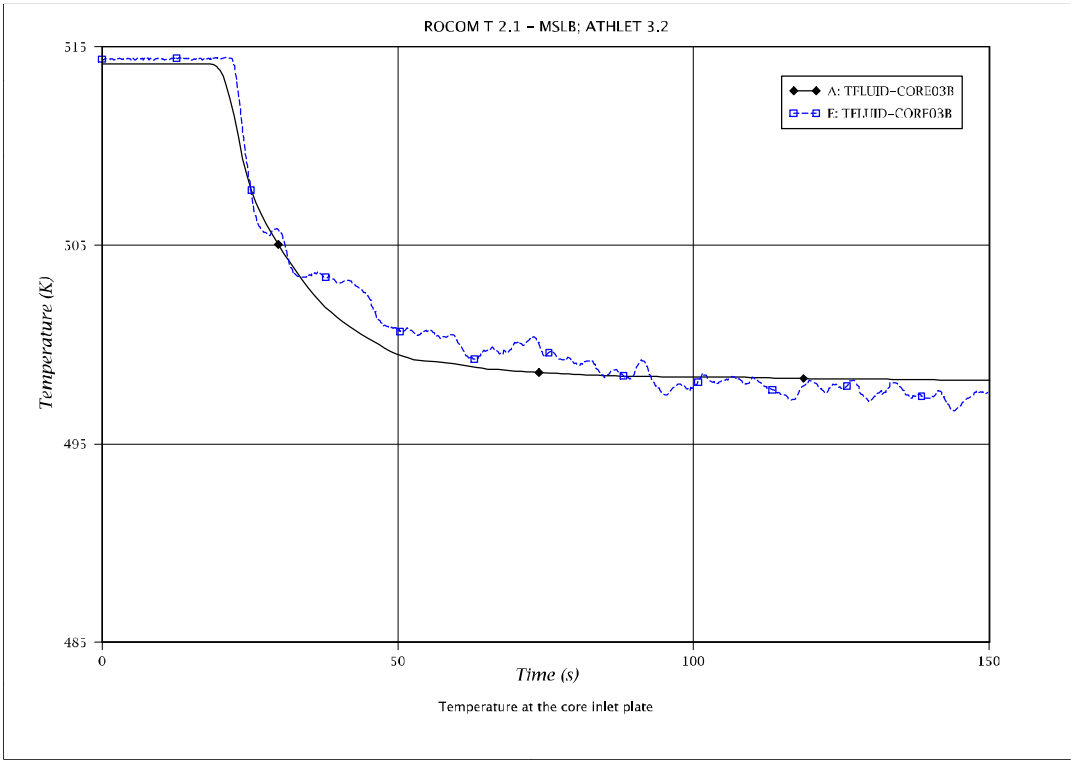

Fig. 5 - 195: Temperature at core inlet: channel 3A to channel 3B

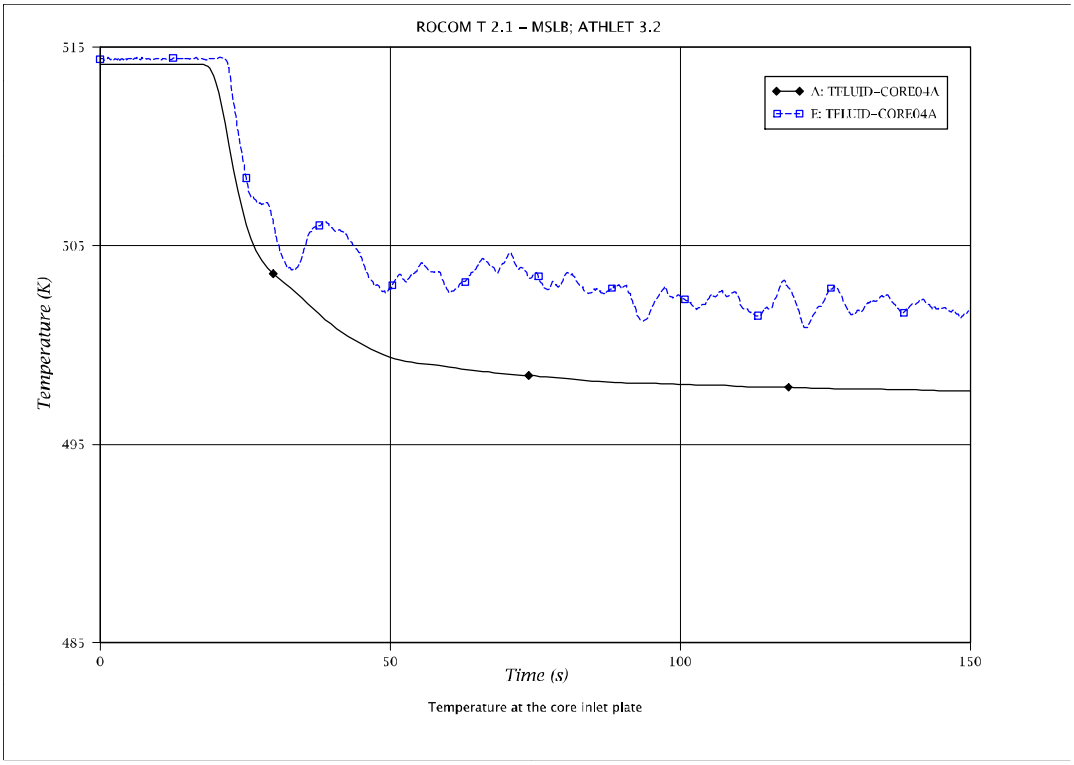

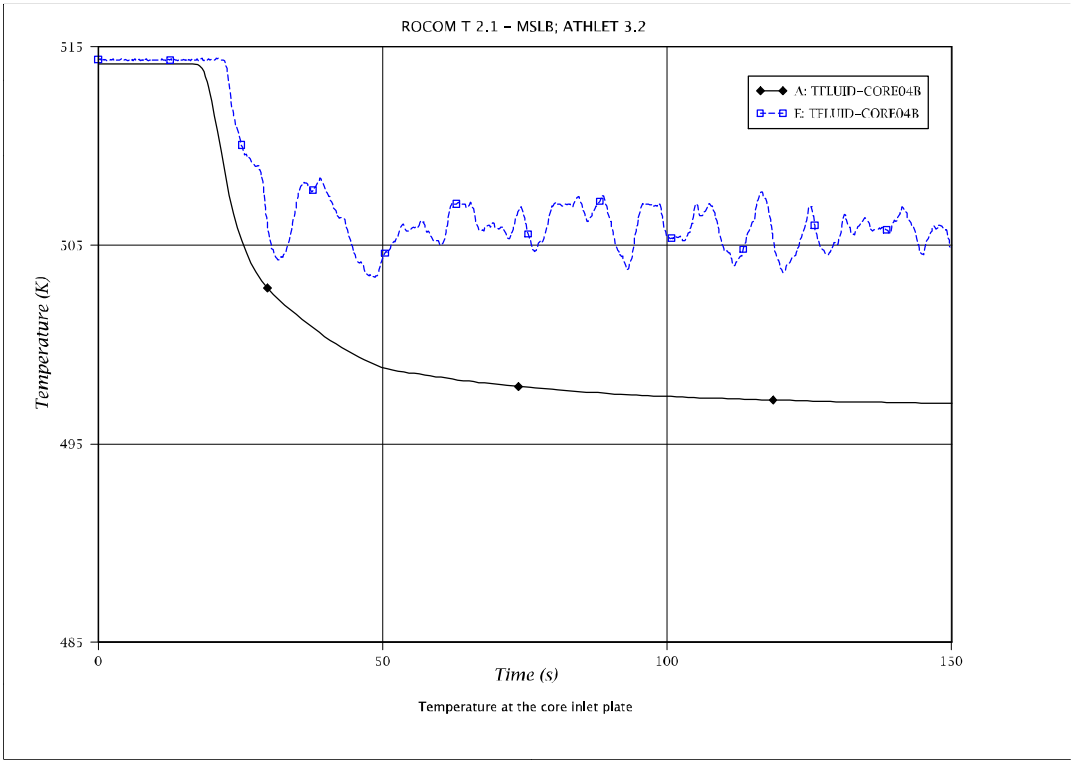

Fig. 5 - 196: Temperature at core inlet: channel 4A to channel 4B

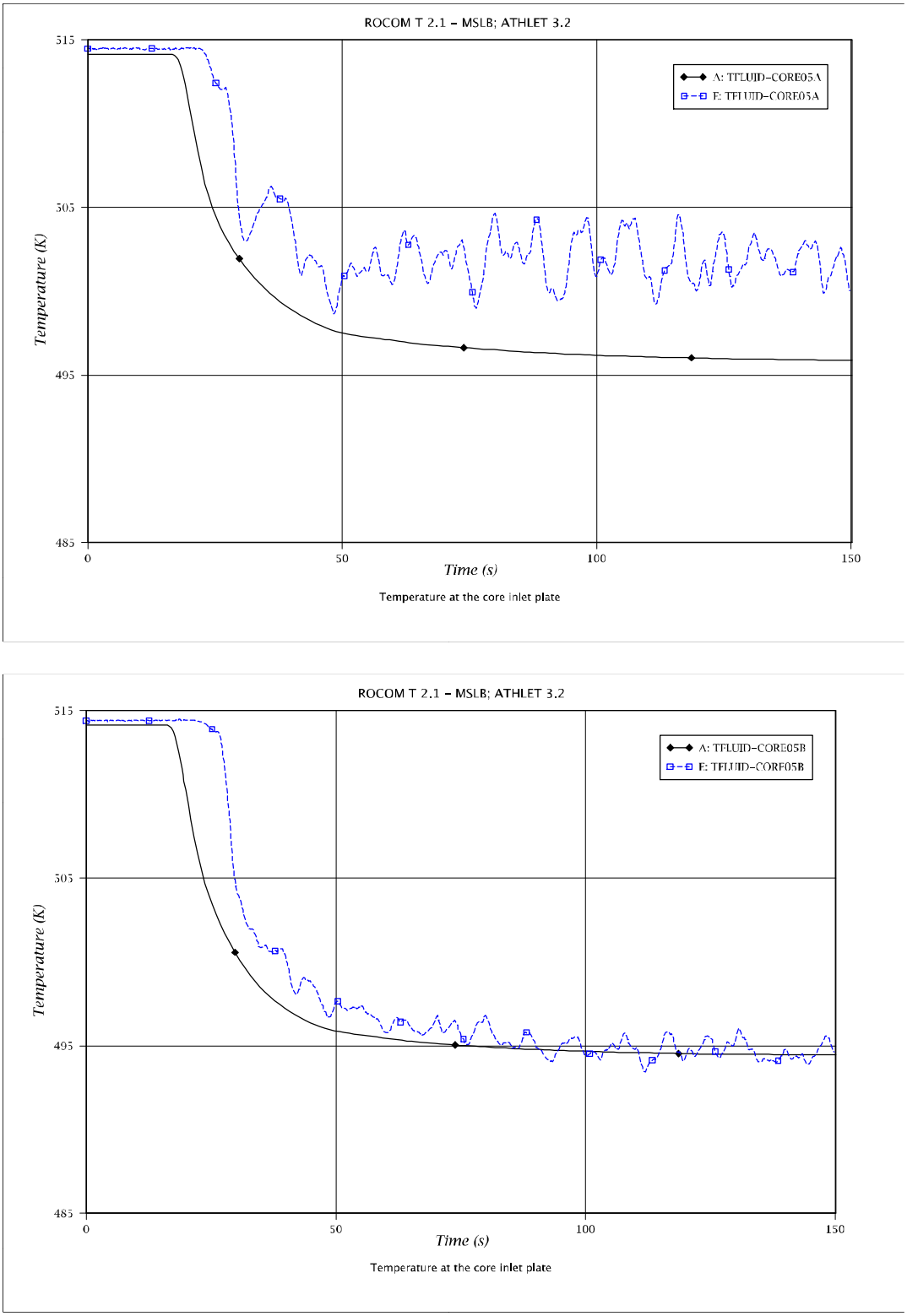

Fig. 5 - 197: Temperature at core inlet: channel 5A to channel 5B

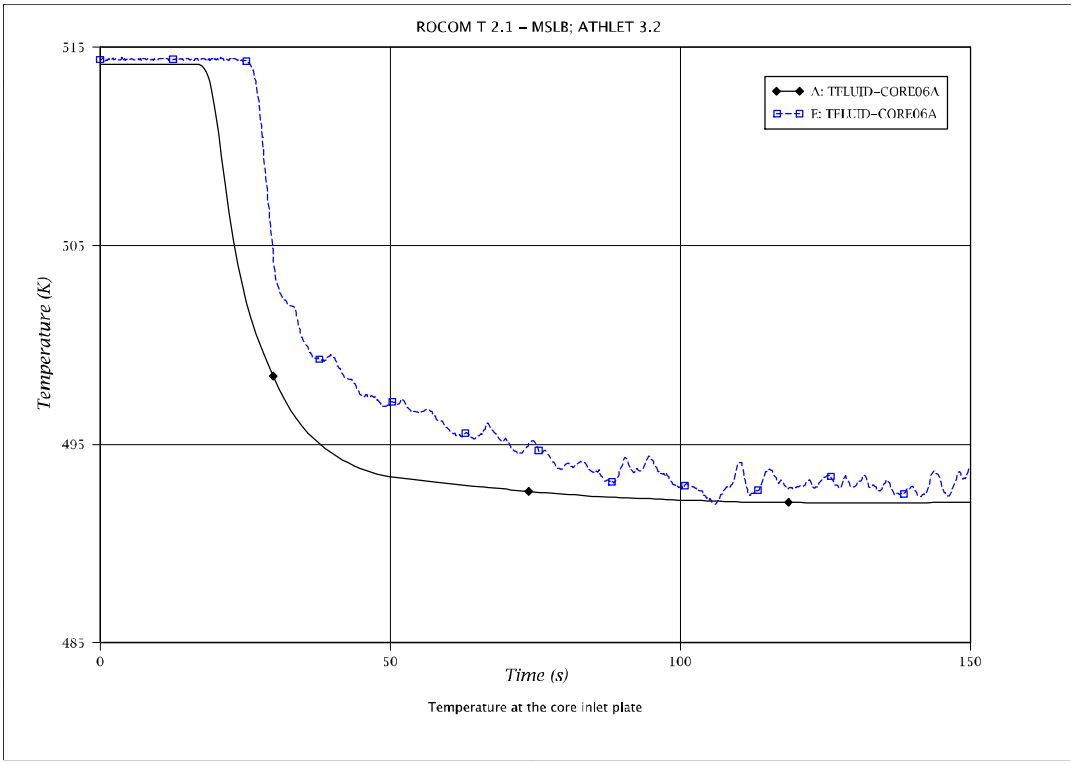

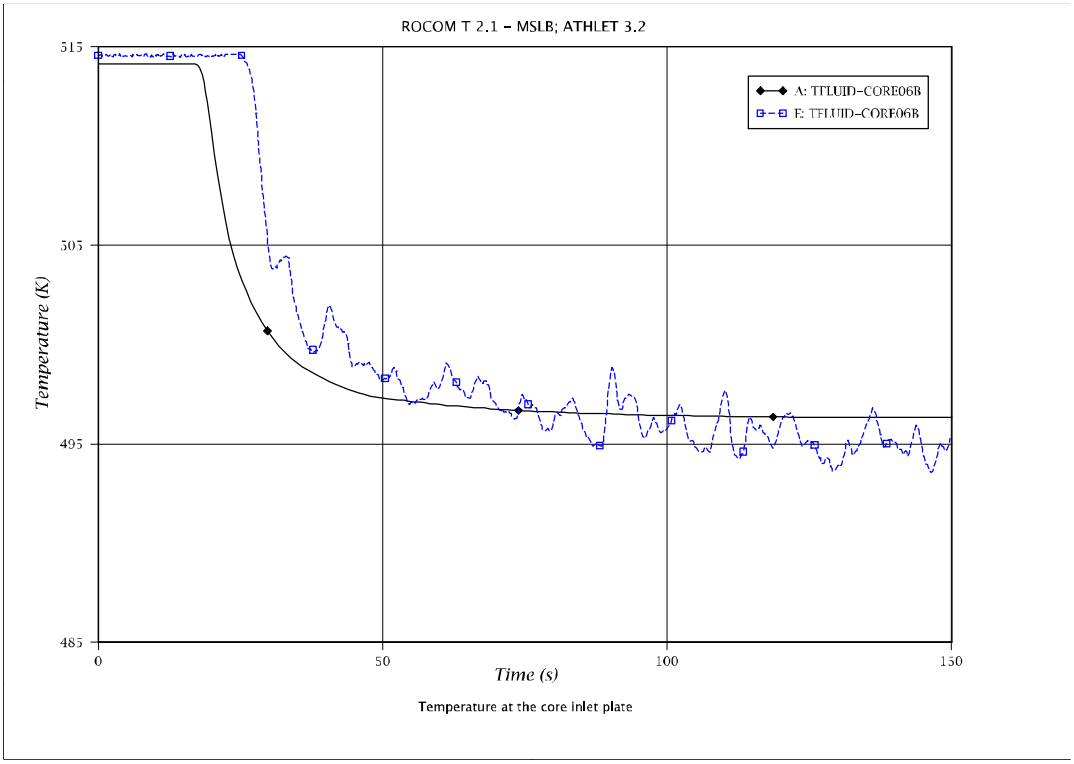

Fig. 5 - 198: Temperature at core inlet: channel 6A to channel 6B

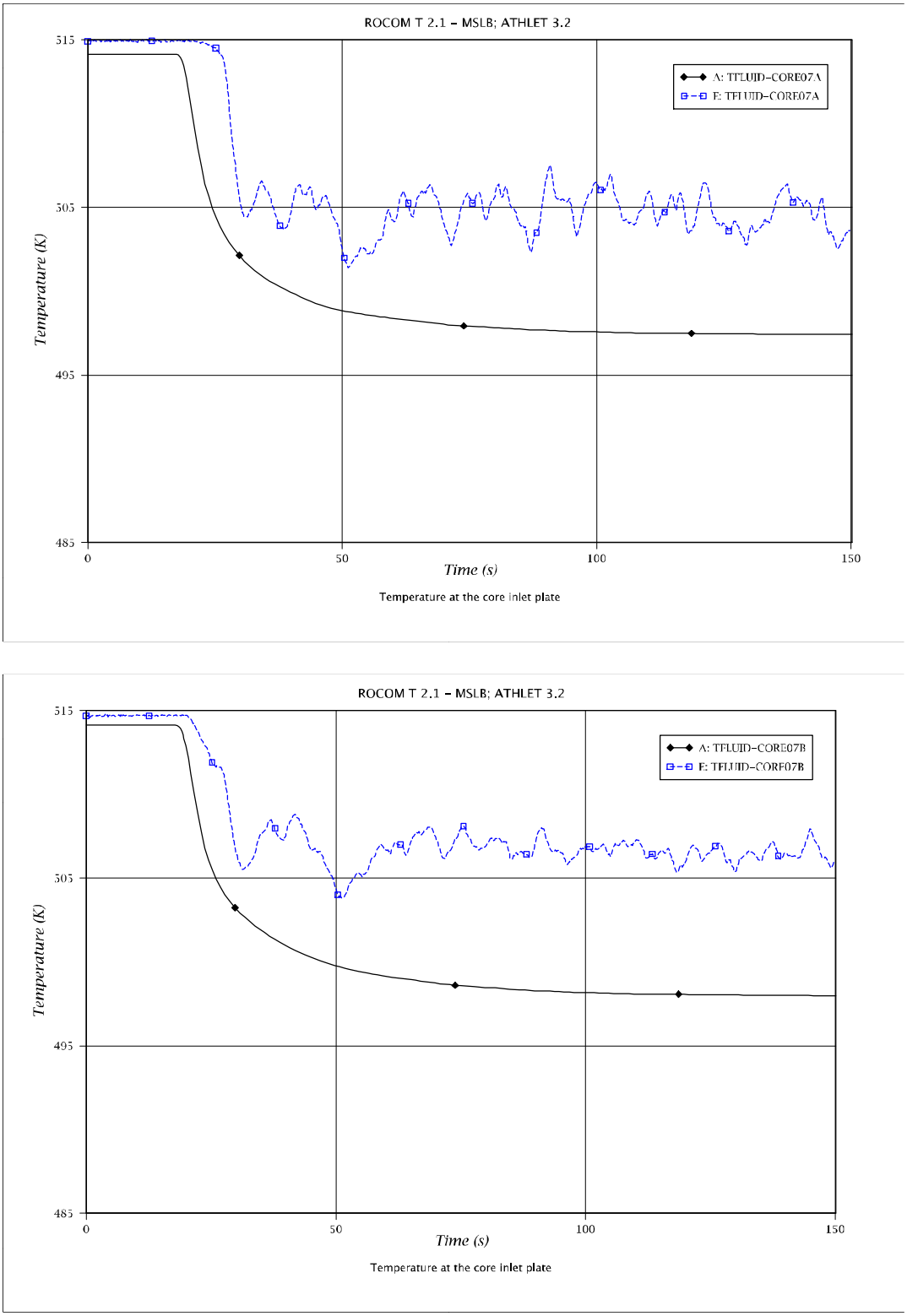

Fig. 5 - 199: Temperature at core inlet: channel 7A to channel 7B

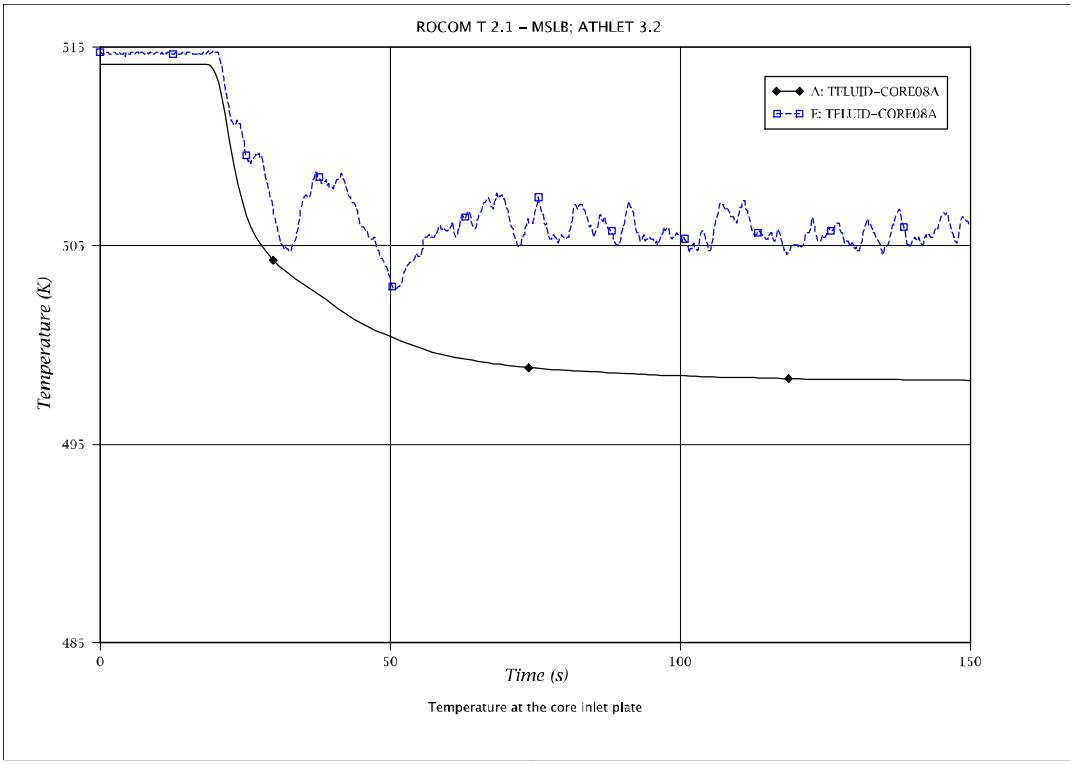

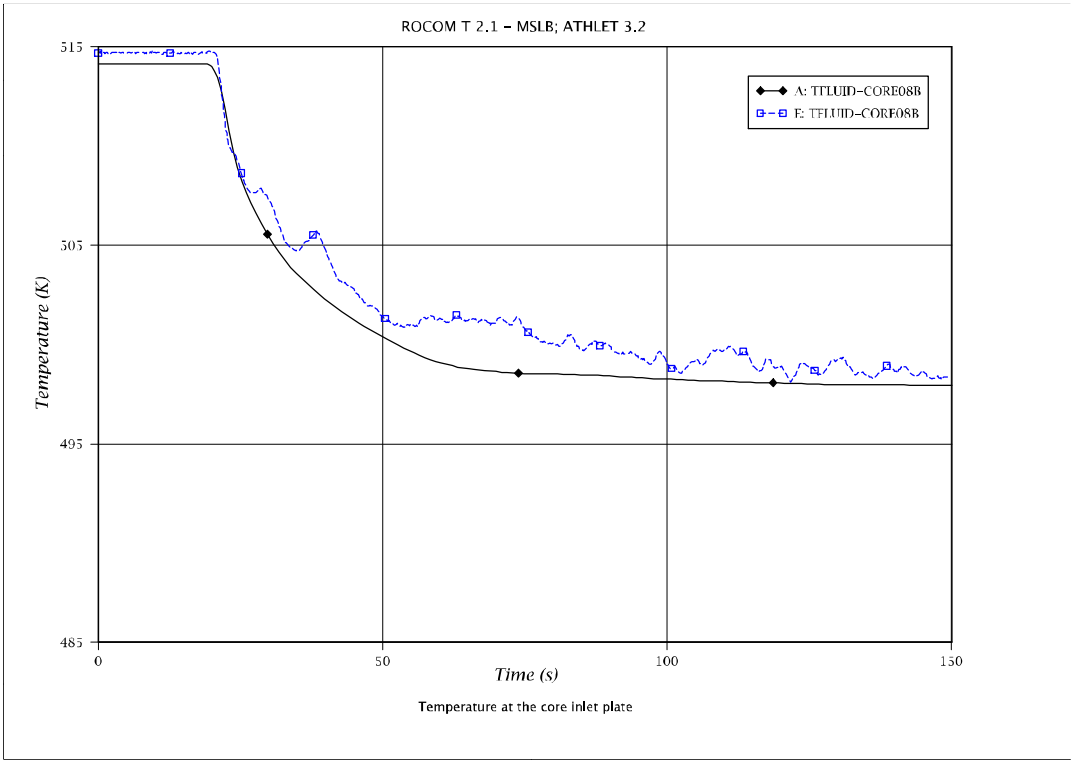

Fig. 5 - 200: Temperature at core inlet: channel 8A to channel 8B

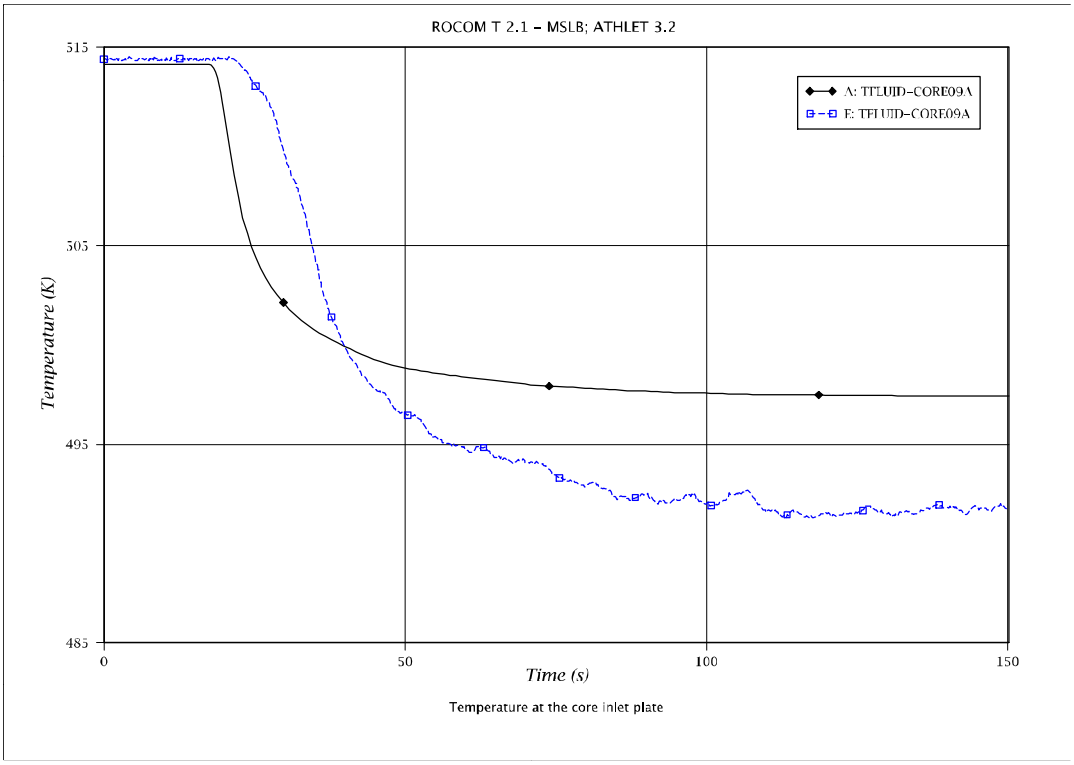

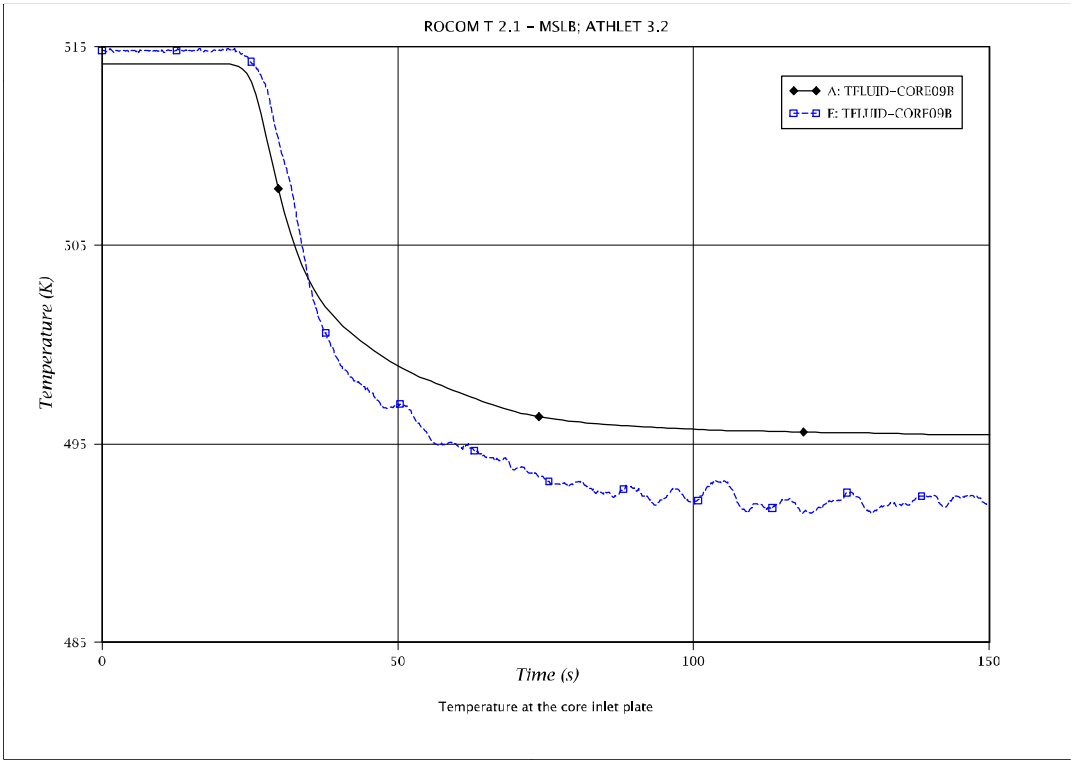

Fig. 5 - 201: Temperature at core inlet: channel 9A to channel 9B

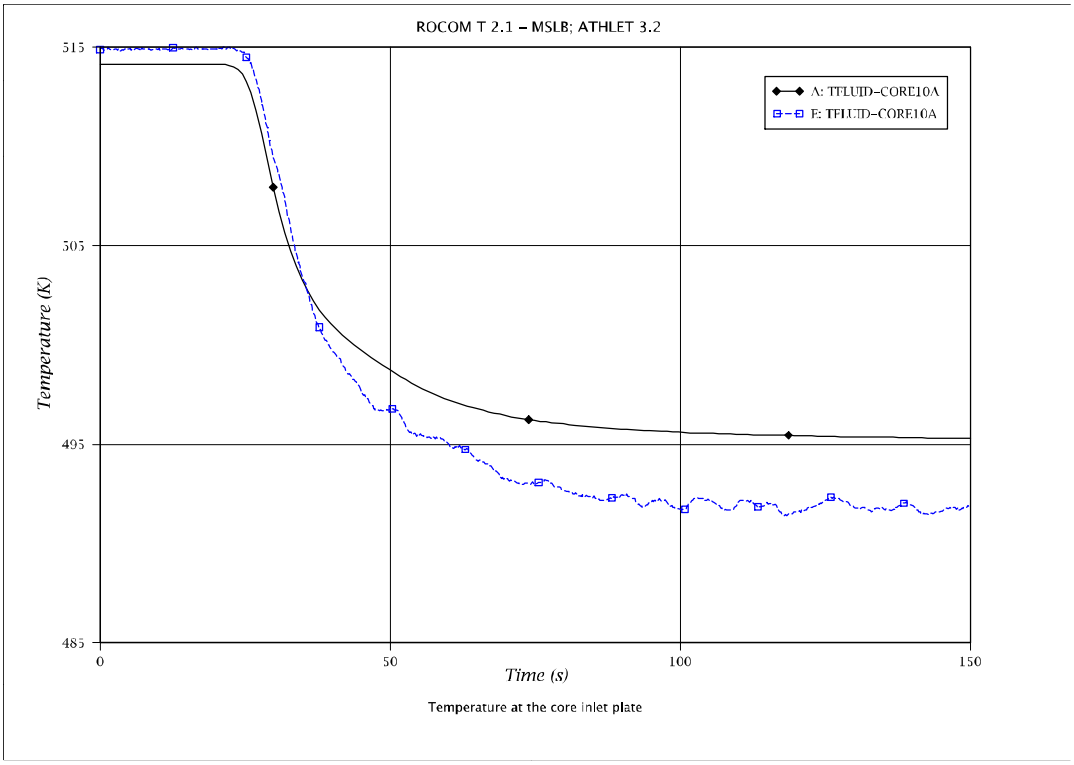

Fig. 5 - 202: U-tube surface temperature at elevation -4923 mm (triple loop)

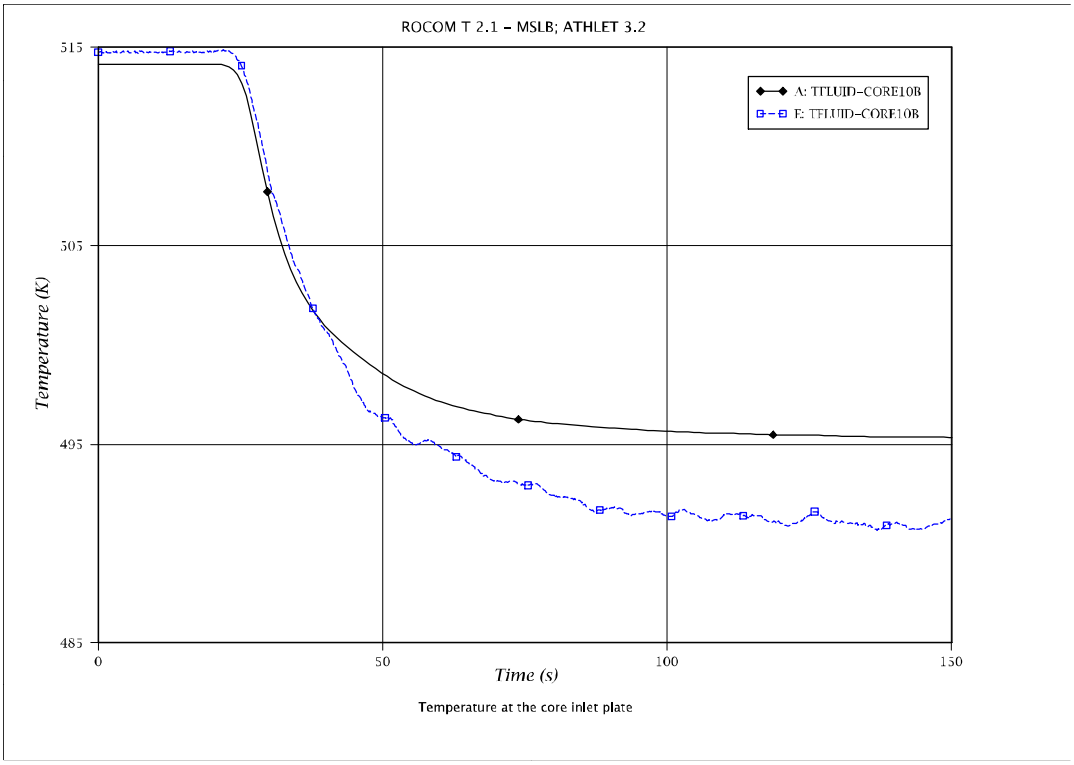

Fig. 5 - 203: Temperature at core inlet: channel 10A to channel 10B

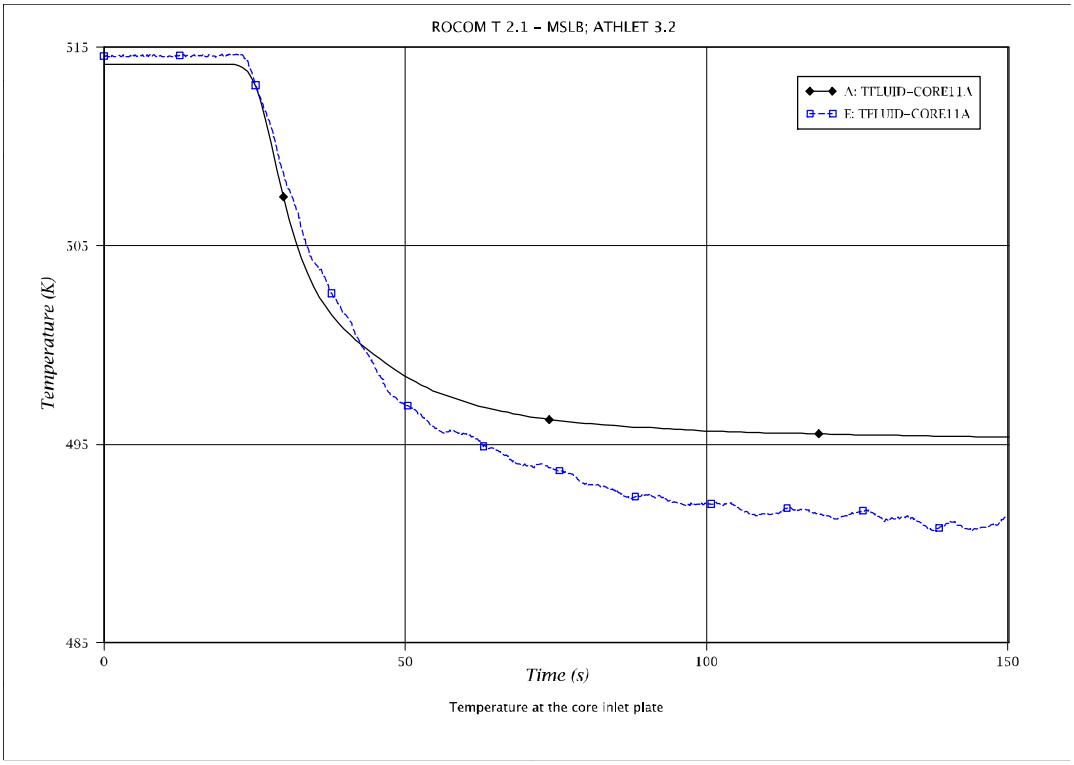

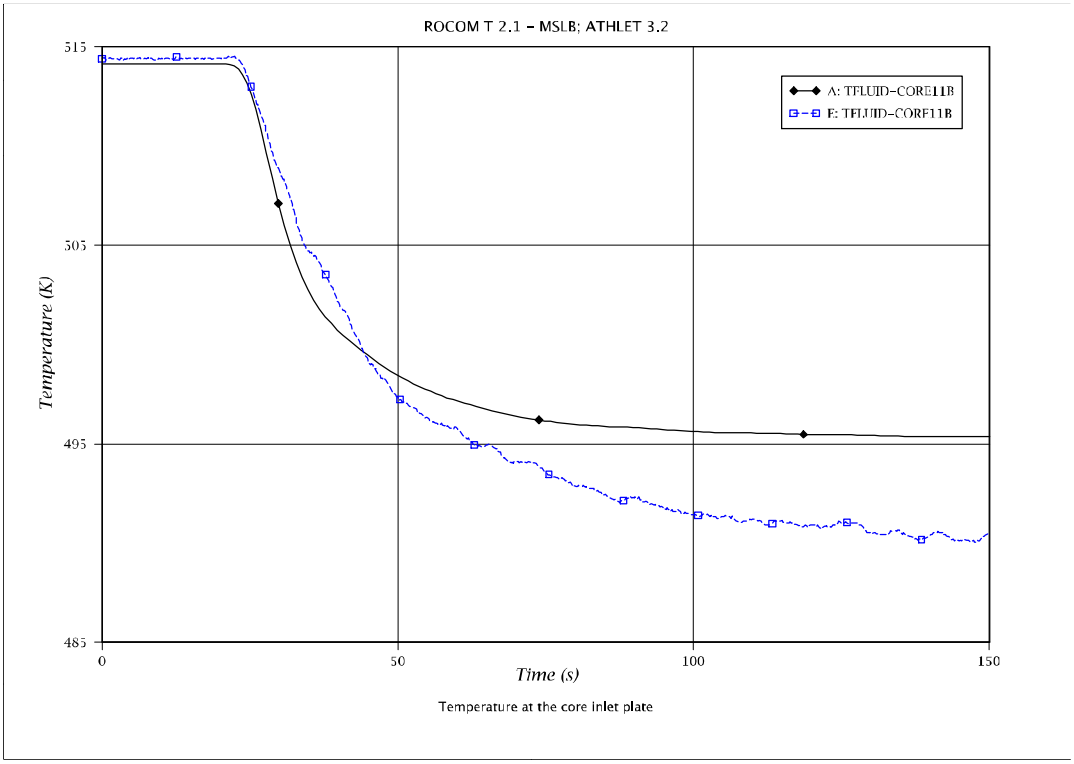

Fig. 5 - 204: Temperature at core inlet: channel 11A to channel 11B

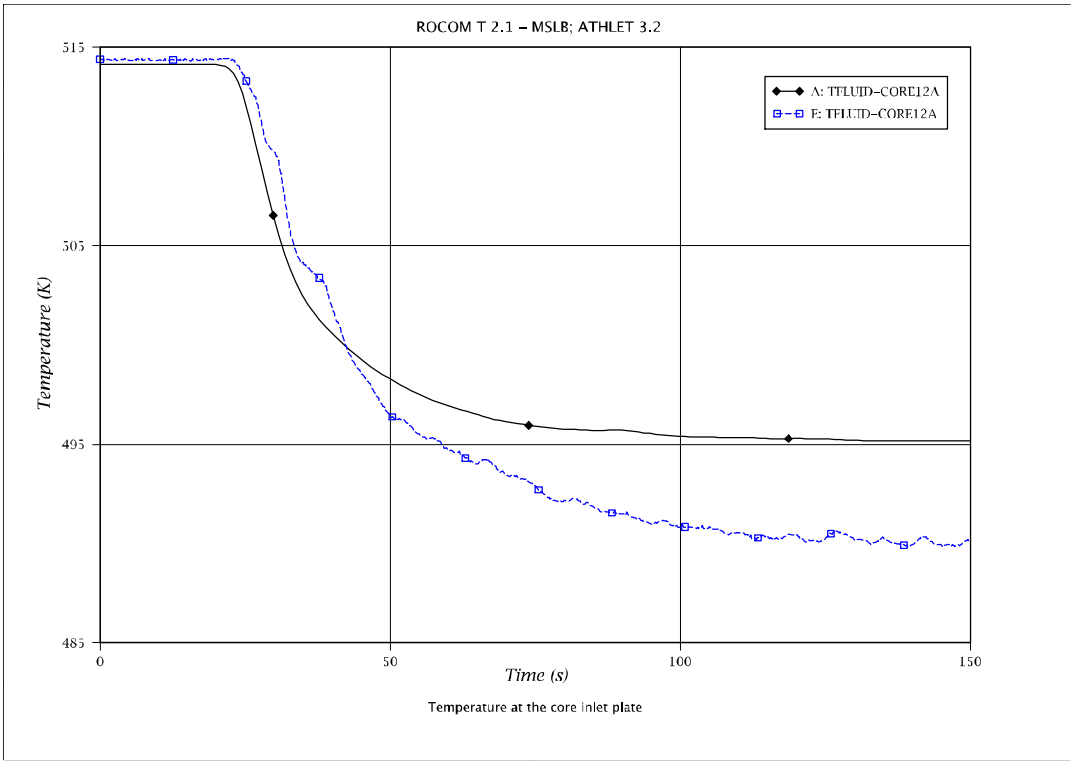

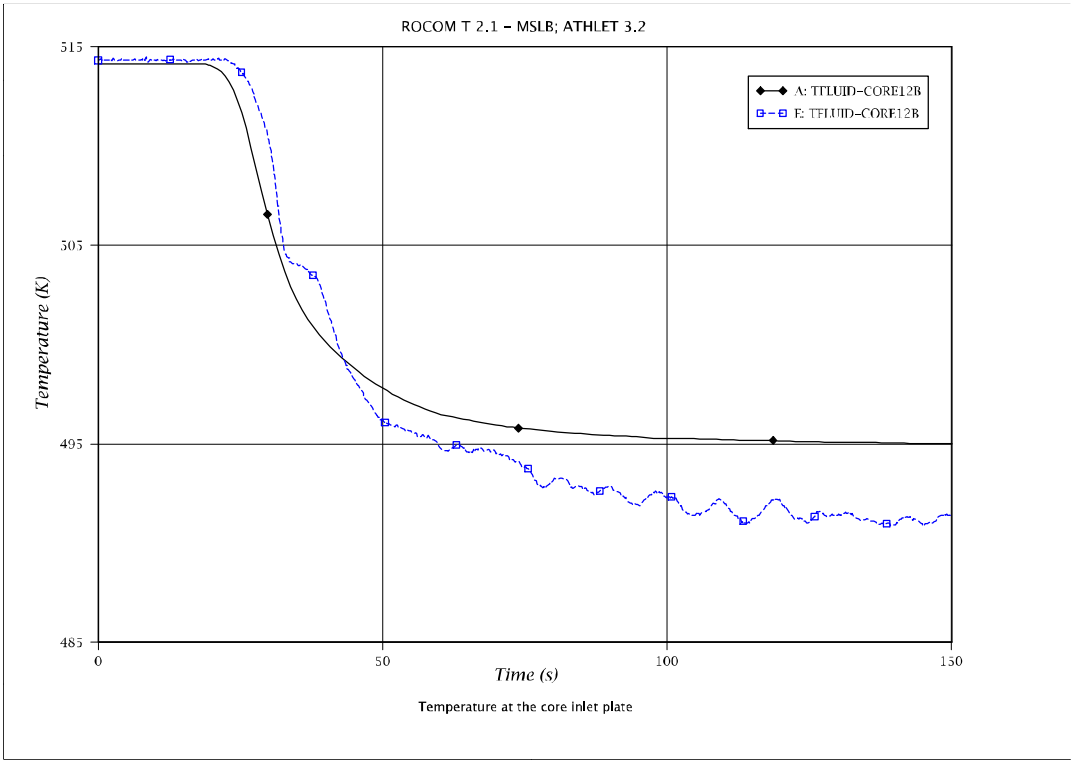

Fig. 5 - 205: Temperature at core inlet: channel 12A to channel 12B

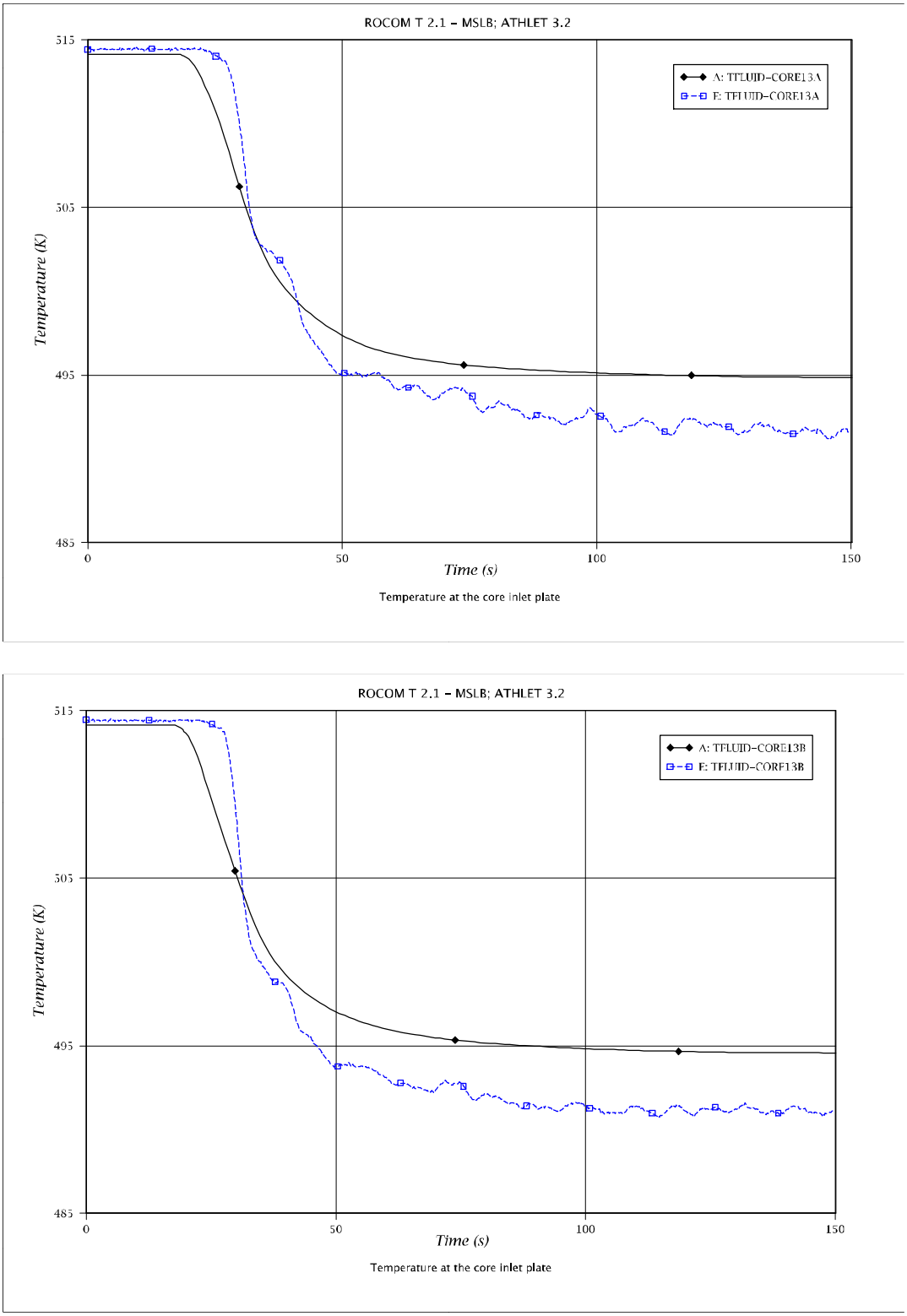

Fig. 5 - 206: Temperature at core inlet: channel 13A to channel 13B

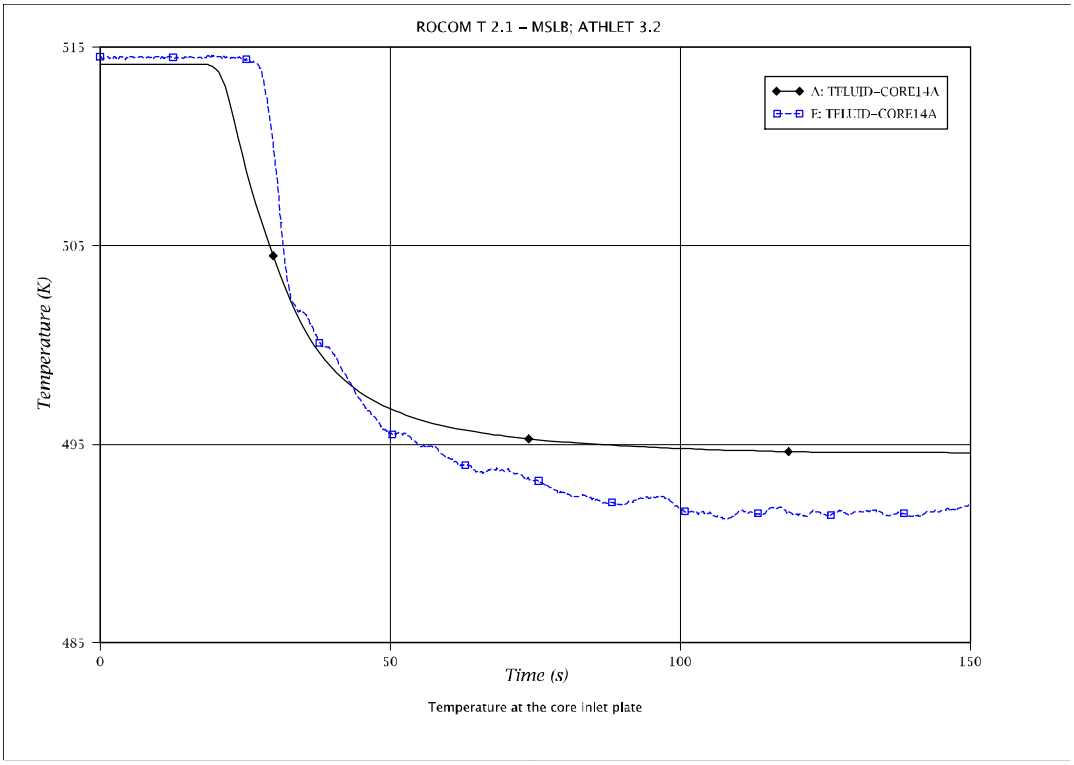

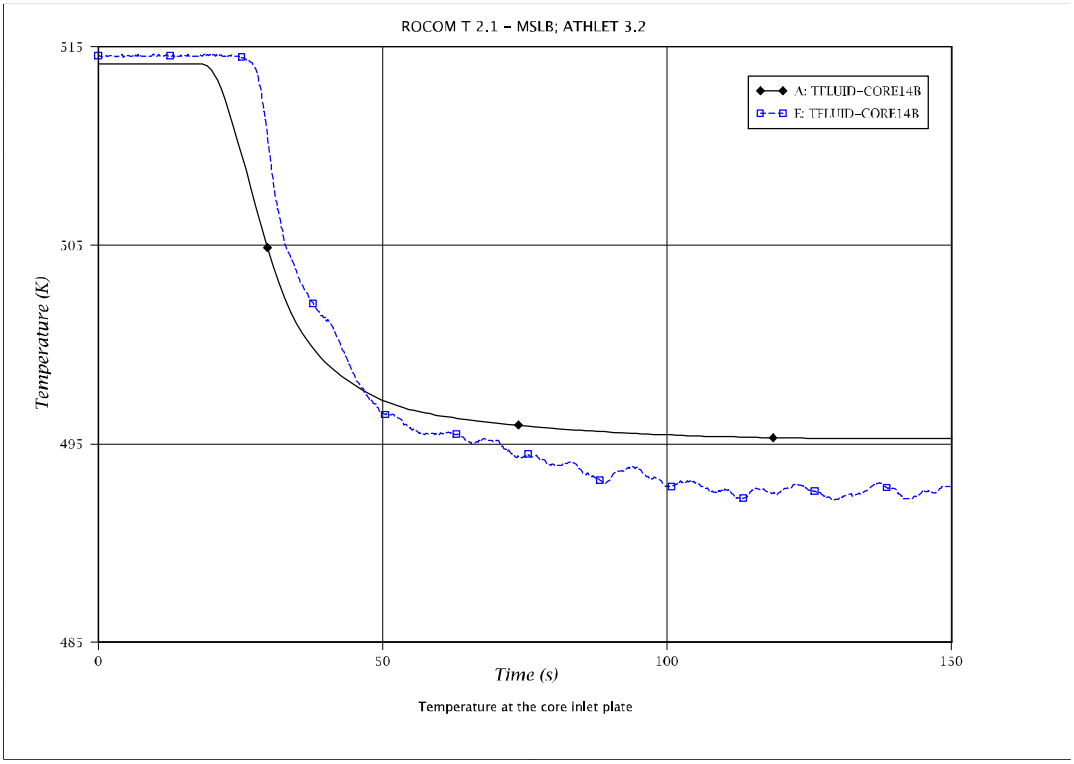

Fig. 5 - 207: Temperature at core inlet: channel 14A to channel 14B

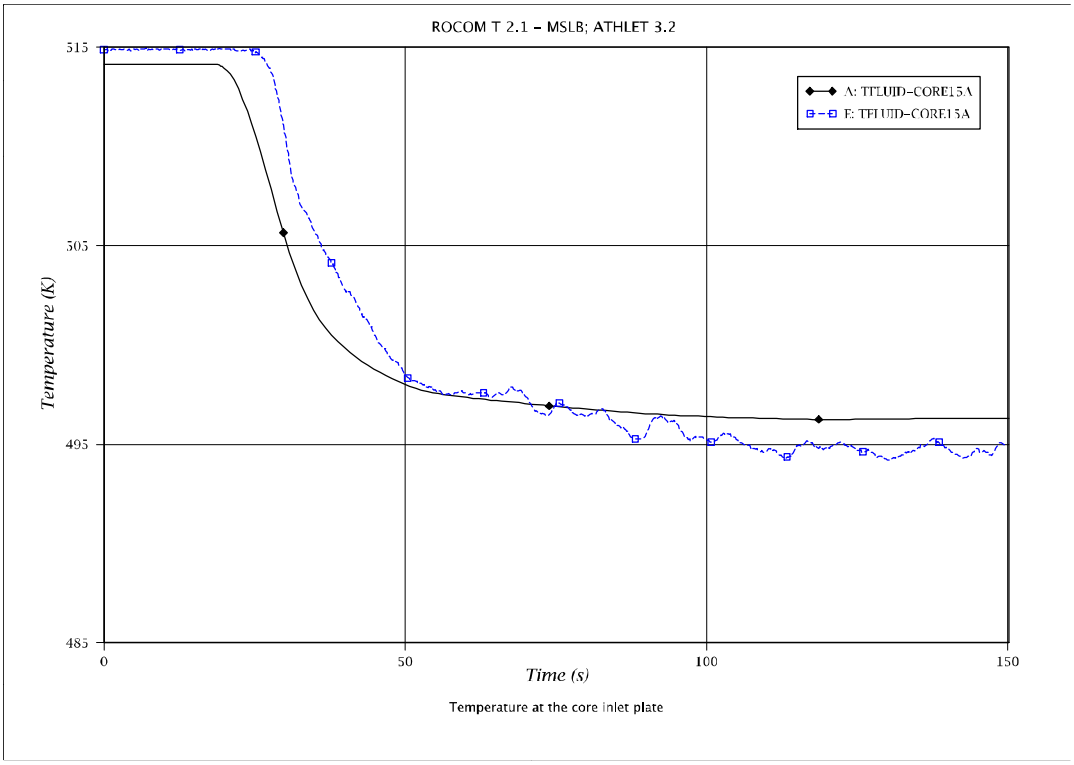

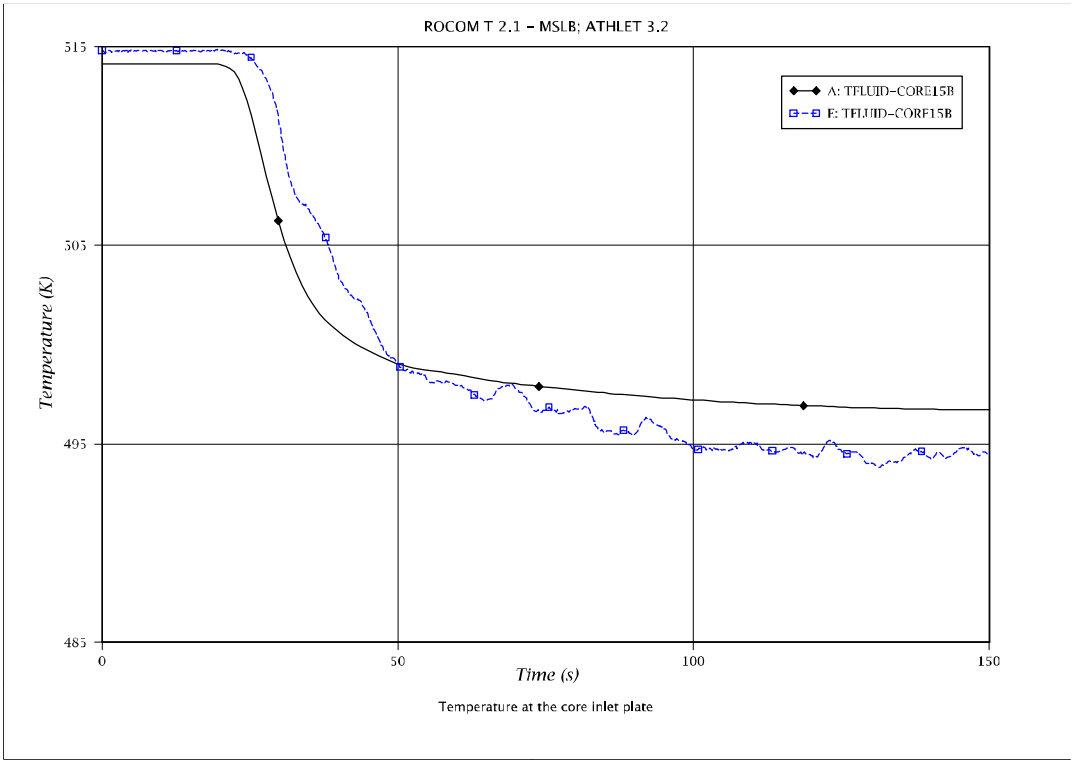

Fig. 5 - 208: Temperature at core inlet: channel 15A to channel 15B

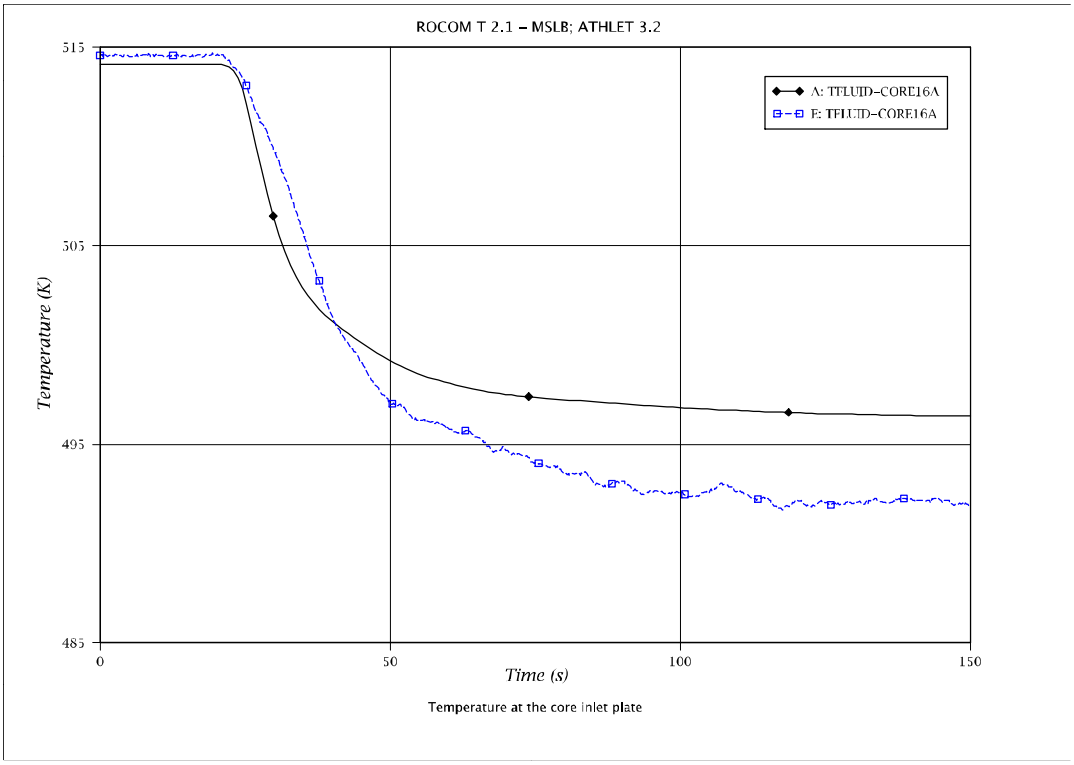

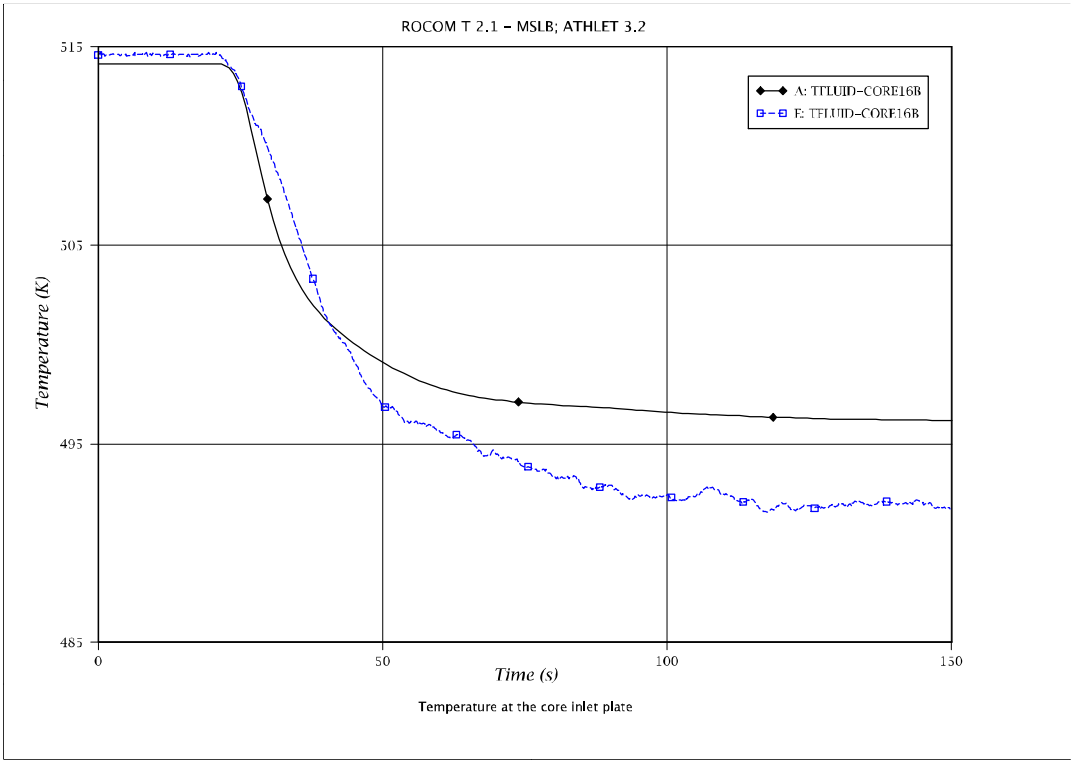

Fig. 5 - 209: Temperature at core inlet: channel 16A to channel 16B

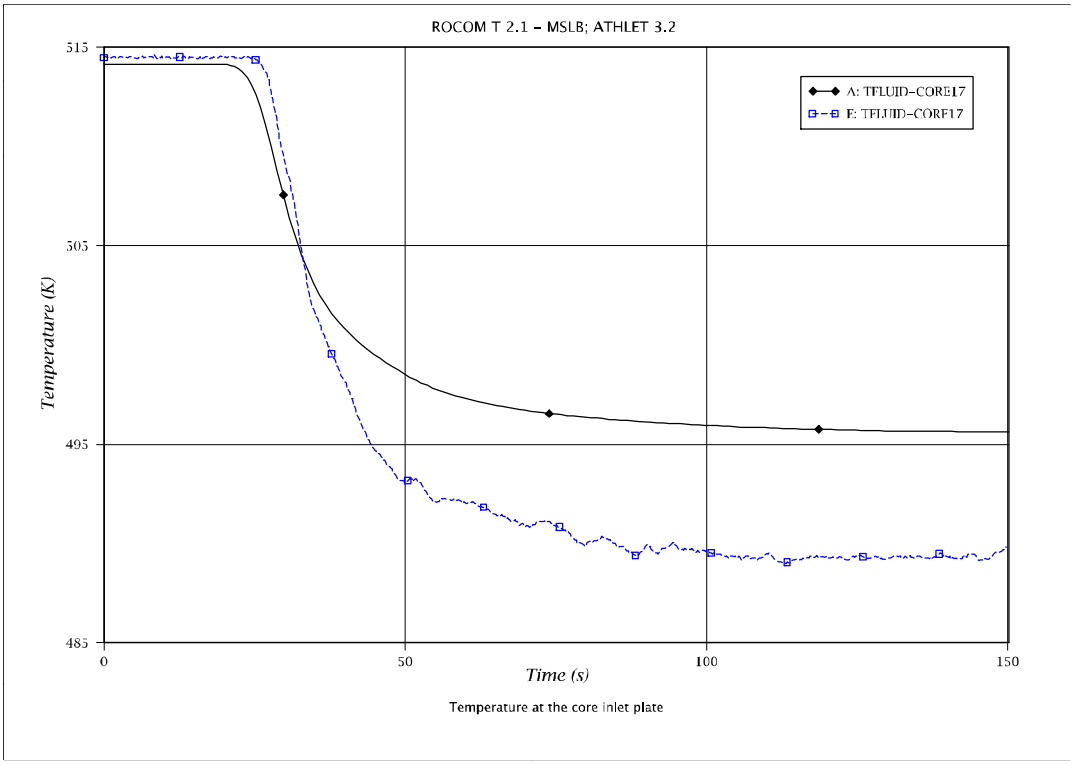

Fig. 5 - 210: Temperature at core inlet: channel 17

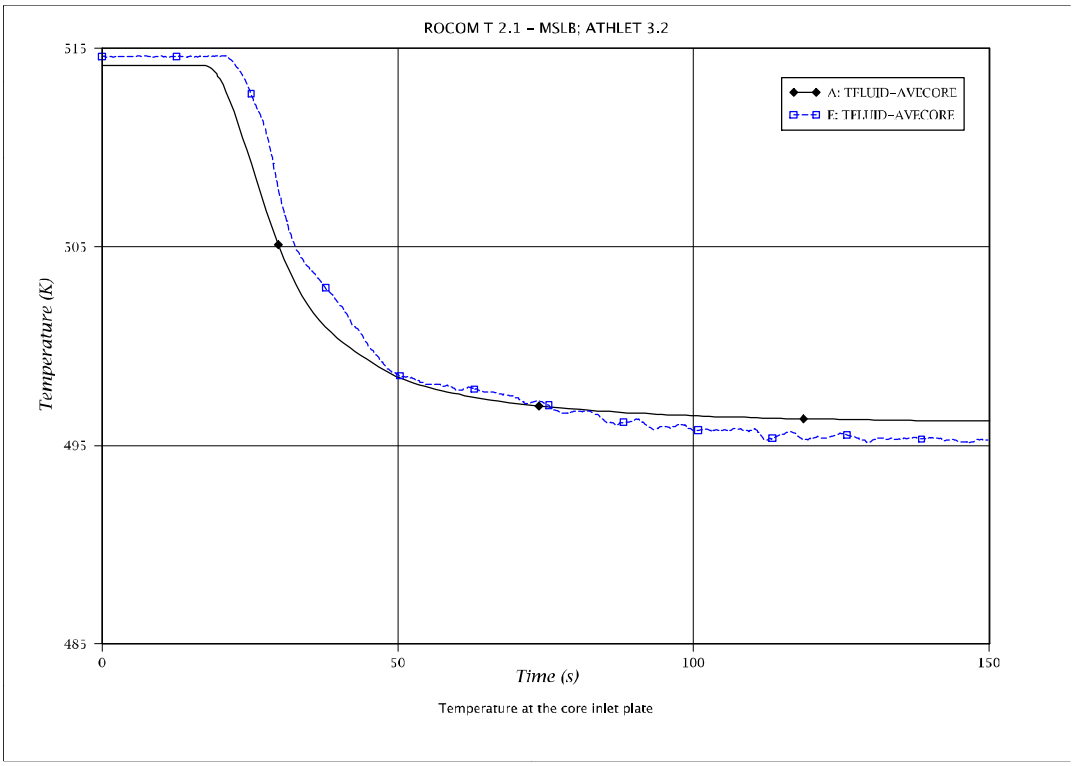

Fig. 5 - 211: Average temperature at core inlet

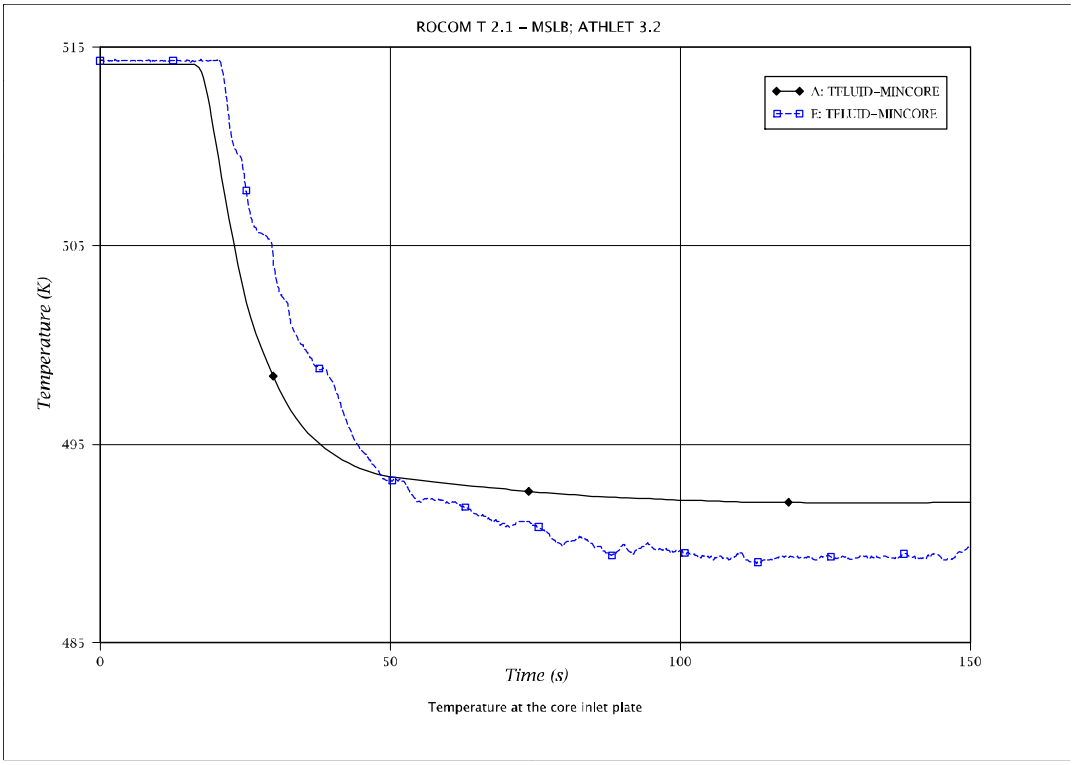

Fig. 5 - 212: Minimum temperature at core inlet

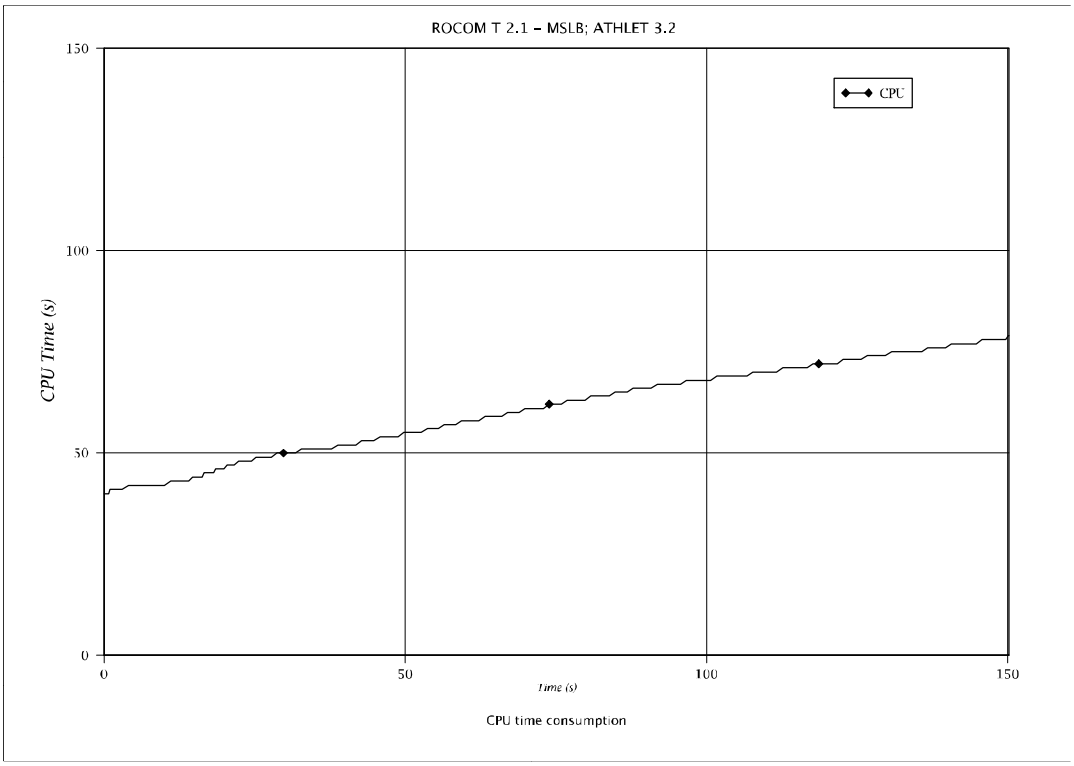

Fig. 5 - 213: CPU time consumption

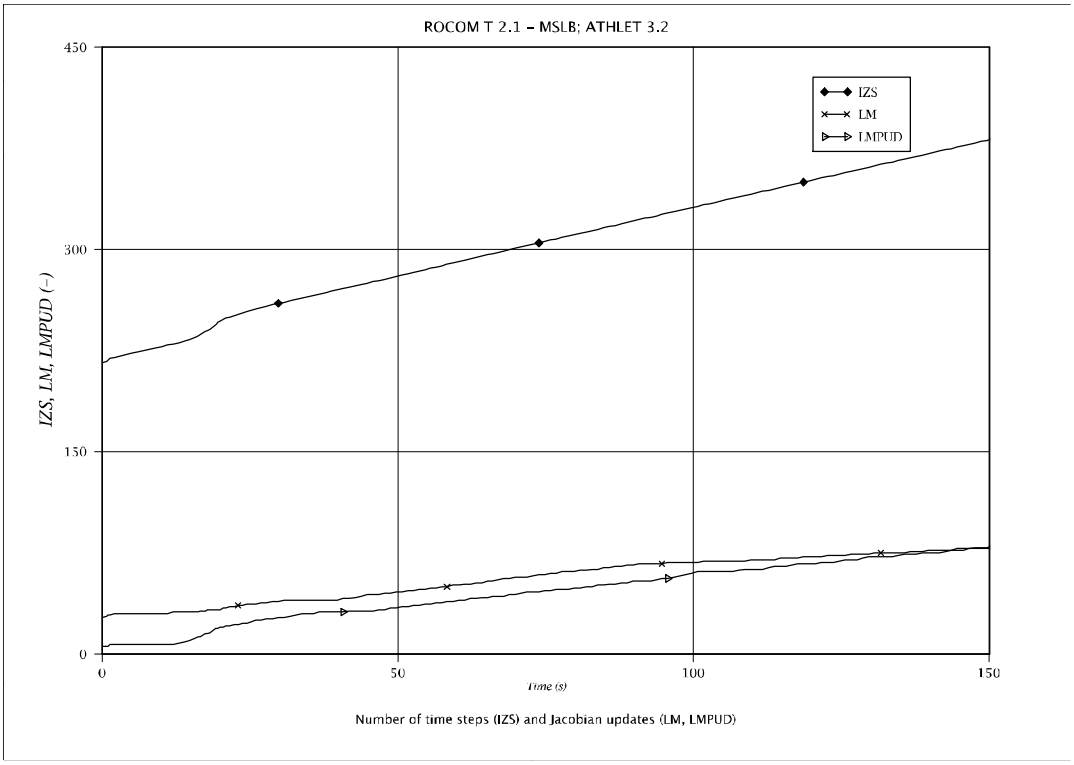

Fig. 5 - 214: Number of time steps (IZS) and Jacobian complete (LM) and partial updates (LMPUD)

6 Uncertainty Evaluation

In computational reactor safety analysis, conservative calculations are replaced by best estimate calculations. Best-estimate calculations are an attempt to predict the thermal-hydraulic behavior of a nuclear power plant under normal and accidental conditions as realistic as the state of knowledge allows. Since a certain time an increasing trend is observed to support the best-estimate calculations with uncertainty analysis. This approach called BEPU (Best Estimate Plus Uncertainty) is introduced to the safety analysis with the aim to increase the quality of the simulations and resulting safety statements.

6.1 Need for Uncertainty Analysis

ATHLET is a thermal-hydraulic system code with best-estimate models for the physical processes. Like in any best-estimate code, the models and methods in ATHLET approximate the physical behavior with more or less accuracy. The comprehensive validation process described in the preceding chapters of this report establishes confidence in the general validity of the models and methods used and provides a qualitative statement on their accuracy.

Best-estimate codes are being applied for reactor safety analysis since several years throughout the OECD-countries. The field of application and the way to account for model uncertainties, however, vary from country to country /BES 96/. In Germany, ATHLET was applied with conservative initial and boundary conditions, thereby introducing a considerable amount of conservatism in the calculation. For future applications, full best-estimate analyses are foreseen. It is mandatory, however, that best-estimate calculations with realistic boundary conditions are supplemented by a quantitative uncertainty analysis. In the US, NRC accepts licensing calculations with best-estimate codes if accompanied by uncertainty analysis /NRC 89/. Also, in European countries there is an increasing trend to apply BEPU approach for the licensing purposes.

There are several sources of uncertainties in code predictions, like the code models, chosen nodalization, initial and boundary conditions, plant state, fuel parameters, scaling and numeri-

cal solution algorithm. Several code correlations are based on measurements, which show a scatter around a mean value. For example, data for two-phase pressure drop show a scatter range of about ± 20 to 30 %. Consequently, a range of values should be taken into account for the respective model parameter instead of one discrete value only. The state of knowledge about all uncertain parameters is described by “subjective” probability distribution. The term “subjective” is used here to distinguish uncertainty due to imprecise knowledge from uncertainty due to stochastic or random variability. Such a distribution express how well the appropriate value of an uncertain parameter of the code application is known in the light of all available evidence according to the state of knowledge experts involved in determination of the probability distribution functions. A state of knowledge based on the minimum information at the parameter level is expressed by uniform distribution.

Stochastic variability due to possible component failures of the reactor plant is not considered in an uncertainty analysis as an input uncertainty. The possible failure of the reactor safety system components is taken into account in a deterministic way, assuming single failure criterion. The probability of system failures is rather a part of probabilistic safety analysis, not of demonstrating the effectiveness of emergency core cooling systems.

The aim of the uncertainty analysis is at first to identify and quantify all potentially relevant uncertain parameters. Their propagation through computer code calculations provides subjective probability distributions (and ranges) for the code results. The evaluation of the margin to a given acceptance criterion, e.g. the maximum fuel rod cladding temperature, should be based on the upper limit of this distribution for the calculated temperatures. Uncertainty analysis is thus needed, if conclusions are to be obtained from best-estimate thermal-hydraulic code calculations, otherwise only single values of unknown accuracy would be available for comparison with the acceptance limits.

An important field of uncertainty and sensitivity analyses is validation and development of the complex numerical codes. In the course of uncertainty and sensitivity analyses performed for experimental tests accuracy of the numerical simulation can be quantitatively estimated. On this basis conclusions can be drown, if the simulations fulfill the criteria of agreement with experimental data and finally, if the expected accuracy of simulation is achieved. The sensitivity analysis enables to identify the input uncertainties which contribute significantly to the uncertainty of the calculated results. In the case of uncertainties related to the code physical models the weak points of the physical models can be identified. On this basis decisions concerning further code development can be performed.

6.2 Methods for Uncertainty Analysis

Methods for the quantification of uncertainties in thermal-hydraulic code calculation have been developed by various institutions. The most frequently applied statistical methods in uncertainty analyses are the input uncertainties propagation methods. The input uncertainties propagation methods consider the effect of uncertainties of input parameters like computer code models, initial and boundary conditions, other application specific input data and parameters of solution algorithms on the calculation results. As the first systematic methodology for performing the uncertainty analysis the CSAU methodology /TEC89/ was introduced by NRC. Among the uncertainty evaluation methods based on input uncertainties propagation the most popular is the method based on Wilks' formula /WIL41/. This method is also called GRS type method since, it was proposed at first by GRS /HOF85/.

Comparisons of functioning and application of different methods for uncertainty analysis were perform in the frame of NEA/CSNI projects: UMS (Uncertainty Methods Study) /WIC 98/, BEMUSE (Best Estimate Methods - Uncertainty and Sensitivity Evaluation) /DEC08/, /PER11/ and PREMIUM (Post-BEMUSE Reflood Models Input Uncertainty Methods) /PRE16/. GRS participated in this international studies using ATHLET and the GRS uncertainty analysis method.

6.3 Description of the GRS Methodology

A methodology for uncertainty and sensitivity analyses has been developed by GRS where the computational effort is independent of the number of uncertain parameters /KRZ94/. The implementation techniques are primarily based on tools from statistics. Statistics is used in order to evaluate the uncertainty and sensitivity with a reasonable number of calculations.

The state of knowledge about all uncertain parameters is described by ranges and probability distributions. In order to get information about the uncertainty of code results, a number of code runs have to be performed. For each of these calculation runs, all identified uncertain parameters are varied simultaneously. Uncertain parameters are uncertain input values, modelling options, initial and boundary conditions, numerical values like convergence criteria and maximum time step, among others. Modelling uncertainties are expressed by adding on or multiplying correlations by a corrective term, or by a set of alternative model formulations. Finding the optimal nodalization to describe the relevant thermal-hydraulic phenomena, is a task of code validation. However, alternative nodalization schemes can be included in the uncertainty analysis.

Code validation results are a fundamental basis to quantify the uncertainty of physical models or their mathematical formulation. Experts specify the ranges and probability distributions of

uncertainties that best express the state of knowledge. The state of knowledge dependence between parameters can be taken into account. Computerized support is provided for an interactive construction of the probability distributions and for the state of knowledge dependence.

In the GRS methodology, all potentially important parameters are included in the analysis, based on judgement of the analyst. The number of calculations to be performed does not grow with the number of parameters. No ranking of input parameters to reduce their number is needed in order to cut computation costs. The reason is the simultaneous variations of all uncertain parameters for each code run, together with the statistical evaluation of these results. The uncertainty and sensitivity results have a well founded probabilistic statistical interpretation.

The number of calculations depends only on the desired probability content and confidence level of the statistical tolerance limits used in the uncertainty statement of the results. The required minimum number n of these calculation runs is given by the Wilks' formula /WIL41/, e.g. for one-sided tolerance limits:

$$1 - \alpha^n \geq \beta \qquad (6-1)$$

where β x 100 is the confidence level (%) that the maximum code result will not be exceeded with a probability of α x 100 (%) of the corresponding output distribution (percentile), which is to be compared to a given acceptance criterion. The confidence level is specified to account for the possible influence of the sampling error due to the fact that the statements are obtained from a random sample of limited size. For two-sided statistical tolerance, the corresponding formula is /SAC84/:

$$1 - \alpha^n - n(1-\alpha)\alpha^{n-1} \geq \beta \qquad (6-2)$$

The minimum number of calculations can be seen in table 6 - 1.

The probabilistic treatment of parameter uncertainties allows to quantify the state of knowledge about them. This means that, in addition to the uncertainty range, the knowledge is expressed by subjective probability density functions or probability distributions. The subjective interpretation of probability is used for a parameter with a fixed but unknown or inaccurately known value. The classical interpretation of probability as the limit of a relative frequency, expressing the uncertainty due to stochastic variability, is not applicable here.

The probabilistic distribution can express that some values in the uncertainty range are more likely the appropriate parameter value than others. In the case that no preferences can be justified, uniform distribution will be specified, i.e. each value between minimum and maximum is

equally likely the appropriate parameter value. As a consequence of this specification of probability distributions of input parameters, the code results also show a subjective probability distribution, from which uncertainty limits or intervals are derived.

Table 6 - 1: Minimum number of calculations n for one-sided and two-sided statistical tolerance limits

	One-sided statistical tolerance limits				**Two-sided statistical tolerance limits**		
β / α	0.90	0.95	0.99		0.90	0.95	0.99
0.90	22	45	230		38	77	388
0.95	29	59	299		46	93	473
0.99	44	90	459		64	130	662

Sensitivity Analysis

Another important feature of the method is that one can determine sensitivity measures of the influence of uncertainties in input parameters on the uncertainties of results. This information can provide guidance as to where to improve the computer code or to perform additional experiments (i.e. improve the state of knowledge) in order to reduce the output uncertainties most effectively. Sensitivity measures like Standardized Rank Regression Coefficients and Correlation Ratios permit a ranking of input uncertainties with respect to their relative contribution to code output uncertainty. The difference to other uncertainty methods is that the ranking is a result of the analysis, not of prior estimates and judgements. Uncertainty statements and sensitivity measures are available simultaneously for all single-valued (e.g. peak cladding temperature) as well as continuous valued (time dependent) output quantities of interest. The GRS method relies only on actual code calculations without using approximations like fitted response surfaces.

The different steps of the uncertainty analysis are supported by the software system SUSA (Software System for Uncertainty and Sensitivity Analyses), also developed GRS and continuously updated incorporating new features /KLO16/.

6.4 Example of Application

In the course of ATHLET validation several uncertainty and sensitivity analyses have been performed. They are related directly to the code development. The sensitivity statements show which models contribute mostly to the uncertainty of the calculations. It indicates the potential code modifications and developments with the aim of improvement of code simulation accuracy.

The uncertainty and sensitivity analyses performed for the code ATHLET include different kinds of thermal-hydraulic experiments but also nuclear reactor applications.:

- Analyses of combined effect tests:
  - FEBA and PERICLES reflooding experiments /SCH 15/, /SKO17/,
  - French OMEGA rod bundle test 9, a blowdown experiment with a PWR type bundle /GLA94a/, /GLA94b/
- Analysis of experiments performed at integral test facilities:
  - PMK experiment “pressurizer surge line break” /HOC01/,
  - LOFT test L2-5 200% cold leg break /GLA01c/, /DEC08/
  - ROSA/LSTF test SB-PV-09 small leak in the reactor upper head /AUC09/, /SKO11/
  - ATLAS experiment 50% break at the DVI line /AUS13a/, /AUS13b/
- Analysis of experiment performed at NACIE test facility with molten metal as cooling medium - calculation of transient behavior of two-phase flow in the closed loop /SCH18/
- Analyses of reactor calculations, e.g.: 5% cold leg break in a German 1300 MW PWR /GLA01b/, 200% cold leg break of Zion Westinghouse type PWR reactors /GLA08/, /SKO09/

To illustrate the application of the GRS methodology, the main results of the uncertainty analysis for the LSTF test SB-CL-18 will be presented in a summarized form. This experiment belongs to the validation matrix of ATHLET, and the corresponding validation calculation with the current code version is described in chap. 5.1.

The main physical phenomena observed during this test were two dry outs of the heater rod bundle simulating the core. The first one was due to water level depression (120-155 s) before the loop seal cleared, and the second one (420-540 s) was due to the loss of water inventory at the break, which was finished by the accumulator injection.

All potentially important uncertain parameters have been included in the uncertainty analysis /GLA01a/. Tables 6 - 2 and 6 - 3 list the selected input parameters, their specified ranges and distribution types. Included are 41 modelling parameters, 4 uncertainties related to the simulation of the bypass flow cross sections in the test vessel, 1 uncertain heater power and 2 uncertain convergence criteria of the numerical integration method of the code. The quantification of the model uncertainties is based on the experience gained from the ATHLET validation.

A total number of 100 ATHLET calculations was performed. According to Wilks' formula (eq. 6 - 2) a minimum of 93 runs are required to establish two-sided tolerance limits with 95% proba-

bility and 95% confidence. Thus, at any time point, at least 95% of the combined influence of all considered uncertainties on the calculated results is within the presented uncertainty range, at a confidence level of at least 95%.

Table 6 - 2: List of uncertain input parameters for LSTF Test SB-CL-18 calculations

No.	Parameter	Ranges		Ref. value	Distribution	Explanation
		min	max			
Critical break flow						
1	DSCON	0.5	3	2.0	Polygonal	Contraction length
2	FD	0.02	0.22	0.02	Polygonal	Weisbach-Darcy wall friction coefficient
3	FF	0.7	1	0.775	Polygonal	Contraction coefficient for steam flow
4	PP	0.98	0.999	0.98	Polygonal	Void transition for contraction coefficient
Evaporation						
5	ZBO	10^8	10^{10}	$5x10^9$	Polygonal	Number of bubbles per unit volume
6	ZT	10^8	10^{10}	$5x10^9$	Polygonal	Number of droplets per unit volume
7	OMTCON	0.5	2	1	Uniform	Direct condensation multiplier
8	TURB	1	50	20	Log-normal	Turbulence factor for evaporation in CDR model
Drift models						
9	ODVRO	0.5	1.5	1	Polygonal	Correction factor for vertical pipes
10	ODBUN	0.3	1.5	1	Normal	Correction factor for vertical bundles
11	ODVKU	0.7	1.3	1	Normal	Correction factor for vertical annulus
12	ODHPI	0.75	2.25	1	Polygonal	Correction factor for horizontal pipes
13	ODHBR	0.5	2	1	Uniform	Correction factor for horizontal cross flow connections
14	ODENT	1	3	1	Uniform	Correction factor for water entrainment in bundles
Two phase pressure drop						
15	ITMPO			1 or 4		Correlation selection (parameters 16 and 17)
16	OFI2H			1	Log-normal	Martinelli-Nelson correlation (ITMPO = 1) - horizontal Chisholm correlation (ITMPO = 4) - horizontal
17	OFI2			1	Log-normal	Martinelli-Nelson correlation (ITMPO = 1) - vertical Chisholm correlation (ITMPO = 4) - vertical
Pressure drop , wall friction						
18	ALAMO	0.01	0.03	0.02	Triangular	Pipe wall friction (ITMPO = 1)
19	ALAMO	0.01	0.03	0.02	Triangular	Rod bundle wall friction (ITMPO = 1)
20	ROUO	10^{-5}	10^{-4}		Polygonal	Pipe wall roughness (ITMPO = 4)
21	ROUO	1.510^{-6}	2.10^{-5}		Polygonal	Rod bundle wall roughness (ITMPO = 4)
Main coolant pump						
22	YHS	Table	Table	Table	Uniform	Two-phase multiplier for head and torque
Bypass flow paths						
23	CSA	0.01	0.6	0.47	Uniform	Bypass flow cross section between upper downcomer and upper plenum
24	CSA	0.2	1	0.62	Uniform	Bypass flow cross section between upper downcomer and upper head
25	ZFFJ/ZFBJ	0.4	2.5	1	Uniform	Correction factor for bypass form loss between rod bundle and upper head
26	ZFFJ/ZFBJ	0.33	3	1	Uniform	Correction factor for bypass form loss between upper plenum and upper head

Table 6 - 3: List of uncertain input parameters for LSTF Test SB-CL-18 calculations (cont.)

No.	Parameter	Ranges		Ref. value	Distribution	Explanation
		min	max			
Pressure drop, momentum term						
27	JDPA				0.25	Momentum flux term HL/UP from HL only (25%)
	JDPA				0.25	Momentum flux term HL/UP not computed (25%)
	JDPA				0.5	Momentum flux term HL/UP in both directions (50%)
28	JDPA				0.25	Momentum flux term CL/DC from CL only (25%)
	JDPA				0.25	Momentum flux term CL/DC not computed (25%)
	JDPA				0.5	Momentum flux term CL/DC in both directions (50%)
29	JDPA				0.5	Momentum flux at rod bundle inlet not computed (50%)
	JDPA				0.5	Momentum flux at bundle inlet in both directions (50%)
Pressure drop, form losses						
30	ZFFJ/ZFBJ	0.667	1.5	1	Uniform	Correction factor for form loss at branches
31	ZFFJ/ZFBJ	0.5	2	1	Uniform	Correction factor for form loss at upper bundle plate
32	ZFFJ/ZFBJ	0.4	2.5	1	Uniform	Correction factor for form loss at DC cross connections
33	ZFFJ/ZFBJ	0.8	1.25	1	Uniform	Correction factor for form loss at surge line
Heat transfer						
34	IHTCI0			1 or 2		Selection of correlations (parameter 35)
35	OHWFB	0.65 0.75	1.3 1.25	1 1	Uniform Polygonal	Correction factor for FB, Dougall-Rohsenow (50%) Correction factor for FB, Condie-Bengston (50%)
36	ICHFI0			0 or 4		Selection of correlations (parameter 37)
37	OTRNB	0.7 0.7	1.3 1.3	1 1	Uniform Uniform	Correction factor for CHF, minimum value (50%) Correction factor for CHF, Biasi correlation (50%)
38	OHWFC	0.85	1.15	1	Uniform	Correction factor for single phase forced convection to water (Dittus-Boelter)
39	OHWNC	0.85	1.15	1	Uniform	Correction factor for single phase natural convection to water (Mc Adams)
40	IHTC30			1 or 2		Selection of correlations (parameter 41)
41	OHVFC	0.8 0.85	1.2 1.25	1 1	Uniform Uniform	Correction factor for single phase forced convection to steam (Dittus-Boelter II , 50%) Correction factor for single phase forced convection to steam (Mc Eligot , 50%)
42	OHWNB	0.8	1.2	1	Uniform	Correction factor for nucleate boiling (mod. Chen)
43	OHWPB	0.75	1.25	1	Uniform	Correction factor for pool film boiling (Bromley)
44	OTMFB	0.9	1.28	1	Uniform	Correction factor for minimum film boiling temperature
45	HTCL0	20	100	50	Uniform	Accumulator walls heat transfer coefficient (W/m^2K)
Convergence criteria, heat power						
46	EPS	10^{-4}	10^{-2}	10^{-3}	Triangular	Convergence criterion (upper local relative error)
47	QROD0/00	0.99	1.01	1	Uniform	Correction factor for heater power (nominal: 10 MW)
48	CLIMX	0.1	1	0.2	Uniform	Correction factor for lower local absolute error for the void fraction (factor 1 : $5x10^{-4}$)

Of special interest is the highest calculated cladding temperature. As it can be seen in fig. 6 - 1, the experimental measurements at the elevation showing the highest temperatures, level 8, are generally inside the calculated uncertainty range. The calculated range of the second heat-up is slightly earlier than measured. The end of this heat-up phase is due to an early accumulator injection start due to a low range of calculated pressure in the primary coolant system.

The measured value for the first peak clad temperature at level 8 is 682 K, and the calculated upper uncertainty limit is 772 K. Sensitivity measures indicate the influence of the uncertainty in input parameters on the first peak clad temperature. For example, fig. 6 - 2 shows the Spearman Rank Correlation Coefficient used as sensitivity measure. The length of the bars indicates the sensitivity of the respective input parameter uncertainty on the result (here the peak clad temperature). The sensitivity measure gives the variation of the results in terms of standard deviations, when the input uncertainty varies by one standard deviation. Positive sign means that input uncertainty and results have the same direction., i.e. an increase of input uncertainty values tends to increase the clad temperature and vice-versa. For negative sign the input uncertainty and the result have opposite direction, i.e. increasing the parameter values tends to decrease the clad temperature and vice versa.

According to these quantities, the most important three parameters are the drift in horizontal pipes, the drift in vertical pipes, and drift in horizontal connections of the heater rod bundle. An increased drift in the horizontal bundle connection (decreased water droplet transport to the hot bundle regions) and increased drift in vertical pipes (impedes loop seal clearance) tend to increase clad temperature, whereas increased drift in the horizontal pipes impedes loop seal filling and results in lower clad temperatures.

A similar analysis can be made for the second peak clad temperature. The most important parameters in this case are the discharge contraction coefficient and drift in the heater rod bundle. An increased contraction coefficient leads to an earlier accumulator injection, and thus tends to decrease the peak clad temperature. A higher drift in the bundle results in increased clad temperatures in the upper bundle region.

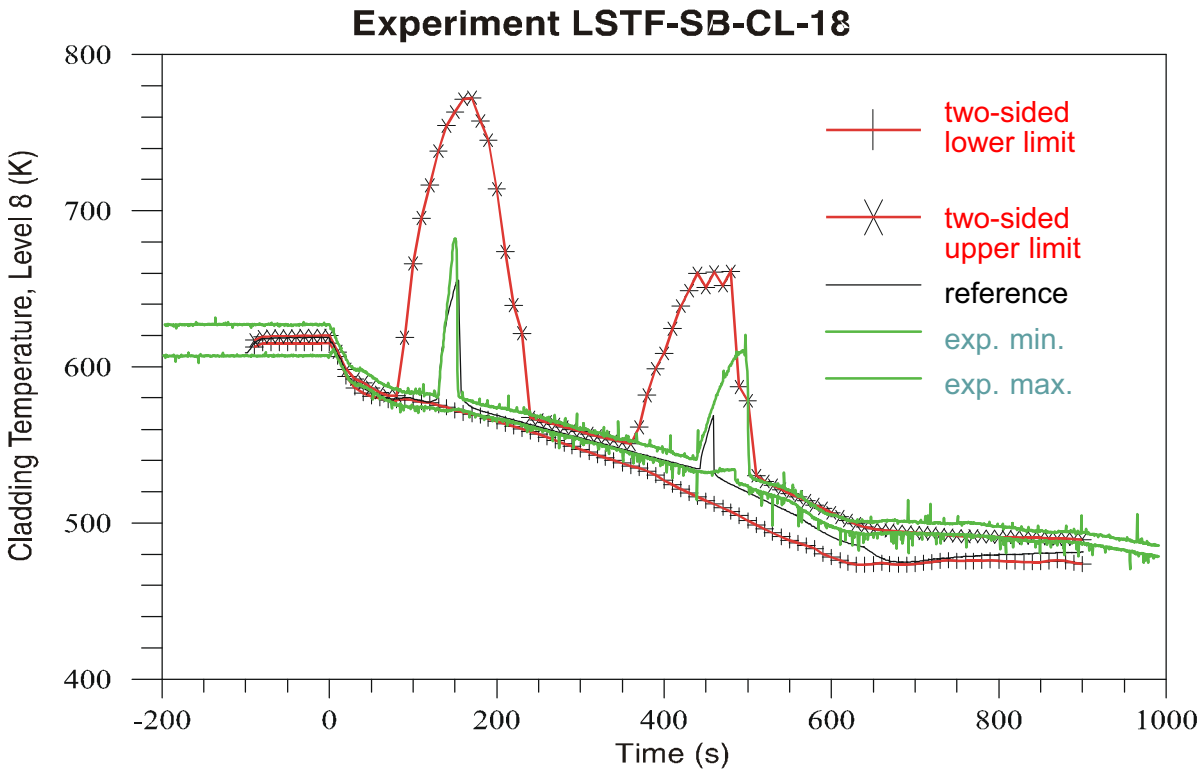

Fig. 6 - 1: Calculated uncertainty range and best-estimate reference calculation compared with measured minimum and maximum values of peak cladding temperatures at level 8 in LSTF Test SB-CL-18.

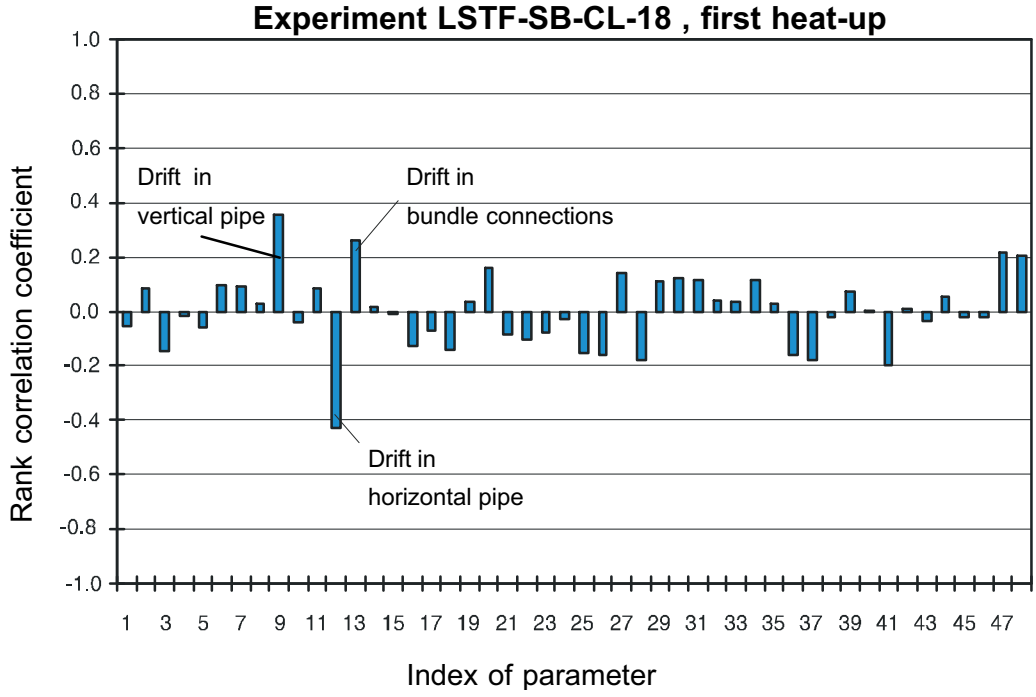

Fig. 6 - 2: Sensitivity measures of the first peak clad temperature for the 48 selected uncertain input parameters for the post-test calculation of LSTF SB-CL-18.

6.5 Conclusions

The validation concept for ATHLET is supported by a methodology to derive uncertainty statements quantifying the combined influence of all potentially important model, nodalization, numerical, and experimental uncertainties of the calculated results.

A significant advantage of this methodology is that no a priori reduction in the number of uncertain input parameters by expert judgement or screening calculations is necessary to limit the calculation effort. All potentially important parameters may be included in the uncertainty analysis. The method accounts for the combined influence of all identified input uncertainties on code results.

The number of calculations needed is independent of the number of uncertain parameters accounted for in the analysis. It does, however, depend on the requested tolerance limits, i.e., the requested probability coverage (percentage) of the combined effect of the quantified uncertainties, and on the requested confidence level (percentage) of the code results. These tolerance limits can be used for quantitative statements about margins to acceptance criteria.

Another important feature of this method is that it provides sensitivity measures of the influence of the identified input parameter uncertainties on the results. The measures allow the derivation of an uncertainty importance ranking, which in turn provides guidance as to where to improve the state of knowledge in order to reduce output uncertainties most effectively, or where to improve code modelling. Different to other known methods, this ranking is a result of the analysis and its inputs, not of an a priori expert judgement. Uncertainty statements and sensitivity measures are available simultaneously for all single-valued parameters (e.g. peak cladding temperature) as well as for the time evolution of output quantities. This method relies only on actual code calculations without the use of approximations like fitted response surfaces.

The specification of ranges and probability distributions of input parameters may have a large influence on the uncertainty of code results, and thus on the quantification of the prediction capability. Current activities in the frame of prediction capabilities of best-estimate codes are emphasizing these specifications. Investigations are underway to transform data measured in experiments and obtained in post-test calculations into thermal-hydraulic modelling parameters with uncertainties. It is more effective to concentrate on those uncertainties showing the highest sensitivity measures. The state of knowledge about uncertain parameters has to be further improved, and suitable experimental as well as analytical information has to be selected.

The GRS method has been used in different applications by various international institutions, e.g. in the frame of the OECD Uncertainty Methods Study /WIC98/. Based on an increasing experience with generic applications to experiments and reactor transients, the method will allow the quantification of uncertainties in future ATHLET reactor calculations.

7 References

/ADA84/ J. P. Adams, J. C. Birchley:
Quick-Look Report on OECD LOFT Experiment LP-LB-1
EG&G Idaho, Inc.
OECG LOFT-T-3504, February 1984

/AKS94/ N. Aksan, F. D'Auria, H. Glaeser, R. Pochard, C. Richards, A. Sjöberg:
Separate Effects Test Matrix for Thermal-Hydraulic Code Validation,
Volume I: Phenomena Characterisation and Selection of Facilities and Tests,
Volume II: Facility and Experiment Characteristics.
NEA/CSNI/R(93)14/Part 1 and Part 2, Paris 1994.

/AKS95/ N. Aksan, F. D'Auria, H. Städtke:
User Effects on the Transient System Code Calculations,
NEA/CSNI/R(94) 35, Jan. 1995.

/ANN96/ A. Annunziato, H. Glaeser, J. Lillington, P. Marsili, C. Renault, A. Sjöberg:
CSNI Integral Test Facility Validation Matrix for the Assessment of Thermal-Hydraulic Codes for LWR LOCA and Transients.
NEA/CSNI/R(96) 17, July 1996.

/ANO80/ Y. Anoda, et. al.:
ROSA-III System Description
Japan Atomic Energy Research Institute
JAERI-M 9243, December 1980

/ANO81/ Y. Anoda, et. al.:
ROSA-III System Description for Fuel Assembly No. 4
Japan Atomic Energy Research Institute
JAERI-M 9363, February 1981

/ARI95/ V. Arinine, R. Kirmse, S. Nikonov, O. Sakharova, F. Steinhoff:
Nachrechnung des FIST-Versuchs 6MSB1 mit ATHLET.
GRS Report, GRS-A-2278, August 1995.

/ARN97/ S. Arndt, J. Macek, R. Meca, I. Vojtek, H. Wolff:
Weiterentwicklung und Verifikation von Rechenprogrammen zur Analyse von Störfällen in WWER-Reaktoren. WTZ mit der Tschechischen Republik
GRS-A-2467, Februar 1997

/ATH92/ ATHLET Developer's Manual
GRS Internal Report, May 1992.

/AUS89/ H. Austregesilo et al.:
Auswertung von internationalen Integral- und Einzeleffektversuchen (Abschlussbericht RS 686;
GRS-A-1625; November 1989.

/AUS07/ H. Austregesilo:
Nachrechnung des ROSA/LSTF Versuchs SB-PV-09 mit ATHLET Mod 2.1 Cycle A;
GRS-A-3369; März 2007.

/AUS10/ H. Austregesilo et al.:
Validierung des Rechenprogrammsystems ATHLET / ATHLET-CD
Abschlussbericht, GRS-A-3522; April 2010.

/AUS13/ H. Austregesilo et al.:
Validierung von Rechenprogrammen zur Simulation von Stör- und Unfällen im Reaktorkühlsystem
Abschlussbericht, GRS-A-3706; Juli 2013.

/AUS13a/ H. Austregesilo et al.:
Teilnahme am Internationalen Standardproblem ISP-50 mit ATHLET
GRS Report, GRS-A-3685; März 2013.

/AUS13a/ H. Austregesilo et al.:
Teilnahme am Internationalen Standardproblem ISP-50 mit ATHLET
GRS Report, GRS-A-3685; März 2013.

/AUS13b/ H. Austregesilo, T. Skorek, Ph. Schöffel:
Simulation of the international standard problem ISP-50 with the system code ATHLET
Proc. Of the 15th International Topical Meeting on Nuclear Thermal-Hydraulics, NURETH-15, Pisa Italy May 2013.

/BAE96/ L.E. Pomier Baez, P Dräger:
TPTF Experiments Post Test Calculation with ATHLET/MOD 1.1C.
GRS Report, GRS-A-2358, March 1996.

/BES96/ D. Bessette:
Status Report on the Use of Best-Estimate Methodology in Safety Analysis and Licensing,
Report by the Task Group on Thermal-Hydraulic Applications (TG-THA of PWG-2),
OECD/NEA/CSNI, July 1996.

/BOR93/ J. T. Bornemann:
Nachrechnung des Integral-Versuches ROSA-III Run 971 mit ATHLET/MOD1.0 - Cycle E.
TÜV Bayern, TÜV-1500881 May 1993.

/BUC15/ S. Buchholz, D. von der Cron, A. Schaffrath:
System codes improvements for modelling passive safety systems and their validation;
Eurosafe Forum; Brussels, Belgium; 2015

/BUR01/ M. J. Burwell:
Nachrechnung des Einzeleffektversuchs UPTF TRAM C2 Run 7a und 9a mit ATHLET;
GRS-A-2871; März 2001

/BUR03/ M. J. Burwell:
Nachrechnung des Einzeleffektversuchs UPTF TRAM C3 (Run 13a, 14a) mit ATHLET;
Technischer Bericht GRS-A-3123; Juli 2003

/BUR85/ M. J. Burwell, P. Romstedt:
Critical flow calculation and the evaluation of the critical plane location in a nozzle with a 1-D two phase flow model
Paper submitted to the “1985 European Two Phase Flow Group Meeting”, Southampton, England, June 4^{th} - 7^{th} , 1985

/BUR89/ M. J. Burwell:
Post-test calculation of the LOBI experiment A2-81 with ATHLET
GRS Report, GRS-A-1569, May 1989.

/BUR92/ M. J. Burwell:
Post-Test Calculation of UPTF-Test 30 with ATHLET
GRS Report, GRS-A-1890, March 1992.

/BUR94/ M. J. Burwell:
Nachrechnung des UPTF-TRAM A6 Run 01C Versuches mit ATHLET.
GRS Report, GRS-A-2126, May 1994.

/BUT84/ J. D. Burtt:
International Standard Problem 13 (LOFT Experiment L2-5)
Final Comparison Report
NUREG/CR-4115, December 1984.

/CEC90/ Commission of the European Communities:
Comparative calculations on selected two-phase flow phenomena using major PWR system codes
EUR 12901; Brussels, Luxembourg, 1990

/CEU15/ S. Ceuca, P. Pandazis:
Nachrechnung der ROCOM-Versuche 2.1 und 2.2 mit ATHLET unter Anwendung des 2D/3D-Modells im Ringraum und unteren Plenum
Technische Notiz TN-RCM-15/01; GRS; März 2015.

/CHO12/ K. Y. Choi et al.:
International Standard Problem No. 50
Final Integration Report
Nuclear Energy Agency NEA / CSNI / R(2012)6, Feb. 2012

/CLE92/ P. Clement, T. Chataing, R. Deruaz:
OECD/NEA/CSNI International Standard Problem No. 27, BETHSY Experiment 9.1B, 2”Cold Leg Break Without HPSI and With Delayed Ultimate Procedure, Comparison Report, Volumes 1 and 2,
NEA/CSNI/R(R92) 20, Nov. 1992.

/CRO15/ D. von der Cron, H. V. Hristov, A. Seubert:
Modeling of the Thermal Hydraulics of Very-High-Temperature Reactors with the System Code ATHLET
Proc. of the NURETH-16 conference, Chicago, USA, 2015.

/CSN87/ CSNI Code Validation Matrix of Thermo-Hydraulic Codes for LWR LOCA and Transients.
CSNI Report 132, March 1987.

/CSN89/ Thermohydraulics of Emergency Core Cooling in Light Water Reactors; a State-of-the-Art Report by a Group of Experts of the NEA Committee on the Safety of Nuclear Installations.
CSNI Report No. 161, October 1989.

/DEC08/ A. de Crecy et al.:
Uncertainty and sensitivity analysisof the LOFT L2-5 tests: Results of the BE-MUSE programme
Nuclear Engineering and Design, Vol. 238, pp. 3561-3578, Dec. 2008.

/DEL11/ A. Del Nevo et al.:
Analytical Exercise on OECD / NEA / CSNI PKL-2 Project Test G.3.1:
Main Steam Line Break Transient in PKL III Facility
OECD /NEA / CSNI PKL-2 Project, TH / PKL-2 / 02 (10), March 201

/DRÄ00/ P. Dräger, W. Horche, Z. Jakubowski, W.Pointner:
Störfallsimulator Unterweser - Qualifikation der Datenbasis.
GRS Report, GRS-A-2802, March 2000

/DRÄ02/ P. Dräger:
Störfallsimulator Philippsburg 2, Qualifikation der Datenbasis
GRS-A-3064; Juni 2002

/DRÄ91/ P. Dräger:
Nachrechnung des Integralexperiments LOFT-LP-SB-3 mit ATHLET.
GRS Report, GRS-A-1764, April 1991.

/DRÄ98/ P. Dräger:
Nachrechnung des Versuchs UPTF/TRAM A7 (Run 1A) mit ATHLET.
GRS Report, GRS-A-2557, Jan. 1998.

/ELE95/ Russian Standard Safety Problem No. 1 (SSP-1) on ISB-WWER Test Facility
2.4% Small Leak From the Upper Plenum of the Reactor
Final Report 3.433 (in Russian language)
Electrogorsk Research & Engineering Centre on Nuclear Plants Safety,
Electrogorsk, Russia, 1995.

/ELE97/ Russian Standard Safety Problem No. 2 (SSP-2) on ISB-WWER Test Facility
11% Leak From the Upper Plenum of the Reactor With Subsequent Trip of Circulation Pumps
Final Report 2.468 (in Russian language)
Electrogorsk Research & Engineering Centre on Nuclear Plants Safety,
Electrogorsk, Russia, 1997.

/FEI93/ L. Fei, Th. Thiele:
Nachrechnung des Versuches UPTF-TRAM A2 mit dem Systemcode ATHLET.
Dr. Pitscheider Ingenieur-Büro, Report Nr. 9308, 1993.

/FES93/ M. Fessel, B. Kraus, W. Lischke, B. Vandreier:
Beiträge zur Verifikation des Rechencodes ATHLET: Analyse der Experimente am Einzelrohrversuchsstand HORUS I.
HTWS Zittau, Project BMFT-150 0856 0, June 1993.

/FJO94/ A. Fjodorov, B. Kraus, W. Lischke, Th. Schöße:
Analyse der Experimente am Einzelrohrversuchsstand HORUS II.
Hochschule für Technik, Wirtschaft und Sozialwesen TWS Zittau/Görlitz (FH),
Report THZ-61205-13, September 1994.

/FJO96/ A. Fjodorov, W. Lischke:
Kondensation von Wasserdampf-Inertgas-Gemischen - Analyse der Experimente am Versuchsstand HORUS II mit den ATHLET-Code Versionen MOD 1.1 Cycle B und C.
Hochschule für Technik, Wirtschaft und Sozialwesen TWS Zittau/Görlitz (FH), Report THZ-61205-15, Mai 1996.

/FJO98/ A. Fjodorow, W. Lischke:
Modell zur Berechnung von Wärmeübergangskoeffizienten bei der Kondensation in horizontalen Rohren für den ATHLET-Code;
Hochschule Zittau/Görlitz (FH); IPM-610205-04; Februar 1998

/GAR73/ R.W. Garner:
Comparative Analyses of Standard Problems, Standard Problem 1 (Straight Pipe Depressurization Experiments)
Aerojet Nuclear Company Interim Report I-212-74-5.1, October 1973

/GAS91/ H. Gasteiger:
Post Test Calculation of UPTF Test 18 with the Code System ATHLET/FLUT.
TÜV Bayern, June 1991

/GAS93/ H. Gasteiger:
Nachrechnung des Integral-Versuches ROSA-III Run 912 (5%-Bruch der Treibwasserschleife ohne Anregung des Hochdruck-Kernsprühsystems) mit ATHLET/MOD1.0 - Cycle E.
TÜV Bayern, TÜV-1500881, May 1993.

/GAX95/ M. P. Gashenko, A. P. Proshutinsky, E. Stolyarov, I. V. Elkin:
ISB-WWER: Description and Geometrical Characteristics, Measurement System Description, Heat Losses.
Electrogorsk Research & Engineering Centre on Nuclear Plants Safety, Electrogorsk, Russia, 1995.

/GAX97/ M. P. Gashenko, A. P. Proshutinsky, E. Stolyarov, I. V. Elkin:
The Russian Standard Problem No. 2 (SSP-2) at the Test Facility ISB-WWER Final Report (in Russian language)
Electrogorsk Research & Engineering Centre on Nuclear Plants Safety, Electrogorsk, Russia, 1997

/GEP90/ J. Geppert, G. Höppner, J. E. Miró:
Nachrechnung des LOBI-Versuches BT-01 (Frischdampfleitungsleck) mit dem Systemcode ATHLET.
GRS Report, GRS-A-1679, June 1990.

/GEP96/ J. Geppert, F. Steinhoff:
Nachrechnung des Integralexperiments PKL III B 1.2 mit ATHLET.
GRS Report, GRS-A-2337, Feb. 1996.

/GLA01a/ H. Glaeser, E. Hofer, B. Krzykacz-Hausmann, J. Leffer, T. Skorek:
Einfluss von Modellparametern auf die Aussagesicherheit von ATHLET-Rechenergebnissen zum Integralexperiment LSTF-SB-CL-18
GRS-A-2941, Juli 2001

/GLA01b/ H. Glaeser, E. Hofer, B. Krzykacz-Hausmann, J. Leffer, T. Skorek:
Einfluss von Modellparametern auf die Aussagesicherheit von ATHLET-Rechenergebnissen zum 5%-Leck im kalten Strang eines Druckwasser-Reaktors
GRS-A-2942, August 2001

/GLA01c/ H. Glaeser, E. Hofer, A. Hora, B. Krzykacz-Hausmann, J. Leffer, T. Skorek:
Einfluss von Modellparametern auf die Aussagesicherheit des Thermohydraulik-Rechenprogramms ATHLET
GRS-A-2963, September 2001

/GLA08/ H. Glaeser, B. Krzykacz-Hausmann, W. Luther, S. Schwarz, T. Skorek:
Methodenentwicklung und exemplarische Anwendungen zur Bestimmung der Aussagesicherheit von Rechenprogrammergebnissen
GRS-A-3443, November 2008

/GLA94a/ H. Glaeser, E. Hofer, M. Kloos, T. Skorek:
Unsicherheits-und Sensitivitätsuntersuchungen von Analysen mit Thermaohydraulik-Rechenprogrammen.
GRS-A-2177, Juli 1994.

/GLA94b/ H. Glaeser, E. Hofer, M. Kloos, T. Skorek:
Uncertainty and sensitivity analysis of a post-experiment calculation in thermal hydraulics,
Reliability Engineering and System Safety 45 (1994) 19 - 33; 1994.

/GOC00/ U. Gocht, W. Lischke, A. Schaffrath:
Beiträge zur Validierung des Thermohydraulikcodes ATHLET anhand der Nachrechnungen der Experimente an der Versuchsanlage HORUS II;
Hochschule Zittau/Görlitz (FH); IPM-610208-03; August 2000.

/GRS13/ Maßnahmen zur Qualitätssicherung bei der Erstellung von Computerprogrammen in der GRS (QM-Richtlinie Programmentwicklung);
QM-Handbuch, Teil 3: Fachanweisung 3 *Fachliche Qualitätssicherung von Arbeitsergebnissen*, Anlage IV; GRS; 2013.

/GYO95/ C. Györi, W. Horche, I. Trosztel:
ATHLET-Verifikation und Einsatz für Störfallanalysen des WWER-440.
GRS Report, GRS-A-2293, October 1995.

/HOB89/ W. Hobbhahn, J.P. Weber, A.Forge, M. Mezza, R. Pochard, A. Porrachia:
Code Comparison based on a Neptunus Pressurizer Experiment.
Proc. NURETH-4, Karlsruhe, Vol. I, 10-13.10.1989.

/HOC01/ W. Horche, A. Guba, I. Trosztel, H. Glaeser, E. Hofer, B. Krykacz:
Untersuchungen zur Weiterentwicklung und Verifikation von ATHLET zur Analyse von WWER-Anlagen.
WTZ mit der Republik Ungarn - Abschlußbericht (Band 2).
GRS Report, GRS-A-2886, Feb. 2001.

/HOC95/ W. Horche, W. Kauer, Th. Lehnart, L. Roßner:
Qualifikation der Datenbasis für das KKW Brokdorf mit dem Programmsystem ATLAS.
GRS Report, GRS-A-2323, Dezember 1995.

/HOC98/ W. Horche, Z. Jakubowski, W. Pointner:
Qualifikation der Datenbasis für das KKW Neckar (GKN-2) mit dem Programmsystem ATLAS.
GRS Report, GRS-A-2541, Jan. 1998.

/HOC99/ W. Horche et al.:
Untersuchungen zur Weiterentwicklung und Verifikation von ATHLET zur Analyse von WWER-Anlagen (Band 1);
GRS-A-2798; Dezember 1999

/HOF85/ E. Hofer et al.:
Uncertainty and Sensitivity Analysis of Accident Consequence Submodels.
Proc. of ANS/ENS International Topical Meeting on Probabilistic Safety Mathods and Applications, San Francisco 1985.

/HOL16/ T. Hollands et al.:
Validierung von Rechenprogrammen zur Simulation des Reaktorkühlkreislaufs unter Stör- und Unfallbedingungen
GRS Report, GRS-404 (partly restricted), July 2016.

/HOP87/ G. Höppner, D. Pietrzak:
ALMOD4 Qualification with LOBI Experiment A2-90.
GRS Report, GRS-A-1351, July 1987.

/HOP93/ G. Höppner, F. Steinhoff:
ATHLET-Nachrechnung eines Ausfalls der Hauptwärmesenke in einem SWR.
GRS Report, GRS-A-2100, Dezember 1993.

/HOR09/ W. Horche
Modellierung des ROCOM-Versuchsstandes und Nachrechnungen von Experimenten aus der Serie T6655 mit ATHLET
GRS Report, GRS-A-3453, Januar 2009.

/HRI15/ H. V. Hristov et al.:
Numerical Analyses on the Safety Aspects of KASOLA test facility
Proc. of the NURETH-16 conference, Chicago, USA, 2015.

/HRU92/ M. Hrubisko:
Nachrechnung des ROSA III Versuchs Run 984 mit dem Rechenprogramm ATHLET.
GRS Report, GRS-A-1981, December 1992.

/HRU93/ M. Hrubisko, W. Pointner:
Nachrechnung des ROSA III Versuchs Run 952 mit ATHLET.
GRS Report, GRS-A-2084, November 1993.

/HRU95/ M. Hrubisko:
Nachrechnung des FIST-Versuchs 6SB2C mit ATHLET.
GRS Report, GRS-A-2276, August 1995.

/IAE95/ Simulation of a Loss of Coolant Accident Without High Pressure Injection But With Secondary Feed and Bleed
Results of the Fourth Standard Problem Exercise on the Simulation of Loss of Coolant Accidents
IAEA Technical Co-operation Project RER/9/004
IAEA-TECDOC-848, November 1995

/JAE85/ ROSA-IV Large Scale Test Facility (LSTF) System Description
The ROSA-IV Group
JAERI-M 84-237, January 1985

/JAE89/ ROSA-IV / LSTF 5% Cold Leg Break LOCA Experiment Run SB-CL-18
Data Report
The ROSA-IV Group
JAERI-M 89-027, March 1989

/JAE89a/ LSTF Instrumentation for Run SB-CL-18
Amendment to System Description (JAERI-M 84-237) and Data Report (JAERI-M 89-027)
JAERI Handout at 1st ISP-26 Workshop, March 9-10, 1989.

/KHR15/ N. Khrennikov et al.:
Application of 3-D coupled code QUABOX/CUBBOX-ATHLET for RBMK-1000 vapor reactivity coefficient measurements;
Annals of Nuclear Energy 84 (2015) 200-224, 2015.

/KIR87/ R. Kirmse, P. K. Malhotra:
Post-Test-Analyses of GE-VESSEL Blowdown Tests #5803-2 (Bottom Leak) and #5702-16 (Top Leak) with ATHLET.
GRS Report, GRS-A-1354, July 1987.

/KIR89/ R. Kirmse:
Auswertung von LOBI Experimenten im Rahmen des “Share Cost Action Research Programme” der Europäischen Gemeinschaft
Abschlussbericht RS 739.
GRS Report, GRS-A-1585, June 1989.

/KIR96/ R. Kirmse, V. Pechterev, F. Steinhoff, A. Suslov:
Nachrechnung des Experiments UPTF TRAM B1, Versuchsläufe B1a-2a, B1b-3c und B1b-2a mit ATHLET.
GRS Report, GRS-A-2377, July 1996.

/KLI08/ S. Kliem, T. Sühnel, U. Rohde, T. Höhne, H.-M. Prasser, F.-P. Weiss:
Experiments at the mixing test facility ROCOM for benchmarking of CFD-codes, Nuclear Engineering and Design, Vol. 238, Issue 3, pp. 566-576 (2008),
/OEC12/ https://www.oecd-nea.org/jointproj/pkl-2.html

/KLI12/ S. Kliem, R. Franz:
OECD PKL2 Project – Final Report on the ROCOM Tests, HZDR Institute Report, Dresden, Germany (2012)

/KLO16/ M. Kloos:
SUSA Version 4.0, Software for Uncertainty and Sensitivity Analyses, User's Guide and Tutorial
GRS-P-5, Rev. 2, GRS, Garching, 2016.

/KOL11/ N. Kolev et al.:
VVER-1000 Coolant Transient Benchmark, Phase 2 (V1000CT-2), Summary Results of Exercise 2 and Exercise 3;
NEA/NSC/DOC(2011)3; 2011.

/KRE01/ E. Krepper, F. Schäfer:
Verifikation des ATHLET-Rechenprogrammes anhand der Nachanalyse zweier Experimente an der CCTF-Versuchsanlage;
FZR-315; Forschungszentrum Rossendorf e.V.; März 2001

/KRE96/ E. Krepper:
Post Test Calculations for a Small Break LOCA Experiment at the Integral Test Facility ISB-VVER using the Thermalhydraulic Code ATHLET.
Jahrestagung Kerntechnik (1996) 122-125.

/KRE98a/ E. Krepper, F Schäfer:
Verifikation des ATHLET-Rechenprogramms im Rahmen der externen Verifikationsgruppe ATHLET: BETHSY Test 5.2c - Totalverlust des Speisewassers.
FZ Rossendorf, FZR-231, August 1998.

/KRE98b/ E. Krepper, F Schäfer:
Verifikation des ATHLET-Rechenprogramms im Rahmen der externen Verifikationsgruppe ATHLET: BETHSY Test 9.3 - Heizrohrbruch mit Versagen der Hochdruck-Noteinspeisung.
FZ Rossendorf, FZR-232, August 1998.

/KRY91/ L. Krey:
Post Test Calculation of CCTF-Test C2-20, Run80 with the Code System ATHLET/FLUT N80a.
TÜV Bayern, June 1991.

/KRZ94/ B. Krzykacz, E. Hofer, M. Kloos:
A Software System for Probabilistic Uncertainty and Sensitivity Analysis of Results from Computer Models,
Proceedings PSAM-II, San Diego, USA, March 20 - 25, 1994.

/KUK92/ Y. Kukita, H. Nakamura, T. Watanabe et al.:
OECD/NEA/CSNI International Standard Problem No. 26, ROSA-4 LSTF Cold Leg Small-Break LOCA Experiment, Comparison Report,
NEA/CSNI/R(R91) 13, Feb. 1992.

/KYN89/ M. Kyncl, R. Kirmse:
Post-test Calculation Report LOBI-MOD2 Test BL-01.
GRS Report, GRS-A-1567, May 1989.

/LAN03/ S. Langenbuch, K.-D. Schmidt, K. Velkov:
Analysis of the pressurized water reactor main steam line break benchmark by the coupled code system ATHLET-QUABBOX/CUBBOX;
Nuclear Technology 142 (2) 124-136, 2003.

/LAN04/ S. Langenbuch, K.-D. Schmidt, K. Velkov:
Analysis of the OECD / NRC BWR Turbine Trip Benchmark by the Coupled Code System ATHLET-QUABBOX/CUBBOX;
Nuclear Science and Engineering 148 (2) 270-280, 2004.

/LAV95/ G. Lavialle, G. Kimber, C. Leveque:
BETHSY International Standard Problem 38, Loss of Residual Heat Removal System During Mid Loop Operation, 1st Workshop Report,
CEA/DRN/STR/LES/95-244, CEA Grenoble, France, Oct. 1995.

/LER02/ G. Lerchl:
Ein Modell zur Simulation des thermischen Mischens im Kaltstrang
GRS, Technische Notiz TN-LER-01/02, Mai 2002

/LER12/ G. Lerchl et al.:
ATHLET Mod 3.0 Cycle A; Validation
GRS-P-1 / Vol. 3, Rev.3; Sept. 2012

/LIE01/ K. Liesch et al.:
Validation Matrix for the Assessment of Thermal-Hydraulic Codes for VVER LOCA and Transients;
NEA/CSNI/R(2001)4

/LIS93/ W. Lischke, B. Vandreier:
Rechnungen zum ISP 33 an der finnischen Versuchsanlage PACTEL.
Hochschule für Technik, Wirtschaft und Sozialwesen TWS Zittau/Görlitz (FH), Report THZ-61205-11, Juli 1993.

/LIS94/ W. Lischke, B. Vandreier:
Nachrechnung der Experimente LOF-01 und LOF-04 (Loss of secondary side feed water) an der finnischen Versuchsanlage PACTEL.
Hochschule für Technik, Wirtschaft und Sozialwesen TWS Zittau/Görlitz (FH), Report THZ-61205-14, December 1994.

/LIS96/ W. Lischke, B. Vandreier:
Nachrechnung des Experimentes LSR-10 (Loop Seal Refilling Test) an der finnischen Versuchsanlage PACTEL mit dem Thermohydraulikcode ATHLET.
Hochschule für Technik, Wirtschaft und Sozialwesen TWS Zittau/Görlitz (FH), Report THZ-61205-16, March 1996.

/LIS97/ W. Lischke, B. Vandreier:
Nachrechnung des Experimentes SBL-22 (Small break loss-of-coolant test) an der finnischen Versuchsanlage PACTEL mit dem Thermohydraulikcode ATHLET.
Hochschule für Technik, Wirtschaft und Sozialwesen TWS Zittau/Görlitz (FH), Report IPM-610205-022, Feb. 1997.

/MOS97/ A. Moskalev, V. Roginskaya, F. Steinhoff:
Nachrechnung des Integralexperiments BETHSY 6.9c mit ATHLET.
GRS Report, GRS-A-2466, March 1997.

/MOS05a/ A. Moskalev, I. Parshikov, D. Soloviev, L. Gilvanov, A. Suslov:
Post-Test Analysis of SBLOCA Experiment with Leak from Cold Leg at the PSB-VVER Test Facility by ATHLET 2.0A Code
Rosatom Software Development Center, Russian Research Center 'Kurchatov Institute', Moscow 2005.

/MOS05b/ A. Moskalev, I. Parshikov, D. Soloviev, L. Gilvanov, A. Suslov:
Post-Test Analysis of Experiment with Two-sided Leak from Hot Leg at the PSB-VVER Test Facility by ATHLET 2.0A Code
Rosatom Software Development Center, Russian Research Center 'Kurchatov Institute', Moscow 2005.

/NAL85/ C. L. Nalczny:
Summary of Nuclear regulatory Commissions LOFT Program
Research Findings.
NUREG/CR-3005, EGG-2231, April 1985.

/NEA00/ CSNI International Standard Problems (ISP), Brief Descriptions
NEA/CSNI/R(2000)5

/NEA89/ CSNI Standard Problem Procedures
CSNI Report No 17, November 1989.

/NEA94/ CSNI International Standard Problems (ISP),
Report of a CSNI Workshop on Uncertainty Analysis Methods,
London, 1 - 4 March 1994, Vol. 1,
NEA/CSNI/R(94) 19, July 1994.

/NIK11/ S. P. Nikonov, K. Velkov, A. Pautz:
Detailed Modeling of KALININ-3 NPP VVER-1000 Reactor Pressure Vessel y the Coupled System code ATHLET/BIPR-VVER
Proc. of the M&C 2011, Rio de Janeiro, Brazil, 2011.

/NRC89/ U.S. Nuclear Regulatory Commission, NRR:
Best-Estimate Calculations of Emergency Core Cooling System Performance,
Regulatory Guide 1.157 (Task RS 701-4), May 1989.

/PAL13/ S. Palazzo, K. Velkov, G. Lerchl and K. van Tichelen:
Analyses of the MYRRHA spallation loop using the system code ATHLET;
Annals of Nuclear Energy 60 (2013) 274-286; 2013.

/PAN15/ P. Pandazis, S. Ceuca, P. Schoeffel, H. Hristov:
Investigation of multidimensional Flow Mixing Phenomena in the Reactor Pressure Vessel with the System Code ATHLET
Proc. NURETH-16, Chicago, 2015.

/PAP12/ A. Papukchiev, et al.:
Multiscale Analysis of a Transient Pressurized Thermal Shock Experiment with the Coupled Code ATHLET - ANSYS CFX;
ATW, International Journal for Nuclear Power, June 2012.

/PAP14/ A. Papukchiev, et al.:
Assessment of Coupled Multiscale and Stand Alone System Code Simulations Based on a Double T-Junction Mixing Experiment;
45th Annual Meeting on Nuclear Technology, Frankfurt, Germany, 2014.

/PAP15/ A. Papukchiev, et al.:
Multiscale Analysis of Forced and Natural Convection Including Heat Transfer Phenomena in the TALL-3D Experimental Facility;
Proc. of the NURETH-16 Conference, Chicago, USA, 2015.

/PAP96/ P. Papadimitriou:
Kondensation an der Einspeisestelle und Modellierung in ATHLET;
Beitrag zu 'Nutzung von UPTF-TRAM-Ergebnissen für Reaktoranalysen mit ATHLET;
UPTF-TRAM Fachtagung V, Mannheim, Deutschland, 15. Oktober 1996.

/PER11/ M. Perez et al.:
Uncertainty and sensitivity analysis of a LB LOCA in a PWR Nuclear Power Plant: Results of the Phase V of the BEMUSE programme.
Nuclear Engineering and Design, Vol. 241, pp. 4206-4222, 2011.

/POI84/ W. Pointner:
Posttest calculation of the LOFT experiment LP-SB-1 with DRUFAN-02.
GRS Report, GRS-A-1047, December 1984.

/POI84a/ W. Pointner:
Posttest calculation of the LOFT experiment LP-SB-2 with DRUFAN-02:
GRS Report, GRS-A-1048, December 1984.

/POI89/ W.Pointner:
Nachrechnung des ROSA III Versuchs Run 983 mit den RechenprogrammenA-THLET und FLUT.
GRS Report, GRS-A-1594, July 1989.

/POI89a/ W. Pointner:
Nachrechnung des ROSA III Versuchs Run 916 mit den Rechenprogrammen ATHLET und FLUT.
GRS Report, GRS-A-1624, November 1989.

/POI91/ W. Pointner:
Wissenschaftlich-technische Zusammenarbeit mit der DDR:
ATHLET Analysen für WWER 440 Reaktoranlagen (Abschlußbericht)
GRS Report, GRS-A-1768, März 1991.

/POI92/ W. Pointner, J. Steinborn:
Vorausrechnung des Integralexperiments BETHSY 9.1.b mit ATHLET.
GRS Report, GRS-A-1949, August 1992.

/POI92a/ W. Pointner, M. Fessel:
Nachrechnung des HDR Versuchs V 21.1 mit dem Rechenprogramm ATHLET
GRS Report, GRS-A-1950, August 1992.

/POI94/ W. Pointner:
Qualifikation der Datenbasis für das KKW Gundremmingen mit dem Programmsystem ATLAS.
GRS Report, GRS-A-2184, September 1994.

/POI96/ W. Pointner:
Störfallsimulator Krümmel - Qualifikation der Datenbasis.
GRS Report, GRS-A-2359, May 1996.

/POI99/ W. Pointner:
Störfallsimulator Philippsburg I - Qualifikation der Datenbasis.
GRS Report, GRS-A-2691, March 1999.

/PRE16/ PREMIUM: A Benchmark on the Quantification of ot the Uncertainty of the Physical models in the System Thermal-Hydraulic Codes - Methodologies and Data Review.
NEA/CSNI/R(2016)9 Report, April 2016.

/PRA03/ H.-M. Prasser, G. Grunwald, T. Höhne, S. Kliem, U. Rohde, F.-P. Weiss:
Coolant mixing in a PWR – deboration transients, breaks and emergency core cooling injection – experiments and analyses, Nuclear Technology, 143,
pp. 37-56 (2003)

/PUR94/ H. Purhonen, J. Kouhia, H. Holmström:
OECD/NEA/CSNI International Standard Problem No. 33, PACTEL Natural Circulation Stepwise Coolant Inventory Reduction Experiment, Comparison Report, Volumes 1 and 2,
NEA/CSNI/R(R94) 24, Dec. 1994.

/REE78/ D. L. Reeder:
LOFT System and Test Description (5.5-Ft Nuclear Core 1 LOCEs).
NUREG/CR-0247, TREE-1208, July 1978.

/RIN01/ F. J. Ringer:
Nachrechnung des Einzeleffektversuchs UPTF 8A mit ATHLET;
GRS-A-2870; März 2001

/RIN01a/ F. J. Ringer:
Nachrechnung des LOBI MOD2 Experiments A1-82
Technischer Bericht GRS-A-3000; Oktober 2001

/RIN03/ F. J. Ringer:
Nachrechnung des Experiments PKL III D 2.2 mit ATHLET
Technischer Bericht GRS-A-3122; Juni 2003

/RIN83/ F. J.Ringer:
Nachrechnung des BATTELLE-Versuchs SL1 mit dem
Rechenprogramm DRUFAN-02.
GRS Report, GRS-A-901, November 1983.

/RIN87/ F. J. Ringer:
Nachrechnung des MARVIKEN - Versuchs NR. 22
mit dem Rechenprogramm ATHLET.
GRS Report, GRS-A-1361, August 1987.

/RIN90/ F. J. Ringer:
OECD-CSNI Internationales Standardproblem Nummer 6 - Nachrechnung des
LSTF-Versuchs SB-CL-18 mit dem Programmsystem ATHLET/FLUT.
GRS Report, GRS-A-1683, June 1990.

/RIN91/ F. J. Ringer:
Nachrechnung des TPTF-Ausdampfversuchs Nr.6 mit dem
5-Gleichungs-Fluiddynamikmodell des Rechenprogramms ATHLET.
GRS Report, GRS-A-1823, August 1991.

/RIN93/ F. J. Ringer:
Nachrechnung des Integralexperiments BETHSY 4.3 b mit ATHLET
GRS Report, GRS-A-2043, June 1993.

/RIN93a/ F. J. Ringer:
Nachrechnung des Integralexperiments BETHSY 5.1a mit ATHLET
GRS Report, GRS-A-2112, December 1993.

/RIN94/ F. J. Ringer:
Nachrechnung des Integralexperiments BETHSY 5.2d mit ATHLET.
GRS Report, GRS-A-2210, October 1994.

/RIN95/ F. Ringer:
Nachrechnung des Integralexperiments PKL III B 4.1 mit ATHLET.
GRS Report, GRS-A-2291, July 1995.

/RIN96/ F. J. Ringer:
Nachrechnung des Integralexperiments PKL III C 1.2 mit ATHLET.
GRS Report, GRS-A-2427, August 1996.

/RUA96/ Y.-Q. Ruan:
On Entropy Balance Analyses of Non-Equilibrium Two-Phase Flow Models for Thermal-Hydraulic Computer Simulation;
Dissertation an der Technischen Universität München, 1996

/SAC84/ L. Sachs:
Applied Statistics.
Springer Verlag, 2nd edition, 1984.

/SAN85/ J. Sanders, E. Ohlmer:
Experimental Data Report on LOBI-MOD2 Test A2-90 (LONOP-ATWS).
Commission of the European Communities, Joint Research Centre,
Ispra Establishment, Report LEC 85-35, Oct. 1985.

/SCA93/ A. Schaffrath, H. Sprünken, A.- K. Krüssenberg, U. Brockmeier:
Verifikation von ATHLET mit Hilfe der Einzeleffekttests ECTHOR
und PATRICIA-SG2.
Ruhr-Universität Bochum, Report RUB E-33, May 1993.

/SCH00/ M. Schall:
Verifikation des ATHLET-Rechenprogramms im Rahmen der externen Verifikationsgruppe ATHLET (Versuche LOFT L2-5 und CCTF C2-12).
Battelle Ingenieurtechnik GmbH, Report BF-R-68.449-01, July 2000.

/SCH89/ M. Schall:
Unabhängige Verifikation des ATHLET-Rechenprogramms am Beispiel von LOBI-Versuchen.
Battelle Institut e. V., Report BF-R-66.762-01, December 1989.

/SCH93/ M. Schall:
Verifikation des ATHLET-Rechenprogramms im Rahmen der externen ATHLET-Verifikationsgruppe.
Battelle Institut e.V., Report BF-R-67.836-01, May 1993.

/SCH94/ M. Schall:
Verifikation des ATHLET-Rechenprogramms durch Nachanalysen von BETHSY-Versuchen (BETHSY 4.1a TC und BETHSY 3.4a).
Battelle Ingenieurtechnik GmbH, Report BF-R-67.836-01, October 1994.

/SCH98/ M. Schall:
Verifikation des ATHLET-Rechenprogramms im Rahmen der externen Verifikationsgruppe ATHLET (Versuche: BETHSY 6.2 TC, BETHSY 7.2c, BETHSY 4.1a, Phase 2).
Battelle Ingenieurtechnik GmbH, Report BF-R-68.355-01, March 1998.

/SCH08/ P. Schöffel:
Nachrechnung des Versuchs UPTF20 mit ATHLET Mod 2.1 Cycle B
GRS Report, GRS-A-3400, Januar 2008.

/SCH12/ P. Schöffel:
Nachrechnung der Versuchsreihe UPTF-TRAM C1 unter Einsatz des neuen ATHLET 2D/3D-Moduls
Technische Notiz TN-SCO-01/12, GRS, Garching, 2012.

/SCH15/ P. Schöffel et al.:
Weiterentwicklung des Systemrechenprogramms ATHLET für Anwendungen in der Reaktorsicherheit;
Abschlussbericht; GRS-387, ISBN 978-3-944161-68-6; 2015.

/SCK98/ H. Schickel, F. Steinhoff:
Wiederholungsrechnungen mit ATHLET zu BETHSY 5.2d, PKL III B 1.2 und UPTF TRAM B1.
GRS Report, GRS-A-2570, April 1998.

/SEN94/ A. Senst, A. Petry:
Nachrechnung des Versuchs PKL III B3.1 mit ATHLET;
GRS-A-2166; April 1994

/SKO88/ T. Skorek, H.-G. Sonnenburg:
ATHLET Calculations of Large Vessel Blowdown Experiments Using a Full-Range Drift-Flux Model;
Proc. Int. Conf. Thermal Reactor Safety, Vol. 5,pp. 1867-1875, Avignon, Oct. 1988

/SKO88a/ T. Skorek:
Calculation of IVO Loop Seal Experiment with ATHLET
GRS, Technische Notiz, TN-SKT-88-1; Mai 1988

/SKO95/ T. Skorek:
Modelling of Two-Phase Flow in Dividing T-Junctions with Horizontal Inlet Pipe
Proc. First Int. Symposium on Two-Phase Flow Modelling and Experimentation, Rome , 1995, pp 339-346.

/SKO09/ T. Skorek:
Uncertainty and Sensitivity Analyses of Experiment and NPP Accidents: Large Break LOCA at Cold Leg of Zion Nuclear Power Plant and Compatison with LOFT Test L2-5
Proc of the 13th Intern. Topical Meeting on Nuclear Reactor Thermal Hydraulics (NURETH13), Kanazawa, Japan, Sept. 27 - Oct. 2, 2009.

/SKO11/ T. Skorek, B. Krzykacz.Hausmann, H. Austregesilo:
Investigation of the Uncertainty of Governing Equation Systems in the Thermal-Hydraulic Calculation,
Proc of the 14th Intern. Topical Meeting on Nuclear Reactor Thermal Hydraulics (NURETH14), Toronto, September 2011.

/SKO17/ T. Skorek:
Input uncertainties in uncertainty analyses of system codes: Quantification of physical model uncertainties on the basis of CET (combined effect tests)
Nuclear Engineering and Design, Vol. 321, pp. 301-317, 2017.

/SON90/ H.-G. Sonnenburg:
Analysis of UPTF 11 (Hot Leg CCF) with a Full-Range Drift-Flux Model.
GRS Report, GRS-A-1681, June 1990.

/SON90a/ H.-G. Sonnenburg, P. N. Prassad:
Analysis of UPTF - Test 26 Run 230 by ATHLET Code
with a Full-Range Drift-Flux Model.
GRS Report, GRS-A-1723, October 1990.

/SON94/ H.-G. Sonnenburg:
Berechnung der Phasendifferenzgeschwindigkeit von Wasser und Dampf in geometrisch unterschiedlich berandeten Kanälen;
Dissertation an der Technischen Universität Berlin, Juni 1994; GRS-109

/STA87/ H. Städtke:
International Standard Problem No. 18
LOBI-MOD2 Small Break LOCA Experiment A2-81
CSNI-133, April 1984.

/STE05/ J. Steinborn:
OECD PSB-VVER Analytical Exercise (AE)
Results of Test 4: Primary to Secondary Leak Post-Test Calculation with ATHLET Computer Code
Participant's Report, December 2005.

/STE94/ J. Steinborn, S. Nikonov:
Voraus-und Nachrechnung des Integralexperimentes PACTEL (ISP-33) mit ATHLET.
GRS Report, GRS-A-2125, May 1994.

/STE95/ J. Steinborn et al.:
Voraus- und Nachrechnung des IAEA Standardproblems SPE-4 mit ATHLET;
GRS-A-2254; Februar 1995

/STE98/ J. Steinborn:
Nachrechnung des 2. Russischen Standardproblems am integralen Versuchsstand ISB-WWER mit ATHLET.
GRS Report, GRS-A-2562, April 1998.

/STE99/ J. Steinborn:
Voraus- und Nachrechnung des 3. Russischen Standardproblems am Integralversuchsstand ISB-WWER mit ATHLET;
GRS-A-2768, November 1999

/STF01/ F. Steinhoff:
Nachrechnung des Versuchs PKL III B4.5 mit ATHLET;
GRS-A-2861; März 2001

/STF02/ F. Steinhoff:
Nachrechnung des Integralexperiments PKL III D2.1 mit ATHLET;
GRS-A-3090; November 2002

/STF04/ F. Steinhoff:
Nachrechnung des Integralexperiments PKL III E2.2 mit ATHLET (Wiederholungsrechnung);
GRS-A-3222; August 2004

/STF06/ F. Steinhoff:
Nachrechnung des Versuchs PKL III E3.1 mit ATHLET;
GRS-A-3298; April 2006

/STF06a/ F. Steinhoff:
Nachrechnung des Versuchs PKL III E2.3 mit ATHLET;
GRS-A-3327; June 2006

/STF89/ F. Steinhoff:
Phasenseparation und Gemischspiegeldynamik bei instationären Zweiphasenströmungen;
Dissertation an der Technischen Universität München, 1989;GRS-73

/STF91/ F. Steinhoff:
Nachrechnung des GERDA-Integral Tests 16 07 02 (20 cm2-Leck im Pumpenbogen) mit dem Rechenprogramm ATHLET.
GRS Report, GRS-A-1828, August 1991.

/STF98/ F. Steinhoff:
Nachrechnung des Integralexperiments PKL III C 5.2 mit ATHLET.
GRS Report, GRS-A-2606, September 1998.

/STF99/ F. Steinhoff:
Nachrechnung des Integralexperiments PKL III D 1.2 mit ATHLET.
GRS Report, GRS-A-2766, Dezember 1999.

/STO92/ P. Stolze:
Nachrechnung des TOSHIBA-Blowdown-Versuchs mit dem 5-Gleichungsmodell (ATHLET MOD 1.0-CycleE);
Lehrstuhl für Reaktordynamik und Reaktorsicherheit, Technische Universität München; Garching, Februar 1992

/TEH91/ Technical Program Group: B. Boyack et al.:
Quantifying Reactor Safety Margines: Application of Code Scaling, Applicability and Uncertainty Evaluation Methodology to a Large Break Loss of Coolant Accident
Technical Report NUREG/CR-5249, EG&G, Idaho, Inc. 1989.

/TEH91/ H. Teske:
Nachrechnung des Integralexperiments BETHSY 4.1a mit ATHLET
GRS Report, GRS-A-1829, August 1991.

/TES01/ V. Teschendorff et al.:
Entwicklungsarbeiten für ATHLET - Abschlußbericht RS 1074.
GRS Report, GRS-A-2938, November 2001.

/TES93/ V. Teschendorff, T. Skorek, J. P. Weber:
ATHLET-Verification an HDR-Kondensationsversuchen und Druckhalterversuchen der TH Zittau.
GRS Report, GRS-A-2062, June1993.

/TES95/ V. Teschendorff, F. Steinhoff, H. Glaeser:
ATHLET Validation Using Accident Management Experiments,
7th Int. Conf. on Nuclear Reactor Thermal-Hydraulics (NURETH-7),
Saratoga Springs, NY, USA, 10. - 16. Sept. 1995.

/TES97/ V. Teschendorff et al.:
ATHLET Weiterentwicklung - Abschlußbericht RS 828A.
GRS Report, GRS-A-2506, September 1997.

/THI90/ T. Thiele:
Post Test Calculation of UPTF TEST No. 20 Using Code System ATHLET/MOD1.0-Cycle C;
Pitscheider Ingenieur-Büro, Bericht Nr. 9058, München, 18.12.1990.

/TIB15/ L. Tiborcz:
Validation of the Reflooding Model in the Code ATHLET
Diploma Thesis, Budapest University of Technology and Economics, 2015.

/TRB09/ K. Trambauer et al.:
Weiterentwicklung ATHLET / ATHLET-CD, Abschlußbericht RS 1162.
GRS Report, GRS-A-3461, März 2009.

/TRB96/ K. Trambauer:
Computer and Compiler Effects on Code Results.
CSNI Status Report, July 1996.

/VAN98/ B. Vandreier, W. Lischke:
Nachrechnung der Experimente SIR-20 und SIR-21 (Stepped inventory reduction in low primary pressure) an der finnischen Versuchsanlage PACTEL mit dem Thermohydraulikcode ATHLET.
Hochschule für Technik, Wirtschaft und Sozialwesen TWS Zittau/Görlitz (FH), Report IPM-610205-03, March 1998.

/VAN99/ B. Vandreier, W. Lischke:
Nachrechnung des PACTEL-Experimentes “Small break loss-of-coolant accident' SBL-31 mit dem Thermohydraulikcode ATHLET.
Hochschule für Technik, Wirtschaft und Sozialwesen TWS Zittau/Görlitz (FH), Report IPM-610208-01, March 1999.

/VAN99a/ B. Vandreier, W. Lischke:
Beiträge zur Validierung des Thermohydraulikcodes ATHLET anhand der Nachrechnung des PACTEL-Experimentes SBL-33.
Hochschule Zittau/Görlitz (FH), Report IPM-610208-02, December 1999.

/VEL09/ K. Velkov et al.:
Boron Transient by the GRS Coupled System Codes QUABOX/CUBBOX-ATHLET and TORT-TD/ATHLET.
Annual Meeting on Nuclear Technology, Dresden, Germany, 2009.

/VOJ00a/ I. Vojtek, J. Macek, S. Arndt, M. Bencik, L. Denk, F. Lahovsky, R. Meca, L. Parduba, H Wolff, L. Zezula:
Validierung von Rechenprogrammen zur Analyse von Störfällen in WWER Reaktoren. WTZ mit der Tschechischen Republik.
GRS-A-2850, November 2000

/VOJ00b/ I. Vojtek, D. Panayotov, B. Ilieva, M. Avramova:
Anwendung und Validierung von Rechenprogrammen zur Analyse von Störfällen in WWER Reaktoren. WTZ mit der Bulgarischen Republik.
GRS-A-2874, Dezember 2000

/VOJ01/ I. Vojtek, J. Husarcek, S. Arndt, M. Kristof, M. Ruttkayova, H. Wolff:
Anwendung und Validierung von Rechenprogrammen zur Analyse von Störfällen in WWER Reaktoren. WTZ mit der Slowakischen Republik.
GRS-A-2916, Juni 2001

/VOJ06/ I. Vojtek:
Methodentransfer im Rahmen der internationalen Kooperation des BMWi mit mittel- und osteuropäischen Ländern
(Abschlussbericht RS 1144)
GRS-A-3325, April 2006

/WAH86/ A. Wahba:
GRS-A-1209, April 1986

/WEI00/ J. Weisbrod, H. Unger:
ATHLET Validierung anhand des Einzeleffektexperiments IVO-CCFL, Nachrechnung des Experiments;
RUB E-257; Ruhr-Universität Bochum; Juni 2000

/WEI01/ J. Weisbrod, G. Bakay, H. Unger:
ATHLET Validierung anhand des Integralexperiments UPTF Test 27, Phase B, Nachrechnung des Experiments;
RUB E-269; Ruhr-Universität Bochum; Juni 2001

/WEI02/ J. Weisbrod, H. Unger, H-J Wagner:
ATHLET Validierung anhand von Nachrechnungen der Experimente UPTF Test 6, Test7 und Test Z3;
LEE-11; Ruhr-Universität Bochum; September 2002

/WEI96/ J. Weisbrod, U. Brockmeier:
Verifikation von ATHLET anhand der Nachrechnung der Einzeleffekttests PATRICIA-SG2 und UPTF TRAM-A5.
Ruhr-Universität Bochum, RUB E-145, March 1996.

/WEI98/ J. Weisbrod, H. Unger:
ATHLET-Validierung anhand von Nachrechnungen der Einzeleffekttests CREARE und UPTF Test Nr. 10, Phase B und Phase C.
Ruhr-Universität Bochum, RUB E-212, August 1998.

/WIB06/ A. Wielenberg:
Nachrechnung des Einzeleffektversuchs UPTF Nr. 7
(Gegenströmung im Ringraum) mit ATHLET
GRS-A-3365, October 2006.

/WIB08/ A. Wielenberg:
Nachrechnung des Versuchs PKL III F2.1 (Reflux-Condenser Mode bei Ausfall der Not- und Nachkühlsysteme im 3/4-Loop-Betrieb) mit ATHLET
GRS-A-3401, January 2008.

/WIC94/ T. Wickett, G. Yadigaroglu:
Report of a CSNI Workshop on Uncertainty Analysis Methods,
London, 1 - 4 March 1994, Volumes 1 and 2,
NEA/CSNI/R(94) 20, August 1994.

/WIC98/ T. Wickett, et al.:
Report of the Uncertainty Methods Study for Advanced Best Estimate Thermal Hydraulic Code Applications, Volume 1 (Comparison) and
Volume 2 (Report by the participant institutions)
NEA/CSNI/R(97) 35, 1998.

/WIE00/ H.-D. Wierum:
Verifikation des ATHLET-Rechenprogramms im Rahmen der externen Verifikationsgruppe ATHLET durch Nachanalysen der PKL II-Versuche B-2 und B-5;
Berichts-Nr. 8/2000;
TÜV Hannover/Sachsen-Anhalt; Dezember 2000

/WIE98/ H.-D. Wierum:
Verifikation des ATHLET-Rechenprogramms im Rahmen der externen Verifikationsgruppe ATHLET durch Nachanalysen der PKL III-Versuche B 4.3 und C 6.1 (Abschlußbericht);
TÜV Hannover/Sachsen-Anhalt, Berichts-Nr. 7/98, August 1998

/WIL41/ S.Wilks:
Determination of sample size for setting tolerance limits
Ann. Math. Statistics, Vol. 12, pp. 91-96, 1941

/WIN78/ W. Winkler:
Comparison Report on OECD-CSNI Standard Problem No. 6
CSNI Report No. 30, August 1978

/YON85/ T. Yonomoto, et. al.:
ROSA-III 50% Break Integral Test Run 916
Japan Atomic Energy Research Institute
JAERI-M 85-109, August 1985